Cape Peninsula
University of Technology

Rheological model influence on pipe flow predictions for homogeneous non-Newtonian fluids

By
EMILE VAN DEN HEEVER

Dissertation submitted in fulfilment of the requirements for the degree

Master of Technology: Civil Engineering

in the Faculty of Engineering

at the Cape Peninsula University of Technology

Supervisor: APN. Sutherland

Co-supervisor: Prof. R. Haldenwang

Cape Town

October 2013

Declaration

I, Emile Marcel van den Heever, declare that this research dissertation is my own unaided work. It is being submitted for the MTech Degree at Cape Peninsula University of Technology, Cape Town. It has not been submitted before for any degree or examination in any other University. Furthermore, it represents my own opinions and not necessarily those of the Cape Peninsula University of Technology.

_____

(Signature)

Signed in Cape Town this 28th day of October 2013

Abstract

The reliable prediction of pressure drop versus flow rate for non-Newtonian pipe flow is important in many industrial processes. In laminar flow scale up is straightforward, but transitional velocity and turbulent flow predictions remain a practical problem. Various theoretical models exist, but nothing in literature shows conclusively which of these is the most reliable and consistent, nor is it evident what effect the choice of rheological model has on the predictions. The aim of this work was to i) evaluate the influence of different rheological models when used in existing prediction techniques for non-Newtonian flow ii) characterise each material type using selected (commonly used) rheological models and iii) predict laminar, transitional and turbulent pipe flow characteristics for each material type using existing prediction techniques, for comparison with experimental results.

Only time-independent, homogeneous, non-Newtonian fluids in pipe sizes from 13mm to 200mm were investigated. Rheological models and laminar flow predictions used only the power law, Bingham plastic, Herschel-Bulkley, Casson and Hallbom yield plastic models. The techniques used to predict transitional velocity were Ryan & Johnson, Metzner-Reed, Hedström intersection method, Slatter and Hallbom. For turbulent flow the Newtonian approximation, Dodge & Metzner, Wilson & Thomas, Slatter, Hallbom modified Wilson & Thomas and the Bowen correlation methods were used. The study documents the relevant theory and presents an assessment of the influence of rheology on pipe flow predictions, summarised in terms of the practical performance of the various rheological model/prediction method combinations for the different materials.

In laminar flow at practical pseudo shear rates (*8V/D*; taken as $\geq 40s^{-1}$) the choice of rheological model does not significantly influence pressure drop predictions. For yield-pseudoplastic materials (eg. kaolin) the Hedström intersection and the Slatter Reynolds number method with Bingham plastic or Casson rheology predicted transitional velocity most accurately. For Bingham plastic materials (eg. bentonite) the best predictions were obtained using the Metzner & Reed Reynolds number with Bingham plastic rheology, although similar results were observed for this technique with all rheologies. The transitional velocity for pseudoplastic materials (eg. CMC) was best predicted by the Slatter and Metzner & Reed Reynolds number methods, using power law or Casson rheology.

For turbulent flow of yield pseudoplastic materials the Slatter method using the Casson rheology gave the most accurate predictions overall. Turbulent flow of Bingham plastic materials was best predicted by the Slatter, Hallbom pseudo fluid Nikuradse and Dodge & Metzner methods, using Bingham plastic, Casson or yield plastic rheology. For pseudoplastic materials the Slatter and Wilson & Thomas methods were the most accurate, when used with yield plastic or power law rheology. Transitionalal velocity and turbulent flow predictions for materials with a yield stress vary significantly with rheological model. Laminar data should therefore be examined thoroughly and rheological models fitted with care. For pseudoplastic fluids there is little difference in predictions between the various techniques as long as power law rheology is used.

Acknowledgements

The Almighty God – for the strength and perseverance He has given me through all the challenges I have faced along my long journey in completing this thesis.

Mar. Andrew Sutherland for his amazing supervisory role, dedicated support and belief in my success throughout the process of completing this dissertation.

The FPRC and CPUT for granting me the opportunity to fulfil my studies in non-Newtonian pipeflow.

A thank you to Mume Kabwe and Batthe Kabamba for their assistance with the test work, and analysis.

To my father Reginald van den Heever and my mother Jennifer Theron, thank you for the continued encouragement, motivation and belief.

To Donovan, Emlyn, Grant and JD for their patience and on-going support.

The financial assistance of the National Research Foundation towards this research is acknowledged. Opinions expressed in this thesis and the conclusions arrived at, are those of the author, and are not necessarily to be attributed to the National Research Foundation.

Table of Contents

Page

List of Figures

Page

Appendices

List of Tables

Page

List of symbols

Constants

A	Cross sectional area (m²)
B	Roughness function (-)
C_x	Relative transitional velocity (-)
d	Pressure tapping diameter (m)
d_x	Representative particle size (m)
D	Internal pipe diameter (m)
F	Force (N)
f	Fanning friction factor (-)
g	Gravitational acceleration (m/s²)
ΔH	Difference in height between fluids in manometer tube (m)
He	Hedström number (-)
K	Fluid consistency index (Pa.s^n)
k	Scaling factor for yield plastics (-)
l	Length of pressure tapping (m)
L	Length of pipe or test section (m)
n	Flow behaviour index (-)
M	Mass of material (kg)
p	Point pressure (Pa)
N	Size of population (-)
Δp	Differential pressure between 2 measuring points (Pa)
Q	Volumetric flow rate (m³/s)
r	Localised distance along radius of pipe or concentric cylinder (m)
R	Pipe radius (m)
Re	Reynolds number (-)
u	Localised linear velocity at (r) value (m/s)
U^*	Shear velocity (m/s)
$u+$	Dimensionless velocity (-)
$\bar{u}$	Time averaged axial velocity (m/s)
V	Velocity, mean velocity in a pipe (m/s)
y	Distance from pipe wall = R-r (m)
$y+$	Dimensionless distance from pipe wall (-)
Z	Wall stress ratio (-)

Greek letters

α	Area ratio (-)
β	Flow factor/ drag reduction factor for yield plastics (-)
ε	Effective pipe roughness of pipe wall (m)
η	Effective viscosity (Pa.s)
μ'	Apparent viscosity = τ_w/γ (Pa.s)

μ	Newtonian viscosity (Pa.s)
η_C	Casson plastic viscosity (Pa.s)
η_B	Bingham plastic viscosity (Pa.s)
γ	True shear rate = $-du/dr$ (s^{-1})
Ω	Velocity profile blunting factor
ρ	Density of the fluid (kg/m^3)
κ	Von Karman constant (-)
π	3.141592
τ	Shear stress (Pa)
Ø	Pressure gradient – $\Delta p/L$ (Pa/m)

Subscripts/superscripts

ann	annulus
av	average
BC	Bingham critical value
B	Bingham Plastic
C	Casson
cl	centreline
c or crit	critical
Gen	general
lam	laminar
MR	Metzner & Reed
max	maximum
plug	quantity relating to unsheared plug
p	plastic
r	roughness
shear	quantity referring to sheared annulus
visc	viscous
w	wall / water
y	yield
z	z-axis direction – parallel to flow direction
0	stress value at zero shear rate = Yield plastic yield stress (τ_0)
3	Slatter's Reynolds number (Re_3)
85	85^{th} percentile passing
∞	at infinity

Terms and concepts

Nominal wall shear rate	Measured pipe flow shear rate (*8V/D*).
Apparent viscosity	The ratio of shear stress to shear rate at a nominal value of shear rate.
Boundary layer	Relevant to turbulent flow, the radius where the velocity profiles of the viscous sub-layer and turbulent core intersect.
Constitutive equation	An algebraic equation which describes the flow behaviour of a material.
Viscous sub-layer	The region near wall in turbulent flow where the viscous effects are dominant and inertial effects insignificant.
Non-Newtonian	A fluid which exhibits a non-linear shear rate-shear stress relationship.
Plastic viscosity	The limiting high shear rate viscosity implied by the consistency model for a viscoplastic material (eg. Bingham Plastic).
Reynolds number	A number that represents the ratio of the inertial forces to the viscous forces (dimensionless).
Rheology	The science of the deformation and flow of matter.
Rheological model	A physical mathematical model used to describe the flow behaviour of a material. The resulting model is represented by a constitutive equation.
RMSE	Root mean square error [Equation (3.1)]
Shear rate	The rate of change of shear strain with time.
Shear strain	The relative in-plane displacement of two parallel layers of a material body divided by their separation distance.
Structure	Aggregation due to stable bond formation between particles in suspensions, affecting the rheology of the materials.
Turbulent core	In turbulent flow, the region taking up most of the pipe cross section and flow is dominated by inertial forces.
Viscoplastic	A property in which a material behaves like solid when the stress is below some critical value (yield stress) and flows like a liquid when it is exceeded.
Yield stress	The critical shear stress value which below, an ideal viscoplastic material will not flow, and flows like a liquid once this stress value is exceeded.

Chapter 1 Introduction

The reliable prediction of pressure drop remains one of the most significant practical problems for non-Newtonian fluids flowing in pipes (El-Nahhas & Mostafa, 2006). In laminar flow, this relationship is easily derived from the integration of the Rabinowitsch-Weissenberg equation for any given rheological model. However, the reliable prediction of pipe flow characteristics in transitional and turbulent flow remains a real problem. This chapter outlines the details of the investigation into the effect of the chosen rheological model on pipe flow predictions for non-Newtonian fluids. The research problem is defined, the objectives which were met are given, and the research methodology employed is presented. Assumptions made in conducting the research work are stated here and the study is clearly delineated.

1.1 Background and motivation

The rheology of a material depends on several properties (particle size, shape and distribution; concentration; pH; conductivity) so the most appropriate rheological model to use could vary from material to material (Slatter, 1999). Heywood & Cheng (1984) and Malkin, Masalova, Pavlovski & Slatter (2004) have shown that the choice of rheological model has no significant effect in predicting laminar pipe flow. However, for transitional and turbulent pipe flow this is not necessarily true, and the effect of rheology on predictions in these flow regimes needs to be thoroughly investigated. The literature predominantly considers the pseudoplastic, Bingham plastic and yield pseudoplastic rheological models, while models such as Casson are often overlooked (Wilson & Addie, 2002). Hallbom & Klein (2006) developed a new rheological model based on particle aggregation which they called the yield-plastic model. This model performed well in comparison with limited selected test results, but still needs to be evaluated using a wider range of experimental results.

The aim of this investigation was to determine what effect the choice of rheological model has on predicting pipe flow characteristics in laminar, transitional and turbulent flow. The power law, Bingham plastic, Casson, Herschel-Bulkley and Hallbom rheological models were used in this study. The performance of these material models was evaluated for three materials, namely CMC, bentonite and kaolin (representative of pseudoplastic, Bingham plastic and yield pseudoplastic materials respectively) (Chhabra & Richardson, 2008) for laminar, transitional and turbulent flow.

1.2 Research problem

To investigate the effect of the rheological model on the prediction of laminar, transitional and turbulent pipe flow characteristics of non-settling homogeneous non-Newtonian fluids.

1.3 Research question

Does the choice of rheological model make a significant difference in predicting laminar, transitional and turbulent flow of homogeneous non-Newtonian fluids in pipes in the flow rate and pipe size ranges of practical interest?

1.4 Objectives and outcomes

The aim of this research work was to evaluate the influence of using different rheological models in various existing prediction techniques for non-Newtonian laminar, transitional and turbulent pipe flow. To meet this aim the following objectives were achieved:

- Straight pipe tests for three representative non-Newtonian fluid types, each at three different concentrations, were done in a sufficient number of different pipe diameters to establish experimental flow characteristics in the laminar, transitional and turbulent flow regimes.
- Each material was characterised using the laminar flow pipe data and each of the selected rheological models.
- Predictions for laminar, transitional and turbulent pipe flow were done for each material and each pipe size, using the selected prediction techniques and derived rheologies as applicable.
- Predictions and experimental results were compared and the effect of the rheological model used was assessed, for each material in each pipe size and flow regime.

The research resulted in:

- An assessment of whether or not the choice of rheological model influences the pipe flow predictions in laminar, transitional and turbulent flow.
- A summary of the practical performance of each model in predicting pipe flow characteristics for representative materials in laminar, transitional and turbulent flow.
- Guidelines, documentation, and an extensive set of spreadsheets on experimental and analytical procedures for determining pipe flow characteristics of homogeneous non-Newtonian fluids.

1.5 Significance

It has been shown for laminar flow, over flow rates of practical interest, that the choice of rheological model makes no difference in predicting pipe pressure drops (Heywood & Cheng, 1984; Malkin *et al*., 2004). This research has extended the investigation to transitional and turbulent flows for a range of representative materials, and has shown the influence of rheological model (including yield stress) and Reynolds number, when used with existing prediction techniques, in these flow regimes. This is significant as it directly influences design procedures for production plants and pipelines.

1.6 Delineation

The boundaries considered in conducting the research work are clearly delineated here.

- Newtonian fluids, settling slurries and time dependent fluids are not included in this study.
- Only three concentrations (by volume) per material type were considered. These were 3, 5 and 8% for pseudoplastic material (CMC), 6, 7.34 and 9% for Bingham plastic material (bentonite) and 6, 10 and 15% for yield-pseudoplastic material (kaolin).
- Pipe tests were done only for $13 \leq D \leq 200$mm.
- The nominal wall shear rate range for the pipe tests was $40s^{-1}$ up to the maximum value obtained in each pipe diameter (see Section 1.7).
- Only the power law, Bingham plastic, Casson, Herschel-Bulkley and Hallbom rheological models were used to characterise the materials and for the laminar flow calculations.
- For transitional flow, only the Ryan & Johnson, Metzner-Reed, Hedström intersection method, Slatter and Hallbom models were used in the predictions, and
- Only the Newtonian approximation, Dodge & Metzner, Wilson & Thomas, Slatter, Hallbom and Bowen (scale-up) were used to predict turbulent flow.
- Only *n'* values in the range 0.36 - 1 were used in the Dodge & Metzner turbulent flow analysis.
- Turbulent flow predictions were made over the whole range of experimental values, but the error estimates were based only on shear stress values up to either +25% of the maximum measured laminar shear stress value or the third measured turbulent data point, whichever was greater (see Section 3.2.7)

1.7 Assumptions

The following assumptions were made when the research work was conducted:

- All the fluids tested were assumed to be homogeneous and non-settling.
- The time dependency effect of bentonite was assumed to have been completely removed by pre-shearing.
- The effect of the increase in temperature of the slurry during testing was negligible.
- Based on guidelines given in Brown & Heywood (1991) and Alderman & Heywood (2004), nominal wall shear rate ($8V/D$) values of less than $40s^{-1}$ are of little practical importance in pumping and pipe flow, so data below this value were excluded from the analyses.

1.8 Methodology

Details of the research design, research methodology, data acquisition and data analysis are briefly discussed here. The research design and methodology used were chosen with the research question in mind.

1.8.1 Research design

This was a quantitative study which employed experimental, comparative and secondary data analysis techniques.

1.8.2 Research methodology

Primary data were collected in straight pipe tests over a nominal wall shear rate range of $40s^{-1}$ to the maximum value obtained in each pipe. Each of the rheological models evaluated was fitted to the laminar experimental data for each test material, and each was used in the prediction of laminar, transitional and turbulent pipe flow. The results were compared.

1.8.3 Data

Primary data measured were pressure drop (ΔP) and flow rate (Q), for each material in each pipe diameter, from a minimum nominal wall shear rate ($8V/D$) of $40s^{-1}$. This resulted in a minimum velocity of 0.065m/s (Q = 0.00863l/s) for the 13mm pipe and a velocity of 1.055m/s (Q = 36.89l/s) for the 200mm pipe. Wall shear stress and pseudo-shear rate were derived from the measured pressure drop and flow rate respectively.

1.8.4 Research instruments/ equipment

Data were collected from three different pipe test loops, namely the valve test loop, the large pipes test loop and the flume test loop. The three loops collectively covered a test pipe diameter range of Ø13mm to Ø200mm. These loops used centrifugal and progressive cavity (positive displacement) pumps for which the flow rate could be varied from almost zero to 200l/s. Pressure drops were measured using Fuji differential pressure transducers via solids traps. The differential pressure transducers used on the flume pipe loop were 6kPa and 30kPa, while those used on the valve test loop and large pipes test loop were 6kPa and 130kPa transducers. Flow rates were measured using Krohne or Fuji inline magnetic flow meters, which varied in size from Ø40mm to Ø100mm (appropriate to the test pipe size). These instruments (DP transducers and magnetic flow meters) all output 4 – 20mA signals which were converted to 1 to 5V for input to the data acquisition system. The data acquisition software captured the input voltage signals, applied the calibration factors and exported the measured parameters to an Excel spreadsheet for further analysis. The Malvern Mastersizer 2000 optical unit with Hydro 2000MU accessory was used to measure the particle size distributions of the kaolin and bentonite test slurries.

1.8.5 Analysis and presentation of results

The pipe test data for each pipe test are presented on graphs of wall shear stress (τ_w) vs. nominal wall shear rate (*8V/D*) (pseudo-shear diagrams). The laminar data of each test material was used for the rheological characterisation. The rheological constants were determined by fitting laminar data to appropriate *8V/D* equations for each rheological model, using Excel solver to minimise the sum of the squares of the residual error. Each rheological model is used in the relevant prediction technique to calculate the predicted *ΔP/L* vs. *V* relationship for laminar and turbulent flow, and the critical velocity (V_c) for transitional flow. For laminar and turbulent flow the experimental and predicted results are plotted on graphs of τ_w vs. *8V/D* for comparison and for transitional flow the experimental and predicted results are presented on plots of V_c vs. *D*. Average percentage errors were calculated for all predictions and in this way the performance of the different techniques with rheological model combinations was evaluated.

1.9 Organisation of dissertation

Chapter 2 presents a review of the literature relating to pipe flow of non-Newtonian fluids, covering fluid classification based on different rheological models, the relevant fluid mechanics equations for each material type, and the various techniques used to predict pipe flow in the transition and turbulent flow regimes. Chapter 3 gives the details of the research methodology employed to collect, analyse and present the data. The measured pipe data and rheological characterisation of the materials tested are presented in Chapter 4. The evaluation of the prediction techniques for laminar, transitional and turbulent flow are presented and discussed in Chapter 5. Laminar flow predictions using the various rheological model fits are compared with the experimental data, and pipe flow predictions for transitional and turbulent flow are evaluated against experimental data on plots of V_c vs. *D* and τ_w vs. *8V/D* respectively. The performance of each prediction in laminar, transitional and turbulent flow was evaluated by calculating the average percentage error. In Chapter 6 conclusions are drawn from the findings of the research work and recommendations for future work are made. Additional details and information relevant to the research work conducted are presented in Appendices.

Chapter 2 Literature review and theory

The literature pertinent to Newtonian and time-independent non-Newtonian fluids in laminar, transitional and turbulent flow is presented here. Newtonian theory is initially presented, as this forms the starting point for many non-Newtonian pipe flow models. The constitutive equations considered in this work to describe the rheological behaviour of non-Newtonian fluids, and the transitional and turbulent prediction techniques in which these rheological models are used, are reviewed.

2.1 Fluid behaviour

This section outlines how fluids are classified and defines Newtonian and non-Newtonian fluid behaviour. The micro structure of non-Newtonian fluids and its influence on rheological behaviour of fluids is briefly discussed. Rheology is defined and the views expressed in the literature about the process of rheological characterisation and the choice of rheological model are presented.

2.1.1 Classification of fluids

Fluids are generally classified in two ways - either according to the response of externally applied pressure (i.e. shear stress) or according to the effects produced under the action of an applied shear rate (Chhabra and Richardson, 2008). Metzner (1956) classified the non-Newtonian fluids into three categories: (i) viscoelastic fluids where a part of the stress is recovered after the removal of the shear causing deformation (ii) fluids with shear stress-shear rate relations dependant on the duration of the application of shear (time-dependent fluids) and (iii) fluids with shear-stress shear rate relations independent of the time over which the shear is applied (time-independent fluids). Time-independent fluids are further categorised into shear thinning and shear thickening fluids (Peker & Helvaci, 2008). In this study only time-independent shear-thinning fluids were considered.

2.1.2 Newtonian fluids

Consider a thin layer of fluid between parallel plates as shown in Figure 2.1 distance *dy* apart. For steady state conditions, the fluid experiences shearing due to the application of force *F*, which will be resisted by an equal but opposite force of internal friction within the fluid. For the fluid to be classified as an incompressible Newtonian fluid in laminar flow, the shear stress (τ) must equal the product of the shear rate (γ) and the viscosity of the fluid. The shear rate is expressed as the velocity gradient in the direction perpendicular to that of the shearing force.

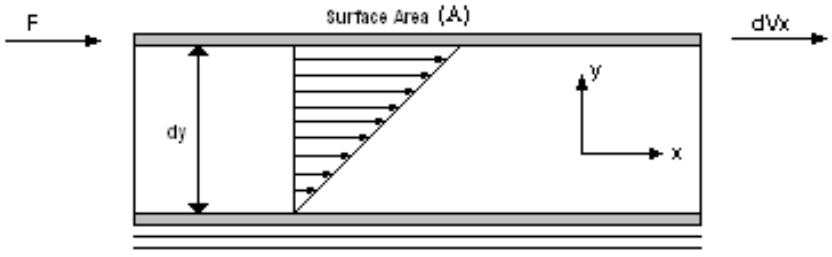

Figure 2.1 Schematic representation of unidirectional shearing flow (Chhabra and Richardson, 2008)

$$\frac{F}{A} = \tau_{yx} \tag{2.1}$$

$$\dot{\gamma} = \left(-\frac{dV_x}{dy} \right) \tag{2.2}$$

$$\mu = \frac{\tau_{yx}}{\dot{\gamma}_{yx}} \tag{2.3}$$

$$\tau_{yx} = \mu \dot{\gamma}_{yx} \tag{2.4}$$

The ratio of the shear stress to the shear rate is called the Newtonian viscosity (μ). It is independent of shear rate (γ_{yx}) or shear stress (τ_{yx}) and depends only on the material at given temperature and pressure. A plot of shear stress (τ_{yx}) and shear rate (γ_{yx}), called the "flow curve" or rheogram, for a Newtonian fluid is therefore a straight line with a slope μ passing through the origin. The single constant μ completely characterises the flow behaviour of a Newtonian fluid at a fixed temperature and pressure (Chhabra and Richardson, 2008).

2.1.3 Non-Newtonian fluid behaviour

A non-Newtonian fluid can be described as a fluid whose rheogram is non-linear and/or does not pass through the origin (Steffe, 1996). The viscosity [Eq. (2.3)] of a non-Newtonian fluid is not constant. It is referred to as the apparent viscosity (Perry, 1997) and is dependent on the shear rate. Several mathematical equations have been derived to describe the rheograms of non-Newtonian fluids, some of which are discussed below.

2.1.4 Structure/ Micro-structure

The rheological properties of suspensions are often related to a vaguely defined property referred to as *structure*. "There is a direct and strong link between the type and extent of non-Newtonian flow behaviour on the one hand, and the response of the structure to externally applied forces on the other" (Chhabra and Richardson, 2008).

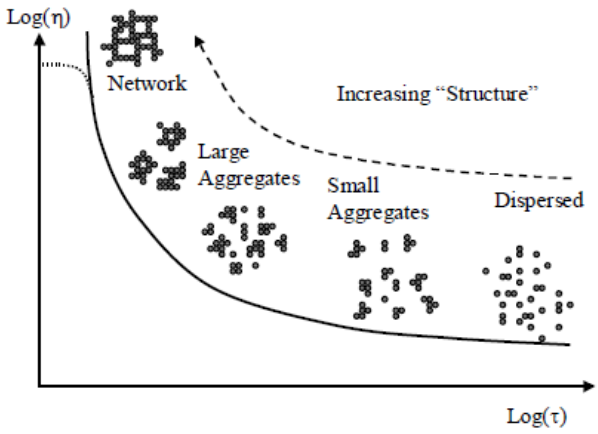

Figure 2.2 The effect of viscous shear stress on particle structure (Hallbom, 2008)

Casson (1959) described structure to be the formation of chains of needle-like ink particles causing an increase in apparent viscosity in much the same way that increasing molecular weight causes an increase in viscosity in polymers. Scott Blair (1967) defined the degree of structure of a slurry as being a function of the number of formed bonds between particles per unit volume, thus a higher bond density would cause a higher apparent viscosity. Hallbom (2008), successfully developed the most recent

rheological model for shear-thinning slurries, and based his work on the theory that at higher shear rates the structure breaks down and particles become fully dispersed enabling the average particle bond strength to increase. He thus defines structure as a property which is related to the average size of the aggregates, which generally decreases as the shear rate increases. This phenomenon is illustrated in Figure 2.2.

2.1.5 Rheology

Rheology is the science of the deformation and flow of matter i.e. it is the study of the manner in which materials respond to applied stress and strain (Steffe, 1996). The rheological properties of fluids are represented by mathematical models so that they are characterised by the model that best describes their behaviour. Common fluid material behaviour is shown in Figure 2.3.

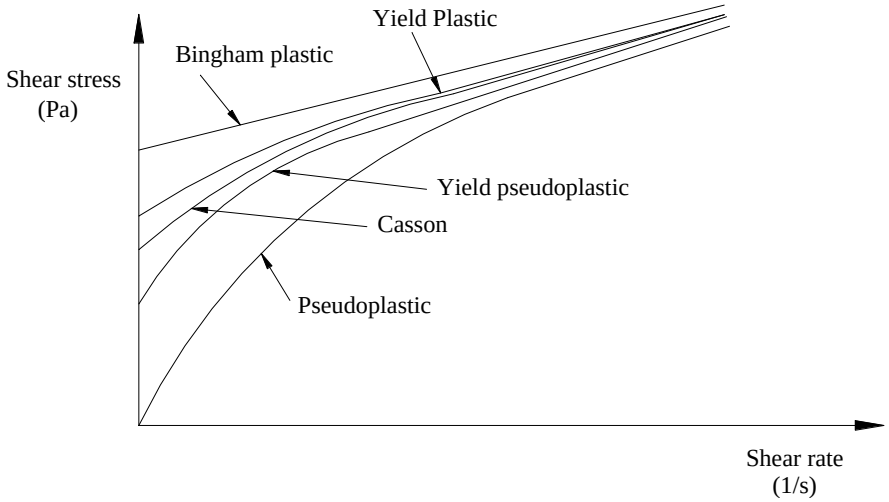

Figure 2.3 Rheological models [Adopted from Chhabra & Richardson (2008); Hallbom (2008)]

2.1.6 Rheological models of time-independent fluids

This group of non-Newtonian fluids is characterised by viscosity relations that are a function of shear rate, but not of time application of shear. The rheological behaviour of these fluids is described by governing relations (constitutive equations), between shear stress (τ) and shear rate (γ). Many non-Newtonian models exist in the literature, but for the purpose of engineering applications only some of the simpler models with only two or three model parameters are considered in this study. These are the Newtonian, power law, Bingham plastic, Herschel-Bulkley, Casson and Hallbom models presented in turn below.

$$\tau = \mathrm{f}(\dot{\gamma}) \tag{2.5}$$

This form of the equation is generally used for simple, unidirectional shear flows of Newtonian and non-Newtonian fluids.

Newtonian

Newtonian fluids are the simplest fluids and described by the equation

$$\tau_w = \mu\dot{\gamma} \tag{2.6}$$

μ is the dynamic viscosity of the fluid and τ_w is the shear stress at the shearing surface (pipe wall).

Power law

The apparent viscosity of many fluids decreases with an increase in shear rate. This is termed shear-thinning rheological behaviour and is described by the power-law model, given by Eq. (2.7)

$$\tau_w = K \dot{\gamma}^n \tag{2.7}$$

The apparent viscosity (μ') is given by

$$\mu' = K \dot{\gamma}^{n-1} \tag{2.8}$$

The variables *K* and *n* are curve fitting parameters known as the fluid consistency index (*K*) and the flow behaviour index (*n*). Shear-thinning behaviour occurs for $n < 1$. Fluids that behave this way are also called pseudoplastic fluids. As the value of *n* decreases, the degree of shear thinning increases. For $n > 1$ shear thickening occurs and such fluids are called dilatant fluids. When $n = 1$, the model reduces to Eq. (2.6) with $K = \mu$ (Newtonian).

Generally, the power-law model applies only over a limited range of shear rates, and the fitted values of *K* and *n* depend on the range of shear rates considered. The value for *K* also depends on the value for *n*, thus *K* values cannot be compared for varying values of *n* (Chhabra and Richardson, 2008).

Bingham Plastic

As originally presented by Bingham in 1922, this is the simplest constitutive equation describing the flow behaviour of a yield stress fluid in one-dimensional shear and is given by (Chhabra & Richardson, 2008)

$$\tau_w = \tau_y + K \dot{\gamma} \tag{2.9}$$

The apparent viscosity is

$$\mu' = K + \left(\frac{\tau_y}{\dot{\gamma}} \right) \tag{2.10}$$

Herschel-Bulkley

The Herschel-Bulkley model (Steffe, 1996) describes shear thinning fluids with a yield stress. At stresses greater than the yield stress, Herschel-Bulkley fluids exhibit shear-thinning behaviour which obeys the power law. The values of *K* and *n* are similar to that for the power law model, and the value for *K* also depends on the value of *n*. The Herschel-Bulkley model reduces to the power law and Bingham plastic model as special cases. The constitutive equation is given by

$$\tau_w = \tau_y + K \dot{\gamma}^n \tag{2.11}$$

The apparent viscosity is

$$\mu' = K \dot{\gamma}^{n-1} + \left(\frac{\tau_y}{\dot{\gamma}} \right) \tag{2.12}$$

Casson

Casson (1959) derived a model similar to that of Herschel-Bulkley model but with more gradual shear thinning effect over the laminar data range. Many food stuffs and biological materials, for example blood and molten chocolate, are appropriately described by this two constant model. τ_C refers to the Casson yield stress and η_C the Casson viscosity. The equation is given by

$$\tau_w^{0.5} = \tau_C^{0.5} + \eta_C^{0.5} \dot{\gamma}^{0.5} \tag{2.13}$$

The apparent viscosity is

$$\mu' = \eta_C \left[\frac{\tau_C^{0.5} + \eta_C \cdot \dot{\gamma}^{0.5}}{\tau_w^{0.5} - \tau_C^{0.5}} \right]^2 \tag{2.14}$$

Hallbom

Hallbom & Klein (2006) developed a three constant yield plastic rheological model based on particle aggregation at increased shear velocities. Once all particles disperse as the shear rate increases, the fluid will reach a minimum value of viscosity which is a fraction or multiple of the carrier fluid. This value of viscosity is referred to as the infinite shear viscosity (μ_∞). The equation is given by

$$\tau_w^{\,k} = \tau_0^{\,k} + \mu_\infty^{\,k} \dot{\gamma}^{k} \tag{2.15}$$

The yield plastic model reduces to the Bingham plastic model if k = 1 and the Casson model if k = 0.5. The three model constants are the scaling factor (k), the yield plastic yield stress (τ_0) and the infinite shear viscosity (μ_∞). The apparent viscosity is given by

$$\mu' = \left[\frac{\tau_0^k}{\dot{\gamma}^k} + \mu_\infty^k \right]^{\frac{1}{k}} \tag{2.16}$$

2.1.7 Rheological characterisation

The rheology of any fluid can be represented by different rheological models (graphical curve fits to the laminar data). The process of rheological characterisation involves fitting a rheological model to laminar flow data to determine the model parameters. The goodness of fit of different models is compared to identify which model best suits the material fluid. The method of Slatter (1994) was used here to characterise the test fluids. In this method the laminar pipe data was plotted as (*8V/D* vs. τ_w) and the models were fitted to the data by minimising the RMSE (root mean square error) for (*8V/D*), corresponding to the experimental wall shear stress values (see Section 3.2.4).

Shear stress and shear rate range

When predicting transitional and turbulent flow from laminar data, it is important to ensure that the laminar data used for rheological characterisation spans the shear stress range for which predictions are required. Shook and Roco (1991) state that viscometric test work should ideally be carried out over the range of shear stresses which will be encountered in practice. i.e. viscometric tests carried out for the prediction of turbulent flow pressure gradients should be performed such that wall shear stresses achieved in laminar flow testing are at least as high as the wall shear stress in turbulent flow which is

being predicted. In practise this is not always possible, even in smaller diameter tubes. Slatter (1997b) suggested that this could be overcome by extrapolating the rheology in laminar flow to higher shear rates so that the required shear stresses in turbulent flow can be achieved, provided the rheological characterisation procedure is accurately carried out.

In contrast to what Slatter (1997b) suggests, Chhabra & Richardson (2008) emphasise that it is important that the maximum shear stress for turbulent predictions as proposed by Shook & Roco (1991) be adhered to. Extrapolating the rheology of the fluid to a wall shear stress higher than actually measured is not a valid practice. This same reasoning is inherent in the theory of Dodge & Metzner (1959) who clearly stated that their turbulent model requires *K'* and *n'* values (Section 2.4.5) to be evaluated from measured laminar data up to the same wall shear stress values for which turbulent flow is to be predicted. Brown & Heywood (1991) also emphasise this point. They suggest that although the extrapolation of rheology data is bad practice, it is still done, prompting the question as to whether or not this is a contributing factor to on-going inaccurate prediction of non-Newtonian turbulent flow (Brown & Heywood, 1991).

Thomas (2000) also showed the importance of ensuring flow curve measurements are made across the relevant shear stress and shear rate range of the application, as this influences which rheological model is most appropriate for the current data. Alderman and Heywood (2004a) suggested that the minimum test value for shear rate can be determined by assuming the lowest flow rate (*Q*) through the largest pipe diameter and the maximum shear rate value by taking the highest *Q* through the smallest pipe diameter.

Yield Stress

Rheological characterisation optimises all of the rheological constants of a given rheological model to best represent the laminar data. The value of τ_y is not necessarily a true value at which the transition from solid to liquid behaviour is initiated (Slatter, 1994). For most viscoplastic fluids a yield value exists either as an engineering reality or an inherent fluid property, but there is still considerable dispute about this issue (Kelessidis, Maglione, Tsamantaki & Aspirtakis, 2006). For the purpose of this study the value of τ_y was taken as best practical approximation of the yield stress, consistent with a pragmatic engineering approach.

2.1.8 Choice of rheological model

Several rheological models are described in the literature, but opinion is divided as to which model works best. Slatter (1999) states that the choice of model is very important not only for rheological characterisation, but also for pipe flow predictions, and suggests that the pseudoplastic and Bingham plastic models are favoured by many researchers. This is in agreement with Wilson & Addie (2002) who state that other models such as Sisko and Casson are often overlooked. Hallbom and Klein (2006) developed a new rheological model which proved accurate in predicting the flow behaviour of kaolin clay suspensions and also presented its advantages over the popular Herschel-Bulkley rheological model. Heywood & Cheng (1984) have shown that the choice of rheological model for predicting of non-Newtonian laminar pipeflow has very little influence on the predicted pressure drop in the pipeflow shear rate range of interest. Malkin *et al.,* (2004), demonstrated by experiment and analysis, for two very different materials, that the choice of rheological model is not crucial for the estimation of pressure drop in laminar pipe flow. Similarly, Mullineux and Simmons (2008) conducted pipe tests with yoghurt, and used the power law and Herschel-Bulkley models to predict laminar pipe flow characteristics. For the shear range of interest there was no significant difference in the predicted results, despite the very

different rheological parameters used in the analyses. Although the choice of rheological model therefore seems relatively unimportant for laminar flow in pipes (at least at practical flow rates) it may be of much more significance in transitional and turbulent pipe flow predictions. Heywood & Cheng (1984) stated that non-Newtonian headloss prediction is far more complicated for turbulent flow than for laminar flow and that many different methods are available, but with little clarity on the choice of method. They found that turbulent predictions for the different methods vary by up to ± 50% and that the uncertainty is compounded by the reliable estimation of the rheological parameters from the laminar data. They concluded that as many different prediction methods should be used as possible, to enable an engineering judgement as to which prediction is most appropriate for a given set of conditions. Litzenberger & Sumner (2004) presented laminar and turbulent data of a clay slurry characterised as both Bingham plastic and Casson material. Turbulent flow predictions using the Wilson & Thomas turbulent model did not coincide for the two rheological models. The Casson model successfully predicted the turbulent pressure drops, but when taking the fluid as a Bingham plastic, turbulent flow pressure gradients were significantly overpredicted. Heywood & Alderman (2003) state preference for the Casson model (over the Bingham plastic and Herschel-Bulkley models) for predicting laminar and turbulent viscoplastic (yielding & shear thinning) non-Newtonian pressure drops. The Casson model has an advantage over the Bingham plastic model for the description of the viscoplastic slurry behaviour because it can predict curvature of the flow curve at lower shear rates. Additional to this, the Casson model enables a direct measure of the yield stress and viscosity, which is not possible with the three-parameter Herschel-Bulkley model (Heywood & Alderman, 2003). This is in line with the objectives of the present study which was to determine whether the choice of rheological model affects the prediction of the transitional velocity and turbulent flow pressure gradients.

2.1.9 Force fitting of models

Consider for example a kaolin slurry which is usually represented accurately by the Herschel-Bulkley model (Slatter, 1994), but which can also be modelled by other rheologies such as power law which has no yield stress, or the Bingham plastic model with no rheogram curvature. This has been demonstrated by Xu, Gillies, Small, & Shook (1993) and Slatter (1994). Xu *et al* (1993) used the Bingham plastic model to characterise the kaolin slurries they tested, and Slatter (1994) demonstrated how the power law, Bingham plastic and Herschel-Bulkley models could be used to characterise kaolin slurries. To force a power law model, yield stress (τ_y) was set to zero and the data fit optimised for K and n. To force a Bingham plastic fit, n was set to unity and the data optimised for τ_y and K. However, the validity of these fits is questionable when used to predict turbulent pressure gradients, as this is where the significance will be observed as illustrated by Slatter (1994), Chara, Vlasak, Severa, Havlik & Vycital (1996), Slatter (1999) and Vlasak & Chara (1999). The value of a rheological model lies not in its ability to fit laminar rheogram data accurately, but rather in whether or not it results in accurate predictions under different flow conditions (Hallbom & Klein, 2009).

2.1.10 Effect of temperature on rheology

Little rigorous detail recording temperature effects on the rheology of slurry is reported in the literature. Metzner (1956) states that although the complexity of some non-Newtonian materials leads to unusual changes in fluid properties with temperature, most non-Newtonian fluids do not show any unusual effects. Thorvaldsen (1996) reported on temperature effects on the rheology of a suspension as follows:

- "For small changes, the flow behavior index (n) may be assumed independent of temperature (Reed, 1954); for larger changes, Vaughn (1956) has reported that flow behavior index increases towards unity i.e. many pseudoplastic materials approach Newtonian behaviour.
- The consistency index (K) frequently changes as rapidly with temperature as the viscosity of the

solvent or suspending medium (Reed, 1954).

- The changes in τ_y with temperature with Bingham plastics have been reported to resemble changes of the flow behavior index (Metzner, 1956)."

2.1.11 Effect of change in concentration on rheology

Metzner (1956) reported that for pseudoplastic fluids, small changes in volumetric concentration won't significantly change the flow behaviour index (*n*), but that larger increases in concentration result in a decrease in *n.* The fluid consistency index (*K*), however, increases rapidly with an increase in concentration. Vlasak & Chara (1999) confirmed these trends for *K* and *n* for yield-pseudoplastics, in addition to a significant increase in τ_y with concentration. Litzenberger & Sumner (2004) and Chhabra & Richardson (2008) also confirmed these observations for yield-pseudoplastic materials.

2.2 Rheometry of non-Newtonian fluids

In order to measure the flow properties of a material, one must use a characterisation device where both shear stress and shear rate can be defined. The science of collecting physical data from tests on a sample of the fluid to establish its unique relationship between shear stress and shear rate is called rheometry (Boger, Scales & Sofra, 2008). The instrument used to measure the rheological properties of a fluid is called a viscometer and can be one of two types; rotational or tube. Only tube viscometers were used in this study.

2.2.1 Tube viscometer

A tube viscometer consists of a straight tube of length (*L*) and inside diameter (*D*) through which a fluid flows at a constant average velocity (*V*) under a known pressure drop (*Δp*) (Nguyen & Boger, 1992). When a fluid flows through a pipe, the velocity is a maximum at the center and the rate of change in fluid velocity normal to the pipe axis [shear rate (γ)] varies from zero at the center to a maximum at the pipe wall. Tube viscometers are therefore restricted to measuring steady shear stress-shear rate properties for time-independent fluids (Chhabra & Richardson, 2008).

Energy loses in tube flow

When a fluid flows in a pipe, energy is expended to overcome viscous frictional forces, which manifests as a head loss (*ΔH*) that can be quantified by measuring the pressure drop over a test section of known length (*L*). The head loss (*ΔH*) is given by the Darcy formula (Massey, 1970).

$$\Delta H = \frac{4fL}{D}\left[\frac{V^2}{2g}\right] \tag{2.17}$$

where *f* is the Fanning friction factor defined as (Massey, 1970)

$$f = \frac{2\tau_0}{\rho V^2} \tag{2.18}$$

Linear shear stress variation in tube flow

Fully developed, steady laminar or turbulent flow of an incompressible fluid in a tube of known radius (*R*) across a known length (*L*) is shown in Figure 2.4a.

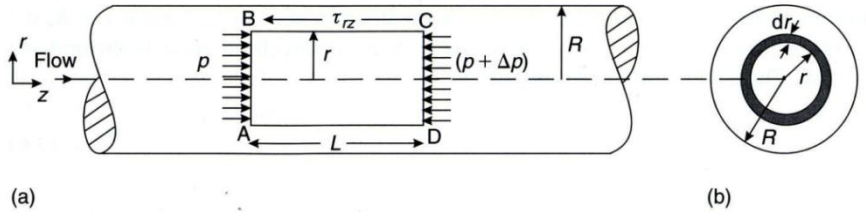

Figure 2.4 Schematic of flow in a tube (Chhabra & Richardson, 2008)

The linear momentum balance (in the direction of flow, z) on a fluid element ABCD of radius (r) and length (L) gives (Chhabra & Richardson, 2008)

$$p(\pi r^2) - (p + \Delta p)(\pi r^2) = \tau_{rz}(2\pi rL) \tag{2.19}$$

from which

$$\tau_{rz} = \left(\frac{r}{2}\right)\left(\frac{-\Delta p}{L}\right) \tag{2.20}$$

Eq. (2.20) gives the linear variation of shear stress across the tube cross-section, increasing from zero at the central axis of the tube (r=0) to a maximum value at the wall of the tube (r=R). The shear stress at the wall of the tube (τ_w) is:

$$\tau_w = \left(\frac{R}{2}\right)\left(\frac{-\Delta p}{L}\right) = \frac{D\Delta p}{4L} \tag{2.21}$$

The shear stress may then be evaluated in terms of shear rate at the wall (γ_w) or $(du/dr)_w$ to yield steady shear stress-shear rate data for the fluid, where u is the z-component of the linear velocity as a function of the radial co-ordinate (r). To develop shear rate equations, a differential flow element (dQ) must be evaluated. Flow rate through the annulus shown in Figure 2.4b is:

$$dQ = 2\pi ru(dr) \tag{2.22}$$

The total volumetric flow rate is therefore:

$$Q = \int_0^R 2\pi ru(r)dr \tag{2.23}$$

Integrating by parts and applying the no slip boundary condition (fluid velocity is zero at the pipe wall)

$$Q = \pi \int_0^R r^2\left(\frac{-du(r)}{dr}\right)dr \tag{2.24}$$

Certain assumptions now need to be made regarding the nature of the flow and of the characteristics of the fluid. For the laminar flow of time-independent fluids, the shear rate ($-du/dr$) is determined only by the value of the corresponding shear stress (τ_{rz}), and the functional relationship can be expressed as (Chhabra & Richardson, 2008):

$$-\frac{du(r)}{dr} = -\frac{dV_z}{dr} = f(\tau_{rz}) \quad \text{[where } u(r) \equiv V_z\text{]} \tag{2.25}$$

The negative sign in Eq. (2.20) is because we assume the positive direction of (τ_{rz}) to be opposite to the direction of flow as indicated in Figure 2.4a. Combining Eq. (2.20) and Eq. (2.21) gives

$$\frac{\tau_{rz}}{\tau_w} = \frac{r}{R} \tag{2.26}$$

or

$$r = R\frac{\tau_{rz}}{\tau_w} \tag{2.27}$$

so for constant values of R and τ_w

$$dr = \left(\frac{R}{\tau_w}\right) d\tau_{rz} \tag{2.28}$$

Combining Eq.(2.25) and Eq. (2.28)

$$du(r) = -f(\tau_{rz})dr = -f(\tau_{rz})\left(\frac{R}{\tau_w}\right)d\tau_{rz} \tag{2.29}$$

and using Eq. (2.27), Eq. (2.24) can be written as

$$Q = -\pi\int_0^{\tau_w}\left(\frac{\tau_{rz}^2}{\tau_w^2}\right)R^2\left(-f(\tau_{rz})\frac{R}{\tau_w}\right)d\tau_{rz} \tag{2.30}$$

where the limits of integration are now 0 to (τ_w). In terms of shear stress and shear rate, the volumetric flow rate is given by:

$$Q = \frac{\pi R^3}{\tau_w^3}\int_0^{\tau_w}\tau_{rz}^2 f(\tau_{rz})d\tau_{rz} \tag{2.31}$$

This equation can be integrated directly for any specific fluid model, f(τ_{rz}) (Chhabra & Richardson, 2008).

2.2.2 Rabinowitsch-Mooney relation

The starting point in the derivation of the Rabinowitsch-Mooney relation is the volumetric flow rate equation [Eq. (2.31)], based on the assumptions that the flow is laminar and steady, end effects are negligible, the fluid is incompressible, fluid properties are not a function of pressure or time, temperature is constant and there is no slip at the wall of the tube (Steffe, 1996).

Writing, Eq. (2.31) as

$$\left(\frac{Q}{\pi R^3}\right)\left(\tau_w\right)^3 = \int_0^{\tau_w} \tau_{rz}^2 f\left(\tau_{rz}\right) d\tau_{rz} \tag{2.32}$$

and applying Leibnitz' rule yields the well known Rabinowitsch-Mooney equation (Chhabra & Richardson, 2008):

$$\dot{\gamma}_w = f\left(\tau_w\right) = \left[\frac{3Q}{\pi R^3}\right] + \tau_w \left\{\frac{d\left(Q/\pi R^3\right)}{d\tau_w}\right\} \tag{2.33}$$

where the derivative is evaluated at a particular value of (τ_w). Eq. (2.33) can also be expressed in terms of apparent wall shear rate (*8V/D*) where V is the mean velocity over the cross section of the pipe.

$$\dot{\gamma}_w = f\left(\tau_w\right) = \left[\left(\frac{3}{4}\right) + \left(\frac{1}{4}\right)\left(\frac{d\left(\ln\left(8V/D\right)\right)}{d\left(\ln\tau_w\right)}\right)\right]\left(\frac{8V}{D}\right) \tag{2.34}$$

The Hagen-Poiseuille equation, which applies to the laminar, fully developed and steady flow of incompressible Newtonian fluids gives the mean velocity, *V* as:

$$V = \left(-\frac{\Delta p}{L}\right)\left(\frac{R^2}{8\mu}\right) \tag{2.35}$$

Rearranging in terms of the wall stress,

$$\left(-\frac{\Delta p}{L}\right)\left(\frac{R}{2}\right) = \tau_w = \mu\left(\frac{8V}{D}\right) \tag{2.36}$$

Thus (*8V/D*) is the true shear rate at the wall for a Newtonian fluid, but Eq. (2.34) shows that a correction factor must be applied for non-Newtonian fluids (Chhabra & Richardson, 2008). Eq. (2.34) may be written in terms of the slope *n'* of the log-log plot of (τ_w) against (*8V/D*). Writing *n'* as

$$n' = \frac{d\ln\tau_w}{d\ln\left(8V/D\right)} \tag{2.37}$$

From Eq. (2.34) and Eq. (2.37) the true shear rate at the wall for a non-Newtonian fluid is

$$\dot{\gamma}_w = \left(-\frac{dV_z}{dr}\right)_w = \left(\frac{8V}{D}\right)\left(\frac{3n'+1}{4n'}\right) \tag{2.38}$$

If the fluid is a power law material, the slope is a constant and *n' = n.* Slight curvature in the logarithmic plot can often be ignored (Steffe, 1996). The correction factor (1+3*n*')/(4*n*'), varies from 1 for a Newtonian fluid, to a maximum of approximately 2 for highly shear thinning fluids (*n*' = 0.2) (Alderman & Heywood, 2004a).

2.2.3 Sources of errors in tube viscometry

Although numerous measurement errors may occur when using tube viscometers [some generally

applicable, others specific (Steffe, 1996)], the most significant sources of errors are end effects and wall slip (Nguyen & Boger, 1992; Chhabra & Richardson, 2008). Alderman and Heywood (2004b) summarise common errors occurring in tube viscometry measurements, and suggest techniques for correcting for them. These are summarised here.

Transitional/ turbulent flow

Tube viscometry is valid only for laminar conditions. Data must therefore be checked to ensure that it is not in the transitional/ turbulent regime. This can be done for instance by calculating the laminar flow limit for the slurry sample and rejecting data that fall beyond this limit. For example, using the Ryan & Johnson transitional flow criterion for a power law fluid

$$\tau_w > \left(\frac{\rho D^2}{8}\right)\left[\frac{\left(\frac{n}{404}\right)*\left[\left(\frac{1+3n}{4n}\right)^2\right]}{\left(\frac{1}{1+2n}\right)^{\left(\frac{n}{1+2n}\right)}\left(\frac{n}{1+n}\right)^{\left(\frac{1}{1+2n}\right)}}\right]\left(\frac{8V}{D}\right)^2 \qquad (2.39)$$

This equation can be plotted as a double logarithmic plot of (τ_w) against ($8V/D$) to give the laminar limit line, which has a slope of 2 as shown in Figure 2.5. Data to the right of the laminar flow limit line as shown in Figure 2.5 must be rejected. Steffe (1996) provides a laminar flow criterion for Bingham fluids.

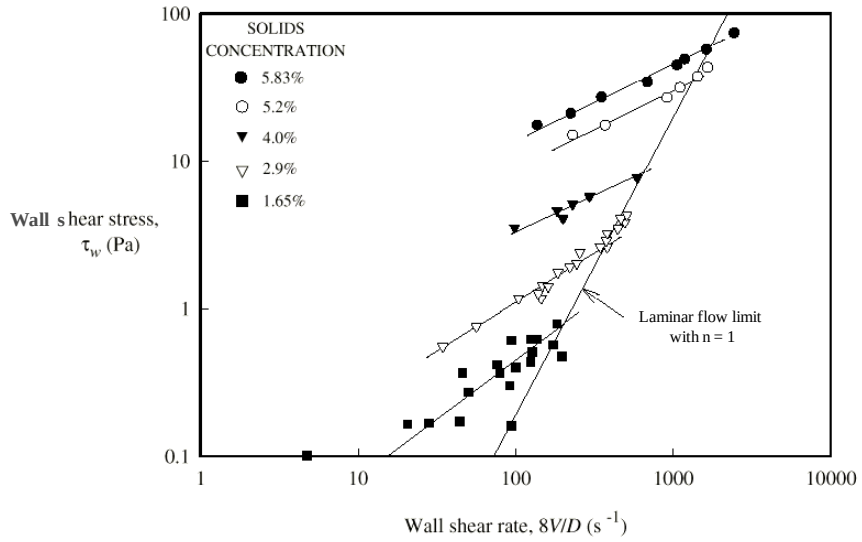

Figure 2.5 Plots of (τ_w) vs. ($8V/D$) for sewage sludge showing the laminar limit (Alderman and Heywood, 2004b)

Alternatively, different size pipes can be used, in which the flow curve data affected by secondary or transitional/turbulent flow (assuming that end effects and wall slip have been accounted for) show up as a deviation from the main curve. This approach was used in this study as the laminar limit approach for all rheological models considered is not documented and the validity of different transitional flow criteria was part of the study.

End effects

End effects manifest as additional pressure drops due to i) viscous or elastic behaviour as the fluid converges at the entrance or diverges at the exit of the pipe or; ii) kinetic energy lost as a result of

streamline rearrangement when the fluid enters and exits the pipe (Alderman and Heywood, 2004b). The pressure loss at the end of the pipe is usually negligible (Steffe, 1996; Chhabra & Richardson, 2008), but the entrance effects are significant and dependent on the type of non-Newtonian fluid (Chhabra & Richardson, 2008). The Bagley method is widely used by many researchers today (Nguyen & Boger, 1992; Steffe, 1996; Alderman and Heywood, 2004b; Chhabra & Richardson, 2008). Details of the correction method are given in both Steffe (1996) and Chhabra & Richardson (2008). Slatter (1994) used 50 diameters before and after the test section to ensure developed flow, while Chhabra & Richardson (2008) suggest that entrance effects can be neglected as long as the *L/D* ratio of the pipe is 100-120.

Wall slip

According to Chhabra & Richardson (2008) the presence of wall slip results in a higher than expected flow rate at a given wall shear stress. Conversely, at a fixed wall shear rate, a lower than expected wall shear stress is encountered. Figure 2.6 schematically shows wall slip. This will manifest as non-collinear laminar flow plots of wall stress (τ_w) against apparent wall shear rate (*8V/D*) for tubes of different diameters, after other effects have been corrected for. To correct for slip the slip velocity (V_s) must be calculated for each diameter and deducted from the measured mean velocity. The procedure to do this is given for example, in Chhabra & Richardson (2008).

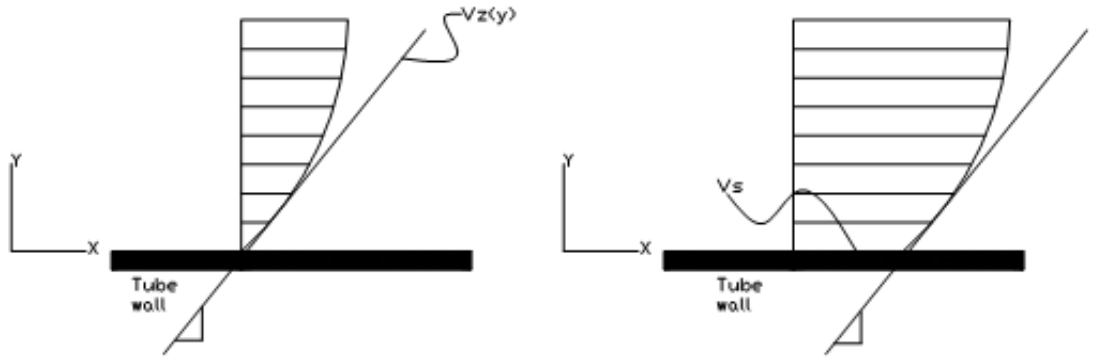

Figure 2.6 Schematics of flow in a tube (Chhabra & Richardson, 2008)

2.3 Laminar flow of a fluid in a pipe

2.3.1 Introduction

A knowledge of the frictional resistance of a fluid as it flows through pipes and fittings (and the rates of mass transfer between the fluid and pipe walls) is important in the design of pipelines. In this section laminar flow in circular closed conduits (round pipes) is considered in detail. For each rheological model the theoretical expressions are given for the fully developed velocity distributions assuming no slip at the wall. The velocity is a maximum at the pipe centre, where the velocity gradient is zero (Knudsen & Katz, 1958).

2.3.2 Velocity profiles and mean velocity equations

Referring to Figure 2.4 and the conditions given in Section 2.2.2, Eq. (2.19) and also the shear stress distribution in a pipe can be described as Eq. (2.20). The two aforementioned equations show the linear variation of the shear stress across the tube cross-section, increasing from zero at the central axis of the tube (*r=0*) to a maximum value at the wall of the tube (*r=R*). This is also illustrated schematically in Figure 2.7 (Chhabra & Richardson, 2008).

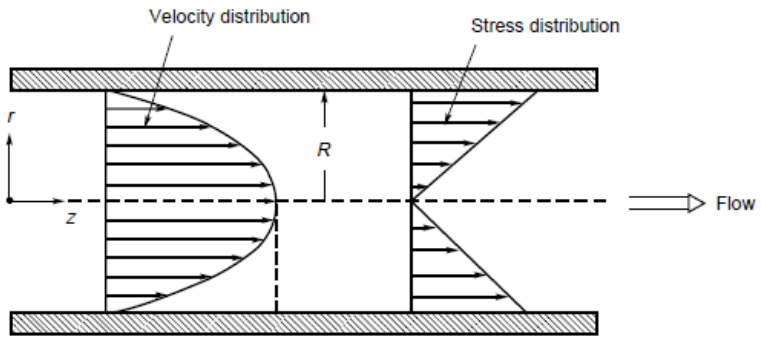

Figure 2.7 Schematic representation of the shear stress and velocity distribution in fully developed laminar flow assuming no slip at the wall and no yield stress (Chhabra & Richardson, 2008)

For fluids without a yield stress, the fully developed velocity profile is also sketched in Figure 2.7, where the velocity decreases from being a maximum at the centre to being zero at the wall, assuming that the no-slip boundary condition applies.

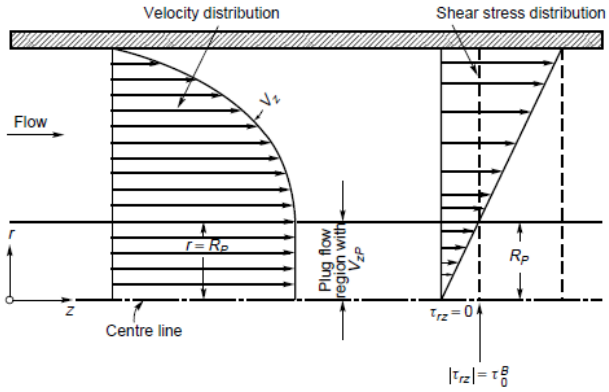

Figure 2.8 Schematic representation of the velocity distribution for laminar flow of a yield stress fluid flowing in a pipe (Chhabra & Richardson, 2008)

For yield stress suspensions part of the material will flow as a solid plug (core) in the part of the pipe ($0 \leq r \leq R_p$) where the stress (τ_{rz}) is less than the yield stress, as shown in Figure 2.8. where R_p is the radius of the plug. Then

$$\frac{R_p}{R} = \frac{\tau_0}{\tau_w} \tag{2.40}$$

or

$$R_p = R\frac{\tau_0}{\tau_w} \tag{2.41}$$

where τ_w is the shear stress at the pipe wall. The velocity in the sheared annulus ($R_p \leq r \leq R$) will decrease from the constant plug velocity to zero at the pipe wall (Slatter, 1994). The expressions for the velocity distributions, bulk flow rate, and apparent shear rate applicable for each material type (rheological model) are as follows:

Herschel-Bulkley model (Peker & Helvaci, 2008)

For yield-pseudoplastic fluids:

$$\tau = \tau_y + K\left(-\frac{dV_z}{dr}\right)^n = \tau_y + K\left(\dot{\gamma}\right)^n \quad \text{for } |\tau| > |\tau_y| \tag{2.11}$$

Thus the velocity distribution of Herschel-Bulkley fluids in the sheared annulus ($R_p \le r \le R$) is given by:

$$V_z = \left(\frac{1}{K}\right)^{1/n} R \frac{n}{(n+1)} \frac{1}{\tau_w} \left[(\tau_w - \tau_y)^{(n+1)/n} - \left(\frac{\tau_w}{R} r - \tau_y\right)^{(n+1)/n} \right] \tag{2.42}$$

The velocity gradient within the plug zone will be zero, so the corresponding velocity $V_{z\ plug}$, in the unsheared plug region ($0 \le r \le R_{plug}$) is obtained by substituting $r = R_p$ in Eq. (2.42) and using (2.41) to yield:

$$V_{zplug} = \left(\frac{1}{K}\right)^{1/n} R \frac{1}{\tau_w} \frac{n}{(n+1)} (\tau_w - \tau_y)^{(n+1)/n} \tag{2.43}$$

The mean velocity for yield stress fluids is obtained by integrating the local velocities in the plug zone [Eq. (2.43)] and the sheared annulus along the walls of the pipe [Eq. (2.42)] over the cross-sectional area

$$V_{av} = \frac{Q}{A} = \frac{\int_0^R 2\pi r V_z dr}{\int_0^R 2\pi r\, dr} = \frac{\int_0^{R_p} 2\pi V_{zp}\, dr + \int_{R_p}^R 2\pi r V_z\, dr}{\int_0^R 2\pi r\, dr} \tag{2.44}$$

to give

$$V_{av} = \left(\frac{1}{K}\right)^{1/n} R \frac{1}{\tau_w^{\,3}} (\tau_w - \tau_y)^{(n+1)/n} \left[\frac{n\tau_w^{\,2}}{(n+1)} - \frac{2n^2\tau_y(\tau_w - \tau_y)}{(n+1)(2n+1)} - \frac{2n^2(\tau_w - \tau_y)^2}{(n+1)(3n+1)} \right] \tag{2.45}$$

or

$$\frac{8V_{av}}{D} = \left(\frac{1}{K}\right)^{1/n} \frac{4}{\tau_w^{\,3}} (\tau_w - \tau_y)^{(n+1)/n} \left[\frac{n\tau_w^{\,2}}{(n+1)} - \frac{2n^2\tau_y(\tau_w - \tau_y)}{(n+1)(2n+1)} - \frac{2n^2(\tau_w - \tau_y)^2}{(n+1)(3n+1)} \right] \tag{2.46}$$

Bingham Plastic fluid model (Peker & Helvaci, 2008)

For Bingham fluids:

$$\tau_w = \tau_0 + K(\dot{\gamma}) \tag{2.9}$$

The velocity distribution is given by:

$$V_{zplug} = \left(\frac{R}{K}\right)\left[\frac{\tau_y^{\,2}}{2\tau_w} + \frac{\tau_w}{2} - \tau_y\right] \quad (0 \le r \le r_{plug}) \tag{2.47}$$

$$V_z = \frac{1}{K}\left[R\left(\frac{\tau_w}{2} - \tau_y\right) - r\left(\frac{\tau_w r}{2R} - \tau_y\right)\right] \quad \text{for } \tau_{plug} \le r \le R \tag{2.48}$$

The mean velocity is:

$$V_{av} = \frac{R\tau_y^{\,4}}{12K\tau_w^{\,3}} + \frac{R\tau_w}{4K} - \frac{R\tau_y}{3K} \tag{2.49}$$

or

$$\frac{8V_{av}}{D} = \frac{\tau_y^{\,4}}{3K\tau_w^{\,3}} + \frac{\tau_w}{K} - \frac{4\tau_y}{3K} \tag{2.50}$$

Power law model or Pseudoplastic fluid behaviour (Peker & Helvaci, 2008)

For power law fluids:

$$\tau_w = K\gamma^n \tag{2.7}$$

The velocity distribution is given by (0 <*r* <*R*):

$$V = \left(\frac{\tau_w}{KR}\right)^{1/n}\left(\frac{n}{n+1}\right)\left(R^{(n+1)/n} - r^{(n+1)/n}\right) \tag{2.51}$$

At r = 0, $V = V_{max}$ where

$$V_{max} = \left(\frac{\tau_w}{KR}\right)^{1/n}\left(\frac{n}{n+1}\right)R^{(n+1)/n} \tag{2.52}$$

and

$$V_{av} = \left(\frac{\tau_w}{K}\right)^{1/n} R\left(\frac{n}{3n+1}\right) \tag{2.53}$$

or

$$\frac{8V_{av}}{D} = 4\left(\frac{\tau_w}{K}\right)^{1/n}\left(\frac{n}{3n+1}\right) \tag{2.54}$$

Casson model (Peker & Helvaci, 2008)

For Casson fluids:

$$\tau_w^{0.5} = \tau_C^{0.5} + \eta_C^{0.5}\gamma^{0.5} \tag{2.13}$$

The velocity distribution is given by:

$$V_{zplug} = \frac{R\tau_w}{4\eta_C}\left[2 - \frac{2}{3}\left(\frac{\tau_C}{\tau_w}\right)^2 + \frac{16}{3}\left(\frac{\tau_C}{\tau_w}\right)^{1/2} + 4\left(\frac{\tau_C}{\tau_w}\right)\right] \quad (0 \le r \le r_{plug}) \tag{2.55}$$

$$V_z = \frac{R\tau_w}{4\eta_C}\left[\frac{16}{3}\left(\frac{\tau_C}{\tau_w}\right)^{1/2}\left(\left(\frac{r}{R}\right)^{3/2} - 1\right) + 4\left(\frac{\tau_C}{\tau_w}\right)\left(1 - \frac{r}{R}\right) + 2\left(1 - \left(\frac{r}{R}\right)^2\right)\right] \quad (r_{plug} \le r \le R) \tag{2.56}$$

The mean velocity is:

$$V_{av} = \frac{R\tau_w}{4\eta_C}\left[1 - \frac{16}{7}\left(\frac{\tau_C}{\tau_w}\right)^{1/2} + \frac{4}{3}\left(\frac{\tau_C}{\tau_w}\right) - \frac{1}{21}\left(\frac{\tau_C}{\tau_w}\right)^4\right] \tag{2.57}$$

or

$$\frac{8V_{av}}{D} = \frac{\tau_w}{\eta_C}\left[1 - \frac{16}{7}\left(\frac{\tau_C}{\tau_w}\right)^{\frac{1}{2}} + \frac{4}{3}\left(\frac{\tau_C}{\tau_w}\right) - \frac{1}{21}\left(\frac{\tau_C}{\tau_w}\right)^4\right] \tag{2.58}$$

Hallbom model

The constitutive equation for yield-plastic fluids is given by (Hallbom, 2008):

$$\tau_w{}^k = (\tau_0)^k + (\mu_\infty)^k (\dot{\gamma})^k \tag{2.15}$$

Hallbom's yield plastic model cannot be integrated analytically for arbitrary values of *k,* to yield the mean velocity equation, so the velocity distribution cannot be derived. An approximation is thus required (Hallbom, 2008), which results in the mean velocity being given for a known pressure drop by:

$$V_{av} = \frac{D}{8}\left(\frac{\tau_0}{\mu_\infty}\right)\left[\frac{(1 - Z^k)^{3/(1+k)}}{Z}\right] \tag{2.59}$$

or

$$\frac{8V_{av}}{D} = \left(\frac{\tau_0}{\mu_\infty}\right)\left[\frac{(1 - Z^k)^{3/(1+k)}}{Z}\right] \tag{2.60}$$

where

$$Z = \frac{\tau_0}{\tau_w} = \frac{R_p}{R} \tag{2.61}$$

Alternatively, if the mean velocity is known and the pressure drop needs to be estimated, the following equation should be used:

$$\tau_w^k = \left(\frac{8V}{D}\right)^k \mu_\infty^k + \left[\frac{4}{(1+k)}\tau_0^k\right] \tag{2.62}$$

Hallbom (2008) states that the use of Eq. (2.62) rather than Eq. (2.60) to estimate nominal wall shear rate (*8V/D*) for a known pressure drop results in significant under-estimation of *8V/D.*

2.4 Transitional flow of fluids in a pipe

The flow of any fluid in a pipeline is laminar at low velocities and turbulent at high velocities, so it is logical to assume that there is some intermediate velocity (or velocity range) at which flow changes from laminar to turbulent. This transitional velocity (often referred to as the critical velocity) is important as it defines the regions in which laminar or turbulent pipe flow equations should be used. There are several models available in the literature, some of which some are presented below.

2.4.1 Two transition points

Frigaard and Nouar (2003) suggest that one reason why the discrepancy between theoretical and experimental values for transition is still not fully resolved is due to the inability to differentiate between the two transition points. Work done by Peixinho, Nouar, Desaubry & Théron (2005) on the transitional and turbulent flow of yield stress fluids in a pipe concluded that transition for the yield stress fluid takes place in two stages. First, the experimental velocity profile departs slightly from the laminar theoretical solution, but the fluctuations remain at a laminar level in a flow zone around the axis and increase slightly around this zone. Then with increasing Reynolds number, turbulent spots filling up the whole section appear, and inside the spots the plug zone is disrupted due to large velocity variations. Hallbom (2008) also established two distinct definitions for transition based on Newtonian behaviour. The first he describes as the onset of instability in the laminar flow, characterised by the first appearance of eddies (instability point transition). The second, is at a higher velocity where the pressure gradient deviates significantly from the laminar flow pressure gradient (break point transition). Perhaps the most obvious weakness with simplistic formulas such as single critical Reynolds numbers available in literature, is that turbulent transition occurs over a wide range of Reynolds numbers and not at a single number (Güzel, Burghelea, Frigaard & Martinez, 2009).

2.4.2 The effect of yield stress on critical velocity

The wall shear stress required to produce the critical velocity in larger pipe diameters reduces asymptotically towards a value dominated by the yield stress (Slatter, 1997a). He suggests that the viscous stresses caused by the fluid consistency index (K) become insignificant and the behaviour is controlled by the yield stress and flow behaviour index (n). This produces a horizontal asymptote which the critical velocity approaches, and is independent of both the fluid consistency index and pipe diameter. This effect is illustrated in Figure 2.9.

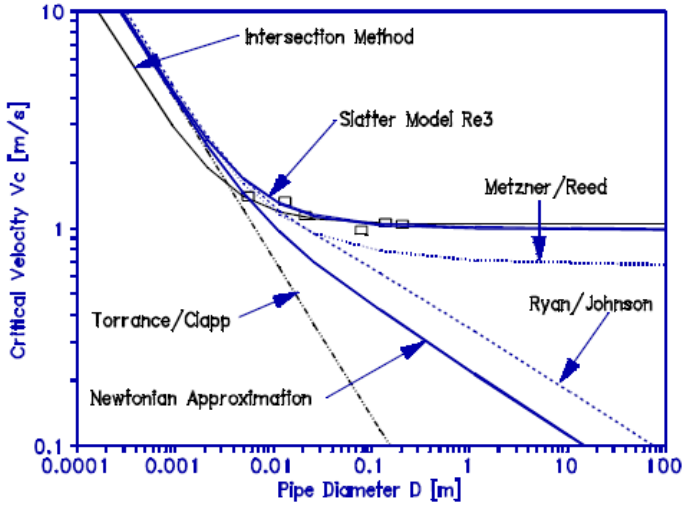

Figure 2.9 Illustration of critical velocity vs. pipe diameter showing the horizontal and oblique asymptotes (Slatter, 1997a)

The experimental data used by Slatter (1997a), shows a definite horizontal trend when plotted on log-log axis as presented in Figure 2.9. Some techniques such as the Intersection method and Slatter model are able to follow this trend, whilst others such as Ryan & Johnson, Torrance/Clapp and Newtonian approximation do not. According to Slatter, it is the effect of the yield stress which allows certain techniques to approach this horizontal asymptote. Slatter concludes that for large pipe diameters (He > 1.5 x 10^5) the yield stress causes the critical velocity to be independent of the pipe diameter.

2.4.3 Definitions of Reynolds number in transitional/turbulent flow

Reynolds number is the ratio of momentum flux by convective mechanism (τ_t) to the flux by molecular mechanism (τ_l) (Peker & Helvaci, 2008) and is also expressed as the ratio of inertial forces to viscous forces (Massey, 1970).

$$Re = \frac{\tau_t}{\tau_l} \approx \frac{inertial \quad forces}{viscous \quad forces} \quad \alpha \quad \frac{\rho D^2 V^2}{D^2 \tau_{visc}} \tag{2.63}$$

or generally

$$Re_{Gen} = \frac{8\rho V^2}{\tau_w} \tag{2.64}$$

This is the general form of the Reynolds number and can be applied for any rheological model. The viscous shear stress is related to the shear rate by the material constitutive rheological equation. Dimensionally, any characteristic velocity divided by a characteristic length can be used as a representative shear rate. According to Peker & Helvaci (2008), it is widely accepted in literature that the flow characteristic (*8V/D*) can be used as the representative shear rate. Hence the viscous shear stress for a Herschel-Bulkley fluid is represented by

$$\tau_w = \tau_y + K\left(\frac{8V}{D}\right)^n \tag{2.65}$$

and using (2.63) and (2.65) results in

$$Re \ \alpha \ \frac{\rho D^2 V^2}{D^2\left[\tau_y + K\left(\frac{8V}{D}\right)^n\right]} \tag{2.66}$$

Choosing the proportionality constant equal to 8 reduces *Re* to the standard form $Re = \rho VD/\mu$ under Newtonian conditions. Thus, for Herschel-Bulkley fluids

$$Re = \frac{8\rho V^2}{\left[\tau_y + K\left(\frac{8V}{D}\right)^n\right]} \tag{2.67}$$

Similarly for the other rheological models considered:

$$Re_{Gen} = \frac{8\rho V^2}{\tau_y + K\left(\frac{8V}{D}\right)} \quad \text{(Bingham Plastic fluid)} \tag{2.68}$$

$$Re_{Gen} = \frac{8\rho V^2}{K\left(\frac{8V}{D}\right)^n} \quad \text{(power law fluid)} \tag{2.69}$$

$$Re_{Gen} = \frac{8\rho V^2}{\left(\tau_C^{0.5} + \eta_C^{0.5}\left(8V/D\right)^{0.5}\right)^2} \quad \text{(Casson fluid)} \tag{2.70}$$

$$Re_{Gen} = \frac{8\rho V^2}{\left(\tau_0^k + \mu_\infty^k\left(8V/D\right)^k\right)^{\frac{1}{k}}} \quad \text{(Hallbom Yield Plastic fluid)} \tag{2.71}$$

Note that the generalised Reynolds number proposed by Torrance (1963) is simply that of a power law fluid, while Re_2 (Slatter, 1994) is the same as Re_{Gen} for a Herschel-Bulkley fluid. Little is found in the literature in which the general form of the Reynolds number is used to predict the experimental transition point. Torrance (1963) presents a transition model using Eq. (2.69) (See Section 2.4.5). Slatter (1994) presents his Re_2 [Eq.(2.67)], but goes on to exclude the unsheared annulus in his analysis of Re_2 and develops his own model, referred to as Re_3. The Slatter Re_2 and Re_3 Reynolds numbers are reviewed in Section 2.4.5.

Masalova, Malkin, Kharatiyan & Haldenwang (2006) investigated the difference between applying the general *Re* for Herschel-Bulkley fluids (Re_{HB}) and the more scientifically refined Re_3, when estimating the transitional velocity for kaolin suspensions. Their findings were such that the differences between the two techniques were significantly minimal and in some instances the general form of Re_{HB} resulted in a smaller error value when compared to the experimental transition data, than that predicted by Re_3. Haldenwang, Sutherland, Fester, Holm, & Chhabra (2012) characterised various concentrations of sewerage sludge using the Bingham Plastic rheological model. They predicted transitional velocities using several Reynolds numbers including the Metzner & Reed Reynolds number, the general *Re* for Bingham fluids (Re_{BP}) and Slatter's Re_3. For their data the general form of the Reynolds number and the Metzner & Reed Reynolds number consistently produced the most accurate prediction of the experimental transitional velocity. Other non-Newtonian Reynolds numbers used in the various transitional velocity prediction techniques are reviewed in Section 2.4.5.

2.4.4 Newtonian transition

In this section work done by various researchers on Newtonian transition is presented. A common approach involved the studying of puffs and slugs (the phenomenon observed at the onset of transitional flow), usually by way of Laser Doppler velocimetry (LDV).

Banfi, Mechili and Henin (1981) used a laser-Doppler velocimeter to investigate transitional pipe flow. They investigated the behaviour of velocity fluctuations as Reynolds numbers increased from 1500 to 4000 and observed that at a Reynolds number of about 2800 the fluctuations reached a maximum.

Darbyshire and Mullin (1995) investigated Newtonian transition pipe flow using constant mass flux induced by pulsating motion of a piston. Transition was induced by singular disturbances into developed Poiseuille flow, using a jet or suction. Their experiments confirmed that turbulent structures could be introduced into laminar flow by injecting disturbances, stirring the supply tank or using sharp flow inlet to the pipe. They also found that turbulent structures could not be maintained below Reynolds numbers of *Re* = 1760. As soon as Reynolds numbers exceed 1800, fairly large disturbances were observed which resulted in sustained transitional flow.

Laser Doppler velocimetry (LDV) measurements of various transition features were presented, including turbulent slugs and equilibrium puffs. Interestingly for both puffs and slugs the mean centre-line velocity decreases during each occurrence. If the flow occurring during the slug is considered to be identical to fully developed pipe flow (Wygnanski and Champagne, 1973) then this could explain the observed blunting of the velocity profile in turbulent flow compared with the laminar flow velocity profile. Klein (1981) reviewed developing turbulent pipe flow and presented the blockage ratio [Eq. (2.72)] as a measure of flow development.

$$B = 1 - \frac{V}{V_{cl}} \tag{2.72}$$

where V is the bulk (mean) velocity and V_{cl} is the mean centreline velocity. This parameter was also considered by others (Pullum, Rudman, Graham, Downie, Battacharya, Chryss & Slatter, 2001) to be best suited to indicating the onset of transition. Another important outcome from their work was that the distance for fully developed turbulent flow could well exceed 140 pipe diameters. It was concluded that the beginning and end of transition was well illustrated on a plot of the blockage ratio against a Reynolds number defined using flow distance rather than pipe diameter.

This brief review of some existing literature shows that transition to turbulence in pipe flow has been an active research topic for many years and remains so. Transition is characterised by turbulent puffs and slugs that are interspersed with intervals of laminar flow, giving rise to the phenomenon of intermittency. Both experimental and computational approaches have been used to investigate these flows, with the advent of direct numerical simulation (DNS) providing greater insight into the details of puffs and slugs (Pullum *et al.*, 2001).

2.4.5 Non-Newtonian transition models/criterion

The following section reviews the non-Newtonian transition criterion used in this study. The constitutive equations are presented in terms of friction factors and Reynolds numbers.

Newtonian Approximation

The generally accepted criterion for laminar–turbulent transition of Newtonian fluids is straight forward: transition occurs when *Re* = 2100 (Hallbom, 2008), which is undoubtedly an over simplification. When a Newtonian fluid flows in a pipe, deviation from true laminar flow may be observed at *Re* = 1225, occasional eddies are observed at *Re* = 2100 and turbulence is usually fully developed by *Re* = 3000, although under special circumstances laminar flow may be observed at Reynolds numbers as high as 50 000 (Govier and Aziz, 1977).

To apply a Newtonian approximation to non-Newtonian fluids, a value for the viscosity is required. This does not make sense for a non-Newtonian fluid, so the viscosity is referred to as an apparent viscosity.

Wilson (1986) describes the apparent viscosity as the point value of the shear stress to the shear rate ratio:

$$\mu' = \frac{\tau_w}{\left[-\frac{du}{dr}\right]_w} \tag{2.73}$$

The Reynolds number is then defined as

$$Re_{Newtonian} = \frac{\rho VD}{\mu'} \tag{2.74}$$

The Newtonian approximation is favoured by many design engineers because of its simplicity and the understanding of the term "viscosity". The only requirement now for the application of the Newtonian model to non-Newtonian fluids is that the value for μ' is not constant for a given fluid and pipe diameter, and needs to be evaluated at a given value for τ_w. Even though favoured by industry, this model does not provide consistent reliable results for materials with a yield stress (Slatter, 1997a). He suggests that the reason for failure is the lack of detail in how the model incorporates the material rheology. Even though it takes the rheology of the material into account by computing the apparent viscosity at a given wall shear stress, it ignores the fact that an unsheared plug exists and how this influences the velocity profile. The Newtonian approximation thus fails to successfully predict transition at larger pipe diameters where the yield stress plays a significant role (Slatter, 1997a). Little is reported on in the literature for use of the Newtonian approximation with the power law rheological model.

Metzner and Reed

Metzner and Reed (1955) developed a generalised Reynolds number for correlating non-Newtonian pipe data, using the Fanning friction factor as their stability parameter. They proposed that non-Newtonian fluids begin to deviate from the laminar flow line at approximately the same Reynolds number as do Newtonian fluids, which for smooth pipes is at f_N = 0.0076, *Re* = 2100.

Following the Rabinowitsch-Mooney derivation for true shear rate at the wall (γ_w) from the nominal shear rate (*8V/D*) (Section 2.2.2), *n'* is the slope of the log-log plot of τ_w vs. (*8V/D*) for time independent non-Newtonian fluids in the laminar region. For pseudoplastic fluids the value for *n*' is constant [Eq. ((2.37))], and the y-intercept of the log-log plot is *ln(K')*. Thus the power law relationship can be written as

$$\tau_w = K'\left(\frac{8V}{D}\right)^{n'} \tag{2.75}$$

Eq. (2.75) is true for any time-independent fluid in fully developed laminar flow, with no slip at the wall. It should be noted that *n'* is only constant for power law fluids, and will have to be evaluated at each (*8V/D*) value for fluids described by other rheological models.

Writing τ_w in terms of the friction factor (*f*) [Eq. (2.18)], Eq. (2.75) becomes

$$f = \frac{2}{\rho V^2} K' \left(\frac{8V}{D} \right)^{n'} \tag{2.76}$$

Metzner & Reed (1955) then defined a friction factor – Reynolds number relationship for laminar flow in the same way as for Newtonian fluids, as

$$f = \frac{16}{Re_{MR}} \tag{2.77}$$

from which the generalised Metzner and Reed Reynolds number was defined as

$$Re_{MR} = \left[\frac{\rho V^{2-n'} D^{n'}}{8^{n'-1} K'} \right] = \frac{8\rho V^2}{K' \left[\frac{8V}{D} \right]^{n'}} \tag{2.78}$$

Metzner and Reed derived their Reynolds number based on experiments with pseudoplastic fluids, for which the values for *K*' and *n*' were often constant. However, *K*' and n' are not constant for Herschel-Bulkley fluids (Slatter, 1994), Bingham plastic fluids (Chhabra & Richardson, 2008) and Casson fluids. For these fluids *K*' and *n*' should thus be evaluated at each value of wall shear stress, which complicates the model. Equations for n' and K' for Bingham plastic, Herschel-Bulkley and Casson fluids are given in Eq. (2.79) to Eq. (2.87). One advantage of this method is that the transition friction factor may be directly determined from pipe test data without knowledge of the fluid's rheology.

Generalised Metzner and Reed for Bingham fluids (Chhabra & Richardson, 2008):

$$n' = \frac{1 - \frac{4}{3}\theta + \frac{\theta^4}{3}}{1 - \theta^4} \tag{2.79}$$

$$K' = \tau_w \left[\frac{K}{\tau_w \left(1 - \frac{4}{3}\theta + \frac{\theta^4}{3} \right)} \right]^{n'} \tag{2.80}$$

where $\theta = (\tau_y / \tau_w)$

Generalised Metzner and Reed for Herschel-Bulkley fluids (Desouky & Al-Awad, 1998):

$$n' = \frac{1}{\lambda_1 + \left(\frac{\lambda 2}{\lambda 3} \right)} \tag{2.81}$$

where:

$$\lambda 1 = -3 + \frac{1+n}{n} \frac{\tau_w}{\tau_w - \tau_y} \tag{2.82}$$

$$\lambda 2 = 2\tau_w \left[+ n \left(\tau_w + 2n\tau_w + n\tau_y \right) \right. \tag{2.83}$$

$$\lambda 3 = \left[+ n \left(+ 2n \left(\tau_w - \tau_y \right)^2 + 2\tau_y \left(\tau_w - \tau_y \right) + n \left(+ 3n \right) + \tau_y^2 \left(+ 2n \right) \left(+ 3n \right) \right. \tag{2.84}$$

$$K' = \frac{\tau_w}{\left\{ \frac{4n}{K^{\frac{1}{n}} \tau_w^3} \left(\tau_w - \tau_y \right)^{1+n/n} \left[\frac{\left(\tau_w - \tau_y \right)^2}{1+3n} + \frac{2\tau_y \left(\tau_w - \tau_y \right)}{1+2n} + \frac{\tau_y^2}{1+n} \right] \right\}^{n'}} \tag{2.85}$$

Generalised Metzner and Reed for Casson fluids:

Following the derivation given in Skellend (1967) for pseudoplastic and Bingham plastic fluids, *n'* and *K'* for Casson fluids were derived as

$$n' = \frac{1 - \frac{16}{7}\left(\frac{\tau_C}{\tau_w}\right)^{\frac{1}{2}} + \frac{4}{3}\left(\frac{\tau_C}{\tau_w}\right) - \frac{1}{21}\left(\frac{\tau_C}{\tau_w}\right)^4}{1 - \frac{8}{7}\left(\frac{\tau_C}{\tau_w}\right)^{\frac{1}{2}} + \frac{1}{7}\left(\frac{\tau_C}{\tau_w}\right)^4} \tag{2.86}$$

and

$$K' = \tau_w \left\{ \frac{\tau_C}{\tau_w \left[1 - \frac{16}{7}\left(\frac{\tau_C}{\tau_w}\right)^{\frac{1}{2}} + \frac{4}{3}\left(\frac{\tau_C}{\tau_w}\right) - \frac{1}{21}\left(\frac{\tau_C}{\tau_y}\right)^4 \right]} \right\}^{n'} \tag{2.87}$$

Dodge & Metzner (1959) developed their critical Reynolds number by plotting the friction factor of power law fluids against generalised Reynolds number. The values of critical Reynolds number determined from their charts agreed with those obtained from the chart developed by Metzner and Reed (1955). The Reynolds number defined by Metzner and Reed was generalised by Kozicki, Chou and Tiu (1966) to apply to laminar flows of purely viscous non-Newtonian fluids through ducts of arbitrary cross-section. This generalisation has made this approach popular and it is now widely used. Slatter (1997a) and Slatter & Wasp (2000) showed that the Metzner & Reed approach accurately predicts the experimental transition data for yield-pseudoplastic and Bingham plastic rheologies respectively. Slatter (1997a) showed that the Metzner & Reed approach is successful for small pipe diameters ($D \leq 25$mm). For large pipe diameters this technique responded positively to the presence of a yield stress and also produced reliable predictions for $n \leq 0.7$ (Slatter, 1997a). Slatter and Wasp (2000) showed that although the approach is successful at smaller diameters, prediction errors increase to 30% for larger diameters and at Hedström numbers > 1×10^8.

Torrance

Torrance (1963) investigated the turbulent flow of yield pseudoplastic fluids, using the Clapp Reynolds number (Slatter, 1994). Transition was assumed to occur at *Re* = 2100, where

$$Re_{Torr} = \frac{8\rho V^2}{K\left[\frac{8V}{D}\right]^n} \tag{2.88}$$

which ignores the effect of the yield stress. This model was unsuccessful when applied to the data of Slatter (1994) and El-Nahhas, El-Hak, Rayan, Vlasak and El-Sawaf (2004). Note that Re_{Torr} is identical to Re_{Gen} for pseudoplastic (power law) fluids [Eq. (2.69)].

Slatter

Slatter (1994) developed a Reynolds number for the flow of Herschel-Bulkley type fluids that places emphasis on the yield stress. The derivation of the Reynolds number, defined as Re_3, was based on the assumption that inertial and viscous forces are determined only by the part of the material that is undergoing shearing, thus excluding the unsheared plug.

There is the implicit assumption that viscous forces are represented by the nominal wall shear rate of ($8V/D$) rather than the true value given of Eq.(2.38). Furthermore, although Slatter (1994, 1999) argued that plug flow does not contribute to the inertial and viscous forces, this assumption is open to criticism and is at best an empiricism without theoretical justification (Haldenwang *et al.,* 2012). Laminar flow was taken to cease at a critical value of Re_3 = 2100.

Slatter Reynolds number for Herschel-Bulkley, Bingham and Pseudoplastic fluids

Slatter (1994) starts the derivation of his transition model (Re_3) by defining a Reynolds number Re_2 given by Eq. (2.89), which is identical to the generalised Reynolds number for Herschel-Bulkley fluids given in Section 2.4.3.

$$Re_2 = \frac{8\rho V^2}{\left[\tau_y + K\left(\frac{8V}{D}\right)^n\right]} \tag{2.89}$$

The radius of the plug (R_p) is given by Eq. (2.41) and the plug velocity ($V_{z\,plug}$) by Eq. (2.43).

The area of the annulus is therefore:

$$A_{ann} = \pi\left(R^2 - R_{plug}^2\right) \tag{2.90}$$

In deriving Re_3 the characteristic dimension D_{shear} was taken as:

$$D_{shear} = D - D_{plug} \tag{2.91}$$

and the mean fluid velocity in the annulus, V_{ann}, is:

$$V_{ann} = \frac{Q_{ann}}{A_{ann}} \tag{2.92}$$

where

$$Q_{ann} = Q - Q_{plug} \tag{2.93}$$

and

$$Q_{plug} = V_{z\,plug} A_{plug} \tag{2.94}$$

so using the form of Eq. (2.89), Re_3 is given by

$$Re_3 = \frac{8\rho V_{ann}^2}{\tau_y + K\left[\frac{8V_{ann}}{D_{shear}}\right]^n} \tag{2.95}$$

This expression can be used to represent both Herschel-Bulkley, Bingham plastic (n=1) and pseudoplastic (τ_y = 0) behaviour (Slatter & Wasp, 2000).

Slatter Reynolds number for Casson fluids

For Casson fluids Eq. (2.13) can be integrated to obtain the plug velocity [$V_{z\,plug}$ in Eq.(2.55)] as:

$$V_{z\,plug} = \frac{R\tau_w}{4\eta_C}\left[2 - \frac{2}{3}\left(\frac{\tau_C}{\tau_w}\right)^2 - \frac{16}{3}\left(\frac{\tau_C}{\tau_w}\right)^{1/2} + 4\left(\frac{\tau_C}{\tau_w}\right)\right] \tag{2.96}$$

and Re_3 given by:

$$Re_3 = \frac{8\rho V_{ann}^2}{\left[\sqrt{\tau_C} + \sqrt{\eta_C\left(\frac{8V_{ann}}{D_{shear}}\right)}\right]^2} \tag{2.97}$$

In his further work on the transition of Herschel-Bulkley fluids (Slatter, 1997a) shows the use of Re_3 gives the most reliable transitional velocity predictions over a wide range of pipes. At small pipe diameters (<25mm), all approaches except the Hedström intersection method (see below) agree with experimental data. At larger diameters, only the Slatter, Metzner & Reed and Intersection method (using Wilson and Thomas turbulence model) predict transition reliably, with Re_3 being most reliable.

Detailed comparisons between the predictions of Slatter's Reynolds number Re_3 and pipe data (Chhabra & Richardson, 2008) show an improvement in the prediction of transition models compared to the Metzner & Reed Reynolds number. The critical values based on Re_{MR} were 20-25% lower than those of Re_3 and the two criteria coincide for power law fluids. From both Slatter (1997a) and Chhabra & Richardson (2008), it is shown the critical velocity is unaffected by the yield stress in small diameters. However, both the yield stress and flow behaviour index (n) play an increasingly greater role in determining the transitional velocity with increasing pipe diameter. It is apparent that both the yield stress and shear-thinning behaviour stabilises the flow, which delays the break-down of laminar flow (Chhabra & Richardson, 2008).

Güzel *et al.* (2009) contradict the existence of the unsheared plug during transitional flow of yield stress

fluids. Their experimental work, together with experiments by Peixinho *et al.* (2005), contribute to the evidence that the plug region thins out to such an extent that the Reynolds stresses can break it before transition commences.

Ryan and Johnson

"Two identical predictions for transitional Reynolds numbers were formulated by Ryan & Johnson (1959) and Hanks (1963), using two totally different approaches" (Nouar & Frigaard, 2001). Ryan and Johnson (1959) suggested using the ratio of input energy to dissipation energy for an element of fluid as the stability parameter. Considering the energy equation for a linear two-dimensional disturbance, they examined the situations where the energy of a disturbance increases or decreases with time. The rate of increase of kinetic energy is equal to the difference between the rate at which energy is converted from the basic flow to the disturbance via a Reynolds shear stress term. A ratio *Z* was formed as the rate of increase in energy to the rate at which energy is dissipated, which varies with radial position (*r*), so their approach can be considered a local approach. They assumed that transitional instabilities will first appear at the radial position where *Z* is a maximum, for all purely viscous non-Newtonian fluids. Further they assumed that instability occurs when this maximal value of *Z* exceeds a critical number Z_{crit} regardless of the exact fluid type. The critical number was determined from the transition of Newtonian flow and is Z_{crit} = 808 (Ryan and Johnson, 1959). The stability parameter *Z* is given by:

$$Z = -\frac{Ru\rho}{\tau_w}\frac{du}{dr} \tag{2.98}$$

For fixed values of *R*, ρ and τ_w the Ryan and Johnson function can be written as

$$Z = constant * u\left[-\frac{du}{dr}\right] \tag{2.99}$$

with shape (for a typical yield-pseudoplastic fluid) as shown in Figure 2.10. The parameter *Z* is zero at the pipe wall and at the pipe centre, and is a maximum at a radial position r_{crit} at which the end of the laminar region can be determined using the velocity profile equation. The r_{crit} values for Newtonian, Herschel-Bulkley, Bingham Plastic and power law are (Güzel *et al*, 2009):

$$r_{crit} = \frac{R}{\sqrt{3}} \qquad \text{Newtonian fluids} \tag{2.100}$$

$$r_{crit} = R\left[\frac{\tau_y}{\tau_w} + \left(1 - \frac{\tau_y}{\tau_w}\right)\left(\frac{1}{n+2}\right)^{n/(n+1)}\right] \qquad \text{Herschel-Bulkley fluids} \tag{2.101}$$

$$r_{crit} = R\left[\frac{\tau_y}{\tau_w} + \left(1 - \frac{\tau_y}{\tau_w}\right)\left(\frac{1}{\sqrt{3}}\right)\right] \qquad \text{Bingham plastic fluids} \tag{2.102}$$

$$r_{crit} = R\left(\frac{1}{n+2}\right)^{n/(n+1)} \qquad \text{power law fluids} \tag{2.103}$$

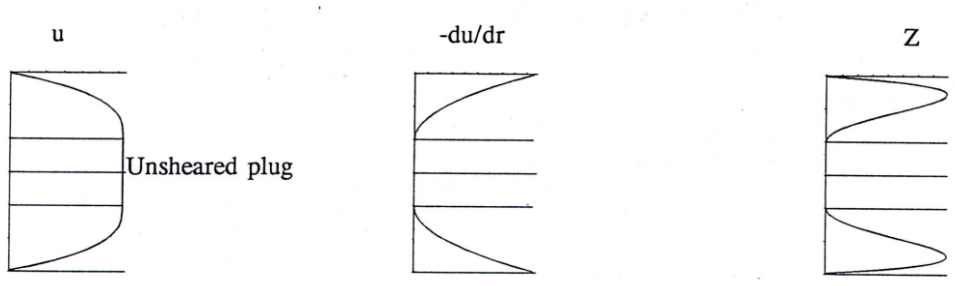

Figure 2.10 Velocity, shear rate and Ryan & Johnson Z function distributions across a pipe section (Slatter, 1994)

For Newtonian flow Z_{crit} = 808 at *Re*= 2100 and it was assumed that all fluids obtain this value of Z_{crit} at transition.

With the development of Re_3 Slatter (1994) concluded the work he conducted on Herschel-Bulkley fluids that the value for Z_{max} is not based on a constant value at the critical point of transition, but increases with Hedström number. Slatter (1997a) investigated the effect of yield stress on the transition of yield pseudoplastics and concluded that the Ryan and Johnson criterion didn't perform well for larger pipe diameters, even though it incorporates the effect of the yield stress. Slatter and Wasp (2000) investigated the transition of yield stress fluids but for Bingham plastics, and again the Ryan and Johnson criterion fared worse at higher Hedström numbers, which are highly dependent on pipe diameter.

Hedström Intersection method

Hedström (1952) developed a criterion for yield stress fluids, postulating that transition occurs at the point of intersection of the laminar and turbulent friction factor curves. He argued that in fully turbulent flow the effect of yield stress is negligible and so used the Nikuradse Newtonian turbulent flow friction factor. More commonly, this approach is known as the intersection method (Güzel *et al*, 2009).

The intersection method is a practical approach only requires the use of standard non-Newtonian laminar flow and Newtonian turbulent flow pressure gradient equations (Slatter, 1997a). However, it is evident from the literature that this criterion underestimates the observed transitional velocity (Hallbom, 2008). Non-Newtonian turbulent models may be used to give somewhat more reliable results, for example Xu *et al* (1993), Slatter (1997a) and Slatter & Wasp (2000).

The success of this approach depends on the turbulent model used. Xu *et al* (1993), Slatter (1997a) and Slatter & Wasp (2000) all made use of the Wilson and Thomas turbulent model and obtained reliable results. Hallbom (2008) used the Knudsen & Katz (1958) Newtonian turbulent equation, but used his own infinite shear rate viscosity instead of the constant Newtonian viscosity. Shook & Roco (1991) state that the success of this method is based on the empirical fact that for most non-Newtonian slurries, especially those which can be characterised using the Bingham plastic model, the abrupt increase in head loss at the laminar/ turbulent transition (characteristic of Newtonian flow) is absent.

This approach is purely a practical one and cannot explain the flow behaviour as does the Newtonian Reynolds number approach, which works from the fundamental definition regarding inertial and viscous forces (Slatter, 1997a). This method is therefore incompatible with Newtonian behaviour, where the critical point is not the intersection of the laminar and turbulent theoretical lines.

Hallbom transition criteria

Hallbom (2008) first defines two distinct transition points namely instability point transition and the pressure break point transition. The instability point transition is characterised by the first appearance of eddies in laminar flow, while the pressure break point transition point is defined as the point where the flow deviates significantly from the laminar flow pressure gradient. The transition point referred to in the model presented by Hallbom (2008) is the pressure break point transition, as this is the point of interest to pipeline engineers, and he presents two models to describe this pressure break point transition for yield plastic materials. The first is an intersection method which takes transition to occur at the intersection of the laminar flow curve [Eq. (2.60)] and the turbulent flow curve [Eq. (2.105)]. The second model is an explicit algebraic equation which uses the same criterion as his intersection method, but incorporates the Hedström number approach.

Method 1: Intersection criterion

The Hallbom (2008) transition criterion is an improvement on that of Hedström (1952) who assumed that transition occurs at the intersection of the Bingham plastic laminar flow curve and the pseudo-fluid turbulent flow curve which is not correct, even for a Newtonian fluid. If the Newtonian fully turbulent flow curve of Knudsen-Katz is extended back to the laminar flow curve for a Newtonian fluid, they intersect at $Re \approx 1500$, well below the generally accepted $Re \approx 2100$.

Hallbom (2008) presents the Newtonian laminar and turbulent friction factors as $f_{lam} = 0.0076$ and $f_{turb} \approx 0.0100$ respectively. He then concludes that Newtonian transition can be assumed to occur at a velocity corresponding to a point at which the smooth wall fully turbulent flow friction factor is 130% of the laminar flow friction factor. Therefore, for a given flow rate and pipe size the pressure gradient is directly proportional to the friction factor (Hallbom, 2008). For a Newtonian fluid flowing in a pipe it is expected that the pressure gradient will follow the laminar flow curve to a velocity where the fully turbulent pressure gradient is about 130% of the laminar flow pressure gradient. Increasing the flow rate further causes the pressure-gradient to "break" (deviate from the laminar flow curve) and increase rapidly towards the fully turbulent flow curve, which it will follow once the velocity exceeds ~ 150% of the "break-point" velocity. This criterion forms the basis of the yield plastic transition models. So:

$$f_{turb} = 1.3 f_{lam} \tag{2.104}$$

Hallbom elected to use the Knudsen-Katz friction factor to describe turbulent flow and so gives his critical friction factor as

$$f_C = \frac{0.046 / 1.3}{Re_p^{0.2}} = \frac{0.0354}{Re_p^{0.2}} \tag{2.105}$$

where Re_p is the plastic Reynolds number given by:

$$Re_p = \frac{\rho V D}{\mu_\infty} \tag{2.106}$$

Transition then occurs when the laminar flow curve for yield plastics [Eq. (2.60)] intercepts the transition curve [Eq. (2.105)]. This intercept can be found graphically or by numerical iteration.

Method 2: Explicit algebraic equation based on the Hedström number

Hallbom (2008) generalised the same dimensionless groups used to describe the transition of Bingham plastics, for yield plastics, by using the infinite shear rate viscosity (μ_∞) of the fully dispersed suspension. At the critical transitional velocity $Re_p = Re_{pC}$ and $f = f_C$ so by Eq. (2.60) and Eq. (2.105), and noting

$$He = 0.5 Z f Re_{pC}^2 \tag{2.107}$$

Hallbom (2008) derived

$$He = \frac{Re_{pC}^{1.8}}{56.5}\left(1 - \left(\frac{2084}{Re_{pC}}\right)^{0.8(1-k/3)}\right)^{\frac{1}{k}} \tag{2.108}$$

When He = 0 (i.e. a Newtonian fluid), Eq.(2.108) predicts the critical Re to be 2084 (≈ 2100). Hallbom's transition model has not been extensively tested to date, but was found to agree well with the predictions of Slatter & Wasp (2000) and Wilson & Thomas (2006) when evaluated against kaolin pipe flow data. Even though the three criteria predicted transition in the same range of 1.25 to 1.35 m/s Hallbom (2008) says that the transitional velocity calculated by his yield plastic model is still somewhat conservative, as it is intended to predict the velocity below which transition will occur.

Yield stress criterion: Slatter and Wasp

Slatter (1997a) investigated the effect of yield stress on the laminar/turbulent transition of yield pseudoplastics. He established that the relationship between the critical velocity and pipe diameter is an appropriate way of investigating the effect of yield stress on transition. He concluded that at small diameter pipes (<25mm), the yield stress becomes insignificant and the behaviour is controlled by the fluid consistency index (K) and the flow behaviour index (n), producing an oblique asymptote on a plot of V_c vs. D, which is independent of the yield stress (Figure 2.9).

From Govier & Aziz (1972) and Slatter (1997a), for larger pipe diameters the behaviour is controlled by yield stress (τ_y) and the flow behaviour index (n), producing a horizontal asymptote on a plot of V_c vs. D which is independent of both the fluid consistency index (K) and pipe diameter. Thus it became apparent that for Bingham plastic fluids in larger pipe diameters i.e. high Hedström numbers ($He > 10^5$) the transitional velocity is equal to a constant value, dependant only on the yield stress and density of the fluid (Slatter & Wasp, 2000).

$$V_{crit} = C_x\sqrt{\left(\frac{\tau_y}{\rho}\right)} \qquad He \geq 10^5 \tag{2.109}$$

where C_x is a dimensionless quantity referred to as the relative transitional velocity.

Later Slatter and Wasp (2000) proposed a correlation for the critical Reynolds number for Bingham plastics based on different ranges of Hedström number. The aim of this approach was to develop simple criteria for practical design use, based on a generalised comparison of the most accurate theoretical approaches and extensive databases. To achieve this, they used the simplest rheological model incorporating yield stress, i.e. the Bingham plastic model. This led to the formulation of a critical velocity criterion over three different ranges of Hedström number, as follows:

$$Re_{BC} = \frac{\rho V_c D}{K} \tag{2.110}$$

$$He = \frac{\rho D^2 \tau_{yB}}{K^2} \tag{2.111}$$

Low range (*He* < 1700):

$$Re_{BC} = 2100 \quad ; \quad V_c = \frac{2100\,K}{\rho D} \tag{2.112}$$

Intermediate range (1700 <*He*< 10^5):

$$Re_{BC} = 155\,He^{0.35} \quad ; \quad V_c = \frac{155\,\tau_y^{0.35} K^{0.35}}{\rho^{0.65} D^{0.3}} \tag{2.113}$$

High range (*He* ≥ 10^5):

$$Re_{BC} = 26\,He^{0.50} \quad ; \quad V_c = C_x \sqrt{\left(\frac{\tau_y}{\rho}\right)} = 26\sqrt{\left(\frac{\tau_y}{\rho}\right)} \tag{2.114}$$

Yield stress criterion: Wilson and Thomas

Wilson and Thomas (2006) extended their analysis of turbulent flow (Wilson & Thomas, 1985; Thomas & Wilson, 1987) to transitional flow of Bingham plastics. They showed that there is a thickening of the sub-layer for turbulent Bingham flow, and therefore a direct relationship between yield stress and the transitional velocity, and concurred with Slatter and Wasp (2000) that the conditions at transition depend only on the Hedström number (Güzel *et al*, 2009). Their equations for the critical velocity for the three different Hedström number ranges are:

Low range (*He* < 1700):

$$Re_{BC} = 2100 \Big/ \left\{10 + 8.3\left(10^{-8}\right) He^{1.3}\right\} \tag{2.115}$$

Intermediate range (1700 <*He*< 10^5):

$$Re_{BC} = 80\,He^{0.40} \tag{2.116}$$

High range (*He* ≥ 10^5):

$$Re_{BC} = 25\,He^{0.50} \tag{2.117}$$

In terms of the dimensionless measure C_x as described by Slatter and Wasp (2000), which Wilson and Thomas (2006) refer to as the relative transitional velocity, the critical velocity at high Hedström numbers can be described as;

$$V_c = C_x\sqrt{\left(\frac{\tau_y}{\rho}\right)} \quad = \quad 25\sqrt{\left(\frac{\tau_y}{\rho}\right)} \qquad He \geq 10^5 \tag{2.118}$$

Wilson and Thomas (2006) compared their model to that of Thomas (1963), which predicts a value of C_x = 30 at He = 10^4, dropping to a value of 19 at $He \geq 10^8$. This was later proven to be incorrect by Slatter (1997), who found the C_x value = 16.2 for $He > 10^5$, rather than 30 as reported by Thomas (1963). Since Eq. (2.118) is so close to Eq. (2.114), experimental values were only compared with Eq. (2.118).

2.5 Newtonian turbulent flow

Newtonian turbulent flow is characterised by the presence of random fluctuations in velocity and pressure. Even when the mean flow is only along the length of the pipe, there are likely fluctuations present in other directions, and the flow behaviour is extremely complex. Equations of motion must be time averaged to yield meaningful practical results. Analysis and results are for these temporal means (Slatter, 1994).

In turbulent flow, elements of the fluid follow irregular fluctuating paths caused by moving eddies. The average velocity increases from zero at the wall, (no slip) to a maximum at the centreline. Although the mean velocity within the fluid is parallel to the wall, the instantaneous velocity fluctuates in both magnitude and direction with time. The turbulent fluctuations cancel out over a relatively short period of time, so the time averaged axial velocity ($\bar{u}$) must be considered. A basic parameter in the turbulent group [$\overline{(\tau_w/\rho)}$] which has the dimension of velocity, is known as the shear velocity and denoted by U_* [Eq. (2.119)]. To simplify calculations, the time-averaged velocity ($\bar{u}$) and the distance from the pipe wall (y=R-r) may be put into dimensionless form using the shear velocity (U_*), which is a function of wall shear stress.

$$U_* = \sqrt{\frac{\tau_w}{\rho}} \qquad \textit{(Shear velocity)} \tag{2.119}$$

$$u^+ = \frac{\bar{u}}{U_*} = \bar{u}\sqrt{\frac{\rho}{\tau_w}} \quad \textit{(Dimensionless velocity)} \tag{2.120}$$

$$y^+ = \frac{y\rho\rho_*}{\mu} \qquad \textit{(Dimensionless distance from wall)} \tag{2.121}$$

The analysis that follows (Section 2.5.1) applies to an incompressible Newtonian fluid in fully developed, steady turbulent flow, with constant density (ρ) and viscosity (μ). The instantaneous axial velocity (u) at any point in the turbulent flow field is taken as the sum of the average velocity ($\bar{u}$) and the velocity due to the erratic turbulent fluctuations (u').

$$u = \bar{u} + u' \tag{2.122}$$

2.5.1 Newtonian turbulence velocity profile

In turbulent flow Eq. (2.3) no longer applies, because the turbulent fluctuations exchange slow and fast moving fluid across surfaces within the flow. This momentum transfer sets up Reynolds' stresses which dominate the purely viscous stresses, except near the pipe wall (Wilson, Addie, Sellgren & Clift, 2006). In fully developed turbulent flow, three flow zones are evident. The turbulent core occupies most of the

central area around the pipe axis and is characterised by turbulent eddies. In the vicinity immediately adjacent to the wall is the viscous sub-layer. Between the turbulent core and the viscous sub-layer is a transition area referred to as the boundary layer (Douglas, Gasiorek & Swaffield, 1995).

Turbulent core

Momentum transfer in the turbulent core is primarily due to inertial mixing, with viscous effects playing an insignificant role. There is a wide range of eddy sizes, from large scale rotations down to the energy dissipative scale. Velocity fluctuations associated with the turbulent eddies have the same order of magnitude as the shear velocity, and so in fully turbulent flow the velocity gradient (du/dr) is directly proportional to U_* and inversely proportional to the 'mixing length'. This length is related to the size of the turbulent eddies and was first described by Prandtl in 1921 (Wilson *et al.*, 2006). Using Prandtl's mixing length theory the velocity profile in the turbulent core can be modelled as

$$U_* = \kappa y \frac{d\bar{u}}{dy} \tag{2.123}$$

$$d\bar{u} = \frac{U_*}{\kappa}\frac{dy}{y} \tag{2.124}$$

For turbulent flow near a pipe wall the mixing length is evaluated as (κy) where y is the distance from the pipe wall and κ is von Karman's constant. For an incompressible liquid, the density is constant therefore at any given wall stress, the shear velocity is constant and Eq. (2.124) can be integrated to give

$$\bar{u} = \frac{U_*}{\kappa} ln(y) + C_0 \tag{2.125}$$

with

$$C_0 = C_1 - \frac{1}{\kappa} ln\left(\frac{\mu}{U_* \rho}\right) \tag{2.126}$$

and C_1 being another constant, then dividing through by U_*gives

$$\frac{\bar{u}}{U_*} = \frac{1}{\kappa} ln\left(\frac{yU_*\rho}{\mu}\right) + C_1 \tag{2.127}$$

The values for κ and C_1 must be determined from experiments and different researchers have used different values for these constants. Von Karman proposed κ= 0.4 to 0.41 and C_1= 5.5 to 5.7, whilst Nikuradse used κ = 0.407 and C_1 = 5.66 for Newtonian fluids. If $\bar{u}/U_* = u^+$ and $yU_*\rho/\mu = y^+$ then

$$u^+ = 2.457\, ln(y^+) + 5.66 = 2.457\, ln(10 y^+) \quad \text{for Nikuradse} \tag{2.128}$$

$$u^+ = 2.5\, ln(y^+) + 5.5 = 2.5\, ln(9.025\, y^+) \quad \text{for von Karman} \tag{2.129}$$

Eq. (2.127) is referred to as the *universal velocity distribution* (Douglas *et al.,* 1995). Thomas and Wilson (1987), Slatter (1994) and Wilson *et al.* (2006) use the constants of von Karman in their analysis, but Hallbom (2008) elects to use Nikuradse's constants in his turbulent model.

The viscous sub-layer

Maximum turbulent eddy sizes decreases as the pipe wall is approached, presumably due to the presence of the pipe wall which restricts the fluid's ability to rotate. At small distances from the pipe wall (y^+) the scale of the smallest and largest eddies coincide and within this interface the fluid is unable to rotate, so it is parallel to the wall and effectively laminar. As viscosity is dominant in this region, (du/dy) must be equal to (τ_0/μ) [Eq.(2.3)] which gives a linear variation of u with y, equivalent to the statement that $u^+ = y^+$ at small values of y^+ (≤ 5). The viscous sub-layer therefore extends from the smooth wall at $y^+ = 0$ to about $y^+ = 5$ as illustrated in Figure 2.11 (Wilson *et al.,* 2006).

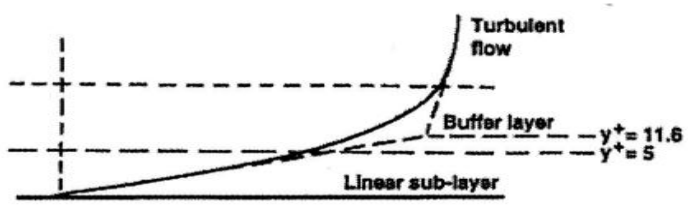

Figure 2.11 Newtonian velocity distribution near the wall (Wilson *et al.,* 2006)

In this region the wall shear stress is

$$\tau_w = \mu\left(\frac{du}{dy}\right)_w = \frac{\mu\bar{u}}{y} \tag{2.130}$$

Combining Eq. (2.129) with Eq.(2.120) and Eq.(2.121) gives

$$u^+ = \sqrt{u^+ y^+} \tag{2.131}$$

so the velocity profile for the viscous sub-layer is

$$u^+ = y^+ \tag{2.132}$$

The boundary/buffer layer

At the interface between a fluid and a surface in relative motion a condition known as 'no-slip' dictates equivalence between fluid and surface velocities. Away from the surface the fluid velocity rapidly increases and the zone in which this occurs is known as the boundary layer. Its definition is fundamental to all calculations of surface drag and viscous forces (Douglas, Gasiorek & Swaffield, 1995). The boundary layer is characterised by a shift from laminar to fully turbulent flow and exists in the range of 5 <y^+< 30 (Steffe, 1996), (Hallbom, 2008). Thus the location of the boundary layer is at the intersection of the viscous sub-layer and the turbulent core velocity curves as illustrated in Figure 2.. The intersection may be found by equating Eq. (2.128) and Eq. (2.132) for Nikuradse's constants, and Eq. (2.129) with Eq. (2.132) for von Karman's constants resulting in:

$$y^+ = 2.457 \ln(10 y^+) = 11.7 \quad \text{for Nikuradse} \tag{2.133}$$

$$y^+ = 2.5 \ln(9.025 y^+) = 11.6 \quad \text{for von Karman} \tag{2.134}$$

Expressed in the widely accepted format using van Karman's constants as

$$\delta = \frac{11.6\mu}{\rho.U_*} \tag{2.135}$$

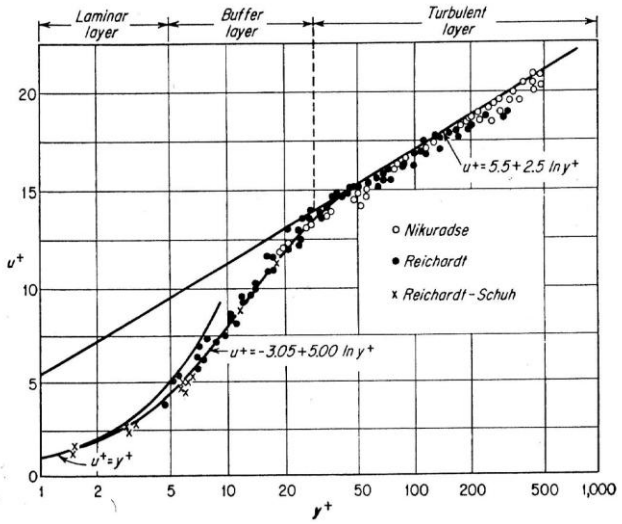

Figure 2.12 Velocity distribution for turbulent flow in pipes (Knudsen & Katz, 1958)

2.5.2 Newtonian turbulence pressure gradient

The flow velocity through the pipe in turbulent flow is calculated in much the same way as laminar flow, the difference being that the time averaged velocity ($\bar{u}$) is used instead of the instantaneous local velocity of the fluid. Referring back to Figure 2.4, the flow rate in the annulus between *r* and *r+dr* is

$$dQ = \bar{u}(2\pi r)dr \tag{2.136}$$

and the total flow rate through the pipe (*r=0* to *r=R*) is

$$Q = \int dQ = \int_0^R \bar{u}(2\pi r)dr = V\pi R^2 \tag{2.137}$$

so the mean velocity *V* (independent of the fluid's rheology) is then:

$$V = \frac{2}{R^2}\int_0^R \bar{u}\,r.dr \tag{2.138}$$

As most of the flow is in the turbulent core (due to it having a much higher average velocity and surface area compared to the viscous sub-layer) it may reasonably be assumed that the velocity profile of the turbulent core extends to the pipe wall. The viscous sub-layer occupies a negligible portion of the cross-sectional area and its presence can be ignored for the purpose of integration (Slatter, 1994). The velocity variation across the pipe is a function of radius so that Eq. (2.120), (2.133) and (2.138) (Nikuradse constants) results in

$$\frac{V}{U_*} = 2.457\ln\left[\left(\frac{D\rho U_*}{\mu}\right)(.12)\right] \tag{2.139}$$

which can be written equivalently as

$$\frac{1}{\sqrt{f}} = -4.0 \log\left(\frac{1.26}{Re\sqrt{f}}\right) = 4.0 \log\left(Re\sqrt{f}\right) - 0.4 \qquad (2.140)$$

Eq. (2.139) is the Nikuradse equation for Newtonian turbulent flow in smooth pipes. According to Govier & Aziz (1972) the Nikuradse equation correlates extremely well with all reliable Newtonian flow data in the range 3 000 <*Re* < 3 000 000. This equation is known as Prandtl's universal law of friction for smooth pipes (Slatter, 1994).

2.5.3 Surface roughness and drag

Following Slatter (1994), the thickness of the viscous sub-layer plays an important role in determining what type of turbulent flow conditions apply (smooth, rough, or partially rough wall turbulent flow). The surface of a pipe contains microscopic protrusions, (asperities) random in both height (ε) and position. If the viscous sub-layer covers the largest of the asperities, surface roughness does not influence the flow and smooth wall turbulence equations apply. If the sub-layer thickness is less than the smallest asperities which then protrude into the turbulent core, the flow is considered to be rough-wall turbulent flow and the asperities cause additional drag (Massey, 1970). Between these two extremes some of the asperities protrude into the turbulent core and some remain below the viscous sub-layer, resulting in so-called partially rough-wall turbulent flow.

2.5.4 Newtonian turbulent flow models

Colebrook-White

Equation (2.140) only applies to 'hydraulically smooth' pipes. For larger values of ε the relative roughness (ε/D) significantly influences pipe friction. In fully rough turbulent flow viscosity no longer plays a role and the friction equation depends only on ln(D/ε). The transition between smooth and rough wall turbulent flow was first investigated by Colebrook and later by Colebrook and White (Slatter, 1994) resulting in the Colebrook-White equation.

$$\frac{1}{\sqrt{f}} = -4 \log\left(\frac{\varepsilon}{D} + \frac{1.26}{Re\sqrt{f}}\right) \qquad (2.141)$$

Knudsen and Katz

Knudsen and Katz (1958), developed a simple relationship between the Reynolds number and friction factor, given by Eq.(2.141), which they compared with the models of Blasius, Drew *et al*, Nikuradse and von Karman [in Knudsen and Katz (1958)], showing good agreement with all up to Reynolds numbers of 10^7, except for the Blasius correlation which deviated from the other methods at *Re* > 100 000.

$$f = \frac{0.046}{Re^{0.2}} \quad (3000 \le \mathrm{Re} \le 3\mathrm{x}10^6) \qquad (2.142)$$

2.6 Non-Newtonian turbulent flow

Sewage sludge, china clay, coal and mineral suspensions are often transported in large diameter pipes in turbulent flow, so a significant amount of research has gone into developing generalised approaches for predicting turbulent flow pressure drop in pipes, mostly using the power law, Bingham plastic and

Herschel-Bulkley rheological models (Chhabra & Richardson, 2008). Just as many equations are available for the prediction of Newtonian turbulent flow friction factors, there are numerous equations for time-independent non-Newtonian fluids, most of which are based on experimental findings combined with dimensional analysis (Chhabra & Richardson, 2008). To date though, there are no guidelines in the literature indicating which method to adopt for a given set of conditions.

For turbulent flows in pipes, various semi-empirical models have been used to describe the local momentum transport and velocity distribution, hence overall friction loss. According to Slatter (1994) non-Newtonian turbulent models can be divided into three categories, these being (i) models with a strong analytical approach such as that of Torrance (1963) and Wilson and Thomas (1985), (ii) models which adapt a purely empirical approach such as Bowen (1961) and (iii) models lying between these two approaches such Dodge & Metzner (1959). These models as well as those of Slatter (1994) and Hallbom (2008) (both analytical) are reviewed next.

2.6.1 Non-Newtonian turbulent models

Newtonian approximation

For turbulent flow of Newtonian fluids in a hydraulically smooth walled pipe the mean velocity can be obtained by Eq. (2.139) if Nikuradse's constants are used. Equation (2.139) is given equivalently by Slatter (1994) if von Karman's constants are used

$$\frac{V_N}{U_*} = 2.5 \ln\left(\frac{\rho R U_*}{\mu'}\right) + 1.75 \tag{2.143}$$

For non-Newtonian fluids the use of a single viscosity is not appropriate, so an apparent viscosity (μ') is defined as:

$$\mu' = \frac{\tau_w}{\left(-\frac{du}{dr}\right)_w} \tag{2.144}$$

μ' must be evaluated at each value of τ_w as shown in Figure 2.13. The Newtonian approximation does not include the premise that the sub-layer thickens in non-Newtonian turbulent flow resulting in the drag reduction effect as proposed by Wilson & Thomas (1985).

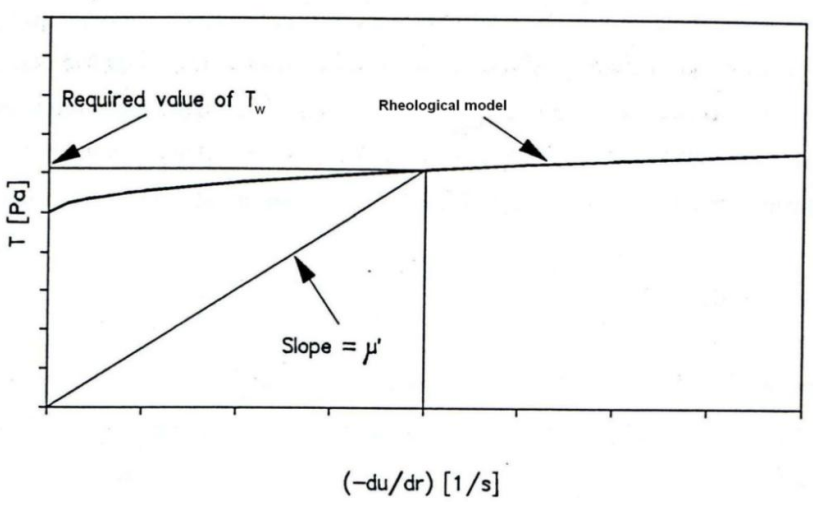

Figure 2.13 Illustration of apparent viscosity - μ' (Slatter, 1994)

Torrance turbulent model

Torrance (1963) developed a relationship between the friction factor and Reynolds number for yield pseudoplastic fluids. Using the mixing length theory of Prandtl, which considers that the laminar and turbulent components of shear stress as additive and neglecting the wall layers (viscous sub-layer and boundary layer), he derived the mean velocity for turbulent flow in smooth pipes is given as:

$$\frac{V}{U_*} = \frac{3.8}{n} + \frac{2.8}{n} ln\left(1 - \frac{\tau_0}{\tau_w}\right) + \frac{2.78}{n} ln\left(\frac{V_*^{2-n}\rho R^n}{K}\right) - 4.17 \qquad (2.145)$$

Although Torrance (1963) based his work on the yield-pseudoplastic model, his definition of Reynolds number [Eq. (2.88)] does not include yield stress. Slatter (1994) compared turbulent flow data of a yield pseudoplastic material with predictions using his own model, Torrance (1963) and Wilson & Thomas (1985). At low shear rates Torrance (1963) showed good agreement with the experimental as well as the results of Slatter (1994) and Wilson & Thomas (1985). Slatter, Mollagee and Petersen (1997) compared turbulent predictions of various turbulent techniques using different rheological models. The average errors for the Torrance (1963) method were 11% for Bingham plastic, 35% for pseudoplastic and for 15% for yield-pseudoplastic. El-Nahhas, El-Hak, Rayan & Elsawaf (2005) compared their new turbulent flow approximation to the models of Torrance (1963), Wilson & Thomas (1987) and Slatter (1994) for kaolin slurries modelled with the yield pseudoplastic model. The Torrance prediction was in close agreement with the prediction of Wilson & Thomas (1985), and both models were considered as being able to reliably predict the experimental data. The similarity between the results obtained by Torrance (1963) and Wilson & Thomas (1985) are because both models treat the slurry as a continuum.

Bowen scale-up method

Bowen (1961) observed that no universal correlation had been suggested for turbulent non-Newtonian fluids. Even though correlations existed, many only correlated specific test data. Bowen observed that on a logarithmic plot of τ_w vs. ($8V/D$) the turbulent branches for different pipe sizes are straight, almost parallel to each other. Based on a Blasius form friction factor, Bowen (1961) wrote

$$\tau_w = A\frac{V^b}{D^c} \qquad (2.146)$$

where *A, b* and *c* are fluid constants to be determined from experimental measurements in smaller tubes (Chhabra & Richardson, 2008), from which turbulent flow in larger pipes can then be predicted. The procedure for the scale-up method is given in (Chhabra & Richardson, 2008).

Bowen's scale-up method produces good correlation of non-Newtonian turbulent flow pipe data which could be regarded as evidence that the viscous characteristics of a slurry are unimportant in turbulent flow (Slatter, 1994). Bowen's method is useful when scale up is required for turbulent predictions (smaller to large pipe diameters) for the same material, and when the rheological properties of a material is not available, or cannot easily be determined.

Dodge & Metzner

Dodge & Metzner (1959) developed equations to describe the velocity profile of power law fluids in turbulent pipe flow. Small errors in their equations were corrected by Skelland (1967) and the final equations are:

For the viscous sub-layer and turbulent core

$$u^+ = y^{+\,1/n} \tag{2.147}$$

$$u^+ = \frac{5.66}{n^{0.75}} \log y^+ - \frac{0.566}{n^{1.2}} + \frac{3.475}{n^{0.75}}\left[1.960 + 0.815n - 1.628n \log\left(3 + \frac{1}{n}\right)\right] \tag{2.148}$$

where y^+ incorporates the flow behaviour index (n) and the consistency coefficient (K) needed for the consideration of power law fluids:

$$y^+ = y^n u_*^{2-n}\left(\frac{\rho}{K}\right) \tag{2.149}$$

Constants were obtained from friction factor measurements so the thickness of the viscous sub-layer was not obtained (Steffe, 1996). This lead to their correlation for turbulent flow based on the Metzner and Reed (1955) laminar flow model [Eq.(2.78)]. Their turbulent flow correlation is the equivalent of the von Karman smooth wall turbulent flow equation and reverts back to Newtonian form for $K' = \mu$ and $n' = 1$. In its final form the Dodge & Metzner (1959) model is given by:

$$\frac{1}{\sqrt{f}} = \frac{4}{n'^{0.75}} \log\left(Re_{MR} f^{(2-n')/2}\right) - \frac{0.4}{n'^{0.2}} \tag{2.150}$$

Eq. (2.150) can be used with fluids described by other rheological models if the values for K' and n' (see Section 2.4.5) are evaluated at the relevant value of the wall shear stress for the computation of Re_{MR}. This reasoning is based on the fact that in turbulent flow, the effects of the molecular viscosity are only significant in close proximity to the pipe wall (Pilehvari & Serth, 2005). The Dodge & Metzner model is based on experimental results in the range $2900 \leq Re_{MR} \leq 36\,000$ and $0.36 \leq n' 1$, so care must be taken to not exceed these limits during the application of this model, which could render the results invalid. Brown & Heywood (1991) acknowledge this fact, but report that in the pipeline engineering industry, n' values are obtained from laminar data at wall shear stress values well below the relevant wall stress values for turbulent flow. The reasons for this are either because the turbulent prediction is required for the same pipe or the shear thinning properties of the material preclude obtaining sufficiently high wall stress values even in smaller pipes. Brown & Heywood (1991) cite Heywood & Richardson (1978) and Kemblowski & Kolodziejski (1973) on the effects of evaluating n' from wall stress values lower than those required for the turbulent flow prediction. These results show that the Dodge & Metzner correlation can significantly underpredict turbulent friction factor values. Brown & Heywood (1991) conclude that as long as the correlation is used within the limitations stipulated by the authors it can be used with confidence.

Slatter *et al* (1997) applied the Dodge & Metzner correlation to slurries characterised as Bingham plastic, pseudoplastic and yield-pseudoplastic materials. Their results showed that the correlation performed best using the yield-pseudoplastic rheology (average error = 18%). For the pseudoplastic rheology it was similar to the models of Torrance (1963) and Wilson and Thomas (1985) (average error = 35%) and using the Bingham plastic model gave an average error of 20%.

Wilson and Thomas turbulent model

Wilson & Thomas (1985) and Thomas & Wilson (1987) developed a turbulent model for the prediction of non-Newtonian flow based on the drag reduction phenomenon. This model predicts that the occurrence of smaller turbulent eddies at the wall increases as the size of the viscous sub-layer increases, by a ratio (α) called the area ratio (see Figure 2.14).

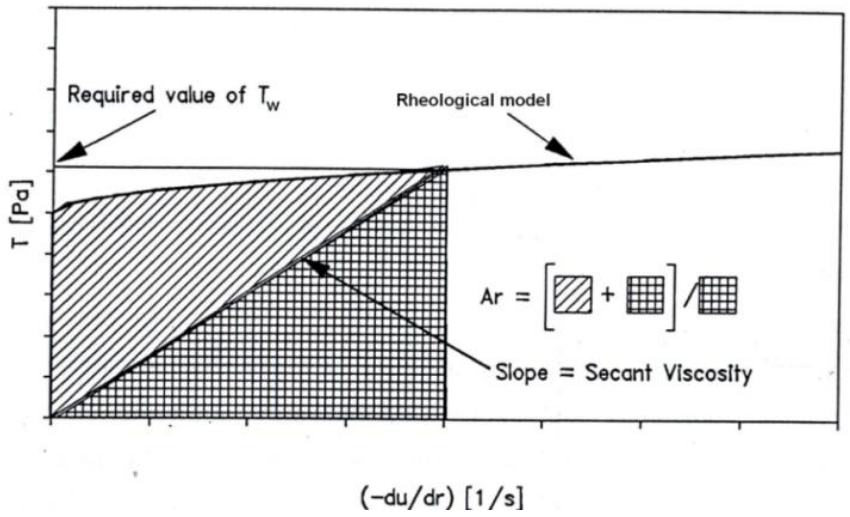

Figure 2.14 Illustration of the area ratio (Slatter, 1994)

This in turn increases the through-put velocity, decreases the friction factor and causes blunting of the velocity profile (Wilson & Thomas, 2006), collectively known as the drag reduction effect. The area ratio (α) is the ratio of the non-Newtonian and assumed Newtonian rheogram areas at a given wall shear stress (Slatter, 1994) as illustrated in Figure 2.14. α must be evaluated for each different rheological model applied, as given in Eq. (2.151) to Eq. (2.154) for the rheological models considered here.

$$\alpha_{HB} = 2\left[\frac{1+\frac{\tau_y}{\tau_w}n}{1+n}\right] \quad \text{[for yield pseudoplastic fluids]} \tag{2.151}$$

$$\alpha_{PL} = 2\left[\frac{1}{1+n}\right] \quad \text{[for pseudoplastic fluids]} \tag{2.152}$$

$$\alpha_{BP} = \left[1+\frac{\tau_y}{\tau_w}\right] \quad \text{[for Bingham plastic fluids]} \tag{2.153}$$

$$\alpha_{Casson} = 1+\left[\frac{2}{3}\right]\sqrt{\frac{\tau_C}{\tau_w}}+\left[\frac{1}{3}\right]*\left(\frac{\tau_C}{\tau_w}\right) \quad \text{[for Casson fluids]} \quad \text{(Wilson \& Addie, 2002)} \tag{2.154}$$

The non-Newtonian viscous sub-layer thickness is then

$$\delta_{NN} = \alpha\,\delta_N \tag{2.155}$$

where (δ_N) is the Newtonian viscous sub-layer thickness. The non-Newtonian velocity distribution is

$$u^+ = \frac{u}{U_*} = 2.5\,ln\left(\frac{\rho U_* y}{\mu'}\right) + 5.5 + 11.6\left(\alpha - 1\right) - 2.5\,ln\left(\alpha\right) \tag{2.156}$$

and the mean velocity (V) resulting from the thickened viscous sub-layer is given by

$$\frac{V}{U_*} = \frac{V_N}{U_*} + 11.6\left(\alpha - 1\right) - 2.5\,ln\,\alpha - \Omega \tag{2.157}$$

V_N is the mean velocity for the equivalent smooth-wall flow of a Newtonian fluid with viscosity (μ'). Thomas & Wilson (2006) describe the ratio of the mean Newtonian velocity (V_N) to the shear velocity (U_*) as

$$\frac{V_N}{U_*} = 2.5\,ln\left(\frac{\rho D U_*}{\mu'}\right) \tag{2.158}$$

The Wilson & Thomas (1985) mean velocity equation for non-Newtonian turbulent flow is finally

$$V = 2.5U_*\,ln\left(D\rho U_* \big/ \mu'\right) + U_*\left[1.6\left(\alpha - 1\right) - 2.5\,ln\left(\alpha\right) - \Omega\right] \tag{2.159}$$

In Eq. (2.159) Ω takes account of blunting of the velocity profile near the pipe centre line. It depends only on (τ_y/τ_w) and is expressed as:

$$\Omega = 2.5\,ln\left(1 - \frac{\tau_y}{\tau_w}\right) - 2.5\frac{\tau_y}{\tau_w}\left(1 + 0.5\frac{\tau_y}{\tau_w}\right) \tag{2.160}$$

The prediction of partially rough wall turbulent flow can be accommodated by the model by using pipe roughness when determining the Newtonian velocity component. According to Slatter (1994) this is only approximate, as the interaction between the pipe roughness and the viscous sub-layer will clearly be different when the thickened viscous sub-layer is present. The partially rough wall variation of the model is used in this study.

Wilson and Thomas (2006) note that in the part of the flow nearest to the pipe axis, some change in the velocity profile result from a non-zero τ_y, but the effect on the velocity is very small, and add that whether or not such blunting actually exists remains a moot point. Work done by Slatter (1994) using kaolin slurries and the yield-pseudoplastic rheology shows that predictions using the Wilson & Thomas (1985) method are almost identical to those of Torrance, and that both models accurately predict turbulent flow at low velocities. Deviation occurs from experimental data as flow velocities increase. Test done by Chara *et al* (1996) on kaolin and fly ash slurries also show the predictions of the Wilson & Thomas (1985) method as well as those of Slatter (1994) closely match experimental data when the yield-pseudoplastic rheology is used in the correlation, as opposed to their proposed constant value for n = 0.77. Slatter *et al.* (1997) compared several turbulent models with slurries modelled using pseudoplastic, Bingham plastic and yield-pseudoplastic rheologies, of which Wilson & Thomas (1985) was one of them. The analysis shows that the Wilson & Thomas (1985) method performed worst when the yield pseudoplastic rheology was applied to all models, with an average error of 27%, and best with an average error of 11% when the Bingham plastic rheology was applied. Using the pseudoplastic rheology it failed, together with the Torrance (1963) and Dodge & Metzner (1957) methods having an error of 35%.

Chilton and Stainsby (1998) evaluated models for turbulent flow with the conclusion that the models which assume a negligible thickness of the viscous sub-layer and in which the turbulent eddy viscosity dominates the molecular viscosity over the majority of the pipe cross-sectional area cannot be valid for non-Newtonian flow. This is especially true for fluids with a yield stress or with very low *n* values. They recommend the Wilson and Thomas (1985) and the Thomas & Wilson (1987) models as the best available analytical model for Herschel-Bulkley fluids in highly turbulent flows (Peker & Helvaci, 2008).

Contrary to Chilton and Stainsby (1998), Xu *et al.* (1993) have shown some cases where the Wilson and Thomas model has failed to accurately predict the turbulent behaviour of slurries. Based on these findings, Bartosik, Hill, and Shook (1997) suggests that when the Wilson and Thomas model fails, this may be as a result of the continuous flow medium which this method employs. The assumption that the fluid is a continuum has been challenged by Slatter, Thorvaldsen & Petersen (1996).

Slatter turbulent model

Slatter (1994) developed an alternative theory for turbulent flow of non-Newtonian slurries based on the particle roughness turbulence effect combined with the Newtonian approach. Slatter (1994) assumed that the roughness effect is caused by the solid particles in the slurry, and scaled the distance with the particle dimension (d_x) responsible for the turbulence. This approach differs from all other approaches to non-Newtonian turbulent flow modelling in its accommodation of the continuum breakdown near the pipe wall due to the physical size of the solid particles present in the material. He also made the assumption that plug flow does not occur in the turbulent core after analysing the experimental results obtained by Park, Mannheimer, Grimley & Morrow (1989) and Xu *et al.* (1993).

A roughness Reynolds number was formulated to incorporate particle roughness effect and to indicate whether smooth wall or fully developed rough wall turbulent flow exists. For the kaolin slurries investigated, $d_x = d_{85}$ was found to be a good representation of the turbulent roughness size effect of the solid particles. If the pipe roughness is larger than the d_{85} value, then the pipe roughness value prevails (Slatter, 1994).

The velocity distribution is logarithmic and similar to the classical Newtonian turbulent velocity distribution over the entire core region. Slatter (1994) applied von Karman's constant (A = 0.4), and used d_{85} as the representative particle size, resulting in the mean velocity over the cross section of the pipe equal to:

$$\frac{V}{U_*} = \frac{1}{0.4} ln\left(\frac{R}{d_{85}}\right) + B - 3.75 \qquad (2.161)$$

Experimental data were used to correlate the roughness function B against the roughness Reynolds number. In case of smooth wall turbulent flow ($Re_r \leq 3.32$) the average velocity is given as:

$$V = U_*\left[2.5\ln\left(\frac{R}{d_{85}}\right) + 2.5\ln \mathrm{Re}_r + 1.75\right] \quad \text{for } \mathrm{Re}_r \leq 3.32 \qquad (2.162)$$

In rough wall turbulent flow ($Re_r > 3.32$) the average velocity is given as:

$$V = U_* \left[2.5 \ln\left(\frac{R}{d_{85}} \right) + 4.75 \right] \quad \text{for } \mathrm{Re}_r > 3.32 \tag{2.163}$$

where Re_r is:

$$\mathrm{Re}_r = \frac{8\rho U_*^{\,2}}{\left[\tau_y + K\left(\frac{8U_*}{d_{85}} \right)^n \right]} \quad \text{for Herschel-Bulkley Fluids} \tag{2.164}$$

$$\mathrm{Re}_r = \frac{8\rho U_*^{\,2}}{\left[\tau_y + K\left(\frac{8U_*}{d_{85}} \right) \right]} \quad \text{for Bingham plastic fluids} \tag{2.165}$$

$$\mathrm{Re}_r = \frac{8\rho U_*^{\,2}}{\left[K\left(\frac{8U_*}{d_{85}} \right)^n \right]} \quad \text{for power law fluids} \tag{2.166}$$

$$\mathrm{Re}_r = \frac{8\rho U_*^{\,2}}{\left[\tau_C^{1/2} + \eta_C^{1/2} \left(\frac{8U_*}{d_{85}} \right)^{1/2} \right]^2} \quad \text{for Casson fluids} \tag{2.167}$$

$$\mathrm{Re}_r = \frac{8\rho U_*^{\,2}}{\left[\tau_0^k + \mu_\infty^k \left(\frac{8U_*}{d_{85}} \right)^k \right]^{\frac{1}{k}}} \quad \text{for Hallbom (2008) yieldplastic fluids} \tag{2.168}$$

Vlasak & Chara (1999) conclude that the Slatter (1994) model can accurately predict the flow behaviour of kaolin slurries in turbulent flow, and yields results similar to those of Wilson & Thomas (1985). They point out that both models are very sensitive to changes in the *n* value. El-Nahhas *et al* (2005) have shown that the Slatter (1994) model predicts turbulent flow of kaolin slurries better than the models of Torrance (1963) and Wilson & Thomas (1985) which produce similar results. The authors conclude that the reason for this is that the Slatter model departs from the continuum theory, which the other two models employ, and incorporates the effect of particle roughness turbulence on the boundary layer. Results presented in Slatter *et al* (1997) indicate that the Slatter (1994) model predicted turbulent data for kaolin slurries characterised with the pseudoplastic, Bingham plastic and yield-pseudoplastic rheologies better than the predictions of the Torrance (1963), Dodge & Metzner (1959), Wilson & Thomas (1985) and Chilton & Stainsby (1998) models. An average error of 6% was obtained for the Slatter predictions using each of the rheologies.

Hallbom turbulent model

Hallbom (2008) published two turbulent flow models. The first model is based on the drag reduction model of Wilson and Thomas (1985), Thomas and Wilson (1987) and Wilson *et al* (2006), using the

Wilson and Thomas (1985) smooth wall (SW) turbulent model, modified to incorporate the yield plastic rheological parameters. The second model is termed the pseudo fluid approximation for partially rough wall (PRW) turbulence and fully rough wall (FRW) turbulence. In this model Hallbom (2008) combines the standard Newtonian equations of Nikuradse for SW and FRW turbulent flow, in the same way as Colebrook (Douglas *et al*, 1995) formulated his PRW turbulent model for turbulent Newtonian fluids, but uses his infinite shear viscosity (μ_∞) in formulating his Re_P instead of the apparent viscosity (μ').

Modified Wilson and Thomas drag reduction model (SW turbulent flow)

Hallbom's first turbulent flow model is a modification of the Wilson and Thomas (1985) drag reduction model. The first modification is in the choice of Newtonian turbulent flow constants. Wilson and Thomas (1985) used the von Karman constant, but Hallbom (2008) used the constants of Nikuradse and incorporated his yield plastic rheological model by claiming that any rheological model with a limiting high shear rate or infinite shear rate viscosity (μ_∞) can be accounted for by replacing the apparent viscosity (μ') with the infinite shear rate viscosity (μ_∞). He also used his Plastic Reynolds number [Eq.(2.106)] and the Fanning friction factor to give

$$\sqrt{\frac{2}{f_N}} = 2.457 ln\left[1.12 Re_p \left(\sqrt{\frac{f_N}{2}}\right)\right] + 2.457 ln(\beta) \tag{2.169}$$

where β is the drag reduction factor given by:

$$\beta = \left(\frac{\mu_\infty}{\eta}\right)\frac{e^{4.76(\alpha-1)}}{\alpha} \tag{2.170}$$

Eq. (2.169) can be equally written as:

$$\frac{1}{\sqrt{f_N}} = -4.0 log\left(\frac{1.26}{Re_p \sqrt{f_N}}\right) + 4.0 log(\beta) \tag{2.171}$$

The first term in the equation is identical to the Nikuradse equation for smooth wall Newtonian turbulent flow (Douglas *et al*, 1995), except that Re_P is used. The second term accounts for the rheology related to drag reduction.

According to the yield plastic model the infinite shear rate viscosity is constant for a given fluid, thus the non-Newtonian consistency only affects β. When β > 1 there is a reduction in the pressure gradient and when β < 1, there is an increase in the pressure gradient (drag augmentation). When β = 1, the second term in Eq. (2.169) becomes zero and there is no drag effect (Hallbom, 2008). Newtonian turbulence then ensues.

In order to determine the drag reduction factor (β) it is necessary to determine the viscosity ratio (μ_∞/η) and the area ratio (α), both of which depend on the consistency of the fluid. For the yield plastic model the viscosity ratio may be found directly using the apparent viscosity vs. shear stress plot from the basic form of the model. The viscosity ratio is defined in Eq. (2.172) where *Z* is the stress ratio defined earlier in Eq. (2.61).

$$\left(\frac{\mu_\infty}{\eta}\right) = \left(1 - Z^k\right)^{\frac{1}{k}} \tag{2.172}$$

The area ratio (α) is defined as for the Wilson & Thomas (1985) model (see Figure 2.14), given for the yield plastic materials as:

$$\alpha_{YP} = 1 + Z^k - \frac{1-k}{1+k} Z^k \left(1 - Z^k\right) \tag{2.173}$$

For Bingham and Casson fluids, Eq. (2.173) results to:

$$\alpha_{BP} = 1 + Z \qquad \text{[Bingham plastic fluid]} \tag{2.174}$$

$$\alpha_{Casson} = 1 + \frac{2}{3} Z^{1/2} + \frac{1}{3} Z \qquad \text{[Casson fluid]} \tag{2.175}$$

As both the area ratio and viscosity ratio are functions of only the stress ratio (Z) and the scaling factor (k), the drag reduction factor (β) can also be determined directly as a function of these two quantities. This is an approximation, with acceptable engineering accuracy (Hallbom, 2008). In terms of Z and α, β is approximated by:

$$\beta \approx e^{4.76^k} \left(1 - Z^k\right)^{\left(\frac{2}{k} - 0.5 Z^k\right)} \tag{2.176}$$

Pseudo-fluid approximation (PRW turbulent flow)

According to Hallbom (2008), engineers often ignore the drag reduction (i.e. assume β = 1). This "pseudo-fluid" approximation has long been in use for Bingham plastics for example (Hedström, 1952). Hallbom (2008) also notes that according to Govier & Aziz (1972), on the basis of the data from several research groups, it seems well established that at (Re_p) values above the critical Reynolds number, and well after some transition range, the friction factor for Bingham plastics is only dependant on (Re_p) and the pipe roughness. For the smooth pipes the f_N - Re_p relationship is very similar to that for Newtonian fluids. This is true for all yield plastics if μ_∞ is equal to the dispersed viscosity. Hallbom (2008) therefore proposes that the infinite shear rate viscosity may be used with any standard Newtonian turbulent flow equation, such as the Nikuradse equation.

$$\frac{1}{\sqrt{f_N}} = -4.0 \log\left(\frac{1.26}{Re_p \sqrt{f_N}}\right) \tag{2.177}$$

Both the modified Wilson and Thomas model and the pseudo-fluid approximation were in good agreement with the experimental data for the fluids he tested. For partially rough wall (PRW) turbulence, Hallbom elected to use the Colebrook-White approach (based on good published theoretical and experimental agreement) and suggests Eq. (2.178) for yield plastics.

$$\frac{1}{\sqrt{f_N}} = -4.0 \log\left(\frac{1.26}{Re_p \sqrt{f_N}} + \frac{\varepsilon}{3.7D}\right) \tag{2.178}$$

2.6.2 Conclusion

The literature review has shown that significant study of non-Newtonian fluid flow has been undertaken by many researchers. Some of the resulting theories, which provide the foundation for this investigation, have been presented.

Laminar flow and rheology

Several rheological models are available to describe the properties of non-Newtonian fluids. The constitutive equations for five of these models which were used in this study have been presented along with the derived bulk flow rate equations for each, used for rheological characterisation. The same characterisation method as used by Slatter (1994) was used here. The opinions of the literature on rheological characterisation, the significance of shear rate and shear stress range, and the choice of rheological model have been reviewed. Tube viscometry was used in this study. The commonly encountered errors and fundamental equations pertinent to this form of viscometry are presented.

Transitional flow

Non-Newtonian transitional flow is an on-going research problem since for many slurries transition does not occur "abruptly" as for Newtonian fluids, but over a shear rate range, which makes prediction more difficult. Hallbom (2008) suggests two transition points which need to be identified, an instability point transition and break point transition. Transitional flow, or the onset of transition can be modelled using various Reynolds numbers and/or other criterion that have been presented in the literature. The generally accepted premise is that transition occurs at Re = 2100 and in the case of the Ryan & Johnson (1959) criterion, Z_{max} = 808. Some of the available criteria and Reynolds numbers have been selected and presented, their fundamental differences discussed and their performance against experimental data reviewed.

Turbulent flow

The analysis of non-Newtonian turbulent flow starts with an understanding of Newtonian turbulent flow. The smooth-wall Newtonian theories of Nikuradse and von Karman are presented with reference to the viscous sub-layer, boundary layer, and turbulent core. Partially rough wall Newtonian turbulent flow can be modelled using the Colebrook-White equation which is a combination of smooth wall and rough wall turbulent flow.

Many turbulent flow correlations have been developed in the literature, each with its own fundamental approach. With several rheological models available to describe material properties, it can be difficult to know which rheological model to combine with which turbulent flow correlation to ensure accurate predictions for a specific material. Several turbulent flow correlations have been presented including the purely empirical approach of Bowen (1961), the model of Slatter (1994) which challenges the continuum approximation, and also the more recently developed model of Hallbom (2008). Their performance against experimental data was reviewed and key aspects of each approach were identified. "The question arises: in view of the wide variation in predictions of f, which of these predictive methods should be adopted for general use? Until a comprehensive comparison is undertaken using a large number of experimental data covering a variety of fluid types, this question will remain unanswered." (Heywood & Cheng, 1984; Brown & Heywood, 1991). This work is an attempt to partially address this issue.

Chapter 3 Research method

This chapter presents details of the apparatus, experimental procedures and materials used to gather data for the evaluation of the rheological models with respect to pipeflow. Included too are descriptions of the operating procedures for the instruments and equipment used, and the rheological characterisation procedure applied to the measured experimental data.

3.1 Research design

The research design technique used for this study was quantitative experimental research. Laboratory tests were conducted to measure actual pipeflow data (ΔP-Q), and theoretical predictions (all flow regimes) were compared with these data. This was done for three typical non-Newtonian materials each at three different concentrations, using selected well known prediction models from the literature.

3.2 Data acquisition and analysis

Primary data was collected using straight pipe tests from a minimum nominal wall shear rate of $40s^{-1}$ up to the maximum value obtained in each pipe. $40s^{-1}$ corresponds to a minimum velocity of 0.065m/s (Q = 0.00863 l/s) in the diameter 13mm pipe and 1.055m/s (Q = 36.89 l/s) in the diameter 200mm pipe. Each of the selected rheological models was fitted to the laminar experimental data of each material, and then used (as applicable) in the prediction of transitional and turbulent pressure drops for each material and all test pipes.

3.2.1 Materials tested

The test fluids represented three common non-Newtonian material types, these being pseudoplastic (CMC), Bingham plastic (bentonite) and yield pseudoplastic (kaolin). Water was used to "calibrate" the different test loops.

Carboxyl methyl cellulose (CMC)

Granular CMC was dissolved in municipal tap water to form a CMC in water solution. Solutions of CMC are stable between pH of 2 and 10. Below pH 2, precipitation of the solids occurs, and above pH 10 the 'viscosity' decreases rapidly (Kabwe, 2009). The pH of the solutions tested for this study was 9.0 at 20 °C. CMC was tested at concentrations of 3%, 5% and 8% by volume.

Kaolin

The kaolin used in this test work was supplied by Serina Kaolin (Pty) Ltd., and mixed with tap water to form the suspension. Concentrations of 6%, 10% and 15% by volume were tested.

Bentonite

Ocean Bentonite H.V. (drilling grade) is a high yield, rapid gelling product suitable for applications in civil engineering and exploration drilling. Bentonite suspensions exhibit time-dependant behaviour, so for the purpose of this study pre-shearing was required prior to pipe test measurements. Volumetric concentrations of 6%, 7% and 9% were tested.

3.2.2 Primary data acquired

Pipe test data was collected for each material at each concentration as flow rate (Q) vs. differential pressure (ΔP) and plotted as pressure gradient ($\Delta P/L$) vs. velocity (V), as shown for example in Figure

3.1. Data from individual pipe sizes are observed as separate plots. Pressure gradient increases as pipe diameter decreases.

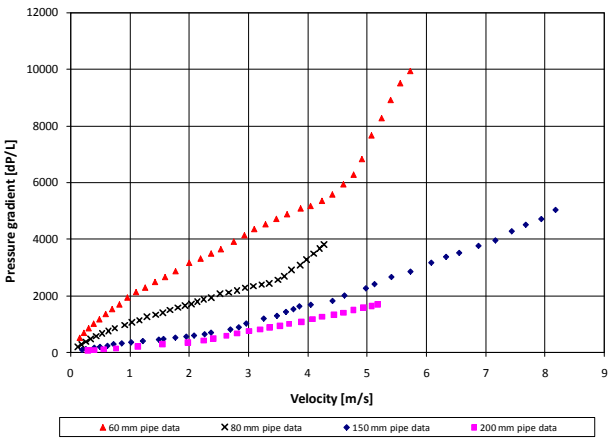

Figure 3.1 Plot of pressure gradient ($\Delta P/L$) vs. velocity (V) for 5% CMC in four different pipe diameters

The ΔP and V data were then converted to wall shear stress (τ_w) [Eq. (2.21)] and pseudo shear rate ($8V/D$) and plotted on a pseudo-shear diagram as τ_w vs. $8V/D$. The temperature of the test fluid in each test was regulated via the heat exchanger (<10°C) to preclude any possible effects on rheology.

3.2.3 Presentation of data on pseudo-shear diagram

For steady, fully developed incompressible flow, in the absence of wall slip and end effects, the laminar flow data from all pipes (i.e. different pipe diameters) is coincident when plotted on the pseudo-shear diagram.

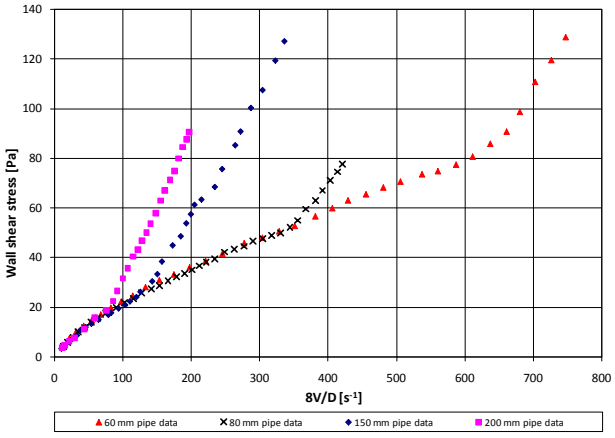

Figure 3.2 Pseudo-shear diagram for 5% CMC for four different pipe diameters

Turbulent flow manifests as a “sudden” increase in the slope of the plot and occurs at increasing values of ($8V/D$) as the pipe diameter decreases. A typical pseudo-shear diagram (5% CMC) is presented in Figure 3.2.

3.2.4 Rheological characterisation

Rheological characterisation requires fitting the experimental laminar flow data from all the test pipes to rheological models to determine the model constants. The approach of Lazarus and Slatter (1988) and Slatter (1994) was used here for rheological characterisation. For each different material (type,

concentration) laminar data were extracted, from *8V/D* of ± 40s^{-1} up to the highest available laminar flow data point. This *N* number of data points were plotted on a pseudo-shear diagram of τ_w vs. *8V/D* and checked for colinearity. The appropriate nominal wall shear rate (*8V/D*) equation for the selected rheological model (see Section 2.3.2) was used to calculate (*8V/D*) at each experimental (τ_w) value for each of the *N* data points. The values for the rheological constants were obtained using Excel's solver, minimising the sum of the root mean square error (RMSE), given by Eq. (3.1), where *N* is the number of data points and *p* the number of model parameters (Kelessidis & Maglione, 2006). The smaller the RMSE value, the better the fit of the rheological model to the data.

$$RMSE_{(N-p)} = \sqrt{\frac{\sum_{i=1}^{N}\left[\left(\frac{8V}{D}\right)_{iobs} - \left(\frac{8V}{D}\right)_{icalc}\right]^2}{N\text{-}p}} \tag{3.1}$$

3.2.5 Laminar flow predictions

The fitted rheological constants for each model were used to predict (for each pipe size) the laminar flow velocity and $(8V/D)_{calc}$ corresponding to a given wall shear stress (τ_w). These values were plotted on the pseudo-shear diagram [τ_w vs. $(8V/D)_{calc}$] and compared with the experimental data. Each prediction was evaluated on the basis of Eq. (3.2):

$$Ave\%E = \sqrt{\left[\frac{\left(\frac{8V}{D}\right)_{icalc} - \left(\frac{8V}{D}\right)_{iexp}}{\left(\frac{8V}{D}\right)_{iexp}}\right]^2} * 100 \tag{3.2}$$

3.2.6 Transition point predictions

For transitional flow a critical velocity (single point) was calculated for each pipe diameter, using each applicable transition technique for each derived rheological model. These values were compared to the experimental transition points which were taken as the last $(8V/D)_{exp}$ point in the laminar flow data before a deviation towards turbulence was observed (similar to what Hallbom (2008) describes at the break-point transition). The predicted transition $(8V/D)_{calc}$ value was evaluated by comparison with experimental values using Eq.(3.2). Transitional velocity predictions, together with the experimental data points, are presented on graphs of critical velocity (V_c) vs. pipe diameter (*D*).

3.2.7 Turbulent flow predictions

For turbulent flow, an $(8V/D)_{calc}$ value for a given experimental wall shear stress value was predicted using each turbulent technique for each turbulent data point, in each pipe size, for each of the derived rheological models (as applicable). These calculated $(8V/D)_{calc}$ values were plotted on pseudo-shear diagrams for comparison with the experimental turbulent data. As for laminar and transitional flow, each prediction was evaluated by calculating the average percentage error of the model using Eq.(3.2).

Typical laminar, transitional and turbulent pipeflow predictions for a yield stress slurry are shown in Figure 3.3. As stated in Section 2.1.7 the material rheology should not be extrapolated to the much higher shear rates for turbulent flow predictions. However (Brown & Heywood, 1991), this is not without difficulty because sometimes the pressure gradient is flat and the higher shear rates are not attainable in laminar flow in the test equipment. In this work turbulent predictions were done and

results plotted for shear stresses corresponding to the experimental values (i.e. the rheology *was* extrapolated), but when comparing and evaluating the different turbulent flow predictions, errors (deviation of predicted from experimental values) were compared only for points up to an arbitrary upper shear stress limit. This arbitrary limit was set to one of

- 1.25 times the highest experimental laminar shear stress value
- the third measured turbulent value if 125% of the highest experimental laminar shear stress value was still too low

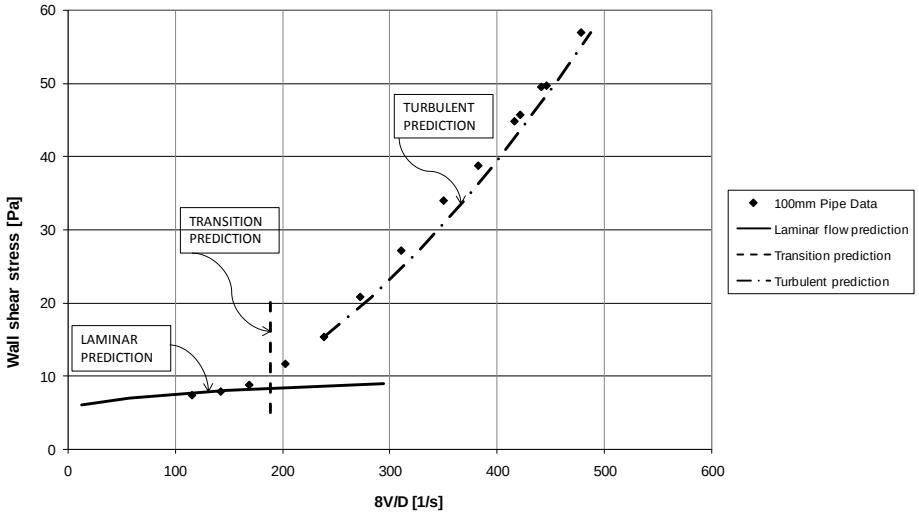

Figure 3.3 Typical pipeflow predictions for a yield stress slurry in a 100mm pipe showing all flow regimes

3.3 Test Apparatus

The apparatus used in conducting the experimental work for this research were the valve test loop, the large pipes test loop and the flume pipe loop. This section describes these apparatus in detail, as well as the instrumentation and data acquisition units used to capture the test data.

3.3.1 Pipe test loops

The valve test loop

This pipe loop consists of six PVC pipes with diameters ranging from 50mm to 110mm OD. Each pipe length is 25m long to ensure fully developed flow before each test section. Fluid is drawn from a 1.7m^3 mixing tank, and pumped by a progressive cavity pump, driven by a 5.5kW motor at up to 11l/s (39.6 m^3/h). A double pipe heat exchanger maintains the slurry at a constant temperature. Flow rate is measured by one of two magnetic flow meters (depending on which pipes are in use) namely the SAFMAG: 110mm ID, Model No. 100A2NESSR0032 or the KROHNE: 50mm ID, Model No. IFC 010D. Thermocouples measure the temperature of the slurry at the heat exchanger exit (just prior to entering the test section), and at the return to the mixing tank (end of the test section). A 500 litre weigh tank and load cell can be used to calibrate the flow meters. The loop is shown schematically in Figure 3.4.

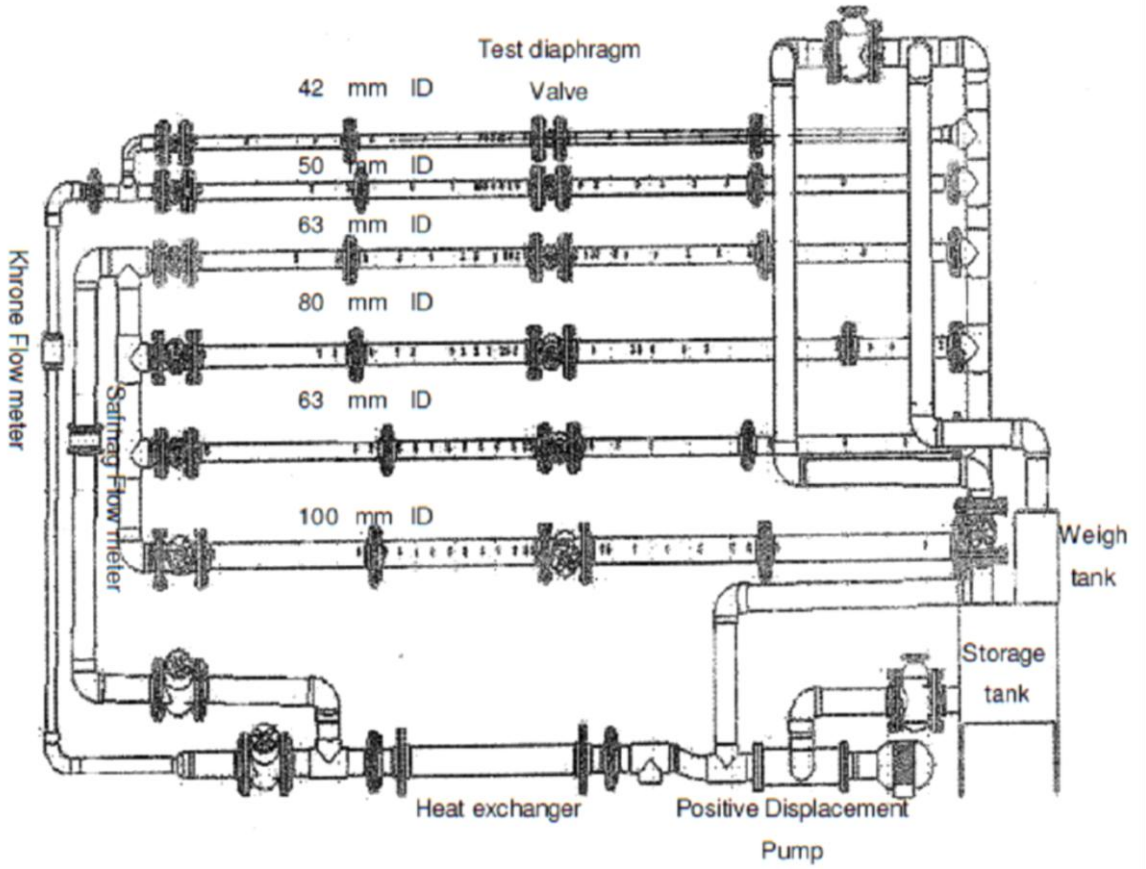

Figure 3.4 Schematic of the valve test loop (Kabwe, 2009)

The large pipes test loop

The large pipes test loop as shown schematically in Figure 3.5 has four different test pipe diameters namely 65, 80, 150 and 200mm. Slurry is pumped through the 65 and 80mm test pipes by a 4x3 Warman centrifugal pump with a maximum capacity of 80l/s (288m³/h) driven by a 55kW motor and inverter. The larger 150 and 200mm test pipes are supplied by 8x6 GIW centrifugal pump with a maximum capacity of 140l/s (504m³/h) driven by a 96KW motor and inverter. The system is fed from an open 4.5m³ conical-bottom tank, fitted with a mixer, into which the fluid is discharged after circulating through the loop. The flow parameters measured on the large pipes loop are flow rate, pressure drop and temperature. Flow rate is measured using 80mm and 150mm magnetic flow meters located in vertical return pipes. In each test pipe the pressure drop is measured using differential pressure transducers via solids traps. The test sections are preceded by unobstructed straight pipe of at least 50 pipe diameters to ensure fully developed flow. The temperature of the slurry is monitored using temperature probes, fitted along each test pipe. Temperature is regulated using a double pipe heat exchanger in which the cooling water flow rate can be controlled to prevent any excessive increases in slurry temperature during testing.

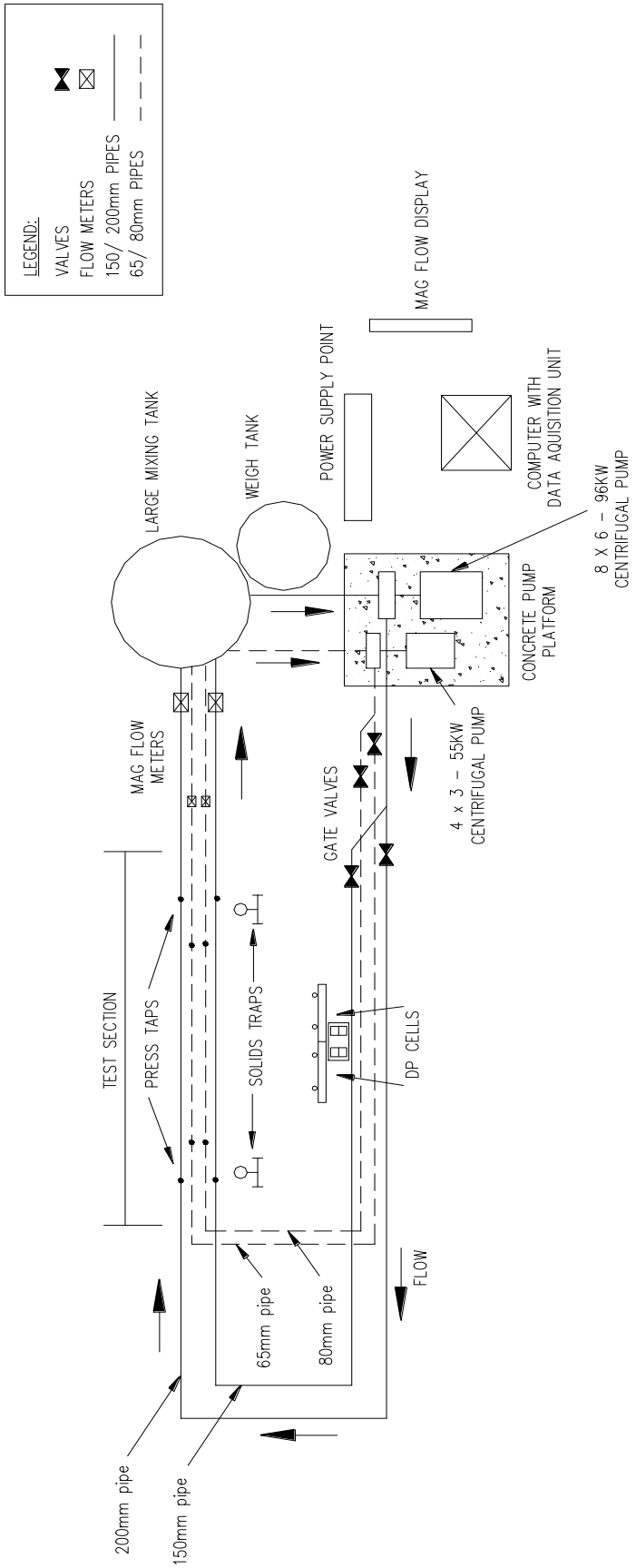

Figure 3.5 Schematic plan view of the large pipes test loop

The Flume pipeloop

The flume pipe loop consists of three PVC test pipes of 13, 28 and 80mm diameter, through which fluid is pumped by a 100mm progressive cavity displacement pump controlled by a variable speed drive. The pump delivers a maximum flow rate of 25l/s up to a maximum pressure of 30 bar and is driven by a 17kW motor. Each pipe has an inline magnetic flow meter. The system is fed from a 500 litre weigh tank which is suspended over the mixing tank and agitator via a load cell and pivot. The weigh tank is used to calibrate the flow meters. Slurry temperature is monitored using a temperature probe situated at the end of the heat exchanger. A schematic diagram of the flume pipe rig is presented in Figure 3.6.

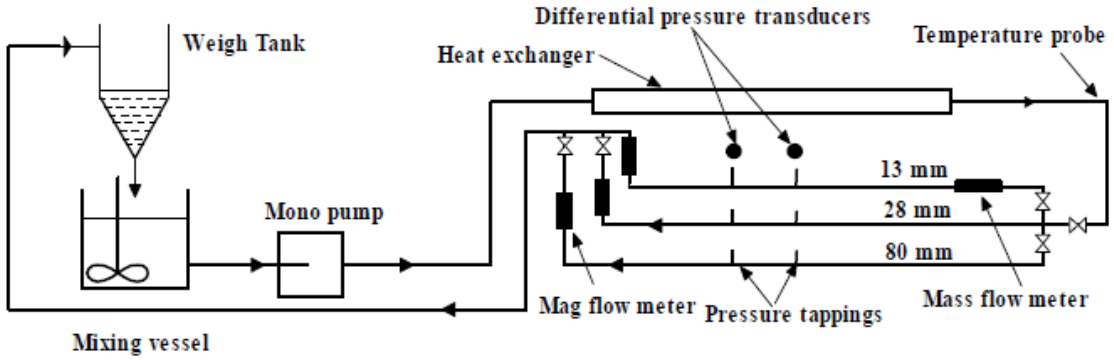

Figure 3.6 Schematic representation of the flume pipe loop (Haldenwang, 2003)

Pressure tappings and solid traps

The differential pressure transducers on all the pipe test loops are connected to the test pipe sections via solid traps (Figure 3.7) and static pressure tappings ($l/d \geq 6$) located in the pipe walls, separated by the test length distance for the specific pipe.

Each pressure tapping is connected to the solids trap via a control valve. Clear water lines connect the traps to the differential pressure transducer (Slatter, 1994). Details of the arrangement between the test pipe, pressure tapping and solids trap are illustrated in Figure 3.7.

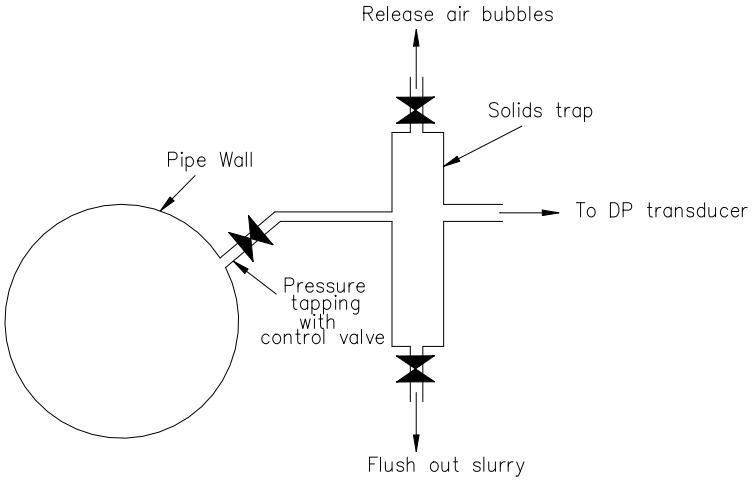

Figure 3.7 Detail of the connection between pipe, pressure tapping, and solid trap (Slatter, 1994)

3.3.2 Instrumentation

The instrumentation used to measure differential pressure (DP transducer), flow rate (magnetic flow meter) and mass (load cell), during the straight pipe experiments are described in the section below.

Malvern particle size analyser

The Malvern Mastersizer is a high precision instrument used to measure particle size distribution. The instrument has three lenses and produces particle size distributions based on particle volume. The instrument specifications are as follows:

Name: Particle size analyser: Malvern Hydro 2000MU
Dispersion type: Wet
Capacity: 600 – 1000ml
Dispersion mechanisms: Continuously variable pump / stirrer and ultrasonication
Maximum particle size: 1000 – 1500μm, depending on particle shape and density

Particle size analysis was carried out on the kaolin and Bentonite slurries to determine the d_{85} representative particle size.

Differential pressure transducers

The differential pressure transducers used on the pipe test loops are the Fuji Electric version 25.0, Model No. IKKW35VI-AKCYYAA [DP]. Two transducers were used on each test loop. The maximum ranges for the transducers used on the valve test loop and the large pipes test loop were 6kPa and 130kPa. The flume pipe loop used a 6kPa and a 32kPa transducer. All the transducers output 4 to 20mA DC with an accuracy of 0.1% of full scale.

Magnetic flow meters

Krohne Aquaflux and SAFMAG magnetic flow meters are fitted in the test loops. They are calibrated by the manufacturers and nominal factory calibration settings were used when conducting the tests. The accuracy of the flow meters is specified by the manufacturer as 0.5% for V > 0.5m/s and (0.25/V)% for V < 0.5m/s, where V is the average fluid velocity through the flowmeter. Flow meter accuracy therefore deteriorates quite rapidly as the nominal wall shear rate values decrease below $\pm 50 s^{-1}$ (see Appendix D), and this, in addition to the reasons stated in Section 1.7, is why the minimum nominal wall shear rate was limited to $40 s^{-1}$.

3.3.3 Data acquisition unit (DAQ)

An HP 3421A data acquisition unit (DAQ) was used on each test loop to sample signals from the instrumentation. Prior to sampling, the 4 to 20mA signals from the instruments were converted to 1 to 5V by high precision 250Ω resistors. The DAQ was controlled by an HP-II serial interface loop, and the system was driven by a custom Microsoft® Visual Basic program, which recorded to disc the raw data, applied the calibration constants (See Section 3.6) and wrote the experimental values to an Excel spreadsheet for further analysis, as illustrated in Figure 3.8.

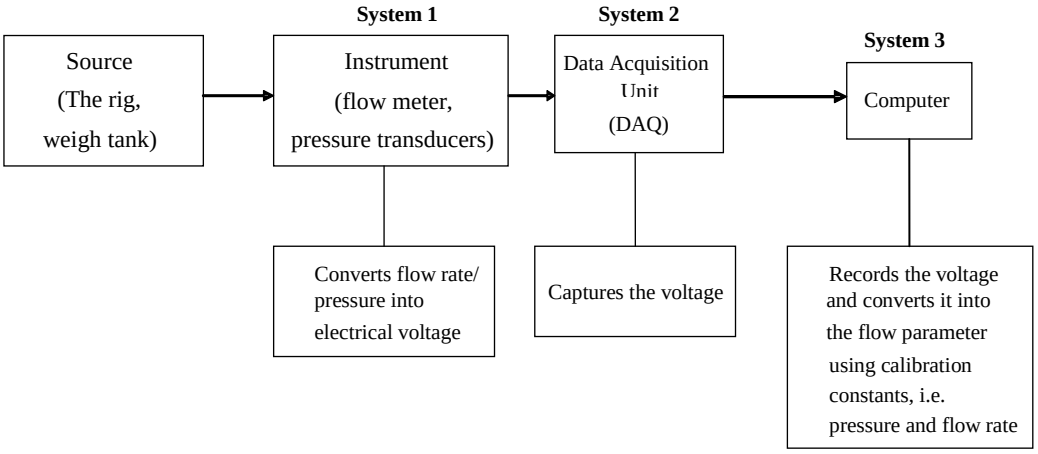

Figure 3.8 Line diagram of the data measuring system used during pipe tests

3.4 Measurable quantities

Determined quantities such as pipe diameter, wall shear stress and nominal wall shear rate are dependent on the product of one or more measured quantities. In this section the equations used to determine the uncertainties are presented. If the result (X) (dependant variable) is in the form of a product of the primary variables raised to some power i.e.

$$X = x_1^{a_1}.x_2^{a_2}.x_3^{a_3}.....x_n^{a_n} \tag{3.3}$$

then the uncertainty in the result, ΔX, is given by (Holman, 2001)

$$\left(\frac{\Delta X}{X}\right)^2 = \sum_{i=1}^{n}\left(\frac{a_i \Delta x_i}{x_i}\right)^2 \tag{3.4}$$

3.4.1 Internal pipe diameter

The diameters of the test pipes were determined by measuring the mass of water (M_w) within a measured length of the pipe (the distance between selected pressure tappings) L. The diameter of the pipe was then calculated as (Slatter, 1994):

$$D = \sqrt{\left(\frac{4M_w}{\rho_w \pi L}\right)} \tag{3.5}$$

By Eq. (3.4) and Eq. (3.5) the uncertainty in pipe diameter was determined as (for a given ρ_w):

$$\left(\frac{\Delta D}{D}\right)^2 = \left(\frac{1}{2}\frac{\Delta M_w}{M_w}\right)^2 + \left(-\frac{1}{2}\frac{\Delta L}{L}\right)^2 \tag{3.6}$$

Weight/Mass

The mass of all samples was measured using a scale graduated in grams. The absolute error on measurements (ΔM_w) = 0.001kg.

Axial distance/ Length

Axial distances and lengths were measured using a measuring tape divided in mm increments. The absolute error on measurements (ΔL) = 0.001m.

The combined experimental errors calculated for each of the pipes in the test loops are presented in Table 3.1.

Table 3.1 Combined experimental errors in the valve, flume and large pipes test loops pipe diameters

VALVE TEST LOOP		FLUME PIPE LOOP		LARGE PIPES TEST RIG	
Average internal diameter (mm)	**Experimental error (%) [ΔD/D]**	**Average internal diameter (mm)**	**Experimental error (%) [ΔD/D]**	**Average internal diameter (mm)**	**Experimental error (%) [ΔD/D]**
42.10	0.63	13.32	0.106	57.68	0.23
52.80	0.32	28.11	0.05	81.20	0.31
63.10	0.45	80.88	0.017	150.60	0.17
80.40	0.22			211.00	0.12
97.20	0.37				

3.4.2 Wall shear stress

Differential pressure was measured using the differential pressure transducers described in Section 3.3.2. The differential pressure transducers used are accurate to 0.1% of full scale. Wall shear stress was calculated using Eq. (2.21) so errors in wall shear stress are given by Eq. (3.7), and were estimated to vary between 0.2 and 3%. The results for the combined errors analysis for wall shear stress calculations for all pipe test lengths, on each of the test rigs, are presented in Appendix D.

$$\left(\frac{\Delta\tau_w}{\tau_w}\right)^2 = \left(\frac{\Delta D}{D}\right)^2 + \left(\frac{\Delta(\Delta P)}{\Delta P}\right)^2 + \left(-\frac{\Delta L}{L}\right)^2 \tag{3.7}$$

3.4.3 Nominal wall shear rate

The volumetric flow rate was measured using the magnetic flow meters described in Section 3.3.2. The accuracy of the flow meters as stipulated by the manufacturer is 0.5% of actual flow. Errors in calculated nominal wall shear rate ($8V/D$) are estimated by Eq. (3.8) [$8V/D = 32Q/\pi D^3$], and varied from 0.5 to 4% in the nominal wall shear rate range considered in this work. The results for the combined errors analysis for wall shear rate calculations, for all pipe test lengths, on each of the test rigs, are presented in Appendix D.

$$\left(\frac{\Delta 8V/D}{8V/D}\right)^2 = \left(\frac{\Delta G}{G}\right)^2 = \left(\frac{\Delta Q}{Q}\right)^2 + 9\left(\frac{\Delta D}{D}\right)^2 \tag{3.8}$$

where $G = 8V/D$

3.5 Test procedures

This section presents details of the water and straight pipe rheology tests conducted in the three test loops.

3.5.1 Water tests

Before slurry tests in were done in any of the pipe loops, the validity of the system (instrumentation, pipes and data acquisition) was verified by comparing the water test results for each pipe with the Colebrook-White equation [Eq. (2.141)]. The procedure followed for the water tests was as described in Haldenwang (2003).

Pipe roughness

The hydraulic pipe roughness (ε) for each diameter was estimated from the water pipe tests by optimising the value for (ε) in the Colebrook-White equation to obtain the "best fit" of the water test data to the Colebrook-White equation. This hydraulic roughness value (ε) was taken as the actual pipe roughness for that specific pipe. These pipe roughness values were used in the partially rough walled turbulent flow prediction method of Wilson & Thomas (1985) and the Hallbom (2008) Nikuradse pseudo-fluid method. They were also used as the (d_{85}) value in the Slatter method for the CMC analyses (as CMC does not contain solid particles, but chain-like molecules instead) and thus the pipe roughness needed to be used instead of the particle roughness (Slatter, 1994). Since the viscous sub-layer is thicker for non-Newtonian fluids than for Newtonian fluids, the pipe-roughness effect is expected to be small for time-independent fluids (Chhabra & Richardson, 2008).

Example water test results (one pipe on each of the test loops) are presented in Figure 3.9, Figure 3.10 and Figure 3.11. All the water test results are given in Appendix C. The hydraulic pipe roughness values for all test pipes on the three test loops are presented in Table 3.2,
Table 3.3 and Table 3.4.

Valve test loop

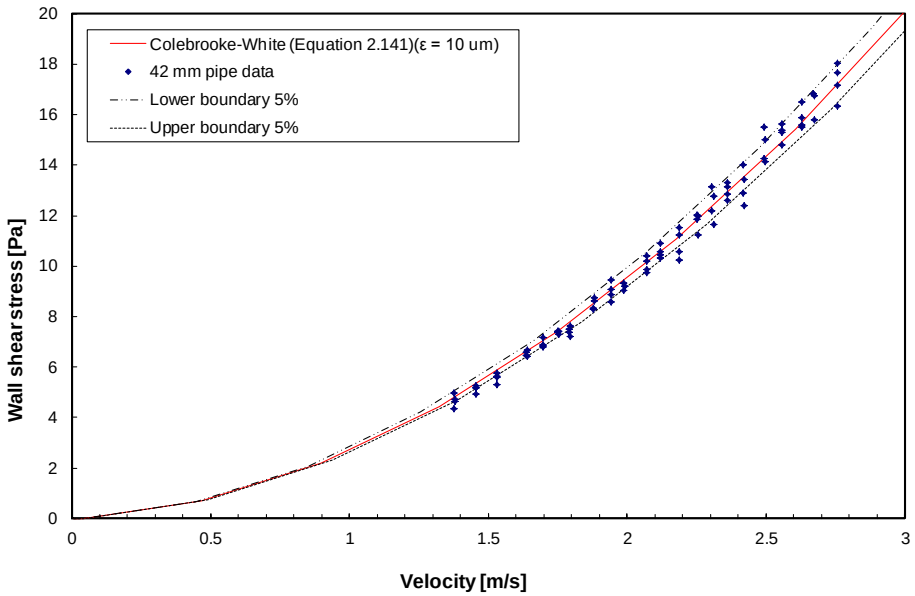

Figure 3.9 Experimental results vs. Colebrook-White prediction for diameter 42mm test pipe on the valve test loop

Table 3.2 Pipe roughness values for pipes on the valve test loop

Pipe size (mm)	Internal diameter (mm)	Pipe Roughness (μm)
42	42.12	10
52	52.80	4
63	63.08	25
80	80.43	18
100	97.17	21

Large pipes test loop

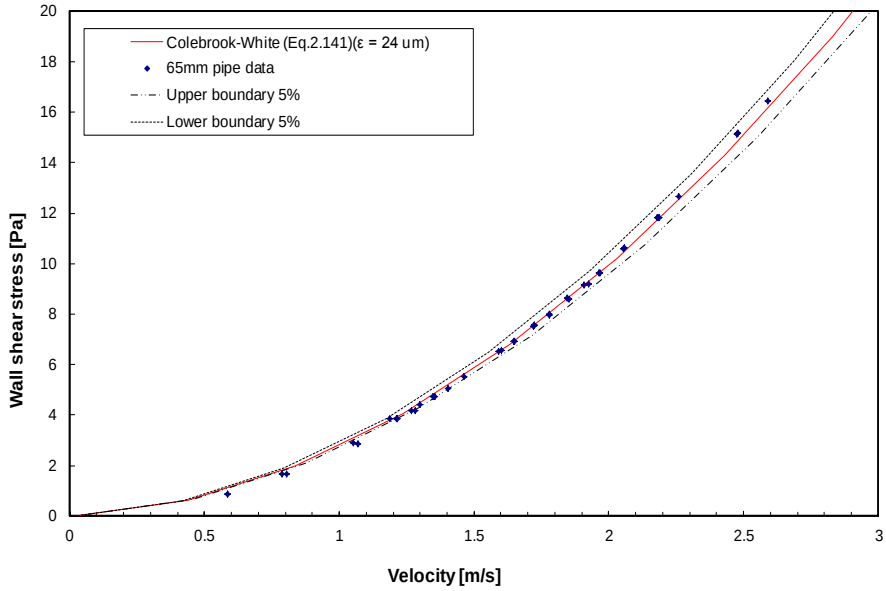

Figure 3.10 Experimental results vs. Colebrook-White prediction for diameter 65mm test pipe on the large pipes test loop

Table 3.3 Pipe roughness values for pipes on the large pipes test loop

Pipe size (mm)	Internal diameter (mm)	Pipe Roughness (μm)
65	57.68	24
80	81.20	44
150	150.60	31
200	211.00	20

The Flume test loop

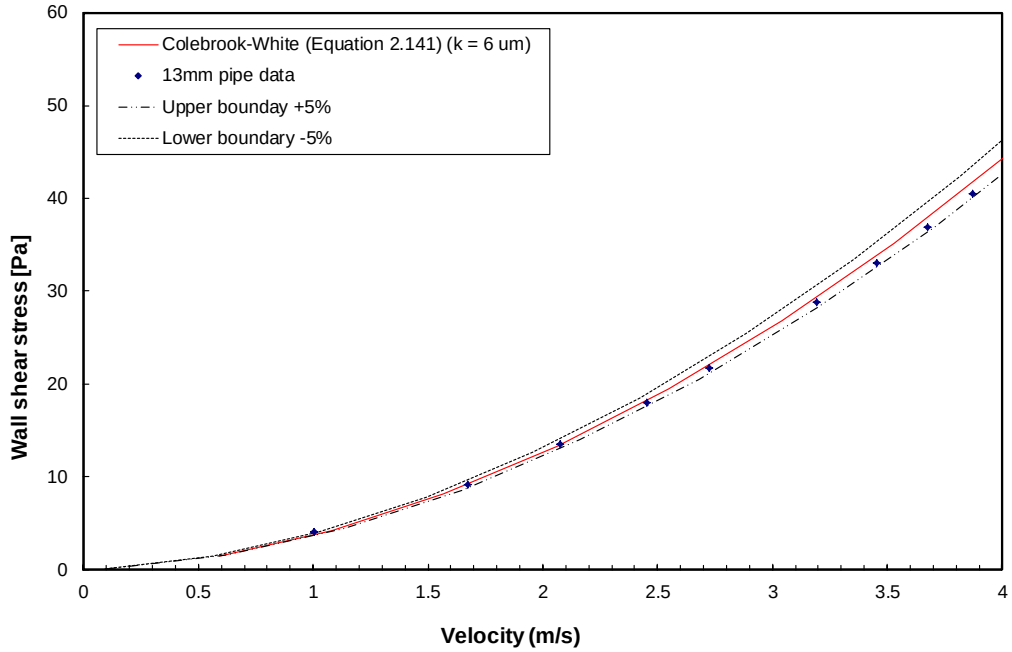

Figure 3.11 Experimental results vs. Colebrook-White prediction for diameter 13mm test pipe on the flume test loop

Table 3.4 Pipe roughness values for pipes on the flume test loop

Pipe size (mm)	Internal diameter (mm)	Pipe Roughness (μm)
13	13.32	6
28	28.11	8
80	80.88	0

3.5.2 Slurry tests

Once the reliable the operation of each test loop was verified through the (Colebrook-White) water tests, the slurry pipe tests were conducted as described in Appendix A.

3.5.3 Particle size testing (Malvern particle size analyser)

The particle size distributions for kaolin and bentonite were determined using a Malvern Hydro 2000MU. The calibration of the instrument was confirmed using standard calibration particles by the laboratory technician. The purpose of the particle size analysis was to determine the d_{85} representative particle size for the Slatter (1994) turbulent analysis. The particle size distributions produced by the Malvern sizer does not necessarily agree with results obtained by other methods, so any comparisons of particle size distributions should be made with due caution (Slatter, 1994). The particle size distributions and the values for the 85th percentile passing (d_{85}) are presented in Figure 3.12 and Figure 3.13.

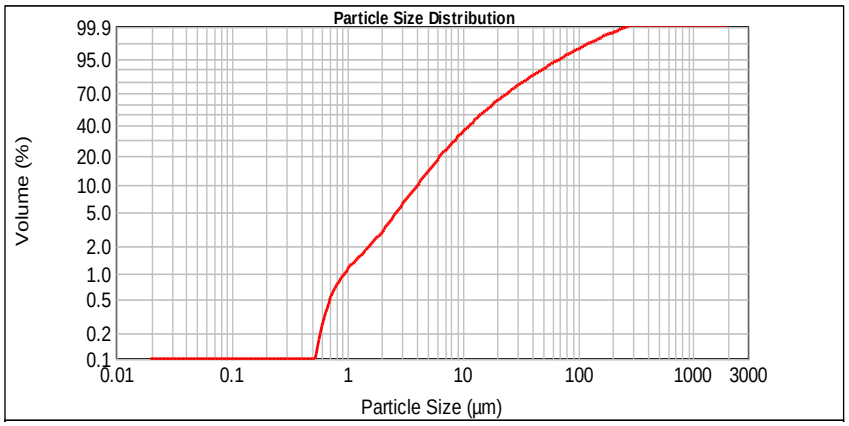

Figure 3.12 Particle size distribution for bentonite – d_{85} = 42µm

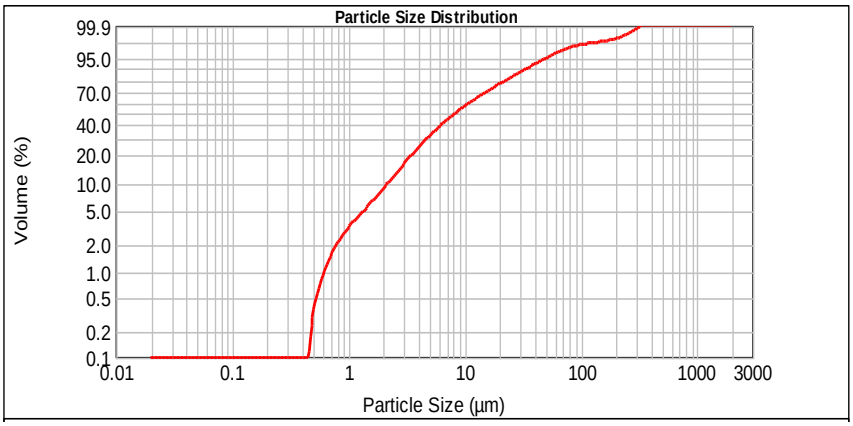

Figure 3.13 Particle size distribution for kaolin – d_{85} = 28µm

3.6 Calibration of instrumentation and verification of test loops

The purpose of the instrument calibrations was to establish the functional relationship between the instrument voltage output and the actual value of the measured quantity. The calibration procedures for the instrumentation described in Section 3.3.2 is presented here. All instruments were calibrated before each new set of tests were conducted and those calibration values used at that time of testing.

The response of the instruments used in this experimental work is linear, so calibration constants were derived from a least squares linear ($y = mx + c$) regression analysis of the calibration test data using Excel (Holman, 2001). The goodness of the fit to the data is represented by the correlation coefficient ($0 \leq r^2 \leq 1$). The closer r^2 is to 1 the better the fit (indicating that a greater proportion of variance is accounted for by the model) (Kirkup, 2002). Calibrations were accepted for $0.999 < r^2 < 1$.

3.6.1 Differential pressure transducer calibration

For the calibration of the differential pressure transducers a hand-held pump with an independently calibrated digital manometer was used to apply a pressure difference across the transducer, and the hand-held communicator and digital manometer were used to read the resulting pressure values. The procedure is described in Appendix B.

Setting the DP transducer range limits and calibrating

Before calibration commences, the range for each DP transducer was set to values appropriate for the pipe tests to be done, and the pressure transducers were then calibrated for each of these ranges.

The DP transducers for each pipe test loop were calibrated for the following ranges:

DP transducer: 0kPa to 6kPa (low - all rigs)
DP transducer: 0kPa to 32kPa (high - flume pipe loop)
DP transducer: 0kPa to 130kPa (high - large pipes test loop rig & valve test loop)

Calibration of all instruments was repeated at regular intervals. An example calibration curve for the 6kPa DP transducer on the valve test loop is presented in Figure 3.14. Other calibration results were similar.

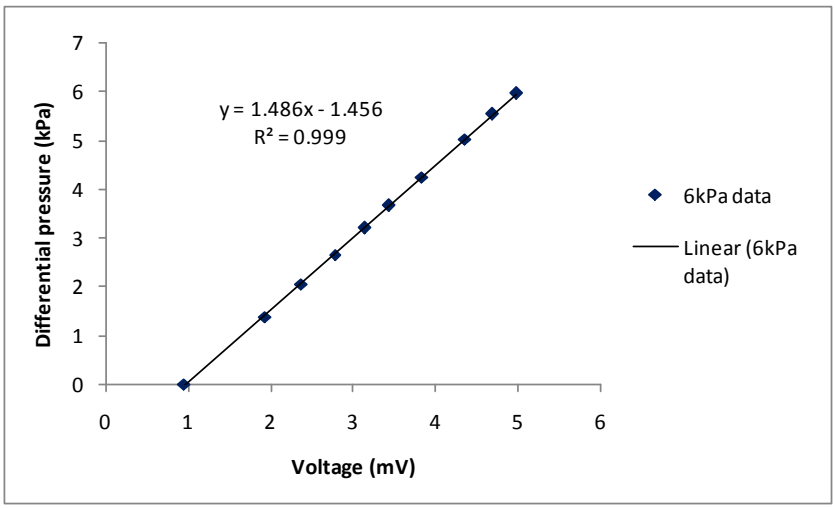

Figure 3.14 Calibration constants for 6kPa DP transducer used on the valve test loop

3.6.2 Flow meter calibration

The factory calibration values are incorporated into the instrument at manufacture so the flow meter reading as displayed on the digital display is taken as the "true" reading which is captured by the data acquisition system. The flow meters were "calibrated" only to verify the factory set constants provided by the manufacturer, to ensure reasonable accuracy even at the lowest nominal wall shear rate value of $\pm 40 s^{-1}$. The Krohne flow meter used on the valve test loop was calibrated to a maximum range of 4.4l/s and the results of the linear regression analysis on the calibration data is presented in Figure 3.15. Refer to Appendix B for the details of the flow meter verification procedure.

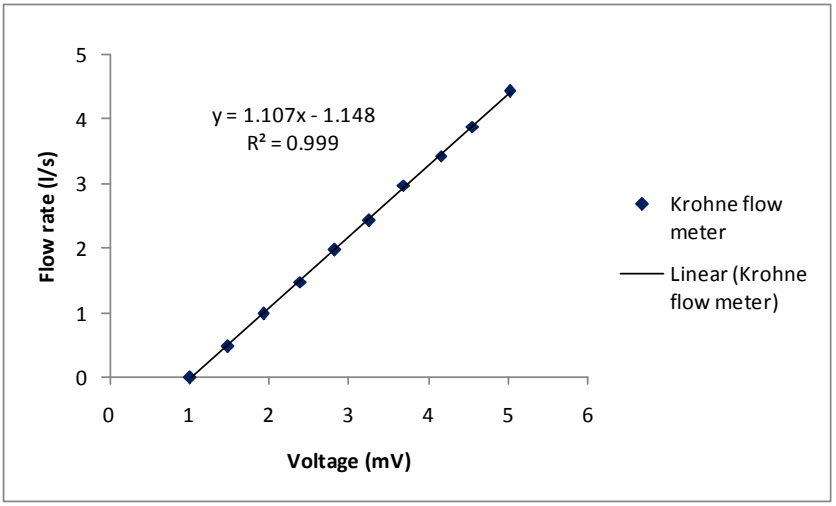

Figure 3.15 Calibration constants for (4.4l/s) Krohne flow meter used on the valve test loop

3.7 Conclusion

This chapter has highlighted the equipment, apparatus, and processes applied to the test material and data in conducting the research work. The experimental equipment and instrumentation used for the reliable collection of pipeline test data for non-Newtonian slurries over a wide range of pipe sizes were described. The three primary test apparatus (valve test loop, large pipes test loop and flume test loop) used for the collection of pipe test data were described and the procedures for using these apparatus for slurry testing were presented. Examples of data presentation on pseudo-shear diagrams were presented. Calibration procedures used were presented to show that accurate slurry measurements were made to determine the relevant rheological properties.

Results of the water tests were presented which confirmed the correct operation of all the pipe test rigs. Error analyses to quantify the expected combined errors for the measured quantities were conducted. The nominal wall shear rate error was estimated to be between 0.2 and 4% for values >40s^{-1}. For the wall shear stress errors were estimated to vary between 0.2 and 3%. The test materials used for this work were three concentrations of kaolin, bentonite and CMC. The physical properties of these materials have been described and the procedure for determining the rheological properties presented. The results of the straight pipe tests and rheological characterisation for all material concentrations are presented in Chapter 4.

Chapter 4 Results and discussion - Pipe tests and rheological characterisation

The aim of this study was to determine what influence the choice of rheological model has on pipe flow predictions in the different flow regimes. In this chapter the results from the pipe tests conducted with all the slurries at all test concentrations are presented. Measured pipe data (*ΔP* and *Q*) was used to calculate (τ_w) and (*8V/D*) as described in Section 3.2.2, which was then plotted as wall shear stress (τ_w) against nominal wall shear rate (*8V/D*). Colinearity of the laminar data for all pipe sizes was observed for all the pipe tests conducted, indicating that wall slip and end effects were never present, and so were not accounted for in the analyses. Laminar flow data were extracted to perform the rheological characterisations, as described in Section 3.2.4. Each material was characterised using each rheological model. The derived rheological constants for each rheological model are tabulated, and presented graphically for each material. These rheological parameters were used to predict laminar, transitional and turbulent flow, which is presented in Chapter 5.

4.1 Effect of temperature

Test material temperature was recorded with pipe flow data for each test. In all tests the change in temperature over the duration of the test was <10°C. Given the findings on the effect of temperature on material rheology (Section 2.1.10) and the fact that no changes in measured data were observed (test points done randomly, and repeated) for any of the materials tested, temperature effects were assumed to be negligible.

4.2 Kaolin

4.2.1 6% kaolin

Figure 4.1a below presents the data for 6% kaolin slurry pumped through pipes of 42, 52, 63, 80, 97 and 150mm diameter (pseudo shear diagram), and Figure 4.1b shows the rheological model fits to the laminar data of the 6% kaolin.

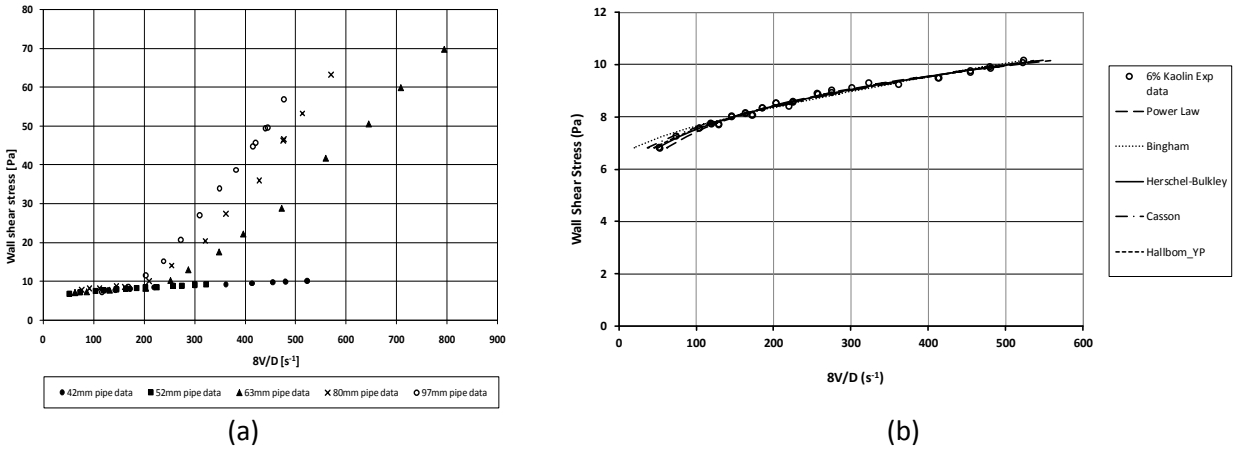

(a) (b)

Figure 4.1 (a) Pseudo shear diagram and (b) rheological model fits to 6% kaolin laminar data

The laminar data shows good agreement with the analysis of Rabinowitsch and Mooney (Chhabra & Richardson, 2008). The change from laminar to turbulent flow is evident as a sharp increase in velocity gradient plotted as *8V/D*, where the data deviates from the laminar flow line. The individual turbulent branches decrease in pipe diameter with increasing *8V/D* (Chhabra & Richardson, 2008). Turbulence was

not achieved in the 42mm and 52mm diameter pipes. The derived rheological constants for each rheological model are tabulated in Table 4.1. The goodness of each model fit to the laminar data was represented and ranked by the RMSE values [Eq. (3.1)].

Table 4.1 Rheological model constants for 6% kaolin

Model	Rheological Constants			RMSE	Ranking
	τ_y	K	n		
Herschel-Bulkley	3.9	0.502	0.361	13.9	1
Bingham Plastic	6.3	0.00443	-	19.6	5
Power law	-	2.797	0.182	14.8	3
	τ_C	η_C			
Casson	5.2	0.00083	-	14.9	4
	τ_0	μ_∞	k		
Hallbom_YP	4.4	0.000096	0.310	14.1	2

4.2.2 10% kaolin

Figure 4.2a presents the test data for 10% kaolin tested in the 42, 52, 63, 80, 97 and 150mm diameter pipes (pseudo shear diagram) and Figure 4.2b shows the rheological model fits to the 10% kaolin laminar data.

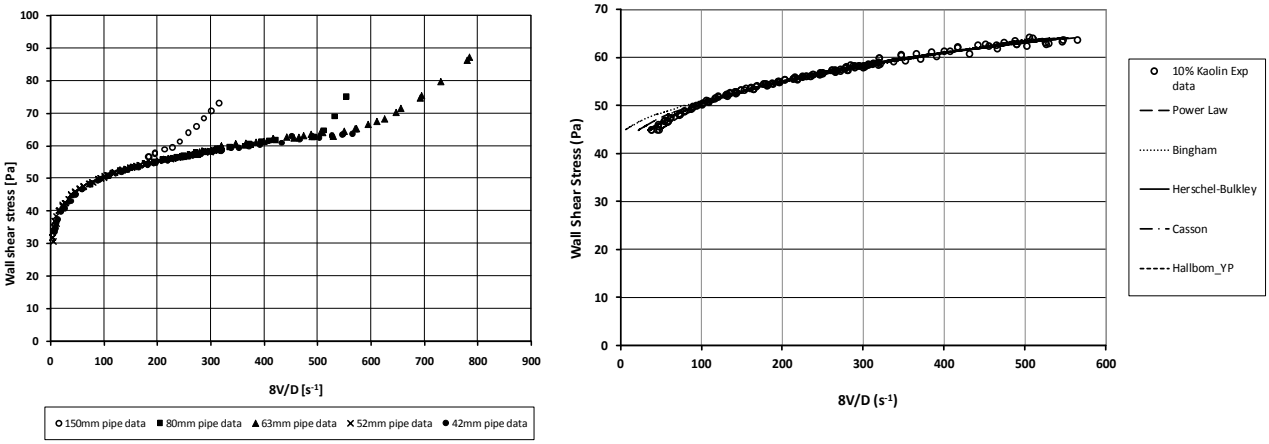

(a) (b)

Figure 4.2 (a) Pseudo shear diagram and (b) rheological model fits to 10% kaolin laminar data

Turbulent flow was not achieved in the 42 and 52mm diameter pipes for 10% kaolin. The laminar data of these two pipes were used for rheological characterisation of the material, and the turbulent data in the larger diameter pipes were used to evaluate transitional and turbulent flow predictions. The derived rheological constants and the RMSE values are presented in Table 4.2. The goodness of each model fit to the laminar data was represented and ranked by the RMSE values [Eq. (3.1)].

Table 4.2 Rheological model constants for 10% kaolin

Model	Rheological Constants			RMSE	Ranking
	τ_y	K	n		
Herschel-Bulkley	27.4	3.959	0.312	14.7	1
Bingham Plastic	43.2	0.0213	-	21.1	5
Power law	-	22.229	0.147	15.6	3
	τ_C	η_C			
Casson	37.3	0.00322	-	16.2	4
	τ_0	μ_∞	k		
Hallbom_YP	29.1	0.000066	0.250	14.7	2

4.2.3 15% kaolin

Figure 4.3a presents the test data for 15% kaolin from the 63, 80, 150 and 200mm diameter pipes on a pseudo shear diagram. The rheological model fits to the 15% kaolin laminar data are presented in Figure 4.3b.

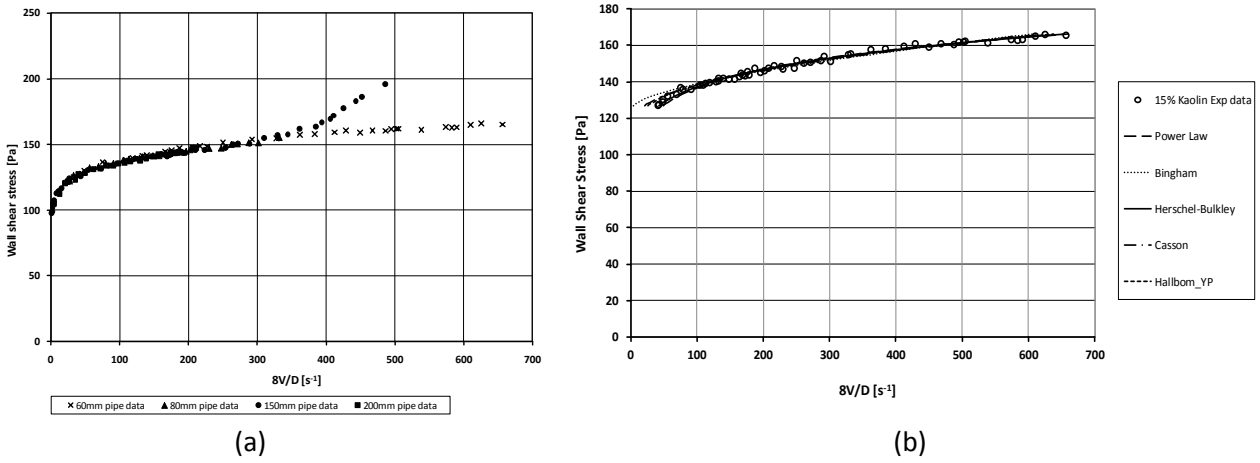

(a) (b)

Figure 4.3 (a) Pseudo shear diagram and (b) rheological model fits to 15% kaolin laminar data

From the data plots it is clear that the yield stress for this concentration kaolin was significantly higher than for the 6 and 10% mixtures. The derived rheological constants for each rheological model are given in Table 4.3. The goodness of each model fit to the laminar data was represented and ranked by the RMSE values [Eq. (3.1)].

Table 4.3 Rheological model constants 15% kaolin

Model	Rheological Constants			RMSE	Ranking
	τ_y	K	n		
Herschel-Bulkley	61.6	25.908	0.184	20.6	1
Bingham Plastic	124.1	0.0296	-	29.1	5
Power law	-	75.408	0.1033	20.7	2
	τ_C	η_C			
Casson	112.1	0.00324	-	23.7	4
	τ_0	μ_∞	k		
Hallbom_YP	105.9	0.000312	0.330	22.5	3

4.2.4 Summary – model fits to kaolin data

From Figure 4.1 to Figure 4.3 and Table 4.1 to Table 4.3, it is evident that kaolin is a material with a significant yield stress and a degree of flow curve curvature, which can be described by the Herschel-Bulkley (incorporating Bingham plastic and power law, (Chhabra & Richardson, 2008)), Casson or Hallbom (Hallbom, 2008) models.

Best fitting model

Based on the calculated RMSE values, the Herschel-Bulkley rheological model best represents the 6, 10 and 15% kaolin laminar data. The least representative fit for all concentrations was found to be the Bingham plastic model, mainly due to its inability to model the curvature in the laminar data, especially in the lower shear rate range. The power law, Casson and Hallbom models also fit the laminar data reasonably well as seen in Figure 4.1 to Figure 4.3, and by the RMSE values given in Table 4.1 to Table 4.3.

4.3 Bentonite

4.3.1 6% bentonite

Figure 4.4 presents the test data for 6% bentonite slurry tested in the 13, 28 and 80mm diameter pipes (pseudo shear diagram) as well as the rheological model fits to the 6% bentonite laminar data.

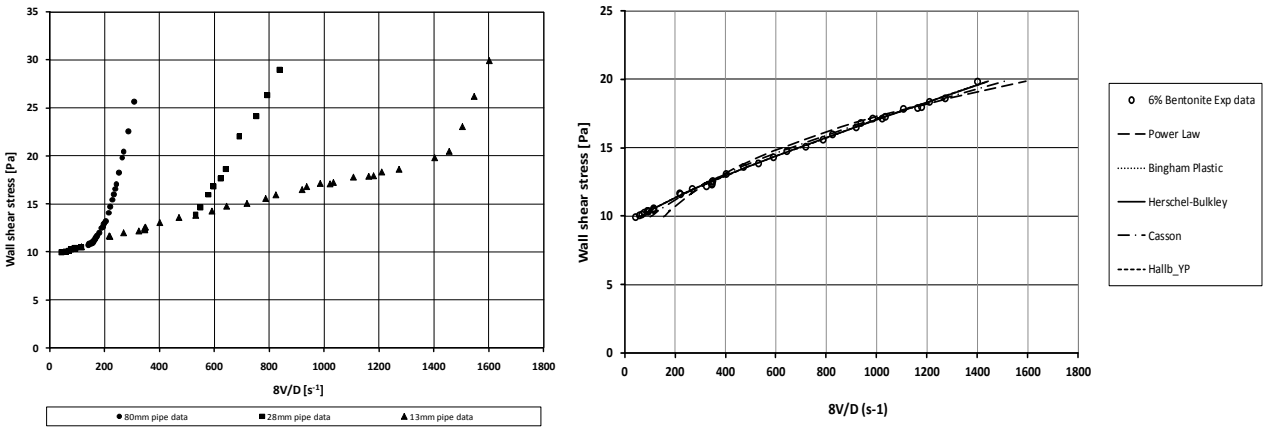

(a) (b)

Figure 4.4 (a) Pseudo shear diagram and (b) rheological model fits to 6% bentonite laminar data

From the laminar data of bentonite, it is evident that the material has a yield stress, and the laminar data for all pipe sizes coincide in a straight line. This is typical of Bingham plastic behaviour (Chhabra & Richardson, 2008). Turbulence is achieved in each pipe size and is evident as the singular turbulent branches deviating from the laminar flow data. The derived rheological constants and the RMSE values are presented in Table 4.4. The goodness of each model fit to the laminar data was represented and ranked by the RMSE values [Eq. (3.1)].

Table 4.4 Rheological model constants for 6% bentonite

Model	**Rheological Constants**			**RMSE**	**Ranking**
	τ_y	K	n		
Herschel-Bulkley	8.5	0.00605	1.000	18.4	3
Bingham Plastic	8.5	0.00605		18.7	1
Power law	-	1.935	0.297	68.2	5
	τ_C	η_C			
Casson	6.3	0.001796		35.7	4
	τ_0	μ_∞	k		
Hallbom_YP	8.9	0.00561	1.000	18.2	2

4.3.2 7.34% bentonite

Figure 4.5a presents the test data for 7.34% bentonite tested in the 60, 80 and 150mm diameter pipes (pseudo shear diagram). Figure 4.5b shows the rheological model fits to the 7.34% bentonite laminar data. The derived rheological constants and RMSE values are presented in Table 4.5.

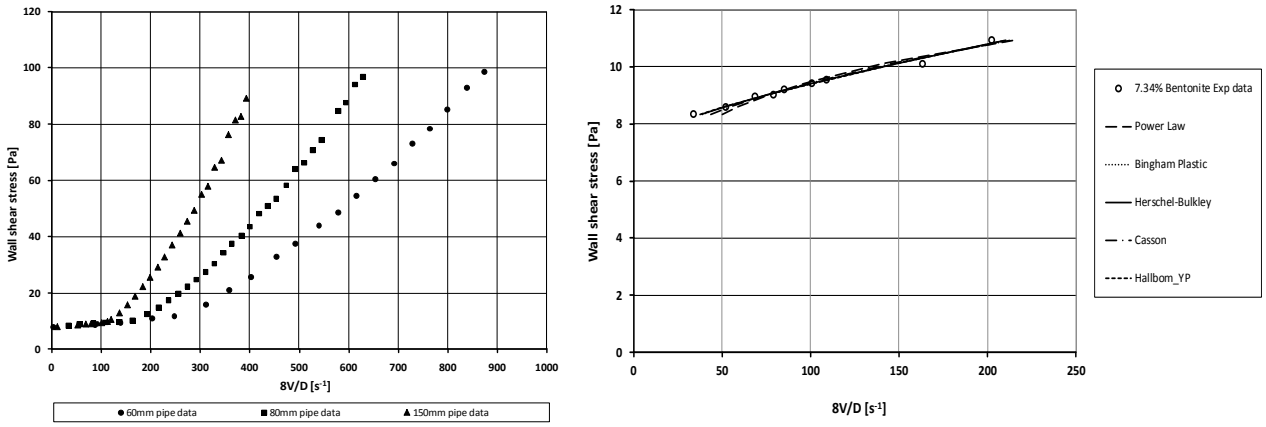

(a) (b)

Figure 4.5 (a) Pseudo shear diagram and (b) rheological model fits to 7.34% bentonite laminar data

The goodness of each model fit to the laminar data was represented and ranked by the RMSE values [Eq. (3.1)].

Table 4.5 Rheological model constants for 7.34% bentonite

Model	Rheological Constants			RMSE	Ranking
	τ_y	K	n		
Herschel-Bulkley	6.95	0.0107	1.000	7.3	3
Bingham Plastic	6.95	0.01074	-	6.8	1
Power law	-	3.501	0.187	12.2	5
	τ_C	η_C			
Casson	5.7	0.00207	-	8.8	4
	τ_0	μ_∞	k		
Hallbom_YP	7.3	0.01002	1.000	7.1	2

4.3.3 9% bentonite

Figure 4.6 presents the test data for 9% bentonite from the 60, 80 and 150mm diameter pipes (pseudo shear diagram) and the rheological model fits to the 9% bentonite laminar data.

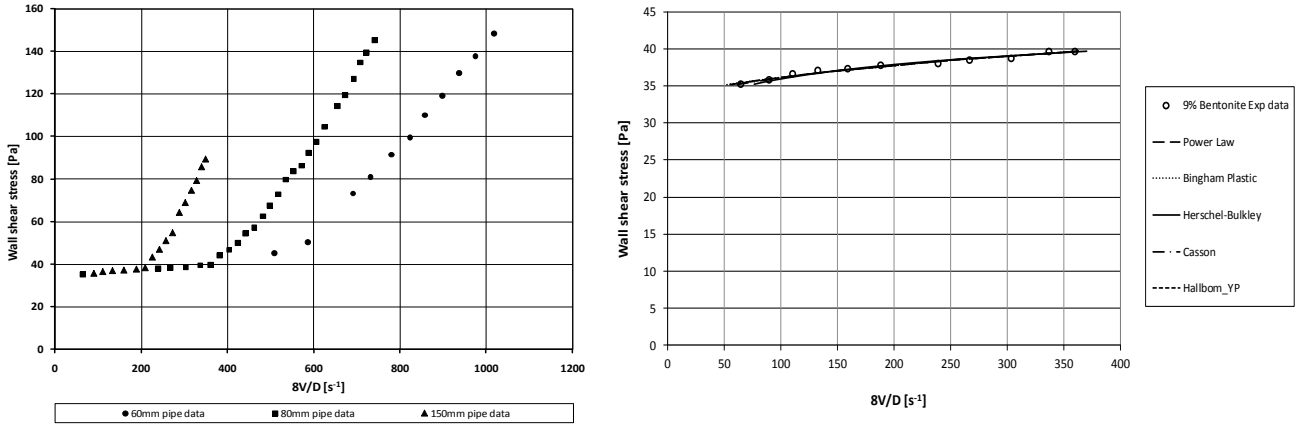

(a) (b)

Figure 4.6 (a) Pseudo shear diagram and (b) rheological model fits to 9% bentonite laminar data

The test results for both the 7.34% and 9% bentonite slurry show typical behaviour of bentonite in pipe flow. The laminar data for all pipe sizes coincide on a straight line, and a yield stress is observed. Turbulence is achieved in all pipe sizes and is evident as the individual branches of data deviating from the laminar data. The derived rheological constants and the RMSE values are presented in Table 4.6. The goodness of each model fit to the laminar data was represented and ranked by the RMSE values [Eq. (3.1)].

Table 4.6 Rheological model constants for 9% bentonite

Model	Rheological Constants			RMSE	Ranking
	τ_y	K	n		
Herschel-Bulkley	32.4	0.0175	0.849	16.0	3
Bingham Plastic	32.9	0.00576	-	15.2	1
Power law	-	22.864	0.0753	19.4	5
	τ_C	η_C			
Casson	30.5	0.000461	-	15.6	2
	τ_0	μ_∞	k		
Hallbom	32.3	0.00112	0.589	16.1	4

4.3.4 Summary – model fits to bentonite data

The results shown in Figure 4.4, Figure 4.5 and Figure 4.6 as well as Table 4.4, Table 4.5 and Table 4.6 indicate that bentonite can be represented by the Bingham plastic rheological model, due to its linear laminar data profile and presence of a yield stress.

Best fitting model

Based on RMSE values shown in Table 4.4 to Table 4.6 the Bingham plastic model best fits the 6% bentonite laminar flow data. The Hallbom and Herschel-Bulkley models both reduced to the Bingham plastic model. Any of these models could thus be used. The same result was observed for the 7.34% and 9% data. The power law model gives the worst fit to the bentonite data due to its rheogram curvature and absence of yield stress.

Rheology observations

The 6% bentonite had a different dry density to the 7.34% and 9% materials (different suppliers), so rheological comparisons are only made between the 7.34% and 9% concentrations. This "anomaly" in the material is apparent from the observation that the yield stress value of the 6% bentonite lies between the yield stress values of the 7.34 and 9% bentonite, not below them as would reasonably be expected.

4.4 CMC (Carboxyl Methyl Cellulose)

4.4.1 3% CMC

Figure 4.7a presents the test data for 3% CMC tested in the 60, 80 and 150mm diameter pipes (pseudo shear diagram). Figure 4.7b shows the rheological model fits to the 3% CMC laminar data.

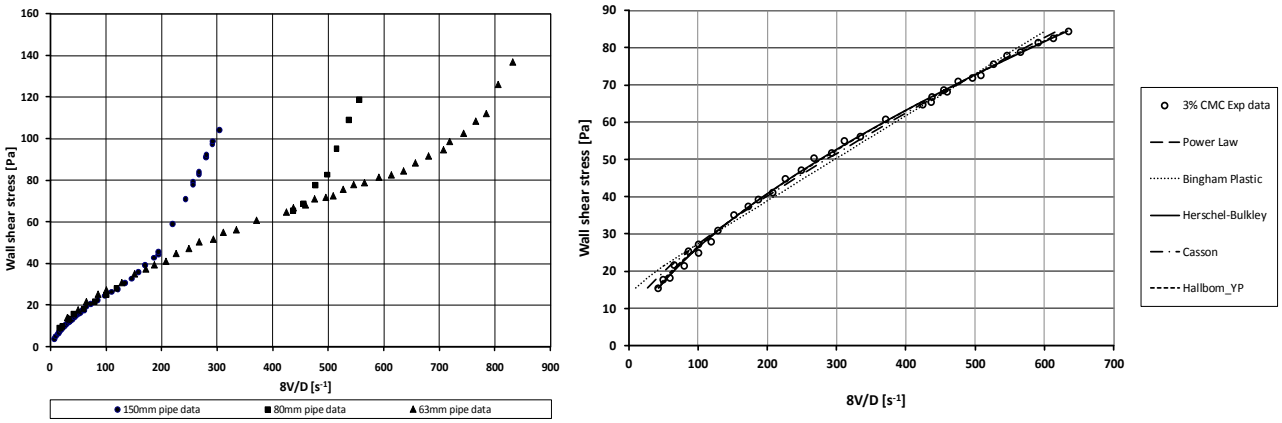

(a) (b)

Figure 4.7 (a) Pseudo shear diagram and (b) rheological model fits to 3% CMC laminar data

The pseudo shear diagram for the 3% CMC shows typical pseudoplastic behaviour i.e. laminar data curvature and no yield stress. Turbulent flow was reached in all pipe sizes and is observed as individual branches deviating from the laminar flow data line. The derived rheological constants as well as the goodness of the model fits [RMSE Eq. (3.1)] to the data are presented in Table 4.7. The goodness of each model fit to the laminar data was represented and ranked by the RMSE values [Eq. (3.1)].

Table 4.7 Rheological model constants for 3% CMC

Model	Rheological Constants			RMSE	Ranking
	τ_y	K	n		
Herschel-Bulkley	0.0	1.321	0.631	7.0	2
Bingham Plastic	12.3	0.113	-	19.4	5
Power law	-	1.321	0.631	6.9	1
	τ_C	η_C			
Casson	5.2	0.0705	-	11.2	4
	τ_0	μ_∞	k		
Hallbom_YP	0.01	0.0029	0.113	7.2	3

4.4.2 5% CMC

Figure 4.8a below shows the data for 5% CMC pumped through the 60, 80, 150 and 200mm diameters pipes (pseudo shear diagram) and the rheological model fits to the 5% CMC laminar data is presented in Figure 4.8b.

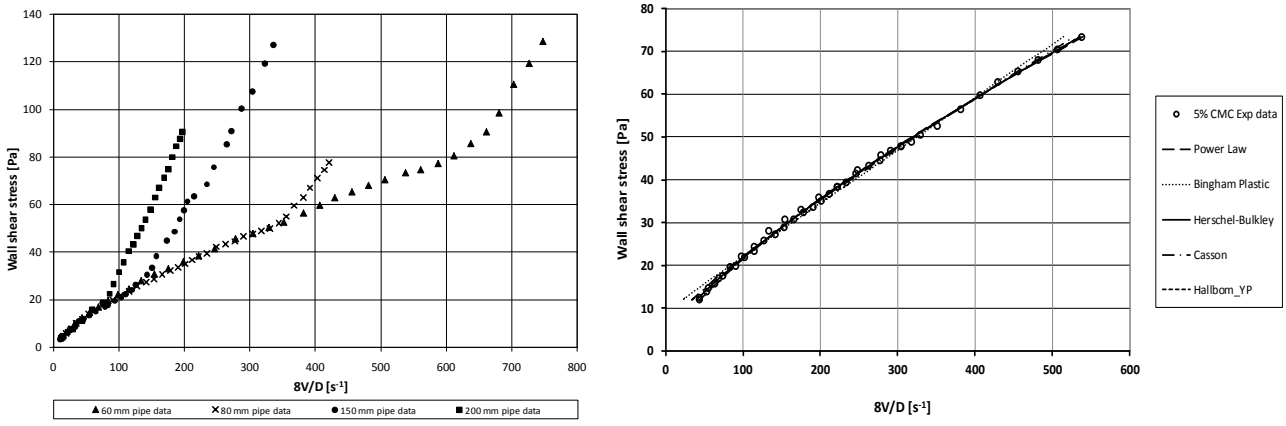

(a) (b)

Figure 4.8 (a) Pseudo shear diagram and (b) rheological model fits to 5% CMC laminar data

5% CMC represents pseudoplastic behaviour in laminar flow. Laminar data coincides well for all pipe sizes, and turbulent flow data is obtained in each pipe diameter. The derived rheological constants for each model are tabulated in Table 4.8. The goodness of each model fit to the laminar data was represented and ranked by the RMSE values [Eq. (3.1)].

Table 4.8 Rheological model constants for 5% CMC

Model	Rheological Constants			RMSE	Ranking
	τ_y	K	n		
Herschel-Bulkley	1.9	0.511	0.776	4.3	2
Bingham Plastic	7.4	0.124		10.1	5
Power law	-	0.705	0.728	4.7	3
	τ_C	η_C			
Casson	2.3	0.0884		5.2	4
	τ_0	μ_∞	k		
Hallbom_YP	0.1	0.0388	0.221	4.2	1

4.4.3 8% CMC

Figure 4.9a shows the test data for 8% CMC tested in the 42, 52, 63 and 150mm pipe diameters (pseudo shear diagram). From this diagram, it is clear that turbulent flow was not obtained in the 42, 52 and 63mm diameter pipes, due to pumping limitations for this material. The laminar data of the 42 and 52mm pipe diameters were used for rheological characterisation and the turbulent flow data from the 150mm pipe diameter only was compared with transitional and turbulent flow predictions. Figure 4.9b shows the rheological model fits to the 8% CMC laminar data.

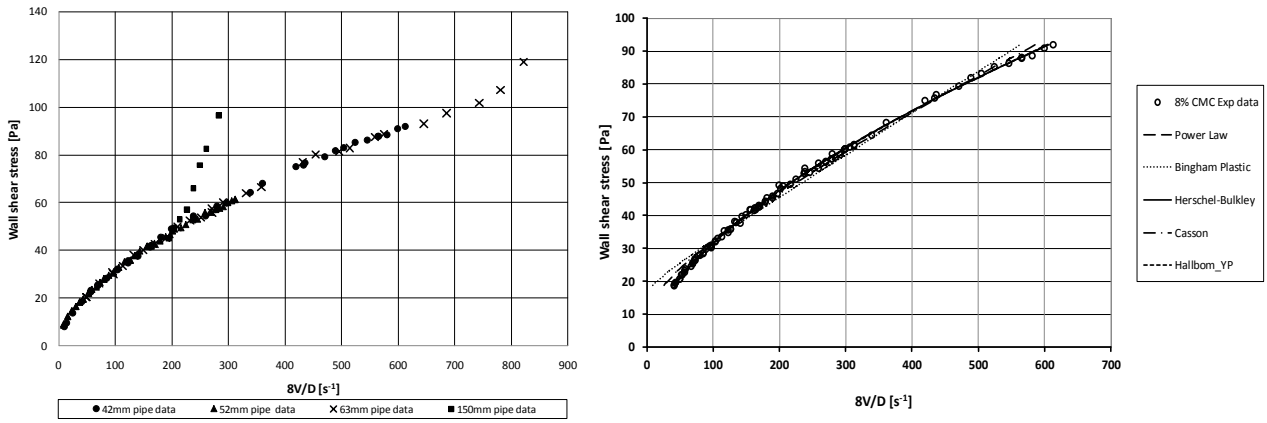

(a) (b)

Figure 4.9 (a) Pseudo shear diagram and (b) rheological model fits to 8% CMC laminar data

The derived rheological constants for each model are tabulated in Table 4.9. The goodness of each model fit to the laminar data was represented and ranked by the RMSE values [Eq. (3.1)].

Table 4.9 Rheological model constants for 8% CMC

Model	Rheological Constants			RMSE	Ranking
	τ_y	K	n		
Herschel-Bulkley	0.0	1.871	0.593	4.8	2
Bingham Plastic	15.2	0.127	-	18. 7	5
Power law	-	1.871	0.593	4.7	1
	τ_C	η_C			
Casson	6.9	0.0742	-	9.9	4
	τ_0	μ_∞	k		
Hallbom_YP	0.002	0.0005	0.089	4.9	3

4.4.4 Summary – model fits to CMC data

CMC is known as a material that has no yield stress, but degree of rheogram curvature. It is a typical pseudoplastic material known to be best characterised by the power law model.

Best fitting model

In this work, 3% and 8% concentrations of CMC were best modelled using the power law rheological model, based on the RMSE values shown in Table 4.7 to Table 4.9. The Herschel-Bulkley model gave identical results as it reduced to the power law in the curve fitting process, as expected in the absence of yield stress (Slatter, 1994). Interestingly, for the 5% CMC laminar flow data the Herschel-Bulkley and Hallbom yield plastic models are almost identical, yielding slightly better RMSE values than the power law model fit, so any of these models could be used. The power law model was taken as the representative rheological model for the 5% CMC solution. The least appropriate model for characterising the CMC material was the Bingham plastic model, due to its incorporation of a yield stress and lack of curvature.

4.5 Force fitted rheological models

The three test materials used in this study (kaolin, bentonite and CMC) can be characterised using the Herschel-Bulkley, Bingham Plastic and power law rheological models respectively. It has been shown in the literature (see Section 2.1.9) that models which are not necessarily the best fit to a set of laminar flow data can be used to characterise a material to a certain degree of accuracy by forcing a fit. This is demonstrated by Slatter (1994) and for example by considering Figure 4.9 and Table 4.9 for the 8% CMC of this work, where the differences in the fit between the forced Bingham plastic model fit and the more appropriate power law model are clear. The effect of force fitting rheological models is evaluated in Chapter 5 when considering transitional and turbulent predictions.

4.6 Effect of concentration

Laminar flow results from the three concentrations of kaolin tested were used to investigate the effect of concentration on the rheological parameters (τ_y, K, n) of the Herschel-Bulkley, Bingham plastic and power law models. Increasing the concentration of the suspension results in an increase in viscous stresses among particles, hence increased laminar wall shear stresses, for a given (laminar) flow rate. This effect is shown in Figure 4.10 in which test data for the three concentrations of kaolin from the same diameter 150mm pipe are shown. In turbulent flow the inertial forces are dominant, thus there is no significant increase in wall shear stress (Slatter, 1994) and the turbulent data for each concentration tend to converge with increasing flow rate.

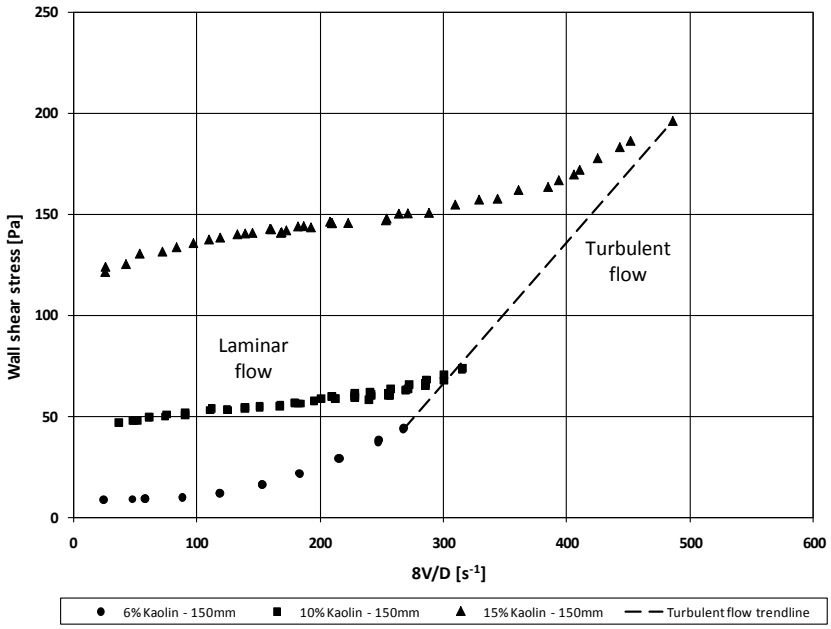

Figure 4.10 Effect of concentration on wall shear stress of a kaolin slurry in a diameter 150mm pipe

Table 4.10 Effect of concentration on rheological parameters of HB, BP and PL models

Model	Concentration	Rheological Constants		
		τ_y	*K*	*n*
Herschelle-Bulkley	6%	3.9	0.502	0.361
	10%	27.4	3.959	0.312
	15%	61.6	25.908	0.184
Bingham Plastic	6%	6.3	0.00443	1
	10%	43.2	0.0213	1
	15%	124.1	0.0296	1
Power Law	0%	0.0	0.00089	1.000
	6%	0.0	2.797	0.182
	10%	0.0	22.229	0.147
	15%	0.0	75.408	0.1033

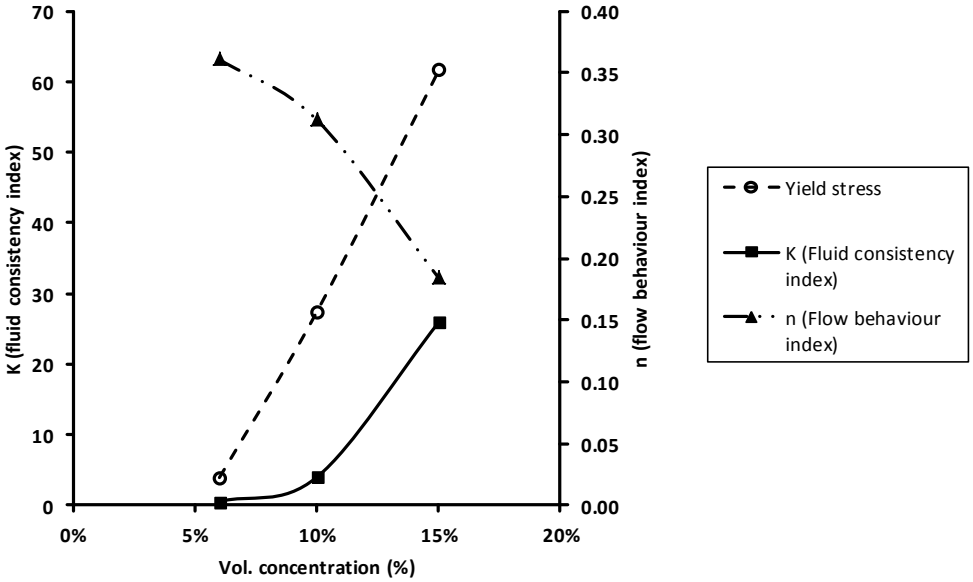

Figure 4.11 Effect of concentration on HB rheological parameters of kaolin

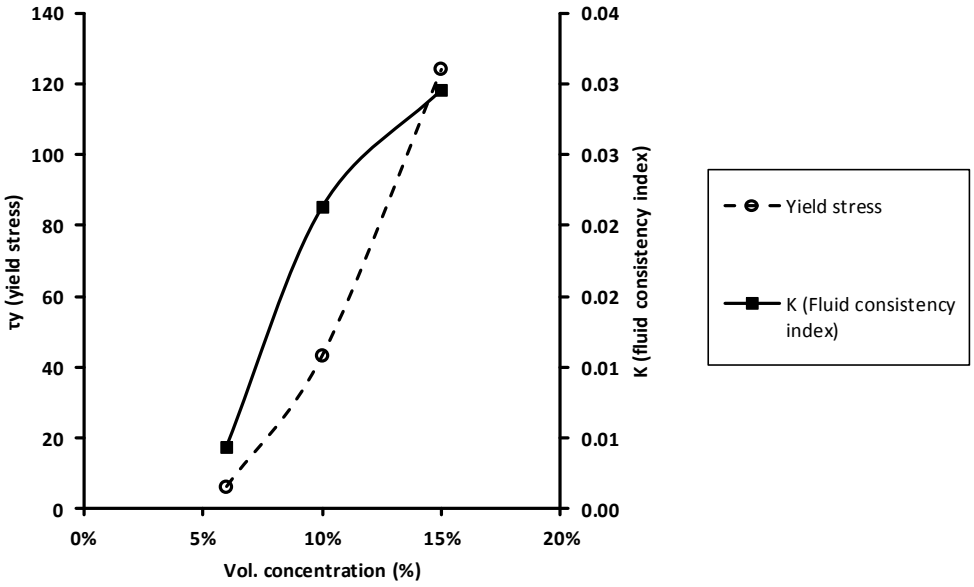

Figure 4.12 Effect of concentration on BP rheological parameters of kaolin

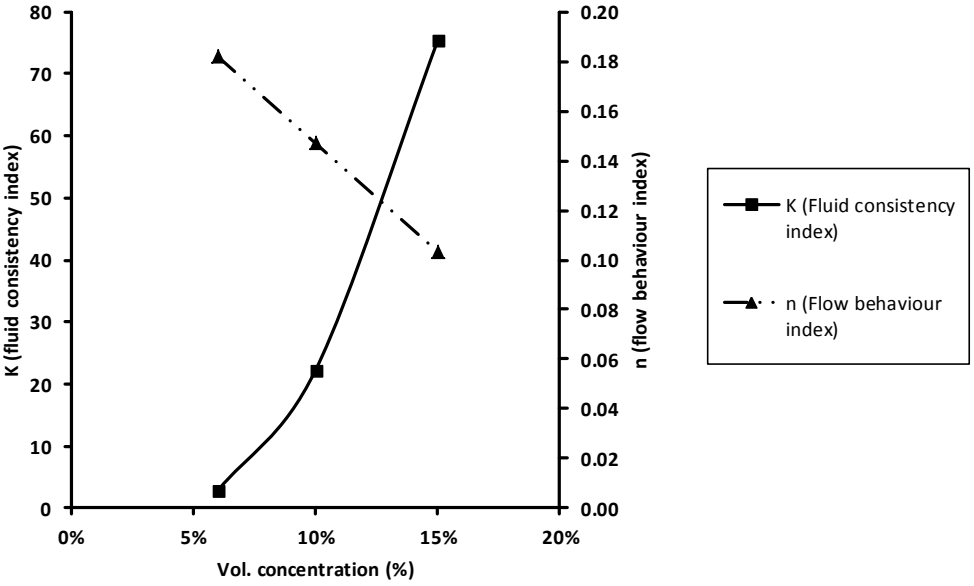

Figure 4.13 Effect of concentration on PL rheological parameters of kaolin

An increase in concentration of a non-Newtonian material has a significant effect on its rheological constants, as illustrated in Figure 4.11 to Figure 4.13 for the Herschel-Bulkley, Bingham plastic and power law models. In this case the fluid consistency index (*K*) increases significantly with an increase in concentration and the flow behaviour index (*n*) gradually decreases from 1. These trends are in line with the findings of Metzner (1956), Vlasak & Chara (1999), Chhabra & Richardson (2008) and Litzenberger & Sumner (2004), as discussed in Section 2.1.11.

4.7 Conclusion

The pipe test data has been presented on pseudo-shear diagrams for all material test concentrations. Turbulent flow was not reached in some of the smaller test pipe diameters, but this did not prove to be

a significant problem as the small pipe data is needed for rheological characterisation which requires only laminar flow data. Laminar data for each test material was extracted for rheological characterisation. The nominal wall shear rate for each test ranged from a practical minimum of $40s^{-1}$ to the highest attainable shear rate in laminar flow. In doing the rheological characterisation the RMSE as per Kelessidis & Maglione (2006) was used to assess goodness of fit. Considering this together with simplistic engineering design requirements (number of fitted parameters in model) suggested that the Herschel-Bulkley, power law and Bingham plastic rheological models best characterised the kaolin, CMC and bentonite test materials respectively. Note though that on the same basis some of the other rheological models also closely fitted the data and could just as well have been chosen. The rheological model parameters are sensitive to changes in concentration of the material. The effect of concentration on the parameters has been discussed and graphically illustrated using one of the kaolin materials as an example. No temperature effects on rheology were observed and it was concluded that for the tests of this work the small changes in temperature over the duration of each test had a negligible effect on the material rheology. The derived rheological parameters were used for the prediction of laminar, transitional and turbulent flow, for comparison with measured turbulent data in the cases in which experimental turbulent pipe flow was achieved. These predictions are presented and discussed in Chapter 5.

Chapter 5 Results and discussion - Pipe flow predictions

This chapter presents the analysis of the pipe test results and predictions of the pumping characteristics of all test materials in laminar, transitional and turbulent flow. The different prediction techniques are compared for each rheological model, material concentration and pipe size. The results are presented graphically as plots of (τ_0) vs. (*8V/D*) and discussed. Each prediction was evaluated by calculating the average percentage difference from the experimental data.

5.1 Laminar flow

This section presents the results and discussion of the laminar flow data analysis for the different rheological models. For each pipe test laminar data from at least two of the smaller pipes were used for rheological characterisation, but the test data of all the pipes i.e. including the larger pipe size data are included for comparison with the fitted models. In some pipe tests all the pipe data (including the larger diameter pipes) were used for rheological characterisation in which case no differentiation is made between smaller and larger diameters. In laminar flow there is no prediction as such, just the fitting of the data to the different rheological models, which simply reproduces the data in accordance with the goodness of the original fit.

5.1.1 Kaolin

Figure 5.1 presents the data, fits for all models and the average errors (in %) [Eq. (3.2)], for the laminar flow of all the kaolin concentrations.

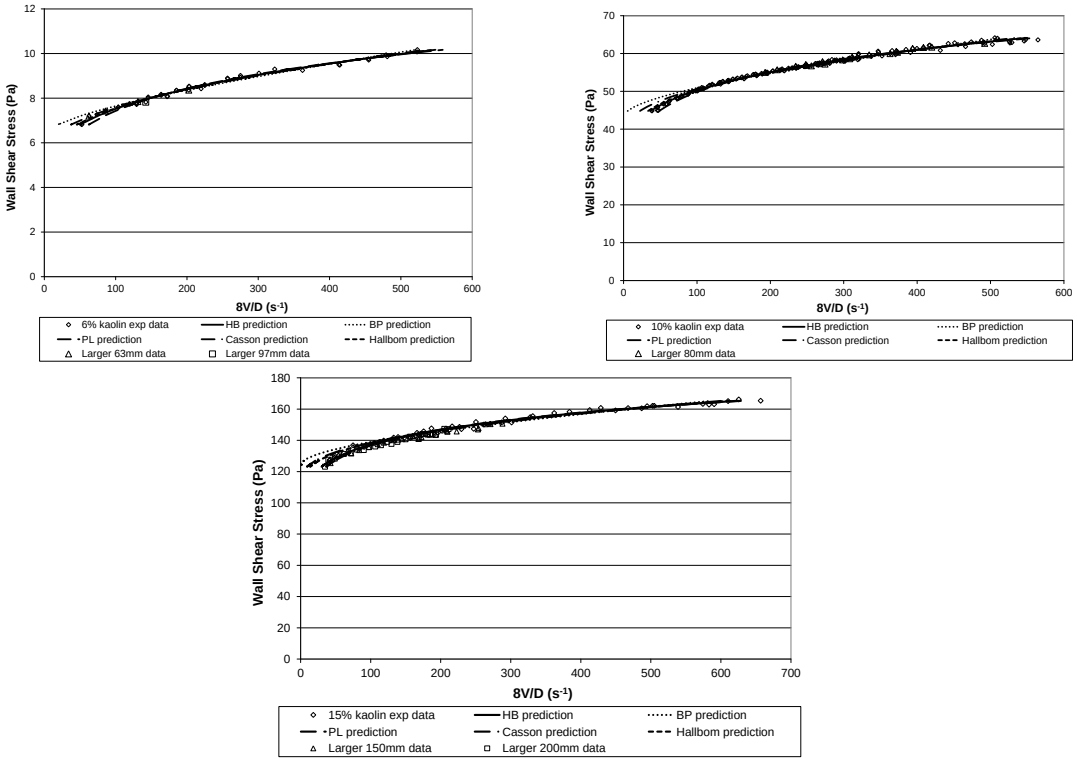

KAOLIN	HB	BP	PL	CASS	HALB
6%	4.776	10.518	6.652	6.200	4.966
10%	3.480	10.660	5.062	6.315	4.011
15%	8.737	20.258	9.126	14.246	13.431

Figure 5.1 6%, 10% and 15% kaolin laminar pipe flow predictions and average % error – all rheological models

The fits plotted in Figure 5.1 show close agreement between all models and the experimental data. Based on the average % error value, the Herschel-Bulkley model best fits the laminar data of the kaolin. The Bingham plastic model is the least accurate due to the inability of this model to adapt to the shear thinning property (rheogram curvature) of the kaolin slurry, especially in the lower shear rate range. If the lower shear rate range is excluded (take the minimum as say 200s^{-1}, more representative of practical pumping) then even by visual inspection of Figure 5.1 it is clear that there is very little difference between the five proposed models.

5.1.2 Bentonite

The results for the laminar flow predictions of all bentonite concentrations are presented in Figure 5.2, including data from the larger diameter 150mm pipe for the 7.34% concentration. All rheological model predictions were evaluated by calculating the average % error and the results are shown in the table in Figure 5.2.

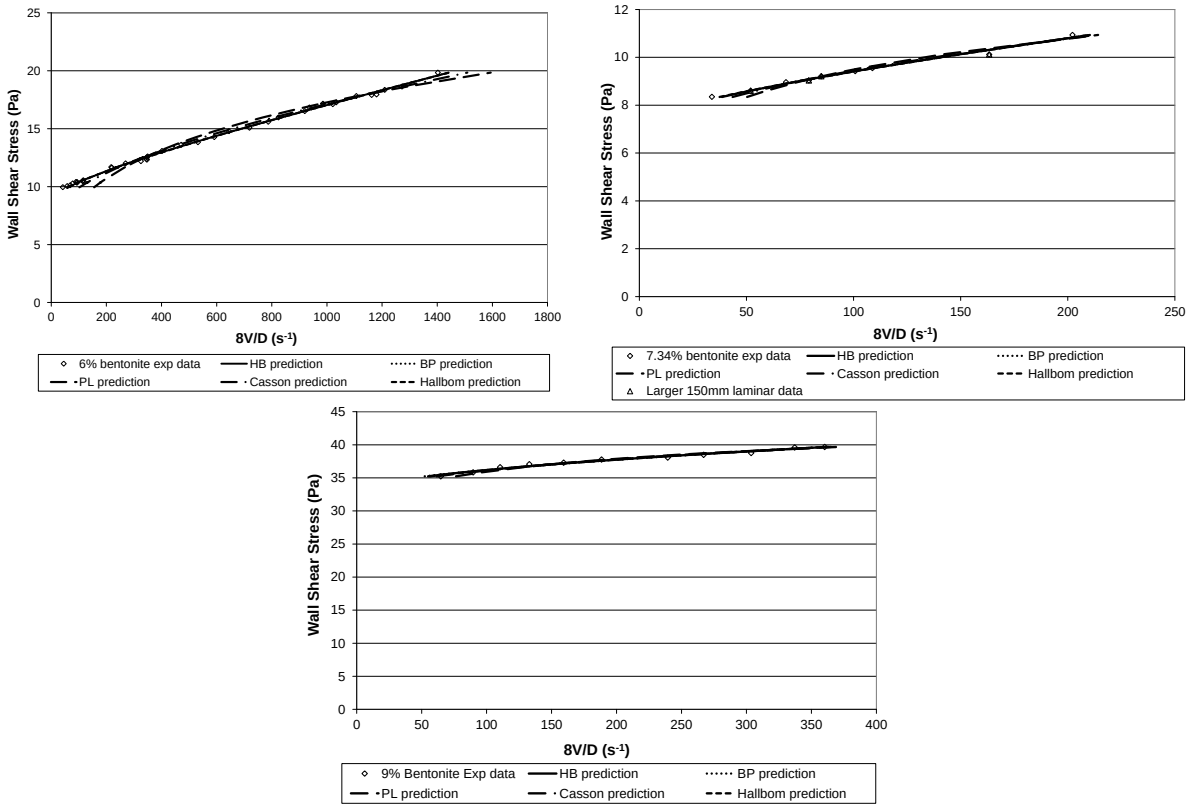

BENTONITE	HB	BP	PL	CASS	HALB
6%	5.464	5.465	36.531	17.900	4.867
7.34%	4.310	4.310	11.349	7.126	4.088
9%	7.676	8.156	8.498	6.478	7.404

Figure 5.2 6%, 7.34% and 9% bentonite laminar pipe flow predictions and average % error – all rheological models

The Bingham plastic, Herschel-Bulkley, and Hallbom yield plastic model predictions all agree well with the bentonite data, and all are similar to each other, as seen by the almost equal deviations from the experimental values for these three models. The Herschel-Bulkley and Hallbom models reduce exactly to the Bingham plastic model for n = 1 and k = 1 respectively. The power law and Casson models predict the bentonite laminar flow data less well, particularly for the 6% and 7.34% concentrations. The main reason for this is the rheogram curvature for shear thinning materials which these two models include,

but is not present in the laminar bentonite data. Additionally the power law model does not include a yield stress, which bentonite is known to exhibit.

5.1.3 CMC

The results for the laminar predictions of all the CMC solutions are presented in Figure 5.3, and the average % error for each model presented in the table. For the 3% and 5% concentrations the data for the diameter 150mm (3%) and 150mm and 200mm (5%) are included in Figure 5.3 for comparison with the rheological model predictions.

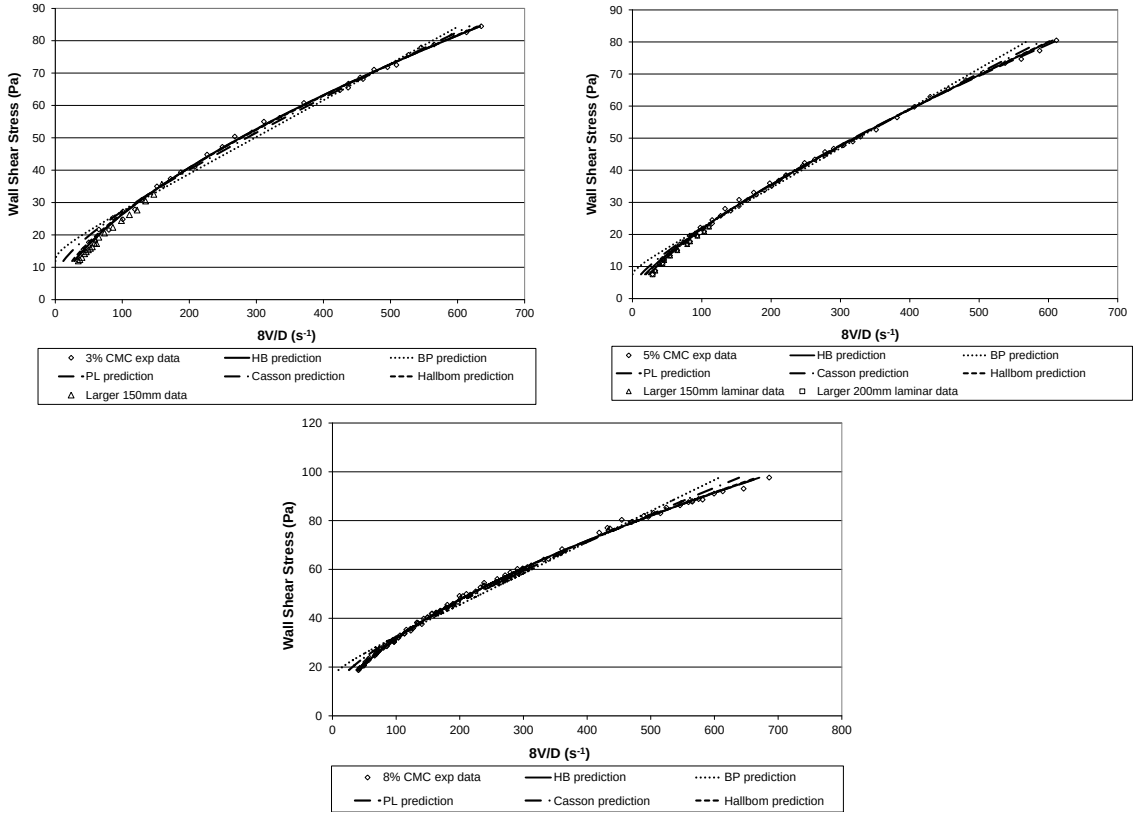

CMC	HB	BP	PL	CASS	HALB
3%	6.195	26.271	6.195	15.977	7.915
5%	4.543	14.017	3.275	7.561	4.329
8%	1.992	13.066	1.992	6.742	2.169

Figure 5.3 3%, 5% and 8% CMC laminar pipe flow predictions and average % error – all rheological models

As shown in Figure 5.3 good agreement is found between the laminar pipe flow predictions for CMC using the power law, Herschel-Bulkley and Hallbom models. Based on the value of the average % error across all concentrations, the power law is most suited for the laminar prediction of CMC slurries, as expected. The Herschel-Bulkley model and the Hallbom model converge to the power law model.

The Bingham plastic is the least suitable model to predict laminar pipeflow for a CMC slurry. It shows the highest average percentage error for all concentrations as illustrated in the table in Figure 5.3, whilst the underprediction of the nominal wall shear rate in the higher and lower shear rate domain is significant. Predictions using the Casson model also show quite significant deviation from the experimental values. The curvature which the Casson model does incorporate results in a slightly better prediction than the Bingham plastic model.

5.1.4 Laminar flow conclusion

Based on the analysis of the laminar flow predictions it is evident that little difference exists between the predictions from the models over the shear rate range ($40s^{-1}$ to $1000s^{-1}$). The rheological models which best predicted the laminar flow of the materials considered were those which are known to describe a particular material best, such as the Herschel-Bulkley rheological model for kaolin, the Bingham plastic rheological model for bentonite and the power law rheological model for CMC. This conclusion was based on the errors for each prediction (difference between experimental and calculated values). Although some instances occur where other models appear to fit the experimental data slightly more accurately (such as the Casson and Hallbom models for bentonite slurries) extensive use of these models is not apparent in the literature.

5.2 Transitional flow

The analysis of the transitional flow results are presented and discussed in this section. Results are presented graphically as critical velocity (V_c) vs. internal pipe diameter (D). This method reveals the strengths and weaknesses of the various transition techniques, indicates the behavioural change between small and larger pipe diameters and is of practical use in slurry pipeline design. Graphs are presented for all the transition techniques using each rheological model (if possible) and the data is evaluated by comparing each experimental V_c value to the predicted values. An absolute percentage error for each prediction is tabulated for the purpose of evaluation, comparison and discussion. As stated previously, each transitional velocity prediction technique is evaluated against an experimental transitional velocity taken as the last laminar data point in the test pipe data set. No claim is made that this is the absolute transitional velocity. It is widely accepted that transition occurs over a Reynolds number range. It was done this way for consistency and to prevent bias. Recommendations as to the best transitional flow prediction technique and rheological model combination to use are based on absolute error values as well as consistency of predictions across all concentrations and pipe sizes.

The results of the analysis are presented for each test material as follows; first one technique is applied using all the rheological models to emphasise the effect the rheological model on a particular technique and to identify which rheology is best suited to a particular technique for a specific test material. Secondly the most successful rheological model is then applied to all techniques and plotted against experimental data to identify which technique and rheology combination best suits a specific test material.

5.2.1 Kaolin

The transitional results for all kaolin test concentrations are discussed here, but only the 6% results presented as similar observations were made for the other concentrations. The results for the 10% and 15% test concentrations can be found in Appendix E. Conclusions are, however, based on the results of all three test concentrations in all pipe sizes. Error values for the predictions were determined from experimental V_c values obtained in three pipe diameters. Calculated V_c values for two additional pipe diameters (40mm and 350mm) are included to get a better idea of the trend of the prediction techniques.

One technique plotted for all rheologies

Transitional velocities are first presented for each prediction technique individually, using each rheological model. The results of the predictions are presented graphically as V_c vs. D and compared to the experimental data.

Slatter

Figure 5.4 presents the V_c predictions and average errors (in %) for the Slatter technique in all pipe sizes using each rheology.

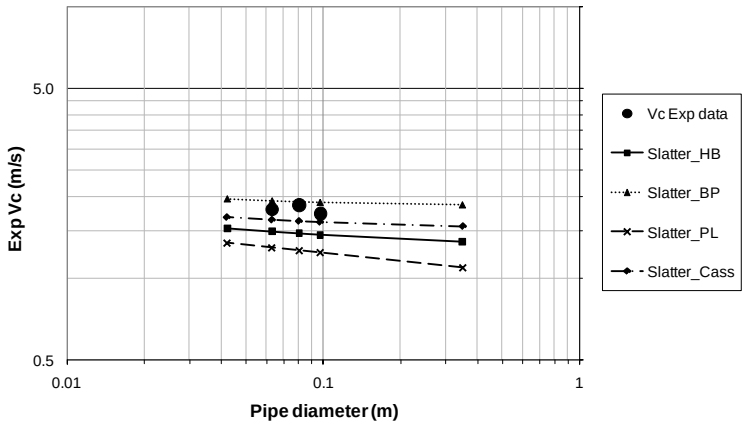

Diameter	Critical velocity (Exp) m/s	Vc Error values - SLATTER Re3 HB m/s	BP m/s	PL m/s	CASS m/s
350mm		1.363	1.868	1.097	1.558
100mm	1.728	1.446	1.907	1.247	1.616
		-16.3%	10.3%	-27.8%	-6.5%
80mm	1.864	1.462	1.917	1.271	1.628
		-21.5%	2.9%	-31.8%	-12.6%
63mm	1.794	1.484	1.932	1.302	1.647
		-17.3%	7.7%	-27.4%	-8.2%
40mm		1.525	1.965	1.356	1.684
	Ave	-18.4%	7.0%	-29.0%	-9.1%

Figure 5.4 Transitional velocity and average % error for 6% kaolin using the Slatter technique – all rheologies

From Figure 5.4 it is clear that the power law rheology is inappropriate in predicting transitional velocity for 6% kaolin, as it greatly underpredicts the value of V_c and does not approach a horizontal asymptote for larger pipe diameters. The Herschel-Bulkley, Bingham plastic and Hallbom rheologies (which all include a yield stress) seem to approach a horizontal asymptote as describe by Slatter (1997a). This is in line with the conclusion of Slatter (1997a) that the approaching of a horizontal asymptote by his techniques is due to the incorporation of the yield stress. The most accurate predictions are based on the Bingham plastic rheology, closely followed by the Casson rheology. Although the Herschel-Bulkley model best describes the 6% kaolin slurry in laminar flow it surprisingly results in underprediction of the transitional velocity when using Slatter's method.

Metzner & Reed

Figure 5.5 presents the V_c predictions and average errors (in %) for the Metzner & Reed technique in all pipe sizes using each rheology.

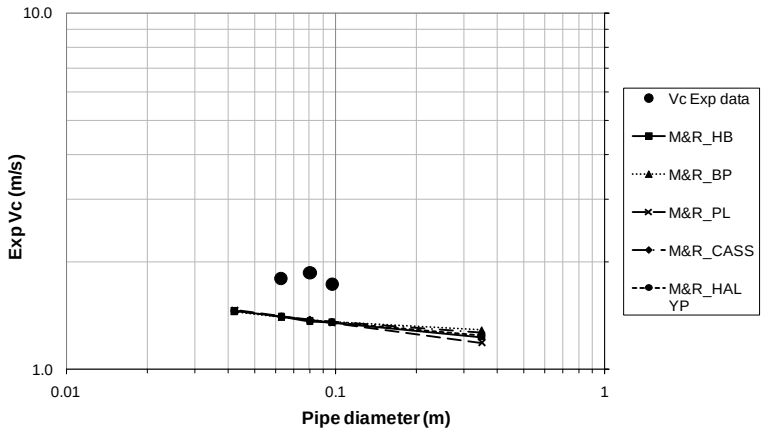

Diameter	Critical velocity (Exp) m/s	Vc Error values - M&R				
		HB m/s	BP m/s	PL m/s	CASS m/s	HAL_YP m/s
350mm		1.231	1.290	1.183	1.262	1.243
100mm	1.728	1.352	1.360	1.345	1.356	1.354
		-21.8%	-21.3%	-22.2%	-21.5%	-21.7%
80mm	1.864	1.363	1.376	1.371	1.376	1.375
		-26.9%	-26.1%	-26.5%	-26.2%	-26.2%
63mm	1.794	1.404	1.401	1.404	1.403	1.404
		-21.7%	-21.9%	-21.7%	-21.8%	-21.7%
40mm		1.460	1.452	1.462	1.457	1.458
	Ave	-23.5%	-23.1%	-23.5%	-23.2%	-23.2%

Figure 5.5 Transitional velocity and average % error for 6% kaolin using the Metzner & Reed technique – all rheologies

The Metzner & Reed technique significantly underpredicts V_c for the kaolin data and is quite insensitive to material rheology. At diameters below 100mm there is excellent agreement between all the rheologies, so for these diameters any rheological model could be used if this technique is preferred. Average errors are in the range of 16.5% to 23.5% for all concentrations using any rheology. As the pipe size increases, the effect of yield stress on V_c becomes more significant (Slatter, 1997a) and discrepancies between the models become more apparent. The predicted value of V_c when using the yield stress rheological models does seem to be tending towards an asymptote.

Generalised Reynolds number

Figure 5.6 presents the V_c predictions and average errors (in %) for the generalised Reynolds number approach in all pipe sizes using each rheology.

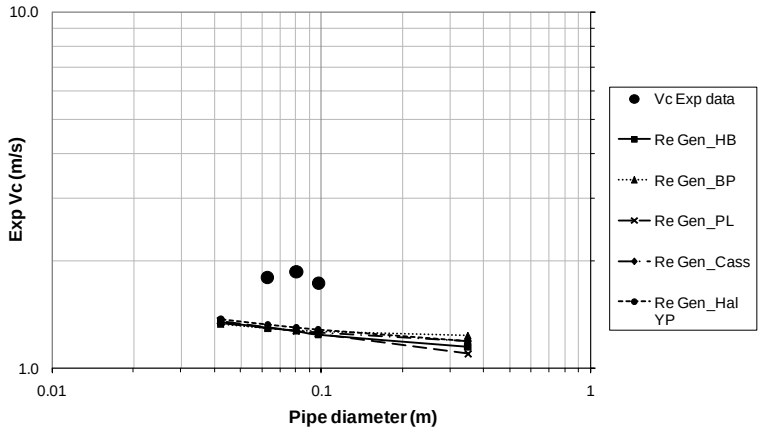

Diameter	Critical velocity (Exp) m/s	Vc Error values - Generalised Re				
		HB m/s	BP m/s	PL m/s	CASS m/s	HAL_YP m/s
350mm		1.148	1.236	1.097	1.189	1.191
100mm	1.728	1.242	1.268	1.247	1.259	1.283
		-28.1%	-26.6%	-27.8%	-27.2%	-25.8%
80mm	1.864	1.272	1.277	1.271	1.274	1.301
		-31.7%	-31.5%	-31.8%	-31.6%	-30.2%
63mm	1.794	1.299	1.292	1.302	1.296	1.326
		-27.6%	-27.9%	-27.4%	-27.7%	-26.1%
40mm		1.348	1.328	1.356	1.340	1.373
	Ave	-29.2%	-28.7%	-29.0%	-28.8%	-27.3%

Figure 5.6 Transitional velocity and average % error for 6% kaolin using the generalised Reynolds number approach – all rheologies

V_c predictions using the generalised Reynolds number approach are similar to those using the Metzner & Reed criterion. Again using the Bingham plastic model gives the best predictions for larger pipe diameters, but the Hallbom rheology is minimally better for the smaller pipe diameters. For smaller pipe diameters (say < 100mm) any of the rheologies can be used. However, the technique is still not suitable for predicting transition for kaolin materials. The generalised Reynolds number approach predicts transitional velocities slightly worse than for the Metzner & Reed criterion, with error values in the range 27% to 28%.

Hedström intersection method

Figure 5.7 presents the V_c predictions and average errors (in %) for the Hedström intersection method in all pipe sizes using each rheology.

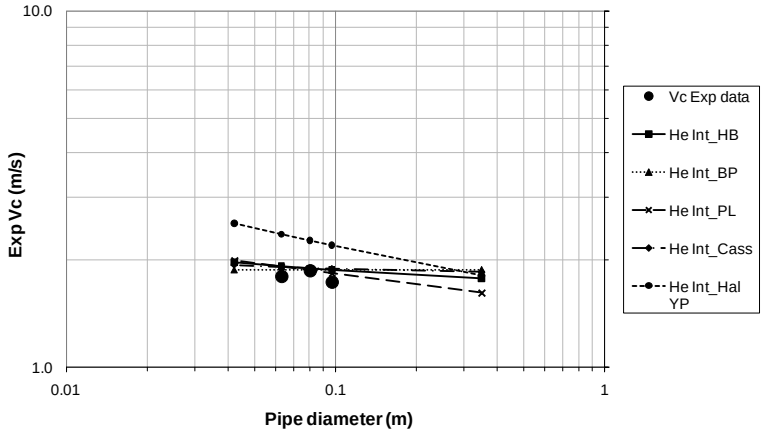

Diameter	Critical velocity (Exp) m/s	Vc Error values - He Intersection				
		HB m/s	BP m/s	PL m/s	CASS m/s	HAL_YP m/s
350mm		1.773	1.878	1.613	1.847	1.806
100mm	1.728	1.874	1.872	1.834	1.886	2.201
		8.4%	8.3%	6.1%	9.1%	27.3%
80mm	1.864	1.893	1.871	1.869	1.894	2.270
		1.6%	0.4%	0.3%	1.7%	21.8%
63mm	1.794	1.920	1.871	1.916	1.907	2.366
		7.0%	4.3%	6.8%	6.3%	31.9%
40mm		1.970	1.874	1.995	1.932	2.540
	Ave	5.7%	4.3%	4.4%	5.7%	27.0%

Figure 5.7 Transitional velocity and average % error for 6% kaolin using the Hedström intersection method – all rheologies

The Hedström intersection method predicts V_c successfully, with good agreement observed between the rheologies except for the yield plastic rheology, which significantly overpredicts the transitional velocity and does not approach a horizontal asymptote. Predictions using the Bingham plastic rheology are the most accurate, but show an almost horizontal trend. The power law model also does not approach a horizontal asymptote, but shows accurate predictions for the three pipe sizes, almost identical to those for Bingham plastic. Similar error values are obtained for the Herschel-Bulkley and Casson rheology predictions although they have very different trends. The results obtained for the different techniques are similar in the diameter range tested here, but can vary significantly for smaller or larger diameters. This intersection criterion takes the velocity at which the Wilson & Thomas turbulent curve (also a prediction) and the laminar curve (a fit) intersect, and so is highly dependent on the quality of those approximations.

Ryan & Johnson criterion

Figure 5.8 presents the V_c predictions and average % error for the Ryan & Johnson criterion in all pipe sizes using each rheology.

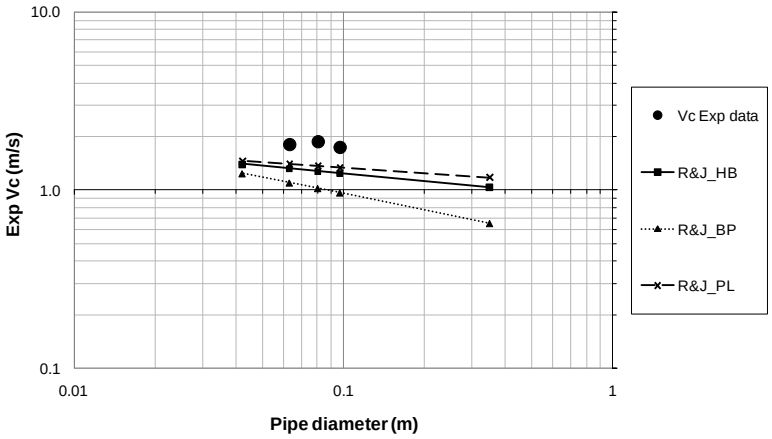

Diameter	Critical velocity (Exp) m/s	Vc Error values - R&J HB m/s	BP m/s	PL m/s
350mm		1.039	0.646	1.176
100mm	1.728	1.242	0.964	1.338
		-28.1%	-44.2%	-22.6%
80mm	1.864	1.276	1.021	1.363
		-31.5%	-45.2%	-26.8%
63mm	1.794	1.321	1.098	1.397
		-26.4%	-38.8%	-22.1%
40mm		1.400	1.238	1.455
	Ave	-28.7%	-42.7%	-23.9%

Figure 5.8 Transitional velocity and average % error for 6% kaolin using the using Ryan & Johnson criterion – all rheologies

The Ryan and Johnson criterion is probably the most sophisticated of the techniques presented as it incorporates specific details of the yield stress using a stability function approach and it also acknowledges plug flow theory. It is thus surprising that transitional velocity predictions do not approach the horizontal asymptote using any of the rheological models in the criterion. In this case using the Bingham plastic rheology results in worse predictions than the Herschel-Bulkley or power law rheologies. For this technique using the power law rheology gives the closest predictions, but with a 23% average error it is not regarded as reliable. The criterion significantly underpredicts the experimental transitional velocities for all rheologies.

Newtonian Approximation

Figure 5.9 presents the V_c predictions and average error (in %) for the Newtonian approximation technique in all pipe sizes using each rheology.

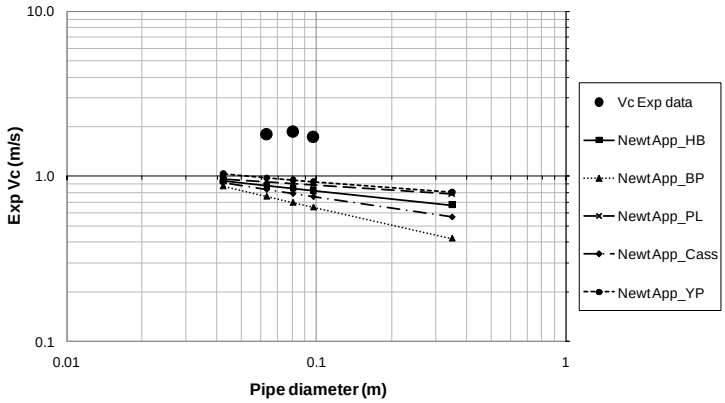

Diameter	Critical velocity (Exp) m/s	Vc Error values - Newt Approx				
		HB m/s	BP m/s	PL m/s	CASS m/s	HAL_YP m/s
350mm		0.669	0.420	0.782	0.566	0.797
100mm	1.728	0.820	0.650	0.889	0.750	0.922
		-52.5%	-62.4%	-48.6%	-56.6%	-46.6%
80mm	1.864	0.846	0.695	0.906	0.783	0.945
		-54.6%	-62.7%	-51.4%	-58.0%	-49.3%
63mm	1.794	0.880	0.757	0.929	0.829	0.976
		-50.9%	-57.8%	-48.2%	-53.8%	-45.6%
40mm		0.941	0.874	0.967	0.912	1.033
	Ave	-52.7%	-61.0%	-49.4%	-56.1%	-47.2%

Figure 5.9 Transitional velocity and average % error for 6% kaolin using the Newtonian approximation technique – all rheologies

The Newtonian approximation technique significantly underpredicts the critical velocity of the kaolin slurry when used with all the rheological models. The technique shows errors of between 47% and 60% for the 6% concentration even though the viscosity is evaluated at the appropriate wall shear stress value. This is due to the fact that the Newtonian approximation ignores the details of how the yield stress influences the transition i.e. the existence of the unsheared plug is ignored. There is a noticeable similarity between the results produced by the Newtonian approximation and the Ryan & Johnson technique, in that both techniques underpredict V_c, using power law rheology gives the most accurate results and using the Bingham plastic rheology gives the worst results. None of the predictions showed any tendency towards a horizontal asymptote as pipe diameter increased.

Torrance

Figure 5.10 presents the V_c predictions and average error (in %) for the Torrance criterion in all pipe sizes using each rheology.

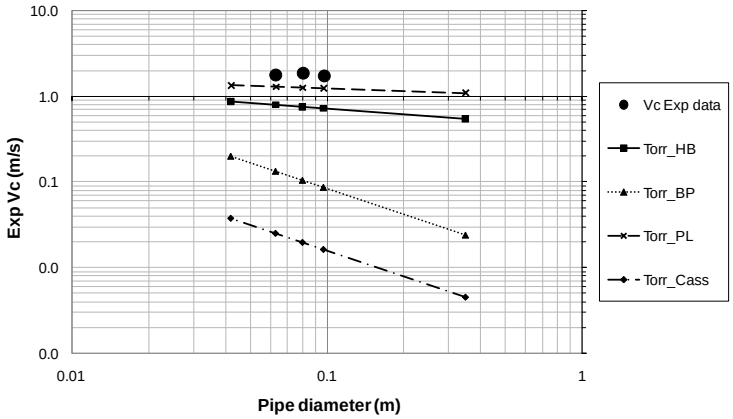

Diameter	Critical velocity (Exp) m/s	Vc Error values - Torrance			
		HB m/s	BP m/s	PL m/s	CASS m/s
350mm		0.547	0.024	1.097	0.005
100mm	1.728	0.725	0.087	1.247	0.016
		-58.0%	-95.0%	-27.8%	-99.1%
80mm	1.864	0.756	0.105	1.271	0.020
		-59.4%	-94.4%	-31.8%	-98.9%
63mm	1.794	0.798	0.134	1.302	0.025
		-55.5%	-92.5%	-27.4%	-98.6%
40mm		0.872	0.201	1.356	0.038
	Ave	-57.7%	-93.9%	-29.0%	-98.9%

Figure 5.10 Transitional velocity and average % error for 6% kaolin using the Torrance criterion – all rheologies

The Torrance criterion gives poor predictions of the transitional velocity for kaolin for all rheologies, again due to not incorporating yield stress. In this case the power law rheology resulted in the smallest average error of 29% over the pipe sizes tested, but this is not acceptable for engineering design.

Hallbom

Figure 5.11 presents the V_c predictions and average error (in %) for the Hallbom technique in all pipe sizes using each rheology.

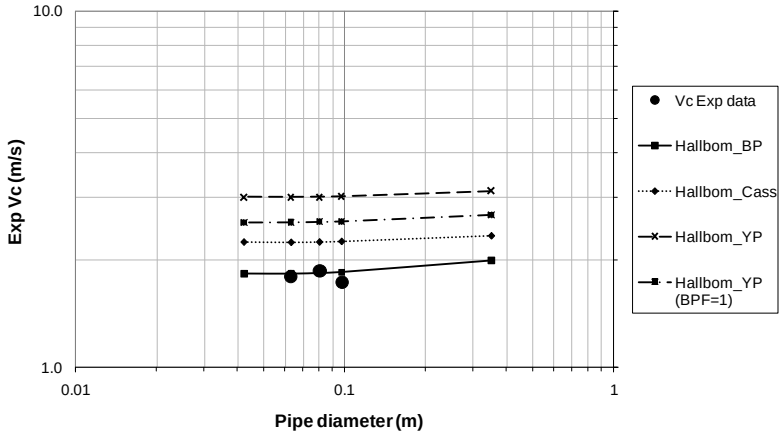

Diameter	Critical velocity (Exp) m/s	Vc Error values - Hallbom Trans			
		BP m/s	CASS m/s	HAL_YP (BPF=1.3) m/s	HAL_YP (BPF=1) m/s
350mm		1.994	2.335	3.126	2.671
100mm	1.728	1.846	2.256	3.012	2.564
		6.8%	30.5%	74.3%	48.3%
80mm	1.864	1.835	2.249	3.005	2.556
		-1.5%	20.7%	61.3%	37.2%
63mm	1.794	1.826	2.244	3.001	2.549
		1.8%	25.1%	67.3%	42.1%
40mm		1.828	2.248	3.004	2.547
	Ave	2.4%	25.4%	67.6%	42.5%

Figure 5.11 Transitional velocity and average % error for 6% kaolin using the Hallbom criterion – all rheologies

The Hallbom transition criterion shows interesting results for the kaolin predictions. For all rheologies except the Bingham plastic, the transitional velocity is greatly overpredicted. Hallbom based his criterion on the fact that transition is assumed to occur at a velocity where smooth wall turbulent flow friction factor is 130% of the laminar flow friction factor. The significant overprediction of the criterion in this case could be due to the over compensation of 30% on the friction factor. Reducing the BPF (break point factor = 1.3) to 1.0 reduced the values of the predicted transitional velocities, but they remained significantly high, as seen in Figure 5.11. Using the Bingham plastic rheology gave good agreement with experimental values of V_c for smaller diameter pipes, but as pipe diameter increased, so did the predicted value of V_c. This is in contrast to the expectation that V_c decreases with D and approaches a horizontal asymptote (Metzner & Reed, 1955; Slatter, 1997a). The technique cannot be regarded as reliable for predicting transitional velocities of kaolin slurries.

One rheology plotted for all techniques

Following the presentation and evaluation of the different V_c prediction techniques for each considered

rheology, the results are now presented in terms of the most successful rheological models for all techniques. Based on the results shown in Figure 5.4 to Figure 5.11, the most appropriate rheological model appeared to be the Bingham plastic, but only marginally so and largely due to it approaching a horizontal asymptote best as pipe diameter increased. This is surprising, as the Bingham plastic rheological model is the least representative of the kaolin 6% laminar data (see Table 4.1 to Table 4.3).
For pipe diameters < 100mm the choice of rheological model makes very little difference. The Ryan & Johnson, Torrance and Newtonian approximation techniques work best using the power law model, but with average error values of 23%, 29%, and 49% respectively for the 6% concentration, these techniques are unable to predict the transitional velocity. The rheological model which best fits the laminar data for this test concentration and which gave the most consistent results for all the transitional velocity prediction techniques was the Herschel-Bulkley model. Based on these findings, predictions using the Herschel-Bulkley and Bingham plastic rheologies are presented below for all techniques.

Herschel-Bulkley

Figure 5.12 presents the V_c predictions and average % error for the Herschel-Bulkley rheology in all pipe sizes using all techniques.

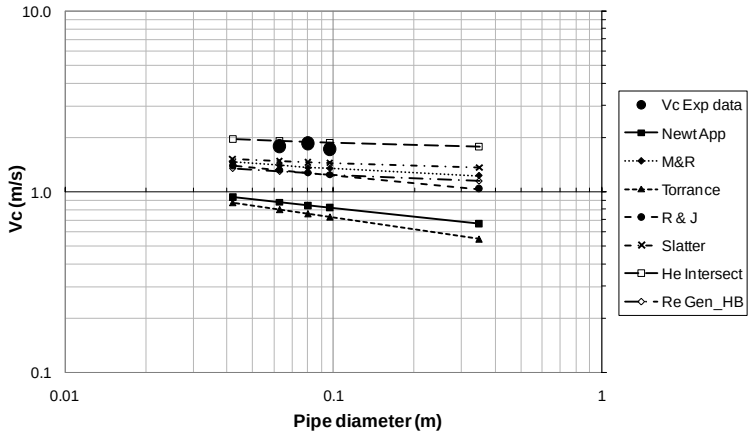

Diameter	Critical velocity (Exp) m/s	Critical velocity Error values - HB - All Techniques						
		Newt App m/s	M & R m/s	Torr/ Clapp m/s	Ryan & John m/s	Slatter m/s	Intersect	Re_Gen
350mm		0.669	1.231	0.547	1.039	1.363	1.773	1.148
100mm	1.728	0.820	1.352	0.725	1.242	1.446	1.874	1.242
		-52.5%	-21.8%	-58.0%	-28.1%	-16.3%	8.4%	-28.1%
80mm	1.864	0.846	1.363	0.756	1.276	1.462	1.893	1.272
		-54.6%	-26.9%	-59.4%	-31.5%	-21.5%	1.6%	-31.7%
63mm	1.794	0.880	1.404	0.798	1.321	1.484	1.920	1.299
		-50.9%	-21.7%	-55.5%	-26.4%	-17.3%	7.0%	-27.6%
40mm		0.941	1.460	0.872	1.400	1.525	1.970	1.348
	Ave	-52.7%	-23.5%	-57.7%	-28.7%	-18.4%	5.7%	-29.2%

Figure 5.12 Transitional velocity and average % error for 6% kaolin (Herschel-Bulkley rheology – all techniques)

Bingham Plastic

Figure 5.13 presents the V_c predictions and average % error for the Bingham plastic rheology in all pipe sizes using all techniques.

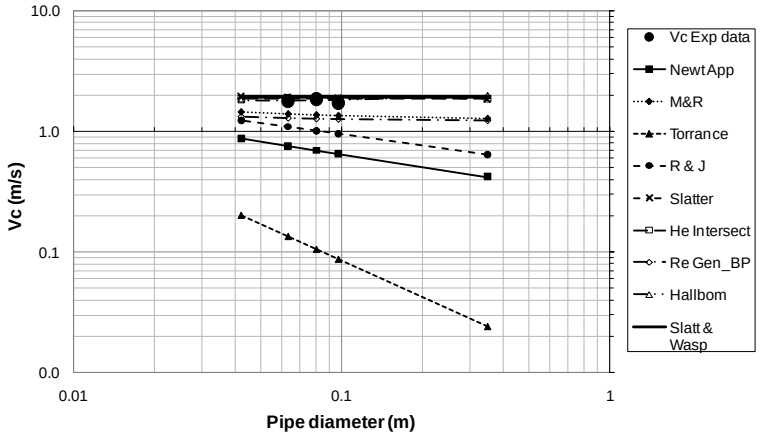

Diameter	Vc (Exp) m/s	Critical velocity Error values - BP - All Techniques								
		Newt App m/s	M & R m/s	Torr/ Clapp m/s	Ryan & John m/s	Slatter m/s	Intersect m/s	Re_Gen m/s	Hallbom m/s	S&W m/s
350mm		0.420	1.290	0.024	0.646	1.868	1.878	1.236	1.994	1.963
100mm	1.728	0.650	1.360	0.087	0.964	1.907	1.872	1.268	1.846	1.963
		-62.4%	-21.3%	-95.0%	-44.2%	10.3%	8.3%	-26.6%	6.8%	13.6%
80mm	1.864	0.695	1.376	0.105	1.021	1.917	1.871	1.277	1.835	1.963
		-62.7%	-26.1%	-94.4%	-45.2%	2.9%	0.4%	-31.5%	-1.5%	5.4%
63mm	1.794	0.757	1.401	0.134	1.098	1.932	1.871	1.292	1.826	1.963
		-57.8%	-21.9%	-92.5%	-38.8%	7.7%	4.3%	-27.9%	1.8%	9.5%
40mm		0.874	1.452	0.201	1.238	1.965	1.874	1.328	1.828	1.963
	Ave	-61.0%	-23.1%	-93.9%	-42.7%	7.0%	4.3%	-28.7%	3.4%	9.5%

Figure 5.13 Transitional velocity and average % error for 6% kaolin (Bingham plastic rheology – all techniques)

From Figure 5.12 and Figure 5.13 it is evident that the intersection method and the Slatter criterion produce reasonably accurate transitional velocity predictions for both the Bingham plastic and Herschel-Bulkley rheologies. The relative success of the Slatter model can be attributed to the incorporation of the yield stress. The intersection method showed good results for all rheologies, as seen in Figure 5.7 and is in line with results obtained by other researchers such as Xu *et al* (1993) and Slatter (1997a) in their work with kaolin slurries. Slatter (1997a) states that the intersection method yields good results when the *n* values are in the range of 0.7 – 1.6, which might explain the success in using the Bingham plastic model, although the *n* value for Herschel-Bulkley model is 0.36. When using the Bingham plastic rheology the Hallbom transition and Slatter & Wasp criteria are also applicable. Hallbom's criterion gives good predictions when using the Bingham plastic rheology, but relatively poor predictions when using his own yield plastic rheology (see Figure 5.11). The Slatter & Wasp high Hedström number criterion also results in good predictions. This simplified technique, which depends only on the yields stress of the fluid, was developed for large pipes and Bingham plastic fluids, but predicted V_c fairly well for all three pipe sizes tested, with the highest deviation from experimental values being 13.6% in the 100mm diameter pipe.

Cross-plot and summary

Figure 5.14 presents the plot of $V_{c(calc)}$ vs. $V_{c(exp)}$ for each technique using each rheology in all pipe sizes.

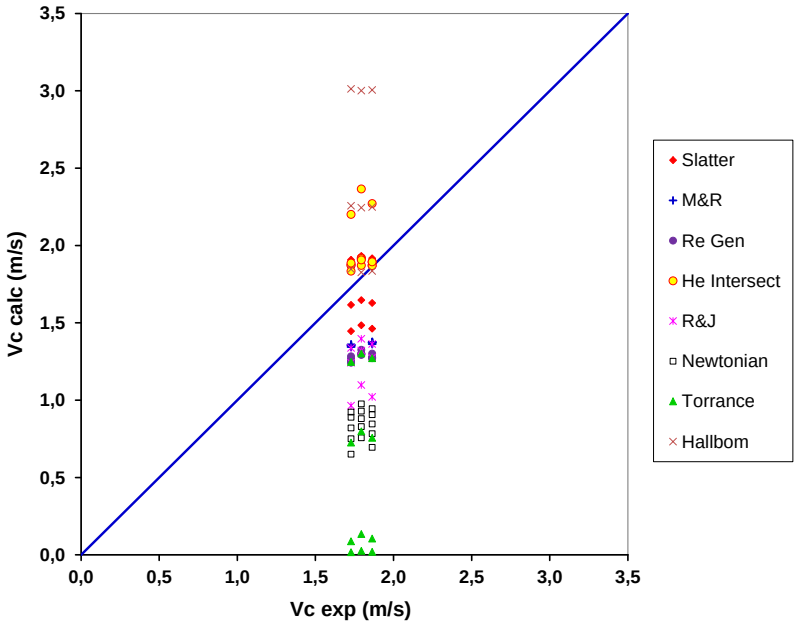

Figure 5.14 All transitional velocity prediction techniques using all rheologies, in the diameter 60mm, 80mm and 100mm pipes - 6% kaolin

Based on analysis of the results for all test concentrations of kaolin, the Hedström intersection method using the Bingham plastic and/or Casson rheologies consistently predicts the transitional velocity of the kaolin slurry most accurately (4.3% to 15.1% error). The predicted V_c tends towards a horizontal asymptote as pipe diameter increases as proposed by Metzner & Reed (1955) and Slatter (1997a). Note again that the intersection method calculations in this study used the Wilson and Thomas turbulent correlation. Different results may be obtained for different turbulent models. The next most accurate model was found to be that of Slatter (1994), also using the Bingham plastic and/or Casson rheologies (5.8% to 17% error). His criterion performed well with all rheologies except power law. There is a noticeable similarity between the Metzner & Reed and the Re_{Gen} approaches. Both these criteria underpredict the kaolin data by 21% to 28% and close correlation between predictions is observed for all rheological models.

Similarities exist between the Ryan & Johnson and the Newtonian approximation techniques. Both techniques follow the same oblique asymptote parallel to each other, performing best using the power law model and worst using the Bingham model, exactly opposite to the performance of the other techniques evaluated. The reasons for this are given by Slatter (1997a) as the inability for the Newtonian approximation to incorporate the details of the yield stress in the formulation, and that the correct estimation of the apparent viscosity is not sufficient for the accurate prediction of transitional velocities in yielding slurries. It is thus surprising that the Ryan & Johnson is so unsuccessful in its predictions since it incorporates the specific details of the yield stress in the formulation.

For Bingham plastic rheology, and for $He > 10^5$ the Slatter & Wasp prediction of the transitional velocity is best for the 6% and 10% kaolin slurry and produces an error of 20% for the 150mm pipe diameter for the 15% concentration. The Hallbom technique shows good results for Bingham plastic rheology only, significantly overpredicting V_c for all the other rheologies. The overall good performance when using the Bingham plastic rheology is surprising as this rheology worst represents the 6% kaolin laminar data.

The critical velocity increases with decreasing pipe diameter, and the prediction techniques, with the exception of Hallbom and Hedström intersection, approach the experimental data as well as each other.

The Hedström intersection method shows various trends for the different models as the diameter decreases while Hallbom's technique is excluded from further comment as it was found to be unviable for transitional velocity predictions for kaolin slurries.

For specific results of the various techniques combined with different rheologies, refer to the relevant sections presented. The plots of $V_{c(calc)}$ vs. $V_{c(exp)}$ for the 10% and 15% kaolin concentrations are shown in Figure 5.15 and Figure 5.16 below. The full results and data analysis of the various techniques and rheological model combinations are given in Appendix E.

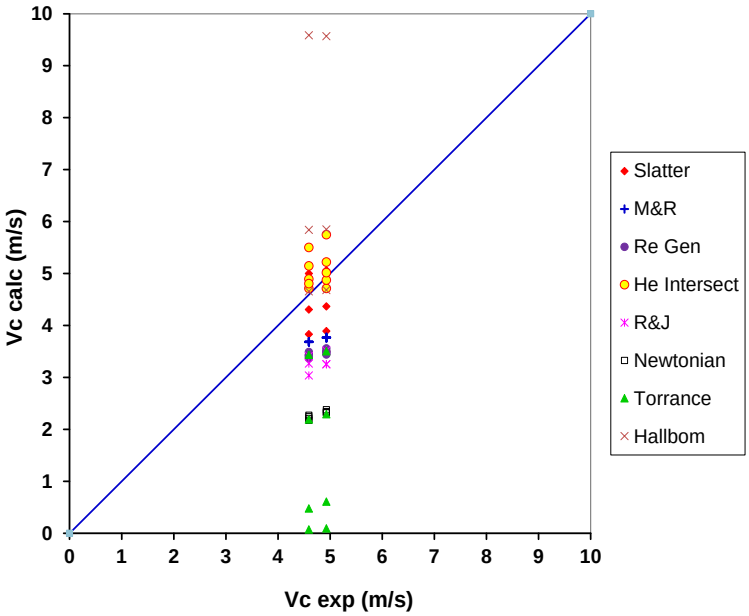

Figure 5.15 All transitional velocity prediction techniques using all rheologies, in the diameter 63mm and 80mm pipes - 10% kaolin

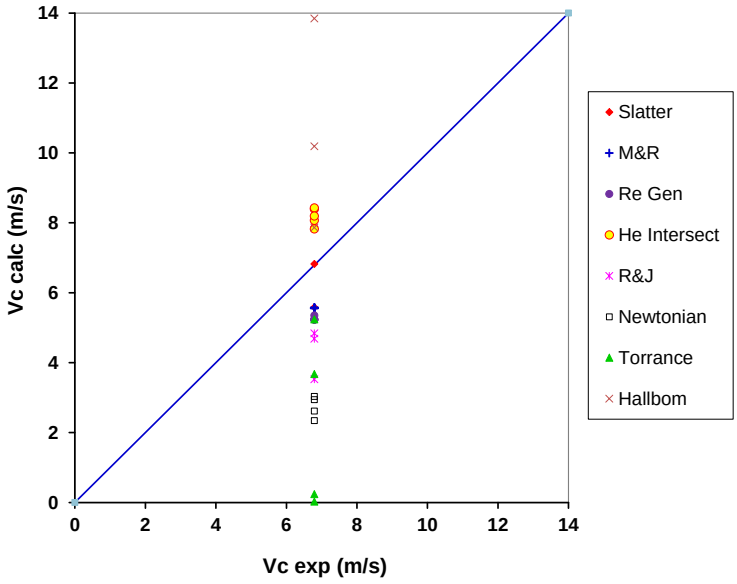

Figure 5.16 All transitional velocity prediction techniques using all rheologies, in the diameter 150mm pipe - 15% kaolin

Effect of concentration and diameter on V_c– kaolin

The effect of concentration and diameter on predicted V_c is shown in Figure 5.17, using the Bingham plastic rheology with the Hedström intersection method. This combination of rheology and technique is shown here as it best predicted the kaolin transitional velocities.

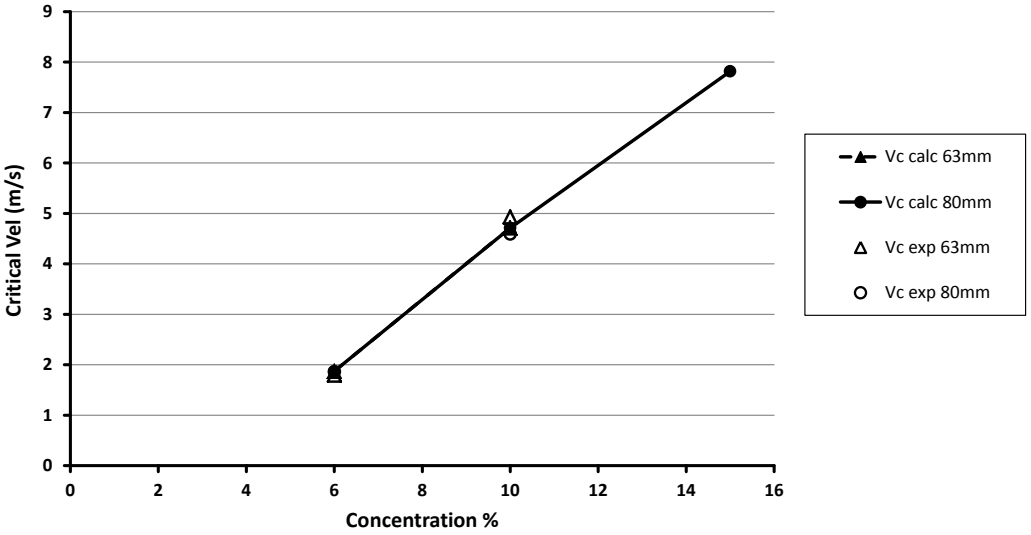

Figure 5.17 Effect of concentration and pipe diameter on the critical velocity of all kaolin test concentrations

Both the experimental and predicted V_c results presented in Figure 5.17 show a significant increase in critical velocity with an increase in concentration, but pipe diameter independence. This effect is attributed to increased slurry density and in turn the yield stress which results in the V_c approaching a constant value in larger pipe diameters irrespective of pipe size. This is in line with the findings of El-Nahhas, El-Hak, Rayan, Vlasak and El-Sawaf (2004), Slatter & Wasp (2000) and Slatter (1997a). Experimental V_c values for the 60 and 80mm diameter pipes were not obtained for the 15% kaolin.

5.2.2 Bentonite

The transition results for all bentonite test concentrations are discussed here, but only the 7.34% results presented as similar observations were made for the other concentrations. The results for the 6% and 9% test concentrations can be found in Appendix F. Conclusions are, however, based on the results of all three test concentrations in all pipe sizes. Error values for the predictions were determined from experimental V_c values obtained in three pipe diameters, however, calculated V_c values were obtained for an additional pipe diameter (350mm) to get a better idea of the trend of the prediction techniques.

One technique plotted for all rheologies

Transitional velocities are first presented for each prediction technique individually, using each rheological model. The results of the predictions are presented graphically as V_c vs. D and compared to the experimental data on the same graph.

Slatter

Figure 5.18 presents the V_c predictions and average error (in %) for the Slatter technique in all pipe sizes using each rheology.

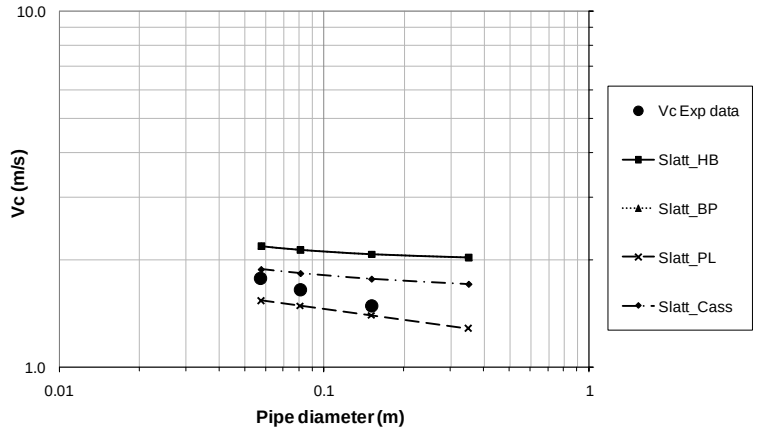

Diameter	Critical velocity (Exp) m/s	Vc Error values - SLATTER Re3 HB m/s	BP m/s	PL m/s	CASS m/s
60mm	1.784	2.198	2.198	1.546	1.889
		23.2%	23.2%	-13.3%	5.9%
80mm	1.658	2.145	2.145	1.493	1.839
		29.4%	29.4%	-9.9%	11.0%
150mm	1.489	2.085	2.085	1.401	1.773
		40.0%	40.0%	-5.9%	19.1%
350mm	0.000	2.040	2.040	1.285	1.714
	Ave	30.9%	30.9%	-9.7%	12.0%

Figure 5.18 Transitional velocity and average % error for 7.34% bentonite using the Slatter technique – all rheologies

The 7.34% bentonite experimental data does not show any significant yield stress effect over the test range, since there is no indication of V_c approaching a horizontal asymptote, unlike the 9% data as shown in Appendix F. Predictions of V_c using the Slatter criterion are somewhat surprising. Those using the power law rheology which worst describes the 7.34% bentonite laminar data, give the smallest overall error in predicted transitional velocity using the Slatter model, but show a continuous downward linear trend with increasing pipe diameter. Using the Bingham plastic rheology, which best describes the laminar data for the 7.34% bentonite, or the Herschel-Bulkley rheology, result in the worst V_c predictions by the Slatter model. The Casson rheology produces more acceptable errors of 3.2% to 12%for the three bentonite concentrations. The yield stress models though tend to a horizontal asymptote.

Metzner & Reed

Figure 5.19 presents the V_c predictions and average error (in %) for the Metzner & Reed technique in all pipe sizes using each rheology.

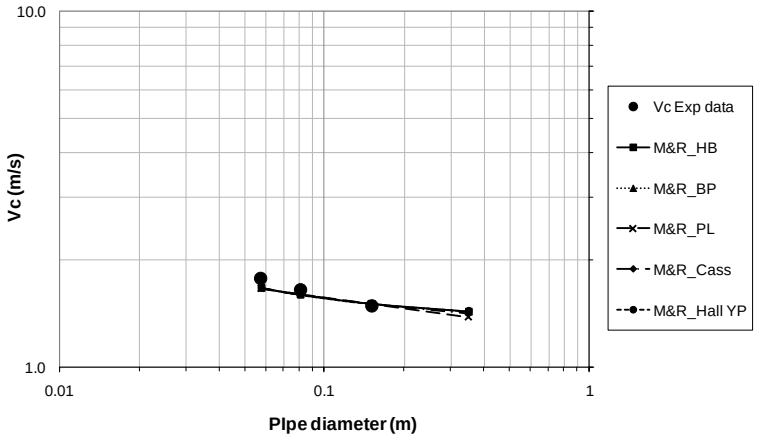

Diameter	Critical velocity (Exp) m/s	Vc Error values - M&R				
		HB m/s	BP m/s	PL m/s	CASS m/s	HAL_YP m/s
60mm	1.784	1.677	1.677	1.668	1.672	1.678
		-5.9%	-5.9%	-6.5%	-6.2%	-5.91%
80mm	1.658	1.603	1.603	1.610	1.606	1.603
		-3.3%	-3.3%	-2.8%	-3.1%	-3.3%
150mm	1.489	1.511	1.511	1.511	1.512	1.510
		1.5%	1.5%	1.5%	1.5%	1.4%
350mm		1.436	1.436	1.386	1.421	1.439
	Ave	-2.60%	-2.60%	-2.61%	-2.62%	-2.59%

Figure 5.19 Transitional velocity and average % error for 7.34% bentonite using the Metzner & Reed technique – all rheologies

V_c predictions for the 7.34% bentonite using the Metzner & Reed technique show consistency and good accuracy with the experimental transitional velocity values. The criterion follows the data trend well and starts approaching a horizontal asymptote at the larger pipe diameters. All the rheologies can be used with this criterion to predict the transition velocity for this 7.34% bentonite and also the 6% and 9% concentrations. In this case the power law rheology gave the greatest error of 6.5% in the diameter 63mm pipe.

Generalised Reynolds number

Figure 5.20 presents the V_c predictions and average error (in %) for the generalised Reynolds number approach in all pipe sizes using each rheology.

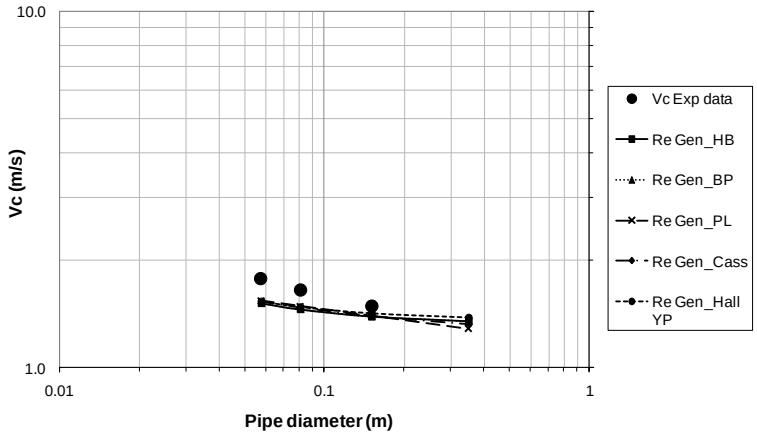

Diameter	Critical velocity (Exp) m/s	Vc Error values - Generalised Re				
		HB m/s	BP m/s	PL m/s	CASS m/s	HAL_YP m/s
60mm	1.784	1.521	1.521	1.546	1.532	1.538
		-14.7%	-14.7%	-13.3%	-14.1%	-13.78%
80mm	1.658	1.460	1.460	1.493	1.475	1.482
		-11.9%	-11.9%	-9.9%	-11.0%	-10.6%
150mm	1.489	1.394	1.394	1.401	1.396	1.421
		-6.4%	-6.4%	-5.9%	-6.2%	-4.6%
350mm		1.352	1.352	1.285	1.325	1.381
	Ave	-11.0%	-11.0%	-9.7%	-10.5%	-9.7%

Figure 5.20 Transitional velocity and average % error for 7.34% bentonite using the generalised Reynolds number approach – all rheologies

Good agreement in predicted V_c values is shown when using any of the rheologies with the General Reynolds number approach. The Hallbom criterion appears to best model the transition data and also most closely approaches a horizontal asymptote. The Hallbom yield plastic rheology also described the 7.34% laminar data well (Section 4.3.1). Once again the power law model shows reasonable agreement with the lower pipe sizes, but does not tend to a horizontal asymptote with increasing diameter.

Hedström intersection method

Figure 5.21 presents the V_c predictions and average error (in %) for the Hedström Intersection method in all pipe sizes using each rheology.

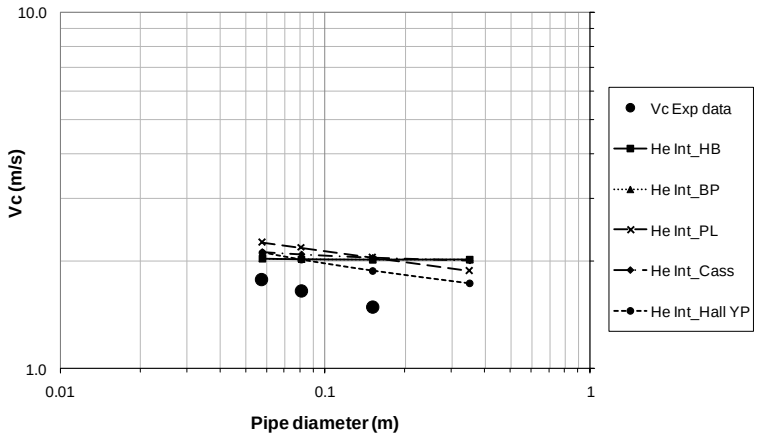

Diameter	Critical velocity (Exp) m/s	Vc Error values - He Intersection				
		HB m/s	BP m/s	PL m/s	CASS m/s	HAL_YP m/s
60mm	1.784	2.038	2.038	2.264	2.131	2.122
		14.2%	14.2%	26.9%	19.5%	18.96%
80mm	1.658	2.027	2.027	2.186	2.097	2.022
		22.3%	22.3%	31.9%	26.5%	22.0%
150mm	1.489	2.020	2.020	2.051	2.052	1.883
		35.7%	35.7%	37.8%	37.8%	26.5%
350mm		2.022	2.022	1.881	2.012	1.734
	Ave	24.1%	24.1%	32.2%	27.9%	22.5%

Figure 5.21 Transitional velocity and average % error for 7.34% bentonite using the Hedström Intersection method – all rheologies

Contrary to the 6% kaolin results, for the 7.34% bentonite the intersection method is unable to accurately predict the transitional velocity, using any rheology. The closest predictions are those of the model of Hallbom. Predictions using the intersection method depend not so much on the properties of the material, but are very dependent on the intersection of the laminar and turbulent flow curves. The

accuracy of the prediction should therefore be evaluated in conjunction with, particularly, the turbulent flow prediction. This method is not useful for the prediction of transional velocity for the bentonite slurries that were tested.

Ryan & Johnson criterion

Figure 5.22 presents the V_c predictions and average error (in %) for the Ryan & Johnson criterion in all pipe sizes each rheology.

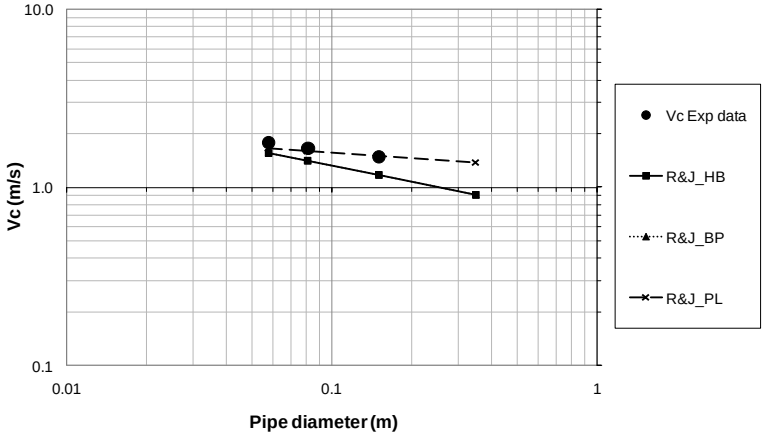

Diameter	Critical velocity (Exp) m/s	Vc Error values - R&J HB m/s	BP m/s	PL m/s
60mm	1.784	1.570	1.570	1.666
		-12.0%	-12.0%	-6.6%
80mm	1.658	1.419	1.419	1.609
		-14.4%	-14.4%	-3.0%
150mm	1.489	1.181	1.181	1.510
		-20.7%	-20.7%	1.4%
350mm		0.914	0.914	1.384
	Ave	-15.7%	-15.7%	-2.7%

Figure 5.22 Transitional velocity and average % error for 7.34% bentonite using the Ryan & Johnson criterion – all rheologies

For the 7.34% bentonite the Ryan & Johnson criterion does not produce good results using the Herschel-Bulkley or Bingham plastic (which for the 7.34% bentonite are exactly equal) rheologies. The Ryan & Johnson criterion incorporates the yield stress, but all the predictions show a continuous downward linear trend. From Figure 5.22, it is clear that the power law model is the most accurate (2.7%) in predicting V_c , which is surprising. It was also the rheology that gave the best accuracy for the 6% concentration (4%), but its use for the 9% concentration led to a prediction error of 34%.

Newtonian Approximation

Figure 5.23 presents the V_c predictions and average error (in %) for the Newtonian Approximation technique in all pipe sizes using each rheology.

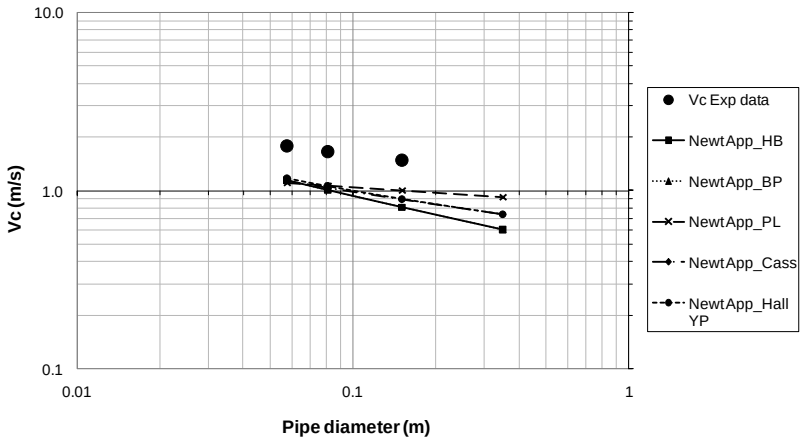

Diameter	Critical velocity (Exp) m/s	Vc Error values - Newt Approx				
		HB m/s	BP m/s	PL m/s	CASS m/s	HAL_YP m/s
60mm	1.784	1.156	1.156	1.111	1.133	1.185
		-35.2%	-35.2%	-37.7%	-36.5%	-33.55%
80mm	1.658	1.016	1.016	1.072	1.039	1.070
		-38.7%	-38.7%	-35.3%	-37.3%	-35.5%
150mm	1.489	0.813	0.813	1.006	0.895	0.907
		-45.4%	-45.4%	-32.4%	-39.9%	-39.1%
350mm	0.000	0.607	0.607	0.923	0.739	0.742
	Ave	-39.8%	-39.8%	-35.1%	-37.9%	-36.0%

Figure 5.23 Transitional velocity and average % error for 7.34% bentonite using the Newtonian Approximation technique – all rheologies

As for the 6% kaolin material, the Newtonian approximation gives better results using the power rheology and worst for the Bingham plastic rheology. No approach to a horizontal asymptote is observed. The Casson and Hallbom rheologies shows close agreement, and all models (except Hallbom) appear to intersect at a diameter of 60mm to give the same critical velocity of 1.1m/s. Error values range between 35% and 40% so this criterion is not useful in predicting the transition for this material test concentration using any of the rheologies.

Torrance

Figure 5.24 presents the V_c predictions and average error (in %) for the Torrance criterion in all pipe sizes using each rheology.

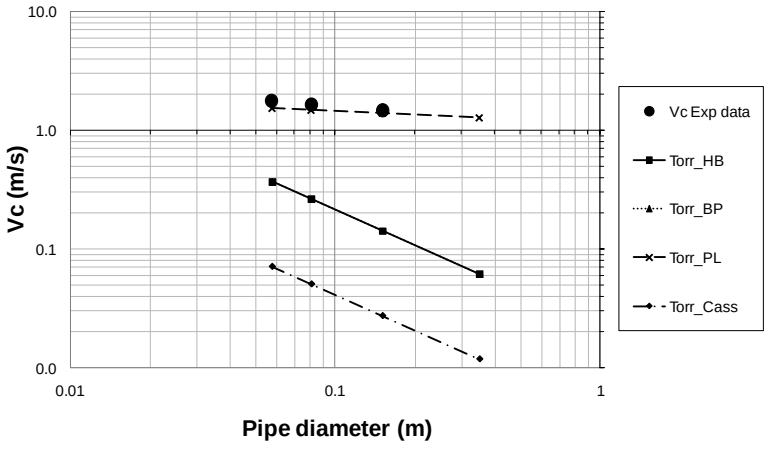

Diameter	Critical velocity (Exp) m/s	Vc Error values - Torrance			
		HB m/s	BP m/s	PL m/s	CASS m/s
60mm	1.784	0.374	0.374	1.546	0.072
		-79.0%	-79.0%	-13.3%	-96.0%
80mm	1.658	0.265	0.265	1.493	0.051
		-84.0%	-84.0%	-9.9%	-96.9%
150mm	1.489	0.143	0.143	1.401	0.028
		-90.4%	-90.4%	-5.9%	-98.1%
350mm		0.062	0.062	1.285	0.012
	Ave	-84.5%	-84.5%	-9.7%	-97.0%

Figure 5.24 Transitional velocity and average % error for 7.34% bentonite using the Torrance criterion – all rheologies

The Torrance criterion is only able to predict reasonable transitional velocities for 7% bentonite using the power law rheology. Using the Herschel-Bulkley, Bingham Plastic and Casson rheologies yields errors of between 79% and 98% and are unsuitable for use with the Torrance criterion, which was formulated for pseudoplastic materials. Similar levels of inaccuracy are observed for the 6% and 9% test concentrations.

Hallbom

Figure 5.25 presents the V_c predictions and average error (in %) for the Hallbom criterion in all pipe sizes using each rheology.

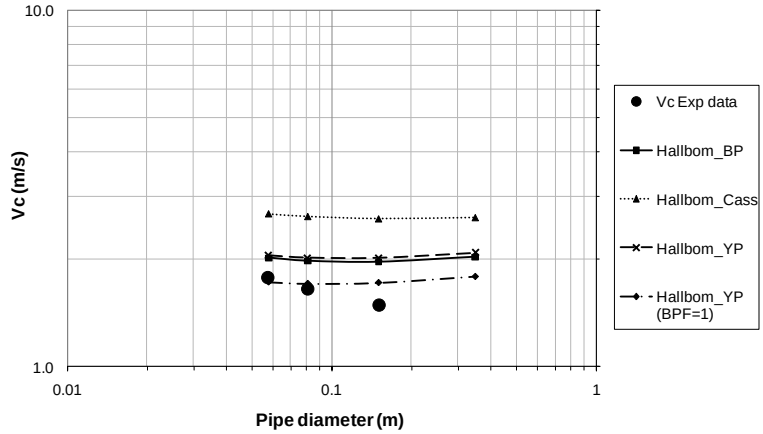

Diameter	Critical velocity (Exp) m/s	Vc Error values - Hallbom Trans			
		BP m/s	CASS m/s	HAL_YP m/s	HALL_YP (BPF=1) m/s
60mm	1.784	2.021	2.687	2.056	1.730
		13.3%	50.6%	15.28%	-3.03%
80mm	1.658	1.983	2.640	2.025	1.713
		19.6%	59.2%	22.2%	3.3%
150mm	1.489	1.971	2.600	2.022	1.723
		32.4%	74.6%	35.8%	15.7%
350mm		2.032	2.621	2.091	1.792
		21.8%	61.5%	24.4%	5.3%

Figure 5.25 Transitional velocity and average % error for 7.34% bentonite using the Hallbom criterion – all rheologies

The Hallbom criterion overpredicts the transition data and shows a completely different (upward) trend as the pipe diameter increases. Reducing the BPF (break point factor) to unity simply scales the predicted V_c values, and the criterion is not considered useful for the prediction of transitional velocities for bentonite slurries. Similar results are observed for the 6% concentration whilst the results for the 9% follow the experimental data trend better and show more consistent predictions (see Appendix F).

One rheology plotted for all techniques

Following the presentation and evaluation of the different V_c prediction techniques for each considered rheology, the results are now presented in terms of the most successful rheological models for all techniques. Based on the observations in Figure 5.18 to Figure 5.25, the most appropriate rheology for the Slatter, Ryan & Johnson, Newtonian, and Torrance criterion, is the power law model. For Metzner & Reed, Re_{Gen} and the Hedström intersection methods using the Hallbom yield plastic rheology was most successful. The rheological model which best describes the laminar data for the 7.34% bentonite is the Bingham plastic model. Based on these findings the predictions of V_c using the Bingham plastic, power law and Hallbom rheologies are now presented for all the transitional velocity criteria.

Bingham plastic

Figure 5.26 presents the V_c predictions and average % error for the Bingham plastic rheology in all pipe sizes using all techniques.

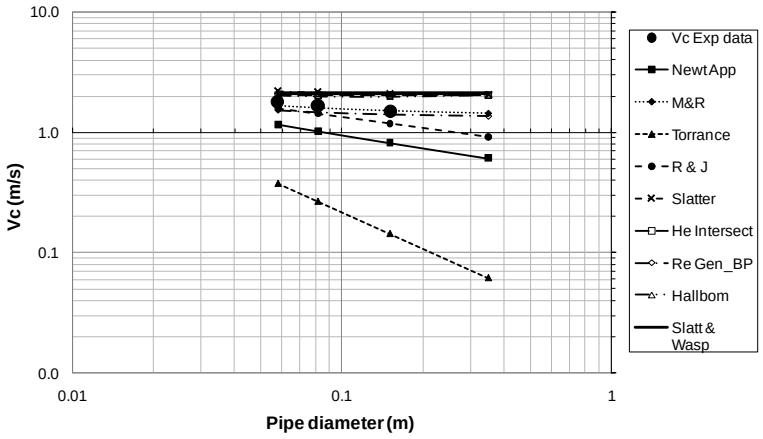

Diameter	Vc (Exp) m/s	Critical velocity error values - BP - All Techniques								
		Newt App m/s	M & R m/s	Torr/ Clapp m/s	Ryan & John m/s	Slatter m/s	Intersect m/s	Re_Gen m/s	Hallbom m/s	S&W m/s
60mm	1.784	1.156	1.677	0.374	1.570	2.198	2.038	1.521	2.021	2.119
		-35.2%	-5.9%	-79.0%	-12.0%	23.2%	14.2%	-14.7%	13.3%	18.8%
80mm	1.658	1.016	1.603	0.265	1.419	2.145	2.027	1.460	1.983	2.119
		-38.7%	-3.3%	-84.0%	-14.4%	29.4%	22.3%	-11.9%	19.6%	27.9%
150mm	1.489	0.813	1.511	0.143	1.181	2.085	2.020	1.394	1.971	2.119
		-45.4%	1.5%	-90.4%	-20.7%	40.0%	35.7%	-6.4%	32.4%	42.3%
350mm	0.000	0.607	1.436	0.062	0.914	2.040	2.022	1.352	2.032	2.119
	Ave	-39.8%	-2.6%	-84.5%	-15.7%	30.9%	24.1%	-11.0%	21.8%	29.7%

Figure 5.26 Transitional velocity and average % error for 7.34% bentonite (Bingham plastic rheology – all techniques)

Referring to Figure 5.26, when using the Bingham plastic rheology it is clear that the Metzner & Reed criterion most accurately predicts the transitional velocity values and trend, with errors ranging between 1.5% and 5.9%. The generalised Reynolds number approach gives predictions similar to the Metzner & Reed criterion, with error values in the range of 6.4% to 14.7%. The Ryan & Johnson, Newtonian approximation, and Torrance criteria all significantly underpredict the transitional velocity of this material when using the Bingham plastic rheology. The simplified technique of Slatter & Wasp (2000), which was developed for Bingham plastic slurries, is not successful for this Bingham plastic material, overpredicting transitional velocities quite significantly. Similar overpredictions were found with Slatter's (1994) and Hallbom's (2008) criteria.

Power law

Figure 5.27 presents the V_c predictions and average % error for the power law rheology in all pipe sizes using all techniques.

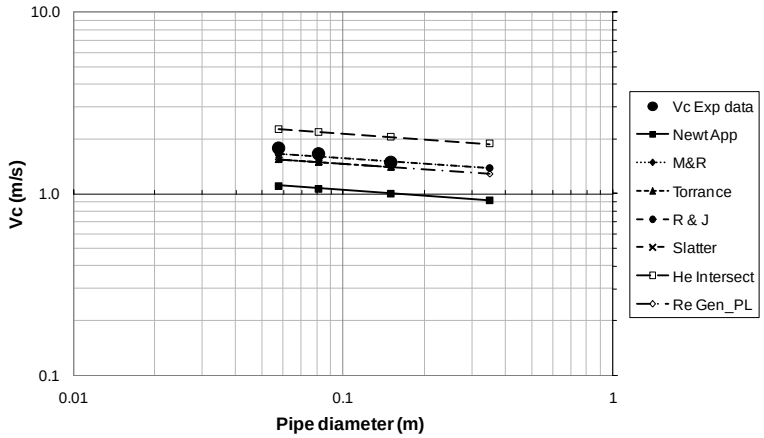

Diameter	Vc (Exp) m/s	Critical velocity Error values - PL - All Techniques						
		Newt App m/s	M & R m/s	Torr/ Clapp m/s	Ryan & John m/s	Slatter m/s	Intersect m/s	Re_Gen m/s
60mm	1.784	1.111	1.668	1.546	1.666	1.546	2.264	1.546
		-37.7%	-6.5%	-13.3%	-6.6%	-13.3%	26.9%	-13.3%
80mm	1.658	1.072	1.610	1.493	1.609	1.493	2.186	1.493
		-35.3%	-2.8%	-9.9%	-3.0%	-9.9%	31.9%	-9.9%
150mm	1.489	1.006	1.511	1.401	1.510	1.401	2.051	1.401
		-32.4%	1.5%	-5.9%	1.4%	-5.9%	37.8%	-5.9%
350mm	0.000	0.923	1.386	1.285	1.384	1.285	1.881	1.285
	Ave	-35.1%	-2.6%	-9.7%	-2.7%	-9.7%	32.2%	-9.7%

Figure 5.27 Transitional velocity and average % error for 7.34% bentonite (power law rheology – all techniques)

The power law rheology is reasonably successful in predicting transitional velocities when used with all the techniques except the Newtonian approximation and the Hedström intersection method. The most accurate results are obtained with the Metzner & Reed and Ryan and Johnson criterion with error values between 1.4% and 6.6%. No tendency towards a horizontal asymptote is observed in Figure 5.27 for all techniques, as expected, since the power law does not include the yield stress in the rheology.

Hallbom yield plastic

Figure 5.28 presents the V_c predictions and average % error for the Hallbom yield plastic rheology in all pipe sizes using all techniques.

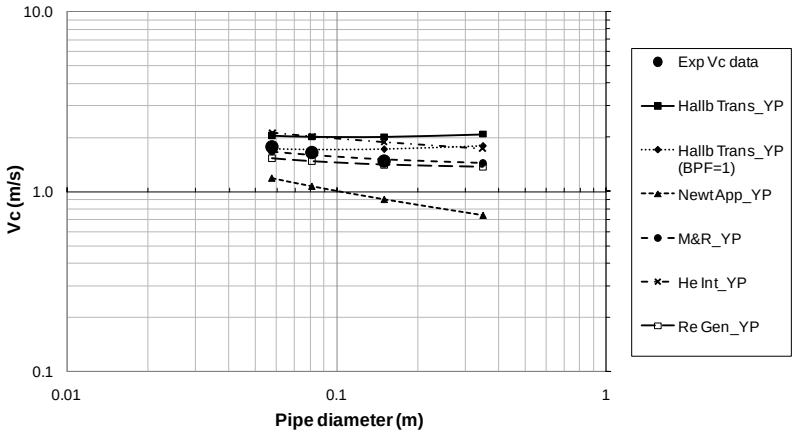

Diameter	Vc (Exp) m/s	Critical velocity Error values - Hallbom YP - All Techniques					
		Hallb_Trans m/s	**Hallb_Trans (BPF = 1)** m/s	He Int_YP m/s	M&R_YP m/s	Re_Gen_YP m/s	NEWT_YP m/s
60mm	1.784	2.056	1.730	2.122	1.678	1.538	1.185
		15.3%	-3.0%	19.0%	-5.9%	-13.8%	-33.5%
80mm	1.658	2.025	1.713	2.022	1.603	1.482	1.070
		22.2%	3.3%	22.0%	-3.3%	-10.6%	-35.5%
150mm	1.489	2.022	1.723	1.883	1.510	1.421	0.907
		35.8%	15.7%	26.5%	1.4%	-4.6%	-39.1%
350mm	0.000	2.091	1.792	1.734	1.439	1.381	0.742
	Ave	24.4%	**5.3%**	22.5%	-2.6%	-9.7%	-36.0%

Figure 5.28 Transitional velocity and average % error for 7.34% bentonite (Hallbom yield plastic rheology – all techniques)

The yield plastic rheology works best with the Metzner & Reed and the generalised Reynolds number prediction techniques, as to be expected from observing Figure 5.19 & Figure 5.20. Once again Hallbom's transition criteria shows an upward trend with increasing pipe diameter, which contradicts the accepted theory that the critical velocity decreases with an increase in pipe diameter, and approaches a constant value for larger pipe diameters for yield stress fluids (Slatter, 1997a); (Slatter & Wasp, 2000); (Wilson & Thomas, 2006). Reducing the BPF to unity just scales down the predicted V_c values. %. This criterion is not useful for predicting the critical velocity for this material. The Hedström intersection method overpredicts experimental V_c values with errors of 19% to 26% whilst the Newtonian Approximation underpredicts V_c data significantly showing errors of 33 to 39%.

Cross plot and summary

Figure 5.29 presents the plot of $V_{c(calc)}$ vs. $V_{c(exp)}$ for each technique using each rheology in all pipe sizes.

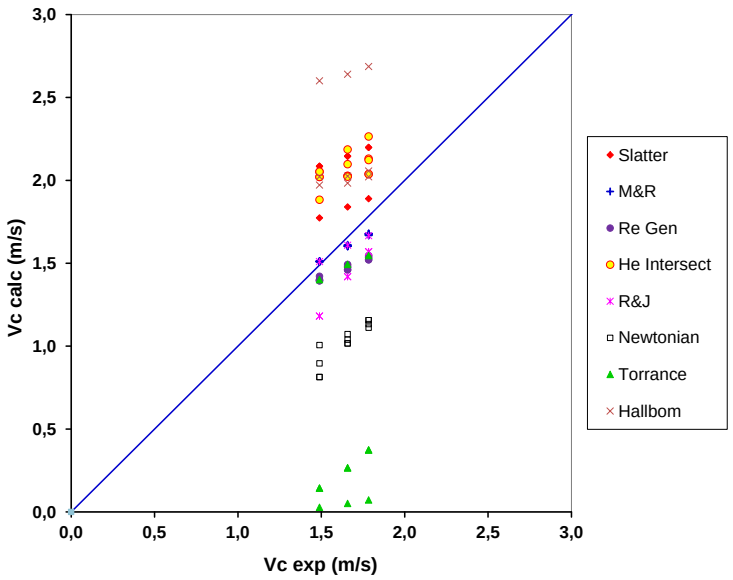

Figure 5.29 All transitional velocity prediction techniques using all rheologies, in the diameter 60mm, 80mm and 150mm pipes – 7.34% bentonite

The results for all bentonite concentrations indicate that the Metzner & Reed approach using Bingham plastic rheology is the most suitable for predicting transitional velocities, although little variation with rheology is observed in the results across all the pipe diameters. Average errors ranged between 0.6% and 16.5% and the criterion also tends to a horizontal asymptote for larger pipe diameters (except when using the power law rheology) as described by Metzner & Reed (1951), Slatter (1997a), Slatter & Wasp (2000) and Wilson & Thomas (2006). The next most consistent criterion was the Slatter Reynolds number approach using the Casson rheology, which produced errors in the range of 3.2% to 12%. Similar results are obtained by the generalised Reynolds number approach, with errors of between 8.4% and 19.7% using the yield plastic rheology, and is also able to follow the horizontal asymptote trend for larger diameters (again with the exception of the power law model). The Newtonian approximation and the Ryan and Johnson techniques both show a continuous linear drop in V_c with increasing pipe diameter which is unrealistic.

Using the power law rheology, the Metzner & Reed, Slatter, generalised Reynolds number, Newtonian approximation and Ryan & Johnson methods all produced reasonably accurate V_c predictions. In some instances the Ryan & Johnson technique with this rheology produced very good results (errors <5%), but was not consistent for all the concentrations. The Hallbom yield plastic rheology gave good results when used in the Metzner & Reed and generalised Reynolds number approaches, but cannot be recommended for use with the other techniques to predict bentonite transitional velocities.

The prediction techniques generally predicted an increase in critical velocity with decreasing pipe diameter and more accurate results for the smaller pipe diameters except for the Hedström intersection method. This technique shows various trends for the different rheological models as the pipe diameter decreases. The worst overall predictions for bentonite transition were produced by the Hedström intersection method, Newtonian approximation, Torrance and Hallbom criteria. These techniques are unable to predict transitional velocities for the bentonite using any of the rheologies, and are not recommended.

The cross-plots for the 6% and 9% concentrations are shown in Figure 5.30 and Figure 5.31 below. All the results and data analysis are given in Appendix F.

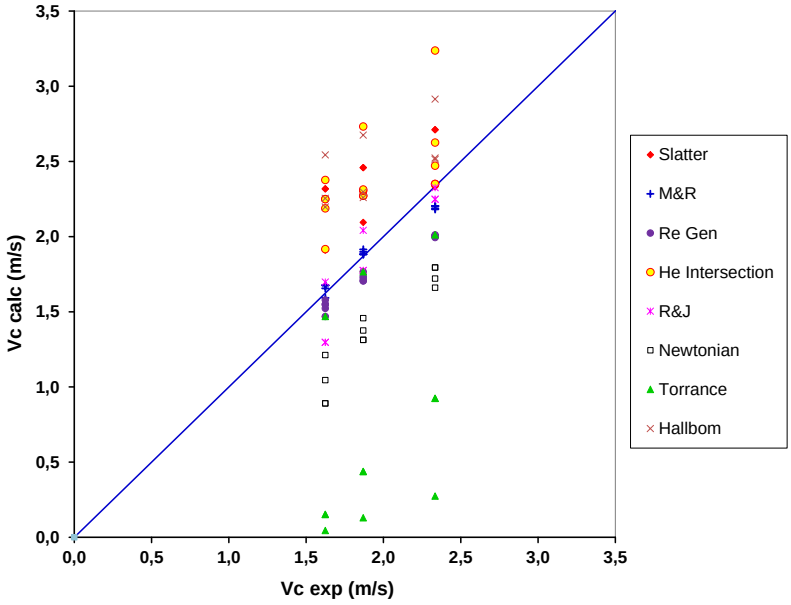

Figure 5.30 All transitional velocity prediction techniques using all rheologies, in the diameter 13mm, 28mm and 80mm pipes – 6% bentonite

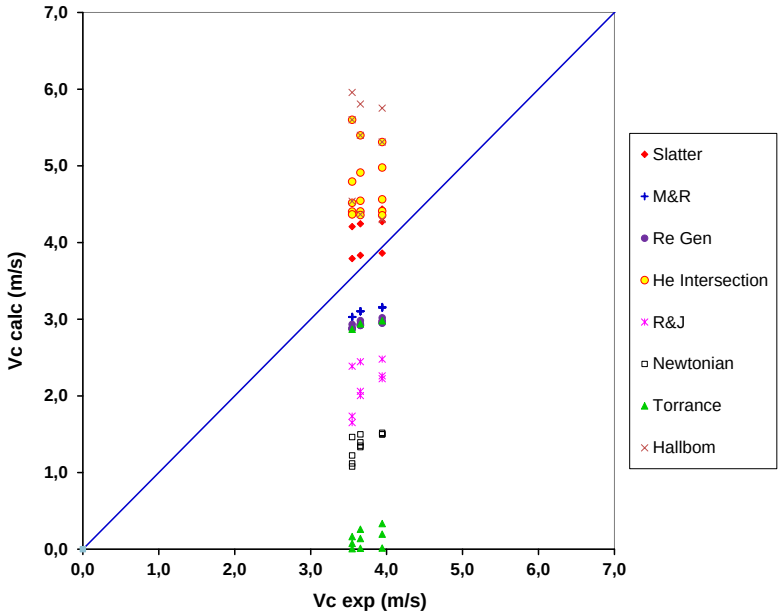

Figure 5.31 All transitional velocity prediction techniques using all rheologies, in the diameter 60mm, 80mm and 150mm pipes – 9% bentonite

Effect of concentration and diameter– bentonite

The effect of concentration and diameter on predicted V_c values is shown in Figure 5.32, using the Bingham plastic rheology in the Metzner & Reed prediction technique, since overall this combination of rheology and technique gave the best bentonite transitional velocity predictions.

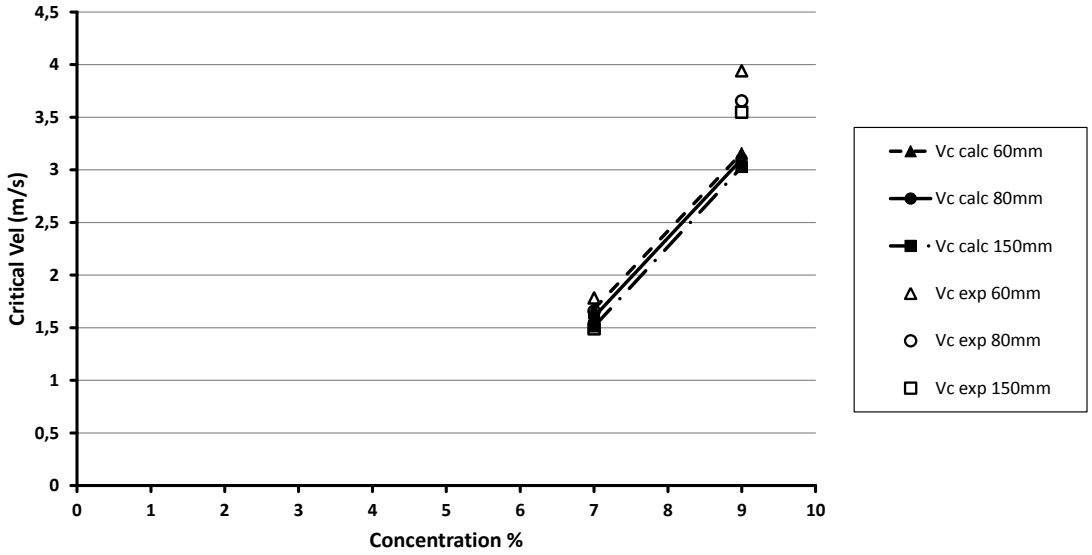

Figure 5.32 Effect of concentration and pipe diameter on the critical velocity of all bentonite test concentrations.

From Figure 5.32 it is clear that the V_c increases with concentration, but both the predicted and experimental results show very little pipe diameter dependence, similar to the results of kaolin. This is again attributed to the influence of the yield stress on the V_c and is in line with the findings of Slatter (1997a), El-Nahhas *et al* (2004) and Chhabra & Richardson (2008). V_c for the 80mm pipe for the 6% bentonite is not included here because it had a different dry density to that of the 7.34% and 9% bentonite (different supplier), so it could not be directly compared to the 7.34% and 9% for concentration effects.

5.2.3 CMC

The transitional results for all CMC test materials are discussed in this section, but only the 5% results are presented as similar observations were made for the other concentrations. The results for the 3% and 8% CMC are given in Appendix G. However conclusions are based on the results of all three test concentrations in all pipe sizes. Error values for the predictions were determined from experimental V_c values obtained in three pipe diameters, however, calculated V_c values were obtained for an additional pipe diameter (400mm) to get a better idea of the trend of the prediction techniques.

One technique plotted for all rheologies

Transitional velocities are first presented for each prediction technique individually, using each rheological model. The results of the predictions are presented graphically as V_c vs. D and compared to the experimental data on the same graph.

Slatter

Figure 5.33 presents the V_c predictions and average error (in %) for the Slatter technique in all pipe sizes using each rheology.

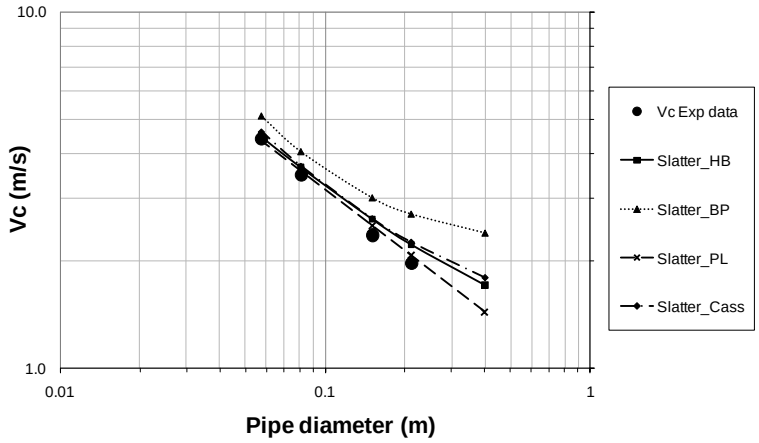

Diameter	Critical velocity (Exp) m/s	Vc Error values - SLATTER Re3 HB m/s	BP m/s	PL m/s	CASS m/s
200mm	1.978	2.228	2.714	2.078	2.258
		12.6%	37.2%	5.1%	14.2%
150mm	2.367	2.626	3.015	2.520	2.630
		10.9%	27.4%	6.5%	11.1%
80mm	3.496	3.670	4.064	3.589	3.697
		5.0%	16.3%	2.7%	5.8%
60mm	4.410	4.476	5.121	4.365	4.620
		1.5%	16.1%	-1.0%	4.8%
400mm		1.713	2.400	1.441	1.794
	Ave	7.5%	24.3%	3.3%	8.9%

Figure 5.33 Transitional velocity and average % error for 5% CMC using the Slatter technique – all rheologies

The 5% CMC test material is best modelled using the power law model as would be expected. The experimental transitional velocities shown in Figure 5.33 decrease linearly with increasing pipe diameter. They do not approach a horizontal asymptote with the increase in pipe diameter, as was observed for the yield stress materials. The Slatter technique gives good agreement for all rheologies for pipe diameters up to about 150mm diameter, after which V_c predictions using the yield stress rheologies tend to flatten out. This is especially so for the Bingham plastic rheology (least representative rheology for the 5% CMC) which also overpredicts V_c significantly more than the other rheologies, most likely due to the higher τ_y value from the fit to the laminar flow data. When using the power law rheology the Slatter technique is effectively the same as the generalised Reynolds number approach or the Torrance criterion. Any of the rheologies (except the Bingham plastic) could be used with this technique for this CMC concentration with confidence up to a pipe diameter of 200mm, after which the yield stress effect becomes too significant. Similar levels of accuracy are observed for the 3% and 8% concentrations using the Slatter technique with the Casson rheology.

Metzner & Reed

Figure 5.34 presents the V_c predictions and average error (in %) for the Metzner & Reed technique in all pipe sizes using each rheology.

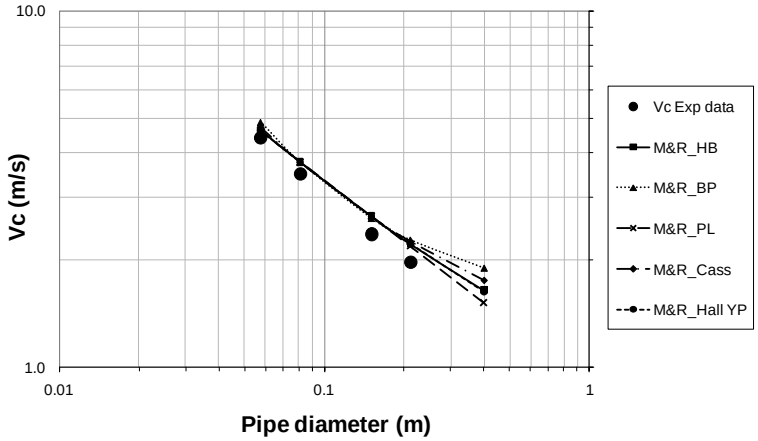

Diameter	Critical velocity (Exp) m/s	Vc Error values - M&R				
		HB m/s	BP m/s	PL m/s	CASS m/s	HAL_YP m/s
200mm	1.978	2.221	2.278	2.187	2.260	2.225
		12.3%	15.2%	10.6%	14.3%	12.50%
150mm	2.367	2.654	2.622	2.652	2.655	2.657
		12.1%	10.8%	12.1%	12.2%	12.3%
80mm	3.496	3.772	3.768	3.777	3.764	3.770
		7.9%	7.8%	8.0%	7.7%	7.8%
60mm	4.410	4.627	4.883	4.594	4.711	4.639
		4.9%	10.7%	4.2%	6.8%	5.2%
400mm		1.646	1.899	1.516	1.758	1.629
	Ave	9.3%	11.1%	8.7%	10.2%	9.5%

Figure 5.34 Transitional velocity and average % error for 5% CMC using the Metzner & Reed technique – all rheologies

The Metzner & Reed technique shows good agreement between all the rheologies over a wide range of pipe sizes. Predictions are particularly good for the 5% CMC test concentration as expected since the criterion was developed for power law fluids which CMC is representative of. Although the power model is best suited to predict the transitional velocity using the Metzner & Reed criterion, any of the rheological models can be used with confidence up to a pipe diameter of 200mm, after which the predicted values of V_c start flatten out way from the experimental trend. Similar levels of consistency and accuracy are observed for the 3% and 8% concentrations for this technique.

Generalised Reynolds number

V_c predictions using the generalised Reynolds number approach show excellent agreement with experimental values for all the models up to pipe diameter of 200mm in all concentrations. For D > 200mm, as with the Metzner & Reed criterion, V_c predictions for this technique using the yield stress rheologies start to flatten out away from the experimental and power law prediction trend. Up to a pipe diameter of 200mm any rheology can be used with the generalised Reynolds number approach with confidence.

Figure 5.35 presents the V_c predictions and average error (in %) for the generalised Reynolds number approach in all pipe sizes using each rheology.

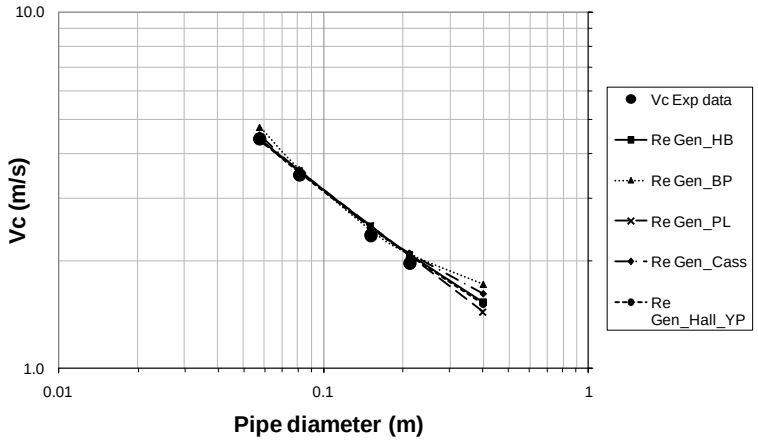

Diameter	Critical velocity (Exp) m/s	Vc Error values - Generalised Re				
		HB m/s	BP m/s	PL m/s	CASS m/s	HAL_YP m/s
200mm	1.978	2.091	2.091	2.078	2.109	2.077
		5.7%	5.7%	5.1%	6.7%	5.00%
150mm	2.367	2.510	2.441	2.520	2.495	2.487
		6.1%	3.2%	6.5%	5.4%	5.1%
80mm	3.496	3.588	3.622	3.589	3.590	3.549
		2.6%	3.6%	2.7%	2.7%	1.5%
60mm	4.410	4.410	4.764	4.365	4.528	4.382
		0.0%	8.0%	-1.0%	2.7%	-0.6%
400mm		1.532	1.720	1.441	1.622	1.514
	Ave	3.6%	5.1%	3.3%	4.4%	2.7%

Figure 5.35 Transitional velocity and average % error for 5% CMC using the generalised Reynolds number approach – all rheologies

Hedström intersection method

Figure 5.36 presents the V_c predictions and average error (in %) for the Hedström intersection method in all pipe sizes using each rheology.

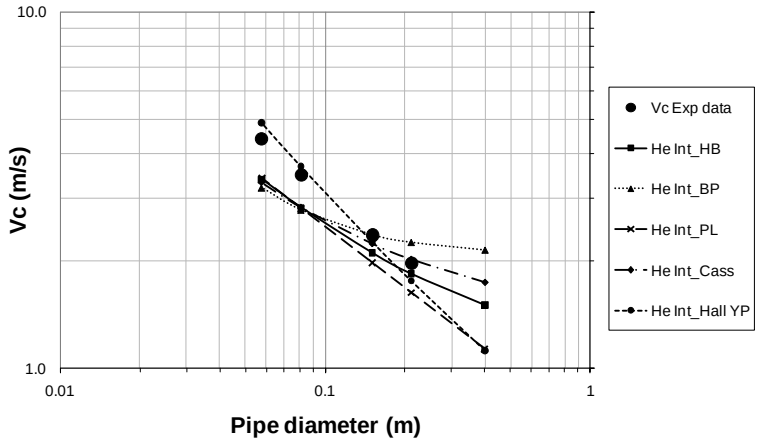

Diameter	Critical velocity (Exp) m/s	Vc Error values - He Intersection				
		HB m/s	BP m/s	PL m/s	CASS m/s	HAL_YP m/s
200mm	1.978	1.845	2.256	1.633	2.023	1.760
		-6.7%	14.1%	-17.4%	2.3%	-11.00%
150mm	2.367	2.112	2.370	1.981	2.239	2.264
		-10.7%	0.1%	-16.3%	-5.4%	-4.4%
80mm	3.496	2.832	2.785	2.821	2.831	3.683
		-19.0%	-20.3%	-19.3%	-19.0%	5.3%
60mm	4.410	3.400	3.216	3.432	3.324	4.893
		-22.9%	-27.1%	-22.2%	-24.6%	11.0%
400mm		1.508	2.146	1.133	1.743	1.121
	Ave	-14.8%	-8.3%	-18.8%	-11.7%	0.2%

Figure 5.36 Transitional velocity and average % error for 5% CMC using the Hedström Intersection criterion – all rheologies

The Intersection method of Hedström is a practical approach which predicts the transitional velocity as the velocity at the intersection of the laminar and turbulent friction factor curves, assuming a reasonable turbulent flow prediction. The effect of the yield stress at larger diameters is more prominent on this technique than that for the other techniques discussed earlier. In this case, using the yield plastic rheology, which also represented the 5% CMC laminar data very well, gives predictions closest to the experimental values. The power law model underpredicts the transitional velocities with this criterion, but follows the experimental trend quite well. Use of the other rheologies in the Hedström intersection method does not give reliable predictions of V_c.

Ryan & Johnson criterion

Figure 5.37 presents the V_c predictions and average error (in %) for the Ryan & Johnson criterion in all pipe sizes using each rheology.

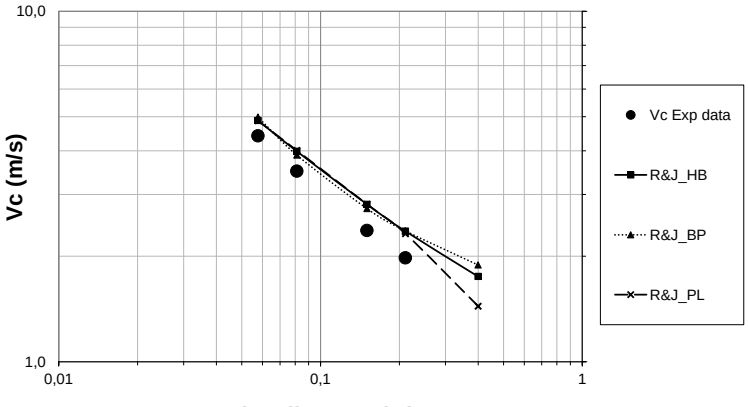

Diameter	Critical velocity (Exp) m/s	Vc Error values - R&J		
		HB m/s	BP m/s	PL m/s
200mm	1.978	2.357	2.362	2.319
		19.2%	19.4%	17.3%
150mm	2.367	2.812	2.734	2.813
		18.8%	15.5%	18.9%
80mm	3.496	3.984	3.887	4.006
		14.0%	11.2%	14.6%
60mm	4.410	4.880	4.987	4.873
		10.6%	13.1%	10.5%
400mm		1.750	1.888	1.441
	Ave	15.6%	14.8%	15.3%

Figure 5.37 Transitional velocity and average % error for 5% CMC using the Ryan & Johnson criterion – all rheologies

The Ryan and Johnson criterion overpredicts the transitional velocities for 5% CMC by 10% - 20% across the range of pipe sizes tested. Up to a pipe diameter of 200mm the criterion predicts V_c independently of which rheology is used, but for D > 200mm the Herschel-Bulkley and Bingham plastic rheologies deviate from the $V_c - D$ experimental data and power law rheology prediction.

Newtonian Approximation

Figure 5.38 presents the V_c predictions and average error (in %) for the Newtonian approximation technique in all pipe sizes using each rheology.

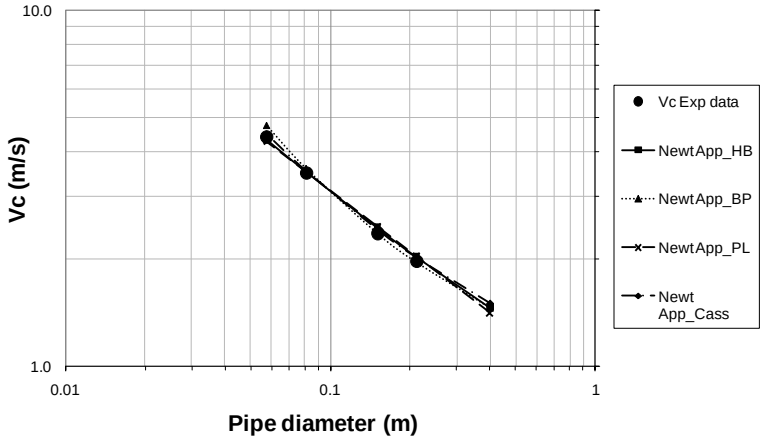

Diameter	Critical velocity (Exp) m/s	Vc Error values - Newt Approx				
		HB m/s	BP m/s	PL m/s	CASS m/s	HAL_YP m/s
200mm	1.978	2.034	1.959	2.038	2.027	2.011
		2.9%	-0.9%	3.1%	2.5%	1.71%
150mm	2.367	2.455	2.362	2.472	2.427	2.420
		3.7%	-0.2%	4.5%	2.5%	2.3%
80mm	3.496	3.528	3.598	3.521	3.543	3.479
		0.9%	2.9%	0.7%	1.4%	-0.5%
60mm	4.410	4.342	4.754	4.283	4.492	4.309
		-1.5%	7.8%	-2.9%	1.8%	-2.3%
400mm		1.464	1.457	1.413	1.509	1.452
	Ave	1.5%	2.4%	1.3%	2.1%	0.3%

Figure 5.38 Transitional velocity and average % error for 5% CMC using the Newtonian approximation technique – all rheologies

The Newtonian approximation technique accurately predicts the transitional velocities for 5% CMC for all rheological models for all the pipe diameters up to 200mm. There is no significant difference in V_c predictions between the rheologies used, and all follow the experimental data precisely. However, the predictions deteriorate significantly for the 3% CMC (10.6% error) and 8% CMC (16.9% error) concentrations, so this technique is inconsistent and not favoured.

Torrance

Figure 5.39 presents the V_c predictions and average error (in %) for the Torrance criterion in all pipe sizes using each rheology.

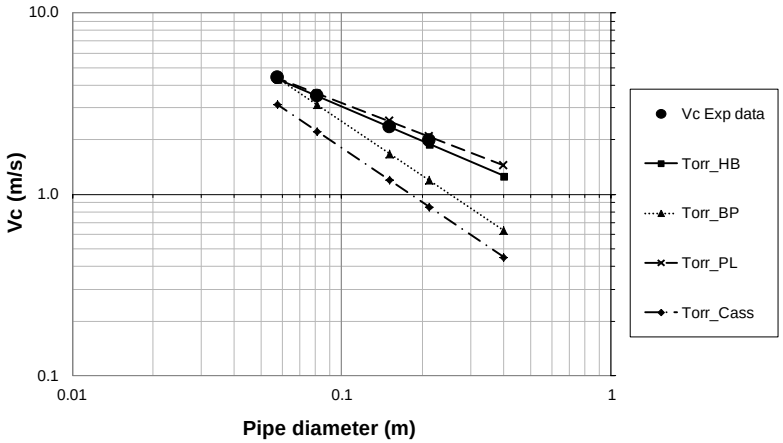

Diameter	Critical velocity (Exp) m/s	Vc Error values - Torrance			
		HB m/s	BP m/s	PL m/s	CASS m/s
200mm	1.978	1.897	1.195	2.078	0.854
		-4.1%	-39.6%	5.1%	-56.8%
150mm	2.367	2.349	1.674	2.520	1.196
		-0.8%	-29.3%	6.5%	-49.4%
80mm	3.496	3.476	3.105	3.589	2.219
		-0.6%	-11.2%	2.7%	-36.5%
60mm	4.410	4.318	4.371	4.365	3.124
		-2.1%	-0.9%	-1.0%	-29.2%
400mm		1.264	0.630	1.441	0.450
	Ave	-1.9%	-20.2%	3.3%	-43.0%

Figure 5.39 Transitional velocity and average % error for 5% CMC using the Torrance criterion – all rheologies

For the 5% CMC power law material the Herschel-Bulkley and power law rheologies are very similar, and when used with the Torrance transitional velocity criterion, produce very similar V_c predictions. This is to be expected, as the Torrance criterion applies specifically to power law fluids. Using the Casson and Bingham plastic rheological models with the Torrance criterion results in significant inaccuracy in V_c predictions, due to the inappropriate inclusion of a yield stress. For the 3% and 8% concentrations less accurate predictions are obtained with average errors of 7.2% and 13% respectively.

Hallbom

Figure 5.40 presents the V_c predictions and average error (in %) for the Hallbom criterion in all pipe sizes using each rheology.

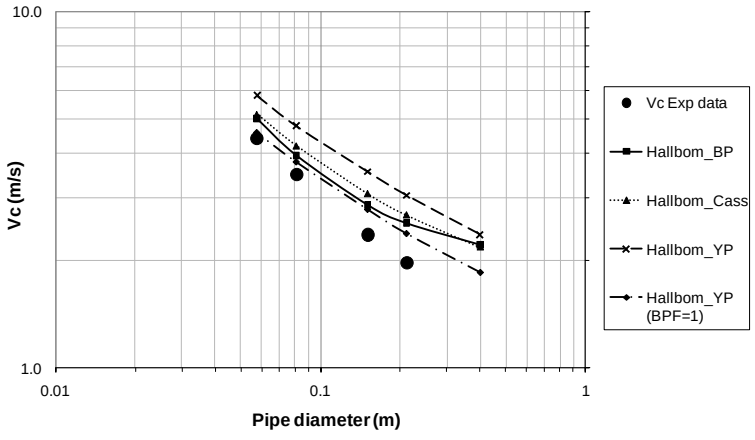

Diameter	Critical velocity (Exp) m/s	Vc Error values - Hallbom Trans			
		BP m/s	CASS m/s	HAL_YP m/s	HAL_YP (BPF=1) m/s
200mm	1.978	2.546	2.688	3.053	2.380
		28.7%	35.9%	54.37%	20.36%
150mm	2.367	2.867	3.086	3.558	2.783
		21.2%	30.4%	50.3%	17.6%
80mm	3.496	3.959	4.207	4.782	3.783
		13.2%	20.3%	36.8%	8.2%
60mm	4.410	5.031	5.159	5.826	4.574
		14.1%	17.0%	32.1%	3.7%
400mm		2.211	2.182	2.367	1.851
	Ave	19.3%	25.9%	43.4%	12.5%

Figure 5.40 Transitional velocity and average % error for 5% CMC using the Hallbom criterion – all rheologies

Hallbom's criterion overpredicts the transitional velocity for 5% CMC significantly, as it did for the kaolin and bentonite slurries, but does follow the experimental trend of the non-yielding pseudoplastic material quite well. Reducing the BPF to unity and using the yield plastic rheology gave more acceptable predictions, but still showed increasing overprediction of V_c with increasing pipe diameter. This technique could be used for CMC materials using the yield plastic rheology, provided that the BPF is set to unity and not 1.3 as suggested by Hallbom (2008), but is not the recommended technique.

One rheology plotted for all techniques

Following the presentation and evaluation of the different V_c prediction techniques for each considered rheology, the results are now presented in terms of the most successful rheological models for all techniques. Based on the results shown in Figure 5.33 to Figure 5.40, the most appropriate rheology for the 5% CMC for use in any of the techniques is power law, as would be expected. With this in mind, V_c predictions for all the techniques using the power law rheology are presented in Figure 5.41.

Power law

Figure 5.41 presents the V_c predictions and average % error for the power law rheology in all pipe sizes using all techniques.

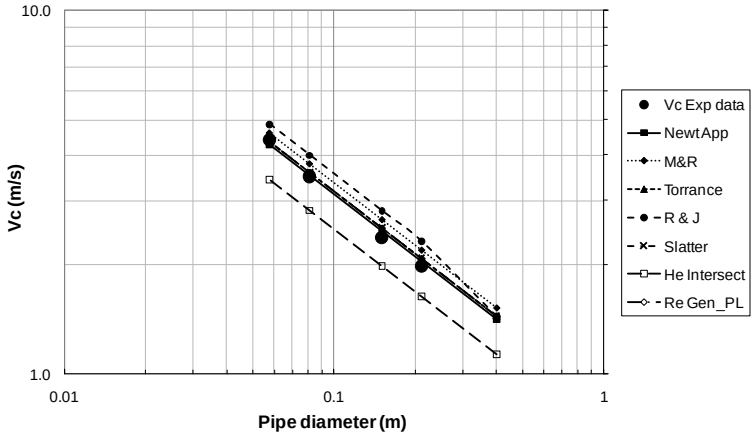

Diameter	Critical velocity (Exp) m/s	Critical velocity Error values - PL - All Techniques						
		Newt App m/s	M & R m/s	Torr/ Clapp m/s	Ryan & John m/s	Slatter m/s	Intersect	Re_Gen
200mm	1.978	2.038	2.187	2.078	2.319	2.078	1.633	2.078
		3.1%	10.6%	5.1%	17.3%	5.1%	-17.4%	5.1%
150mm	2.367	2.472	2.652	2.520	2.813	2.520	1.981	2.520
		4.5%	12.1%	6.5%	18.9%	6.5%	-16.3%	6.5%
80mm	3.496	3.521	3.777	3.589	4.006	3.589	2.821	3.589
		0.7%	8.0%	2.7%	14.6%	2.7%	-19.3%	2.7%
60mm	4.410	4.283	4.594	4.365	4.873	4.365	3.432	4.365
		-2.9%	4.2%	-1.0%	10.5%	-1.0%	-22.2%	-1.0%
400mm		1.413	1.516	1.441	1.441	1.441	1.133	1.441
	Ave	1.3%	8.7%	3.3%	15.3%	3.3%	-18.8%	3.3%

Figure 5.41 Transitional velocity and average % error for 5% CMC (power law rheology – all techniques)

The Hedström intersection method and Ryan & Johnson criterion under and overpredict the transitional velocity respectively, although they do follow the data trend. Any of the other techniques could be used to predict the transitional velocity of the 5% CMC, all showing excellent agreement with the experimental data. Considering all concentrations, the Slatter and Metzner & Reed techniques were the most consistently accurate with the power law rheology.

Cross plot and summary - CMC

Figure 5.42 to Figure 5.42Figure 5.44 present plots of $V_{c(calc)}$ vs. $V_{c(exp)}$ for the CMC material for each technique using each rheology in all pipe sizes. The CMC material is best represented by the power law rheology. Considering all the CMC results it is concluded that the Slatter and Metzner & Reed methods using either the power law or Casson rheology consistently produce the most accurate transitional velocity predictions, with errors in the range of 1% to 9%. The generalised Reynolds number approach gives similar results and produces errors in the range of 2.7% to 12.7%. The Ryan & Johnson and Newtonian approximation techniques show inconsistent results across the three concentrations. Ryan & Johnson using the power law rheology produces average errors of 0.4% and 6.3% for the 8% and 3% concentrations respectively, however produces 15.3% for the 5% concentration. The Newtonian approximation produces 1.3% error for the 5% concentration but 10.6% and 16.9% error for the 3% and 8% concentrations respectively. The intersection method and Hallbom transition technique are unable to reliably predict transition for pseudoplastic materials (CMC).

The Hedström intersection method underpredicts V_c, and when using the yield stress rheology deviates significantly (upward on the $V_c - D$ diagram) for the larger diameters. Only the Hallbom yield plastic rheology is applicable with this technique for the CMC. The Torrance approach produces reasonable V_c predictions provided the power law rheology is used. Hallbom's method overpredicts the transitional velocity significantly for all applicable rheologies, and is worst when using his own yield plastic rheology. Adjusting the BPF (break point factor) to unity essentially reduces his method to the Hedström intersection method between a Knudsen & Katz (1958) turbulent prediction and the yield plastic laminar curve. This improved the results for the smaller diameter pipes, but still resulted in overpredictions for the larger diameter pipes. All the results for the 3% and 8% CMC concentrations and are presented in Appendix G.

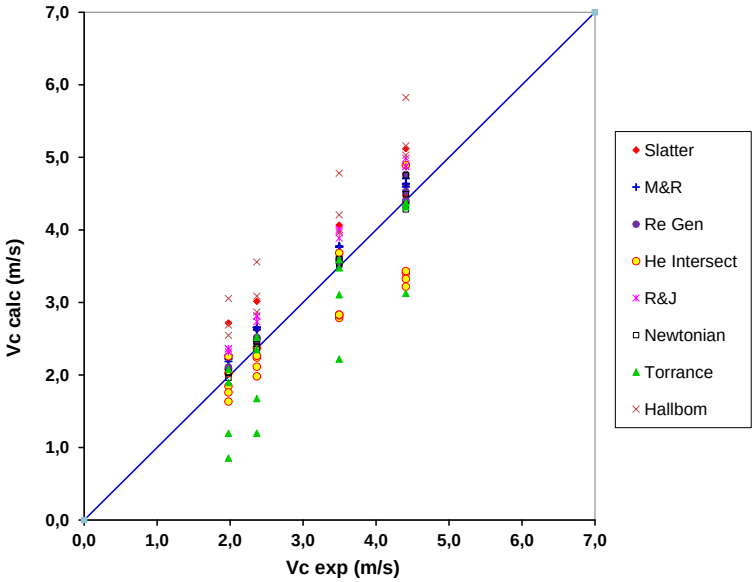

Figure 5.42 All transitional velocity prediction techniques using all rheologies, in the diameter 60mm, 80mm, 150mm and 200mm – 5% CMC

Figure 5.43 and Figure 5.44 below present the plots of $V_{c(calc)}$ vs. $V_{c(exp)}$ for the 3% and 8% concentrations respectively.

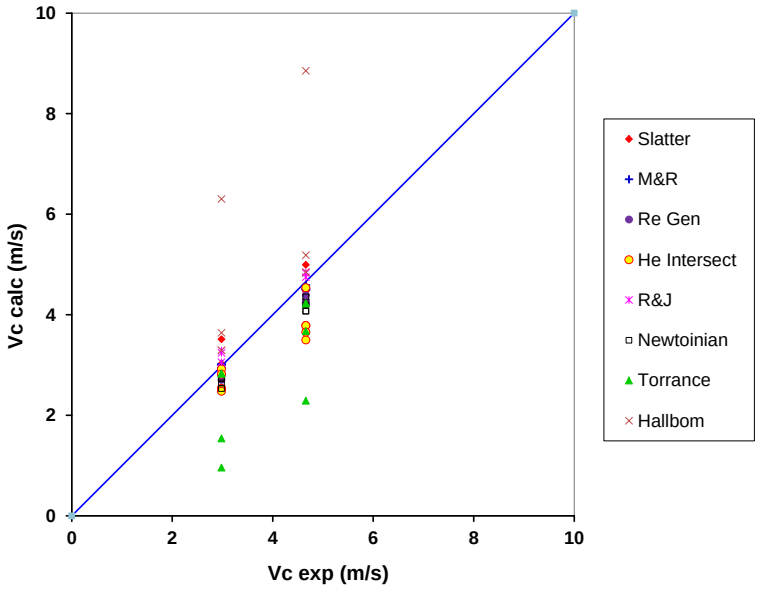

Figure 5.43 All transitional velocity prediction techniques using all rheologies, in the diameter 63mm and 150mm pipes – 3% CMC

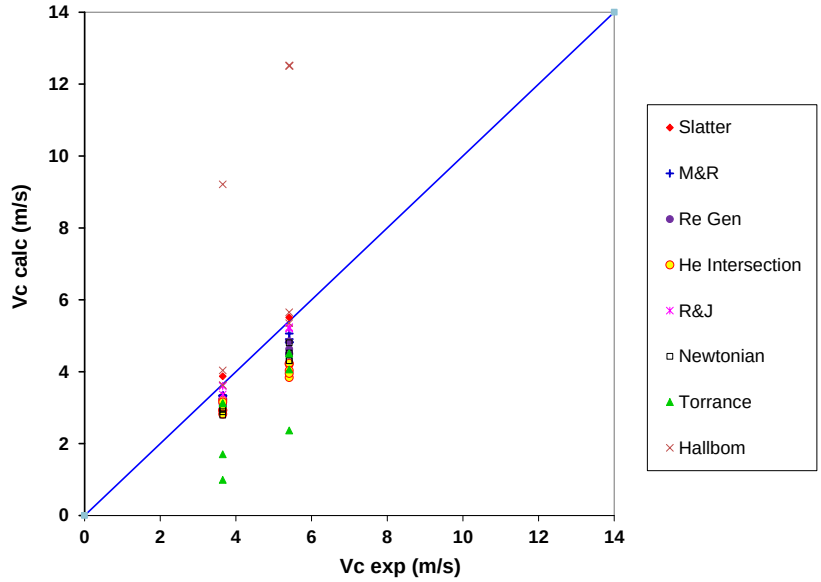

Figure 5.44 All transitional velocity prediction techniques using all rheologies, in the diameter 63mm and 150mm pipes – 8% CMC

Effect of concentration and diameter – CMC

The effect of concentration and diameter on predicted V_c is shown in Figure 5.45, using the power law rheology with the Newtonian approximation technique. This combination of rheology and technique is shown here as it best predicted the CMC transitional velocities.

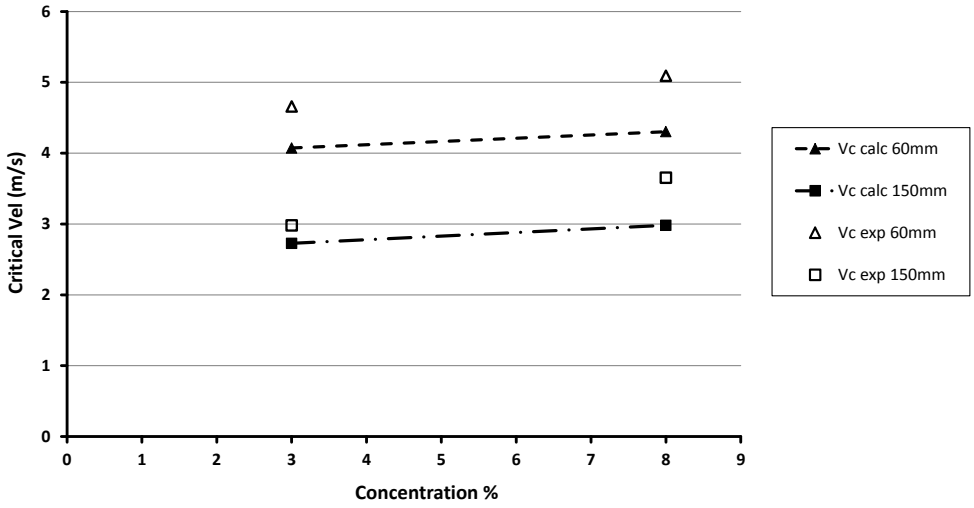

Figure 5.45 Effect of concentration and pipe diameter on the critical velocity of all CMC test concentrations.

From Figure 5.45 its clear that the critical velocity increases moderately with increasing concentration. A clear diameter effect is also observed, unlike for the yield stress fluids (kaolin and bentonite) presented earlier. This implies that the critical velocity decreases with an increase in pipe diameter, opposite to what was observed for yield stress fluids where the critical velocity approached a constant value for larger pipe diameters in yield stress fluids (Slatter, 1997a; El-Nahhas *et al,* 2004 and Chhabra & Richardson, 2008). The 5% CMC was obtained from a different supplier (different dry density) and was not tested in corresponding diameter pipe sizes, so it was not included in Figure 5.45 for comparison with the 3% and 8% concentrations.

5.2.4 Transition conclusion

The results of the transitional velocity predictions for the three test materials, using all the prediction techniques combined in turn with the applicable rheologies, have been presented and discussed. This sub-section briefly reviews the outcomes. Transitional velocity prediction techniques were evaluated against values taken as the velocity corresponding to the last laminar flow data point. This was done simply to enable a consistent reference (datum) for comparison – it does not imply this is the critical transitional velocity, as it is acknowledged that transition occurs over some finite velocity range.

Laminar flow kaolin data was best represented by the Herschel-Bulkley rheological model. However, using either Bingham plastic or Casson rheology with the Hedström intersection or the Slatter Reynolds number criterion gave the most consistent and accurate agreement with experimental data. The Metzner & Reed method and the generalised Reynolds number approach also showed close agreement with experimental values for all the rheologies, but both underpredict the V_c. The Newtonian approximation, Ryan & Johnson and Torrance approaches were not able to predict the transitional velocities for kaolin slurries. Hallbom's prediction method shows reasonable agreement only when using the Bingham plastic rheology, but predicts increasing values of V_c with increasing pipe diameters and so is deemed unreliable. The simplified approach of Slatter & Wasp which applicable only for Bingham plastic rheology also gave good results for the kaolin slurries, with error values between 5% and 13% for the pipe diameters tested. This method must be used cautiously though due to the simplifications assumed, and is only applicable for $He > 10^5$.

Bentonite slurry is best described by the Bingham plastic rheological model. With regard to the V_c prediction techniques the Metzner & Reed method produced the most consistent and accurate results for bentonite using this rheology. Predictions showed good agreement with experimental values for all rheologies and the yield stress effect was apparent. The next best technique/rheology combination is the Slatter technique using the Casson rheology. The Hedström intersection, Newtonian approximation and Torrance methods failed to predict the experimental transitional velocities. Hallbom's method again proved unreliable in the prediction of transitional velocities for bentonite as it over estimates the V_c values and predicts increasing critical velocity with increasing pipe diameter. The Slatter & Wasp criterion also failed to predict transitional velocities for bentonite slurry with any accuracy, showing errors in the range 18% to 42%, even though the Bingham plastic rheology is best suited to this material.

CMC is a power law material, and the power law rheological model is therefore the best model to represent it. Notwithstanding this, considering the results of all CMC concentrations it can be concluded that the Slatter and Metzner & Reed methods using either the power law or Casson rheology consistently produce the most accurate transitional velocity predictions. The generalised Reynolds number approach produces similarly accurate results when using all rheologies. The Ryan & Johnson and Newtonian approximation techniques show inconsistent results across the three CMC concentrations. The Hedström intersection method underpredicted V_c for all rheologies except the Hallbom yield plastic rheology. For CMC the Hallbom technique followed the experimental data trend, and did not predict increasing V_c with increasing pipe diameter as it did for the kaolin and bentonite slurries. The technique still overpredicted transitional velocity, but for smaller diameters with the BPF equal to unity, it reverts to the Hedström intersection method using the Knudsen & Katz turbulent model and gave errors in the range 3% to 8% for the diameter 60 and 80mm pipes. The power law rheology yields the most accurate results for the prediction of transition data in CMC test materials.

The yield stress effect on transitional velocity was observed and illustrated for the kaolin and bentonite

test materials, as seen in the plots of V_c vs. D where V_c approached a horizontal asymptote as D increased (Slatter, 1997a). Predictions for CMC showed no such trend.

The effect of concentration and pipe diameter on V_c was shown for each of the test materials and concentration, and supported the theory that critical velocity depends on concentration, but becomes independent of D for large pipe diameters in yield stress fluids (Slatter & Wasp, 2000). Conversely its dependence on pipe diameter for non-yield stress fluids like CMC was also apparent.

5.3 Turbulent flow

Presented in this section are the results, analysis and discussion of the turbulent pipe flow predictions for the kaolin, bentonite and CMC test materials. Experimental results and predictions from each pipe diameter are presented as plots of τ_w vs. ($8V/D$).

The accuracy of each technique was evaluated by calculating the errors (deviation of predicted from experimental, calculated as normalised RMSE values) for each set of results. These values are tabulated below each turbulent prediction plot for easy reference. Only turbulent data points which fall within the shear stress range as defined in Section 3.2.7 were included in the error estimates, although turbulent predictions and experimental data were plotted for the entire experimental turbulent data range. In addition to how closely the predictions match the experimental data, the slopes of the turbulent flow predictions were also compared to those of the experimental data, to get an indication of the reliability of the predictions at higher shear rates. Some of the predictions show good accuracy at low turbulent shear stresses, but deviate significantly from experimental values at higher shear stresses. In these instances the calculated error value for the lower shear stress turbulent data (as given here) may be unrepresentative of the model performance and thus misleading. Such behaviour was taken into account in the evaluation of the different prediction techniques. Recommended turbulent prediction technique/ rheological model combinations were based on absolute error values as well as consistency of predictions across all concentrations for all pipe sizes.

5.3.1 Kaolin

The turbulent analysis and results for the kaolin test concentrations are presented and discussed in this section. Only the results for the 6% kaolin are presented here. Conclusions are, however, based on the results of all three test concentrations in all pipe sizes. Results for the 10% and 15% concentrations are given in Appendix H.

One technique plotted for all rheologies

To see the effect of rheology on the prediction technique the turbulent results are first presented as plots of predicted τ_w vs. ($8V/D$) for one prediction technique in one diameter pipe, for all applicable rheologies. Experimental values are also shown on the plots.

Wilson and Thomas

Figure 5.46 presents the turbulent predictions and average error (in %) for kaolin in three pipe sizes using the Wilson & Thomas method with each rheological model in turn. A large variation is observed between the predictions based on the different rheological models, and the slopes of the predicted flow curves are very different from that of the experimental data, with the exception of the Casson rheology.

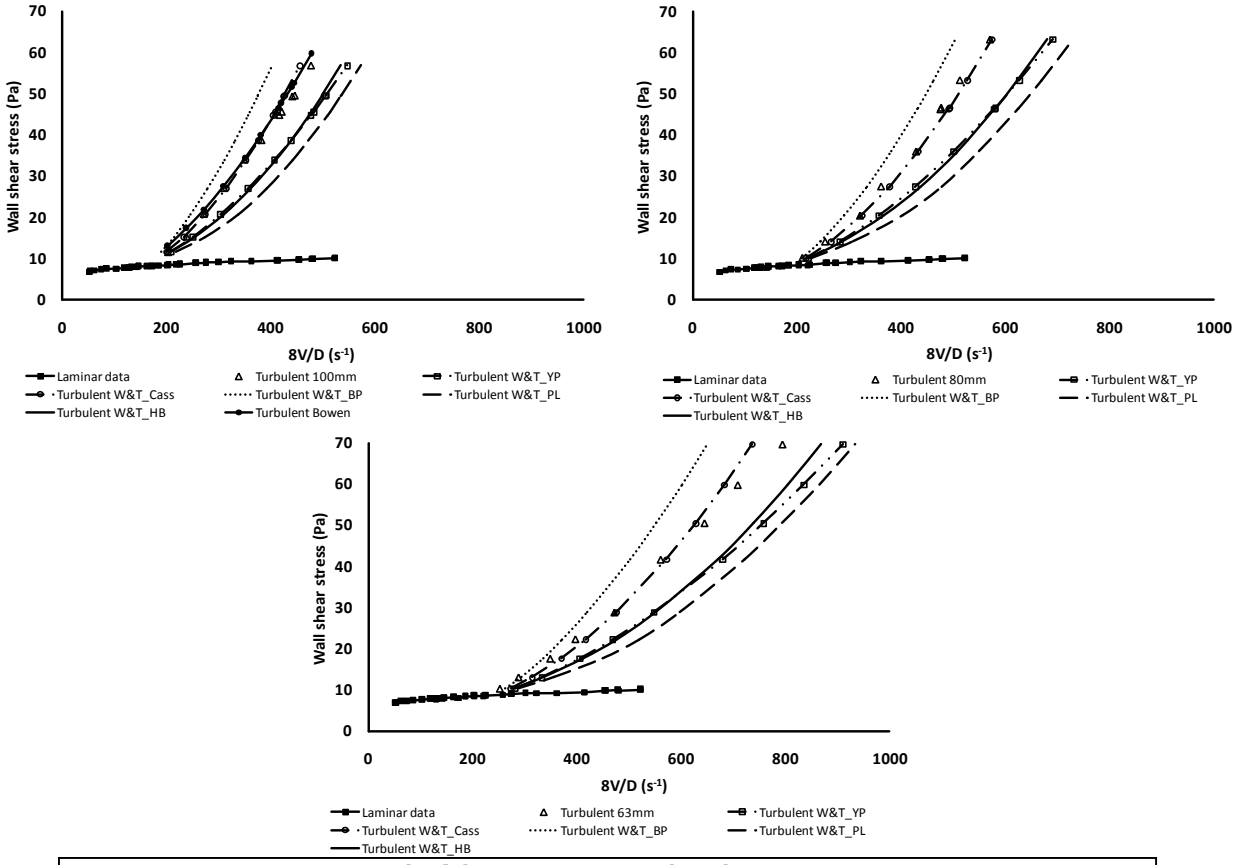

(8V/D) RMSE values - W&T(PRW) method						
Pipe diameter	**HB**	**BP**	**PL**	**CASS**	**HALL_YP(SW)**	**BOWEN (To)**
100mm	7.8%	8.7%	15.5%	1.5%	6.3%	10.3%
80mm	11.2%	4.3%	18.3%	3.0%	9.5%	N/A
63mm	15.4%	3.3%	22.1%	7.8%	14.4%	N/A
Ave	**11.5%**	**5.4%**	**18.6%**	**4.1%**	**10.1%**	**10.3%**

Figure 5.46 Turbulent flow predictions and average % error for 6% kaolin using the Wilson & Thomas method – all rheologies

The Bingham plastic rheology overpredicts the turbulent shear stresses, and the overprediction worsens with increasing (*8V/D*). Although the use of Bingham plastic rheology shows a low error value, this error was calculated using only the lower turbulent data (See Section 3.2.7). Using the power law rheology, the Wilson & Thomas (1985) method constantly underpredicts the turbulent flow curve. Predictions using the Herschel-Bulkley rheology lie between the Bingham plastic and power law predictions, but still below the experimental data. This in line with other findings for clay slurries using the Wilson & Thomas technique combined with these rheologies (Brown & Heywood, 1991; Chilton & Stainsby, 1996; Slatter *et al*, 1997; Slatter, 1999; El-Nahhas *et al*, 2005). For this material the most accurate predictions with this technique were obtained using the Casson rheology, in terms of both values and the slope of the turbulent flow curve. Average errors obtained for each concentration were 4.1% for the 6%, 3.6% for the 10% and 12.4% for the 15% concentrations. The yield plastic rheology also gave reasonable results when used with this technique, especially for the 6% and 10% kaolin cocncentrations, with average errors of 10.1% and 15.9% respectively.

The Hallbom (2008) turbulence technique is effectively just a modification of the Wilson & Thomas (1985) model using the yield plastic rheology, for smooth wall turbulent flow. This method gave similar results using the Herschel-Bulkley and yield plastic rheology, since the yield plastic and Herschel-Bulkley rheologies produced almost identical fits (See Figure 5.46).

The Wilson and Thomas method is sensitive to the rheological model used (El-Nahhas et al, 2004) and more specifically to the value of *n* (Vlasak & Chara, 1999). This is illustrated by the variation in turbulent predictions, as shown in Figure 5.46 between the power law model (*n*= 0.182), Bingham plastic (*n* = 1), Herschel-Bulkley (*n*=0.3) and yield plastic (*k* = 0.3) rheologies, even though the rheological model fits to the 6% kaolin laminar data are almost identical. The variations arise as a result of the extention of the laminar data to the much higher turbulent shear stress values to be accommodated. Considering the rheological model fits to the 6% kaolin laminar data shown in Figure 4.1 Section 4.2.1, it can be seen that the different rheological models correlate very well across the laminar regime (50 to 550s^{-1}), but when extended to the much higher turbulent shear stress values, they differ considerably. Considering Figure 5.46 the maximum shear stress obtained was about 70Pa. Extending each rheological model to this turbulent shear stress value results in the plots shown in Figure 5.47. Clearly for a given wall shear stress the predicted turbulent average velocity will vary with rheological model.

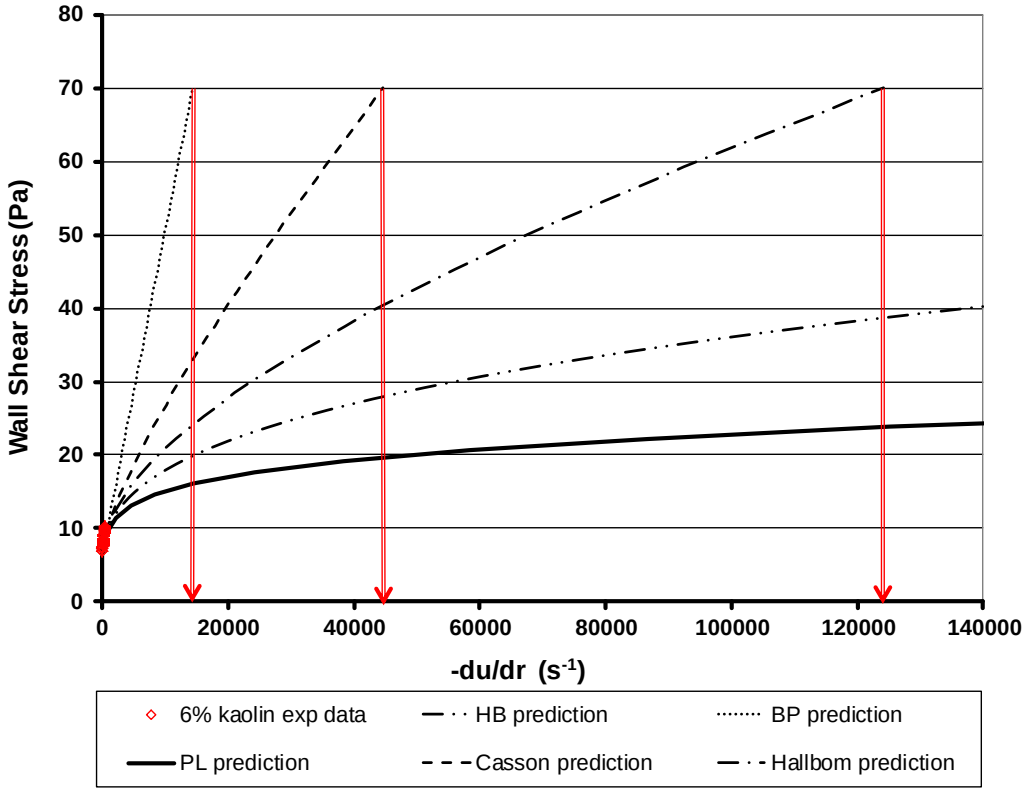

Figure 5.47 Effect of extrapolating the laminar rheological model fits to the maximum turbulent shear stress obtained for 6% kaolin

The Wilson & Thomas method is also sensitive to changes in pipe roughness as this influences the thickening of the viscous sub-layer (drag reduction). For non-Newtonian turbulent flow a thickening of the viscous sub-layer occurs so the effect of pipe roughness can only be approximate (Slatter, 1994) and also small (Chhabra & Richardson, 2008). Even so, errors of up to 5% were observed for some of the kaolin test results when the pipe roughness was not used in the predictions. Generally the turbulent predictions were less accurate when the pipe roughness was not incorporated.

Slatter

Figure 5.48 presents the turbulent predictions and average error (in %) for kaolin in three pipe sizes using the Slatter method with each rheological model in turn.

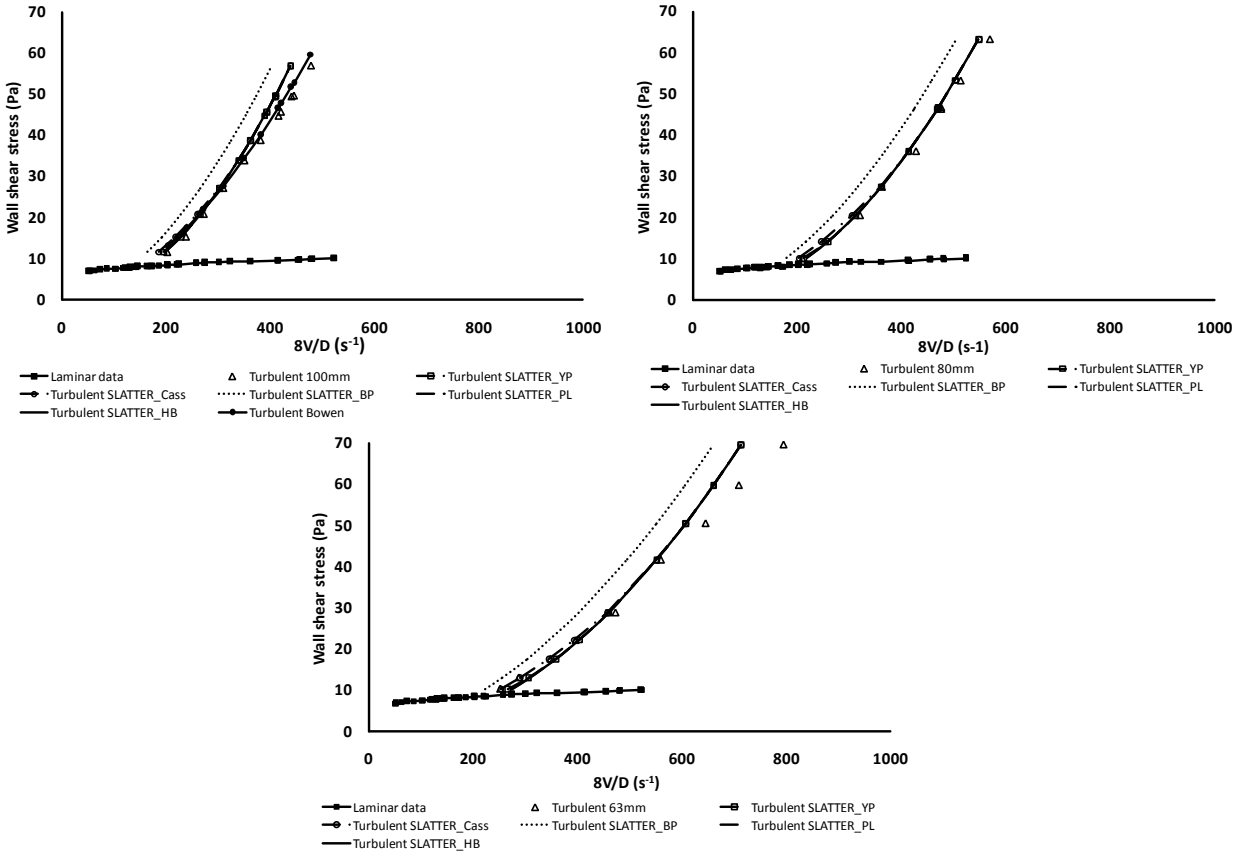

(8V/D) RMSE values - Slatter method						
Pipe diameter	**HB**	**BP**	**PL**	**CASS**	**HALL_YP**	**BOWEN (To)**
100mm	3.2%	18.0%	3.2%	7.3%	3.8%	10.3%
80mm	3.1%	15.1%	3.1%	3.8%	2.0%	N/A
63mm	6.4%	11.6%	6.4%	0.8%	5.1%	N/A
Ave	**4.2%**	**14.9%**	**4.2%**	**3.9%**	**3.6%**	**10.3%**

Figure 5.48 Turbulent flow predictions and average % error for 6% kaolin using the Slatter method – all rheologies

The Slatter turbulent flow prediction method is the only one that does not consider the slurry to be a continuum, by taking into account the particle roughness effect in turbulent flow. The technique gave accurate results for all rheologies except Bingham plastic, for which it overpredicted turbulent shear stresses, as for the Wilson & Thomas method. For all the rheologies the slopes of the predicted flow curves are consistent with the experimental data. Reasons for the good slope and experimental data correlation for this technique is due to the inclusion of the particle roughness effect in the formulation (Slatter *et al*, 1997). The identical results obtained when using the Herschel-Bulkley or power law rheology are due to the roughness function (*B*) [See Eq.(2.161)] which reduces to a constant when the roughness Reynolds number is greater than 3.32, implying fully rough wall turbulent flow. This was the case for both the Herschel-Bulkley and power law rheologies, so the turbulent velocity was no longer dependant on fluid rheology. This was also the case for the 10% and 15% kaolin concentrations.

The Slatter method gave the most accurate results when using the Hallbom yield plastic and Casson rheologies. The accuracy in the predictions could have resulted from a combination of the particle roughness effect and the way these rheological models adapt their apparent viscosity at increased shear rates. The Hallbom rheology approaches a constant value for apparent viscosity defined by the rheological characterisation as μ_∞. The Casson model also gives a direct measure of the higher shear rate viscosity (η_C), which the Herschel-Bulkley model is not able to (Heywood & Alderman, 2003). Other models such as the Herschel-Bulkley and power law models approach a zero shear rate viscosity at very

high shear rate values which results in the underprediction of shear stresses at higher shear rates. This is the reason for the underprediction of the kaolin turbulent data in the work done by Chilton & Stainsby (1996) and probably also for the results of El-Nahhas *et al.* (2005) when using the Slatter model with the Herschel-Bulkley rheology. The sensitivity of the Slatter technique to the rheological model used was not apparent for the 6% and 15% kaolin as the roughness function reduced the friction factor to a constant value. However, the effect was observed for the 10% kaolin concentration which showed differences in the predictions between the Bingham plastic, power law and Herschel-Bulkley rheologies similar to those of the Wilson & Thomas technique. The result for the 10% and 15% test concentrations can be referred to in Appendix H.

Hallbom: Smooth wall turbulence – modified Wilson & Thomas method

Figure 5.49 presents the turbulent predictions and average error (in %) for kaolin in three pipe sizes using the Hallbom modified Wilson & Thomas method with each rheological model in turn.

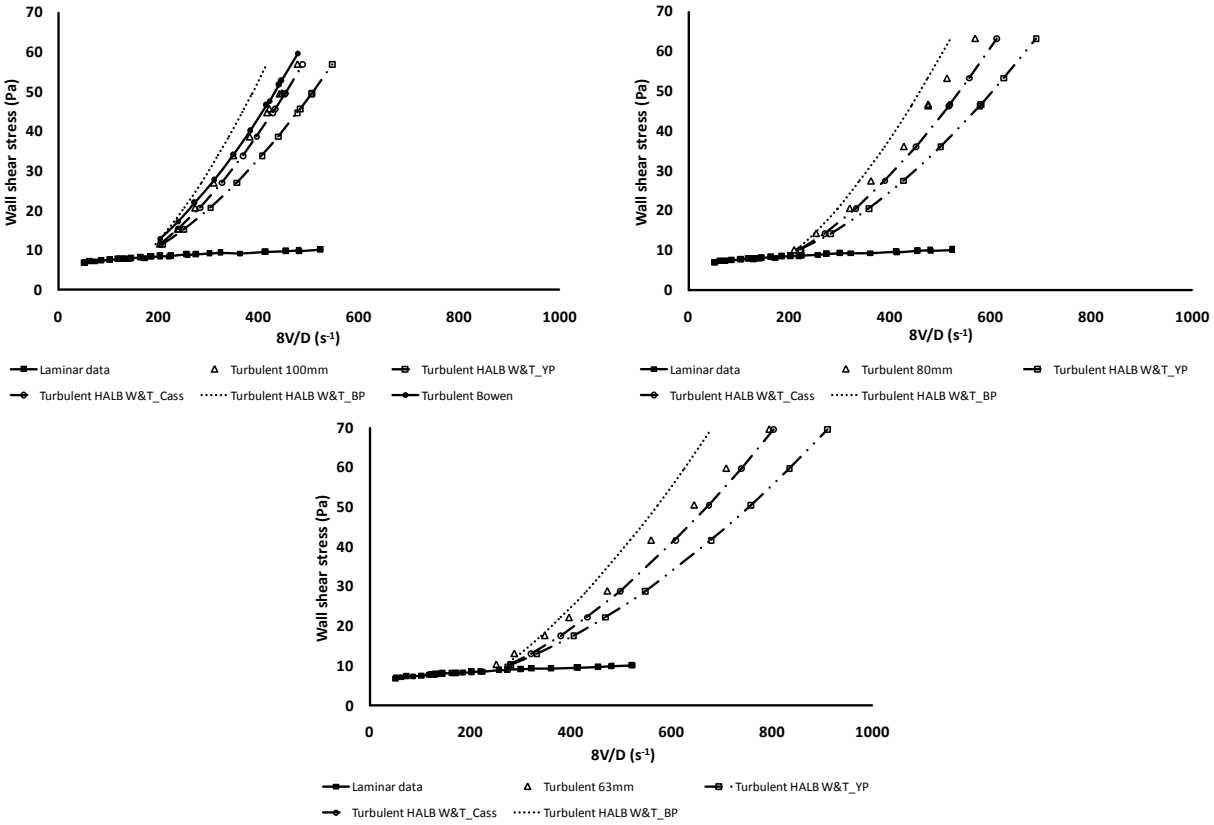

(8V/D) RMSE values - Hallbom_Mod W&T (SW)				
Pipe diameter	**BP**	**CASS**	**YP**	**BOWEN (To)**
100mm	6.9%	1.3%	6.3%	10.3%
80mm	4.1%	5.1%	9.5%	N/A
63mm	4.3%	10.3%	14.4%	N/A
Ave	**5.1%**	**5.6%**	**10.1%**	**10.3%**

Figure 5.49 Turbulent flow predictions and average % error for 6% kaolin using the Hallbom modified Wilson & Thomas method – all rheologies

Hallbom's smooth wall modified Wilson & Thomas technique produced reasonably accurate results using all the rheologies, but was best for the Casson rheology. The lower average error for the Bingham plastic rheology is not representative of the performance of the rheology as the slope of the predicted turbulent flow curve is too high, and the prediction becomes increasingly inaccurate with increasing shear rate. Bingham plastic rheology, the least appropriate for the kaolin material was unable to follow

the rheogram curvature, resulting in an over estimation of wall shear stress as shear rate increases (in laminar flow). Extrapolating this result to the required turbulent shear stress then underpredicts the velocity. The Casson model follows the laminar data trend well and so gives consistently reliable results for all concentrations, even at the higher shear rates. The yield plastic model underpredicts the shear stresses and does not follow the data trend well especially for the 6% and 15% concentrations, although for the 10% concentration the error was only 6.7%.

Hallbom: Partially rough wall turbulence (pseudofluid) - using Nikuradse turbulent equation

Figure 5.50 presents the turbulent predictions and average error (in %) for kaolin in three pipe sizes using the Hallbom pseudo fluid Nikuradse method with each rheological model in turn.

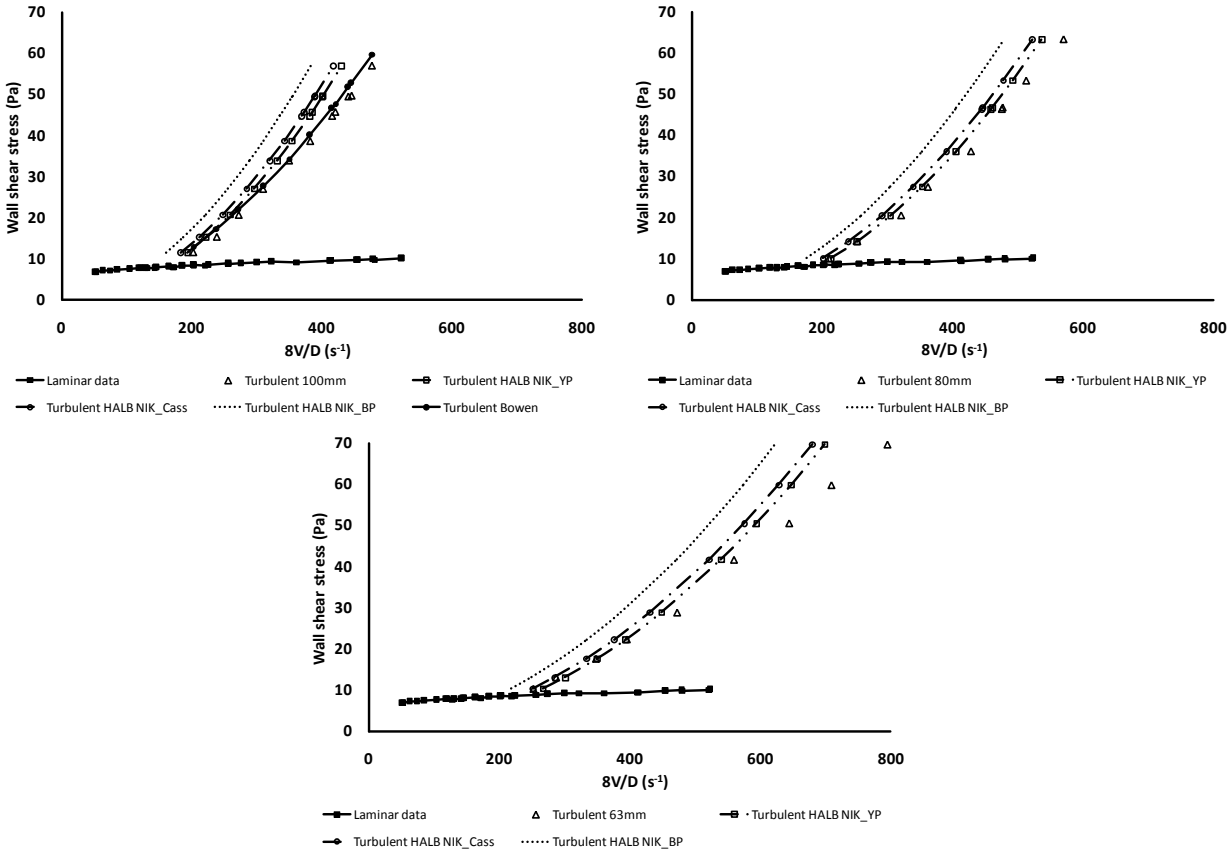

(8V/D) RMSE values - Hallbom_Nikuradse				
Pipe diameter	**BP**	**CASS**	**YP**	**BOWEN (To)**
100mm	20.4%	10.1%	5.5%	10.3%
80mm	17.5%	6.3%	2.5%	N/A
63mm	14.0%	1.8%	3.8%	N/A
Ave	**17.3%**	**6.0%**	**3.9%**	**10.3%**

Figure 5.50 Turbulent flow predictions and average % error for 6% kaolin using the Hallbom pseudo fluid Nikuradse method – all rheologies

This approach by Hallbom incorporates pipe roughness in the turbulent flow analysis via the Nikuradse Newtonian approach, using the appropriate rheological model (Bingham plastic, Casson or yield plastic). The technique gave good turbulent predictions using the Casson and yield plastic rheologies and was consistent for all concentrations, but when using the Bingham plastic rheology the turbulent shear stresses were again overpredicted. The results from this technique showed a similar trend to those of the Slatter technique for the common rheologies. Similar results were obtained for the 10% and 15% kaolin and are given in Appendix H. These finding are in line with the result reported by Hallbom (2008).

Dodge and Metzner

The Dodge and Metzner approach has two restrictions which make comparison with the other techniques difficult. The first is that the values of *n*' and *K*' must be evaluated at the same shear stress in laminar flow for which the turbulent prediction is required. This is extremely difficult to achieve in practice, as very small pipe sizes are required. It was not achieved in this work. Secondly the validity of the method is limited to $0.36 \leq n \leq 1.0$ (Chhabra & Richardson, 2008).

To avoid excessive extrapolation of the laminar data, comparison of predictions with experimental turbulent data were limited to either the maximum shear stress obtained in laminar flow or alternatively 1.25 times this value for any data set (see Section 3.2.7). This resulted in a low unusable turbulent shear stress experimental range in some cases, insufficient to achieve valid *n*' values. Some *n*' values in the range 0.36 – 0.39 still resulted in absurd predictions. The Dodge & Metzner technique therefore could not be used for any of the kaolin turbulent predictions over the same turbulent experimental data range as used for the other prediction techniques.

Newtonian Approximation

Figure 5.51 presents the turbulent predictions and average error (in %) for kaolin in three pipe sizes using the Newtonian Approximation method with each rheological model in turn.

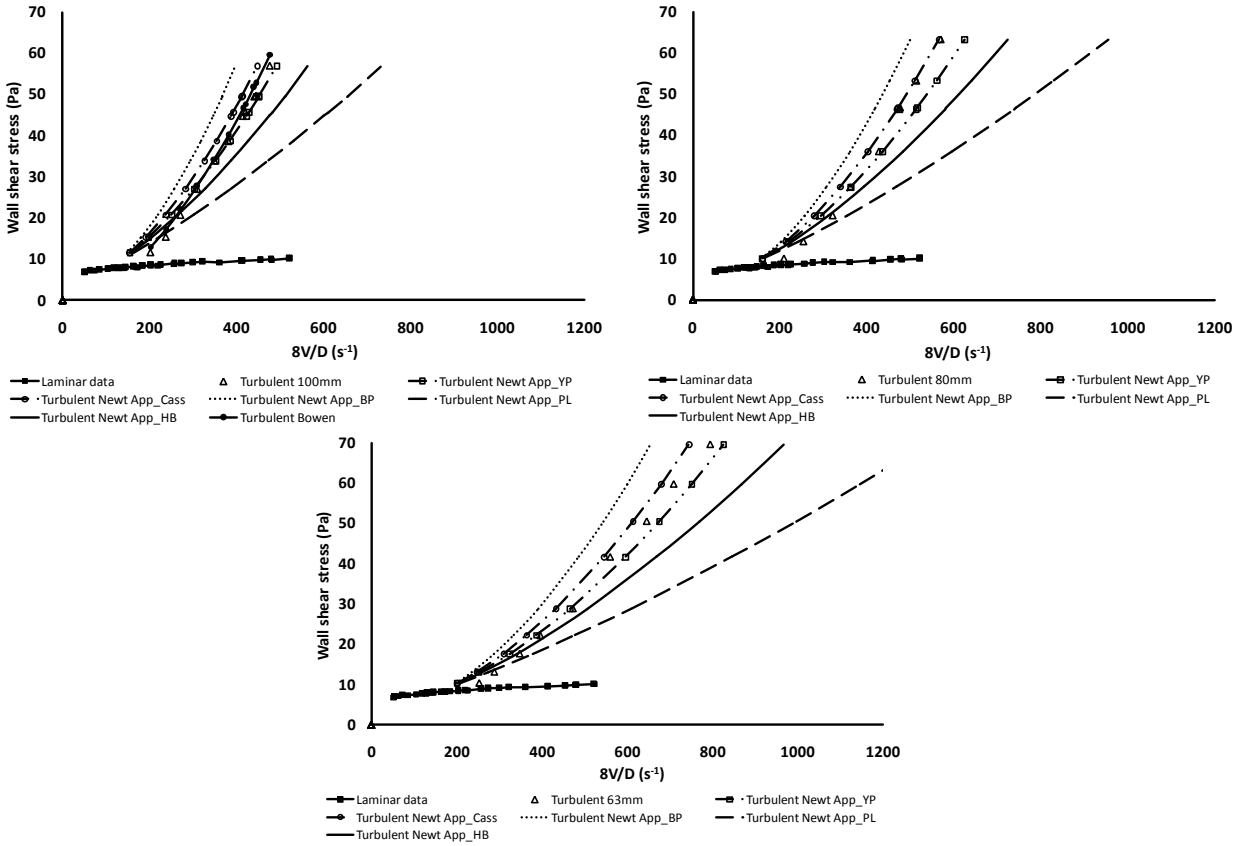

(8V/D) RMSE values - Newtonian approximation method						
Pipe diameter	**HB**	**BP**	**PL**	**CASS**	**HALL_YP**	**BOWEN (To)**
100mm	12.6%	23.3%	12.3%	18.8%	16.1%	10.3%
80mm	12.1%	21.8%	12.3%	17.7%	15.5%	N/A
63mm	10.3%	19.2%	10.4%	15.2%	13.4%	N/A
Ave	**11.7%**	**21.4%**	**11.6%**	**17.2%**	**15.0%**	**10.3%**

Figure 5.51 Turbulent flow predictions and average % error for 6% kaolin using the Newtonian Approximation method – all rheologies

The Newtonian approximation shows varying results for the kaolin turbulent predictions for the different rheologies. At the lower turbulent shear stresses the technique overpredicts the experimental wall shear stress data. The Casson, yield plastic and Bingham plastic rheologies follow the slope of the experimental data best, but the Bingham plastic rheology overpredicted turbulent τ_w the most. The Herschel-Bulkley and power law rheologies produce much flatter slopes for the turbulent predictions and as a result, underpredict the turbulent τ_w significantly. Based on the results the power law rheology is the least suitable rheology when using this technique and the Casson rheology best. Similar results were obtained for the 10% and 15% kaolin (see Appendix H), except that for all rheologies the technique predicts a much lower turbulent velocity than the experimental data. The consistent underprediction of the turbulent velocity when using the Newtonian approximation could be attributed to the increasing viscous sub-layer thickness during non-Newtonian turbulent flow, and subsequent increase in throughput velocity for a given wall shear stress (Wilson & Thomas, 1985). This phenomenon is not considered when using the standard Newtonian theory (see Section 2.6.1) applied in this technique. These results are in line with those of Wilson & Addie (2002) for the turbulent predictions of clay slurries using different turbulent prediction methods which do and do not include the sub-layer thickening.

Torrance

Figure 5.52 presents the turbulent predictions and average error (in %) for kaolin in three pipe sizes using the Torrance method with each rheological model in turn.

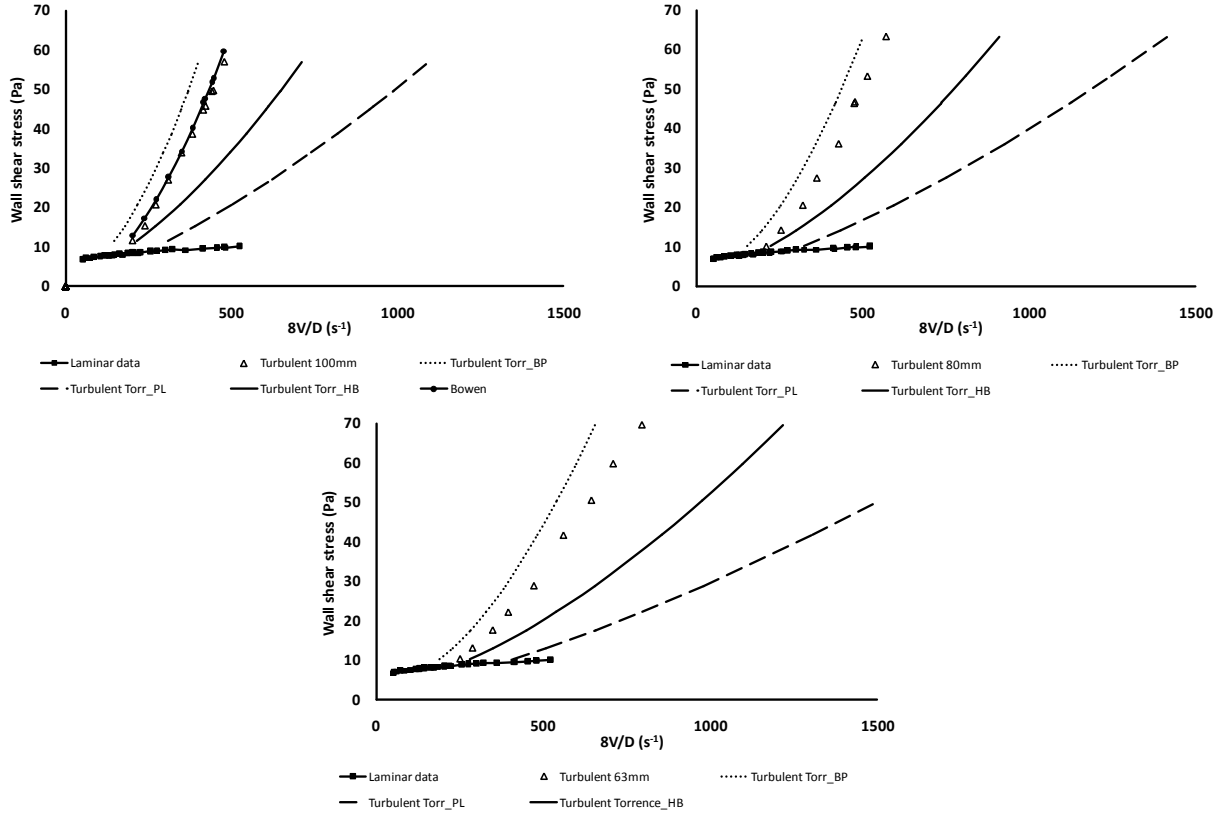

(8V/D) RMSE values - Torrance method				
Pipe diameter	**HB**	**BP**	**PL**	**BOWEN (To)**
100mm	15.4%	24.3%	66.5%	10.3%
80mm	17.1%	23.2%	70.1%	N/A
63mm	20.7%	21.2%	76.2%	N/A
Ave	**17.8%**	**22.9%**	**71.0%**	**10.3%**

Figure 5.52 Turbulent flow predictions and average % error for 6% kaolin using the Torrance method – all rheologies

Predictions using the Torrance technique vary significantly with rheology. Using the Bingham plastic rheology overpredicts the turbulent shear stress data, using the power law rheology grossly underpredicts shear stresses, using the Herschel-Bulkley rheological model also underpredicts shear stresses giving a turbulent flow curve approximately equidistant from those of the other two rheologies. The significant differences between the predictions show the sensitivity of the Torrance method to rheology. Similar results were obtained for the 10% and 15% kaolin (see Appendix H). The sensitivity of the technique to rheology is likely due to inclusion of n in the von Karman constant formulation (κ = 0.36n), illustrating its dependence on the viscous characteristics of the fluid. Due to the inaccurate and inconsistent predictions obtained with this technique, the Torrance analysis was not extended to the Casson and yield plastic rheologies for this work.

The underprediction of the turbulent wall shear stress using the Herschel-Bulkley rheology with this technique was also found by other researchers, for example El-Nahhas *et al.*, (2005) who got similar results to those of this study. Slatter (1994) achieved reasonable results for the turbulent flow prediction of kaolin using the Herschel-Bulkley model and Torrance approach, achieving an average error of 17%. Better correlation was observed at lower turbulent shear stresses. The Torrance technique, however is unable to model the turbulent data slope using the power law and Herschel-Bulkley rheology and results in order of magnitude errors as the shear rate increases. Using the Bingham plastic rheology was the most consistent and follows the data trend best, but it overpredicts the shear stress significantly. Based on these results and observations, the Torrance technique is not recommended for the prediction of turbulent flow for kaolin slurries.

Bowen scale-up method

Results for the Bowen scale-up method are included in the comparison plots for the different techniques presented in Figure 5.46 to Figure 5.52. The Bowen scale-up technique does not require the rheological properties of a fluid, hence it was not plotted separately for different rheologies. It does require turbulent flow data, for the same fluid from at least two (preferably three) pipes of smaller diameter than that for which the turbulent flow is to be predicted. The technique gave good predictions for the turbulent flow of kaolin and followed the data trend well. An average error of 10% was found for the 6% kaolin and an average error of 3% for the 10% kaolin in the diameter 150mm pipe. It should be ensured that the turbulent data from the smaller pipes are well into the turbulent regime. Ideally the turbulent data branches should be parallel, and the computed value for the constant (c) must not be negative (see Section 2.6.1).

One rheology plotted for all techniques

The analysis now focuses on the individual rheological models plotted for all techniques. The most appropriate rheological model for kaolin was found to be the Herschel-Bulkley model (Section 4.2.1), but based on the results presented in Figure 5.46 to Figure 5.52 this rheology did not necessarily give the best turbulent flow predictions for kaolin. Figure 5.53 to Figure 5.59 show the predictions of each technique using each selected rheology for the 6% kaolin. The results for the 10% and 15% kaolin are given in Appendix H.

Bingham plastic

Figure 5.53 presents the turbulent predictions and average % error for kaolin in three pipe sizes using the Bingham plastic model with each turbulent flow prediction technique.

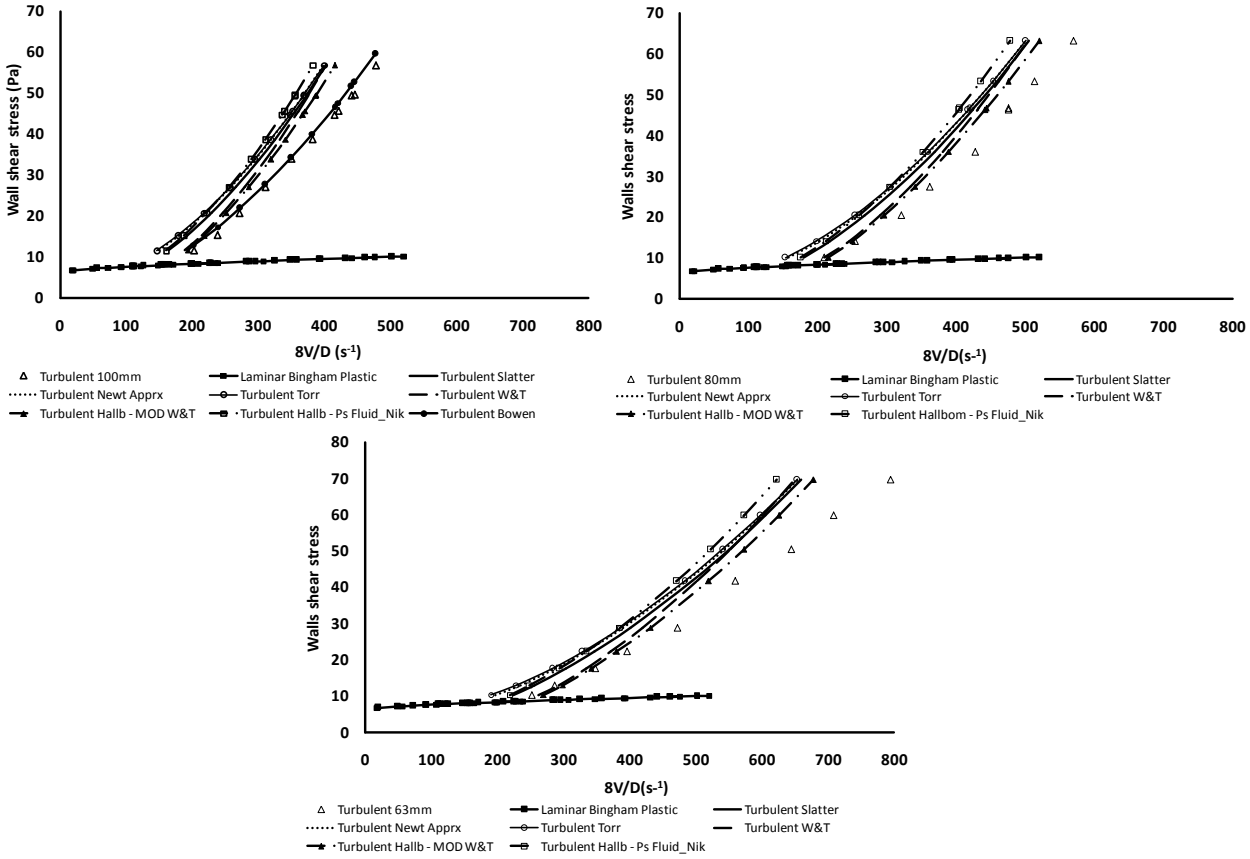

(8V/D) RMSE values - Bingham Plastic								
Pipe diameter	**W&T**	**NEWT**	**TORR**	**D&M**	**SLATT**	**BOWEN (To)**	**MOD_W&T**	**Ps Fld_Nik**
100mm	8.7%	23.3%	24.3%	N/A	18.0%	10.3%	6.9%	20.4%
80mm	4.3%	21.8%	23.2%	N/A	15.1%	N/A	4.1%	17.5%
63mm	3.3%	19.2%	21.2%	N/A	11.6%	N/A	4.3%	14.0%
Ave	**5.4%**	**21.4%**	**22.9%**	**N/A**	**14.9%**	**10.3%**	**5.1%**	**17.3%**

Figure 5.53 6% kaolin turbulent flow predictions and average % error using the Bingham plastic rheology – all techniques

The PRW Wilson & Thomas (1985) and the SW Hallbom (2008) modified Wilson & Thomas techniques best predict the kaolin turbulent flow data using the Bingham plastic rheology, producing nearly identical results. The slight differences observed could be attributed to the way each technique incorporates pipe roughness, and computes the Newtonian velocity component in its formulation. The Wilson & Thomas method uses the varying apparent viscosity and Hallbom uses the constant infinite shear rate viscosity. When using the Bingham plastic rheology all techniques overpredict the pressure drop in turbulent flow, with the exception of the Wilson & Thomas and modified Hallbom techniques, the results are very similar and tightly grouped. Slatter *et al.* (1997) suggests that this is because at higher shear stresses the influence of τ_y decreases as the influence of n increases, due to the nature of the power law part of the relationship. All of the models are based on Newtonian theory and therefore revert to the Newtonian model as the conditions approach Newtonian, which is the case at higher shear stresses for the Bingham plastic model. Similar conclusions were drawn by Heywood & Cheng (1984) who showed that the various predictions approach each other as the conditions approach Newtonian (n approaches unity). This could also explain similarities between the Torrance and Newtonian approximation techniques, as Torrance use the same mixing length model used to derive Newtonian turbulent flow. Similarly the distinct similarity between the Slatter and Nikuradse pseudo fluid methods is assumed to be due to the Newtonian basis of both approaches. These similarities are particularly emphasised in the 10% kaolin results. The 10% and 15% kaolin results are given in Appendix H.

Power law

Figure 5.54 presents the turbulent predictions and average % error for kaolin in three pipe sizes using the power law rheological model with each turbulent flow prediction technique.

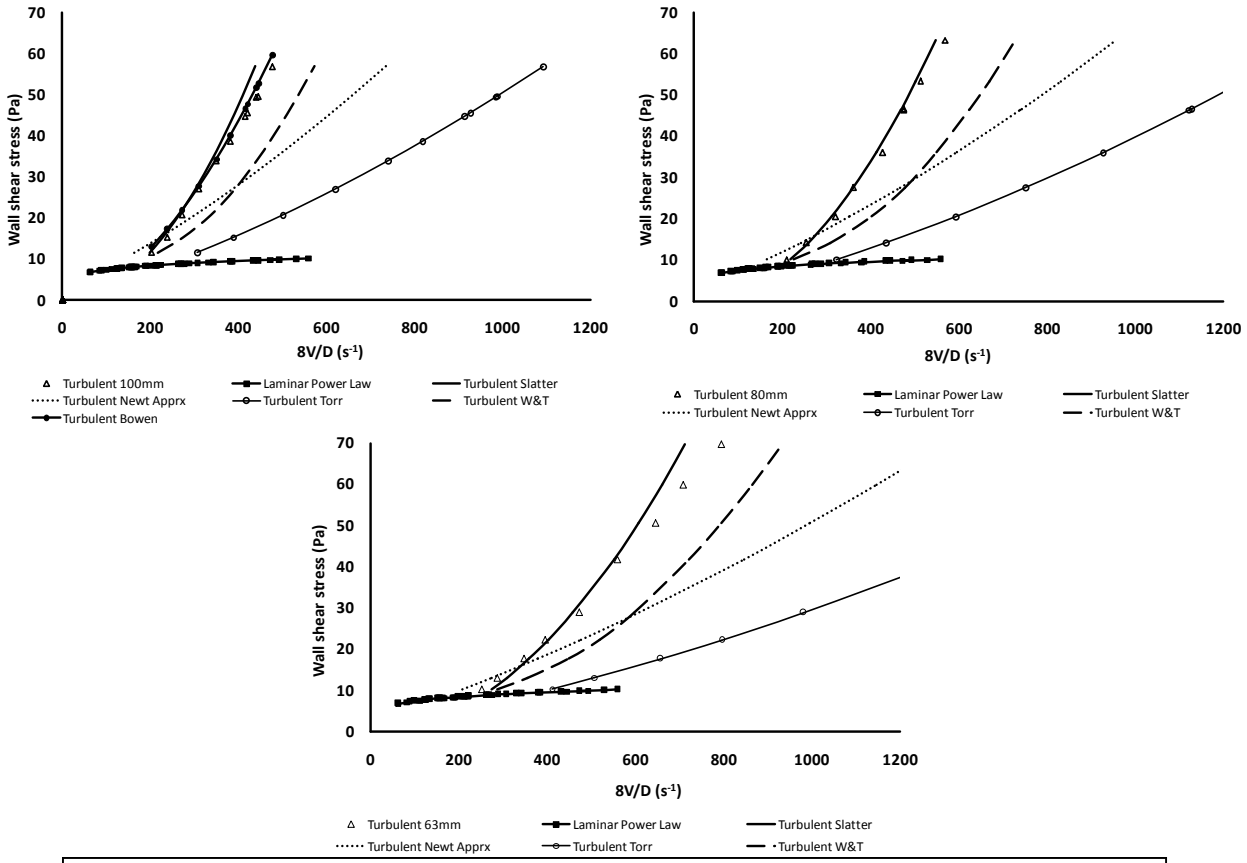

(8V/D) RMSE values - Power Law						
Pipe diameter	**W&T**	**NEWT**	**TORR**	**D&M**	**SLATT**	**BOWEN (To)**
100mm	15.5%	12.3%	66.5%	N/A	3.2%	10.3%
80mm	18.3%	12.3%	70.1%	N/A	3.1%	N/A
63mm	22.1%	10.4%	76.2%	N/A	6.4%	N/A
Ave	**18.6%**	**11.6%**	**71.0%**	**N/A**	**4.2%**	**10.3%**

Figure 5.54 6% kaolin turbulent flow predictions and average % error using the power law rheology – all techniques

The power law rheology proves unsuccessful in predicting kaolin turbulent flow, except when used with the Slatter model. The Wilson & Thomas, Newtonian approximation and Torrance techniques significantly underpredict the turbulent flow shear stress data and show flatter slopes than the experimental turbulent τ_w vs. (*8V/D*). This is likely due to the extrapolation of the laminar data to the much higher shear stress values for turbulent flow. For the power law rheology the smaller the *n* value, the more significant the rheogram curvature is and the more significant the shear thinning effect. This results in higher shear rate values for a given shear stress in laminar flow compared to other rheological models, which is exaggerated when extrapolated to turbulent flow, and results in large prediction errors. The *n* values for the 6%, 10% and 15% kaolin are 0.182, 0.147 and 0.103 respectively, which are quite low. As a result, the error increases significantly with an increase in concentration due to the decreasing value of *n*.

The Slatter model produced fairly accurate predictions in the lower turbulent shear rate range, but as for the other techniques, the slope of the turbulent branch of the τ_w vs. (*8V/D*) curve differs from that of

the experimental data which leads to significant errors in pressure drop predictions as the shear rate increases which vary with pipe diameter. The Slatter model predicts a slightly steeper τ_w vs. (*8V/D*) slope than the experimental data, especially for the 10% and 15% concentrations (Appendix H), but is the preferred technique for the power law rheology. The reason for the better prediction is the influence of the particle roughness which Slatter incorporates (Slatter *et al*., 1997), although this over compensates in the case of the kaolin concentrations, resulting in the steeper predicted τ_w vs. (*8V/D*) slope than that of the experimental data.

Herschel-Bulkley

Figure 5.55 presents the turbulent predictions and average % error for kaolin in three pipe sizes using the Herschel-Bulkley rheological model with each turbulent flow prediction technique.

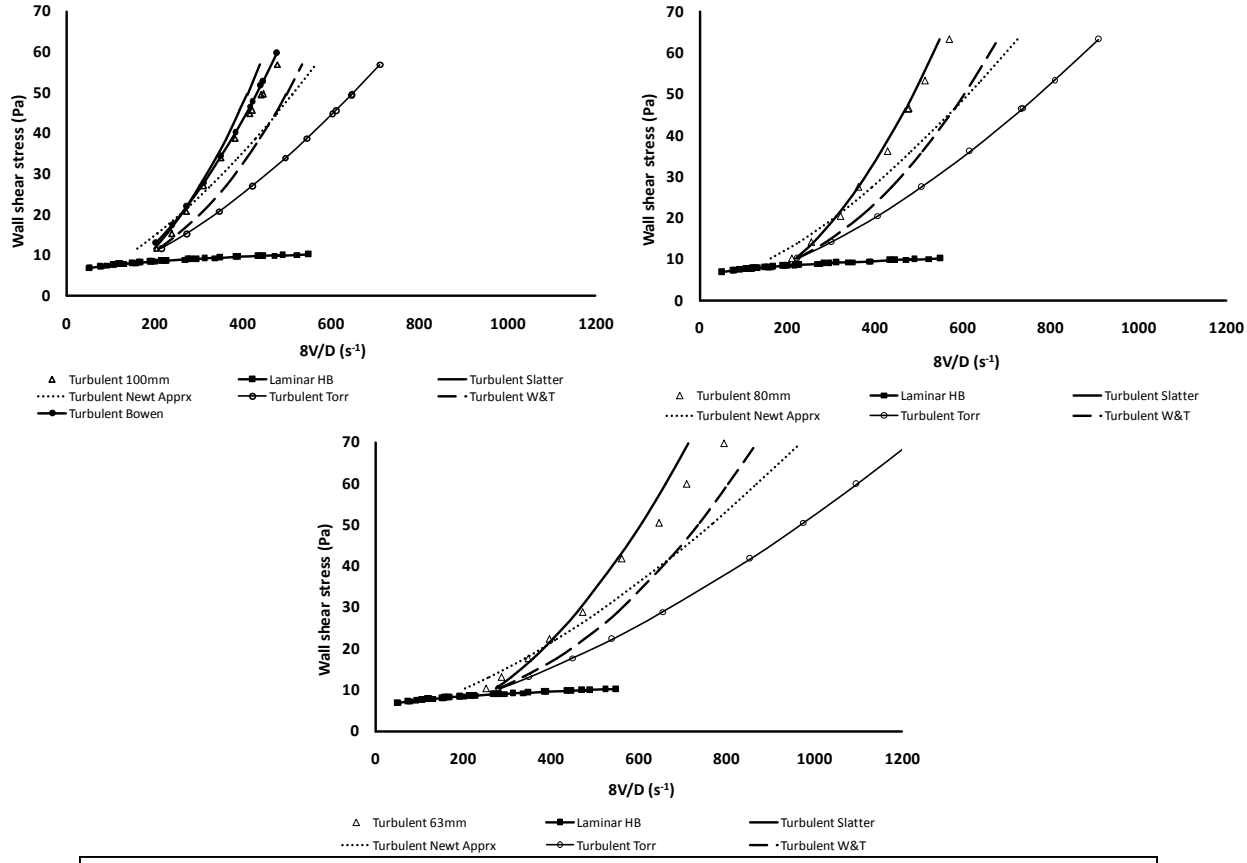

(8V/D) RMSE values - Herschelle-Bulkley						
Pipe diameter	**W&T**	**NEWT**	**TORR**	**D&M**	**SLATT**	**BOWEN (To)**
100mm	7.8%	12.6%	15.4%	N/A	3.2%	10.3%
80mm	11.2%	12.1%	17.1%	N/A	3.1%	N/A
63mm	15.4%	10.3%	20.7%	N/A	6.4%	N/A
Ave	**11.5%**	**11.7%**	**17.8%**	**N/A**	**4.2%**	**10.3%**

Figure 5.55 6% kaolin turbulent flow predictions and average % error using the Herschel-Bulkley rheology – all techniques

The Herschel-Bulkley rheological model best described the kaolin laminar data (lowest error) for all test concentrations. Using this rheology the Wilson & Thomas, Newtonian approximation and Torrance techniques all underpredict turbulent shear stresses to varying degrees. The slopes of the Wilson & Thomas predicted τ_w vs. (*8V/D*) turbulent flow curves are in reasonable agreement with the experimental data, but the Newtonian Approximation and the Torrance predictions have significantly flatter slopes. The predicted results for the 10% and 15% concentrations were better than the 6%

concentration. The average errors for these three techniques for the turbulent pressure drop predictions were 11%, 12%, and 18% respectively for the 6% concentration, 8%, 23% and 14% for the 10% concentration and 21%, 15%, 64% for the 15% test concentration respectively. Predictions using the Herschel-Bulkley rheology with the Slatter technique correlate well with experimental results in the lower turbulent shear stress range for the 6% kaolin, due to the particle roughness influence which the technique adopts. At the higher 10% and 15% concentrations the Slatter technique over compensates for particle roughness and the slope of the predicted τ_w vs. (*8V/D*) curve exceeds that of the experimental data, resulting in the overprediction of the pressure drop at higher shear rates. A similar observation was made for the Bingham rheology. Slatter's technique is, however, still the most successful in predicting the kaolin turbulent flow data with errors of 3% to 6% for the 6% kaolin, 5% to 14% for the 10% concentration and 16% (average) for the 15% kaolin in the diameter 150mm pipe. Similar results to these were obtained by others for example Chilton & Stainsby (1996), Slatter *et al.* (1997), Chilton & Stainsby (1998) and Kumar, Saboo, Sheth, Pilehvari & Serth (2000).

Casson

Figure 5.56 presents the turbulent predictions and average % error for kaolin in three pipe sizes using the Casson rheological model with each turbulent flow prediction technique.

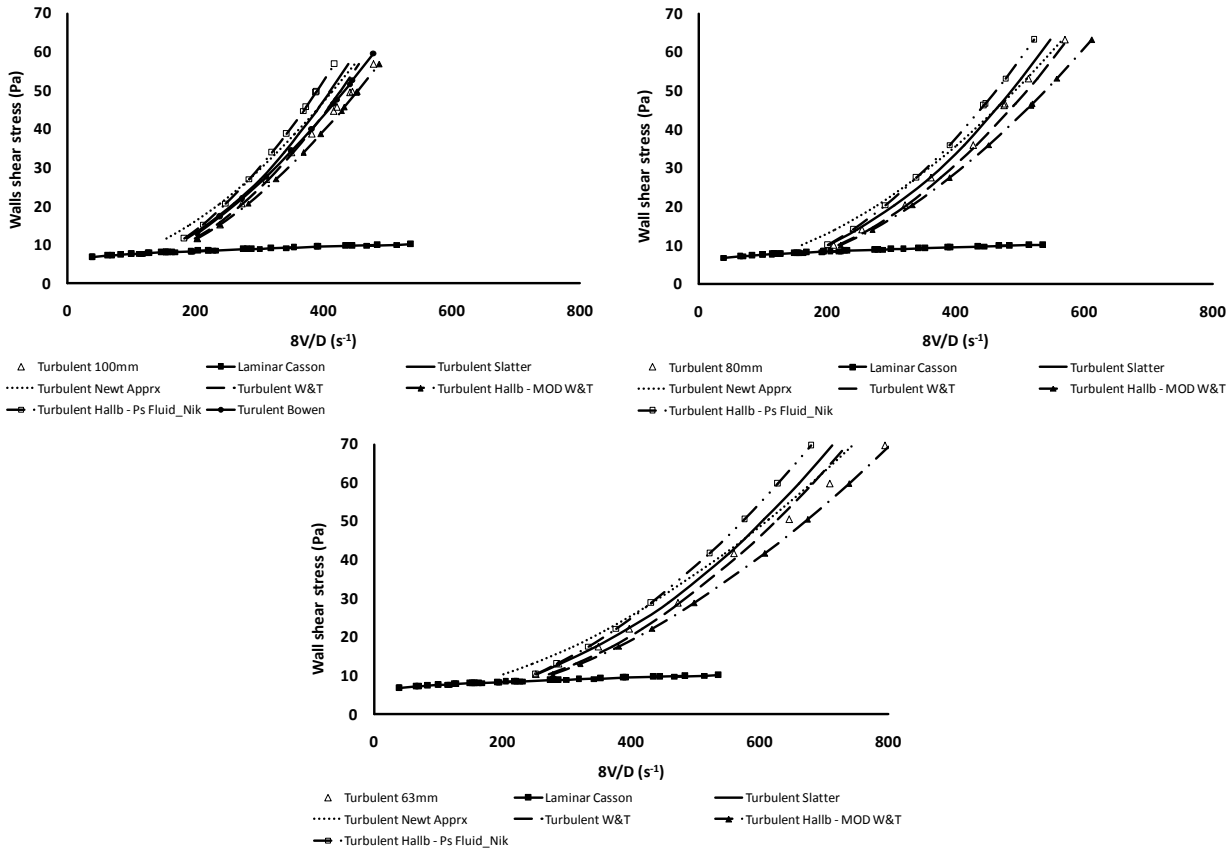

(8V/D) RMSE values - Casson								
Pipe diameter	**W&T**	**NEWT**	**TORR**	**D&M**	**SLATT**	**BOWEN (To)**	**MOD_W&T**	**Ps Fld_Nik**
100mm	1.5%	18.8%	N/A	N/A	7.3%	10.3%	1.3%	10.1%
80mm	3.0%	17.7%	N/A	N/A	3.8%	N/A	5.1%	6.3%
63mm	7.8%	15.2%	N/A	N/A	0.8%	N/A	10.3%	1.8%
Ave	**4.1%**	**17.2%**	**N/A**	**N/A**	**3.9%**	**10.3%**	**5.6%**	**6.0%**

Figure 5.56 6% kaolin turbulent flow predictions and average % error using the Casson rheology – all techniques

Considering the turbulent flow predictions for the 6% kaolin test concentration presented in Figure 5.56, as well as those for the 10% and 15% test concentrations presented in Appendix H, it is seen that using the Casson rheology gave accurate predictions. The Newtonian approximation and Nikuradse PRW pseudofluid method constantly overpredicted the pressure drop, and is not considered to be a reliable techniques using this rheology. Both these techniques do not incorporate drag reduction, by ignoring the thickening of the viscous sub-layer, nor do they include the particle roughness effect. The other techniques showed good agreement between the predicted results and the experimental data. The results vary slightly for the different test concentrations, but the general trend remains consistent. Errors for the 6% and 10% kaolin range from 1% to 10% for all prediction techniques except the Newtonian approximation, and from 1% to 15% for the 15% kaolin. Using the Casson rheology gives predictions that lie between those obtained when using the Bingham plastic rheology (overpredict pressure drop) and the power law and Herschel-Bulkley rheologies (underpredict pressure drop). Similar results were obtained by Wilson & Addie (2002) when comparing the use of power law and Bingham plastic models with the Wilson & Thomas technique to predict turbulent flow of kaolin slurries. Heywood and Alderman (2003) have also confirmed increasing popularity of the Casson model to predict turbulent flow because it gives consistently accurate results.

Predictions by the Wilson & Thomas (1985) and modified Hallbom (2008) methods show close agreement, as for the Bingham plastic rheology. Errors for the 6% and 10% test concentrations using the Wilson & Thomas (1985) technique range between 1.5% and 8%, and between 1.5% and 10% for the modified Hallbom (2008) method. For the 15% kaolin, these techniques underpredict the pressure drop with errors of 12% and 14% respectively for the 150mm diameter pipe. Predictions using the Slatter technique show excellent agreement with the 6% experimental turbulent data, following the values and the slope of the τ_w vs. (*8V/D*) curve accurately. However for the 10% and 15% kaolin slurries the slope of the τ_w vs. (*8V/D*) curve predicted by the Slatter technique is too high, resulting in overprediction of the pressure drop as the shear rate increases, similarly to the Nikuradse PRW pseudofluid method (Hallbom, 2008). The same observation was made earlier for the Bingham plastic rheology. The reasons for this behaviour are presented there.

Hallbom yield plastic

Figure 5.57 presents the turbulent predictions and average % error for kaolin in three pipe sizes using the Hallbom yield plastic rheological model with each turbulent flow prediction technique.

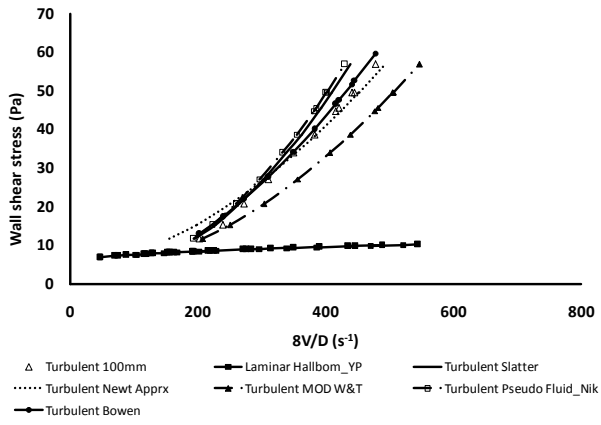

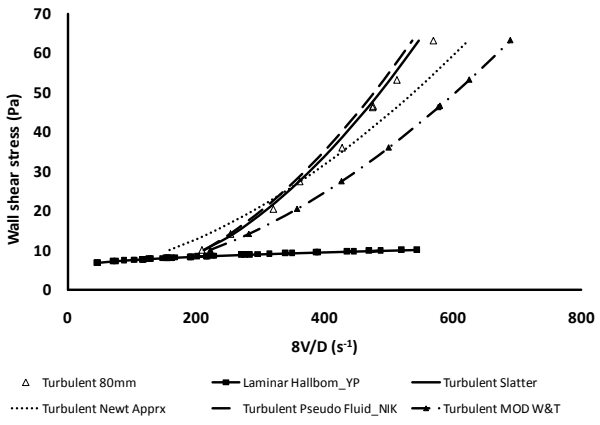

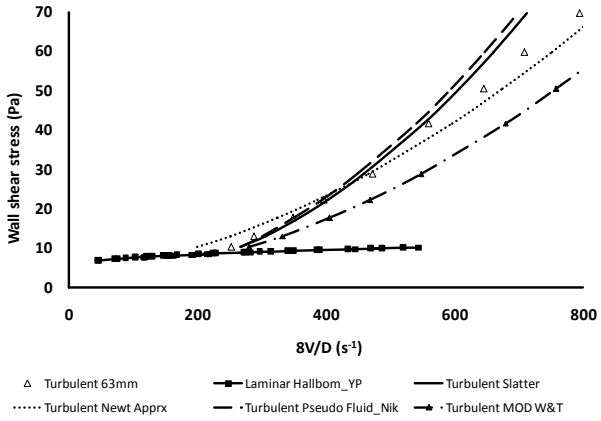

(8V/D) RMSE values - Hallbom_Yield plastic					
Pipe diameter	**MOD_W&T**	**NEWT**	**Ps Fld_Nik**	**SLATT**	**BOWEN (To)**
100mm	6.3%	16.1%	5.5%	5.4%	10.3%
80mm	9.5%	15.5%	2.5%	2.0%	N/A
63mm	14.4%	13.4%	3.8%	5.1%	N/A
Ave	**10.1%**	**15.0%**	**3.9%**	**4.2%**	**10.3%**

Figure 5.57 6% kaolin turbulent flow predictions and average % error using the Hallbom yield plastic rheology – all techniques

Predictions using the yield plastic rheology are very similar to those using the Casson rheology. This is to be expected since the Casson rheological model is a special case of the yield plastic model, and both a direct measure of the viscosity. The yield plastic model of Hallbom is a recent approach and has not been widely quoted in the literature. In this study using this rheology to predict turbulent pressure drops in kaolin slurries with the Hallbom Nikuradse pseudofluid and Slatter technique show good agreement with each other and with the experimental values. For the 6% kaolin errors were in the range of 2% to 6% (Hallbom Nikuradse pseudofluid) and 2% to 5% (Slatter). For the 10% kaolin errors for both techniques were between 6% and 7%. 15% kaolin, which was only tested in the 150mm diameter pipe, shows errors of 14.5% (Hallbom Nikuradse pseudofluid) and 14.2% (Slatter). The Slatter and PRW Hallbom Nikuradse pseudo fluid methods again gave almost identical results, as was observed for the Bingham and Casson rheologies.

Kaolin turbulent flow summary

The experimental and predicted turbulent flow pressure drops for the kaolin slurries, presented above and in Appendix H, indicate that the Slatter turbulent flow prediction model generally gives the most consistently accurate results particularly when used with the Casson rheology (3.9% to 8.5% error). The success is attributed to the inclusion of the particle roughness effect. Most of the techniques considered underpredict the slope of the turbulent τ_w vs. (*8V/D*) curve, but the Slatter technique predicts a steeper slope which more closely matches the experimental data. The Wilson & Thomas (1985), Hallbom (2008) modified Wilson & Thomas and Hallbom (2008) pseudofluid Nikuradse techniques give similar results to the Slatter method, especially when using the Casson or the yield plastic rheological model. The Slatter and Wilson & Thomas models show significant dependence on the value of *n*, thus emphasising the importance of the laminar flow rheological characterisation for use in turbulent flow predictions. The Dodge & Metzner method was not applied to the kaolin data set for comparison due to the restrictions on τ_w imposed by the approach. The Newtonian approximation underpredicts the turbulent shear rate (overpredicts shear stress) data for all rheologies as it ignores the sub-layer thickness in the formulation. The method of Torrance (1963) shows significance dependence on the rheological model used yielding widely varying results for the different models and is not suitable for predicting turbulent flow for kaolin slurries using any of the rheologies considered. Bowen's (1961) method showed good agreement for the

6% and 10% kaolin, with an average error of 10% and 3% respectively, and is independent of the rheological properties of the test fluid.

It seems apparent that for kaolin the Casson rheology is actually best suited for predicting the turbulent flow with all the techniques except with the Newtonian approximation. Using the Bingham plastic rheology constantly overpredicts the turbulent flow pressure drop, while use of the power law rheology vastly underpredicts it. Using the Herschel-Bulkley rheology underpredicts the turbulent flow pressure drops, but the predictions are reasonably accurate and an analysis with this rheology should always be included since it best describes the yield-pseudoplastic material. The yield plastic rheological model of Hallbom produced good agreement with experimental turbulent data when used in the Slatter, Hallbom modified Wilson & Thomas and Hallbom Nikuradse pseudo fluid techniques. The Slatter and Hallbom Nikuradse pseudo fluid techniques, and the Wilson & Thomas and the Hallbom modified Wilson & Thomas techniques gave similar results (values and slopes of τ_w vs. $8V/D$) when using the Casson, Bingham plastic, and Hallbom yield plastic rheologies. This is to be expected as the Casson and Bingham plastic rheologies are both special cases of the yield plastic rheology.

Effect of concentration and pipe diameter

The analyses presented above, for the various combinations of turbulent flow prediction techniques and rheological model revealed on occasion some dependence on slurry concentration and pipe diameter. To try to see this the % error was plotted against pipe diameter for the most appropriate prediction technique, which was the Slatter method in this case of the kaolin slurries. The results for each concentration are plotted separately as shown in Figure 5.58.

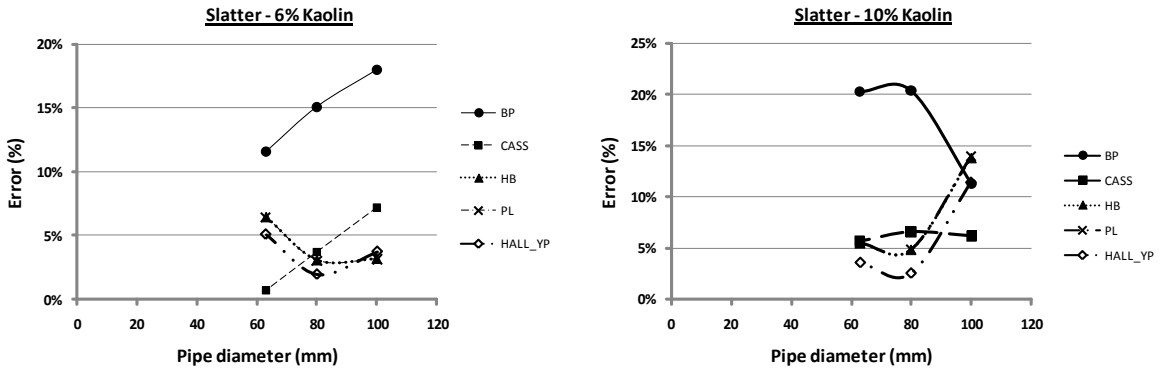

Figure 5.58 Effect of diameter on the % error value for the Slatter method in different pipe sizes at 6% and 10% kaolin concentrations

Unfortunately the plots in Figure 5.58 do not show any clear trends with respect to pipe diameter for either kaolin concentration, so no conclusion can be drawn in this regard. They do indicate though that the Bingham plastic rheology is unsuitable for use in kaolin turbulent flow predictions, but that the other rheologies can be used, generally resulting in errors of up to 15%. Turbulent flow was only achieved in one pipe size (diameter 150mm) for the 15% kaolin so no diameter effects are available for that material.

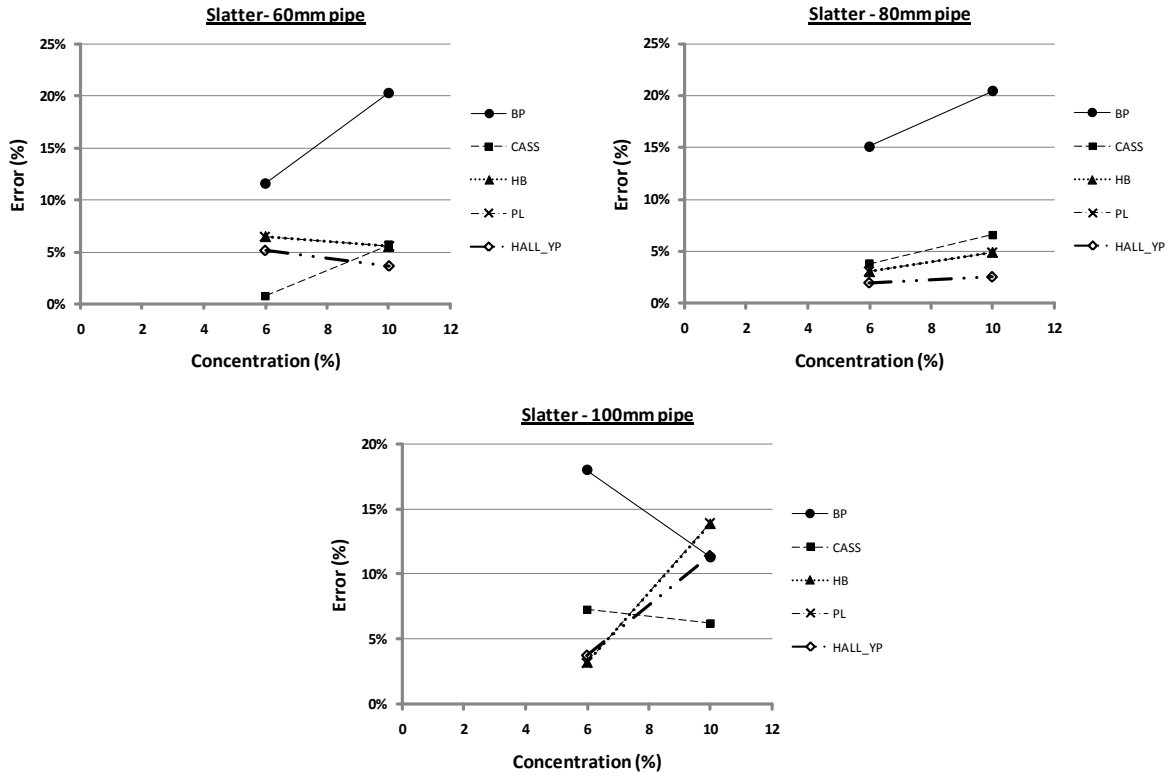

Figure 5.59 Effect of concentration on the % error value for the Slatter method at different kaolin concentrations in the diameter 60mm, 80mm and 100mm pipes

As for the diameter effect plots in Figure 5.58, the concentration effect plots shown in Figure 5.59 for the 60mm, 80mm, and 100mm diameter pipes do not show any clear trends. Although the 80mm pipe results show some consistency, it is inconclusive. Once again the plots show simply that generally the Bingham plastic rheological model is not appropriate for kaolin slurries, but that the other rheological models considered yield results that are within 15% of the experimental values. For the 15% concentration kaolin, turbulent flow was not achieved in the 60, 80 and 100mm diameter pipes and so results for these pipe diameters are absent from Figure 5.59.

5.3.2 Bentonite

The turbulent analysis and results for the bentonite test concentrations are presented and discussed in this section. Only the results for the 7.34% concentration are presented here, but the conclusions are based on results for all concentrations in all pipe sizes. Results for the 6% and 9% concentrations are given in Appendix I.

One technique plotted for all rheologies

The bentonite turbulent flow results are first presented as plots of predicted τ_w vs. (*8V/D*) for a single prediction method in one diameter pipe, for all the applicable rheologies. The experimental points are included in the plots.

Wilson and Thomas

Figure 5.60 presents the turbulent predictions and average error (in %) for bentonite in three pipe sizes using the Wilson & Thomas method with each rheological model in turn.

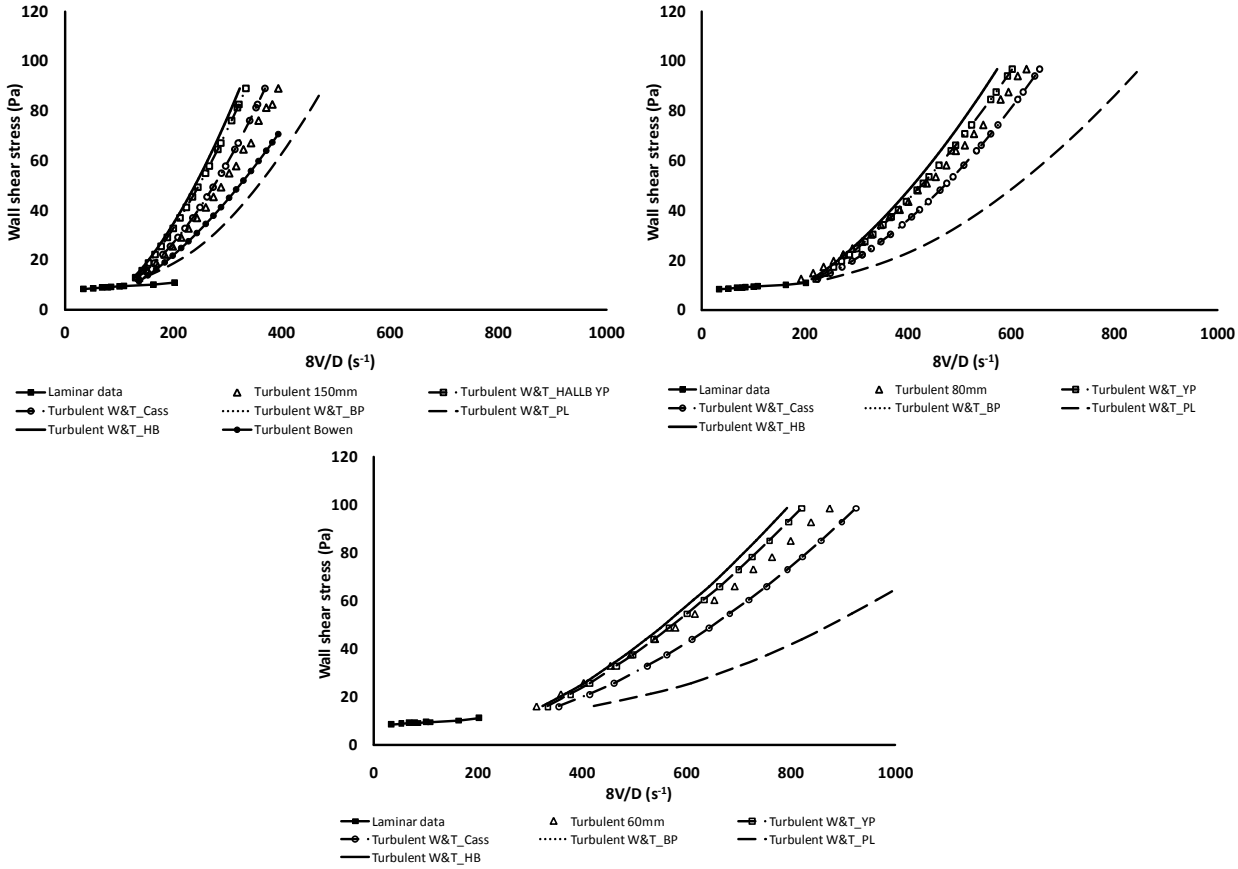

(8V/D) RMSE values - W&T(PRW) method						
Pipe diameter	HB	BP	PL	CASS	HALL_YP(SW)	BOWEN (To)
150mm	9.4%	9.4%	13.3%	2.2%	6.7%	12.2%
80mm	7.5%	7.5%	32.4%	15.7%	11.3%	N/A
60mm	2.0%	2.0%	44.8%	14.4%	4.9%	N/A
Ave	6.3%	6.3%	30.2%	10.8%	7.6%	12.2%

Figure 5.60 7.34% bentonite turbulent flow predictions and average % error using the Wilson & Thomas method – all rheologies

The bentonite slurry laminar data was best described by the Bingham plastic model (Section 4.3). The Herschel-Bulkley, and yield plastic models reduced to the Bingham plastic model for the 6% and 7.34% concentrations. The Herschel-Bulkley and Bingham plastic rheologies gave the same turbulent flow predictions, but the yield plastic rheology gave slightly different predictions due to the different yield stress and infinite shear viscosity. The results, however, are similar.

Referring to Figure 5.60, using the Bingham plastic or Herschel-Bulkley rheology gave the most accurate results for this technique. This was true for all the test concentrations. The predictions for the 7.34% concentration were good with errors between 2% to 10% but for the 6% and 9% concentrations the accuracy deteriorated to between 2% to 19% and 13% to 20% respectively. Generally the Wilson & Thomas method underpredicted the turbulent wall shear stress for all the rheologies for the 6% and 9% concentrations. The prediction results for the 7.34% concentration follow the experimental data and slope much more accurately.

Using the Casson rheology gave predictions which compared only with the diameter 150mm pipe for the 7.34% concentration experimental values. Generally with this rheology the turbulent wall shear stress was underpredicted. Predictions for the diameter 80mm and 150mm pipes for all concentrations using the Casson rheology significantly underpredict the turbulent wall shear stresses.

The power law model is not considered at all suitable for use with the Wilson & Thomas technique giving errors in the diameter 60mm pipe of up to 45% for the 7.34% concentration and 58% for the 9% concentration bentonite (see Appendix I). The main reason for this exaggerated failure is the force fitting of the power law model to the laminar flow data of a material which is not a power law fluid. Extrapolating this power law rheological model to the turbulent flow shear stress values results in unrealistic corresponding *8V/D* values (see Figure 5.47). It was also observed that for the 6% and 7.34% bentonite the Wilson & Thomas technique underpredicts the turbulent shear tresses more and more with increasing diameter.

Slatter

Figure 5.61 presents the turbulent predictions and average error (in %) for bentonite in three pipe sizes using the Slatter method with each rheological model in turn.

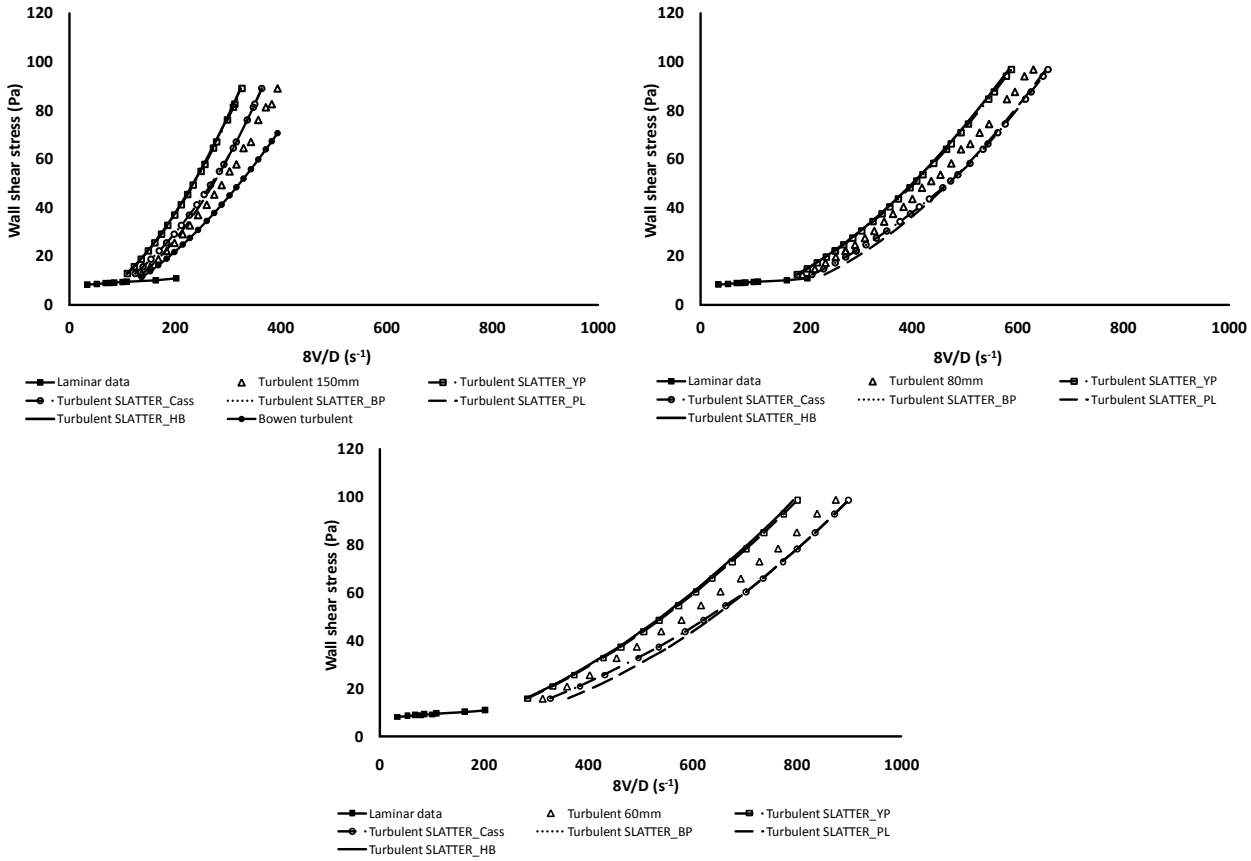

(8V/D) RMSE values - Slatter method						
Pipe diameter	HB	BP	PL	CASS	HALL_YP	BOWEN (To)
150mm	20.2%	20.2%	0.7%	8.7%	19.5%	12.2%
80mm	7.0%	7.0%	18.9%	8.3%	6.1%	N/A
60mm	9.1%	9.1%	15.2%	6.1%	8.2%	N/A
Ave	12.1%	12.1%	11.6%	7.7%	11.3%	12.2%

Figure 5.61 7.34% bentonite turbulent flow predictions and average % error using the Slatter method – all rheologies

The Slatter technique shows good agreement with the slope of the turbulent τ_w vs. (*8V/D*) data for all the rheologies, due to the incorporation of particle roughness in its formulation (Slatter et al, 1997). The most consistent results for all the concentrations were obtained using the Bingham plastic rheology although the Casson rheology shows slightly better predictions in some instances. For the 7.34% bentonite and using the Casson rheology the Slatter method gave errors in the range 6% to 9%. When

using the Bingham plastic, Herschel-Bulkley or yield plastic rheologies it overpredicted the turbulent wall shear stresses by 8% to 20%. For the 6% bentonite the predictions using the Bingham plastic, Herschel-Bulkley and yield plastic rheologies result in errors of 3% to 14% whilst Casson rheology results in predictions: 4% to 10% different to the experimental values. For the 9% concentration Slatter's method with the Bingham plastic rheology gives small errors of 1.7% to 2.7% and with the Herschel-Bulkley rheology errors of 4% to 7%. Using the Casson and yield plastic rheologies results in predictions that are 9% to 13% off the experimental values. Using the power law rheology overall gives the most inaccurate results, constantly underpredicting the turbulent flow data, except in the diameter 150mm pipe for the 7.34% concentration where the error is only 0.7% while all the other rheologies result in significant overprediction of τ_w. It is likely that in this case the experimental results may be wrong. The results indicate that for the lower concentrations the Casson rheology gives better results, and as the concentration increases the Bingham plastic rheology gives more accurate predictions.

Hallbom: Smooth wall turbulence – modified Wilson & Thomas method

Figure 5.62 presents the turbulent predictions and average error (in %) for bentonite in three pipe sizes using the Hallbom modified Wilson & Thomas method with each rheological model in turn.

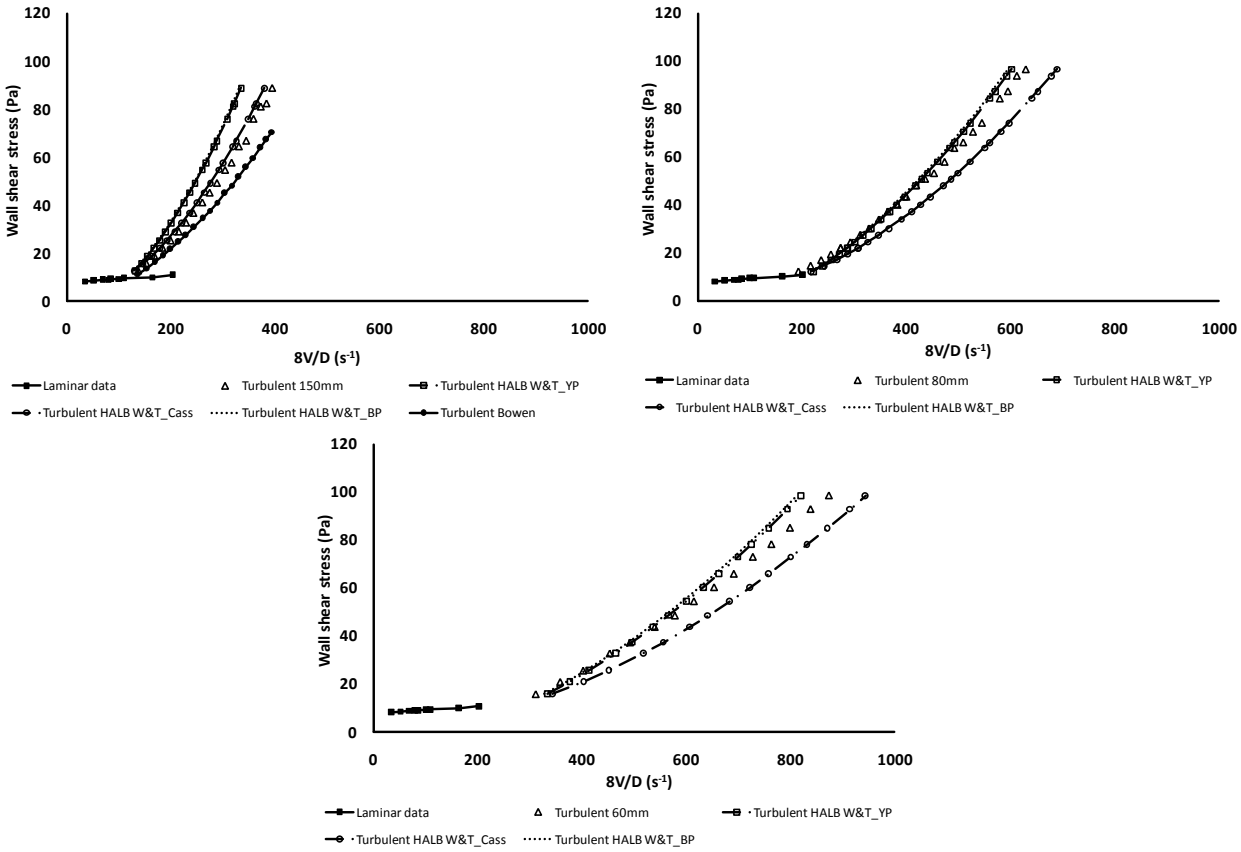

(8V/D) RMSE values - Hallb Mod W&T (SW)				
Pipe diameter	BP	CASS	YP	BOWEN (To)
150mm	7.9%	4.8%	6.7%	12.2%
80mm	9.7%	12.5%	11.3%	N/A
60mm	3.4%	11.6%	4.9%	N/A
Ave	7.0%	9.7%	7.6%	12.2%

Figure 5.62 7.34% bentonite turbulent flow predictions and average % error using the Hallbom modified Wilson & Thomas method – all rheologies

The Hallbom modified Wilson and Thomas technique gives reasonable results using the Bingham plastic rheology, similarly to the Wilson & Thomas method. For the bentonite slurries the yield plastic rheology reverts to the Bingham plastic rheology for the 6% and 7.34% concentrations and to the Casson rheology for the 9% concentration.

For the 6% and 7.34% concentrations, predictions using the Bingham plastic rheology (also the yield plastic rheology) are in good agreement with the experimental values in terms of error values and slope of the τ_w vs. (*8V/D*) curve. This rheology can be used to predict turbulent τ_w with some confidence across the turbulent shear rate range. For the 9% concentration, use of all rheologies underpredicted the turbulent flow τ_w data with errors in excess of 13%. Casson rheology shows slightly lower errors, but the slope of the prediction data does not agree well with the experimental data, so as the shear rate increases the accuracy of the prediction deteriorates significantly (as seen in Figure I.12 in Appendix I). The calculated error value would be larger if all the experimental points were included in its estimate. In this case it is the Bingham plastic which produces the more reliable prediction since it follows the slope of the experimental data more consistently. The slope of the predicted τ_w vs. (*8V/D*) curve should be carefully considered to properly assess the reliability of the prediction at higher shear rates. Using the Bingham plastic (also the yield plastic) rheology overpredicts turbulent τ_w in the 7.34% concentration, whilst all rheologies underpredict turbulent data for the 6% and 9% concentrations. The Bingham plastic rheology generally predicts a higher turbulent wall shear stress than the Casson model and shows a better slope correlation with the experimental data. The Casson model has a flatter slope and underpredicts turbulent wall stress data. This is again assumed to be as a result of the extrapolation of the laminar data.

Hallbom: Partially rough wall turbulence (pseudofluid) – using Nikuradse turbulent equation

Figure 5.63 presents the turbulent predictions and average error (in %) for bentonite in three pipe sizes using the Hallbom pseudo fluid Nikuradse method with each rheological model in turn.

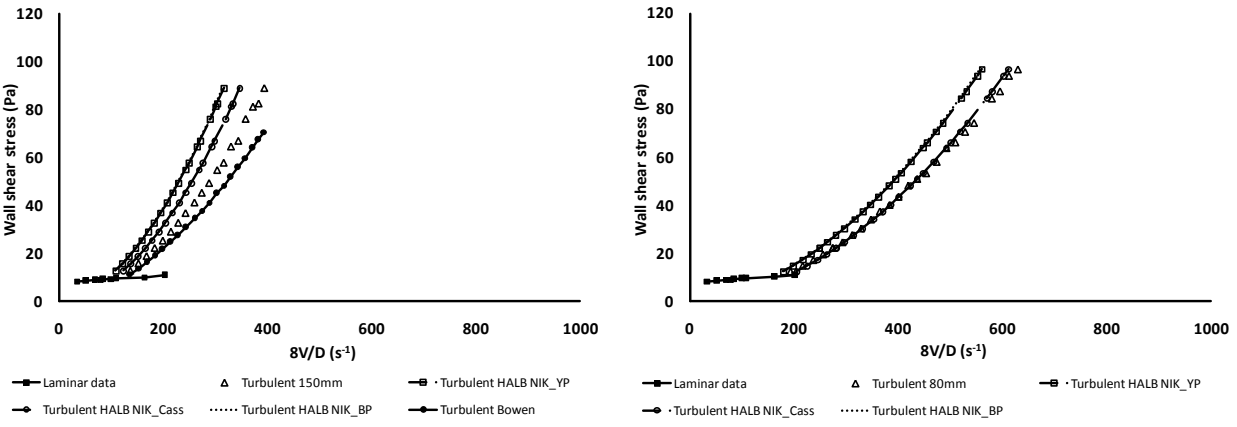

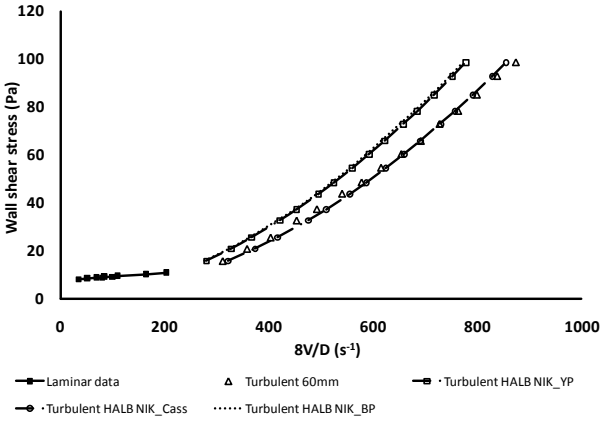

(8V/D) RMSE values - Hallbom_Nikuradse				
Pipe diameter	BP	CASS	YP	BOWEN (To)
150mm	21.3%	10.1%	20.6%	12.2%
80mm	8.7%	4.7%	7.8%	N/A
60mm	10.2%	3.4%	9.4%	N/A
Ave	13.4%	6.1%	12.6%	12.2%

Figure 5.63 7.34% bentonite turbulent flow predictions and average % error using the Hallbom Nikuradse pseudo fluid method – all rheologies

The results for the 7.34% concentration show that using the Casson rheology gave the most accurate results with errors in the range 3% to 10% for all three diameter test pipes. Using the Bingham plastic rheology constantly overpredicted the pressure drops with errors in the range of 9% to 21%. However for the 6% and 9% concentrations using the Bingham plastic rheology gave excellent agreement with the experimental data. The yield plastic rheology was equivalent to the Bingham plastic rheology for the 6% and 7.34% concentrations, and to the Casson rheology for the 9% concentration, and therefore gave very similar results in those cases. Results show that the Hallbom Nikuradse pseudo fluid technique which Hallbom uses to incorporate pipe roughness can be used with confidence for bentonite turbulent flow predictions with the Bingham plastic and Casson rheologies. However, due to inconsistencies between the predictions when using the Casson and Bingham plastic rheologies for the different concentrations, a clear conclusion could not be drawn as to which is better. Both rheologies should be applied and compared with experimental data when this technique is used to predict the turbulent flow of bentonite slurries.

Dodge and Metzner

Figure 5.64 presents the turbulent predictions and average error (in %) for bentonite in the diameter 60mm pipe using the Dodge & Metzner method with each rheological model in turn.

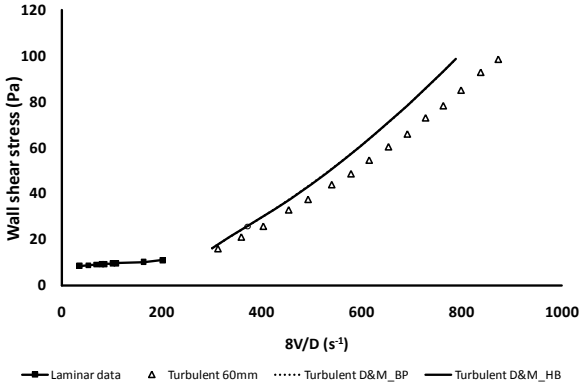

(8V/D) RMSE values - D&M method					
Pipe diameter	HB	BP	PL	CASS	BOWEN (To)
150mm	N/A	N/A	N/A	N/A	12,2%
80mm	N/A	N/A	N/A	N/A	N/A
60mm	5,6%	5,6%	N/A	N/A	N/A
Ave	5,6%	5,6%	N/A	N/A	12,2%

Figure 5.64 7.34% bentonite turbulent flow predictions and average % error using the Dodge & Metzner method – all rheologies

Due to the restrictions described in Section 3.2.7, experimental results for comparison with predictions using the Dodge & Metzner technique were only obtained in the diameter 60mm pipe for the 7.34% concentration and the diameter 13mm pipe the for 6% concentration. For both the 6% and 7.34% concentrations the Herschel-Bulkley rheology reduced to the Bingham plastic form and produced identical results. Predictions for the 7.34% concentration could only be achieved using the Bingham plastic (also Herschel-Bulkley) rheology which produced an error of 5.6% and followed the data slope well. For the 6% concentration, both the Casson rheology and the Bingham plastic rheology gives results that do not follow the experimental data trend accurately. Considering the slope of each predicted curve Bingham plastic rheology will probably produce more accurate results as the shear rate increases, while the Casson rheology will result in predictions that diverge from the experimental data, underpredicting pressure drop significantly. Due to the limitations of the method and few experimental results for only two diameter pipe sizes out of a possible nine, it is impossible to draw any firm conclusions. However, for the predictions which were possible the technique proved successful when using the Bingham plastic rheology, and gave average errors of 5.6% and 6.8% for the 7.34% and 6% concentrations respectively. In conducting the Dodge & Metzner analyses it became clear that *n*' values outside the range of $0.36 \leq n \leq 1$ gave invalid results, and the method must be used with caution for materials characterised with $n' \leq 0.36$.

Newtonian approximation

Figure 5.65 presents the turbulent predictions and average error (in %) for bentonite in three pipe sizes using the Newtonian Approximation method with each rheological model in turn.

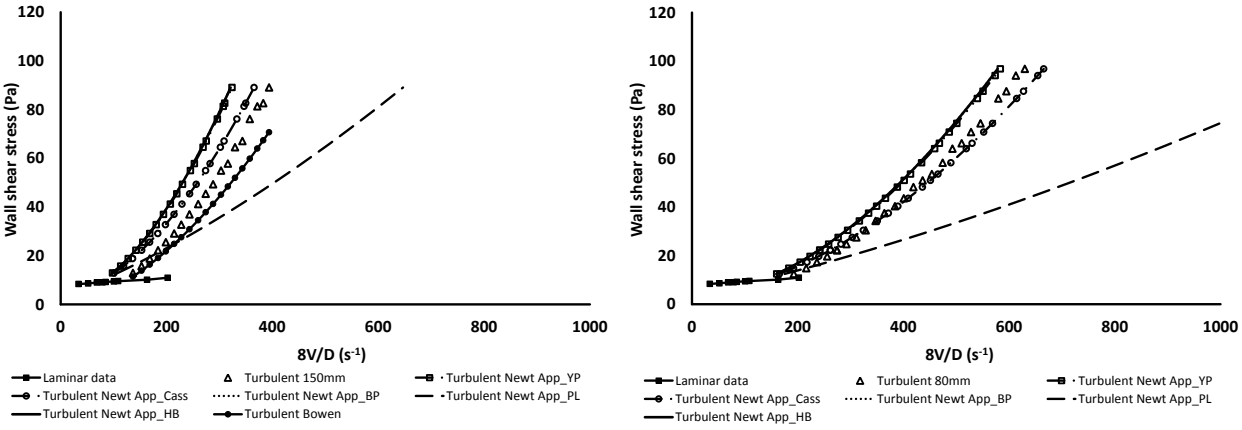

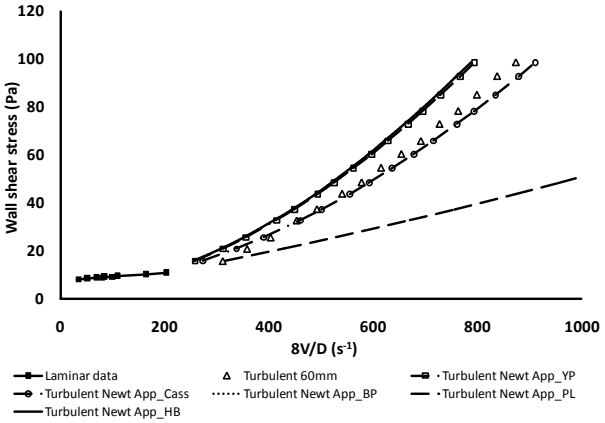

(8V/D) RMSE values - Newtonian Approximation						
Pipe diameter	HB	BP	PL	CASS	HALL_YP	BOWEN (To)
150mm	26.4%	26.4%	12.1%	22.5%	26.1%	12.2%
80mm	15.5%	15.5%	6.0%	11.1%	15.2%	N/A
60mm	14.7%	14.7%	17.5%	7.2%	14.1%	N/A
Ave	18.9%	18.9%	11.9%	13.6%	18.5%	12.2%

Figure 5.65 7.34% bentonite turbulent flow predictions and average % error using the Newtonian approximation method – all rheologies

The Newtonian approximation overpredicts the turbulent wall shear stress data for the 6% and 7.34% concentrations at the lower turbulent wall shear stress values, as it did for the kaolin slurries. Both bentonite and kaolin are yield stress non-Newtonian materials which will exhibit thickening of the viscous sub-layer (Wilson & Thomas, 2006), resulting in a higher throughput velocity. The Newtonian approximation does not account for this and could possibly be the reason that the technique underpredicts the turbulent velocity (overpredicts the pressure drop). For the 7.34% bentonite the Casson model was the most appropriate with predictions following the experimental data slope well and producing the lowest errors of 11% to 23%. The Bingham plastic rheology (also identical Herschel-Bulkley) and the yield plastic rheology, also gave results that follow the experimental slope very well but significantly overpredict the turbulent shear stresses by 15% to 26%. Using the power law rheology resulted in a turbulent prediction with a very flat slope and is not useful with this technique. For the 6% bentonite, using the Casson or Bingham plastic rheologies gave similar results, except for the diameter 13mm pipe where the Bingham plastic rheology followed the experimental data slope much better. Errors were in the range of 11% to 16% (Casson) and 11% to 19% (Bingham plastic). Use of the power law rheology again gave very poor predictions. For the 9% concentration the results vary. Considering both error values and slope of predictions, the Casson rheology gives better results in the diameter 150mm pipe and the Bingham plastic rheology produced better predictions in the diameter 60 and 80mm pipes. Although all rheologies correlate well with the experimental turbulent data at lower turbulent shear rates, as the shear rate increases the Casson rheology predicts a much higher velocity while the Bingham plastic follows the experimental data well. The power law rheology is not suitable to predict bentonite turbulent flow using this technique.

Torrance

Figure 5.66 presents the turbulent predictions and average error (in %) for bentonite in three pipe sizes using the Torrance method with each rheological model in turn.

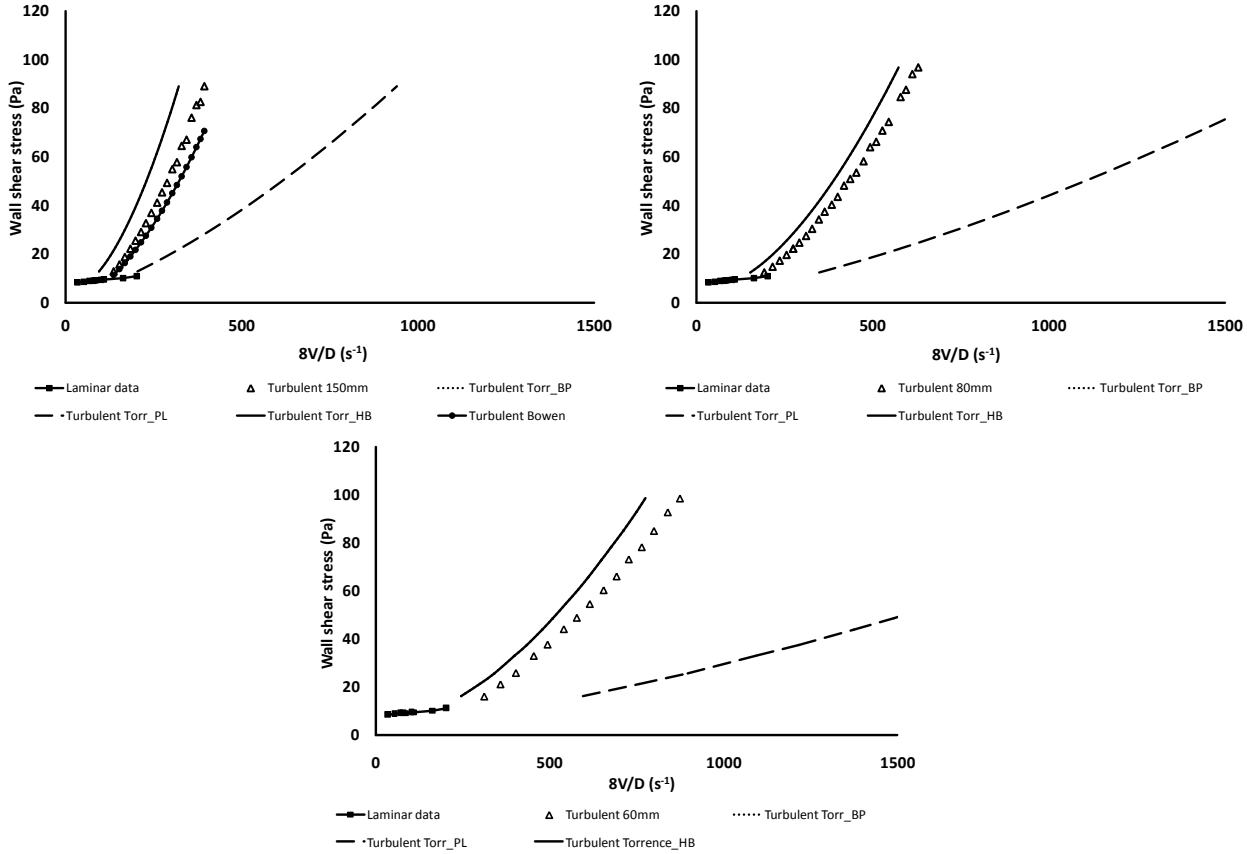

(8V/D) RMSE values - Torrance method				
Pipe diameter	HB	BP	PL	BOWEN (To)
150mm	28.0%	28.0%	58.7%	12.2%
80mm	18.7%	18.7%	88.9%	N/A
60mm	17.8%	17.8%	108.6%	N/A
Ave	21.5%	21.5%	85.4%	12.2%

Figure 5.66 7.34% bentonite turbulent flow predictions and average % error using the Torrance method– all rheologies

For all concentrations the Torrance technique was very inaccurate when using the power law rheology to predict the bentonite turbulent flow with errors up to 300% in the 60mm pipe for the 9% concentration. This is mainly due to the inability of the shear thinning power law rheology to properly model the bentonite material in laminar flow. Extrapolating the poor laminar flow model to the much higher turbulent wall shear stresses results in meaningless predictions, and the Torrance model should not be used with the power law rheology to predict bentonite turbulent flow. Using the Bingham plastic or Herschel-Bulkley rheologies predict the same results for the 6% and 7.34% concentrations but different results for the 9% concentration. In the 6% and 7.34% concentrations, use of the Bingham plastic rheology gives good agreement with the slope of the experimental data, but overpredicts turbulent wall shear stresses with errors of 14% to 24% (6% concentration) and 17% to 28% (7.34% concentration). For the 9% test concentration better results were obtained using the Bingham plastic and Herschel-Bulkley rheologies, which in this case were not the same. Use of the Herschel-Bulkley rheology gave errors in the range 6% to 10%, while use of the Bingham plastic rheology resulted in errors of 8% to 15%. The results emphasise the importance of choosing the correct rheological model for the test material as the laminar flow rheology significantly effects turbulent flow predictions.

Bowen scale-up method

The Bowen method gave good agreement with the experimental results in the diameter 150mm pipe for

the 7.34% and 9% concentrations, with average errors of 12% and 3% respectively. For the 6% concentration the results were less accurate, with an average error of 22% in the diameter 80mm pipe predictions. There is merit to the technique, but the experimental results from the bentonite tests are not consistent across the different concentrations, and so did not enable a thorough evaluation of the method.

One rheology plotted for all techniques

The analysis now focuses on the use of specific rheological models with all techniques. The most appropriate rheological model for bentonite is the Bingham plastic model (Section 4.2.1), but based on the results presented in Figure 5.60 to Figure 5.66 this good agreement with experimental turbulent flow results was also achieved when using the Casson rheology. The Herschel-Bulkley and Hallbom yield plastic rheologies reduced to the Bingham plastic rheology for the 6% and 7.34% concentrations. For the 9% concentration, the yield plastic rheology reduced to the Casson rheology, and the Herschel-Bulkley rheology remained different to both of them. To avoid duplication only results using the Bingham plastic and Casson rheologies are presented now. All the techniques are presented for the 7.34% bentonite concentration using the Bingham plastic and Casson rheologies. Similar results for the 6% and 9% bentonite are given in Appendix I.

Bingham plastic

Figure 5.67 presents the turbulent predictions and average % error for bentonite in three pipe sizes using the Bingham plastic rheological model with each turbulent flow prediction technique.

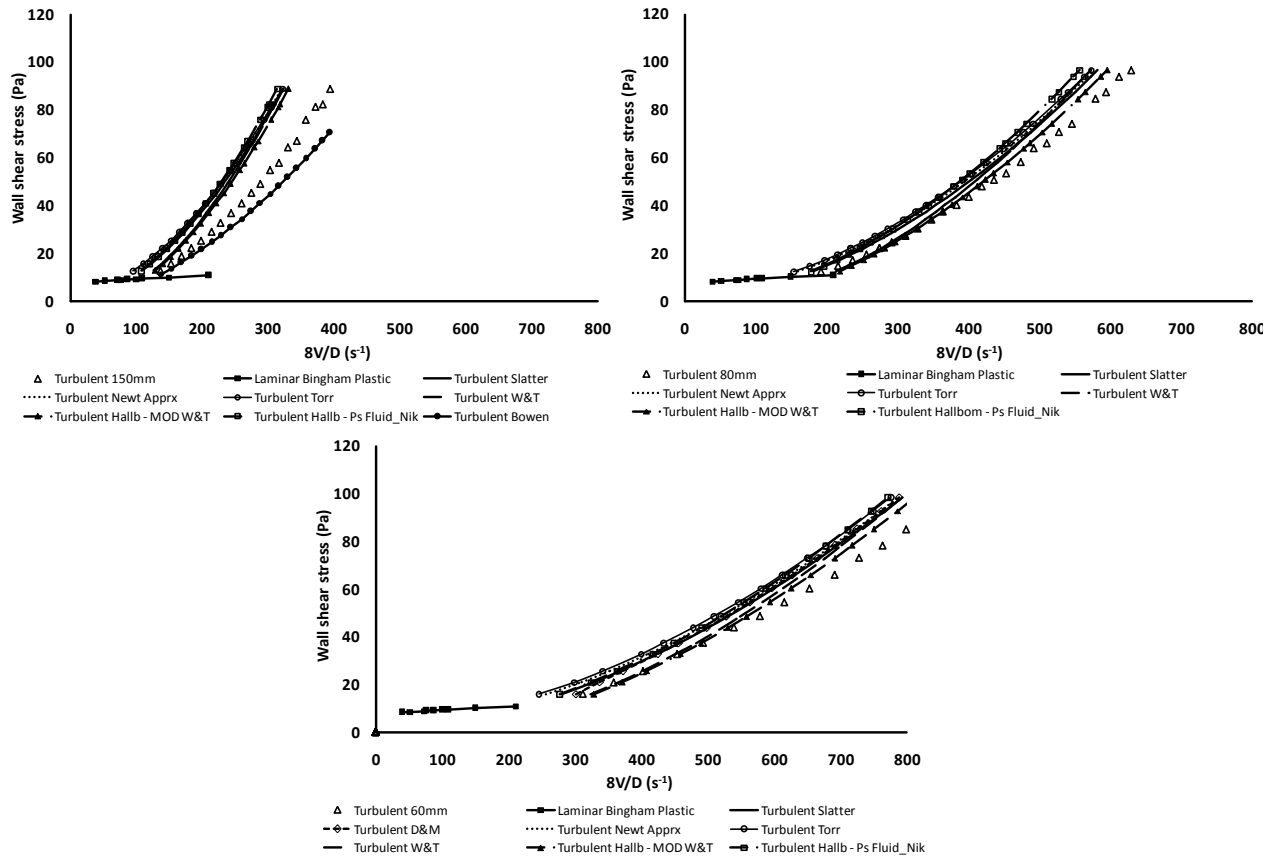

(8V/D) RMSE values - Bingham Plastic								
Pipe diameter	W&T	NEWT	TORR	D&M	SLATT	BOWEN (To)	MOD_W&T	Ps Fld_Nik
150mm	9.4%	26.4%	28.0%	N/A	20.2%	12.2%	7.9%	21.3%
80mm	7.5%	15.5%	18.7%	N/A	7.0%	N/A	9.7%	8.7%
60mm	2.0%	38.5%	17.8%	5.6%	9.1%	N/A	3.4%	10.2%
Ave	6.3%	26.8%	21.5%	5.6%	12.1%	12.2%	7.0%	13.4%

Figure 5.67 7.34% bentonite turbulent flow predictions and average % error using the Bingham plastic rheology – all techniques

From Figure 5.67 it is evident that use of the bentonite rheology generally overpredicts turbulent wall shear stresses for most techniques, as is reported in the literature (Slatter *et al.*, 1997), but there are some exceptions. The predicted results from the different techniques using the Bingham plastic rheology show reasonable agreement with each other, since according to Slatter *et al.* (1997) all the techniques approach the Newtonian model under Newtonian conditions, and for Bingham plastic materials (n = 1) this is at the higher turbulent shear stress values. As for the kaolin results (Section 5.3.1) there are similarities between some of the techniques when using the Bingham plastic rheology and were identified as i) the Torrance model uses the same mixing length theory as for Newtonian turbulent flow, shows similar behaviour to the Newtonian approximation – both methods are unsuccessful and overpredict turbulent shear stresses significantly ii) the Slatter technique, which uses the inverse of the von Karman universal constant in its formulation, consistently gives similar results to the Hallbom Nikuradse pseudo fluid method due to the common Newtonian theory on which they are based and iii) the Wilson & Thomas (uses apparent viscosity in the Newtonian velocity term and includes pipe roughness) and the Hallbom modified Wilson & Thomas method give similar results. The similarity of the predictions using these methods is also apparent for the 9% concentration, and can be seen in Appendix I.

For the 7.34% bentonite results presented in Figure 5.67 the Wilson & Thomas and the Hallbom modified Wilson &Thomas technique gave the most accurate results, with errors of 2% to 9%. For the 6% (now also referring to the Herschel-Bulkley and yield plastic rheology) and 9% bentonite the Slatter and Hallbom Nikuradse pseudo fluid methods gave the best results with errors in the range 3% to 13% (6% bentonite) and 1.5% to 3.5% (9% bentonite). It is clear that some inconsistency exists in the bentonite data and predictions. Even so, any of these techniques will give reasonable predictions for bentonite when using Bingham plastic rheology.

Casson

Figure 5.68 presents the turbulent predictions and average % error for bentonite in three pipe sizes using the Casson rheological model with each turbulent flow prediction technique.

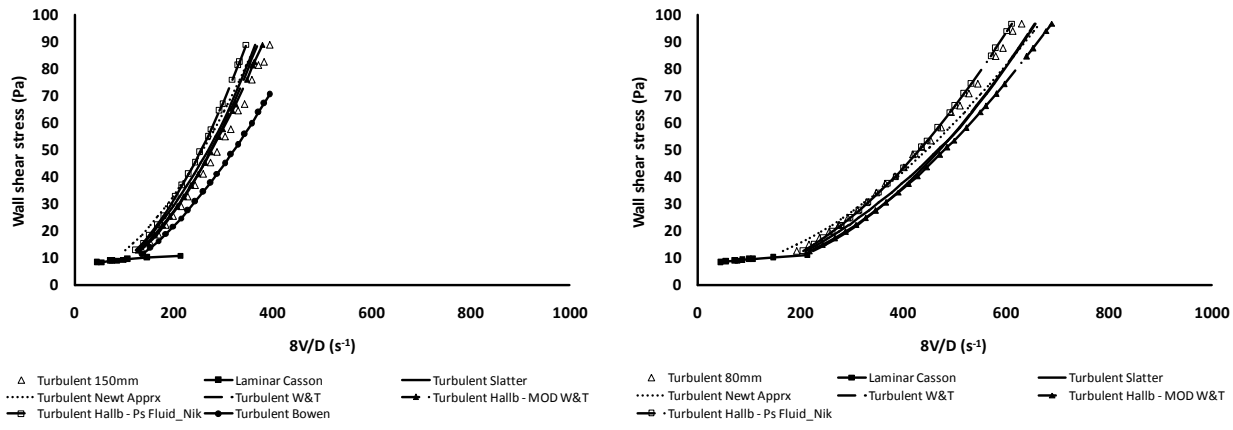

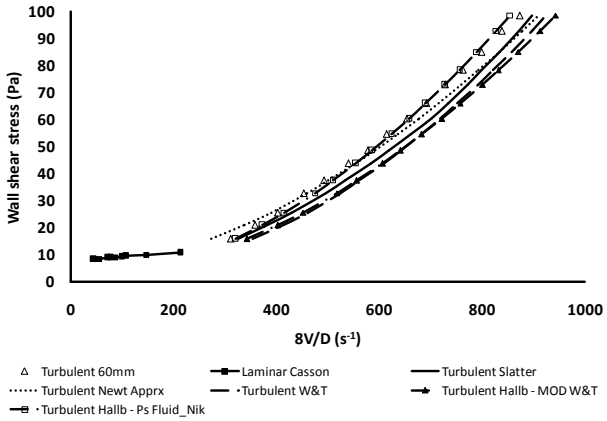

(8V/D) RMSE values - Casson								
Pipe diameter	W&T	NEWT	TORR	D&M	SLATT	BOWEN (To)	MOD_W&T	Ps Fld_Nik
150mm	2.2%	22.5%	N/A	N/A	8.7%	12.2%	4.8%	10.1%
80mm	15.7%	11.1%	N/A	N/A	8.3%	N/A	12.5%	4.7%
60mm	14.4%	33.1%	N/A	N/A	6.1%	N/A	11.6%	3.4%
Ave	10.8%	22.2%	N/A	N/A	7.7%	12.2%	9.7%	6.1%

Figure 5.68 7.34% bentonite turbulent flow predictions and average % error using the Casson rheology – all techniques

When using the Casson rheology for all the bentonite concentrations, the slopes of the predicted τ_w vs. (*8V/D*) curves agree well with experimental results for all the techniques except the Newtonian approximation. The Newtonian approximation overpredicts turbulent shear stresses for the all concentrations at lower turbulent shear rate values, but due to the much flatter slope predicted by this technique it underpredicts the turbulent shear stress data as the shear rate increases. This technique is not recommended to reliably predict bentonite turbulent flow using the Casson rheology. As for the Bingham plastic rheology, a close relation is again observed between the results for the Wilson & Thomas and Hallbom modified Wilson & Thomas techniques using the Casson rheology, for the same reasons. These techniques, however, consistently underpredict the turbulent flow shear stresses for all bentonite concentrations with errors of 11% to 25% across the range.

When using the Casson rheology the Slatter and the Hallbom Nikuradse pseudo fluid methods were successful. These two techniques gave similar predictions when using the Bingham plastic, Casson and Hallbom yield plastic rheologies, as for the kaolin turbulent analysis (Section 5.3.1). For the 6% concentration the Slatter technique was more accurate for all pipe diameters with errors in the range 4% to 10%. In the 7.34% concentration the techniques gave similar results with errors of 6% to 8% (Slatter) and 3% to 10% (Hallbom Nikuradse pseudo fluid). For the 9% concentration the Hallbom Nikuradse pseudo fluid method was better, yielding errors in the range 6% to 10% compared to 9% to 13% for the Slatter method. Either of these methods can be used to achieve accurate and reliable predictions using the Casson rheology for bentonite fluids.

Bentonite turbulent flow summary

Bentonite is best characterised by the Bingham plastic rheological model, although the Casson rheology was also good especially for the higher 9% concentration (See Section 4.3). The Herschel-Bulkley and Hallbom yield plastic rheologies reduced to the Bingham plastic or Casson rheologies for the bentonite test materials and using these models gave the most accurate and reliable turbulent flow predictions. The reason for the success of the Casson rheology is attributed to the Newtonian approach of the model at higher shear stress and shear rate values, exhibiting a constant shear viscosity similar to that of the Bingham plastic model (Heywood & Alderman, 2003). This is what makes the model attractive to many as it can model shear thinning in the lower shear stress and shear rate ranges, and also adapt to a

constant apparent shear viscosity as the shear rate increases.

Use of the power law rheology, which did not describe the bentonite laminar data well (Section 4.3) gave excessively inconsistent and inaccurate results, is completely inappropriate for bentonite turbulent flow predictions.

Considering the different turbulent flow prediction techniques, the Newtonian approximation was unable to produce reliable results due to the flatter slope of the turbulent predictions. The Torrance model failed to predict bentonite turbulent flow, giving large differences in the predictions due to its sensitivity to rheological parameters. The Wilson & Thomas technique (and similarly the Hallbom modified Wilson & Thomas) produced inconsistent results showing good predictions (6% error) for 7.34% bentonite, but errors of 11.6% and 15.3% are obtained for the 6% and 9% concentrations respectively. The Slatter and the Hallbom Nikuradse pseudo fluid methods gave the most reliable and consistently accurate results for the different bentonite slurries, when using either the Bingham plastic, Casson or the yield plastic rheology. Using the Bingham plastic rheology, average errors were between 2.1% and 13.4% and in all cases the slope of the predicted τ_w vs. (*8V/D*) curve followed the experimental values well. Using the Casson rheology the Slatter and the Hallbom Nikuradse pseudo fluid methods gave the best predictions with errors in the range 6.1% to 12.6% across all the tests. For the yield plastic rheology the average errors were 6.1% to 11.3%.

Results of the Bowen scale-up method varied with concentration, but was only possible to apply the method in one pipe size per concentration, making a reliable conclusion difficult. For the 6% concentration in the diameter 80mm pipe the method gave a 22% average error. For the 7.34% and 9% concentrations predictions for the diameter 150mm pipe gave errors of 12% and 3% respectively. The Dodge & Metzner technique was evaluated, and produced good results using the Bingham plastic and Casson rheology for the 7.34% and 6% concentrations producing average errors of 5.6% and 2.6% respectively. Due to the limitations imposed by the technique, no results were possible for the 9% concentration. As the limits of the Dodge & Metzner method are approached, the method fails. Generally, when applied to the bentonite material the different prediction methods gave similar results to those obtained for the kaolin slurries.

Effect of concentration and pipe diameter

The results of the various analyses presented above for bentonite sometimes indicated unexpected changes with concentration and pipe diameter, but it could not be established if these were actual effects or due to experimental inaccuracies. To get some idea though, the % error was plotted against pipe diameter for the Slatter technique for all rheologies. A separate plot for each concentration is presented in Figure 5.69.

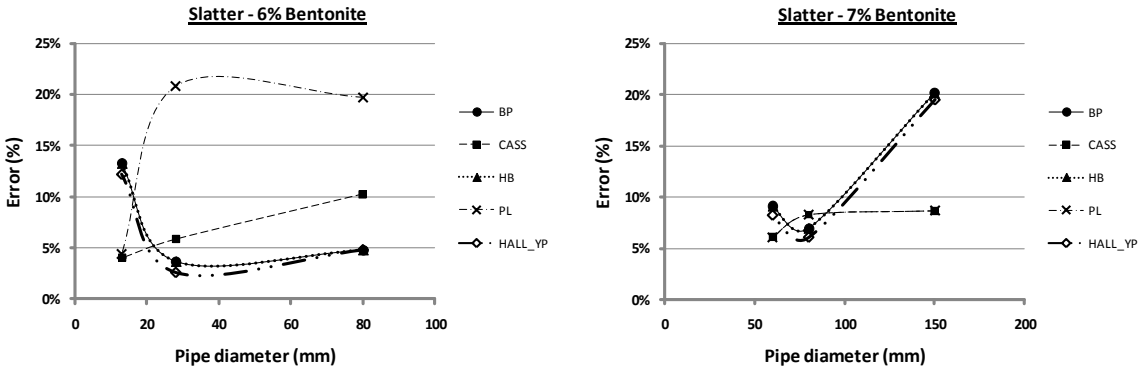

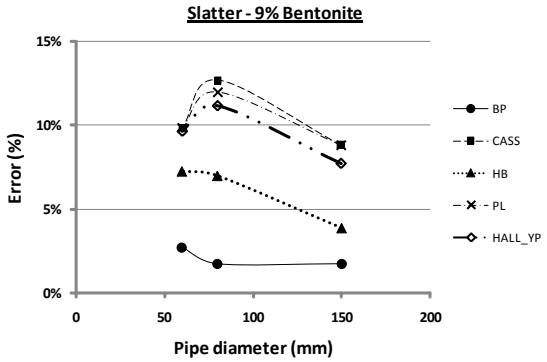

Figure 5.69 Effect of diameter on the % error value for the Slatter method in different pipe sizes at 6%, 7.34% and 9% bentonite concentrations

Referring to Figure 5.69, no trend for the relationships is evident. Once again, the figures only give an indication of the prediction accuracy achieved, in this case greatly influenced by the credibility of the diameter 13mm pipe data for the 6% concentration, and by the diameter 150mm pipe data for the 9% concentration. No conclusion regarding diameter effect can be made based on the results given in Figure 5.69 but the similarities between certain model predictions and the lack of accuracy achieved can be identified.

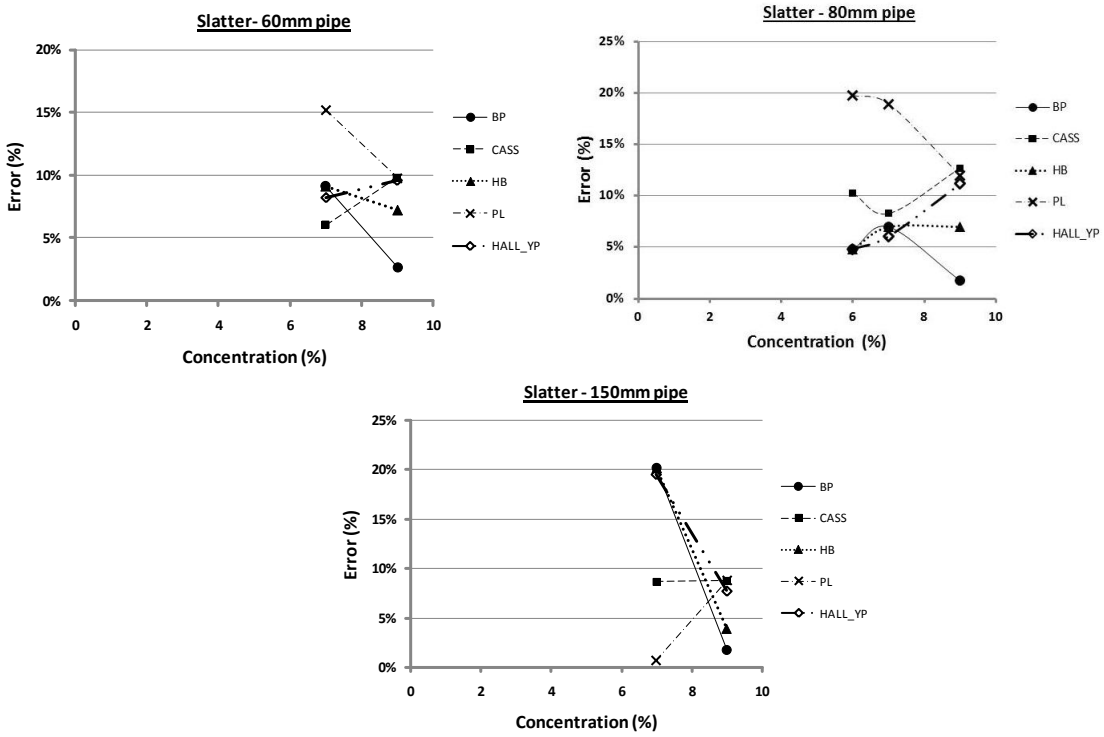

Figure 5.70 Effect of concentration on the % error value for the Slatter method at different bentonite concentrations in the diameter 60mm, 80mm and 150mm pipes

As seen in Figure 5.70, prediction errors for the diameter 60mm and diameter 80mm pipes vary similarly with concentration, but are essentially opposite to the trends shown for the diameter 150mm pipe. Without any further test results it is not possible to reach a meaningful conclusion on the effect, if any, of concentration. Turbulent flow was not achieved in the 60 and 150mm pipe diameters for the 6% bentonite tests so results for those pipes sizes are not available for inclusion in Figure 5.70.

5.3.3 CMC

The turbulent analysis and results for the CMC test concentrations are presented and discussed in this section. Only the results for the 5% CMC are presented here, but the conclusions are based on the results of all three test concentrations in all pipe sizes. Results for the 3% and 8% concentrations are given in Appendix J.

One technique plotted for all rheologies

To see the effect of rheology on the prediction technique the turbulent results are first presented as plots of predicted τ_w vs. (*8V/D*) for one prediction technique in one diameter pipe, for all applicable rheologies. Experimental values are also shown on the plots.

Wilson & Thomas

Figure 5.71 presents the turbulent predictions and average error (in %) for CMC in three pipe sizes using the Wilson & Thomas method with each rheological model in turn.

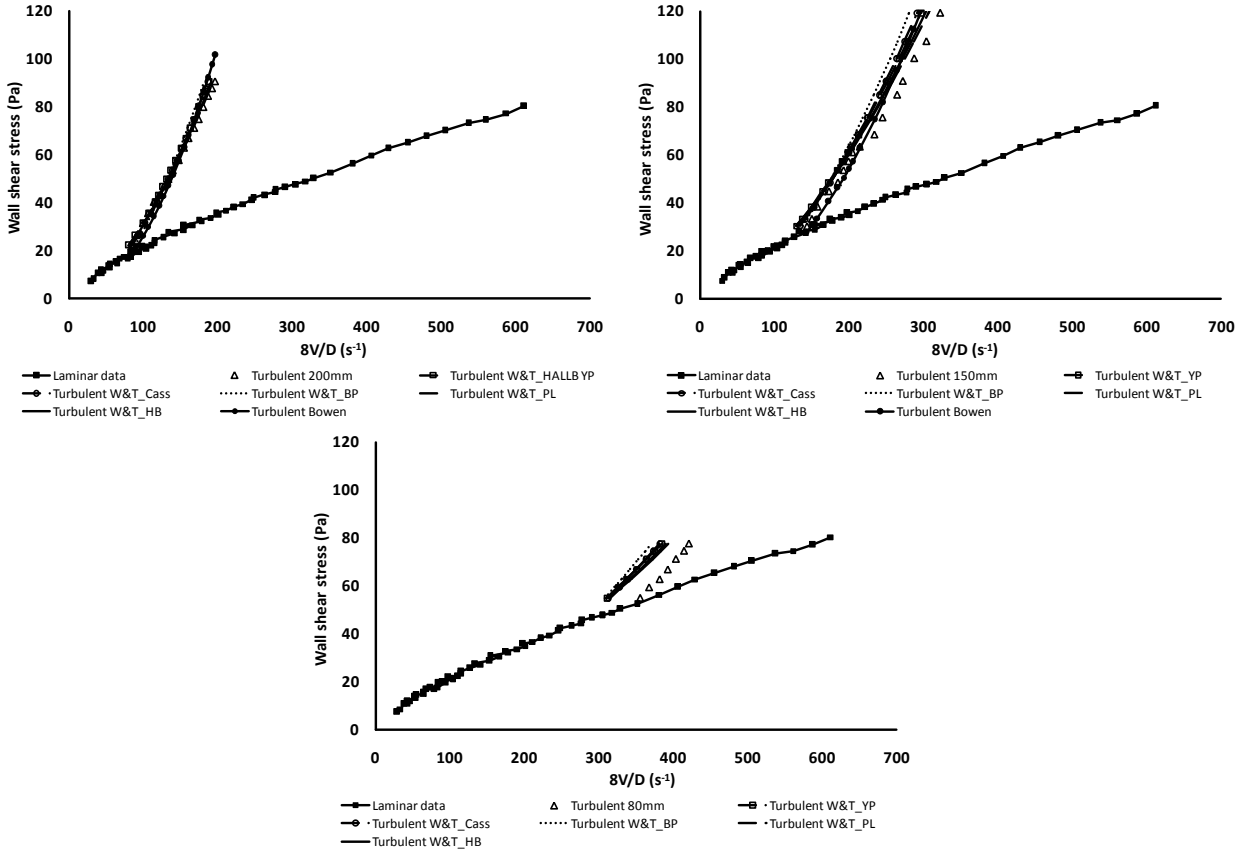

(8V/D) RMSE values - W&T(PRW) method						
Pipe diameter	HB	BP	PL	CASS	HALL_YP(SW)	BOWEN (To)
200mm	1.4%	4.4%	0.9%	2.7%	2.1%	9.1%
150mm	5.4%	6.8%	5.4%	5.8%	6.7%	7.9%
80mm	9.4%	12.8%	8.8%	10.7%	10.6%	N/A
Ave	5.4%	8.0%	5.0%	6.4%	6.5%	8.5%

Figure 5.71 5% CMC turbulent flow predictions and average % error using the Wilson & Thomas method – all rheologies

The CMC laminar flow data was best characterised using the power law rheological model (Section 4.4). The Herschel-Bulkley rheology reduced to the power law model for the 3% and 8% CMC concentrations,

and for the 5% CMC it gave a very low yield stress value and almost identical *n* value to the power law model. The Hallbom yield plastic rheology reduced to a power law form for all the CMC concentrations, giving an almost zero yield stress in each case. Referring to Figure 5.71, it is clear that excellent predictions were obtained using the Wilson & Thomas method with all the rheologies, up to high shear rates. Using the power law rheology produced the most accurate results produced the most accurate results with errors in the range 1% to 9%. Using the Bingham plastic rheology gave the worst results with errors of 10% to 16% across all pipe diameters and concentrations. This was expected as the Bingham plastic rheology is the least appropriate to describe the non-yield stress shear thinning CMC laminar data. Surprisingly though, using the Bingham plastic model still does give fairly accurate predictions. Possibly this is because the CMC material was characterised across the same shear stress range for which the turbulent data would be predicted and so the rheology may be reasonably representative of the fluid behaviour well into turbulent flow, minimising the error caused by extrapolating the laminar flow curve.

Using the Casson model gives marginally better predictions than achieved with the Bingham plastic model, with errors of 2% to 10% for the 3% concentration, 7% to 12% for the 5% concentration and 8% for the 8% CMC. The Casson model includes some shear thinning behaviour, so extrapolating the laminar flow data to the turbulent shear stresses is probably more realistic than in the case of Bingham plastic rheology.

Using the Hallbom yield plastic rheology gave almost identical results to those obtained with the Casson model for the 3% and 5% concentrations, and identical to results when using the Bingham plastic rheology in the 8% concentration, with an error of 10.5% in the diameter 150mm pipe. Predictions for the diameter 80mm pipe for the 3% and 5% concentrations are offset from the experimental data, consistently showing a higher pressure drop, for all rheologies. There appears to be some pipe diameter effect with this technique.

Slatter

Figure 5.72 presents the turbulent predictions and average error (in %) for CMC in three pipe sizes using the Slatter method with each rheological model in turn.

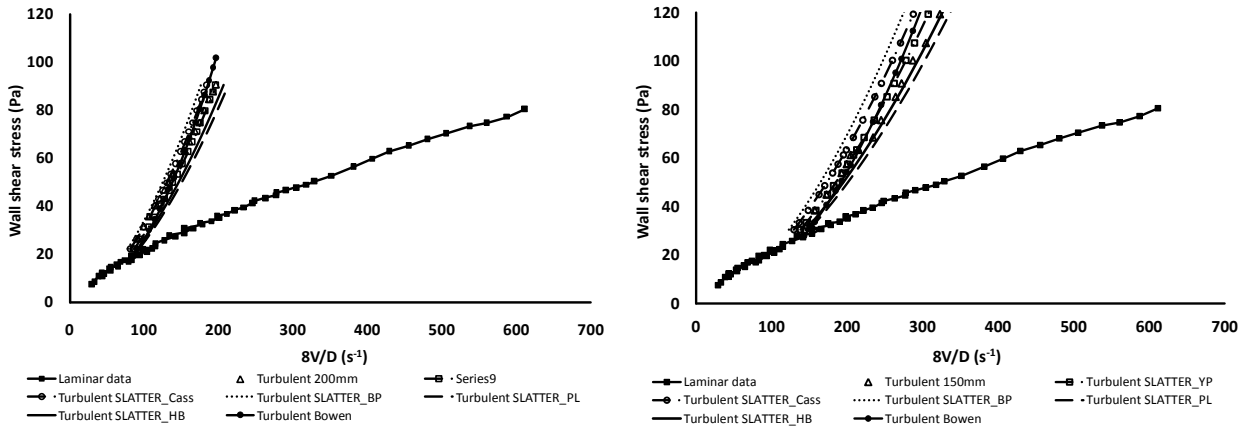

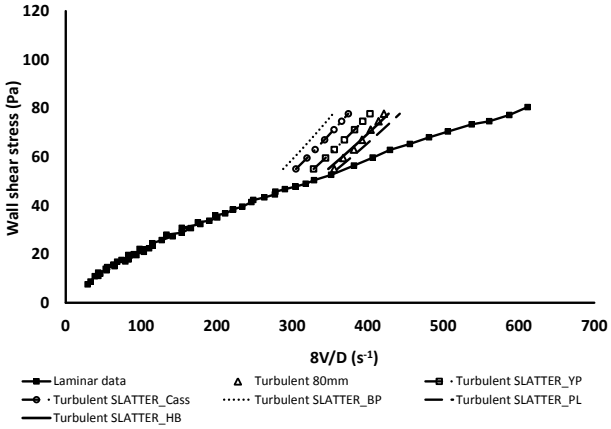

(8V/D) RMSE values - Slatter method						
Pipe diameter	HB	BP	PL	CASS	HALL_YP	BOWEN (To)
200mm	9.9%	7.6%	13.5%	3.2%	3.9%	9.1%
150mm	3.6%	12.5%	6.8%	8.0%	2.3%	7.9%
80mm	1.7%	17.4%	1.6%	12.8%	6.5%	N/A
Ave	5.1%	12.5%	7.3%	8.0%	4.2%	8.5%

Figure 5.72 5% CMC turbulent flow predictions and average % error using the Slatter method – all rheologies

The Slatter method is the only one which does not assume the fluid is to be a continuum by taking into account the particle roughness effect in turbulent flow. CMC does not contain particles however, but is made up of chain like molecules, so in this case the pipe roughness was used instead of particle roughness (Slatter, 1994).

Considering the predictions for the three concentrations of CMC as shown in Figure 5.72 and Appendix J when using the Bingham plastic and Casson rheologies the method overpredicts the shear stresses and gives the most inaccurate results. Use of the Bingham plastic rheology gives errors in the range 15% to 21% for the 3% concentration, 7% to 17% for the 5% concentration and 18% for the 8% concentration. Using the Casson rheology results in errors of 9% to 15% for the 3% concentration, 3% to 12% for the 5% concentration and 11.8% for the 8% concentration.

Using the Hallbom yield plastic rheology the Slatter method showed good agreement with the turbulent flow experimental data with errors of 2.9% to 3.1%, 3.9% to 6.5% and 3.9% for the 3%, 5% and 8% concentrations respectively. Similar, but not so good results were obtained when using the Herschel-Bulkley and power law rheologies. Predictions by the Slatter method also display some diameter effect, except when using the Herschel-Bulkley and power law rheologies.

Hallbom smooth wall turbulence - Modified Wilson & Thomas

Figure 5.73 presents the turbulent predictions and average error (in %) for CMC in three pipe sizes using the Hallbom modified Wilson & Thomas method with each rheological model in turn.

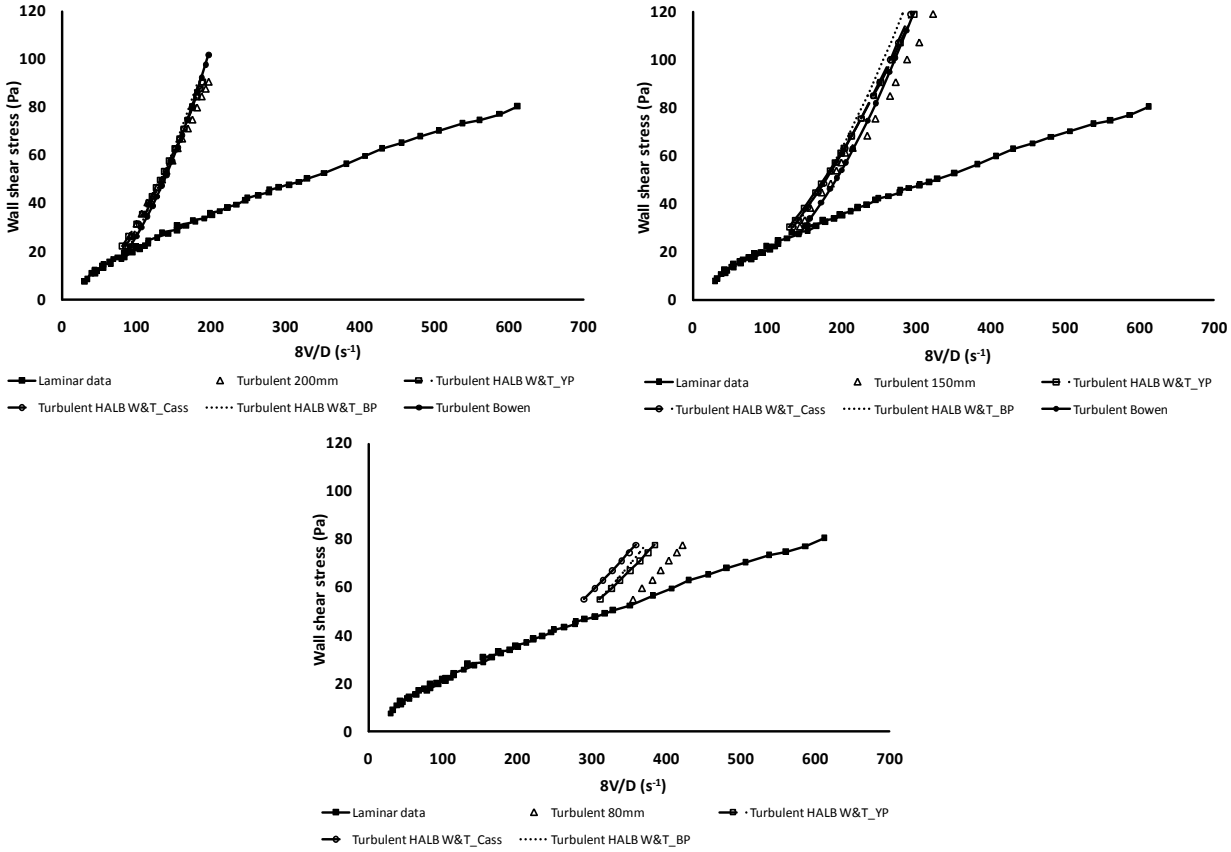

(8V/D) RMSE values - Hallb Mod W&T (SW)				
Pipe diameter	BP	CASS	YP	BOWEN (To)
200mm	4.4%	2.6%	2.1%	9.1%
150mm	6.4%	5.5%	6.7%	7.9%
80mm	12.3%	16.7%	10.6%	N/A
Ave	7.7%	8.2%	6.5%	8.5%

Figure 5.73 5% CMC turbulent flow predictions and average % error using the Hallbom modified Wilson & Thomas method – all rheologies

The turbulent predictions for the smooth wall Hallbom modified Wilson & Thomas method produced almost identical results to the Wilson & Thomas technique presented earlier when using the Bingham plastic, Casson and yield plastic rheologies. The same tendency to overpredict the turbulent shear stresses as diameter increases is apparent for both the 3% and 5% concentrations, as was observed for the Wilson & Thomas method. Use of the Casson and yield plastic rheologies gives equally accurate predictions of turbulent shear stresses for the CMC. With either rheology errors range from 7% to 12% for the 3% concentration. For the 5% concentration use of the Casson rheology results in errors of 2% to 17% whilst using the yield plastic rheology gives errors in the range 2% to 11%. For the 8% concentration the Casson rheology results in better predictions with an 8.3% error in the diameter 150mm pipe compared to a 10.5% error when using the yield plastic rheology.

Hallbom: Partially rough wall turbulence (pseudofluid) – Nikuradse turbulent flow equation

Figure 5.74 presents the turbulent predictions and average error (in %) for CMC in three pipe sizes using the Hallbom pseudo fluid Nikuradse method with each rheological model in turn.

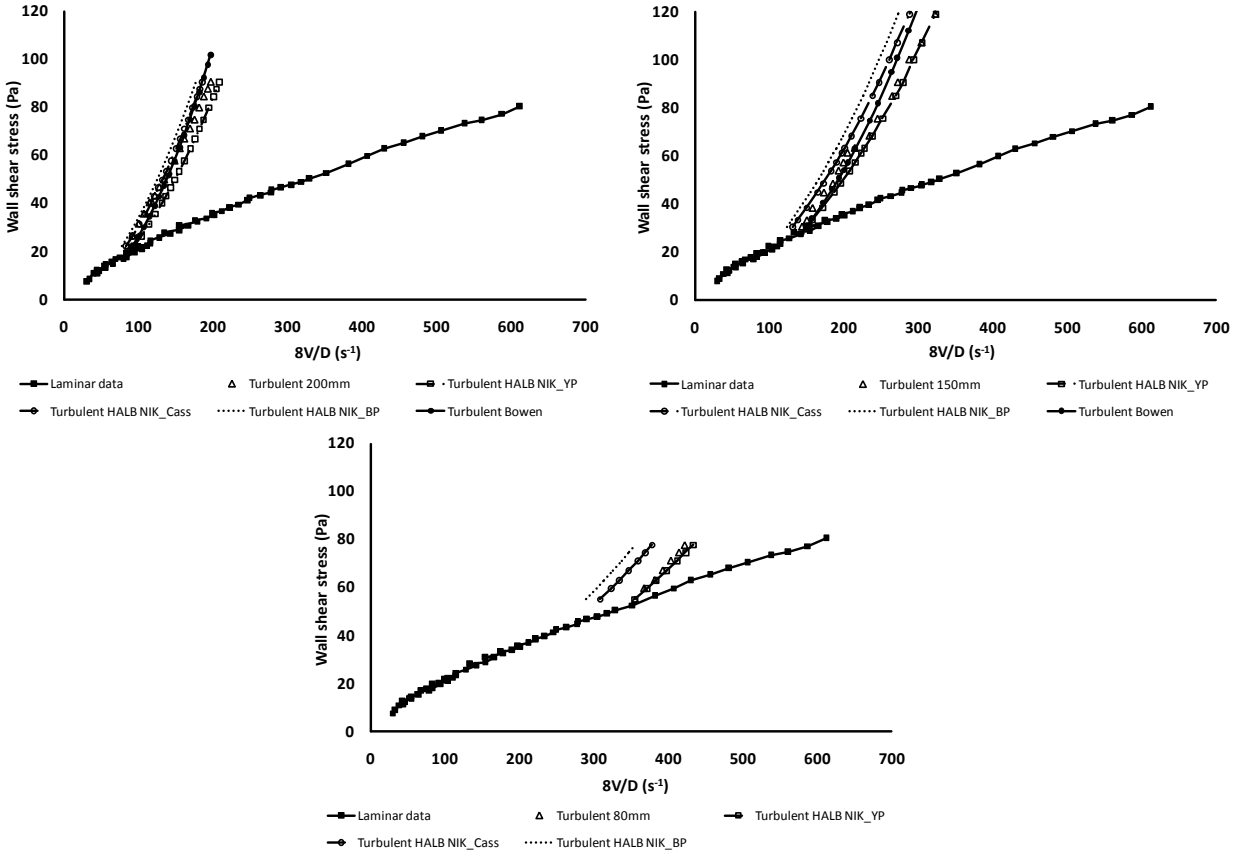

(8V/D) RMSE values - Hallbom_Nikuradse method				
Pipe diameter	BP	CASS	YP	BOWEN (To)
200mm	6.7%	2.1%	9.5%	9.1%
150mm	12.5%	7.5%	4.7%	7.9%
80mm	17.3%	12.1%	0.9%	N/A
Ave	12.2%	7.2%	5.0%	8.5%

Figure 5.74 5% CMC turbulent flow predictions and average % error using the Hallbom (2008) Nikuradse partially rough wall method – all rheologies

The Hallbom pseudo fluid method based on the Nikuradse equation gave reasonably accurate results using either the Casson or the yield plastic rheology. In all cases the predicted and experimental slopes of the τ_w vs. (*8V/D*) curves agree quite well, except when using the Bingham plastic rheology, in which case the slope is a bit high and pressure drops are overpredicted for all concentrations. For the 3% concentration use of the Casson rheology gives the best results with an error range of 9% to 15%. When using the yield plastic rheology shear stresses are underpredicted by 21% to 26%. For the 5% concentration using the yield plastic model gave the most accurate results with errors in the range 0% to 9%, whilst using the Casson rheology gave errors of 2% to 12%. For the 8% concentration using the yield plastic rheology again fails with a large 33% error for the diameter 150mm pipe while using the Casson rheology gave an 11% error. The reason for the inconsistency in the results is not apparent and no clear trend is evident. When using this prediction method, both the Casson and the yield plastic rheologies should be tried, and results compared, as it is not possible to recommend one based on the results presented here.

Dodge & Metzner

Figure 5.75 presents the turbulent predictions and average error (in %) for CMC in three pipe sizes using the Dodge & Metzner method with each rheological model in turn.

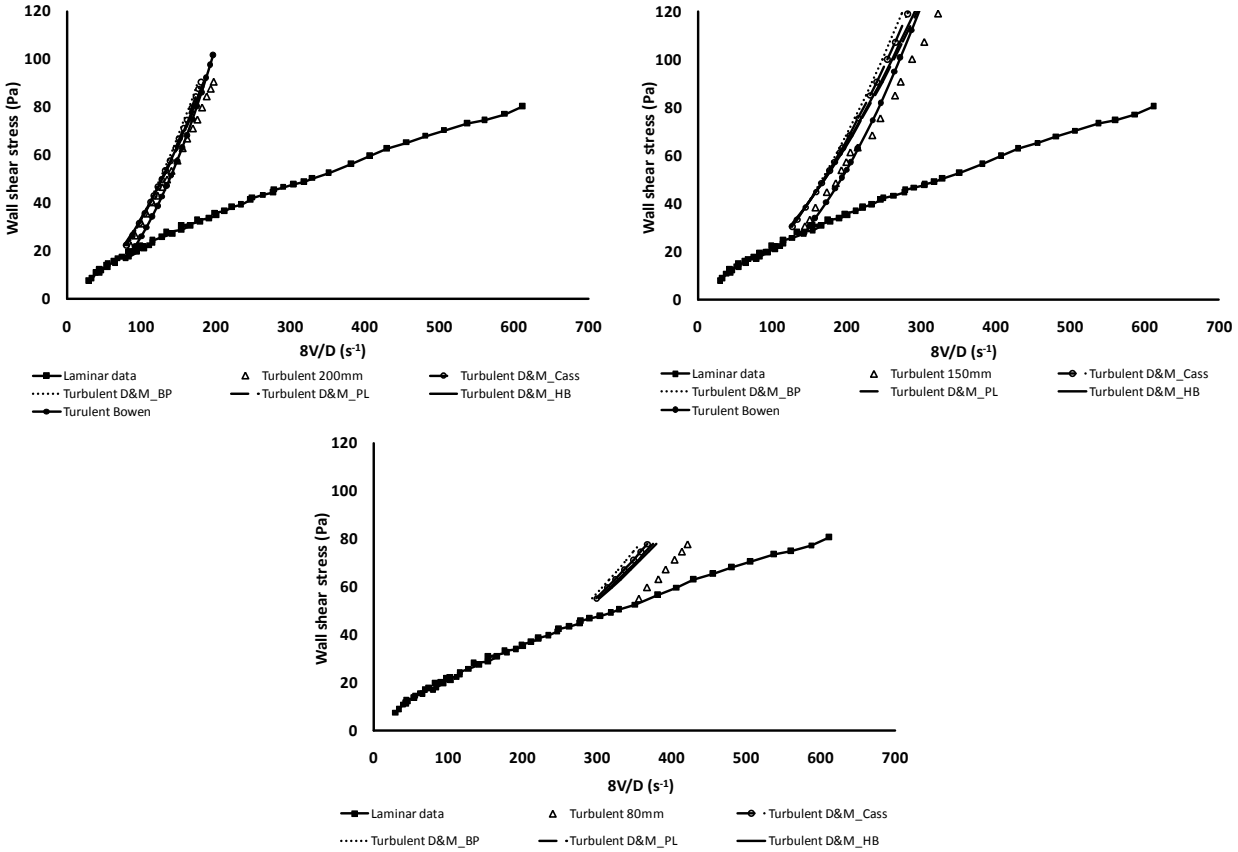

(8V/D) RMSE values - Dodge & Metzner method					
Pipe diameter	HB	BP	PL	CASS	BOWEN (To)
200mm	5.1%	6.9%	4.9%	5.9%	9.1%
150mm	9.6%	11.5%	9.3%	10.3%	7.9%
80mm	12.9%	16.4%	12.2%	14.3%	N/A
Ave	9.2%	11.6%	8.8%	10.2%	8.5%

Figure 5.75 5% CMC turbulent flow predictions and average % error using the Dodge & Metzner method – all rheologies

The Dodge & Metzner method could be applied to all the CMC experimental data as the calculated '*n* values for all experimental data points were in the valid range ($0.36 \leq$ '$n \leq 1$). The Dodge & Metzner technique gave accurate results for the turbulent flow predictions of CMC using the power law and or the Herschel-Bulkley models. Good agreement with the slope of the turbulent τ_w vs. (*8V/D*) data was achieved by the method. Results using the different rheologies agreed well with each other in the lower shear stress range in the larger pipe, but diverged somewhat with increasing (*8V/D*) and decreasing pipe diameter. As for the Wilson & Thomas and Slatter methods there seems to be a diameter effect, with increasing overprediction of τ_w as *D* decreases for all rheologies. When using the power law rheology the Dodge & Metzner predictions differ from experimental values by 9% to 13% for the 3% concentration, 4% to 12% for the 5% concentration and 11.7% for the 8% concentration. This technique was also tried with the Casson rheology and gave predictions that were only marginally better than those obtained using the Bingham plastic rheology, also overpredicting the shear stress more as the shear rate increased. Errors when using Casson rheology were 12% to 17% for the 3% concentration, 5% to 14% for the 5% concentration and 14% for the 8% concentrations. The Dodge & Metzner technique works at the lower turbulent shear stress values, especially for the 5% CMC, but for the 3% and 8% concentrations the method overpredict the turbulent shear stress data and deteriorate as the pipe size decrease in the 3% and 5% concentrations.

Newtonian approximation

Figure 5.76 presents the turbulent predictions and average error (in %) for CMC in three pipe sizes using the Newtonian Approximation method with each rheological model in turn.

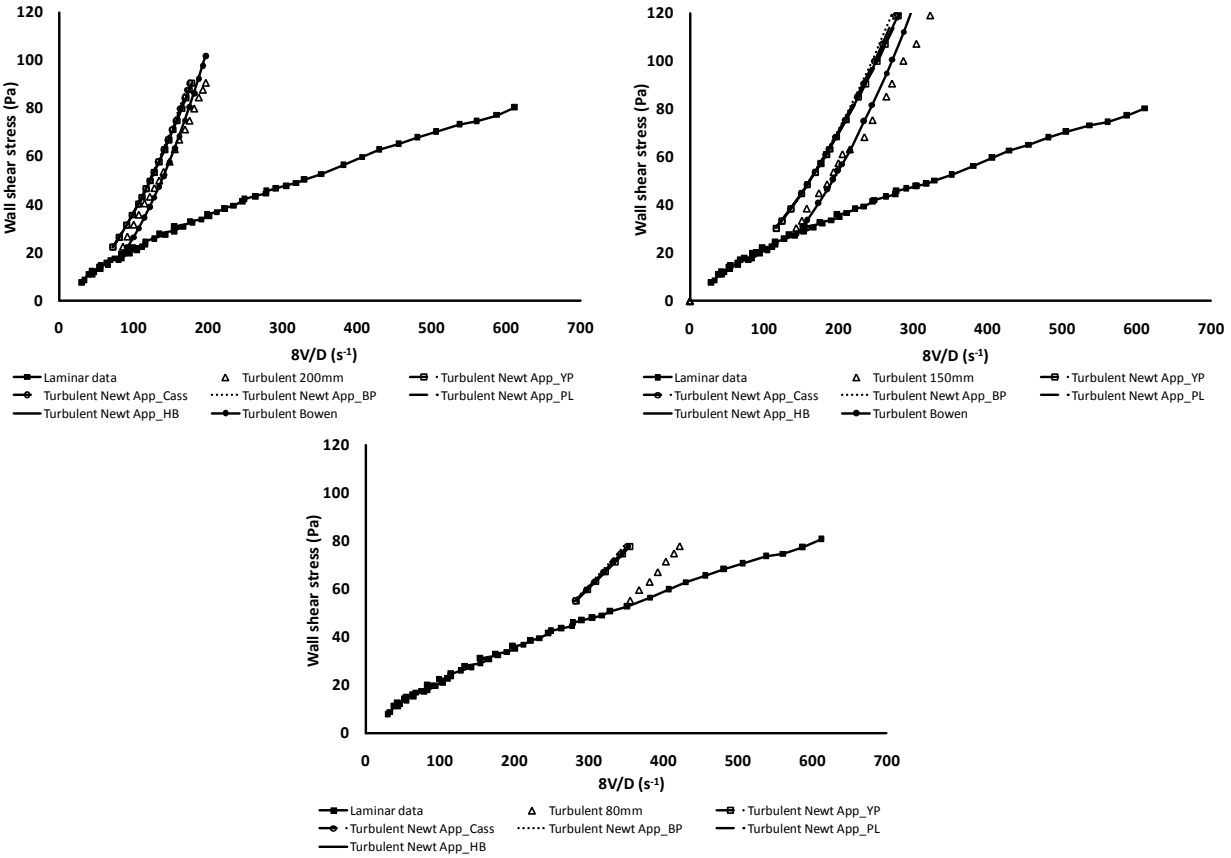

(8V/D) RMSE values - Newtonian Approximation method						
Pipe diameter	HB	BP	PL	CASS	HALL_YP	BOWEN (To)
200mm	9.5%	9.5%	9.4%	9.7%	9.2%	9.1%
150mm	14.4%	14.9%	14.3%	14.6%	14.2%	7.9%
80mm	18.3%	19.3%	18.1%	18.6%	18.0%	N/A
Ave	14.0%	14.5%	13.9%	14.3%	13.8%	8.5%

Figure 5.76 5% CMC turbulent flow predictions and average % error using the Newtonian approximation method – all rheologies

The results presented for the Newtonian approximation in Figure 5.76 show very close agreement for all rheologies in all the pipe sizes and at all concentrations (see Appendix J for 3% and 8% concentration results). The method consistently underpredicts the turbulent velocity, for the same reasons as discussed previously.

For all rheologies this method gave errors of 15% to 23% for the 3% concentration, 9% to 14% for the 5% concentration and 21% in the diameter 150mm pipe for the 8% concentration. Although all rheologies gave almost identical results, the Newtonian approximation is not the most accurate method to use to predict CMC turbulent pressure drops.

Torrance

Figure 5.77 presents the turbulent predictions and average error (in %) for CMC in three pipe sizes using the Torrance method with each rheological model in turn.

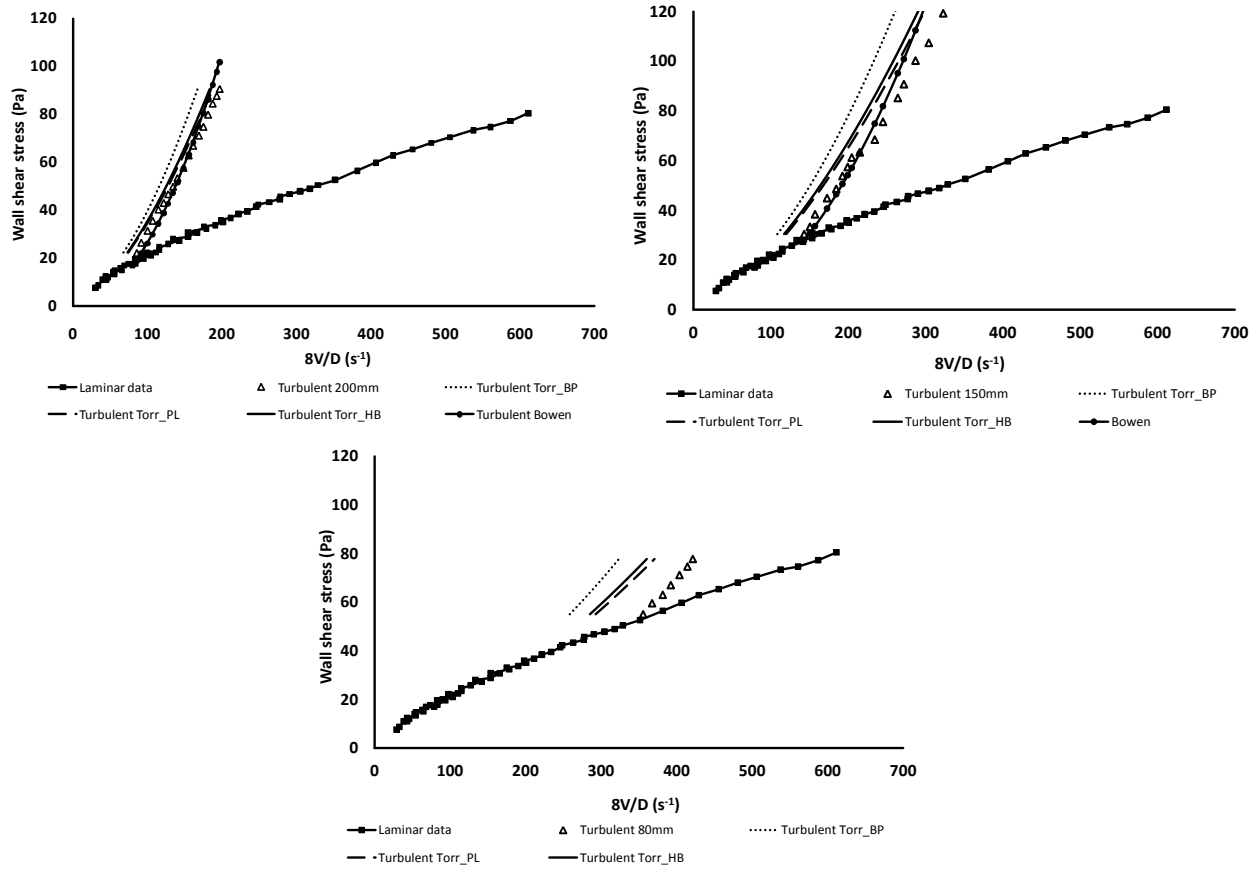

(8V/D) RMSE values - Torrance method				
Pipe diameter	HB	BP	PL	BOWEN (To)
200mm	6.8%	14.2%	4.7%	9.1%
150mm	12.4%	19.7%	10.3%	7.9%
80mm	17.3%	25.4%	15.1%	N/A
Ave	12.2%	19.7%	10.0%	8.5%

Figure 5.77 5% CMC turbulent flow predictions and average % error using the Torrance method – all rheologies

The Torrance turbulent flow prediction gave reasonably reliable CMC predictions of pressure drop when using the power law rheology. For the 5% CMC the fitted Herschel-Bulkley model did not reduce identically to the power law model. In this case use of the power law rheology gave more accurate results with errors of 4% to 15% compared to errors of 7% to 17% for the Herschel-Bulkley rheology. Using the Bingham plastic rheology results in consistent overprediction of the turbulent shear stresses with errors in the range 21% to 28% for the 3% concentration, 14% to 25% for the 5% concentration and 26% for the 8% concentration. In this study the Torrance method has only given acceptable predictions for the CMC material. Based on these results this technique should only be used with the power law rheology for pseudoplastic materials. As for the other techniques, the same diameter effect is present.

Bowen correlation

Results from the Bowen scale-up method are included in Figure 5.71 to Figure 5.77 for the CMC turbulent flow analysis. The technique gave good predictions for the CMC material following the experimental data well in all cases. It gave an average error of 4.3% for the 3% CMC concentration in the diameter 150mm pipe and 9.1% and 7.9% average errors for the 5% concentration in the diameter 200mm and diameter 150mm pipes respectively. When applying this method, care must be exercised that the data from the smaller pipes reasonably meets the requirements on which the method is based.

One rheology plotted for all techniques

The analysis now focuses on the use of specific rheological models with all techniques. The most appropriate rheological model for CMC is the power law model (Section 4.2.1), and use of this model gave the best results, as seen in Figure 5.71 to Figure 5.77. The Herschel-Bulkley and yield plastic rheologies reduced to the power law rheology for the 3% and 8% test concentrations. For the 5% CMC concentration only the yield plastic reduced to the power law model. The Herschel-Bulkley fit resulted in a small yield stress value. Use of the Bingham plastic rheology resulted in the worst turbulent flow predictions for the CMC slurries. To avoid duplication here, only results from using the power law rheology are presented in this section as those obtained when using the Herschel-Bulkley and yield plastic rheologies are similar. All the techniques are presented for the 5% CMC concentration. The results for the 3% and 8% concentrations are given in Appendix J.

Power law

Figure 5.78 presents the turbulent predictions and average % error for CMC in three pipe sizes using the power law rheological model with each turbulent flow prediction technique.

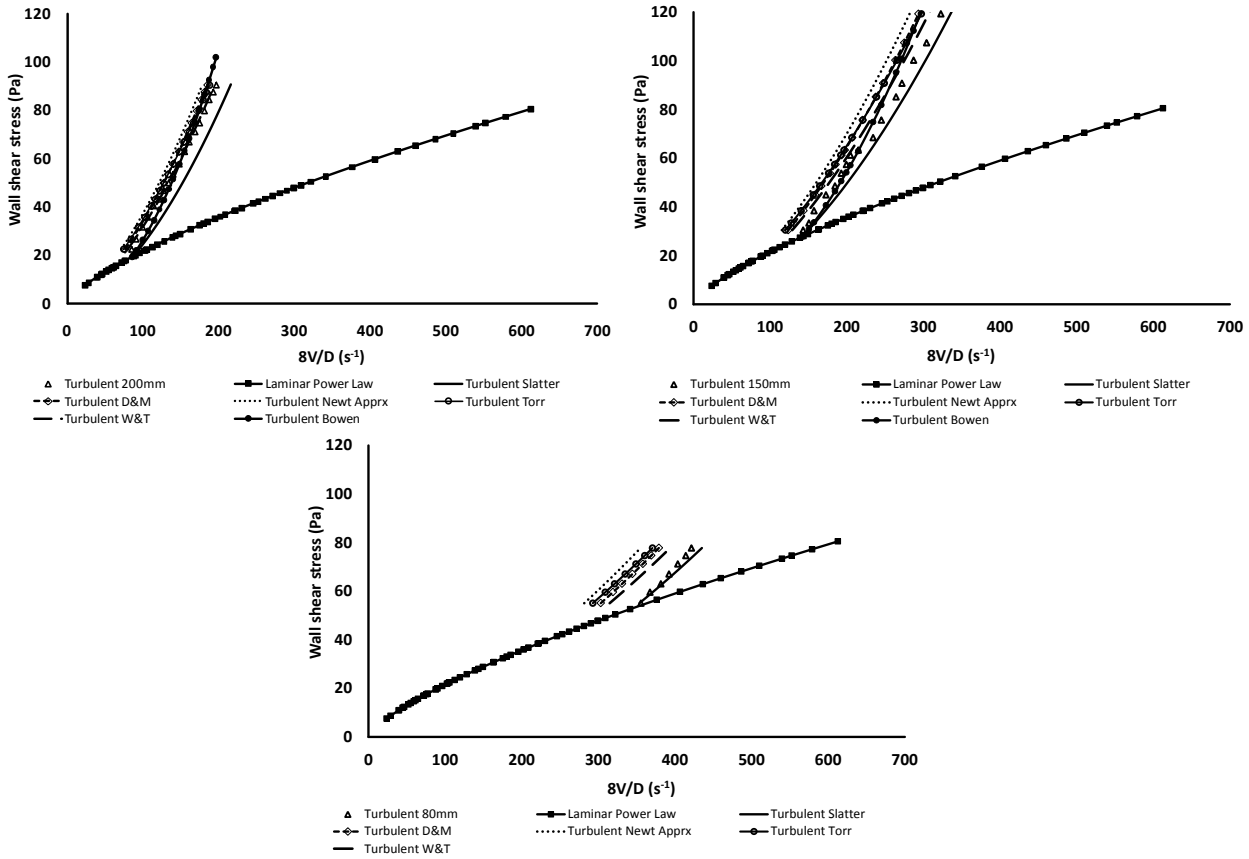

(8V/D) RMSE values - Power Law						
Pipe diameter	W&T	NEWT	TORR	D&M	SLATT	BOWEN (To)
200mm	0.9%	9.4%	4.7%	4.9%	13.5%	9.1%
150mm	5.4%	14.3%	10.3%	9.3%	6.8%	7.9%
80mm	8.8%	18.1%	15.1%	12.2%	1.6%	N/A
Ave	5.0%	13.9%	10.0%	8.8%	7.3%	8.5%

Figure 5.78 5% CMC turbulent flow predictions and average % error using power law rheology – all techniques

The results of the turbulent flow predictions for the three concentrations of the CMC, show that using the power law rheology in the Wilson and Thomas technique gives the most accurate and reliable results. Referring to the results presented for the 5% concentration in Figure 5.78, which is representative of the 3% and 8% concentrations, the values and the slopes of the τ_w vs. (*8V/D*) predicted curves agree well with the experimental values. All techniques overpredict the pressure drops except the Slatter method which underpredicts the shear stresses especially in the diameter 80mm pipe for the 3% and 5% concentrations. The Newtonian approximation significantly overpredicts pressure drops for all concentrations using any of the rheological models. The Dodge & Metzner method produced reasonably accurate results using the Herschel-Bulkley and/or the power law rheology, as the values for *K'* and *n'* were evaluated at the appropriate wall shear stress values for this concentration, and the conditions as stipulated by Dodge & Metzner (1959) were met. The Wilson & Thomas, Slatter or Dodge & Metzner techniques can all be used with power law or Herschel-Bulkley rheology to reliably predict turbulent flow for CMC.

CMC turbulent flow summary

Evaluation of the CMC turbulent flow predictions show that the most successful prediction techniques are the Slatter and Wilson & Thomas methods when combined with the yield plastic and power law rheologies respectively. These two combinations gave errors in the range 3.1% to 7.8% for all concentrations. Predictions from all the techniques, except the Torrance and Hallbom pseudo fluid methods, for all rheologies were reasonably closely grouped, with the Bingham plastic rheology generally resulting in the greatest overprediction of the turbulent shear stresses and the Slatter method generally underpredicting the shear stresses. The Torrance and Hallbom Nikuradse pseudo fluid techniques showed the largest differences with different rheologies especially for the 3% concentration. The Newtonian approximation overpredicts the shear stresses when using all the rheologies, but shows the least sensitivity to the rheological parameters in the 5% concentration. The Newtonian approximation gave errors in the range 9% to 19% for all concentrations. The Dodge & Metzner method gave reasonable predictions when using the power law and Herschel-Bulkley rheologies, with errors of 8.8% to 11.7%, but overpredicted shear stresses for the 3% CMC concentration. The Bowen method resulted in an average error of 4.3% for the 3% CMC test concentration in the diameter 150mm pipe and for the 5% concentration a 9.1% error in the diameter 200mm pipe and a 7.9% error in the diameter 150mm pipe. Shear stress predictions for this 5% CMC and to a lesser degree for the 3% concentration in the smaller diameter 80mm pipe mostly overpredicted the shear stresses. The reason for this could not be established, but may be a diameter effect that the predictions cannot capture.

Effect of concentration and pipe diameter

The analyses presented above for the three concentrations of CMC indicated some behaviour which could suggest both concentration and diameter effects. Some attempt was made to assess these effects by plotting the % error against pipe diameter for one of the most appropriate prediction techniques, namely the Wilson & Thomas method, for all the rheologies considered. A separate plot for each concentration is presented in Figure 5.79 to show the diameter effect, and a separate plot for each diameter in Figure 5.80 to indicate the effect of changing concentration.

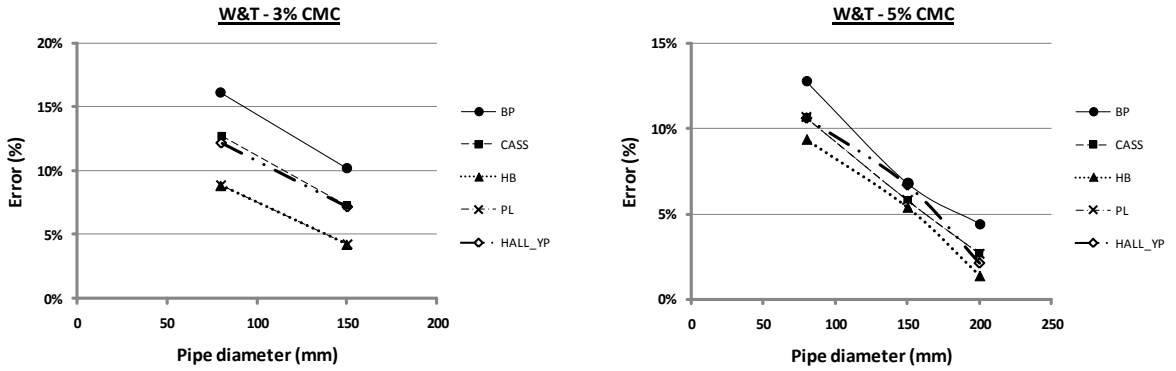

Figure 5.79 Effect of diameter on the % error value for the Wilson & Thomas method in different pipe sizes at 3% and 5% CMC concentrations

The curves shown in Figure 5.79 indicate that the accuracy of the turbulent flow predictions deteriorates as the pipe diameter decreases, both the 3% and 5% concentrations. They also show that for the 5% concentration prediction of turbulent flow is less sensitive to changes in rheological parameters. It seems though that although the levels of accuracy of the predictions change with rheology, the change with pipe diameter remain approximately constant, but different for each concentration. For the 3% CMC the change in error from the diameter 150mm pipe to the diameter 80mm pipe is about 6 to 7%, while for the 5% concentration it is about 4%. With the exception of the Slatter method, all the prediction methods overpredicted shear stresses especially in the diameter 80mm pipe. It can also be seen that the Slatter technique is less sensitive to diameter than the other methods and shows fairly consistent accuracy across all pipe diameters for the 5% CMC concentration (see Figure 5.72). Turbulent flow was only obtained in one pipe size (diameter 150mm) for the 8% CMC, so no diameter effects are available for that material.

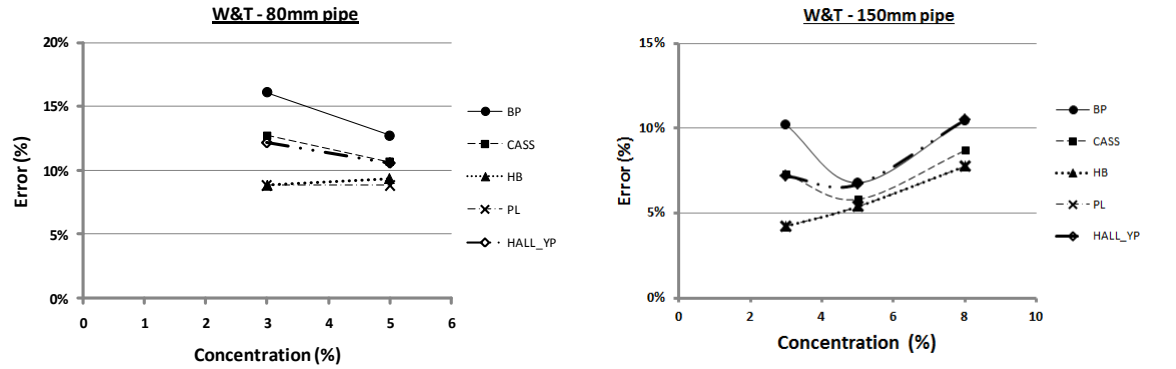

Figure 5.80 Effect of concentration on the % error for the Wilson & Thomas method at different CMC concentrations in the diameter 80mm and 150mm pipes

Referring to the graphs shown in Figure 5.80 it is clear that the 5% concentration generally gave more accurate results for the turbulent predictions than the 3% and 8% concentrations. Overall smaller errors are achieved in the diameter 150mm pipe compared to the diameter 80mm and the variation in prediction errors achieved between the different rheologies are smaller for the 5% and 8% concentration than for the 3% CMC. This could be due to different experimental conditions Turbulent flow was not achieved in the 80mm diameter pipe for the 8% concentration, so no diameter effect comparison is available for this pipe size/material combination.

5.3.4 Turbulent flow conclusion

The results of the turbulent flow predictions for the three test materials using all the considered techniques with the applicable considered rheologies have been presented and discussed. This section gives summary of the outcomes of the turbulent flow analyses.

Three materials, namely kaolin, bentonite and CMC were used in the turbulent study as they are representative of Herschel-Bulkley (yield pseudoplastic), Bingham plastic and power law (pseudoplastic) materials respectively. To ensure accurate and reliable turbulent predictions, it is important that the laminar flow data is correctly and accurately characterised by the most suitable rheological model. This was done and presented in Section 4.2 to Section 4.4.

Choice of rheological model

Each of the turbulent flow predictive techniques uses the rheological parameters of the material in various fundamental ways (see Chapter 2) in their formulation, thus if the rheology of the material is poorly described, accurate predictions cannot be expected. The function defining the laminar flow curve is also used directly to calculate pressure drop values at the much higher shear rate values of turbulent flow by extrapolating it to these higher stresses, and this is not necessarily valid.

Extrapolation and force fitting

The extrapolation of laminar data can result in significantly inaccurate turbulent predictions if an inappropriate rheological model is forced onto a laminar data set. Although several rheological models might appear to fit the experimental data reasonably well in the laminar flow regime, the extrapolation to the higher shear rates of the turbulent flow regime will be very different for each model and not necessarily representative of the material, as seen in Figure 5.47. In this study several different rheological models were used in this way, and the effect of the laminar rheology on turbulent flow predictions evaluated. To minimise extrapolation 'unknowns' the turbulent shear stress range considered was limited as described in Section 3.2.7 and below.

Shear stress range

Ideally the shear stress range for which turbulent flow predictions are required, should be covered in the laminar flow tests. This will ensure that rheological characterisation is done for the entire range of shear stress values and that no extrapolation is required. Doing this, however, poses severe experimental difficulties, as the high shear stresses of turbulent flow then require laminar flow tests in very small diameter pipes at relatively high shear rates (Chhabra & Richardson, 2008). The Dodge & Metzner technique requires that *K'* and *n'* be evaluated from such laminar flow data, otherwise the technique is not strictly valid and can produce spurious results, as was observed for all the kaolin and most of the bentonite slurries considered in this study.

In an attempt to minimise the effect of the extrapolation of laminar data, turbulent predictions were limited to shear stresses of 1.25 times (i.e. 25% greater than) the maximum experimental laminar shear stress value, or to the third measured turbulent value, whichever was greater. Even so, the effects of the extrapolation were still evident, except for the CMC material for which the laminar flow shear stresses obtained are much higher than for kaolin and bentonite, and cover the shear stress range required for turbulent flow predictions. The shear thinning property of CMC and lack of yield stress enabled laminar flow data to be collected at shear stress values corresponding to the turbulent flow. This was particularly clear when using the Dodge & Metzner technique.

Results: kaolin

The turbulent flow prediction results of this study showed the Slatter technique to be the most accurate for kaolin slurry. The success of the Slatter technique is due to the incorporation of particle roughness effects on the velocity gradient in the pipe wall region in turbulent flow. This prediction technique combined with the Casson, closely followed by the yield plastic rheological model, gave the best agreement with the experimental values and slope of the turbulent τ_w vs. (*8V/D*) curves.

The Wilson and Thomas technique, which incorporates thickening of the laminar sub layer, also gave accurate results with the Casson rheology. Similarly the Hallbom pseudo fluid Nikuradse method combined with the Casson or yield plastic rheology consistently gave good turbulent predictions. The Dodge & Metzner method was not applied to the kaolin material due to the limitations imposed by the technique. The Newtonian approximation constantly overpredicted the kaolin turbulent flow pressure drops, probably due to thickening of the viscous sub-layer which is not accounted for in this method. The Torrance method was unable to predict the kaolin turbulent data accurately at all and showed significant dependence on the rheological model used. Bowen's method gave errors of the order of 10% and is a good technique to use if suitable experimental data is available from tests in smaller pipes.

For the kaolin materials, use of the Casson rheology consistently gave the most accurate results even though the Herschel-Bulkley rheology was the most appropriate rheological model for this material. However, use of the Herschel-Bulkley model also gave good predictions and should not be discounted. Using the Bingham plastic model resulted in overprediction of the turbulent shear stresses, whilst use of the power law model underpredicted the stresses. Use of the rheological model of Hallbom (yield plastic) gave good agreement with experimental turbulent data in the Slatter, Hallbom modified Wilson & Thomas and Hallbom pseudofluid Nikuradse techniques.

Results: bentonite

The bentonite slurries tested were best characterised as Bingham plastics, although for the 9% concentration the Casson model fit gave a similar accuracy to the Bingham plastic model. Evaluation of the turbulent flow predictions showed that the Slatter and Hallbom Nikuradse pseudo fluid methods gave the most reliable and accurate results for the different bentonite slurries when combined with the Bingham plastic, Casson or the yield plastic rheologies. These were closely followed by the Dodge & Metzner method Bingham or Casson rheology.

The Wilson & Thomas technique produced inconsistent results showing good predictions (6.3% error) for 7.34% bentonite, but errors of 11.6% and 15.3% for the 6% and 9% concentrations respectively. The Newtonian approximation showed varying results for the different concentrations. For the 6% and 7.34% concentrations the Casson rheology produced good results, and the Bingham plastic overpredicted turbulent pressure drop. For the 9% concentration the Casson rheology underpredicted the turbulent pressure drop significantly and the Bingham plastic produced more accurate results. The Torrance model also failed to predict bentonite turbulence showing large differences in results for the different rheologies. The Bowen method gave varied results for the bentonite concentrations with errors of 22% for the 6% concentration, 12% for the 7.34% concentration and 3% for the 9% concentration. It of course depends on the quality of the experimental data from the smaller pipes.

Use of the Bingham plastic and Casson rheologies gave the most accurate and reliable predictions. The success of the Casson rheology is attributed to the Newtonian tendency of the model at the higher shear stress and shear rate values, where it exhibits a constant shear viscosity, although it incorporates shear

thinning in the lower shear stress and shear rate ranges (Heywood & Alderman, 2003). The Herschel-Bulkley and Hallbom yield plastic rheologies reduced to the Bingham plastic or Casson form for the bentonite test material and so resulted in similar predictions. The power law rheology failed to describe the laminar flow of the bentonite materials and (Section 4.3), and gave excessively inconsistent and inaccurate results. This rheology is completely unsuitable for use in bentonite turbulent flow predictions.

Results: CMC

The CMC material was best described by the power law rheological model, but evaluation of the turbulent flow predictions showed little sensitivity to the rheology, for all the prediction methods. The most accurate turbulent flow prediction technique was the Slatter technique using the yield plastic rheology, closely followed by the Wilson & Thomas method using the power law rheology or the Hallbom modified Wilson & Thomas method combined with the Casson rheology. The Dodge & Metzner technique method produced fair predictions when using the power law rheology, showing errors of 8.8% to 11.7%.

The most appropriate rheologies to use with the suggested turbulent prediction techniques for this material are the power law, yield plastic and Casson rheologies. The yield plastic model is able to adapt very well to the non-yielding pseudoplastic material producing good results in the Slatter and Hallbom modified Wilson & Thomas techniques. This is surprising since the rheological model was developed for yield stress fluids (Hallbom, 2008).

For this material the most inaccurate techniques were the Torrance and Hallbom Nikuradse pseudofluid methods. The Newtonian approximation overpredicted the pressure drops, but not excessively. Bowen's method gave accurate results for the CMC material, with average errors of 4.3% for the 3% CMC concentration in the diameter 150mm pipe and 9.1% and 7.9% in the diameter 150mm and diameter 200mm pipes respectively for the 5% concentration.

5.4 Concluding comment

From this study it is evident that the prediction of turbulent flow of non-Newtonian fluids can be complex and many variables need to be considered. Even with carefully obtained experimental results and attention to detail in the analyses, predictions can differ widely. Although not exhaustive the analyses presented here have been able to identify which combination of rheological model and turbulent flow prediction techniques give acceptable predictions for yield pseudoplastic, Bingham plastic and pseudoplastic materials. This can serve as a good starting point for further more specific and more detailed investigation of the turbulent flow of homogeneous fluids using this approach.

Chapter 6 Conclusions and recommendations

The accurate prediction of pipe flow headloss for non-Newtonian fluids in the laminar, transitional and turbulent flow regimes is still a significant problem. It requires choosing the correct rheological model for the material, and then using it with an appropriate predictive technique. The aim of this work was to evaluate how appropriate/accurate different rheological models are in reproducing non-Newtonian laminar flow, and the influence of each when used in selected transitional and turbulent flow prediction techniques. This chapter presents the conclusions of the study and some recommendations for future research.

6.1 Conclusions

Pipe test were conducted using three non-Newtonian materials representing the pseudoplastic, Bingham plastic and yield pseudoplastic rheologies at three concentrations in laminar, transitional and turbulent flow, in pipes ranging from diameter 13mm to diameter 200mm. A minimum shear rate of $40s^{-1}$ was considered for all pipe tests, corresponding to a velocity of 0.065m/s in the diameter 13mm pipe and 1.055m/s in the diameter 200mm pipe. Turbulent flow predictions were done for all the experimental points, but the errors for each rheological model/technique combination were compared only for shear stress values up to 1.25 times the highest measured laminar flow shear stress, or up to the third measured turbulent point, whichever was greater.

6.1.1 Laminar flow

Rheological characterisation of each material was done using the laminar data and the suitability of each rheological model assessed by comparing the RMSE values of each nonlinear curve fit. On this basis it was concluded that:

- Yield pseudoplastic materials (represented by kaolin) are best described by the Herschel-Bulkley rheological model or Hallbom yield plastic rheological model.
- Bingham plastic type materials (represented by bentonite) are best described by the Bingham plastic rheological model (or the Hallbom yield plastic rheological model which reduces to the Bingham plastic model during the curve fitting).
- Pseudoplastic type materials (represented by CMC) are best described by the power law rheological model (or the Herschel-Bulkley and Hallbom yield plastic rheological models which both reduce to power law during the curve fitting).

The recommended rheological models for use with the materials considered in this study are presented in Table 6.1.

Table 6.1 Recommended rheological models for pseudoplastic, Bingham plastic and yield-pseudoplastic materials

Material type:	Pseudoplastic	Bingham plastic	Yield-pseudoplastic
Most suitable rheology:	Power law, Hallbom yield plastic	Bingham plastic, Hallbom yield plastic	Herschel-Bulkley, Hallbom yield plastic

6.1.2 Transitional velocity (V_c) predictions

The transitional velocity prediction techniques were evaluated against an arbitrarily selected experimental value, chosen as the last laminar data point in the test pipe data set simply to enable a common reference with which to compare the predictions. Conclusions are based on absolute error values and consistency of predictions across all concentrations and pipe sizes.

For yield pseudoplastic materials (eg. kaolin) the Hedström intersection method and the Slatter Reynolds number method, using the Bingham plastic or the Casson rheological model, gave the most accurate critical (transitional) velocity predictions. The Metzner & Reed and generalised Reynolds numbers show close agreement for all rheologies, but underpredict the experimental transitional velocity. The Newtonian approximation, Ryan and Johnson and Torrance techniques are not able to predict the transitional velocity reliably. Hallbom's transition criterion gives acceptable predictions using the Bingham plastic rheology, but fails when using any other rheological model. The Slatter & Wasp method (only applicable to Bingham plastic rheology) also showed good results for the kaolin material with errors ranging from 5% to 13%.

The transitional velocity for Bingham plastic materials (eg. bentonite), is best predicted using the Metzner & Reed Reynolds number with Bingham plastic rheology, although the technique gives similar results for all rheologies. This is closely followed by the Slatter method using the Casson rheology. The Hedström intersection method, Newtonian approximation, Torrance and Hallbom techniques fail to predict the transitional velocity for this type of material. The method of Slatter & Wasp also fails to reliably predict the transitional velocity, with errors in the range 18% to 48%.

For pseudoplastic materials (eg. CMC) the Slatter method and the Metzner & Reed Reynolds number method give the most consistently accurate transitional velocity predictions, when using power law or the Casson rheology, producing errors in the range of 1% to 9%. They are closely followed by the Generalised Reynolds number technique which produces errors in the range of 2.7% to 12.7%. The Ryan & Johnson and Newtonian Approximation techniques show inconsistent results across the three concentrations, whilst the Intersection method and Hallbom transition technique are unable to predict transition for pseudoplastic materials reliably. A summary of the recommended transitional flow technique and rheology combinations for use with the materials considered in this study is presented in Table 6.2. These combinations gave the most consistently accurate results, but it is recommended that the rheological model which best describes the material should also always be included in the analyses with the suggested transitional velocity prediction techniques.

Table 6.2 Recommended transitional flow prediction technique and rheology combination for pseudoplastic, Bingham plastic and yield-pseudoplastic materials

Pseudoplastic		Bingham plastic		Yield-pseudoplastic	
Method	Rheology	Method	Rheology	Method	Rheology
Slatter, Metzner & Reed	Power law, Casson	Metzner & Reed, Slatter	Bingham plastic, Casson	Hedström intersection, Slatter	Bingham plastic, Casson, (Herschel-Bulkley)
				Slatter & Wasp	Bingham plastic

6.1.3 Turbulent flow predictions

Turbulent flow velocity predictions were evaluated against experimental turbulent data in each pipe for each material concentration. Conclusions were based on absolute error values and consistency of predictions across all concentrations and pipe sizes.

For yield pseudoplastic materials slurries (eg. kaolin) the Slatter method using Casson rheology gave the most accurate turbulent flow predictions overall. This was closely followed by the Wilson & Thomas and Hallbom pseudo fluid Nikuradse technique, using the Casson or yield plastic rheology. The Dodge & Metzner method could not be tested due to limitations in the laminar flow data. The Newtonian approximation consistently overpredicts the turbulent pressure drop by an average of 17%. The Torrance method is unable to predict turbulent flow for yield pseudoplastic materials and is very dependent on the rheological model used. Bowen's scale-up method works well, with errors up to 10%.

For the yield pseudoplastic material the Casson and yield plastic rheology gave the most accurate results when used with the various turbulent techniques. However it is recommended that the Herschel-Bulkley rheology (most appropriate rheological model) also be used in turbulent predictions. Using the Bingham plastic rheology overpredicts pressure drop whilst using power law rheology underpredicts the pressure drop. Using Hallbom's yield plastic rheological model with the Slatter and Hallbom modified Wilson & Thomas techniques gives good predictions, with average errors of 4% to 10%.

Turbulent flow for Bingham plastic materials (eg. bentonite) is best predicted by the Slatter, Hallbom pseudo fluid Nikuradse and Dodge & Metzner methods, using the Bingham plastic, Casson or the yield plastic rheologies, with errors in the range 2.1% to 7.7%. For the Dodge & Metzner method only the Casson or Bingham plastic rheology applies since the yield plastic rheology cannot be incorporated into this method. The Newtonian approximation overpredicts pressure drops by an average of 13% whilst the Torrance method fails to predict turbulent flow reliably at all. The Bowen method gives results of varying accuracy, with errors between 3% and 22%, and is very dependent on the quality of the smaller pipe data on which it is based. The rheological models which result in the most accurate turbulent flow predictions for bentonite are the Bingham plastic, Casson and yield plastic models. Use of the power law rheology with any of the prediction techniques fails to give meaningful results for Bingham plastic materials.

For pseudoplastic materials (eg. CMC) the Slatter and the Wilson & Thomas techniques predict turbulent flow most accurately when using the yield plastic and power law rheologies respectively, both showing errors in the range 3.1% to 7.8%. The Hallbom modified Wilson & Thomas technique also produced consistently good results when using yield plastic or Casson rheology (6.5% to 10.5%). The Dodge & Metzner and Torrance methods produced fair predictions only when using the power law rheological model, with errors in the range 8.8% to 11.7% and 10% to 12% respectively. The Newtonian approximation overpredicts pressure drops for this type of material, but Bowen's scale up method accurately predicts the turbulent data for pseudoplastic materials (4% to 9%). The most inaccurate and inconsistent technique is the Hallbom pseudo fluid Nikuradse technique showing errors varying between 5% and 33%. A summary of the recommended turbulent flow technique and rheology combinations for use with the materials considered in this study is presented in Table 6.3. These combinations gave the most consistently accurate results, but it is recommended that the rheological model which best describes the material always included in the analyses as well.

Table 6.3 Recommended turbulent flow prediction technique and rheology combination for pseudoplastic, Bingham plastic and yield-pseudoplastic materials

Pseudoplastic		Bingham plastic		Yield-pseudoplastic	
Method	Rheology	Method	Rheology	Method	Rheology
Slatter, Wilson & Thomas, (Dodge & Metzner)	Yield plastic, Power law, Casson	Slatter, Hallbom pseudo fluid Nikuradse, Dodge & Metzner	Bingham plastic, Casson, yield plastic	Slatter, Wilson & Thomas, Hallbom pseudo fluid Nikuradse	Casson, yield plastic, (Herschel-Bulkley)
Bowen	N/A			Bowen	N/A

6.2 Final Remarks

Results presented in this work have shown the influence of the choice of rheological model (rheological parameters based on laminar flow data) on the predictions of laminar, transitional and turbulent flow of non-Newtonian homogeneous fluids in pipes. For laminar flow in a realistic *8V/D* range, the choice of rheological model does not significantly influence the laminar 'predictions' obtained by each model, which is in line with the findings of Malkin et al (2004).

In transitional and turbulent flow the best rheological model to use with a prediction technique is generally the rheological model which most appropriately describes the test material in laminar flow. However, the use of the Casson rheology for turbulent predictions in Bingham plastic and yield-pseudoplastic fluids gave more accurate results than the generally preferred respective Bingham plastic and Herschel-Bulkley rheological models. This confirms the concern of Wilson & Addie (2000) that rheological models such as Casson are often overlooked. Transitional and turbulent predictions for materials with a yield stress are very dependent on the choice of the rheological model, but for power law fluids (no yield stress) the results are closely grouped.

Spreadsheets were developed for the rheological characterisation of materials and for the analysis of laminar, transitional and turbulent flow of non-Newtonian fluids. These are available for future studies.

6.3 Recommendations

When conducting pipe tests to characterise a material it is very important to do these accurately and to collect data over a sufficiently wide range of pipe sizes and flow rates, with sufficient test points in each flow regime. It is also important to examine all the data carefully to see that it makes sense, and to fit an appropriate rheological model. Some judgement is needed with regard to the choice of the lower and upper *8V/D* values used to 'define' the range of the laminar flow data to be used in the rheological characterisation. The extrapolation of laminar data to the higher shear rate values of turbulent flow should be avoided. Ideally experimental pipe tests should be carried out in smaller diameter tubes at higher *8V/D* values to achieve wall shear stresses which cover the turbulent shear stress range for turbulent flow predictions in larger pipes. It is recognised though, that in many cases it may be very difficult or even impossible to conduct physical tests to high enough wall shear stress values.

It is suggested that further tests be done with the same material types in smaller diameter test pipes in order to obtain sufficiently high laminar flow shear stresses, which will correspond to the higher turbulent shear stress in the larger pipes. This will also allow better evaluation of the Dodge & Metzner (1957) turbulent flow prediction model, which could not be included here for all materials due to its limitations and insufficient test data.

References

Alderman, N. J. and Heywood, N.I. 2004a. Improving slurry viscosity and flow curve measurements, Chem. Eng. Prog., 101(4): 27-32, April.

Alderman, N. J. and Heywood, N.I. 2004b. Making accurate slurry flow curve measurements, Chem. Eng. Prog.: 27-32, May.

Banfi, G.P., De Mechili, R. & Henin, A. 1981. Velocity fluctuation enhancement in the transition to turbulence in a pipe. Journal of Physics D: Applied Physics, 14: 625-632.

Bartosik, A.S., Hill, K.B. & Shook, A.S.1997. Numerical modelling of turbulent Bingham flow. 9th International Conference on Transport and Sedimentation of Solid Particles, Cracow, 2-5 September 1997: 69-81.

Boger, D.V., Scales, P.J. & Sofra, F. 2008. Paste and Thickened Tailings and the Impact on the Development of New Rheological Techniques. Proceedings of the 2008 Paste Conference, Kasane, 5-9 May 2008: 225-236. Australian Centre for Geomatics, Perth: Nedlands, W.A.

Bowen, R.L. 1961. Designing Turbulent Flow Systems. Chemical Engineering, 68(14): 143-150, July 24.

Brown, N. P. & Heywood, N. I. 1991. Slurry Handling: Design of Solid-Liquid systems. Elsevier Science Publishers. England.

Casson, N. 1959. A flow equation for pigment-oil suspensions of the printing ink type. In Mill, C.C. (ed). Rheology of disperse Systems. New York: Pergamon Press: 84-104.

Chara, Z., Vlasak, P., Severa, M. Havlik, V. & Vycital, J. 1996. Flow of dense kaolin and ash slurries in pipes. 13th International Conference on Slurry Handling and Pipeline Transport, Johannesburg, 3-5 September: 75-87.

Chilton, R.A. & Stainsby, R. 1996. Prediction of pressure losses in turbulent non-Newtonian flows: Development and application of a hybrid rheological model. Proceedings of the 13th Conference on the Hydraulic Transport of Solids, Johannesburg, 3-5 September: 21-40.

Chilton, R.A. & Stainsby, R. 1998. Pressure loss equations for Laminar and Turbulent non-Newtonian Pipe flow. Journal of Hydraulic Engineering, 124(5): 522-529.

Chhabra, R.P. and Richardson, J.F. 2008. Non-Newtonian Flow in the Process Industries. 2nd ed. Oxford: Butterworth-Heinemann.

Darbyshire, A.G. & Mullin, T. 1995. Transition to turbulence in constant mass-flux pipe flow. Journal of Fluid Mechanics,289: 83-114.

Desouky, S.E.M. & Al-Awad, M.N. 1998. A new laminar-to-turbulent transition criterion for yield-pseudoplastic fluids. Journal of Petroleum Science and Engineering, 19: 171-176.

Dodge, D.W. and Metzner, A.B. 1959. Turbulent flow of non-Newtonian systems. AIChE Journal, 5(2): 198-204.

Douglas, J.F., Gasiorek, J.M. & Swaffield, J.A.1995. Fluid Mechanics. 3rd ed. Singapore: Longman Publishing Group.

El Nahhas, K., El-Hak, N.G., Rayan, M.A., Vlasak, P. and El-Sawaf, I.A. 2004. The laminar/ turbulent transition condition of non-Newtonian slurries flow in pipes. Proceedings of the 16th Conference on the Hydraulic Transport of Solids, Santiago, 26-28 April: 47-59.

El Nahhas, K., El-Hak, N.G., Rayan, M.A., and El-Sawaf, I. 2005. Flow behaviour of non-Newtonian clay slurries. Proceedings of the 9th International Water Technology Conference, Sharm El-Sheik, Egypt. 47-59.

El-Nahhas, K. & Mostafa, N.H. 2006. Prediction of non-Newtonian Turbulent flow behaviour by a Newtonian approach. 10th International Water Conference, IWTC10, Alexandria, 23-25 March 2006: 479-490.

Frigaard, I.A. & Nouar, C. 2003. On three dimensional linear stability of Poiseuille flow of Bingham fluids. Physics of Fluids, 15(10): 2843-2851.

Govier, G.W. & Aziz, K. 1972. The flow of complex mixtures in pipes. Florida: R.E. Krieger Publishing Co.

Güzel, B., Burghelea, T., Frigaard, I.A. & Martinez, D.M. 2009. Observation of laminar-turbulent transition of a yield stress fluid in Hagen-Poiseuille flow. Journal of Fluid Mechanics, 627: 97-128, January 2009.

Hallbom, D.J. 2008. Pipe flow of homogeneous slurry. Unpublished PhD dissertation, University of British Columbia, Vancouver.

Hallbom, D.J. and Klein, B. 2006. Laminar pipe flow of a yield plastic fluid. JKMRC International Student Conference, Brisbane, Australia.

Hallbom, D.J. and Klein, B. 2009. A physical model for yield plastics. Particulate Science and Technology, 27:1-15.

Haldenwang, R. 2003. Flow of non-Newtonian fluids in open channels. Unpublished DTech dissertation, Cape Peninsula University of Technology, Cape Town.

Haldenwang, R., Sutherland, A., Fester, V., Holm, R.& Chhabra, R. 2012. Sludge pipeflow pressure drop prediction using composite power law friction factor-Reynolds number correlations based on different non-Newtonian Reynolds numbers. Water SA, 38(4) 2012.

Hanks, R.W. 1963. The laminar-turbulent transition for fluids with a yield stress. A.I.Ch.E. Journal, 9: 306-309.

Hedström, B.O.A. 1952. Flow of plastic materials in pipes. Industrial Engineering and Chemistry, 44(3): 652-656.

Heywood, N. I. & Alderman, N. J. 2003. Developments in slurry pipeline technologies. Chem. Eng. Prog., 36-43, April.

Heywood, N. I. & Cheng, D.C-H. 1984. Comparison of methods for predicting headloss in turbulent pipe-flow of non-Newtonian fluids. Trans. Inst. M C. Vol 6, No 1: Jan - Mar.

Heywood, N. I. & Richardson, J.F. 1978. Rheological behaviour of flocculated and dispersed kaolin suspensions in pipe flow. Journal of Rheology, 22(6): 599-613.

Holland, F.A. & Bragg, R. 1995. Fluid Flow for Chemical Engineers. 2nd ed. Great Britain: Edward Arnold Hydrotransport 17. The 17th International conference on the Hydraulic Transport of Solids, Cape Town, 7-11 May 2007: 77-86.

Holman, J.P. 2001. Experimental methods for engineers. 7th edition. McGraw-Hill International Edition. New York.

Kabwe, A.M. 2009. Non-Newtonian loss coefficients for Saunders diaphragm valves, Unpublished MTech dissertation, Cape Peninsula University of Technology, Cape Town.

Kelessidis, V.C. & Maglione, R. 2006. Modelling rheological behaviour of bentonite suspensions as Casson and Robertson-Stiff fluids using Newtonian and true shear rates in Couette viscometry. Powder Technology, 168: 134-147.

Kelessidis, V.C., Maglione, R. Tsamantaki, C. & Aspirtakis, Y. 2006. Optimal determination of rheological parameters for Herschel-Bulkley drilling fluids and impact on pressure drop, velocity profiles and penetration rates during drilling. Journal of Petroleum science and engineering, 53: 203-224.

Kemblowski, Z. & Kolodziejski, J. 1973. Flow resistance of non-Newtonian fluids in transitional and turbulent flow. Int. Chem. Eng,. 13(2): 265-279.

Kirkup, L. 2002. Data analysis with Excel. New York: Cambridge University Press.

Klein, A. 1981. Review: Turbulent developing pipe flow. Transactions of the ASME: Journal of Fluids Engineering, 103: 243-249.

Knudsen, J.G. & Katz, D.L. 1958. Fluid Dynamics and Heat Transfer. New York: McGraw-Hill.

Kozicki, W., Chou, C.H. and Tiu, C. 1966. Non-Newtonian Flow in Ducts of Arbitrary Cross Sectional Shape. Chemical Engineering Science, 21: 665-679.

Kumar, A., Saboo, S., Sheth, S., Pilehvari, A. & Serth, R. 2000. Correlation of Rheometric data and Hydraulic calculations using Rational Polynomials. Chem. Eng. Comm, 183: 99-117.

Lazarus, J. H. and Slatter, P. T. 1988. A method for the rheological characterisation of tube viscometer data, Journal of pipelines, V.7.

Litzenberger, C. G. & Sumner, R.J. 2004. Flow behaviour of clay slurries. 16th International conference on the Hydraulic transport of Solids in Pipes, Santiago. 26-28 April 2004: 75-91.

Malkin, A., Masalova, I., Pavlovski, D., Slatter, P. 2004. Is the choice of flow curve fitting equation crucial for the estimation of pumping characteristics? Applied Rheology, 14(2): 89-95, January 28.
Masalova, I., Malkin, A. Ya., Kharatiyan, E. & Haldenwang, R. 2006. Scaling in pipeline flow of kaolin suspensions. Journal of Non-Newtonian Fluid Mechanics 136: 76-78.

Massey, B.S. 1970. Mechanics of Fluids. 2nd ed. London: van Nostrand Reinold Co.

Metzner, A.B. 1956. Non-Newtonian technology: Fluid mechanics, Mixing, and Heat Transfer. Advances in Chemical Engineering. Drew, T.B. & Hopes, J.W. Jr.: Academic Press: 77-153.

Metzner, A.B. & Reed, J.C. 1955. Flow of Non-Newtonian fluids – correlations of the laminar, turbulent and transition flow regions. A.I.Ch.E. Journal, 1: 434-440.

Mullineux, G. & Simmons, M. 2008. Influence of rheological model on the processing of yoghurt. Journal of Food Engineering, 84(2): 250-257, January 2008.

Nguyen, Q.D. & Boger, D.V.1992 Measuring the flow properties of yield stress fluids. Annual Review of Fluid Mechanics, 24: 47-88.

Nouar, C. & Frigaard, I.A. 2001. Non-linear stability of Poiseuille flow of a Bingham fluid: theoretical results and comparison with phenomenological criteria. Journal of Non-Newtonian Fluid Mechanics, 100: 127-149.

Park J.T., Mannheimer R.J., Grimley T.A., Morrow T.B. 1989. Pipeflow measurements of transparent non-Newtonian slurry. Journal of Fluids Engineering, 111: 331-336.

Peixinho, J., Nouar, C., Desaubry, C. & Theron, B. 2005. Laminar transitional and turbulent flow of yield stress fluid in a pipe. Journal of Non-Newtonian Fluid Mechanics, 128: 172-184.

Peker, S.M. & Helvaci, S.S. 2008. Solid-liquid two phase flow. USA: Elsevier Science and technology.

Perry, R.H. 1997. Perry's Chemical Engineering Handbook. 7thed. New York: McGraw-Hill.

Pullum, L., Rudman, M., Graham, L., Downie, R., Battacharya, S., Chryss, A. & Slatter, P. 2001. AMIRA P599 1st Progress report. March 2001.

Pilehvari, A.A. & Serth, R. W. 2005. Generalised Hydraulic calculation method using Rational Polynomial. Journal of Energy Resources Technology, 127: 15-25, March 2005.

Ryan, N.W. & Johnson, M.M. 1959. Transition from laminar to turbulent flow in pipes. A.I.Ch. E. Journal, 5: 433-435.

Scott Blair, G.W. 1967. A model to describe the flow curves of concentrated suspensions of spherical particles. Rheological Acta, 6(3): 201-202.

Shook, C.A. & Roco, M.C. 1991. Slurry flow: Principles and Practice. Boston: Butterworth-Heinemann.

Skellend, A. H. P. 1967. Non-Newtonian flow and heat transfer, John Wiley and Sons Inc., New York.

Slatter, P.T. 1994. Transitional and turbulent flow of non-Newtonian slurries. Unpublished PhD dissertation, University of Cape Town, Cape Town.

Slatter, P.T. 1997a. The Effect of the Yield Stress on the Laminar/Turbulent transition. Proceedings of the 9th International Conference on Transport and Sedimentation of Solid Particles, Cracow, 2-5 September: 547-561.

Slatter, P.T.1997b. The Rheological characterisation of Sludges. Water Science and Technology, 36(11): 9-18.

Slatter, P.T. 1999. Role of rheology in pipelining of mineral slurries. Cape Technikon, Cape Town.

Slatter, P.T., Mollagee, M. & Petersen, F. W. 1997. Non-Newtonian turbulence – A practical overview. Proceedings of the 9th International Conference on Transport and Sedimentation of Solid Particles, Cracow, 2-5 September 1997: 83-95.

Slatter, P.T., Thorvaldsen, G. S.& Petersen, F. W. 1996. Particle roughness turbulence. Proceedings of the 13th International Conference on Slurry Handling and Pipeline Transport, Johannesburg, 3-5 September.

Slatter, P.T. & Wasp, E.J. 2000. The Laminar/ Turbulent transition in Large pipes. Proceedings of the 10th international Conference on Transport and Sedimentation of Solid Particles, Wroclaw, 4-7 September 2000: 389-399.

Steffe, J. 1996 Rheological Methods in Food Process Engineering. USA: Freeman Press.

Thomas, A. 2000. Relationship between viscometer measurements and laminar and turbulent pipe flow. Proceedings of the 10th International Conference on Transport and Sedimentation of Solid Particles, Wroclaw, 4-7 September 2000. Poland: 13-28.

Thomas, A.D. & Wilson, K.C. 1987. New Analysis of non-Newtonian Turbulent Flow – Yield Power Law Fluids. Canadian Journal of Chemical Engineering, 65:335-338, April 1987.

Thomas, D.G. 1963. Non-Newtonian Suspensions Part 1: Physical properties and laminar transport characteristics. Ind Eng. Chem. 55(11): 18-29.

Thorvaldsen, G. S. 1996. The effect of the particle distribution on non-Newtonian turbulent slurry flow in pipes. Unpublished MTech dissertation, Cape Technikon, Cape Town.

Torrance, B. McK. 1963. Friction Factors for Turbulent non-Newtonian Fluid Flow in Circular pipes. The South African Mechanical Engineer, 13(4): 89-92, November.

Vlasak, P. &Chara, Z. 1999. Laminar and turbulent flow experiments with yield-power law slurries. Powder Technology, 104: 200-206.

Wilson, K. 1986. Modelling the effects of non-Newtonian and time-dependant slurry behaviour. 10th International conference on the Hydraulic transport of Solids in Pipes, Innsbruck, 29-31 October 1986: 283-289. Australia.

Wilson, K.C. & Addie, G. R. 2002. Pipe-flow experiments with a sand-clay mixture. 15th International conference on the Hydraulic transport of Solids in Pipes, Banff. 03-05 June 2002: 577-588.

Wilson, K. & Thomas, A.D. 1985 A new analysis of the turbulent flow of non-Newtonian fluids, Canadian Journal of Chemical Engineering, 63: 539-546.

Wilson, K.C. & Thomas, A.D. 2006. Analytic model of laminar-turbulent transition for Bingham plastics, Canadian Journal of Chemical Engineering, 84(5): 520-526.

Wilson, K.C., Addie, G.R., Sellgren, G.R. & Clift, R. 2006. Slurry transport using centrifugal pumps. 3rd ed. USA: Springer.

Wygnanski, I., Sokolov, M. & Friedman, D. 1975. On transition in a pipe. Part 2: The equilibrium puff. Journal of Fluid Mechanics, 69: 283-304.

Wygnanski, I.J. & Champagne, F.H. 1973. On transition in a pipe. Part 1: The origin of puffs and slugs and the flow in a turbulent slug. Journal of Fluid Mechanics, 59: 281-335.

Xu, J., Gillies, R., Small, M. & Shook, C. 1993. Laminar and turbulent flow of Kaolin Slurries. Proceedings of the 12th International conference on Slurry handling and Transport, Belgium, 28-30 September 1993: 595-613. Hydrotransport 12, BHR Group.

Appendices

Appendix A. Test procedures

Details of the procedures followed for water and slurry tests, as referred to in Chapter 3, are described here.

Material preparation

- Ensure that the system is clean, and free from any insoluble material such as sand and metal.
- Determine the desired concentration of the mixture to be produced.
- Calculate the exact volume of solids (e.g. kaolin powder) and water required to produce the desired volume of slurry.
- Fill the slurry hopper and pipes with 75% of the total volume of water required for the mixture.
- Start the pump and mixer to circulate the water through the pipelines.
- Add the dry material into the system at the top of the slurry hopper.
- While circulating this material through the system, add the remaining water, ensuring that all dry material is rinsed into the hopper.
- Keep circulating the material through the system until the suspension is thoroughly mixed.
- Leave the material to hydrate for 1-2 days (depending on the material type).
- Whilst hydrating, periodically circulate the material through the system to facilitate mixing.
- When the material is properly hydrated testing can begin.

Slurry testing procedure

- Ensure that the pump suction valve is open before the pump motor is started.
- Flush the pressure transducer system (transducers, pipes and traps) to remove all air and/or trapped solid particles, then open the pressure tapping valves.
- Start the test program and input the test parameters.
- Set the pump speed to give the desired flow rate and wait for the flow to stabilise (monitor on the analogue display for the flow meter).
- Once a stable flow rate has been established read the data. Sample sufficient data to ensure satisfactory mean value and standard deviation. Monitor the value to ensure it looks feasible.
- When data for the selected flow rate has been acquired, decrease the flow rate and when stable acquire next set of data.
- Repeat this procedure until sufficient data in all flow regimes have been acquired.
- In the transition region try to decrease the intervals between data points for better definition (identification) of this regime.
- Choose flow rates randomly, and move "up" and "down", monitoring data and equipment at all times.
- Repeat the procedure for all pipe sizes.

Appendix B. Calibration procedures

Calibration procedure for differential pressure transducers

For the calibration of the differential pressure transducers a hand-held pump with a digital manometer was used to apply a pressure difference across the transducer, and the hand-held communicator used to read the resulting pressure values.

Procedure:

- Open the calibration computer program and switch the DAQ to the required channel.
- Set the transducer zero.
- Open each side of the transducer to atmosphere and ensure the diaphragm is dry.
- Connect the Handheld Communicator to the transducers and switch it on.
- Set the transducer to the desired pressure range using the handheld communicator, then set the handheld communicator to data recording mode.
- Read the pressure recorded by the handheld communicator and the voltage recorded by the DAQ. These are the zeros.
- Apply pressure on the high pressure side of the transducer using the handheld pump and record both the pressure and the voltage reading on the handheld communicator and the DAQ, respectively.
- Repeat this procedure, taking about 10 sets of readings and ensuring that the complete range is covered.
- Zero pressure corresponds to 1V and the maximum pressure (set range) to 5V.
- Determine the calibration equation by performing linear regression on the measured pressure and transducer readings.

This calibration equation is then used to determine (from measured voltage) the pressure differential during testing, as seen in Figure B.1.

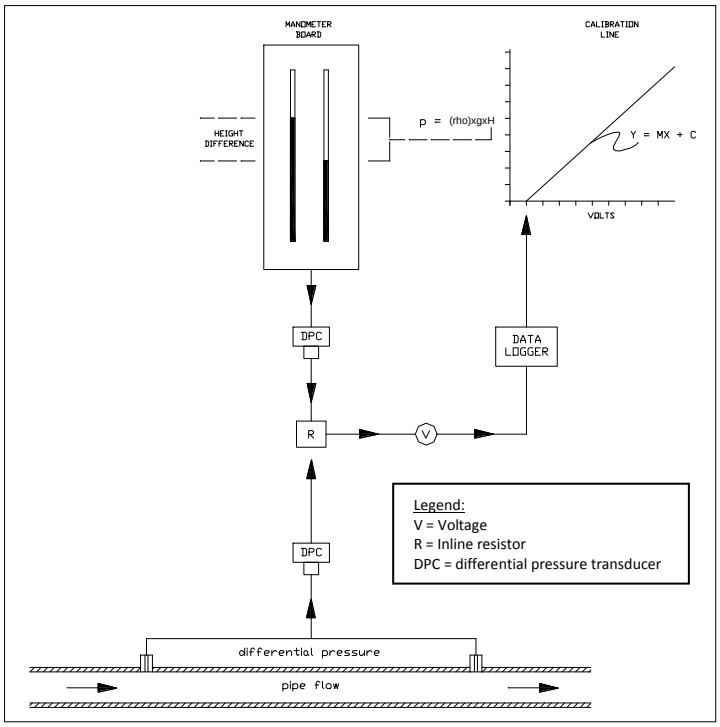

Figure B.1 Schematic diagram of the calibration sequence

Flow meter calibration procedure

Flow meters were calibrated only to verify the manufacturer settings and to check accuracy at the low nominal wall shear rate ($40s^{-1}$). Details of the procedure are described below.

Procedure:

- Open the DAQ program, select the flow meter channel and set the weigh tank sampling rate.
- Pump water through the rig and set the valves to divert the flow through the appropriate flow meter and the weigh tank.
- Close the valve at the bottom of the weigh tank to accumulate water in the tank.
- Start the DAQ program, then stop it when the tank is almost full.
- Record the voltage reading on the DAQ.
- Empty the weigh tank by opening the valve at the bottom of the tank.
- Change the flow rate of water though the rig.
- Repeat step 4 to 7 to record another set of data.
- Repeat the procedure to acquire at least 5 sets of data at differing flow rates.
- The temperature of the water in the hopper is also measured using a thermometer.
- To calculate the flow rate, the following should be considered:
  - Time that registered on the stop watch
  - Temperature as measured by the thermometer
  - Density (ρ) - kg/m^3 @ the temperature measured
  - Volume - mass/ density
  - Flow rate (Q) - Volume/ time
- Repeat the process for ten different flow rate values (calibration points), spread as far across the operating range of flow meters as the system limitations allow.
- Do a linear regression for plot of (voltage) vs. (Q) to yield the calibration constants for the specific pipe.
- This procedure is repeated for all pipe sizes.

Appendix C. Water test results

Water tests were conducted in the straight pipe test sections to establish credibility and accuracy of the testing rigs before tests with non-Newtonian material were conducted. The experimental data for the water pipeline tests were fitted against the Colebrook-White curve. From this analysis the pipe roughness was also obtained. The water test results for all pipe test loops are presented here.

Valve test loop

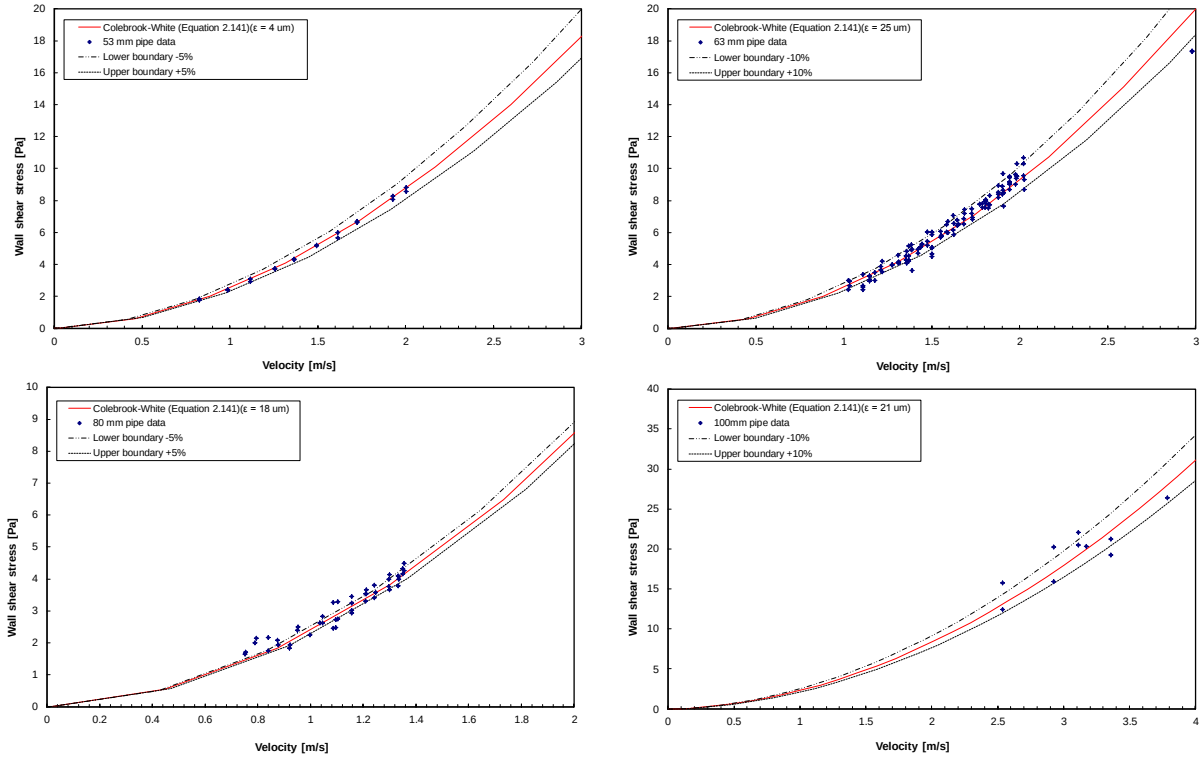

Figure C.1 Experimental results vs. Colebrook-White prediction for diameter 53, 63, 80 and 100mm test pipes on the valve test loop

Flume test loop

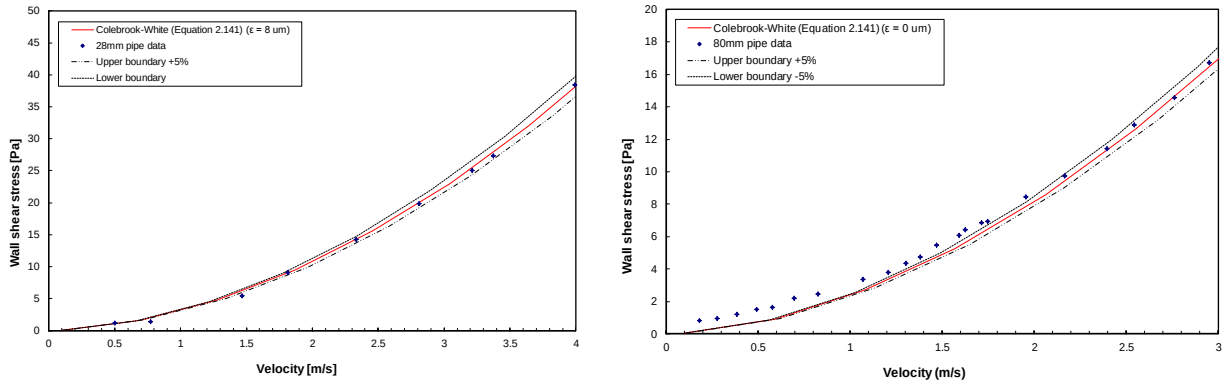

Figure C.2 Experimental results vs. Colebrook-White prediction for diameter 13 and 28mm test pipes on the flume test loop

Large pipes test loop

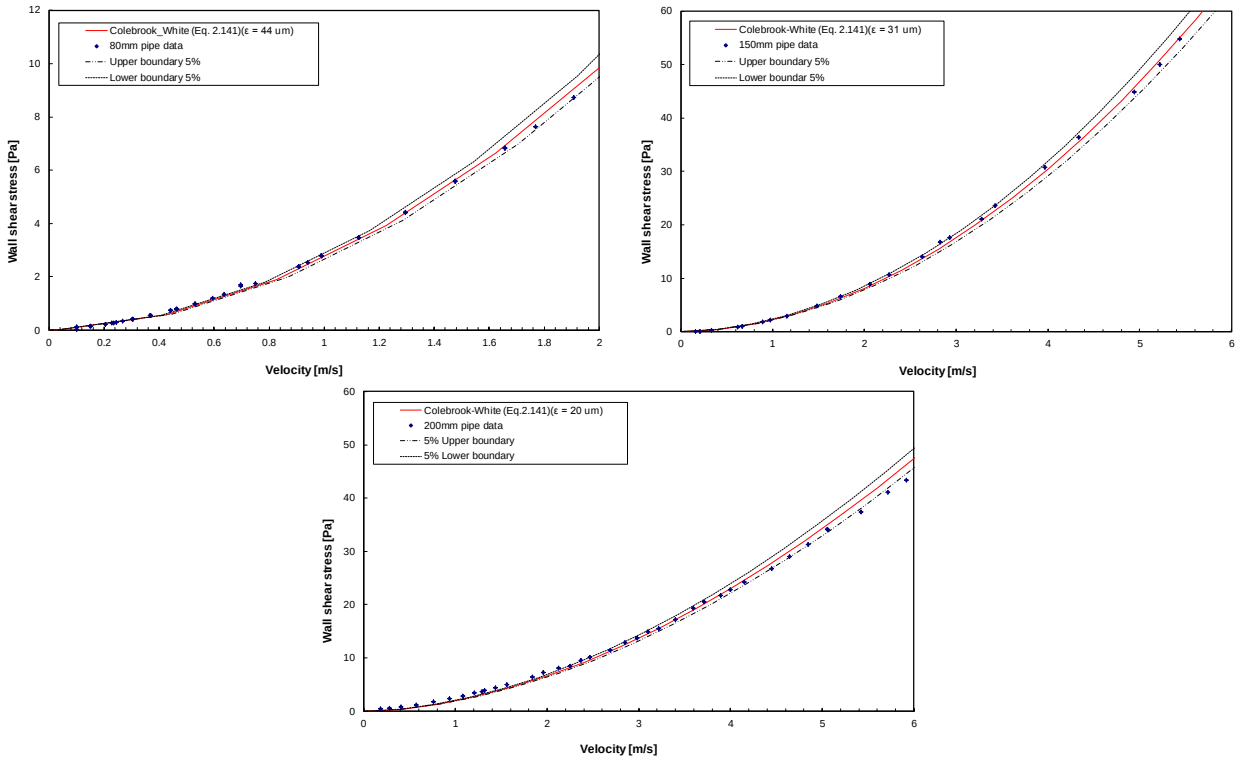

Figure C.3 Experimental results vs. Colebrook-White prediction for diameter 80, 150 and 200mm test pipes on the large pipe test loop

Appendix D. Results for combined experimental error analysis

Flume pipe loop

$$\left(\frac{\Delta\tau_0}{\tau_0}\right)^2 = \left(\frac{\Delta D}{D}\right)^2 + \left(\frac{\Delta(\Delta P)}{\Delta P}\right)^2 + \left(-\frac{\Delta L}{L}\right)^2$$

Ø13mm	ΔP	1000	1325	1650	1975	2300	2625	2950	3275	3600.00	5500	7400	9300	11200	13100	15000.00	17500	20000	22500	25000	27500	30000
	τ_0	3.33	4.41	5.49	6.58	7.66	8.74	9.82	10.90	11.99	18.31	24.64	30.96	37.29	43.62	49.94	58.27	66.59	74.91	83.24	91.56	99.89
$\left(\frac{\Delta\tau_0}{\tau_0}\right)$	%	1.12E-06	1.12E-06	1.12E-06	1.12E-06	1.12E-06	1.12E-06	1.12E-06	1.12E-06	1.12E-06	1.12E-06	1.12E-06	1.12E-06	1.12E-06	1.12E-06	1.12E-06	1.12E-06	1.12E-06	1.12E-06	1.12E-06	1.12E-06	1.12E-06	1.12E-06
		9.00E-04	5.13E-04	3.31E-04	2.31E-04	1.70E-04	1.31E-04	1.03E-04	8.39E-05	6.94E-05	2.98E-05	1.64E-05	1.04E-05	7.17E-06	5.24E-06	4.00E-06	2.94E-06	2.25E-06	1.78E-06	1.44E-06	1.19E-06	1.00E-06
		1.00E-06	1.00E-06	1.00E-06	1.00E-06	1.00E-06	1.00E-06	1.00E-06	1.00E-06	1.00E-06	1.00E-06	1.00E-06	1.00E-06	1.00E-06	1.00E-06	1.00E-06	1.00E-06	1.00E-06	1.00E-06	1.00E-06	1.00E-06	1.00E-06	1.00E-06
		3.004	2.269	1.824	1.526	1.312	1.152	1.027	0.928	0.846	0.565	0.431	0.354	0.305	0.271	0.247	0.225	0.209	0.198	0.189	0.182	0.177
28mm	ΔP	450	844	1238	1631	2025	2419	2813	3206	3600.00	5500	7400	9300	11200	13100	15000.00	17500	20000	22500	25000	27500	30000
	τ_0	3.16	5.93	8.69	11.46	14.23	16.99	19.76	22.53	25.29	38.64	51.99	65.34	78.69	92.04	105.39	122.96	140.53	158.09	175.66	193.22	210.79
$\left(\frac{\Delta\tau_0}{\tau_0}\right)$	%	2.50E-07	2.50E-07	2.50E-07	2.50E-07	2.50E-07	2.50E-07	2.50E-07	2.50E-07	2.50E-07	2.50E-07	2.50E-07	2.50E-07	2.50E-07	2.50E-07	2.50E-07	2.50E-07	2.50E-07	2.50E-07	2.50E-07	2.50E-07	2.50E-07	2.50E-07
		1.78E-04	5.06E-05	2.35E-05	1.35E-05	8.78E-06	6.15E-06	4.55E-06	3.50E-06	2.78E-06	1.19E-06	6.57E-07	4.16E-07	2.87E-07	2.10E-07	1.60E-07	1.18E-07	9.00E-08	7.11E-08	5.76E-08	4.76E-08	4.00E-08
		1.00E-06	1.00E-06	1.00E-06	1.00E-06	1.00E-06	1.00E-06	1.00E-06	1.00E-06	1.00E-06	1.00E-06	1.00E-06	1.00E-06	1.00E-06	1.00E-06	1.00E-06	1.00E-06	1.00E-06	1.00E-06	1.00E-06	1.00E-06	1.00E-06	1.00E-06
		1.338	0.720	0.498	0.384	0.317	0.272	0.241	0.218	0.201	0.156	0.138	0.129	0.124	0.121	0.119	0.117	0.116	0.115	0.114	0.114	0.114
Ø80mm	ΔP	500	498	495	493	490	488	485	483	480.00	733	987	1240	1493	1747	2000.00	2333	2667	3000	3333	3667	4000
	τ_0	10.11	10.06	10.01	9.96	9.91	9.86	9.81	9.76	9.71	14.83	19.95	25.07	30.19	35.32	40.44	47.18	53.92	60.66	67.40	74.14	80.88
$\left(\frac{\Delta\tau_0}{\tau_0}\right)$	%	2.89E-08	2.89E-08	2.89E-08	2.89E-08	2.89E-08	2.89E-08	2.89E-08	2.89E-08	2.89E-08	2.89E-08	2.89E-08	2.89E-08	2.89E-08	2.89E-08	2.89E-08	2.89E-08	2.89E-08	2.89E-08	2.89E-08	2.89E-08	2.89E-08	2.89E-08
		6.40E-05	6.46E-05	6.53E-05	6.60E-05	6.66E-05	6.73E-05	6.80E-05	6.87E-05	6.94E-05	2.98E-05	1.64E-05	1.04E-05	7.17E-06	5.24E-06	4.00E-06	2.94E-06	2.25E-06	1.78E-06	1.44E-06	1.19E-06	1.00E-06
		1.00E-06	1.00E-06	1.00E-06	1.00E-06	1.00E-06	1.00E-06	1.00E-06	1.00E-06	1.00E-06	1.00E-06	1.00E-06	1.00E-06	1.00E-06	1.00E-06	1.00E-06	1.00E-06	1.00E-06	1.00E-06	1.00E-06	1.00E-06	1.00E-06	1.00E-06
		0.806	0.810	0.814	0.818	0.823	0.827	0.831	0.835	0.839	0.555	0.418	0.338	0.286	0.250	0.224	0.199	0.181	0.168	0.157	0.149	0.142

$$\left(\frac{\Delta(8V/D)}{8V/D}\right)^2 = \left(\frac{\Delta G}{G}\right)^2 = \left(\frac{\Delta Q}{Q}\right)^2 + 9*\left(\frac{\Delta D}{D}\right)^2$$

Ø13mm	Q	0.024	0.025	0.026	0.027	0.029	0.030	0.031	0.032	0.033	0.039	0.044	0.050	0.055	0.061	0.066	0.119	0.173	0.226	0.279	0.332	0.385
	V	0.172	0.180	0.188	0.197	0.205	0.213	0.222	0.230	0.238	0.278	0.318	0.357	0.397	0.437	0.476	0.858	1.239	1.620	2.001	2.382	2.763
	$V_{flowmeter}$ = (8V/D)	0.180	0.189	0.198	0.206	0.215	0.224	0.233	0.241	0.250	0.292	0.333	0.375	0.417	0.458	0.500	0.900	1.300	1.700	2.100	2.500	2.900
$\left(\frac{\Delta(8V/D)}{8V/D}\right)$	%	103	108	113	118	123	128	133	138	143	167	191	215	238	262	286	515	744	973	1202	1431	1660
		1.93E-04	1.75E-04	1.60E-04	1.47E-04	1.35E-04	1.25E-04	1.16E-04	1.07E-04	1.00E-04	7.35E-05	5.62E-05	4.44E-05	3.60E-05	2.98E-05	2.50E-05	2.50E-05	2.50E-05	2.50E-05	2.50E-05	2.50E-05	2.50E-05
		1.01E-05	1.01E-05	1.01E-05	1.01E-05	1.01E-05	1.01E-05	1.01E-05	1.01E-05	1.01E-05	1.01E-05	1.01E-05	1.01E-05	1.01E-05	1.01E-05	1.01E-05	1.01E-05	1.01E-05	1.01E-05	1.01E-05	1.01E-05	1.01E-05	1.01E-05
		1.425	1.362	1.305	1.253	1.205	1.162	1.121	1.084	1.049	0.914	0.815	0.739	0.679	0.631	0.593	0.593	0.593	0.593	0.593	0.593	0.593
28mm	Q	1.616	1.711	1.806	1.901	1.996	2.091	2.186	2.281	2.376	2.772	3.168	3.564	3.960	4.356	4.752	13.305	21.858	30.411	38.964	47.517	56.070
	V	2.604	2.757	2.911	3.064	3.217	3.370	3.523	3.676	3.830	4.468	5.106	5.744	6.383	7.021	7.659	21.446	35.233	49.019	62.806	76.593	90.380
	$V_{flowmeter}$ = (8V/D)	0.170	0.180	0.190	0.200	0.210	0.220	0.230	0.240	0.250	0.292	0.333	0.375	0.417	0.458	0.500	1.400	2.300	3.200	4.100	5.000	5.900
$\left(\frac{\Delta(8V/D)}{8V/D}\right)$	%	741	785	828	872	916	959	1003	1046	1090	1272	1453	1635	1817	1999	2180	6105	10029	13953	17878	21802	25726
		2.16E-04	1.93E-04	1.73E-04	1.56E-04	1.42E-04	1.29E-04	1.18E-04	1.09E-04	1.00E-04	7.35E-05	5.63E-05	4.44E-05	3.60E-05	2.98E-05	2.50E-05	2.50E-05	2.50E-05	2.50E-05	2.50E-05	2.50E-05	2.50E-05
		2.25E-06	2.25E-06	2.25E-06	2.25E-06	2.25E-06	2.25E-06	2.25E-06	2.25E-06	2.25E-06	2.25E-06	2.25E-06	2.25E-06	2.25E-06	2.25E-06	2.25E-06	2.25E-06	2.25E-06	2.25E-06	2.25E-06	2.25E-06	2.25E-06	2.25E-06
		1.478	1.397	1.324	1.259	1.200	1.146	1.097	1.052	1.011	0.870	0.765	0.683	0.618	0.566	0.522	0.522	0.522	0.522	0.522	0.522	0.522
Ø80mm	Q	0.322	0.439	0.555	0.672	0.789	0.906	1.023	1.140	1.257	1.466	1.676	1.885	2.094	2.304	2.513	4.775	7.037	9.299	11.561	13.823	16.085
	V	0.063	0.085	0.108	0.131	0.154	0.176	0.199	0.222	0.245	0.285	0.326	0.367	0.408	0.448	0.489	0.929	1.370	1.810	2.250	2.691	3.131
	$V_{flowmeter}$ = (8V/D)	0.064	0.087	0.111	0.134	0.157	0.180	0.204	0.227	0.250	0.292	0.333	0.375	0.417	0.458	0.500	0.950	1.400	1.850	2.300	2.750	3.200
$\left(\frac{\Delta(8V/D)}{8V/D}\right)$	%	6	8	11	13	15	17	20	22	24	28	32	36	40	44	48	92	135	179	223	266	310
		1.53E-03	8.21E-04	5.12E-04	3.49E-04	2.54E-04	1.92E-04	1.51E-04	1.22E-04	1.00E-04	7.35E-05	5.63E-05	4.44E-05	3.60E-05	2.98E-05	2.50E-05	2.50E-05	2.50E-05	2.50E-05	2.50E-05	2.50E-05	2.50E-05
		2.60E-07	2.60E-07	2.60E-07	2.60E-07	2.60E-07	2.60E-07	2.60E-07	2.60E-07	2.60E-07	2.60E-07	2.60E-07	2.60E-07	2.60E-07	2.60E-07	2.60E-07	2.60E-07	2.60E-07	2.60E-07	2.60E-07	2.60E-07	2.60E-07	2.60E-07
		3.907	2.866	2.263	1.870	1.593	1.388	1.230	1.104	1.001	0.859	0.752	0.669	0.602	0.548	0.503	0.503	0.503	0.503	0.503	0.503	0.503

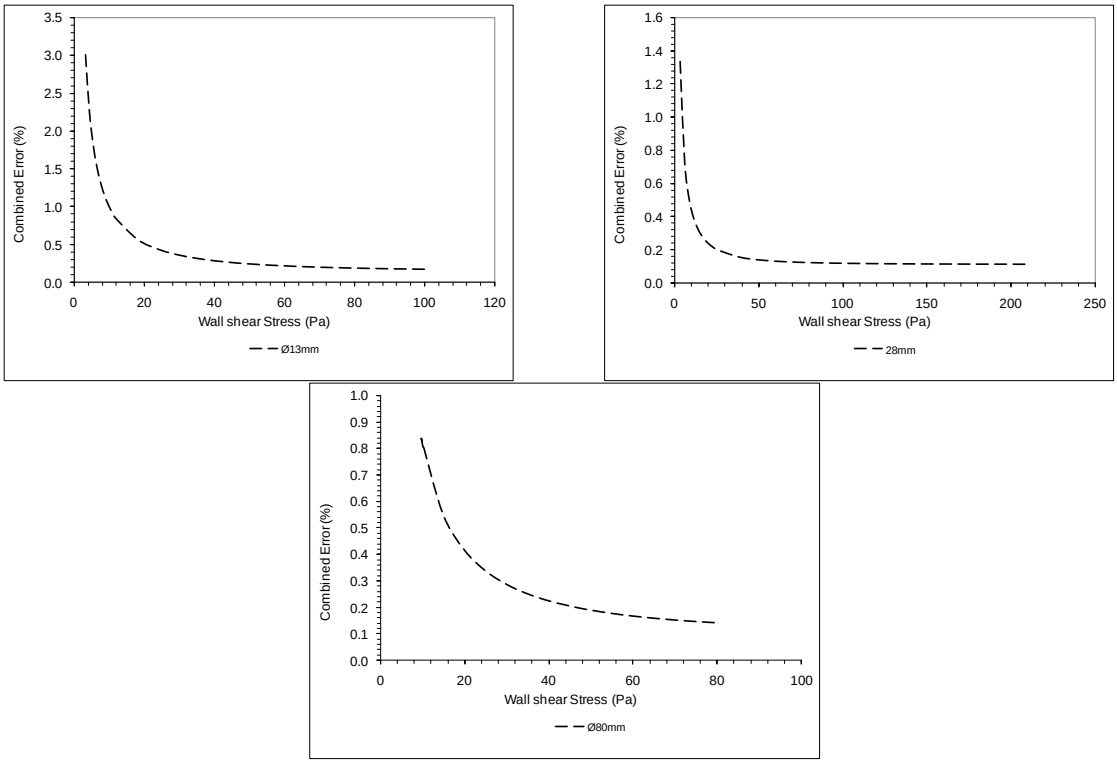

Figure D.1 Combined errors in wall shear stress for diameter 13, 28 and 80mm pipe data on the flume test loop

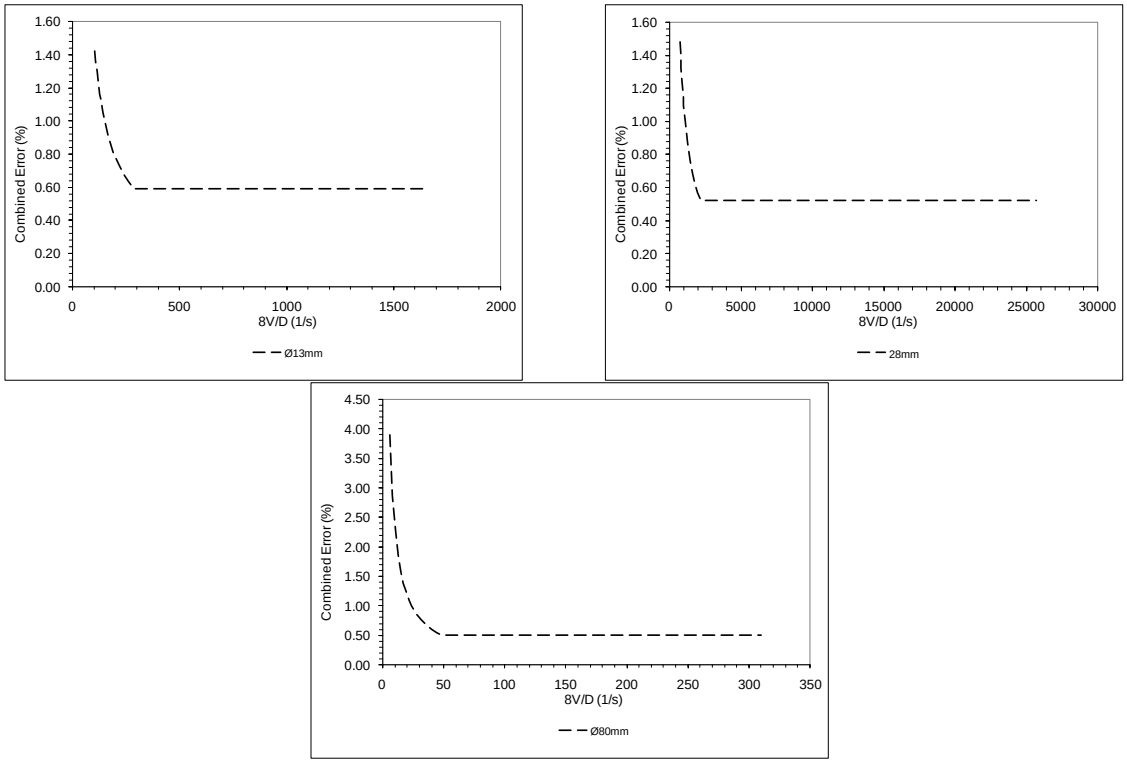

Figure D.2 Combined errors in nominal wall shear rate (*8V/D*) for diameter 13, 28 and 80mm pipe data on the flume test loop

Valve test loop

$$\left(\frac{\Delta\tau_0}{\tau_0}\right)^2 = \left(\frac{\Delta D}{D}\right)^2 + \left(\frac{\Delta(\Delta P)}{\Delta P}\right)^2 + \left(-\frac{\Delta L}{L}\right)^2$$

Ø42mm																			
	ΔP	300	353	405	458	510	563	615	668	720.00	1100	1480	1860	2240	2620	3000.00	3500	4000	4500	5000	5500	6000
	τ_0	5.02	5.90	6.78	7.66	8.54	9.42	10.30	11.17	12.05	18.41	24.78	31.14	37.50	43.86	50.22	58.59	66.96	75.33	83.70	92.07	100.45
$\left(\frac{\Delta\tau_0}{\tau_0}\right)$		3.97E-05	3.97E-05	3.97E-05	3.97E-05	3.97E-05	3.97E-05	3.97E-05	3.97E-05	3.97E-05	3.97E-05	3.97E-05	3.97E-05	3.97E-05	3.97E-05	3.97E-05	3.97E-05	3.97E-05	3.97E-05	3.97E-05	3.97E-05	3.97E-05
	%	4.00E-04	2.90E-04	2.19E-04	1.72E-04	1.38E-04	1.14E-04	9.52E-05	8.08E-05	6.94E-05	2.98E-05	1.64E-05	1.04E-05	7.17E-06	5.24E-06	4.00E-06	2.94E-06	2.25E-06	1.78E-06	1.44E-06	1.19E-06	1.00E-06
		2.53E-06	2.53E-06	2.53E-06	2.53E-06	2.53E-06	2.53E-06	2.53E-06	2.53E-06	2.53E-06	2.53E-06	2.53E-06	2.53E-06	2.53E-06	2.53E-06	2.53E-06	2.53E-06	2.53E-06	2.53E-06	2.53E-06	2.53E-06	2.53E-06
		2.103	1.822	1.618	1.464	1.344	1.249	1.172	1.109	1.057	0.848	0.766	0.725	0.703	0.689	0.680	0.672	0.667	0.663	0.661	0.659	0.657
Ø52mm																						
	ΔP	450	621	793	964	1136	1307	1479	1650	1821.71	2783	3745	4706	5668	6629	7590.46	7325	7060	6795	6530	6265	6000
	τ_0	2.98	4.11	5.25	6.38	7.52	8.65	9.78	10.92	12.05	18.41	24.78	31.14	37.50	43.86	50.22	48.47	46.71	44.96	43.21	41.45	39.70
$\left(\frac{\Delta\tau_0}{\tau_0}\right)$		1.02E-05	1.02E-05	1.02E-05	1.02E-05	1.02E-05	1.02E-05	1.02E-05	1.02E-05	1.02E-05	1.02E-05	1.02E-05	1.02E-05	1.02E-05	1.02E-05	1.02E-05	1.02E-05	1.02E-05	1.02E-05	1.02E-05	1.02E-05	1.02E-05
	%	1.78E-04	9.32E-05	5.73E-05	3.87E-05	2.79E-05	2.11E-05	1.65E-05	1.32E-05	1.08E-05	4.65E-06	2.57E-06	1.63E-06	1.12E-06	8.19E-07	6.23E-07	7.22E-07	7.80E-07	8.44E-07	9.17E-07	1.00E-06	1.00E-06
		2.51E-07	2.51E-07	2.51E-07	2.51E-07	2.51E-07	2.51E-07	2.51E-07	2.51E-07	2.51E-07	2.51E-07	2.51E-07	2.51E-07	2.51E-07	2.51E-07	2.51E-07	2.51E-07	2.51E-07	2.51E-07	2.51E-07	2.51E-07	2.51E-07
		1.372	1.018	0.823	0.701	0.620	0.562	0.519	0.487	0.462	0.389	0.361	0.348	0.341	0.336	0.333	0.334	0.335	0.336	0.337	0.338	0.339
Ø63mm																						
	ΔP	400	440	480	520	560	600	640	680	720.00	1100	1480	1860	2240	2620	3000.00	3500	4000	4500	5000	5500	6000
	τ_0	3.23	3.56	3.88	4.20	4.53	4.85	5.17	5.50	5.82	8.89	11.97	15.04	18.11	21.18	24.26	28.30	32.34	36.38	40.43	44.47	48.51
$\left(\frac{\Delta\tau_0}{\tau_0}\right)$		2.03E-05	2.03E-05	2.03E-05	2.03E-05	2.03E-05	2.03E-05	2.03E-05	2.03E-05	2.03E-05	2.03E-05	2.03E-05	2.03E-05	2.03E-05	2.03E-05	2.03E-05	2.03E-05	2.03E-05	2.03E-05	2.03E-05	2.03E-05	2.03E-05
	%	2.25E-04	1.86E-04	1.56E-04	1.33E-04	1.15E-04	1.00E-04	8.79E-05	7.79E-05	6.94E-05	2.98E-05	1.64E-05	1.04E-05	7.17E-06	5.24E-06	4.00E-06	2.94E-06	2.25E-06	1.78E-06	1.44E-06	1.19E-06	1.00E-06
		2.63E-07	2.63E-07	2.63E-07	2.63E-07	2.63E-07	2.63E-07	2.63E-07	2.63E-07	2.63E-07	2.63E-07	2.63E-07	2.63E-07	2.63E-07	2.63E-07	2.63E-07	2.63E-07	2.63E-07	2.63E-07	2.63E-07	2.63E-07	2.63E-07
		1.567	1.437	1.330	1.240	1.163	1.098	1.041	0.992	0.948	0.709	0.608	0.556	0.526	0.508	0.495	0.484	0.477	0.472	0.469	0.466	0.464
Ø80mm																						
	ΔP	400	393	387	380	374	367	361	354	347.99	532	715	899	1083	1266	1449.95	2208	2967	3725	4483	5242	6000
	τ_0	6.69	6.58	6.47	6.37	6.26	6.15	6.04	5.93	5.82	8.89	11.97	15.04	18.11	21.18	24.26	36.94	49.63	62.31	75.00	87.68	100.37
$\left(\frac{\Delta\tau_0}{\tau_0}\right)$		4.84E-06	4.84E-06	4.84E-06	4.84E-06	4.84E-06	4.84E-06	4.84E-06	4.84E-06	4.84E-06	4.84E-06	4.84E-06	4.84E-06	4.84E-06	4.84E-06	4.84E-06	4.84E-06	4.84E-06	4.84E-06	4.84E-06	4.84E-06	4.84E-06
	%	2.25E-04	2.32E-04	2.40E-04	2.49E-04	2.57E-04	2.67E-04	2.76E-04	2.86E-04	2.97E-04	1.27E-04	7.04E-05	4.45E-05	3.07E-05	2.25E-05	1.71E-05	7.38E-06	4.09E-06	2.59E-06	1.79E-06	1.31E-06	1.00E-06
		6.92E-07	6.92E-07	6.92E-07	6.92E-07	6.92E-07	6.92E-07	6.92E-07	6.92E-07	6.92E-07	6.92E-07	6.92E-07	6.92E-07	6.92E-07	6.92E-07	6.92E-07	6.92E-07	6.92E-07	6.92E-07	6.92E-07	6.92E-07	6.92E-07
		1.518	1.543	1.568	1.594	1.621	1.650	1.679	1.709	1.740	1.153	0.871	0.708	0.602	0.529	0.476	0.359	0.310	0.285	0.271	0.262	0.256
Ø100mm																						
	ΔP	400	407	414	421	428	435	442	449	456.00	697	937	1178	1419	1659	1900.00	2217	2533	2850	3167	3483	3800
	τ_0	6.45	6.56	6.68	6.79	6.90	7.02	7.13	7.24	7.36	11.24	15.12	19.00	22.88	26.76	30.65	35.75	40.86	45.97	51.08	56.19	61.29
$\left(\frac{\Delta\tau_0}{\tau_0}\right)$		1.37E-05	1.37E-05	1.37E-05	1.37E-05	1.37E-05	1.37E-05	1.37E-05	1.37E-05	1.37E-05	1.37E-05	1.37E-05	1.37E-05	1.37E-05	1.37E-05	1.37E-05	1.37E-05	1.37E-05	1.37E-05	1.37E-05	1.37E-05	1.37E-05
	%	2.25E-04	2.17E-04	2.10E-04	2.03E-04	1.97E-04	1.90E-04	1.84E-04	1.79E-04	1.73E-04	7.42E-05	4.10E-05	2.59E-05	1.79E-05	1.31E-05	9.97E-06	7.33E-06	5.61E-06	4.43E-06	3.59E-06	2.97E-06	2.49E-06
		4.41E-07	4.41E-07	4.41E-07	4.41E-07	4.41E-07	4.41E-07	4.41E-07	4.41E-07	4.41E-07	4.41E-07	4.41E-07	4.41E-07	4.41E-07	4.41E-07	4.41E-07	4.41E-07	4.41E-07	4.41E-07	4.41E-07	4.41E-07	4.41E-07
		1.546	1.521	1.497	1.474	1.451	1.430	1.409	1.388	1.368	0.940	0.742	0.633	0.566	0.522	0.491	0.463	0.444	0.431	0.421	0.413	0.408
Ø150mm																						
	ΔP	900	885	870	856	841	826	811	797	781.80	1194	1607	2020	2432	2845	3257.50	3715	4172	4629	5086	5543	6000
	τ_0	8.47	8.33	8.19	8.05	7.91	7.77	7.63	7.49	7.36	11.24	15.12	19.00	22.88	26.76	30.65	34.95	39.25	43.55	47.85	52.15	56.45
$\left(\frac{\Delta\tau_0}{\tau_0}\right)$		2.89E-06	2.89E-06	2.89E-06	2.89E-06	2.89E-06	2.89E-06	2.89E-06	2.89E-06	2.89E-06	2.89E-06	2.89E-06	2.89E-06	2.89E-06	2.89E-06	2.89E-06	2.89E-06	2.89E-06	2.89E-06	2.89E-06	2.89E-06	2.89E-06
	%	4.44E-05	4.59E-05	4.75E-05	4.92E-05	5.09E-05	5.27E-05	5.47E-05	5.67E-05	5.89E-05	2.52E-05	1.39E-05	8.83E-06	6.09E-06	4.45E-06	3.39E-06	2.61E-06	2.07E-06	1.68E-06	1.39E-06	1.17E-06	1.00E-06
		6.24E-08	6.24E-08	6.24E-08	6.24E-08	6.24E-08	6.24E-08	6.24E-08	6.24E-08	6.24E-08	6.24E-08	6.24E-08	6.24E-08	6.24E-08	6.24E-08	6.24E-08	6.24E-08	6.24E-08	6.24E-08	6.24E-08	6.24E-08	6.24E-08
		0.688	0.699	0.710	0.722	0.734	0.746	0.759	0.773	0.786	0.531	0.411	0.343	0.301	0.272	0.252	0.236	0.224	0.215	0.208	0.203	0.199

$$\left(\frac{\Delta(8V/D)}{8V/D}\right)^2 = \left(\frac{\Delta G}{G}\right)^2 = \left(\frac{\Delta Q}{Q}\right)^2 + 9*\left(\frac{\Delta D}{D}\right)^2$$

Ø63mm																				
Q		1.616	1.711	1.806	1.901	1.996	2.091	2.186	2.281	2.376	2.772	3.168	3.564	3.960	4.356	4.752	15.997	27.243	38.488	49.734	60.980	72.225
V		0.517	0.547	0.578	0.608	0.639	0.669	0.699	0.730	0.760	0.887	1.014	1.140	1.267	1.394	1.520	5.119	8.717	12.316	15.914	19.512	23.111
$V_{flowmeter}$ =		0.170	0.180	0.190	0.200	0.210	0.220	0.230	0.240	0.250	0.292	0.333	0.375	0.417	0.458	0.500	1.683	2.867	4.050	5.233	6.417	7.600
(8V/D)		66	69	73	77	81	85	89	93	96	112	129	145	161	177	193	649	1106	1562	2018	2475	2931
$\left(\frac{\Delta(8V/D)}{8V/D}\right)$		2.16E-04	1.93E-04	1.73E-04	1.56E-04	1.42E-04	1.29E-04	1.18E-04	1.09E-04	1.00E-04	7.35E-05	5.63E-05	4.44E-05	3.60E-05	2.98E-05	2.50E-05	2.50E-05	2.50E-05	2.50E-05	2.50E-05	2.50E-05	2.50E-05
	%	1.82E-04	1.82E-04	1.82E-04	1.82E-04	1.82E-04	1.82E-04	1.82E-04	1.82E-04	1.82E-04	1.82E-04	1.82E-04	1.82E-04	1.82E-04	1.82E-04	1.82E-04	1.82E-04	1.82E-04	1.82E-04	1.82E-04	1.82E-04	1.82E-04
		1.996	1.937	1.885	1.840	1.800	1.765	1.733	1.705	1.680	1.599	1.544	1.506	1.477	1.456	1.440	1.440	1.440	1.440	1.440	1.440	1.440
Ø80mm																				
Q		1.616	1.711	1.806	1.901	1.996	2.091	2.186	2.281	2.376	2.772	3.168	3.564	3.960	4.356	4.752	15.997	27.243	38.488	49.734	60.980	72.225
V		0.318	0.337	0.355	0.374	0.393	0.412	0.430	0.449	0.468	0.546	0.623	0.701	0.779	0.857	0.935	3.149	5.362	7.575	9.789	12.002	14.216
$V_{flowmeter}$ =		0.170	0.180	0.190	0.200	0.210	0.220	0.230	0.240	0.250	0.292	0.333	0.375	0.417	0.458	0.500	1.683	2.867	4.050	5.233	6.417	7.600
(8V/D)		31.628	33.488	35.349	37.209	39.070	40.930	42.791	44.651	46.512	54.264	62.015	69.767	77.519	85.271	93.023	313.178	533.333	753.488	973.643	1193.797	1413.952
$\left(\frac{\Delta(8V/D)}{8V/D}\right)$		2.16E-04	1.93E-04	1.73E-04	1.56E-04	1.42E-04	1.29E-04	1.18E-04	1.09E-04	1.00E-04	7.35E-05	5.63E-05	4.44E-05	3.60E-05	2.98E-05	2.50E-05	2.50E-05	2.50E-05	2.50E-05	2.50E-05	2.50E-05	2.50E-05
	%	4.36E-05	4.36E-05	4.36E-05	4.36E-05	4.36E-05	4.36E-05	4.36E-05	4.36E-05	4.36E-05	4.36E-05	4.36E-05	4.36E-05	4.36E-05	4.36E-05	4.36E-05	4.36E-05	4.36E-05	4.36E-05	4.36E-05	4.36E-05	4.36E-05
		1.612	1.538	1.472	1.414	1.361	1.314	1.272	1.233	1.198	1.082	0.999	0.938	0.892	0.856	0.828	0.828	0.828	0.828	0.828	0.828	0.828

Ø42mm																				
Q		0.039	0.096	0.152	0.209	0.265	0.322	0.378	0.434	0.491	0.573	0.654	0.736	0.818	0.900	0.982	1.914	2.847	3.780	4.712	5.645	6.578
V		0.028	0.069	0.109	0.150	0.190	0.231	0.271	0.312	0.352	0.411	0.470	0.528	0.587	0.646	0.705	1.374	2.043	2.713	3.382	4.051	4.721
$V_{flowmeter}$ =		0.020	0.049	0.078	0.106	0.135	0.164	0.193	0.221	0.250	0.292	0.333	0.375	0.417	0.458	0.500	0.975	1.450	1.925	2.400	2.875	3.350
(8V/D)		5	13	21	28	36	44	52	59	67	78	89	100	112	123	134	261	388	515	642	769	897
$\left(\frac{\Delta(8V/D)}{8V/D}\right)$		1.56E-02	2.63E-03	1.04E-03	5.54E-04	3.43E-04	2.33E-04	1.69E-04	1.28E-04	1.00E-04	7.35E-05	5.63E-05	4.44E-05	3.60E-05	2.98E-05	2.50E-05	2.50E-05	2.50E-05	2.50E-05	2.50E-05	2.50E-05	2.50E-05
	%	3.57E-04	3.57E-04	3.57E-04	3.57E-04	3.57E-04	3.57E-04	3.57E-04	3.57E-04	3.57E-04	3.57E-04	3.57E-04	3.57E-04	3.57E-04	3.57E-04	3.57E-04	3.57E-04	3.57E-04	3.57E-04	3.57E-04	3.57E-04	3.57E-04
		12.642	5.465	3.739	3.018	2.646	2.430	2.293	2.202	2.138	2.075	2.033	2.004	1.983	1.967	1.955	1.955	1.955	1.955	1.955	1.955	1.955
Ø52mm																				
Q		0.039	0.096	0.152	0.209	0.265	0.322	0.378	0.434	0.491	0.573	0.654	0.736	0.818	0.900	0.982	1.914	2.847	3.780	4.712	5.645	6.578
V		0.018	0.044	0.069	0.095	0.121	0.147	0.173	0.198	0.224	0.262	0.299	0.336	0.374	0.411	0.448	0.874	1.300	1.726	2.152	2.578	3.004
$V_{flowmeter}$ =		0.020	0.049	0.078	0.106	0.135	0.164	0.193	0.221	0.250	0.292	0.333	0.375	0.417	0.458	0.500	0.975	1.450	1.925	2.400	2.875	3.350
(8V/D)		2.717	6.624	10.530	14.436	18.343	22.249	26.155	30.062	33.968	39.629	45.290	50.952	56.613	62.274	67.936	132.475	197.014	261.553	326.091	390.630	455.169
$\left(\frac{\Delta(8V/D)}{8V/D}\right)$		1.56E-02	2.63E-03	1.04E-03	5.54E-04	3.43E-04	2.33E-04	1.69E-04	1.28E-04	1.00E-04	7.35E-05	5.63E-05	4.44E-05	3.60E-05	2.98E-05	2.50E-05	2.50E-05	2.50E-05	2.50E-05	2.50E-05	2.50E-05	2.50E-05
	%	9.22E-05	9.22E-05	9.22E-05	9.22E-05	9.22E-05	9.22E-05	9.22E-05	9.22E-05	9.22E-05	9.22E-05	9.22E-05	9.22E-05	9.22E-05	9.22E-05	9.22E-05	9.22E-05	9.22E-05	9.22E-05	9.22E-05	9.22E-05	9.22E-05
		12.537	5.217	3.366	2.541	2.086	1.803	1.615	1.483	1.386	1.287	1.218	1.169	1.132	1.104	1.082	1.082	1.082	1.082	1.082	1.082	1.082

Ø100mm																				
Q		1.616	1.711	1.806	1.901	1.996	2.091	2.186	2.281	2.376	2.772	3.168	3.564	3.960	4.356	4.752	13.305	21.858	30.411	38.964	47.517	56.070
V		0.218	0.231	0.243	0.256	0.269	0.282	0.295	0.308	0.320	0.374	0.427	0.481	0.534	0.587	0.641	1.794	2.947	4.101	5.254	6.408	7.561
$V_{flowmeter}$ =		0.170	0.180	0.190	0.200	0.210	0.220	0.230	0.240	0.250	0.292	0.333	0.375	0.417	0.458	0.500	1.400	2.300	3.200	4.100	5.000	5.900
(8V/D)		18	19	20	21	22	23	24	25	26	31	35	40	44	48	53	148	243	338	433	528	622
$\left(\frac{\Delta(8V/D)}{8V/D}\right)$		2.16E-04	1.93E-04	1.73E-04	1.56E-04	1.42E-04	1.29E-04	1.18E-04	1.09E-04	1.00E-04	7.35E-05	5.63E-05	4.44E-05	3.60E-05	2.98E-05	2.50E-05	2.50E-05	2.50E-05	2.50E-05	2.50E-05	2.50E-05	2.50E-05
	%	1.23E-04	1.23E-04	1.23E-04	1.23E-04	1.23E-04	1.23E-04	1.23E-04	1.23E-04	1.23E-04	1.23E-04	1.23E-04	1.23E-04	1.23E-04	1.23E-04	1.23E-04	1.23E-04	1.23E-04	1.23E-04	1.23E-04	1.23E-04	1.23E-04
		1.842	1.778	1.721	1.672	1.628	1.589	1.554	1.522	1.494	1.402	1.340	1.295	1.262	1.237	1.217	1.217	1.217	1.217	1.217	1.217	1.217
Ø150mm																				
Q		1.616	1.711	1.806	1.901	1.996	2.091	2.186	2.281	2.376	2.772	3.168	3.564	3.960	4.356	4.752	13.305	21.858	30.411	38.964	47.517	56.070
V		0.091	0.096	0.101	0.107	0.112	0.117	0.123	0.128	0.133	0.156	0.178	0.200	0.222	0.245	0.267	0.747	1.227	1.707	2.187	2.668	3.148
$V_{flowmeter}$ =		0.170	0.180	0.190	0.200	0.210	0.220	0.230	0.240	0.250	0.292	0.333	0.375	0.417	0.458	0.500	1.400	2.300	3.200	4.100	5.000	5.900
(8V/D)		4.818	5.101	5.385	5.668	5.951	6.235	6.518	6.802	7.085	8.266	9.447	10.628	11.808	12.989	14.170	39.676	65.182	90.688	116.194	141.700	167.206
$\left(\frac{\Delta(8V/D)}{8V/D}\right)$		2.16E-04	1.93E-04	1.73E-04	1.56E-04	1.42E-04	1.29E-04	1.18E-04	1.09E-04	1.00E-04	7.35E-05	5.63E-05	4.44E-05	3.60E-05	2.98E-05	2.50E-05	2.50E-05	2.50E-05	2.50E-05	2.50E-05	2.50E-05	2.50E-05
	%	2.60E-05	2.60E-05	2.60E-05	2.60E-05	2.60E-05	2.60E-05	2.60E-05	2.60E-05	2.60E-05	2.60E-05	2.60E-05	2.60E-05	2.60E-05	2.60E-05	2.60E-05	2.60E-05	2.60E-05	2.60E-05	2.60E-05	2.60E-05	2.60E-05
		1.557	1.480	1.411	1.350	1.295	1.246	1.201	1.160	1.123	0.997	0.907	0.839	0.787	0.747	0.714	0.714	0.714	0.714	0.714	0.714	0.714

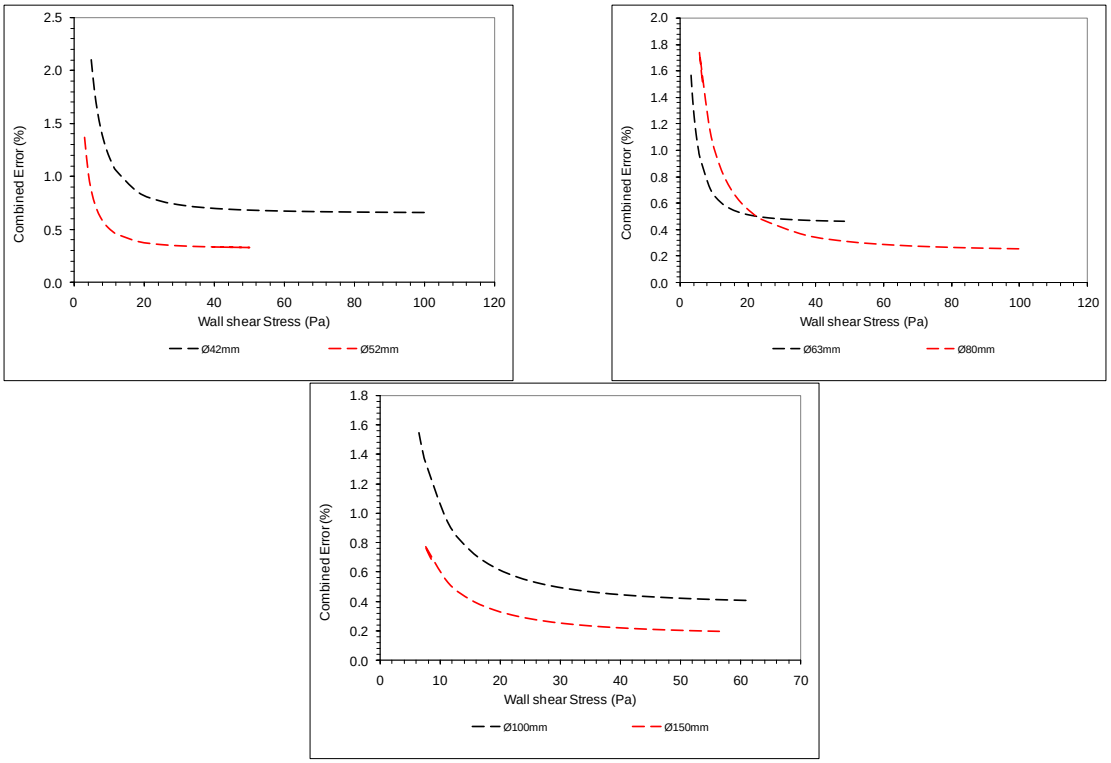

Figure D.3 Combined errors in wall shear stress for diameter 42, 52, 63, 80, 100 and 150mm pipe data on the valve test loop

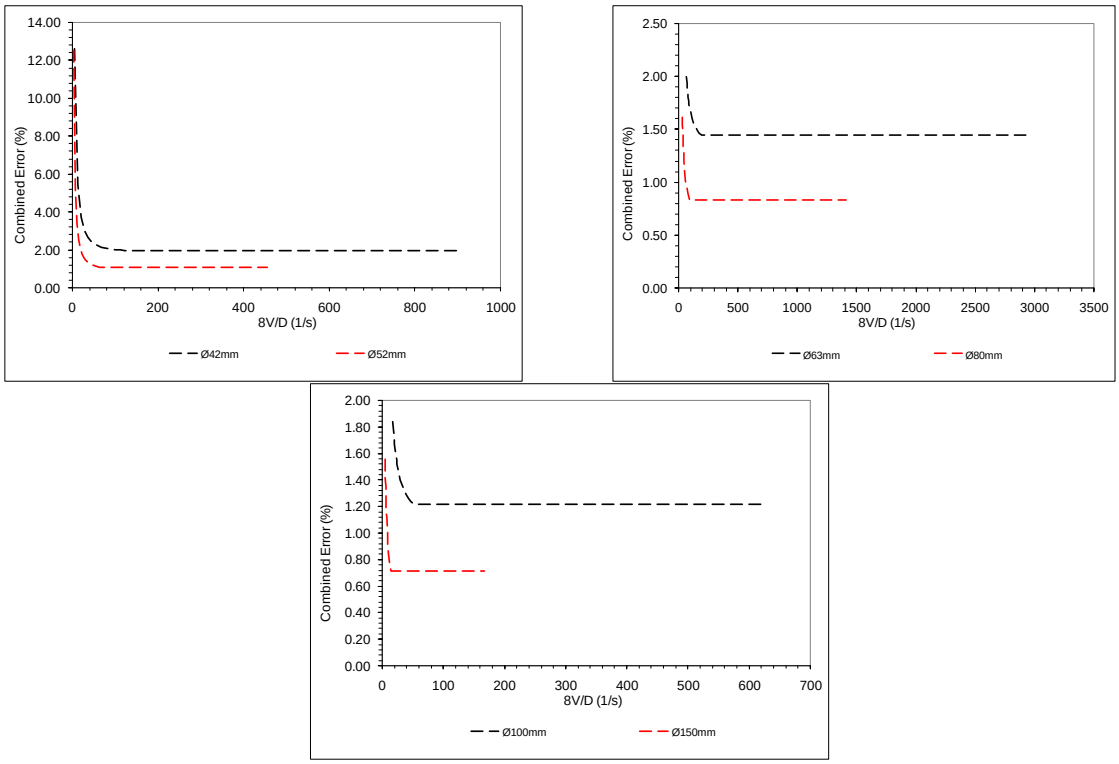

Figure D.4 Combined errors in nominal wall shear rate (*8V/D*) for diameter 42, 52, 63, 80, 100 and 150mm pipe data on the valve test loop

Large pipes test loop

$$\left(\frac{\Delta\tau_0}{\tau_0}\right)^2 = \left(\frac{\Delta D}{D}\right)^2 + \left(\frac{\Delta(\Delta P)}{\Delta P}\right)^2 + \left(-\frac{\Delta L}{L}\right)^2$$

Ø60mm																					
ΔP	1500	1763	2025	2288	2550	2813	3075	3338	3600.00	5500	7400	9300	11200	13100	15000.00	17500	20000	22500	25000	27500	30000
τ_0	7.21	8.47	9.73	11.00	12.26	13.52	14.78	16.04	17.30	26.44	35.57	44.70	53.83	62.97	72.10	84.12	96.13	108.15	120.17	132.18	144.20
	5.29E-06	5.29E-06	5.29E-06	5.29E-06	5.29E-06	5.29E-06	5.29E-06	5.29E-06	5.29E-06	5.29E-06	5.29E-06	5.29E-06	5.29E-06	5.29E-06	5.29E-06	5.29E-06	5.29E-06	5.29E-06	5.29E-06	5.29E-06	5.29E-06
$\left(\frac{\Delta\tau_0}{\tau_0}\right)$	4.00E-04	2.90E-04	2.19E-04	1.72E-04	1.38E-04	1.14E-04	9.52E-05	8.08E-05	6.94E-05	2.98E-05	1.64E-05	1.04E-05	7.17E-06	5.24E-06	4.00E-06	2.94E-06	2.25E-06	1.78E-06	1.44E-06	1.19E-06	1.00E-06
%	1.11E-07	1.11E-07	1.11E-07	1.11E-07	1.11E-07	1.11E-07	1.11E-07	1.11E-07	1.11E-07	1.11E-07	1.11E-07	1.11E-07	1.11E-07	1.11E-07	1.11E-07	1.11E-07	1.11E-07	1.11E-07	1.11E-07	1.11E-07	1.11E-07
	2.013	1.718	1.500	1.332	1.199	1.092	1.003	0.928	0.865	0.593	0.467	0.398	0.355	0.326	0.307	0.289	0.277	0.268	0.262	0.257	0.253
Ø80mm																					
ΔP	888	1043	1199	1354	1509	1665	1820	1976	2131.03	3256	4380	5505	6630	7755	8879.31	10359	11839	13319	14798	16278	17758
τ_0	7.21	8.47	9.73	11.00	12.26	13.52	14.78	16.04	17.30	26.44	35.57	44.70	53.83	62.97	72.10	84.12	96.13	108.15	120.16	132.18	144.19
	9.61E-06	9.61E-06	9.61E-06	9.61E-06	9.61E-06	9.61E-06	9.61E-06	9.61E-06	9.61E-06	9.61E-06	9.61E-06	9.61E-06	9.61E-06	9.61E-06	9.61E-06	9.61E-06	9.61E-06	9.61E-06	9.61E-06	9.61E-06	9.61E-06
$\left(\frac{\Delta\tau_0}{\tau_0}\right)$	4.00E-04	2.90E-04	2.19E-04	1.72E-04	1.38E-04	1.14E-04	9.52E-05	8.08E-05	6.94E-05	2.97E-05	1.64E-05	1.04E-05	7.17E-06	5.24E-06	4.00E-06	2.94E-06	2.25E-06	1.78E-06	1.44E-06	1.19E-06	1.00E-06
%	1.60E-07	1.60E-07	1.60E-07	1.60E-07	1.60E-07	1.60E-07	1.60E-07	1.60E-07	1.60E-07	1.60E-07	1.60E-07	1.60E-07	1.60E-07	1.60E-07	1.60E-07	1.60E-07	1.60E-07	1.60E-07	1.60E-07	1.60E-07	1.60E-07
	2.024	1.731	1.514	1.348	1.217	1.111	1.024	0.952	0.890	0.629	0.512	0.449	0.412	0.387	0.371	0.356	0.347	0.340	0.335	0.331	0.328
Ø150mm																					
ΔP	350	756	1163	1569	1975	2381	2788	3194	3600.00	5500	7400	9300	11200	13100	15000.00	17500	20000	22500	25000	27500	30000
τ_0	3.29	7.11	10.94	14.76	18.58	22.40	26.22	30.05	33.87	51.74	69.62	87.49	105.37	123.24	141.12	164.64	188.16	211.68	235.19	258.71	282.23
	2.89E-06	2.89E-06	2.89E-06	2.89E-06	2.89E-06	2.89E-06	2.89E-06	2.89E-06	2.89E-06	2.89E-06	2.89E-06	2.89E-06	2.89E-06	2.89E-06	2.89E-06	2.89E-06	2.89E-06	2.89E-06	2.89E-06	2.89E-06	2.89E-06
$\left(\frac{\Delta\tau_0}{\tau_0}\right)$	7.35E-03	1.57E-03	6.66E-04	3.66E-04	2.31E-04	1.59E-04	1.16E-04	8.82E-05	6.94E-05	2.98E-05	1.64E-05	1.04E-05	7.17E-06	5.24E-06	4.00E-06	2.94E-06	2.25E-06	1.78E-06	1.44E-06	1.19E-06	1.00E-06
%	6.24E-08	6.24E-08	6.24E-08	6.24E-08	6.24E-08	6.24E-08	6.24E-08	6.24E-08	6.24E-08	6.24E-08	6.24E-08	6.24E-08	6.24E-08	6.24E-08	6.24E-08	6.24E-08	6.24E-08	6.24E-08	6.24E-08	6.24E-08	6.24E-08
	8.573	3.971	2.586	1.920	1.529	1.272	1.090	0.955	0.851	0.572	0.440	0.365	0.318	0.286	0.264	0.243	0.228	0.217	0.210	0.204	0.199
Ø200mm																					
ΔP	313	676	1039	1402	1765	2128	2491	2854	3216.66	4914	6612	8310	10007	11705	13402.77	15636	17870	20104	22338	24571	26805
τ_0	3.29	7.11	10.94	14.76	18.58	22.40	26.22	30.05	33.87	51.74	69.62	87.49	105.37	123.24	141.12	164.64	188.15	211.67	235.19	258.71	282.23
	1.42E-06	1.42E-06	1.42E-06	1.42E-06	1.42E-06	1.42E-06	1.42E-06	1.42E-06	1.42E-06	1.42E-06	1.42E-06	1.42E-06	1.42E-06	1.42E-06	1.42E-06	1.42E-06	1.42E-06	1.42E-06	1.42E-06	1.42E-06	1.42E-06
$\left(\frac{\Delta\tau_0}{\tau_0}\right)$	7.35E-03	1.57E-03	6.66E-04	3.66E-04	2.31E-04	1.59E-04	1.16E-04	8.82E-05	6.94E-05	2.98E-05	1.64E-05	1.04E-05	7.17E-06	5.24E-06	4.00E-06	2.94E-06	2.25E-06	1.78E-06	1.44E-06	1.19E-06	1.00E-06
%	3.98E-08	3.98E-08	3.98E-08	3.98E-08	3.98E-08	3.98E-08	3.98E-08	3.98E-08	3.98E-08	3.98E-08	3.98E-08	3.98E-08	3.98E-08	3.98E-08	3.98E-08	3.98E-08	3.98E-08	3.98E-08	3.98E-08	3.98E-08	3.98E-08
	8.572	3.969	2.583	1.916	1.524	1.266	1.083	0.947	0.842	0.559	0.423	0.344	0.294	0.259	0.234	0.210	0.193	0.180	0.170	0.163	0.157

$$\left(\frac{\Delta(8V/D)}{8V/D}\right)^2 = \left(\frac{\Delta G}{G}\right)^2 = \left(\frac{\Delta Q}{Q}\right)^2 + 9*\left(\frac{\Delta D}{D}\right)^2$$

Ø60mm																					
Q	0.603	0.685	0.767	0.848	0.930	1.012	1.093	1.175	1.257	1.466	1.676	1.885	2.094	2.304	2.513	6.953	11.394	15.834	20.274	24.714	29.154
V	0.231	0.262	0.293	0.325	0.356	0.387	0.418	0.450	0.481	0.561	0.641	0.721	0.802	0.882	0.962	2.661	4.360	6.060	7.759	9.458	11.157
$V_{flowmeter}$ =	0.120	0.136	0.153	0.169	0.185	0.201	0.218	0.234	0.250	0.292	0.333	0.375	0.417	0.458	0.500	1.383	2.267	3.150	4.033	4.917	5.800
(8V/D)	32	36	41	45	49	54	58	62	67	78	89	100	111	122	133	369	605	840	1076	1312	1547
	4.34E-04	3.37E-04	2.69E-04	2.19E-04	1.83E-04	1.54E-04	1.32E-04	1.14E-04	1.00E-04	7.35E-05	5.63E-05	4.44E-05	3.60E-05	2.98E-05	2.50E-05	2.50E-05	2.50E-05	2.50E-05	2.50E-05	2.50E-05	2.50E-05
$\left(\frac{\Delta(8V/D)}{8V/D}\right)$	4.76E-05	4.76E-05	4.76E-05	4.76E-05	4.76E-05	4.76E-05	4.76E-05	4.76E-05	4.76E-05	4.76E-05	4.76E-05	4.76E-05	4.76E-05	4.76E-05	4.76E-05	4.76E-05	4.76E-05	4.76E-05	4.76E-05	4.76E-05	4.76E-05
%	2.195	1.960	1.779	1.634	1.517	1.421	1.341	1.273	1.215	1.100	1.019	0.959	0.914	0.880	0.852	0.852	0.852	0.852	0.852	0.852	0.852
Ø80mm																					
Q	0.603	0.685	0.767	0.848	0.930	1.012	1.093	1.175	1.257	1.466	1.676	1.885	2.094	2.304	2.513	6.953	11.394	15.834	20.274	24.714	29.154
V	0.116	0.132	0.148	0.164	0.180	0.195	0.211	0.227	0.243	0.283	0.324	0.364	0.404	0.445	0.485	1.343	2.200	3.058	3.915	4.772	5.630
$V_{flowmeter}$ =	0.120	0.136	0.153	0.169	0.185	0.201	0.218	0.234	0.250	0.292	0.333	0.375	0.417	0.458	0.500	1.383	2.267	3.150	4.033	4.917	5.800
(8V/D)	11.476	13.030	14.584	16.138	17.692	19.246	20.800	22.354	23.908	27.893	31.877	35.862	39.847	43.831	47.816	132.291	216.765	301.240	385.715	470.189	554.664
	4.34E-04	3.37E-04	2.69E-04	2.19E-04	1.83E-04	1.54E-04	1.32E-04	1.14E-04	1.00E-04	7.35E-05	5.63E-05	4.44E-05	3.60E-05	2.98E-05	2.50E-05	2.50E-05	2.50E-05	2.50E-05	2.50E-05	2.50E-05	2.50E-05
$\left(\frac{\Delta(8V/D)}{8V/D}\right)$	8.65E-05	8.65E-05	8.65E-05	8.65E-05	8.65E-05	8.65E-05	8.65E-05	8.65E-05	8.65E-05	8.65E-05	8.65E-05	8.65E-05	8.65E-05	8.65E-05	8.65E-05	8.65E-05	8.65E-05	8.65E-05	8.65E-05	8.65E-05	8.65E-05
%	2.281	2.057	1.885	1.749	1.640	1.552	1.479	1.417	1.366	1.265	1.195	1.144	1.107	1.078	1.056	1.056	1.056	1.056	1.056	1.056	1.056
Ø150mm																					
Q	3.358	3.490	3.623	3.755	3.888	4.020	4.153	4.285	4.418	5.154	5.890	6.627	7.363	8.099	8.836	31.514	54.192	76.871	99.549	122.228	144.906
V	0.188	0.196	0.203	0.211	0.218	0.226	0.233	0.241	0.248	0.289	0.331	0.372	0.413	0.455	0.496	1.769	3.042	4.315	5.589	6.862	8.135
$V_{flowmeter}$ =	0.190	0.198	0.205	0.213	0.220	0.228	0.235	0.243	0.250	0.292	0.333	0.375	0.417	0.458	0.500	1.783	3.067	4.350	5.633	6.917	8.200
(8V/D)	10	10	11	11	12	12	12	13	13	15	18	20	22	24	26	94	162	229	297	364	432
	1.73E-04	1.60E-04	1.49E-04	1.38E-04	1.29E-04	1.21E-04	1.13E-04	1.06E-04	1.00E-04	7.35E-05	5.63E-05	4.44E-05	3.60E-05	2.98E-05	2.50E-05	2.50E-05	2.50E-05	2.50E-05	2.50E-05	2.50E-05	2.50E-05
$\left(\frac{\Delta(8V/D)}{8V/D}\right)$	2.60E-05	2.60E-05	2.60E-05	2.60E-05	2.60E-05	2.60E-05	2.60E-05	2.60E-05	2.60E-05	2.60E-05	2.60E-05	2.60E-05	2.60E-05	2.60E-05	2.60E-05	2.60E-05	2.60E-05	2.60E-05	2.60E-05	2.60E-05	2.60E-05
	1.411	1.365	1.322	1.282	1.246	1.211	1.180	1.150	1.123	0.997	0.907	0.839	0.787	0.747	0.714	0.714	0.714	0.714	0.714	0.714	0.714
Ø200mm																					
Q	3.358	3.490	3.623	3.755	3.888	4.020	4.153	4.285	4.418	5.154	5.890	6.627	7.363	8.099	8.836	31.514	54.192	76.871	99.549	122.228	144.906
V	0.096	0.100	0.104	0.107	0.111	0.115	0.119	0.123	0.126	0.147	0.168	0.190	0.211	0.232	0.253	0.901	1.550	2.198	2.847	3.496	4.144
$V_{flowmeter}$ =	0.190	0.198	0.205	0.213	0.220	0.228	0.235	0.243	0.250	0.292	0.333	0.375	0.417	0.458	0.500	1.783	3.067	4.350	5.633	6.917	8.200
(8V/D)	3.641	3.784	3.928	4.072	4.215	4.359	4.503	4.647	4.790	5.589	6.387	7.185	7.984	8.782	9.581	34.171	58.761	83.352	107.942	132.532	157.123
	1.73E-04	1.60E-04	1.49E-04	1.38E-04	1.29E-04	1.21E-04	1.13E-04	1.06E-04	1.00E-04	7.35E-05	5.63E-05	4.44E-05	3.60E-05	2.98E-05	2.50E-05	2.50E-05	2.50E-05	2.50E-05	2.50E-05	2.50E-05	2.50E-05
$\left(\frac{\Delta(8V/D)}{8V/D}\right)$	1.27E-05	1.27E-05	1.27E-05	1.27E-05	1.27E-05	1.27E-05	1.27E-05	1.27E-05	1.27E-05	1.27E-05	1.27E-05	1.27E-05	1.27E-05	1.27E-05	1.27E-05	1.27E-05	1.27E-05	1.27E-05	1.27E-05	1.27E-05	1.27E-05
	1.363	1.315	1.271	1.229	1.191	1.155	1.122	1.091	1.062	0.929	0.831	0.756	0.698	0.652	0.614	0.614	0.614	0.614	0.614	0.614	0.614

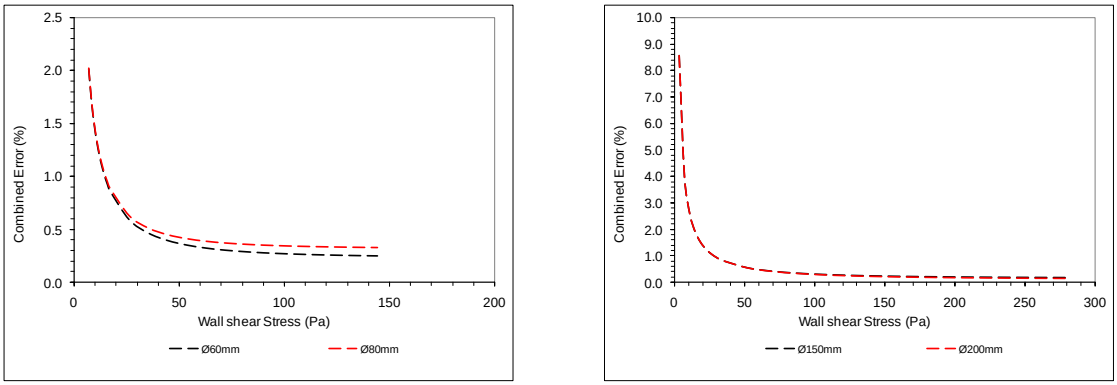

Figure D.5 Combined errors in wall shear stress for diameter 60, 80, 150 and 200mm pipe data on the large pipes test loop

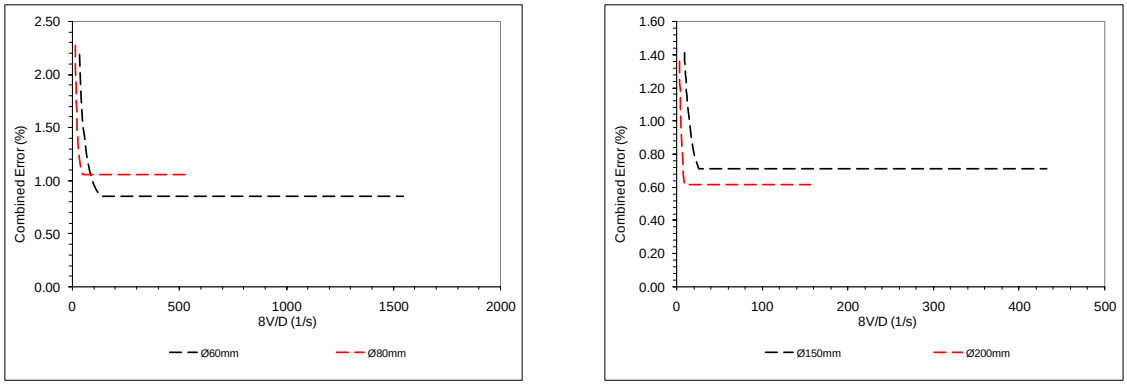

Figure D.6 Combined errors in nominal wall shear rate (*8V/D*) for diameter 60, 80, 150 and 200mm pipe data on the large pipes test loop

Appendix E. Transitional prediction results & analysis: kaolin

The results for the transitional velocity predictions of 10% and 15% kaolin are presented here.

10% kaolin

One technique plotted for all rheologies

Slatter

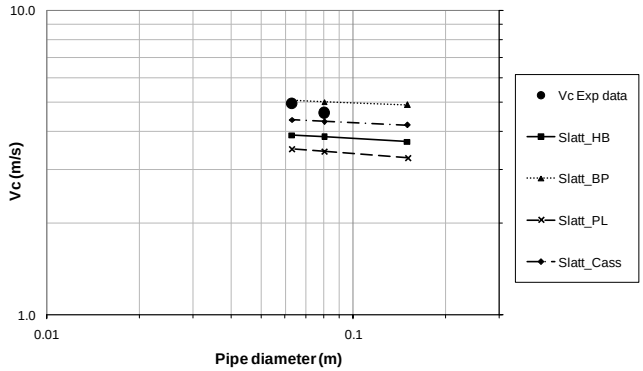

Diameter	Critical velocity (Exp) m/s	Vc Error values - SLATTER Re3 HB m/s	BP m/s	PL m/s	CASS m/s
150mm		3.701	4.885	3.270	4.189
80mm	4.593	3.832	4.998	3.436	4.307
		-16.6%	8.8%	-25.2%	-6.2%
63mm	4.930	3.890	5.063	3.503	4.366
		-21.1%	2.7%	-28.9%	-11.4%
	Ave	-18.8%	5.8%	-27.1%	-8.8%

Figure E.1 Transitional velocity and average % error for 10% kaolin using the Slatter technique – all rheologies

Metzner & Reed

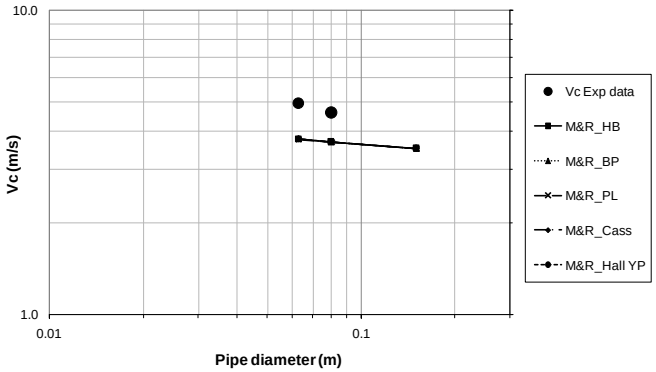

Diameter	Critical velocity (Exp) m/s	Vc Error values - M&R HB m/s	BP m/s	PL m/s	CASS m/s	HAL_YP m/s
150mm		3.509	3.501	3.510	3.506	3.509
80mm	4.593	3.686	3.680	3.689	3.683	3.685
		-19.7%	-19.9%	-19.7%	-19.8%	-19.8%
63mm	4.930	3.763	3.776	3.761	3.767	3.763
		-23.7%	-23.4%	-23.7%	-23.6%	-23.7%
	Ave	-21.7%	-21.6%	-21.7%	-21.7%	-21.7%

Figure E.2 Transitional velocity and average % error for 10% kaolin using the Metzner & Reed technique – all rheologies

Generalised Reynolds number

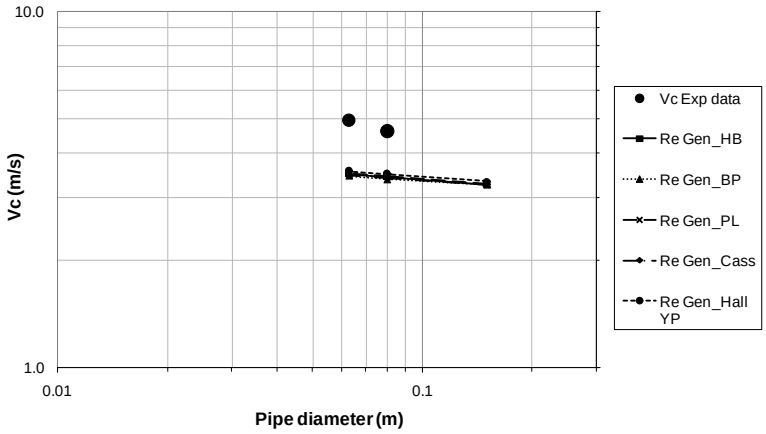

Diameter	Critical velocity (Exp) m/s	Vc Error values - Generalised Re				
		HB m/s	BP m/s	PL m/s	CASS m/s	HAL_YP m/s
150mm		3.264	3.253	3.270	3.258	3.336
80mm	4.593	3.420	3.370	3.436	3.399	3.489
		-25.5%	-26.6%	-25.2%	-26.0%	-24.0%
63mm	4.930	3.488	3.442	3.503	3.469	3.557
		-29.2%	-30.2%	-28.9%	-29.6%	-27.8%
	Ave	-27.4%	-28.4%	-27.1%	-27.8%	-25.9%

Figure E.3 Transitional velocity and average % error for 10% kaolin using the generalised Reynolds number approach – all rheologies

Hedström intersection method

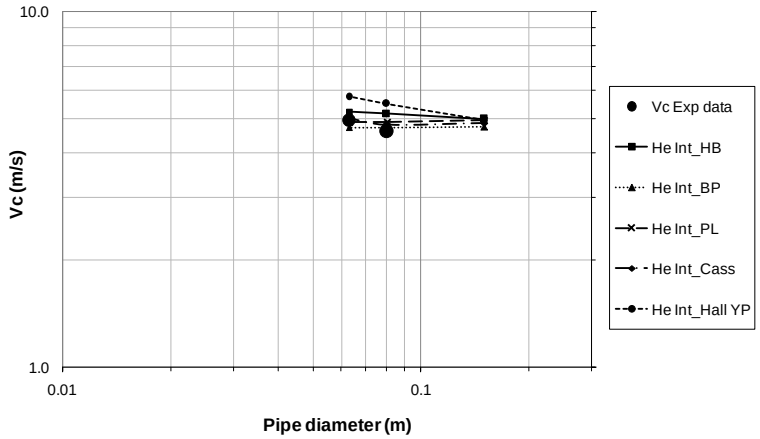

Diameter	Critical velocity (Exp) m/s	Vc Error values - He Intersection				
		HB m/s	BP m/s	PL m/s	CASS m/s	HAL_YP m/s
150mm		4.978	4.732	4.948	4.841	4.929
80mm	4.593	5.146	4.712	4.895	4.804	5.502
		12.0%	2.6%	6.6%	4.6%	19.8%
63mm	4.930	5.221	4.713	4.874	5.017	5.748
		5.9%	-4.4%	-1.1%	1.8%	16.6%
	Ave	9.0%	3.5%	3.8%	3.2%	18.2%

Figure E.4 Transitional velocity and average % error for 10% kaolin using Hedström intersection method – all rheologies

Ryan & Johnson criterion

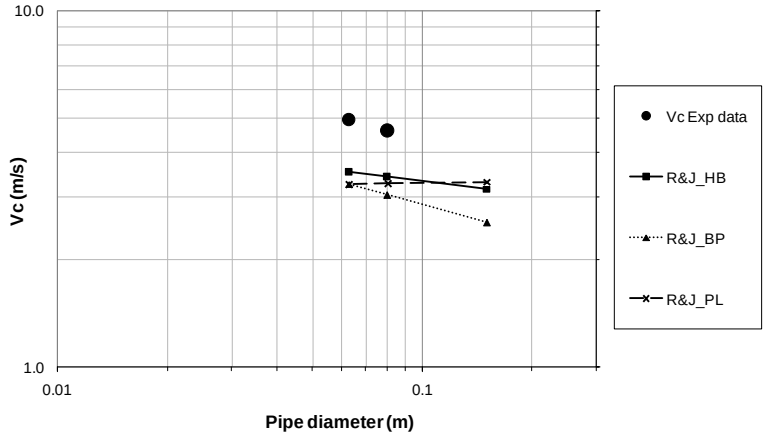

Diameter	Critical velocity (Exp) m/s	Vc Error values - R&J HB m/s	BP m/s	PL m/s
150mm		3.152	2.540	3.302
80mm	4.593	3.412	3.037	3.266
		-25.7%	-33.9%	-28.9%
63mm	4.930	3.519	3.255	3.252
		-28.6%	-34.0%	-34.0%
	Ave	-27.2%	-33.9%	-31.5%

Figure E.5 Transitional velocity and average % error for 10% kaolin using the Ryan & Johnson criterion – all rheologies

Newtonian Approximation

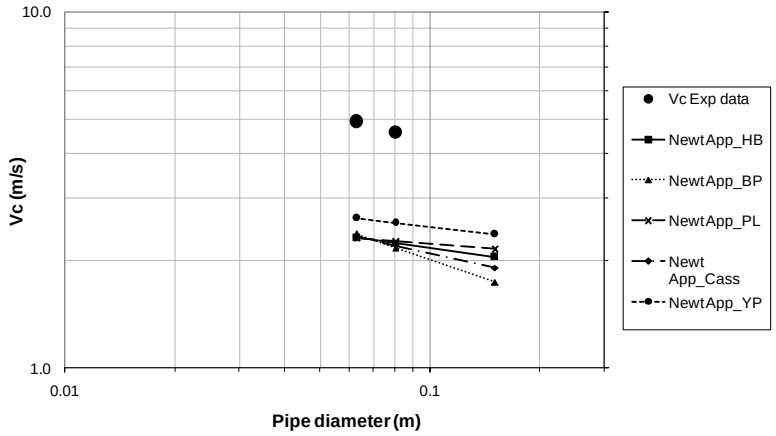

Diameter	Critical velocity (Exp) m/s	Vc Error values - Newt Approx HB m/s	BP m/s	PL m/s	CASS m/s	HAL_YP m/s
150mm		2.051	1.741	2.162	1.911	2.376
80mm	4.593	2.243	2.175	2.272	2.208	2.554
		-51.2%	-52.6%	-50.5%	-51.9%	-44.4%
63mm	4.930	2.323	2.376	2.316	2.339	2.632
		-52.9%	-51.8%	-53.0%	-52.5%	-46.6%
	Ave	-52.0%	-0.4%	1.2%	-52.2%	-45.5%

Figure E.6 Transitional velocity and average % error for 10% kaolin using the Newtonian Approximation approach – all rheologies

Torrance

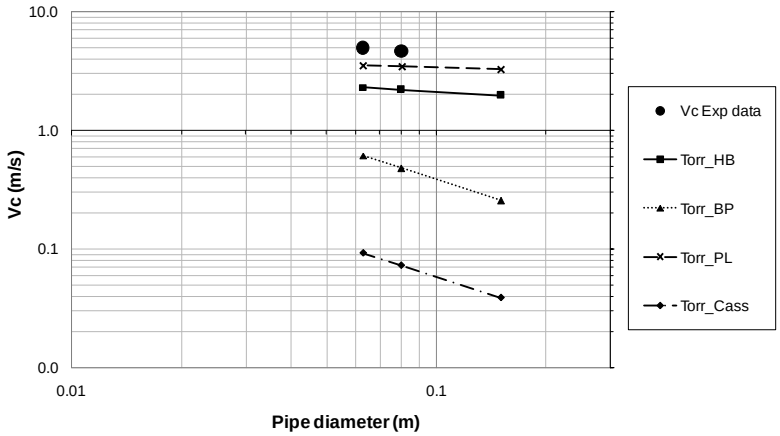

Diameter	Critical velocity (Exp) m/s	Vc Error values - Torrance HB m/s	BP m/s	PL m/s	CASS m/s
150mm		1.951	0.255	3.270	0.039
80mm	4.593	2.191	0.478	3.436	0.072
		-52.3%	-89.6%	-25.2%	-98.4%
63mm	4.930	2.292	0.609	3.503	0.092
		-53.5%	-87.6%	-28.9%	-98.1%
	Ave	-52.9%	-1.0%	1.9%	-98.3%

Figure E.7 Transitional velocity and average % error for 10% kaolin using the Torrance criterion – all rheologies

Hallbom

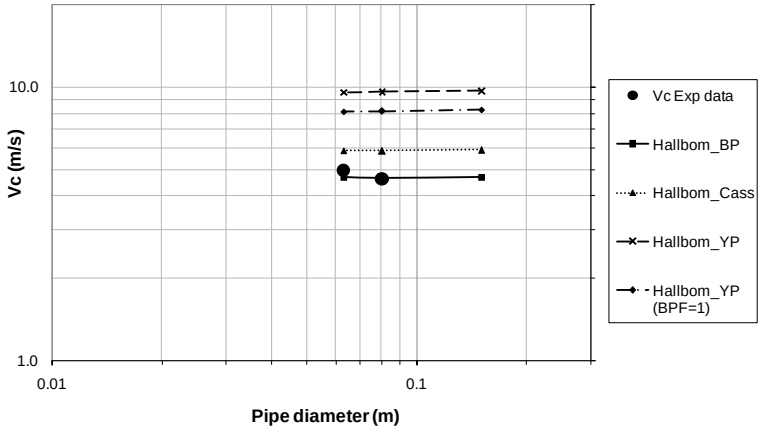

Diameter	Critical velocity (Exp) m/s	Vc Error values - Hallbom Trans HB m/s	BP m/s	PL m/s	CASS m/s	HAL_YP m/s	HAL_YP (BPF=1) m/s
150mm			4.682		5.884	9.675	8.242
80mm	4.593		4.655		5.839	9.585	8.146
			1.3%		27.1%	108.7%	77.4%
63mm	4.930		4.682		5.847	9.568	8.127
			-5.0%		18.6%	94.1%	64.9%
	Ave		-1.8%		22.9%	101.4%	71.1%

Figure E.8 Transitional velocity and average % error for 10% kaolin using the Hallbom criterion – all rheologies

One rheology plotted for all techniques

Herschel-Bulkley

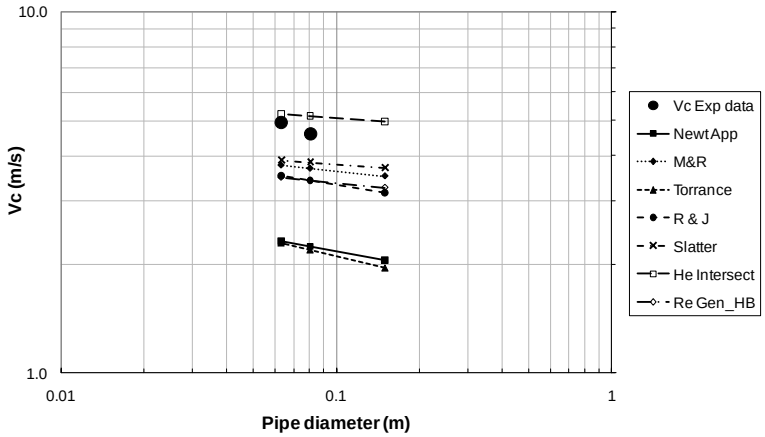

Diameter	Critical velocity (Exp) m/s	Critical velocity Error values - HB - All Techniques						
		Newt App m/s	M & R m/s	Torr/ Clapp m/s	Ryan & John m/s	Slatter m/s	Intersect m/s	Re_Gen m/s
150mm		2.051	3.509	1.951	3.152	3.701	4.978	3.264
80mm	4.593	2.243	3.686	2.191	3.412	3.832	5.146	3.420
		-51.2%	-19.7%	-52.3%	-25.7%	-16.6%	12.0%	-25.5%
63mm	4.930	2.323	3.763	2.292	3.519	3.890	5.221	3.488
		-52.9%	-23.7%	-53.5%	-28.6%	-21.1%	5.9%	-29.2%
	Ave	-52.0%	-21.7%	-52.9%	-27.2%	-18.8%	9.0%	-27.4%

Figure E.9 Transitional velocity and average % error for 10% kaolin (Herschel-Bulkley rheology – all techniques)

Bingham plastic

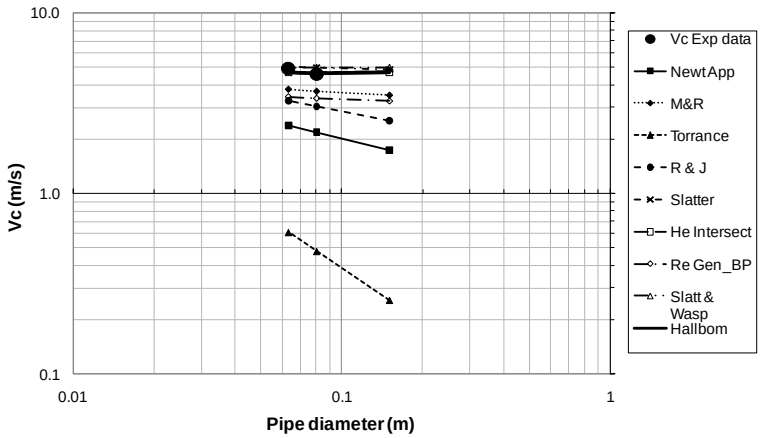

Diameter	Vc (Exp) m/s	Critical velocity Error values - BP - All Techniques						
		Newt App m/s	M & R m/s	Torr/ Clapp m/s	Ryan & John m/s	Slatter m/s	Intersect m/s	Re_Gen m/s
150mm	0.000	1.741	3.501	0.255	2.540	4.885	4.732	3.253
80mm	4.593	2.175	3.680	0.478	3.037	4.998	4.712	3.370
		-52.6%	-19.9%	-89.6%	-33.9%	8.8%	2.6%	-26.6%
63mm	4.930	2.376	3.776	0.609	3.255	5.063	4.713	3.442
		-51.8%	-23.4%	-87.6%	-34.0%	2.7%	-4.4%	-30.2%
	Ave	-52.2%	-21.6%	-88.6%	-33.9%	5.8%	3.5%	-28.4%

Figure E.10 Transitional velocity and average % error for 10% kaolin (Bingham plastic rheology – all techniques)

15% kaolin

One technique plotted for all rheologies

Slatter

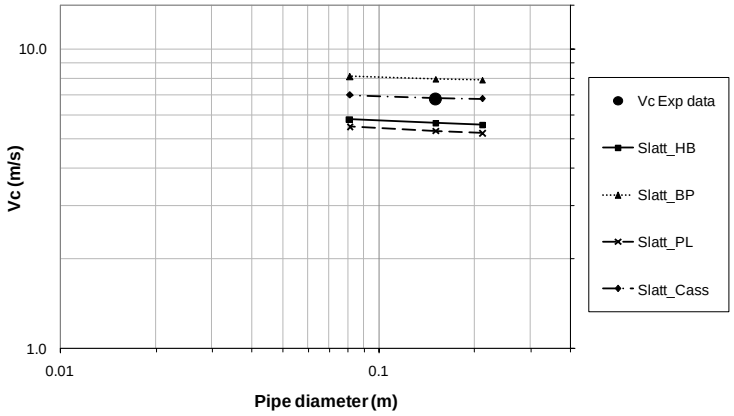

Diameter	Critical velocity (Exp) m/s	Vc Error values - SLATTER Re3 HB m/s	BP m/s	PL m/s	CASS m/s
200mm		5.582	7.891	5.235	6.822
150mm	6.792	5.665	7.946	5.332	6.880
		-16.6%	17.0%	-21.5%	1.3%
80mm		5.829	8.095	5.514	7.020
	Ave	-16.6%	17.0%	-21.5%	1.3%

Figure E.11 Transitional velocity and average % error for 15% kaolin using the Slatter technique – all rheologies

Metzner & Reed

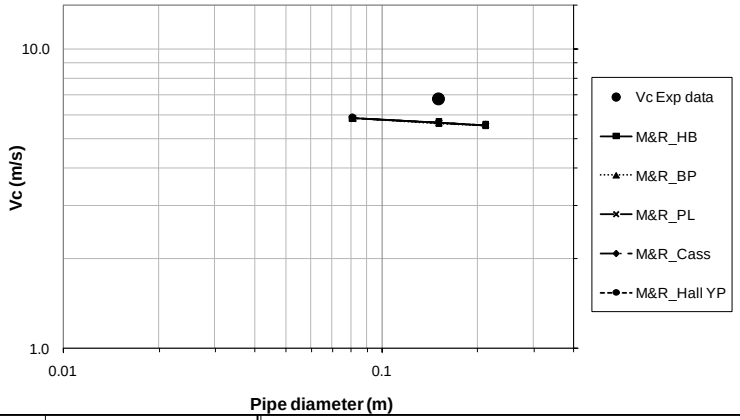

Diameter	Critical velocity (Exp) m/s	Vc Error values - M&R HB m/s	BP m/s	PL m/s	CASS m/s	HAL_YP m/s
200mm		5.572	5.553	5.574	5.562	5.568
150mm	6.792	5.674	5.649	5.678	5.660	5.666
		-16.5%	-16.8%	-16.4%	-16.7%	-16.6%
80mm		5.873	5.893	5.872	5.882	5.877
	Ave	-16.5%	-16.8%	-16.4%	-16.7%	-16.6%

Figure E.12 Transitional velocity and average % error for 15% kaolin using the Metzner & Reed technique – all rheologies

Generalised Reynolds number

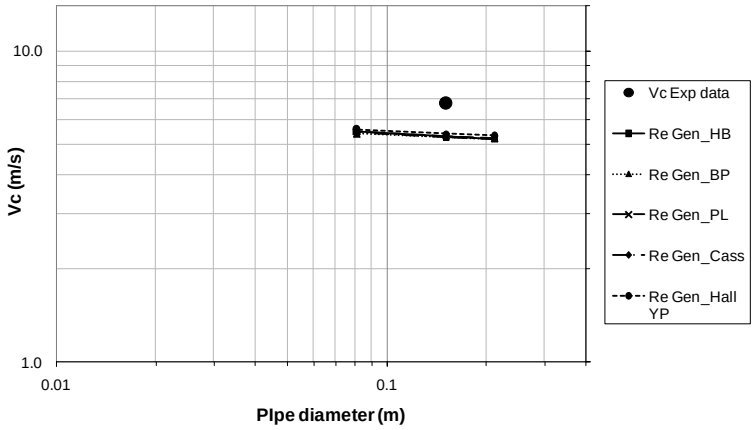

Diameter	Critical velocity (Exp) m/s	Vc Error values - Generalised Re				
		HB m/s	BP m/s	PL m/s	CASS m/s	HAL_YP m/s
200mm		5.232	5.229	5.235	5.225	5.348
150mm	6.792	5.323	5.277	5.332	5.295	5.427
		-21.6%	-22.3%	-21.5%	-22.0%	-20.1%
80mm		5.504	5.425	5.514	5.463	5.601
	Ave	-21.6%	-22.3%	-21.5%	-22.0%	-20.1%

Figure E.13 Transitional velocity and average % error for 15% kaolin using the Generalised Reynolds number approach – all rheologies

Hedström intersection method

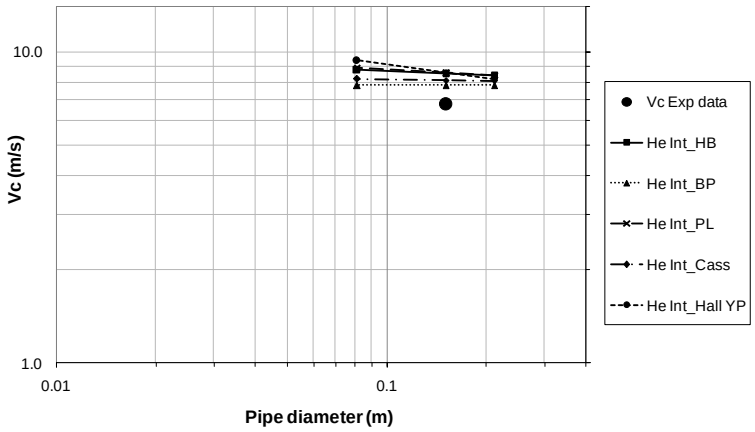

Diameter	Critical velocity (Exp) m/s	Vc Error values - He Intersection				
		HB m/s	BP m/s	PL m/s	CASS m/s	HAL_YP m/s
200mm		8.390	7.823	8.426	8.069	8.193
150mm	6.792	8.512	7.817	8.582	8.108	8.591
		25.3%	15.1%	26.4%	19.4%	26.5%
80mm		8.754	7.816	8.876	8.201	9.395
	Ave	25.3%	15.1%	26.4%	19.4%	26.5%

Figure E.14 Transitional velocity and average % error for 15% kaolin using the Hedström intersection method – all rheologies

Ryan & Johnson criterion

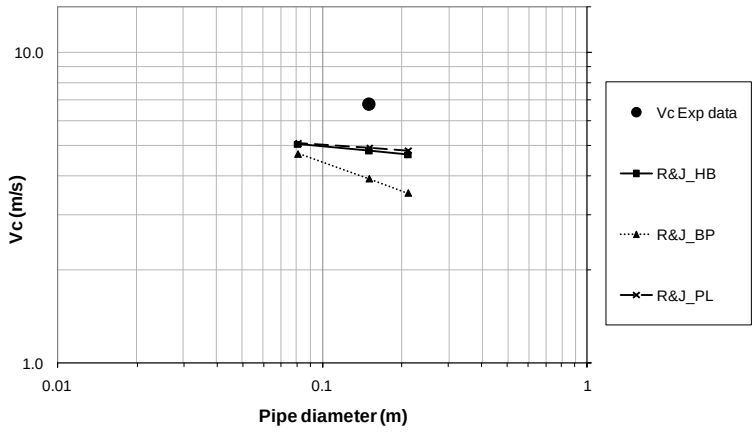

Diameter	Critical velocity (Exp) m/s	Vc Error values - R&J HB m/s	BP m/s	PL m/s
200mm		4.682	3.525	4.839
150mm	6.792	4.811	3.910	4.929
		-29.2%	-42.4%	-27.4%
80mm		5.060	4.711	5.098
	Ave	-29.2%	-42.4%	-27.4%

Figure E.15 Transitional velocity and average % error for 15% kaolin using the Ryan & Johnson criterion – all rheologies

Newtonian Approximation

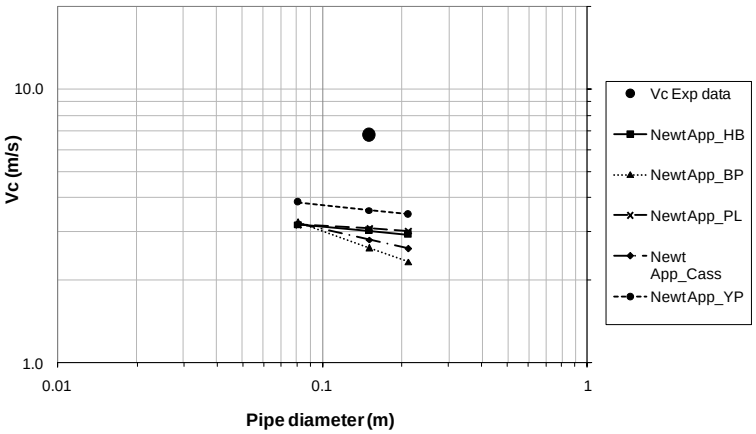

Diameter	Critical velocity (Exp) m/s	Vc Error values - Newt Approx HB m/s	BP m/s	PL m/s	CASS m/s	HAL_YP m/s
200mm		2.942	2.339	3.034	2.614	3.484
150mm	6.792	3.029	2.627	3.090	2.812	3.608
		-55.4%	-61.3%	-54.5%	-58.6%	-46.9%
80mm		3.198	3.262	3.196	3.226	3.862
	Ave	-55.4%	-61.3%	-54.5%	-58.6%	-46.9%

Figure E.16 Transitional velocity and average % error for 15% kaolin using the Newtonian Approximation technique – all rheologies

Torrance

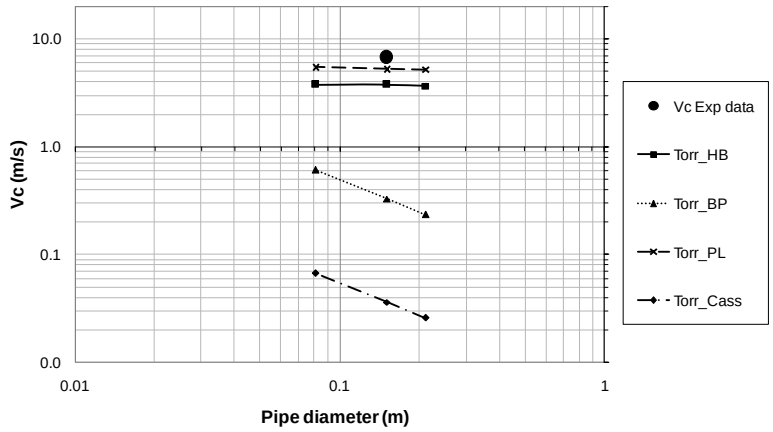

Diameter	Critical velocity (Exp) m/s	Vc Error values - Torrance			
		HB m/s	BP m/s	PL m/s	CASS m/s
200mm		3.674	0.236	5.235	0.026
150mm	6.792	3.801	0.331	5.332	0.036
		-44.0%	-95.1%	-21.5%	-99.5%
80mm		3.801	0.613	5.514	0.067
	Ave	-44.0%	-95.1%	-21.5%	-99.5%

Figure E.17 Transitional velocity and average % error for 15% kaolin using the Torrance criterion – all rheologies

Hallbom

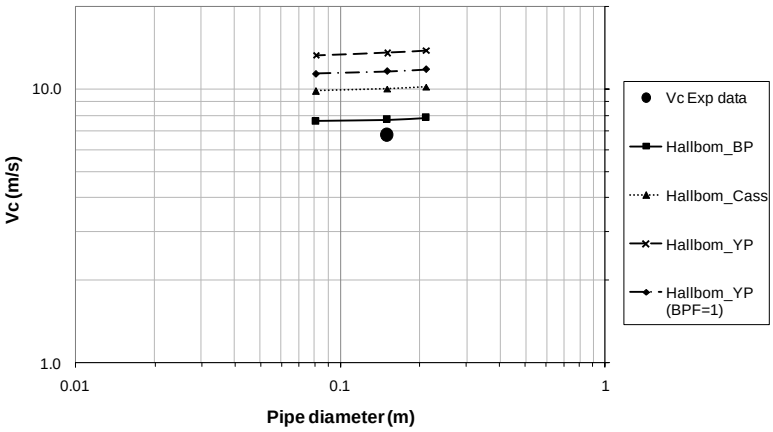

Diameter	Critical velocity (Exp) m/s	Vc Error values - Hallbom Trans			
		BP m/s	CASS m/s	HAL_YP m/s	HAL_YP (BPF=1) m/s
200mm		7.863	10.188	13.844	11.789
150mm	6.792	7.737	10.034	13.557	11.602
		13.9%	47.7%	99.6%	70.8%
80mm		7.619	9.835	13.302	11.359
	Ave	13.9%	47.7%	99.6%	70.8%

Figure E.18 Transitional velocity and average % error for 15% kaolin using the Hallbom criterion – all rheologies

One rheology plotted for all techniques

Herschel-Bulkley

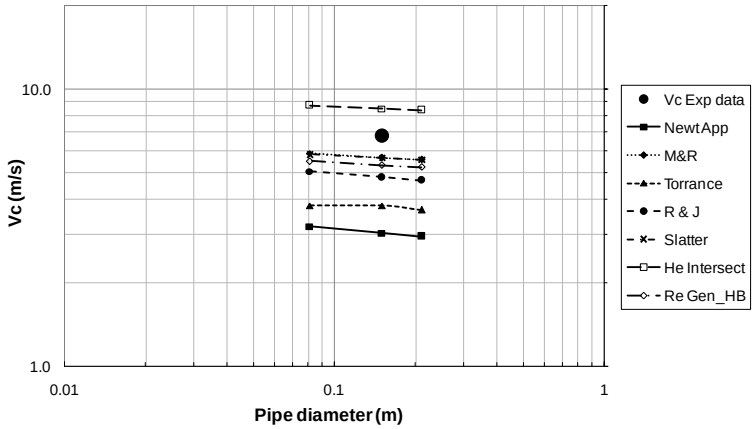

Diameter	Vc (Exp) m/s	Critical velocity Error values - HB - All Techniques						
		Newt App m/s	M & R m/s	Torr/ Clapp m/s	Ryan & John m/s	Slatter m/s	Intersect m/s	Re_Gen m/s
200mm		2.942	5.572	3.674	4.682	5.582	8.390	5.232
150mm	6.792	3.029	5.674	3.801	4.811	5.665	8.512	5.323
		-55.4%	-16.5%	-44.0%	-29.2%	-16.6%	25.3%	-21.6%
80mm		3.198	5.873	3.801	5.060	5.829	8.754	5.504
Ave		-55.4%	-16.5%	-44.0%	-29.2%	-16.6%	25.3%	-21.6%

Figure E.19 Transitional velocity and average % error for 15% kaolin (Herschel-Bulkley rheology – all techniques)

Bingham plastic

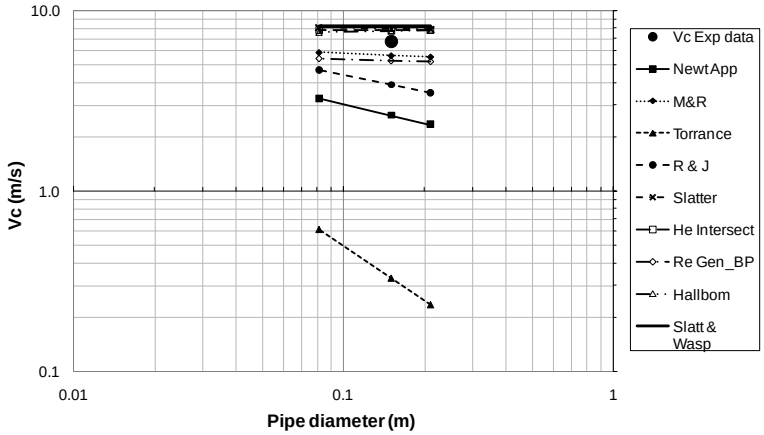

Diameter	Vc (Exp) m/s	Critical velocity Error values - BP - All Techniques							
		Newt App m/s	M & R m/s	Torr/ Clapp m/s	Ryan & John m/s	Slatter m/s	Intersect m/s	Re_Gen m/s	S&W m/s
200mm		2.339	5.553	0.236	3.525	7.891	7.823	5.229	8.199
150mm	6.792	2.627	5.649	0.331	3.910	7.946	7.817	5.277	8.199
		-61.3%	-16.8%	-95.1%	-42.4%	17.0%	15.1%	-22.3%	20.7%
80mm		3.262	5.893	0.613	4.711	8.095	7.816	5.425	8.199
Ave		-61.3%	-16.8%	-95.1%	-42.4%	17.0%	15.1%	-22.3%	20.7%

Figure E.20 Transitional velocity and average % error for 15% kaolin (Bingham plastic rheology – all techniques)

Appendix F. Transitional prediction results & analysis: bentonite

The results for the transitional velocity predictions of 6% and 9% bentonite are presented here.

6% bentonite

One technique plotted for all rheologies

Slatter

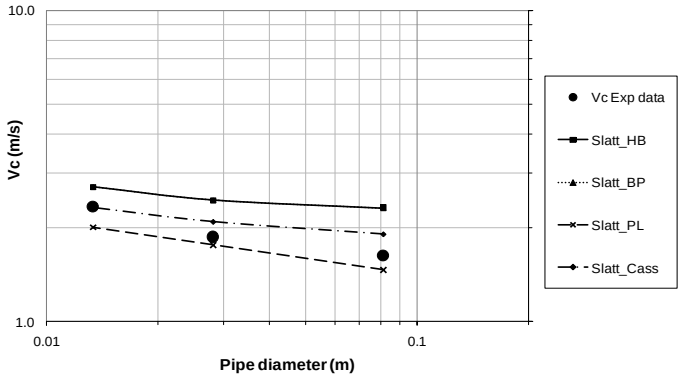

Diameter	Critical velocity (Exp) m/s	Vc Error values - SLATTER Re3 HB m/s	BP m/s	PL m/s	CASS m/s
80mm	1.624	2.317	2.317	1.468	1.910
		42.7%	42.7%	-9.6%	17.6%
28mm	1.870	2.458	2.458	1.766	2.094
		31.5%	31.5%	-5.6%	12.0%
13mm	2.335	2.710	2.710	2.011	2.332
		16.1%	16.1%	-13.9%	-0.1%
	Ave	30.1%	30.1%	-9.7%	9.8%

Figure F.1 Transitional velocity and average % error for 6% bentonite using Slatter's technique – all rheologies

Metzner & Reed

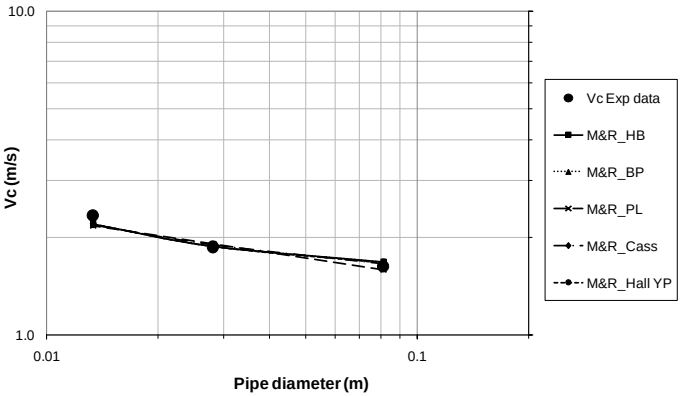

Diameter	Critical velocity (Exp) m/s	Vc Error values - M&R HB m/s	BP m/s	PL m/s	CASS m/s	HAL_YP m/s
80mm	1.624	1.676	1.676	1.592	1.655	1.675
		3.2%	3.2%	-2.0%	1.9%	3.15%
28mm	1.870	1.882	1.882	1.915	1.899	1.882
		0.7%	0.7%	2.4%	1.6%	0.7%
13mm	2.335	2.203	2.203	2.181	2.188	2.203
		-5.6%	-5.6%	-6.6%	-6.3%	-5.7%
	Ave	-0.6%	-0.6%	-2.0%	-0.9%	-0.6%

Figure F.2 Transitional velocity and average % error for 6% bentonite using the Metzner & Reed technique – all rheologies

Generalised Reynolds number

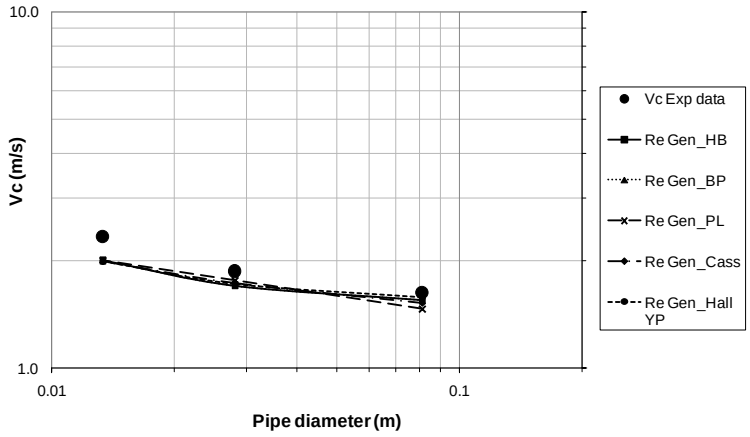

Diameter	Critical velocity (Exp) m/s	Vc Error values - Generalised Re				
		HB m/s	BP m/s	PL m/s	CASS m/s	HAL_YP m/s
80mm	1.624	1.548	1.548	1.468	1.523	1.578
		-4.7%	-4.7%	-9.6%	-6.3%	-2.84%
28mm	1.870	1.705	1.705	1.766	1.735	1.722
		-8.8%	-8.8%	-5.6%	-7.2%	-7.9%
13mm	2.335	2.003	2.003	2.011	2.001	1.994
		-14.2%	-14.2%	-13.9%	-14.3%	-14.6%
	Ave	-9.2%	-9.2%	-9.7%	-9.2%	-8.4%

Figure F.3 Transitional velocity and average % error for 6% bentonite using the Generalised Reynolds number approach – all rheologies

Hedström intersection method

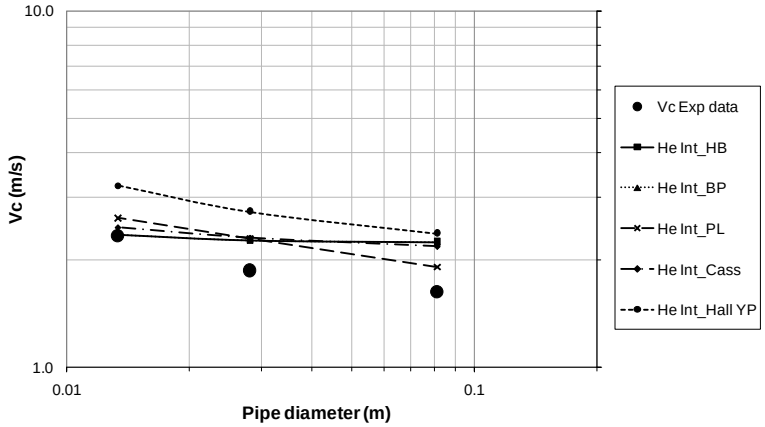

Diameter	Critical velocity (Exp) m/s	Vc Error values - He Intersection				
		HB m/s	BP m/s	PL m/s	CASS m/s	HAL_YP m/s
80mm	1.624	2.249	2.249	1.917	2.188	2.376
		38.4%	38.4%	18.0%	34.7%	46.27%
28mm	1.870	2.271	2.271	2.304	2.313	2.731
		21.5%	21.5%	23.3%	23.7%	46.1%
13mm	2.335	2.349	2.349	2.625	2.471	3.237
		0.6%	0.6%	12.4%	5.9%	38.6%
	Ave	20.2%	20.2%	17.9%	21.4%	43.7%

Figure F.4 Transitional velocity and average % error for 6% bentonite using the Hedström intersection method – all rheologies

Ryan & Johnson criterion

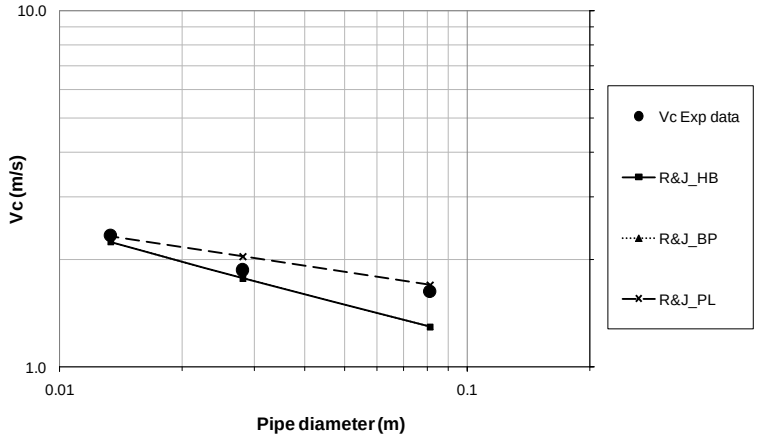

Diameter	Critical velocity (Exp) m/s	Vc Error values - R&J HB m/s	BP m/s	PL m/s
80mm	1.624	1.297	1.297	1.698
		-20.2%	-20.2%	4.5%
28mm	1.870	1.774	1.774	2.041
		-5.1%	-5.1%	9.2%
13mm	2.335	2.248	2.248	2.325
		-3.7%	-3.7%	-0.4%
	Ave	-9.7%	-9.7%	4.4%

Figure F.5 Transitional velocity and average % error for 6% bentonite using the Ryan & Johnson criterion – all rheologies

Newtonian Approximation

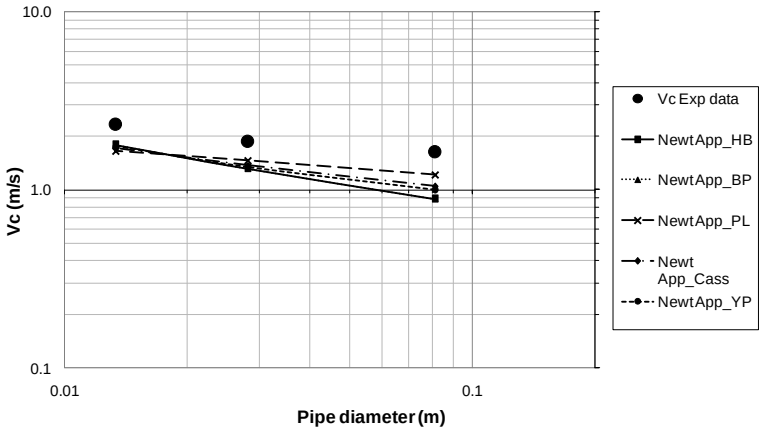

	Diameter m	Critical velocity (Exp) m/s	Vc Error values - Newt Approx HB m/s	BP m/s	PL m/s	CASS m/s	HAL_YP m/s
80mm	0.080879	1.624	0.891	0.891	1.212	1.045	0.997
			-45.2%	-45.2%	-25.4%	-35.6%	-38.64%
28mm	0.028105	1.870	1.313	1.313	1.457	1.375	1.338
			-29.8%	-29.8%	-22.1%	-26.4%	-28.4%
13mm	0.013318	2.335	1.794	1.794	1.660	1.721	1.757
			-23.2%	-23.2%	-28.9%	-26.3%	-24.7%
		Ave	-32.7%	-32.7%	-25.4%	-29.5%	-30.6%

Figure F.6 Transitional velocity and average % error for 6% bentonite using the Newtonian Approximation technique – all rheologies

Torrance

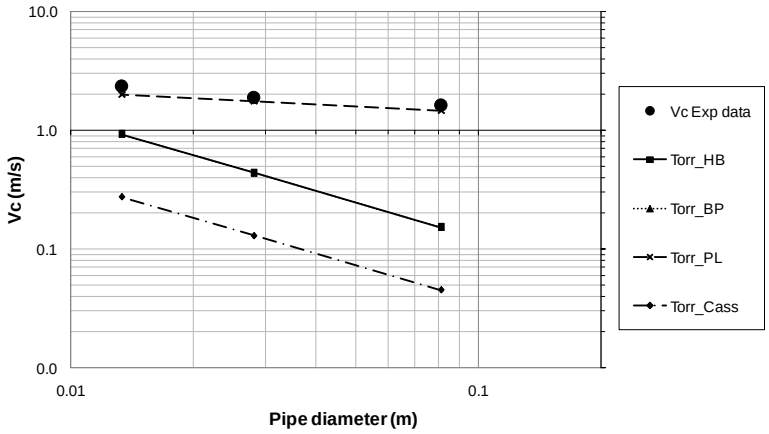

Diameter	Critical velocity (Exp) m/s	Vc Error values - Torrance			
		HB m/s	BP m/s	PL m/s	CASS m/s
80mm	1.624	0.152	0.152	1.468	0.045
		-90.6%	-90.6%	-9.6%	-97.2%
28mm	1.870	0.438	0.438	1.766	0.130
		-76.6%	-76.6%	-5.6%	-93.1%
13mm	2.335	0.924	0.924	2.011	0.274
		-60.4%	-60.4%	-13.9%	-88.3%
	Ave	-75.9%	-75.9%	-9.7%	-92.8%

Figure F.7 Transitional velocity and average % error for 6% bentonite using the Torrance criterion – all rheologies

Hallbom

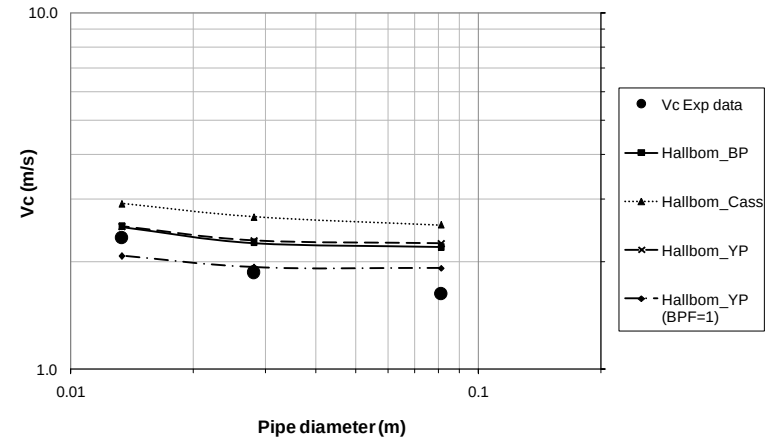

Diameter	Critical velocity (Exp) m/s	Vc Error values - Hallbom Trans					
		HB m/s	BP m/s	PL m/s	CASS m/s	HAL_YP m/s	HALL_YP (BPF=1) m/s
80mm	1.624		2.197		2.543	2.254	1.922
			35.2%		56.5%	38.77%	18.30%
28mm	1.870		2.259		2.674	2.297	1.930
			20.9%		43.0%	22.9%	3.3%
13mm	2.335		2.513		2.914	2.522	2.080
			7.6%		24.8%	8.0%	-10.9%
	Ave		21.2%		41.5%	23.2%	3.5%

Figure F.8 Transitional velocity and average % error for 6% bentonite using the Hallbom criterion – all rheologies

One rheology plotted for all techniques

Bingham plastic

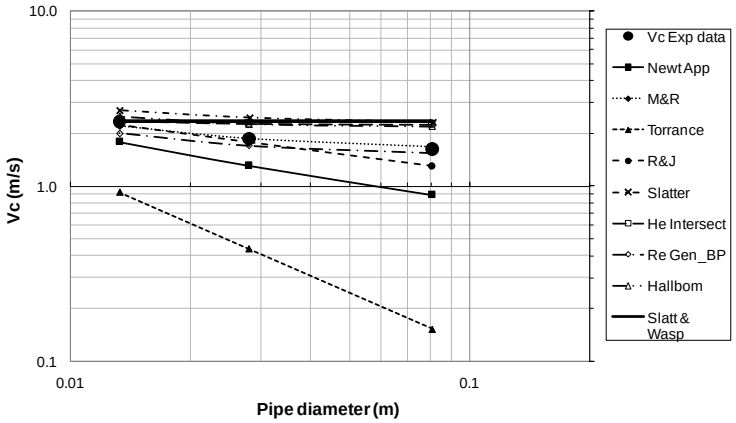

Diameter	Vc (Exp) m/s	Vc Error values - BP - All Techniques							
		Newt App m/s	M & R m/s	Torr/ Clapp m/s	Ryan & John m/s	Slatter m/s	Intersect m/s	Re_Gen m/s	Hallbom m/s
80mm	1.624	0.891	1.676	0.152	1.297	2.317	2.249	1.548	2.197
		-45.2%	3.2%	-90.6%	-20.2%	42.7%	38.4%	-4.7%	35.2%
28mm	1.870	1.313	1.882	0.438	1.774	2.458	2.271	1.705	2.259
		-29.8%	0.7%	-76.6%	-5.1%	31.5%	21.5%	-8.8%	20.9%
13mm	2.335	1.794	2.203	0.924	2.248	2.710	2.349	2.003	2.513
		-23.2%	-5.6%	-60.4%	-3.7%	16.1%	0.6%	-14.2%	7.6%
	Ave	-32.7%	-0.6%	-75.9%	-9.7%	30.1%	20.2%	-9.2%	21.2%

Figure F.9 Transitional velocity and average % error for 6% bentonite (Bingham plastic rheology – all techniques)

Power law

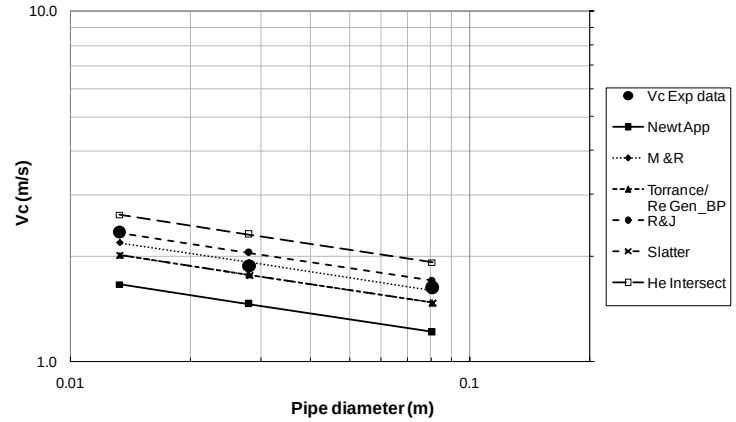

Diameter	Vc (Exp) m/s	Vc Error values - PL - All Techniques						
		Newt App m/s	M & R m/s	Torr/ Clapp m/s	Ryan & John m/s	Slatter m/s	Intersect m/s	Re_Gen m/s
80mm	1.624	1.212	1.592	1.468	1.698	1.468	1.917	1.468
		-25.4%	-2.0%	-9.6%	4.5%	-9.6%	18.0%	-9.6%
28mm	1.870	1.457	1.915	1.766	2.041	1.766	2.304	1.766
		-22.1%	2.4%	-5.6%	9.2%	-5.6%	23.3%	-5.6%
13mm	2.335	1.660	2.181	2.011	2.325	2.011	2.625	2.011
		-28.9%	-6.6%	-13.9%	-0.4%	-13.9%	12.4%	-13.9%
	Ave	-25.4%	-2.0%	-9.7%	4.4%	-9.7%	17.9%	-9.7%

Figure F.10 Transitional velocity and average % error for 6% bentonite (power law rheology – all techniques)

Hallbom yield plastic

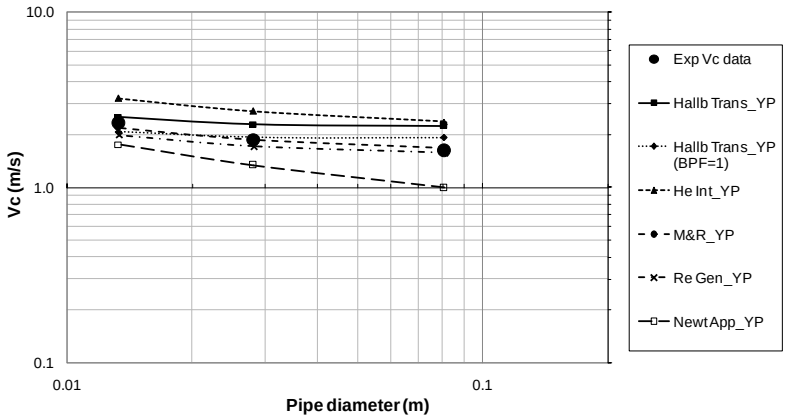

Diameter	Vc (Exp) m/s	Vc Error values - Hallbom_YP - All Techniques					
		Hallb_Trans m/s	Hallb_Trans (BPF = 1) m/s	He Int_YP m/s	M&R_YP m/s	Re_Gen_YP m/s	NEWT_YP m/s
80mm	1.624	2.254	1.922	2.376	1.675	1.578	0.997
		38.8%	18.3%	46.3%	3.1%	-2.8%	-38.6%
28mm	1.870	2.297	1.930	2.731	1.882	1.722	1.338
		22.9%	3.3%	46.1%	0.7%	-7.9%	-28.4%
13mm	2.335	2.522	2.080	3.237	2.203	1.994	1.757
		8.0%	-10.9%	38.6%	-5.7%	-14.6%	-24.7%
	Ave	23.2%	3.5%	43.7%	-0.6%	-8.4%	-30.6%

Figure F.11 Transitional velocity and average % error for 6% bentonite (Hallbom yield plastic rheology – all techniques)

9% bentonite

One technique plotted for all rheologies

Slatter

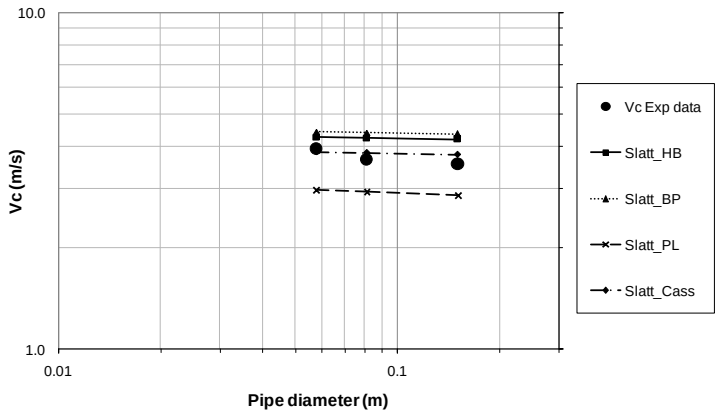

Diameter	Critical velocity (Exp) m/s	Vc Error values - SLATTER Re3			
		HB m/s	BP m/s	PL m/s	CASS m/s
60mm	3.942	4.272	4.435	2.979	3.861
		8.4%	12.5%	-24.4%	-2.1%
80mm	3.656	4.244	4.402	2.939	3.831
		16.1%	20.4%	-19.6%	4.8%
150mm	3.547	4.207	4.360	2.869	3.790
		18.6%	22.9%	-19.1%	6.9%
	Ave	14.4%	18.6%	-21.1%	3.2%

Figure F.12 Transitional velocity and average % error for 9% bentonite using the Slatter technique – all rheologies

Metzner & Reed

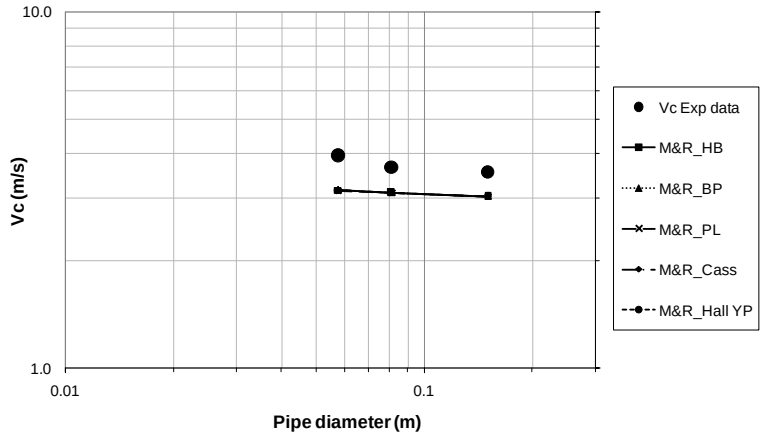

Diameter	Critical velocity (Exp) m/s	Vc Error values - M&R				
		HB m/s	BP m/s	PL m/s	CASS m/s	HAL_YP m/s
60mm	3.942	3.158	3.160	3.147	3.154	3.156
		-19.9%	-19.8%	-20.2%	-20.0%	-19.93%
80mm	3.656	3.103	3.103	3.105	3.104	3.103
		-15.1%	-15.1%	-15.1%	-15.1%	-15.1%
150mm	3.547	3.028	3.028	3.031	3.030	3.029
		-14.6%	-14.6%	-14.6%	-14.6%	-14.6%
	Ave	-16.5%	-16.5%	-16.6%	-16.6%	-16.6%

Figure F.13 Transitional velocity and average % error for 9% bentonite using the Metzner & Reed technique – all rheologies

Generalised Reynolds number

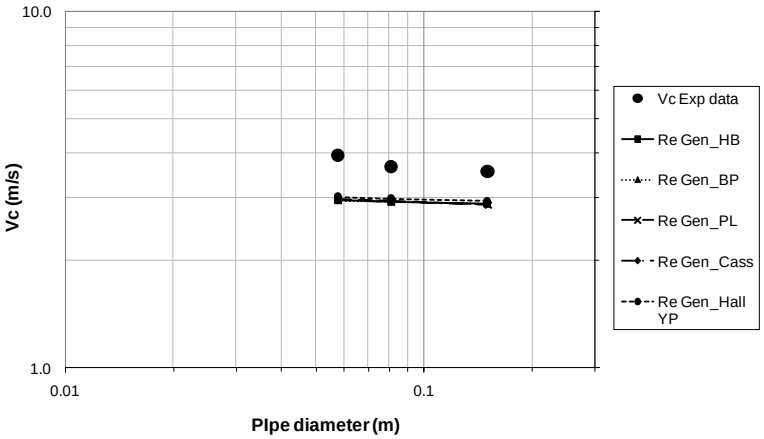

Diameter	Critical velocity (Exp) m/s	Vc Error values - Generalised Re				
		HB m/s	BP m/s	PL m/s	CASS m/s	HAL_YP m/s
60mm	3.942	2.951	2.947	2.979	2.960	3.018
		-25.1%	-25.2%	-24.4%	-24.9%	-23.44%
80mm	3.656	2.919	2.918	2.939	2.925	2.981
		-20.1%	-20.2%	-19.6%	-20.0%	-18.5%
150mm	3.547	2.882	2.885	2.869	2.876	2.932
		-18.8%	-18.7%	-19.1%	-18.9%	-17.4%
	Ave	-21.4%	-21.4%	-21.1%	-21.3%	-19.7%

Figure F.14 Transitional velocity and average % error for 9% bentonite using the Generalised Reynolds number approach – all rheologies

Hedström intersection method

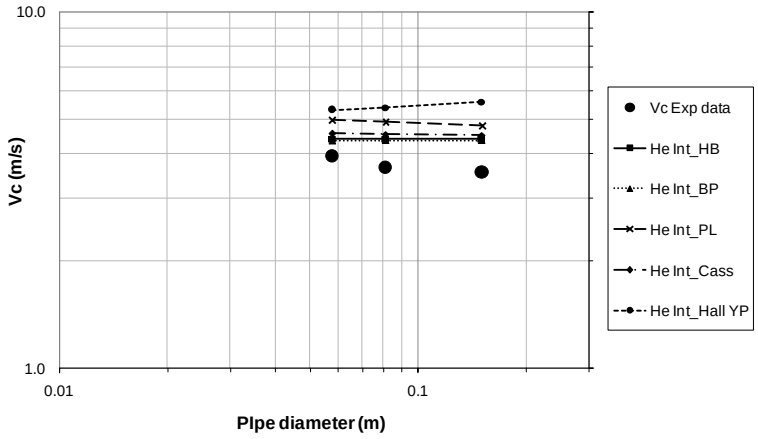

Diameter	Critical velocity (Exp) m/s	Vc Error values - He Intersection				
		HB m/s	BP m/s	PL m/s	CASS m/s	HAL_YP m/s
60mm	3.942	4.410	4.355	4.978	4.563	5.310
		11.9%	10.5%	26.3%	15.8%	34.69%
80mm	3.656	4.405	4.358	4.912	4.544	5.398
		20.5%	19.2%	34.4%	24.3%	47.6%
150mm	3.547	4.403	4.366	4.795	4.517	5.601
		24.1%	23.1%	35.2%	27.3%	57.9%
	Ave	18.8%	17.6%	31.9%	22.5%	46.7%

Figure F.15 Transitional velocity and average % error for 9% bentonite using the Hedström intersection method – all rheologies

Ryan & Johnson criterion

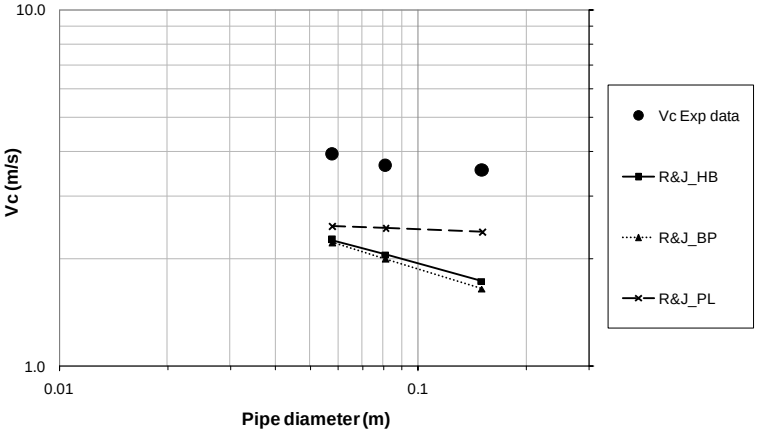

Diameter	Critical velocity (Exp) m/s	Vc Error values - R&J		
		HB m/s	BP m/s	PL m/s
60mm	3.942	2.260	2.224	2.478
		-42.7%	-43.6%	-37.1%
80mm	3.656	2.058	2.003	2.445
		-43.7%	-45.2%	-33.1%
150mm	3.547	1.734	1.651	2.387
		-51.1%	-53.5%	-32.7%
	Ave	-45.8%	-47.4%	-34.3%

Figure F.16 Transitional velocity and average % error for 9% bentonite using the Ryan & Johnson criterion – all rheologies

Newtonian Approximation

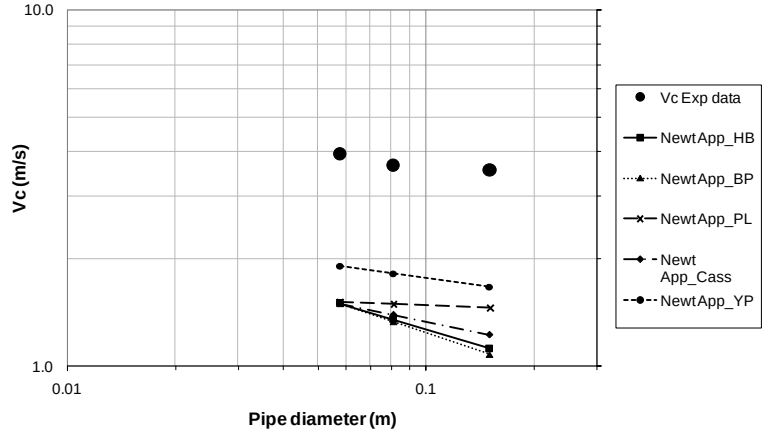

Diameter	Critical velocity (Exp) m/s	Vc Error values - Newt Approx				
		HB m/s	BP m/s	PL m/s	CASS m/s	HAL_YP m/s
60mm	3.942	1.499	1.499	1.518	1.501	1.913
		-62.0%	-62.0%	-61.5%	-61.9%	-51.47%
80mm	3.656	1.349	1.332	1.498	1.394	1.819
		-63.1%	-63.6%	-59.0%	-61.9%	-50.2%
150mm	3.547	1.118	1.079	1.462	1.223	1.670
		-68.5%	-69.6%	-58.8%	-65.5%	-52.9%
	Ave	-64.5%	-65.0%	-59.8%	-63.1%	-51.6%

Figure F.17 Transitional velocity and average % error for 9% bentonite using the Newtonian Approximation technique – all rheologies

Torrance

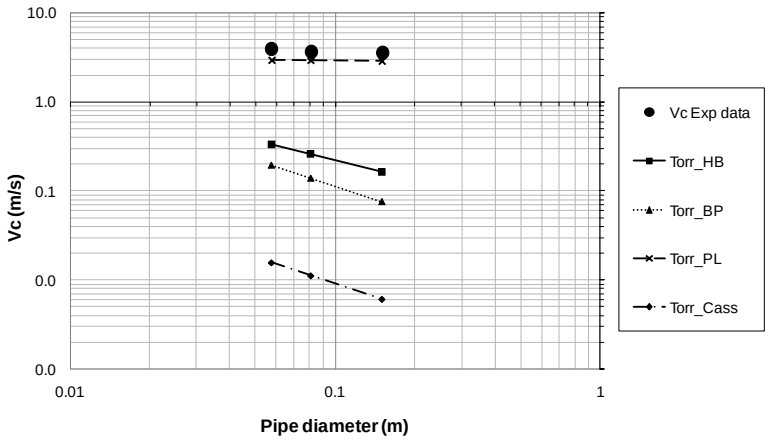

Diameter	Critical velocity (Exp) m/s	Vc Error values - Torrance			
		HB m/s	BP m/s	PL m/s	CASS m/s
60mm	3.942	0.335	0.197	2.979	0.016
		-91.5%	-95.0%	-24.4%	-99.6%
80mm	3.656	0.260	0.140	2.939	0.011
		-92.9%	-96.2%	-19.6%	-99.7%
150mm	3.547	0.165	0.075	2.869	0.006
		-95.3%	-97.9%	-19.1%	-99.8%
	Ave	-93.2%	-96.3%	-21.1%	-99.7%

Figure F.18 Transitional velocity and average % error for 9% bentonite using the Torrance criterion – all rheologies

Hallbom

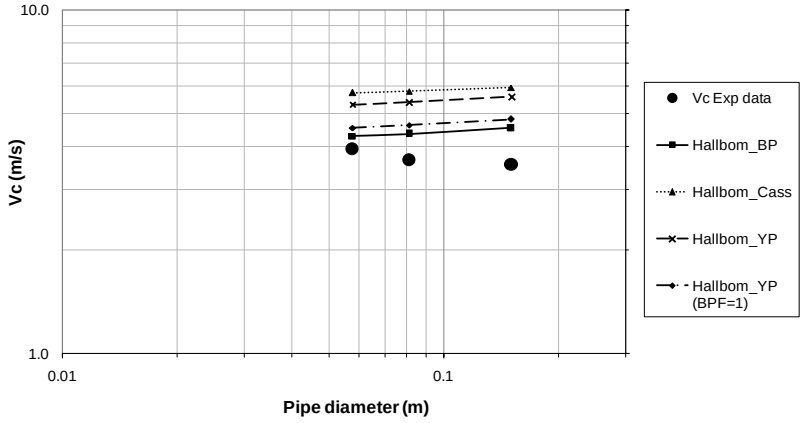

Diameter	Critical velocity (Exp) m/s	Vc Error values - Hallbom Trans			
		BP m/s	CASS m/s	HAL_YP m/s	HALL_YP (BPF=1) m/s
60mm	3.942	4.299	5.751	5.310	4.540
		9.1%	45.9%	34.69%	15.18%
80mm	3.656	4.367	5.806	5.398	4.623
		19.4%	58.8%	47.6%	26.4%
150mm	3.547	4.538	5.957	5.601	4.807
		27.9%	67.9%	57.9%	35.5%
	Ave	18.8%	57.5%	46.7%	25.7%

Figure F.19 Transitional velocity and average % error for 9% bentonite using the Hallbom criterion – all rheologies

One rheology plotted for all techniques

Bingham plastic

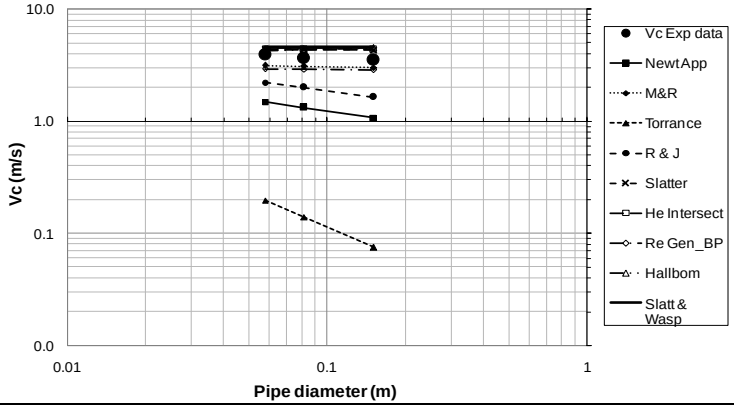

Diameter	Vc (Exp) m/s	Critical velocity Error values - BP - All Techniques								
		Newt App m/s	M & R m/s	Torr/ Clapp m/s	Ryan & John m/s	Slatter m/s	Intersect m/s	Re_Gen m/s	S&W m/s	Hallbom m/s
60mm	3.942	1.499	3.160	0.197	2.224	4.435	4.355	2.947	4.568	4.299492
		-62.0%	-19.8%	-95.0%	-43.6%	12.5%	10.5%	-25.2%	15.9%	9.1%
80mm	3.656	1.332	3.103	0.140	2.003	4.402	4.358	2.918	4.568	4.366538
		-63.6%	-15.1%	-96.2%	-45.2%	20.4%	19.2%	-20.2%	25.0%	19.4%
150mm	3.547	1.079	3.028	0.075	1.651	4.360	4.366	2.885	4.568	4.537554
		-69.6%	-14.6%	-97.9%	-53.5%	22.9%	23.1%	-18.7%	28.8%	27.9%
	Ave	-65.0%	-16.5%	-96.3%	-47.4%	18.6%	17.6%	-21.4%	23.2%	18.8%

Figure F.20 Transitional velocity and average % error for 9% bentonite (Bingham plastic rheology – all techniques)

Power law

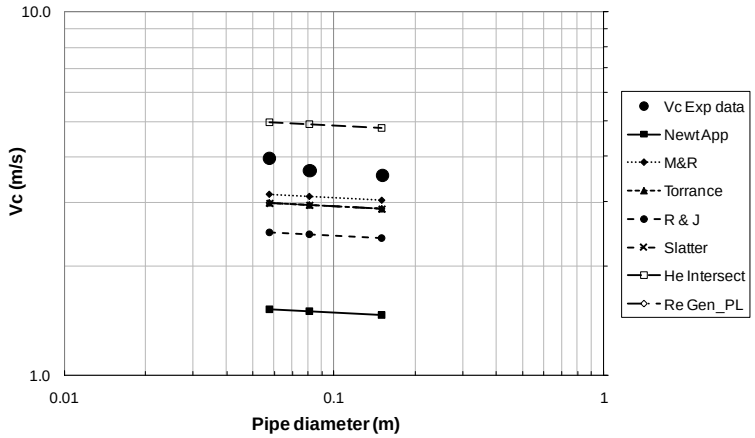

Diameter	Vc (Exp) m/s	Critical velocity Error values - PL - All Techniques						
		Newt App m/s	M & R m/s	Torr/ Clapp m/s	Ryan & John m/s	Slatter m/s	Intersect m/s	Re_Gen m/s
60mm	3.942	1.518	3.147	2.979	2.478	2.979	4.978	2.979
		-61.5%	-20.2%	-24.4%	-37.1%	-24.4%	26.3%	-24.4%
80mm	3.656	1.498	3.105	2.939	2.445	2.939	4.912	2.939
		-59.0%	-15.1%	-19.6%	-33.1%	-19.6%	34.4%	-19.6%
150mm	3.547	1.462	3.031	2.869	2.387	2.869	4.795	2.869
		-58.8%	-14.6%	-19.1%	-32.7%	-19.1%	35.2%	-19.1%
Ave		-59.8%	-16.6%	-21.1%	-34.3%	-21.1%	31.9%	-21.1%

Figure F.21 Transitional velocity and average % error for 9% bentonite (power law rheology – all techniques)

Hallbom yield plastic

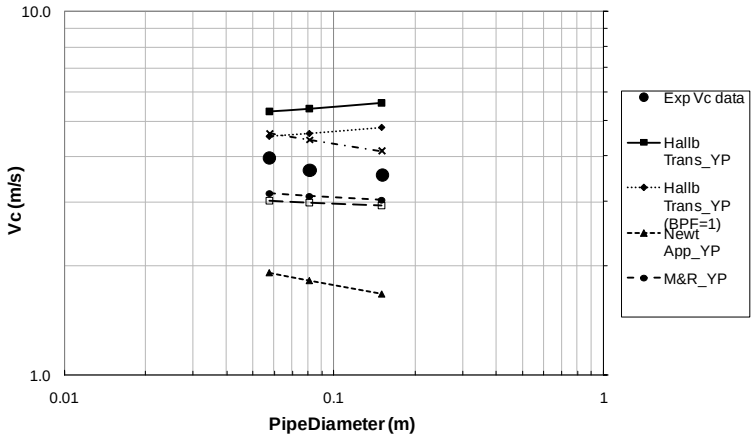

Diameter	Vc (Exp) m/s	Critical velocity Error values - Hallbom_YP - All Techniques					
		Hallb_Trans m/s	Hallb_Trans (BPF = 1) m/s	He Int_YP m/s	M&R_YP m/s	Re_Gen_YP m/s	NEWT_YP m/s
60mm	3.942	5.310	4.540	4.621	3.156	3.018	1.913
		34.7%	15.2%	17.2%	-19.9%	-23.4%	-51.5%
80mm	3.656	5.398	4.623	4.435	3.103	2.981	1.819
		47.6%	26.4%	21.3%	-15.1%	-18.5%	-50.2%
150mm	3.547	5.601	4.807	4.129	3.029	2.932	1.670
		57.9%	35.5%	16.4%	-14.6%	-17.4%	-52.9%
Ave		46.7%	25.7%	18.3%	-16.6%	-19.7%	-51.6%

Figure F.22 Transitional velocity and average % error for 9% bentonite (Hallbom yield plastic rheology – all techniques)

Appendix G. Transitional prediction results and analysis: CMC

The results for the transitional velocity predictions of 3% and 8% CMC is presented here.

3% CMC

One technique plotted for all rheologies

Slatter

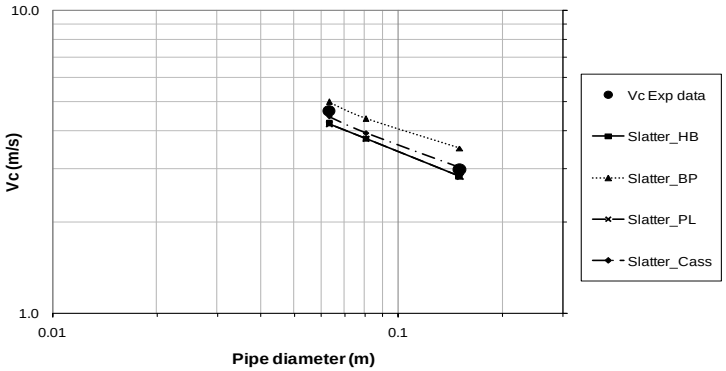

Diameter	Critical velocity (Exp) m/s	Vc Error values - SLATTER Re3			
		HB m/s	BP m/s	PL m/s	CASS m/s
150mm	2.981	2.829	3.511	2.829	3.024
		-5.1%	17.8%	-5.1%	1.5%
80mm		3.778	4.399	3.778	3.946
63mm	4.660	4.226	4.993	4.226	4.469
		-9.3%	7.2%	-9.3%	-4.1%
	Ave	-7.2%	12.5%	-7.2%	-1.3%

Figure G.1 Transitional velocity and average % error for 3% CMC using the Slatter technique – all rheologies

Metzner & Reed

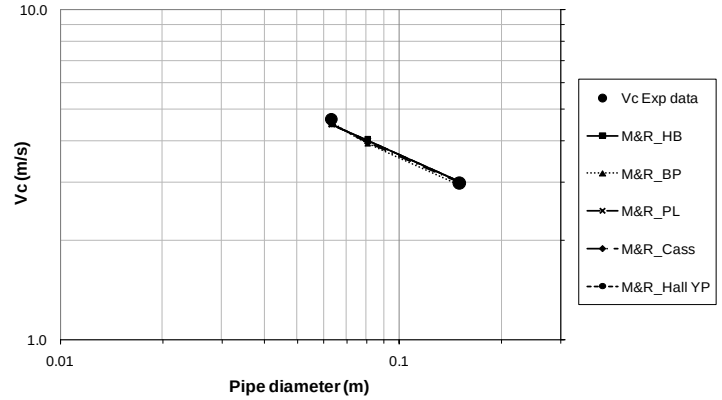

Diameter	Critical velocity (Exp) m/s	Vc Error values - M&R				
		HB m/s	BP m/s	PL m/s	CASS m/s	HAL_YP m/s
150mm	2.981	3.012	2.946	3.012	3.001	3.016
		1.1%	-1.2%	1.1%	0.7%	1.2%
80mm		4.023	3.944	4.023	3.983	4.015
63mm	4.660	4.500	4.589	4.500	4.531	4.504
		-3.4%	-1.5%	-3.4%	-2.8%	-3.3%
	Ave	-1.2%	-1.3%	-1.2%	-1.0%	-1.1%

Figure G.2 Transitional velocity and average % error for 3% CMC using the Metzner & Reed technique – all rheologies

Generalised Reynolds number

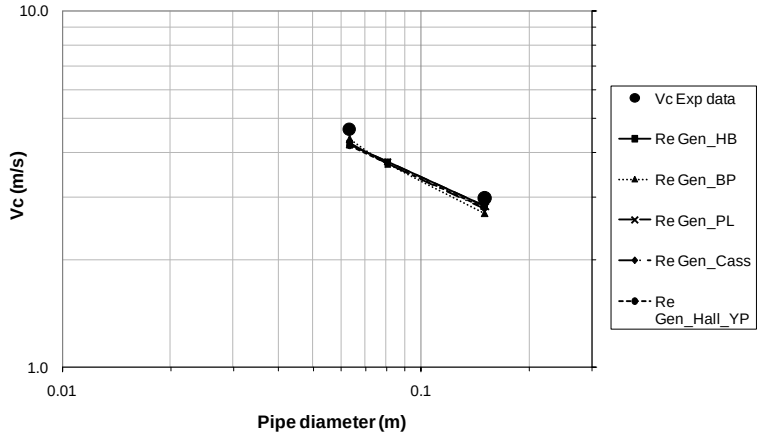

Diameter	Critical velocity (Exp) m/s	Vc Error values - Generalised Re				
		HB m/s	BP m/s	PL m/s	CASS m/s	HAL_YP m/s
150mm	2.981	2.829	2.703	2.829	2.785	2.802
		-5.1%	-9.3%	-5.1%	-6.6%	-6.00%
80mm		3.778	3.727	3.778	3.744	3.737
63mm	4.660	4.226	4.392	4.226	4.283	4.196
		-9.3%	-5.7%	-9.3%	-8.1%	-9.9%
	Ave	-7.2%	-7.5%	-7.2%	-7.3%	-8.0%

Figure G.3 Transitional velocity and average % error for 3% CMC using the Generalised Reynolds number – all rheologies

Hedström intersection method

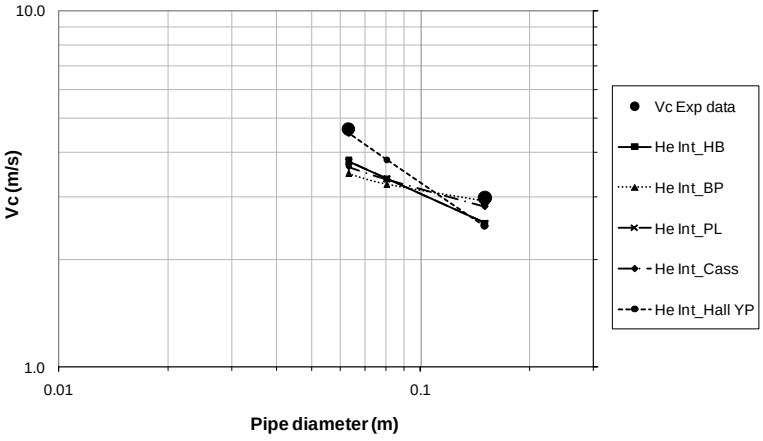

Diameter	Critical velocity (Exp) m/s	Vc Error values - He Intersection				
		HB m/s	BP m/s	PL m/s	CASS m/s	HAL_YP m/s
150mm	2.981	2.533	2.921	2.533	2.819	2.477
		-15.0%	-2.0%	-15.0%	-5.4%	-16.91%
80mm		3.383	3.263	3.383	3.359	3.828
63mm	4.660	3.784	3.499	3.784	3.654	4.538
		-18.8%	-24.9%	-18.8%	-21.6%	-2.6%
	Ave	-16.9%	-13.5%	-16.9%	-13.5%	-9.8%

Figure G.4 Transitional velocity and average % error for 3% CMC using the Hedström intersection method – all rheologies

Ryan & Johnson criterion

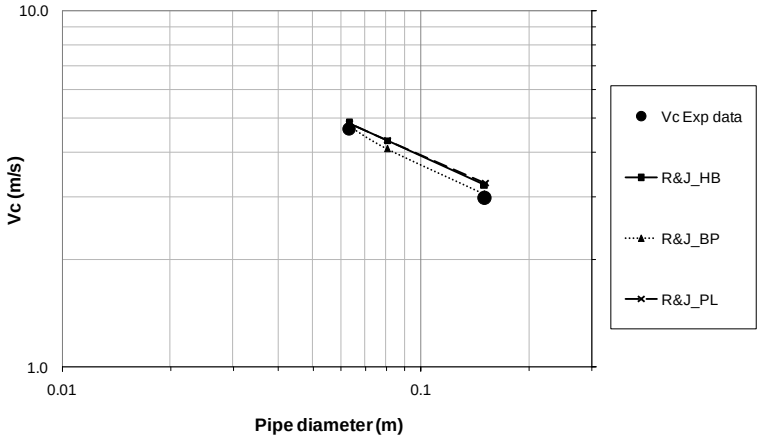

Diameter	Critical velocity (Exp) m/s	Vc Error values - R&J		
		HB m/s	BP m/s	PL m/s
150mm	2.981	3.240	3.054	3.290
		8.7%	2.4%	10.4%
80mm		4.327	4.102	4.339
63mm	4.660	4.840	4.747	4.830
		3.9%	1.9%	3.7%
	Ave	6.3%	2.2%	7.0%

Figure G.5 Transitional velocity and average % error for 3% CMC using the Ryan & Johnson criterion – all rheologies

Newtonian Approximation

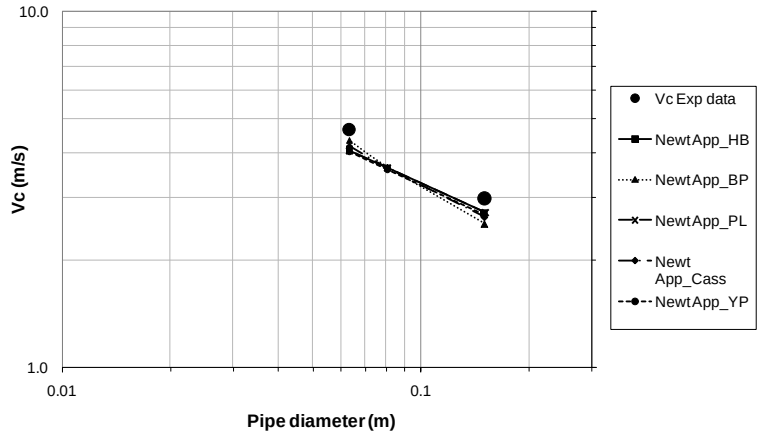

Diameter	Critical velocity (Exp) m/s	Vc Error values - Newt Approx				
		HB m/s	BP m/s	PL m/s	CASS m/s	HAL_YP m/s
150mm	2.981	2.727	2.531	2.727	2.642	2.677
		-8.5%	-15.1%	-8.5%	-11.4%	-10.20%
80mm		3.642	3.665	3.641	3.642	3.590
63mm	4.660	4.073	4.354	4.073	4.194	4.040
		-12.6%	-6.6%	-12.6%	-10.0%	-13.3%
	Ave	-10.6%	-10.8%	-10.6%	-10.7%	-11.8%

Figure G.6 Transitional velocity and average % error for 3% CMC using the Newtonian Approximation technique – all rheologies

Torrance

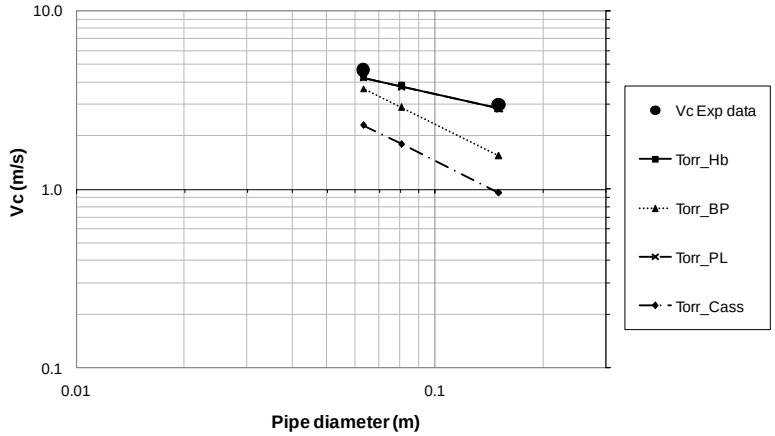

Diameter	Critical velocity (Exp) m/s	Vc Error values - Torrance			
		HB m/s	BP m/s	PL m/s	CASS m/s
150mm	2.981	2.829	1.540	2.829	0.959
		-5.1%	-48.3%	-5.1%	-67.8%
80mm		3.778	2.884	3.778	1.796
63mm	4.660	4.226	3.677	4.226	2.291
		-9.3%	-21.1%	-9.3%	-50.8%
	Ave	-7.2%	-34.7%	-7.2%	-59.3%

Figure G.7 Transitional velocity and average % error for 3% CMC using the Torrance criterion – all rheologies

Hallbom

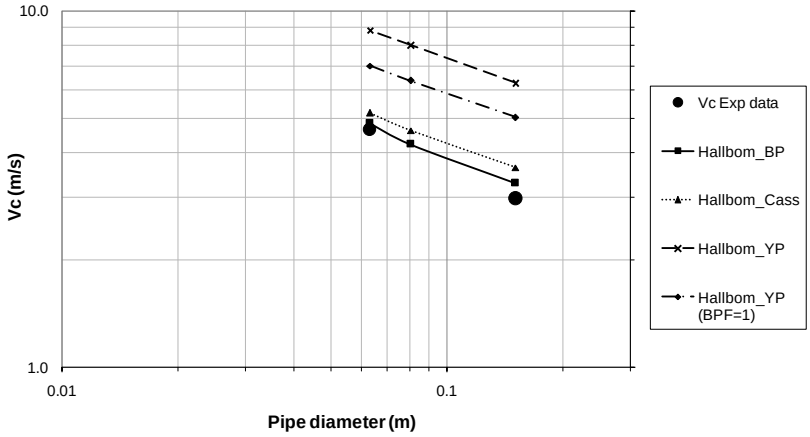

Diameter	Critical velocity (Exp) m/s	Vc Error values - Hallbom Trans			
		BP m/s	CASS m/s	HAL_YP m/s	HAL_YP (BPF=1) m/s
150mm	2.981	3.292	3.639	6.301	5.034
		10.4%	22.1%	111.39%	68.88%
80mm		4.234	4.631	8.032	6.380
63mm	4.660	4.849	5.184	8.852	7.025
		4.1%	11.3%	90.0%	50.7%
	Ave	7.3%	16.7%	100.7%	59.8%

Figure G.8 Transitional velocity and average % error for 3% CMC using the Hallbom criterion – all rheologies

One rheology plotted for all techniques

Power law

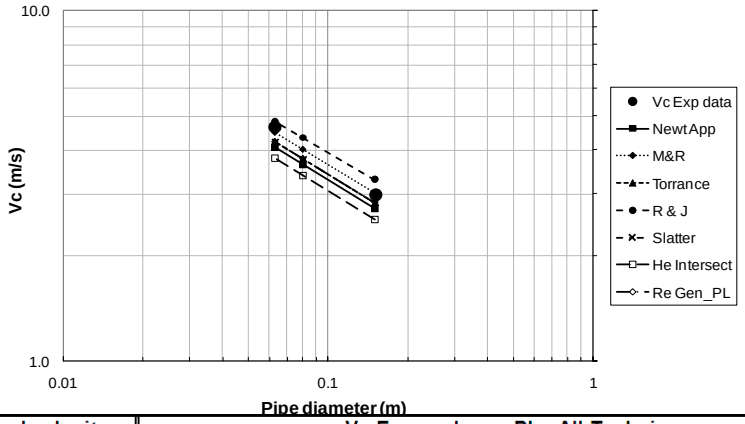

Diameter	Critical velocity (Exp) m/s	Vc Error values - PL - All Techniques						
		Newt App m/s	M & R m/s	Torr/ Clapp m/s	Ryan & John m/s	Slatter m/s	Intersect m/s	Re_Gen m/s
150mm	2.981	2.727	3.012	2.829	3.290	2.829	2.533	2.829
		-8.5%	1.1%	-5.1%	10.4%	-5.1%	-15.0%	-5.1%
80mm		3.641	4.023	3.778	4.339	3.778	3.383	3.778
63mm	4.660	4.073	4.500	4.226	4.830	4.226	3.784	4.226
		-12.6%	-3.4%	-9.3%	3.7%	-9.3%	-18.8%	-9.3%
	Ave	-10.6%	-1.2%	-7.2%	7.0%	-7.2%	-16.9%	-7.2%

Figure G.9 Transitional velocity and average % error for 3% CMC (power law rheology – all techniques)

8% CMC

One technique plotted for all rheologies

Slatter

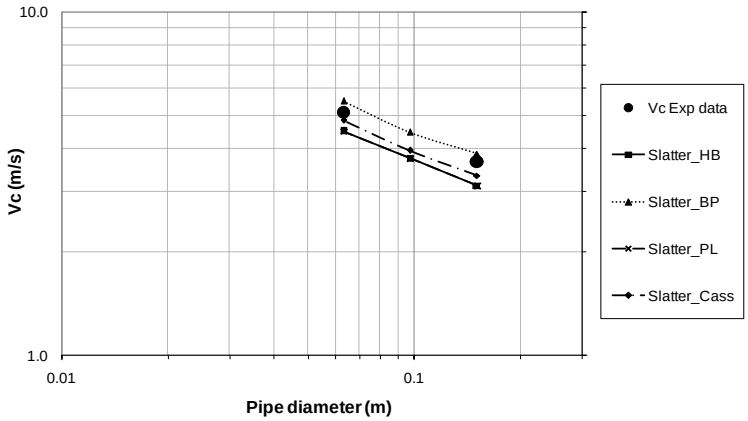

Diameter	Critical velocity (Exp) m/s	Vc Error values - SLATTER Re3			
		HB m/s	BP m/s	PL m/s	CASS m/s
150mm	3.655	3.122	3.870	3.122	3.340
		-14.6%	5.9%	-14.6%	-8.6%
100mm		3.755	4.467	3.755	3.955
63mm	5.093	4.505	5.508	4.505	4.848
		-11.5%	8.1%	-11.5%	-4.8%
	Ave	-13.1%	7.0%	-13.1%	-6.7%

Figure G.10 Transitional velocity and average % error for 8% CMC using the Slatter technique – all rheologies

Metzner & Reed

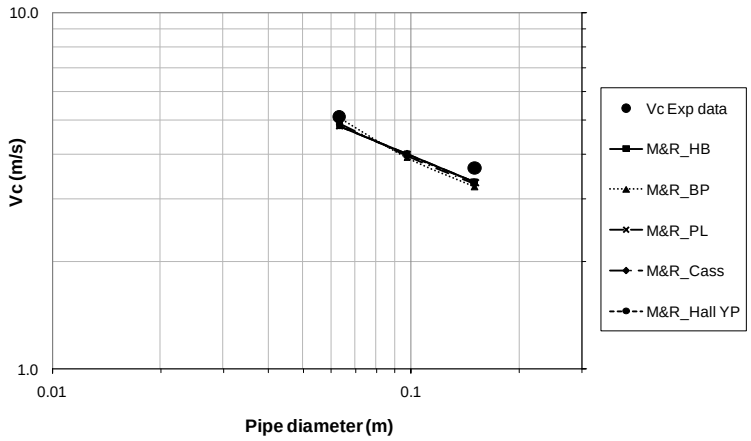

Diameter	Critical velocity (Exp) m/s	Vc Error values - M&R				
		HB m/s	BP m/s	PL m/s	CASS m/s	HAL_YP m/s
150mm	3.655	3.337	3.248	3.337	3.303	3.336
		-8.7%	-11.1%	-8.7%	-9.6%	-8.72%
100mm		4.014	3.926	4.014	3.965	4.006
63mm	5.093	4.816	5.063	4.816	4.907	4.825
		-5.4%	-0.6%	-5.4%	-3.7%	-5.3%
	Ave	-7.1%	-5.9%	-7.1%	-6.6%	-7.0%

Figure G.11 Transitional velocity and average % error for 8% CMC using the Metzner & Reed technique – all rheologies

Generalised Reynolds number

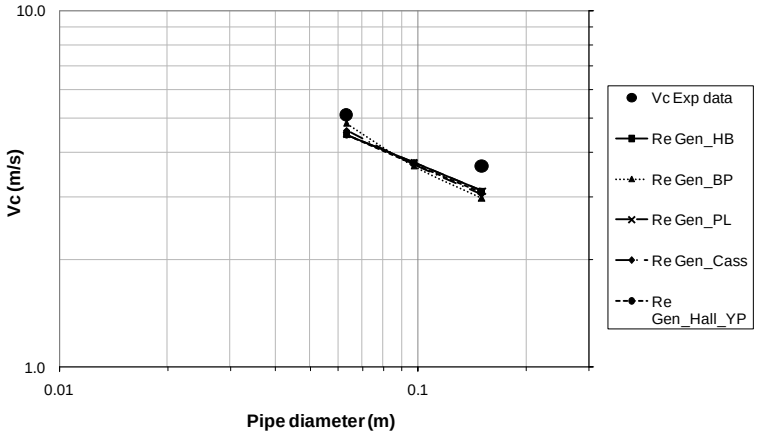

Diameter	Critical velocity (Exp) m/s	Vc Error values - Generalised Re				
		HB m/s	BP m/s	PL m/s	CASS m/s	HAL_YP m/s
150mm	3.655	3.122	2.980	3.122	3.060	3.094
		-14.6%	-18.5%	-14.6%	-16.3%	-15.34%
100mm		3.755	3.674	3.755	3.703	3.718
63mm	5.093	4.505	4.847	4.505	4.627	4.482
		-11.5%	-4.8%	-11.5%	-9.2%	-12.0%
	Ave	-13.1%	-11.6%	-13.1%	-12.7%	-13.7%

Figure G.12 Transitional velocity and average % error for 8% CMC using the Generalised Reynolds number – all rheologies

Hedström intersection method

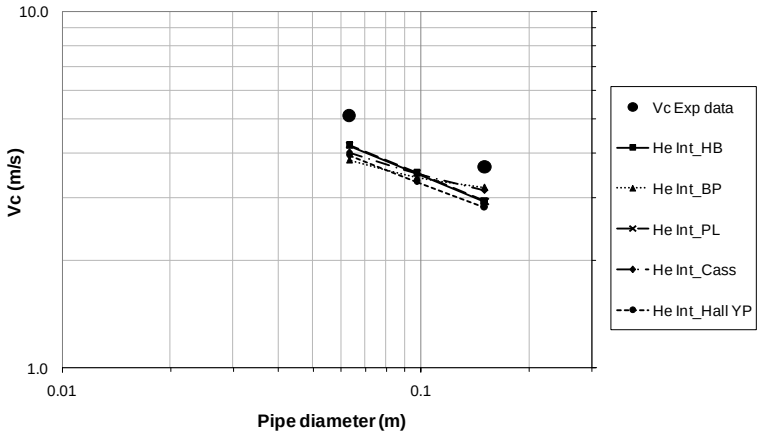

Diameter	Critical velocity (Exp) m/s	Vc Error values - He Intersection				
		HB m/s	BP m/s	PL m/s	CASS m/s	HAL_YP m/s
150mm	3.655	2.925	3.212	2.932	3.154	2.822
		-20.0%	-12.1%	-19.8%	-13.7%	-22.80%
100mm		3.514	3.435	3.527	3.521	3.333
63mm	5.093	4.208	3.838	4.232	4.034	3.951
		-17.4%	-24.6%	-16.9%	-20.8%	-22.4%
	Ave	-18.7%	-18.4%	-18.3%	-17.2%	-22.6%

Figure G.13 Transitional velocity and average % error for 8% CMC using the Hedström intersection method – all rheologies

Ryan & Johnson criterion

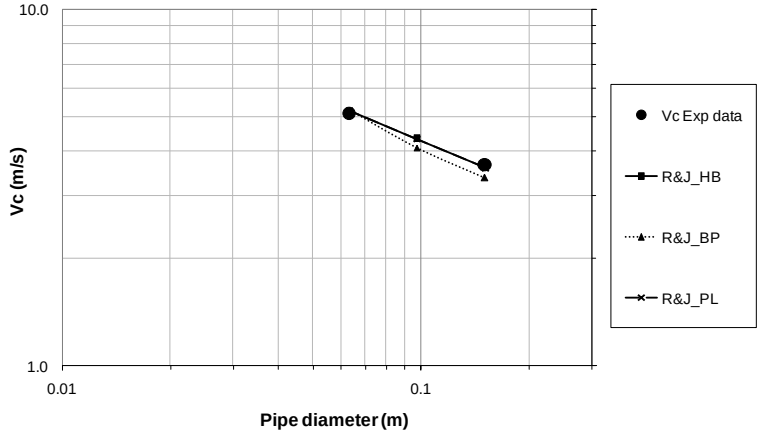

Diameter	Critical velocity (Exp) m/s	Vc Error values - R&J		
		HB m/s	BP m/s	PL m/s
150mm	3.655	3.604	3.367	3.604
		-1.4%	-7.9%	-1.4%
100mm		4.336	4.092	4.336
63mm	5.093	5.202	5.236	5.202
		2.2%	2.8%	2.2%
	Ave	0.4%	-2.5%	0.4%

Figure G.14 Transitional velocity and average % error for 8% CMC using the Ryan & Johnson criterion – all rheologies

Newtonian Approximation

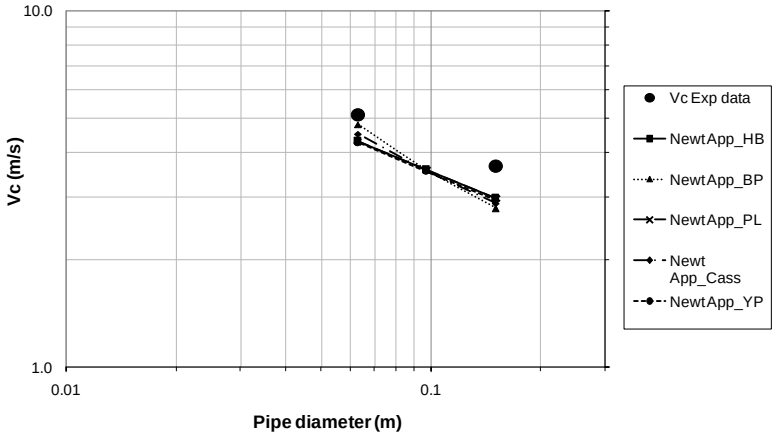

Diameter	Critical velocity (Exp) m/s	Vc Error values - Newt Approx				
		HB m/s	BP m/s	PL m/s	CASS m/s	HAL_YP m/s
150mm	3.655	2.982	2.792	2.982	2.886	2.932
		-18.4%	-23.6%	-18.4%	-21.0%	-19.77%
100mm		3.587	3.577	3.587	3.565	3.536
63mm	5.093	4.304	4.805	4.304	4.519	4.276
		-15.5%	-5.7%	-15.5%	-11.3%	-16.0%
	Ave	-16.9%	-14.6%	-16.9%	-16.1%	-17.9%

Figure G.15 Transitional velocity and average % error for 8% CMC using the Newtonian Approximation technique – all rheologies

Torrance

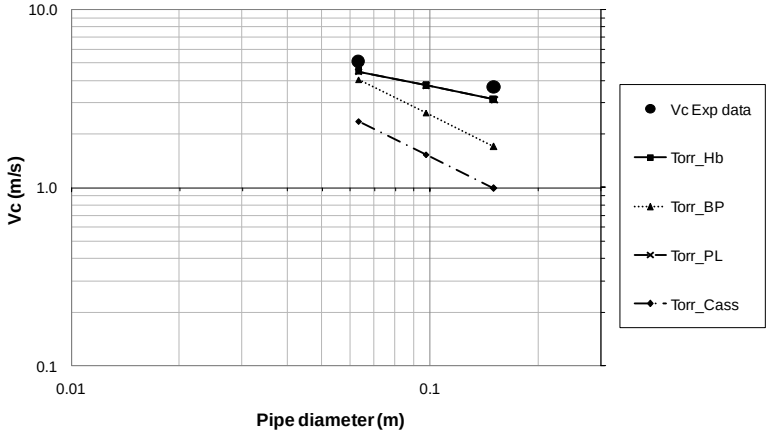

Diameter	Critical velocity (Exp) m/s	Vc Error values - Torrance			
		HB m/s	BP m/s	PL m/s	CASS m/s
150mm	3.655	3.122	1.701	3.122	0.991
		-14.6%	-53.5%	-14.6%	-72.9%
100mm		3.755	2.636	3.755	1.535
63mm	5.093	4.505	4.060	4.505	2.365
		-11.5%	-20.3%	-11.5%	-53.6%
	Ave	-13.1%	-36.9%	-13.1%	-63.2%

Figure G.16 Transitional velocity and average % error for 8% CMC using the Torrance criterion – all rheologies

Hallbom

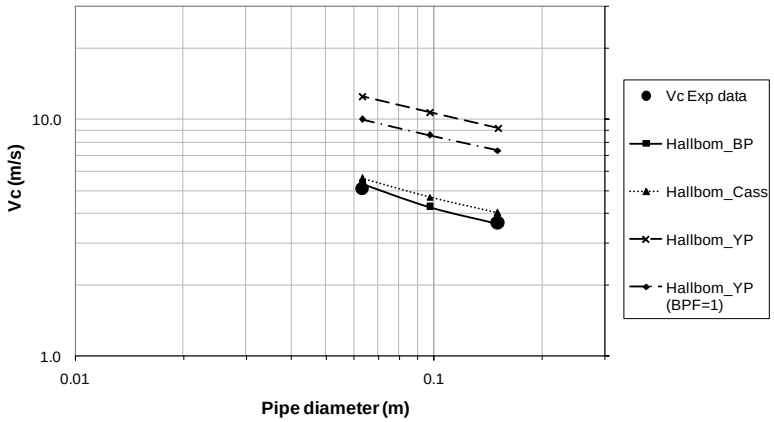

Diameter	Critical velocity (Exp) m/s	Vc Error values - Hallbom Trans			
		BP m/s	CASS m/s	HAL_YP m/s	HAL_YP (BPF=1) m/s
150mm	3.655	3.629	4.033	9.211	7.398
		-0.7%	10.4%	152.03%	102.43%
100mm		4.266	4.700	10.718	8.584
63mm	5.093	5.349	5.653	12.509	9.990
		5.0%	11.0%	145.6%	96.2%
	Ave	2.2%	10.7%	148.8%	99.3%

Figure G.17 Transitional velocity and average % error for 8% CMC using the Hallbom criterion – all rheologies

One rheology plotted for all techniques

Power law

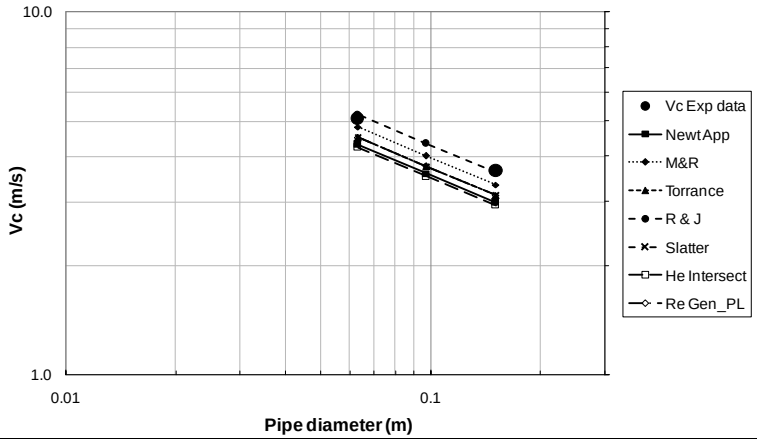

	Diameter m	Critical velocity (Exp) m/s	Critical velocity Error values - PL - All Techniques						
			Newt App m/s	M & R m/s	Torr/ Clapp m/s	Ryan & John m/s	Slatter m/s	Intersect m/s	Re_Gen m/s
150mm	0.1506	3.655	2.982	3.337	3.122	3.604	3.122	2.932	3.122
			-18.4%	-8.7%	-14.6%	-1.4%	-14.6%	-19.8%	-14.6%
100mm	0.09717		3.587	4.014	3.755	4.336	3.755	3.527	3.755
63mm	0.06308	5.093	4.304	4.816	4.505	5.202	4.505	4.232	4.505
			-15.5%	-5.4%	-11.5%	2.2%	-11.5%	-16.9%	-11.5%
		Ave	-16.9%	-7.1%	-13.1%	0.4%	-13.1%	-18.3%	-13.1%

Figure G.18 Transitional velocity and average % error for 8% CMC (power law rheology – all techniques)

Appendix H. Turbulent flow analysis and results: kaolin

The results for the 10% and 15% kaolin turbulent flow predictions are presented here.

10% kaolin

One technique plotted for all rheologies

Wilson & Thomas

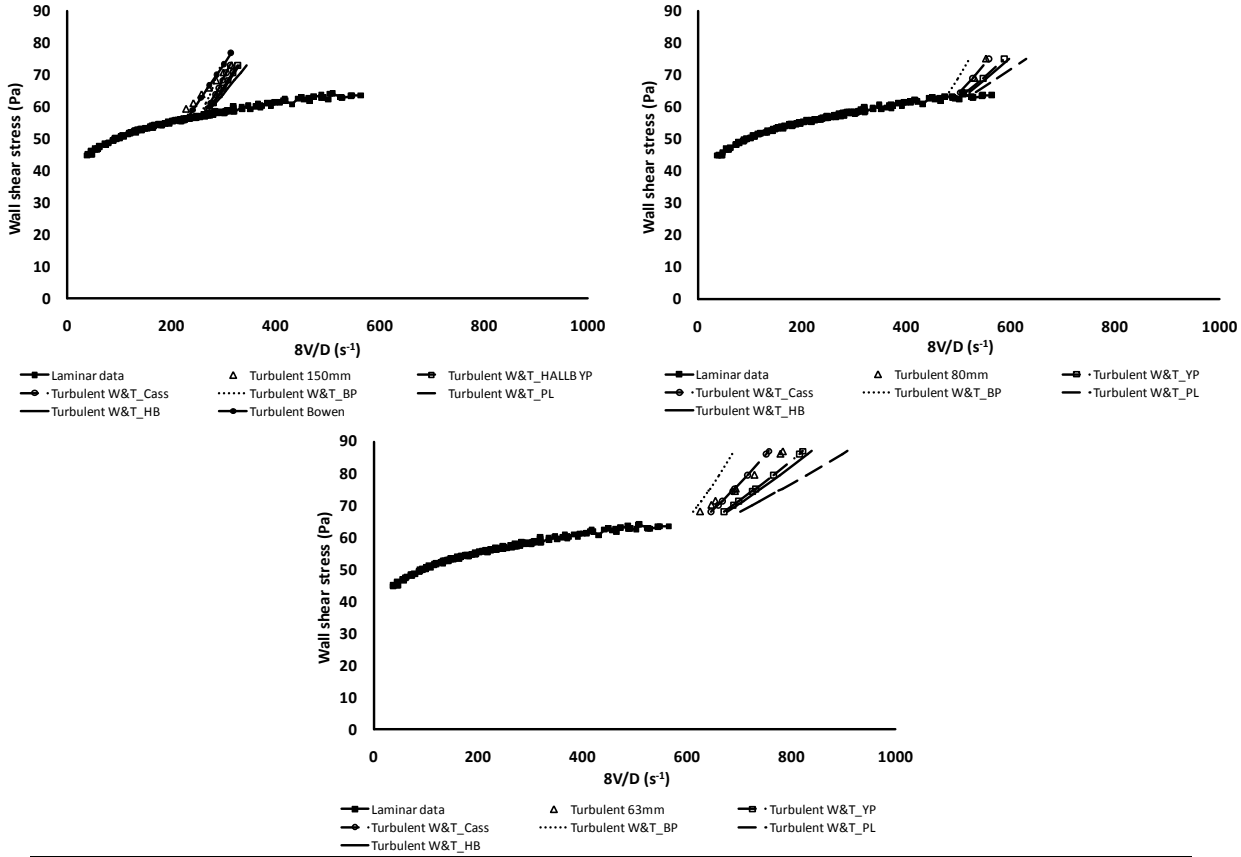

(8V/D) RMSE values - W&T(PRW) method						
Pipe diameter	HB	BP	PL	CASS	HALL_YP(SW)	BOWEN (To)
100mm	11.6%	6.4%	14.4%	7.9%	10.8%	3.2%
80mm	4.6%	5.9%	8.7%	1.2%	3.3%	N/A
63mm	7.4%	5.6%	12.7%	1.7%	5.9%	N/A
Ave	7.9%	6.0%	11.9%	3.6%	6.7%	3.2%

Figure H.1 Turbulent flow predictions and average % error for 10% kaolin using the Wilson & Thomas method – all rheologies

Slatter

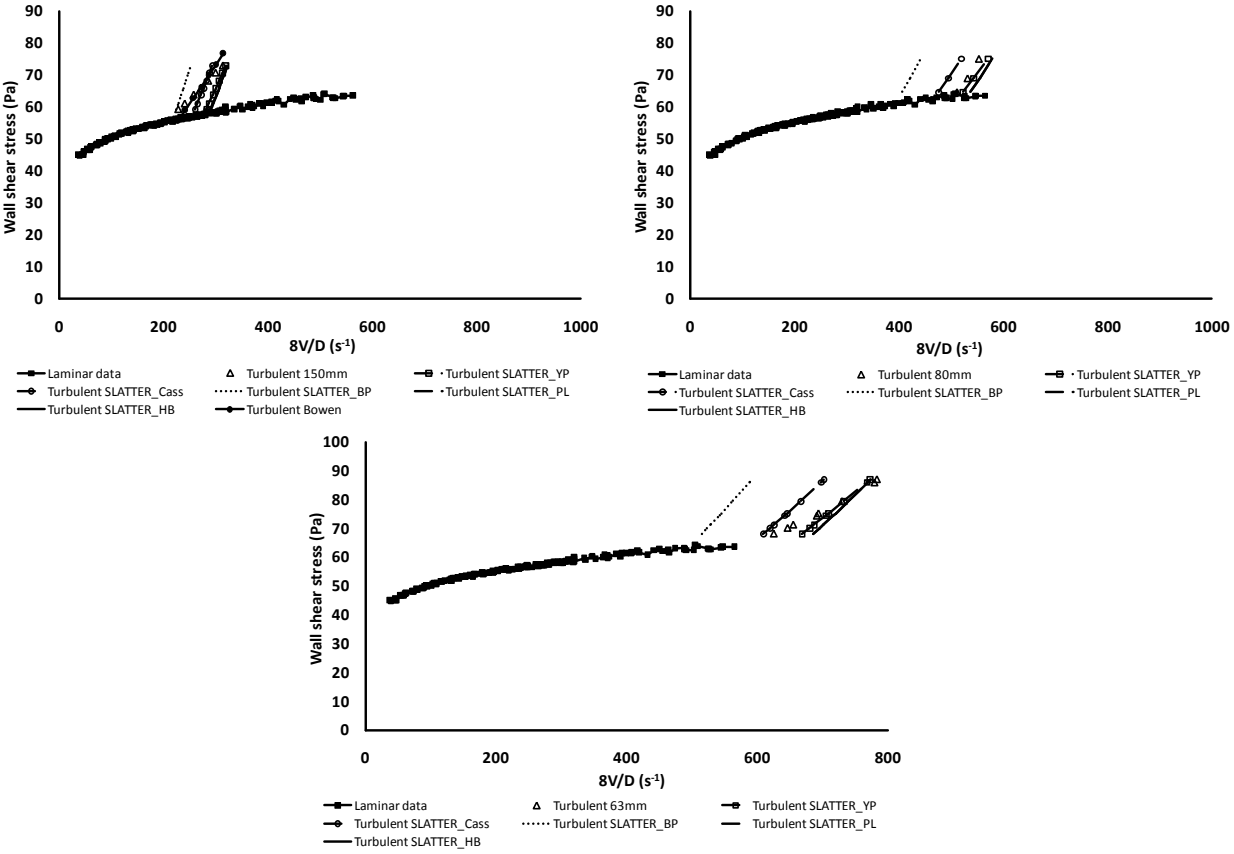

(8V/D) RMSE values - Slatter method						
Pipe diameter	HB	BP	PL	CASS	HALL_YP	BOWEN (To)
100mm	13.9%	11.3%	14.0%	6.2%	11.4%	3.2%
80mm	4.9%	20.4%	4.9%	6.6%	2.6%	N/A
63mm	5.5%	20.3%	5.5%	5.7%	3.6%	N/A
Ave	8.1%	17.4%	8.1%	6.2%	5.9%	3.2%

Figure H.2 Turbulent flow predictions and average % error for 10% kaolin using the Slatter method – all rheologies

Hallbom: Smooth wall turbulence – Modified Wilson & Thomas

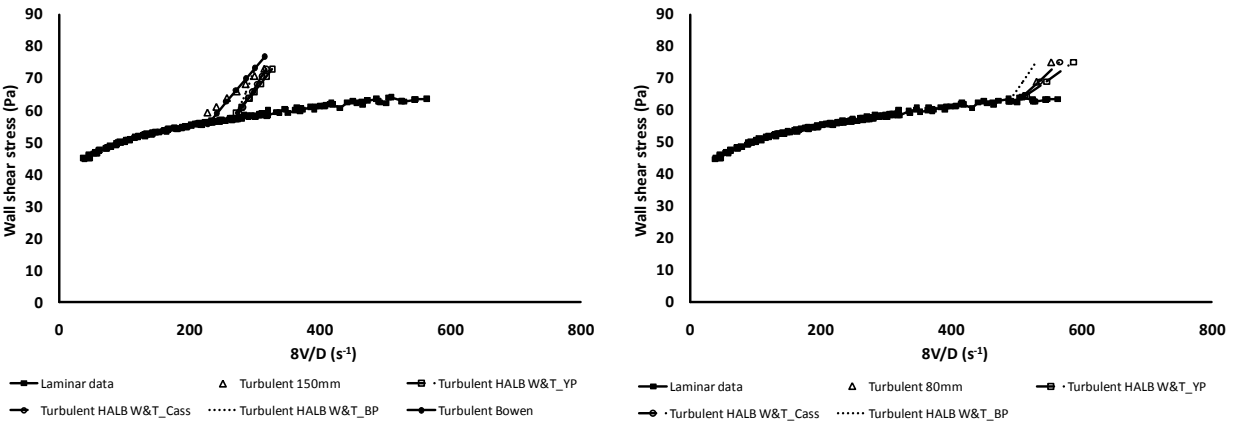

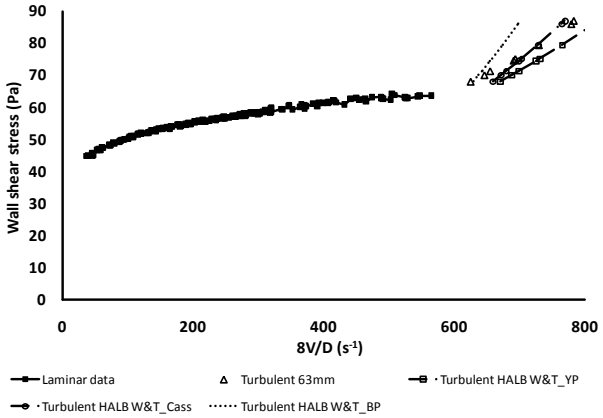

(8V/D) RMSE values - Hallbom_Mod W&T (SW)				
Pipe diameter	BP	CASS	YP	BOWEN (To)
100mm	8.1%	9.9%	10.8%	3.2%
80mm	3.6%	1.2%	3.3%	N/A
63mm	3.7%	2.6%	5.9%	N/A
Ave	5.1%	4.6%	6.7%	3.2%

Figure H.3 Turbulent flow predictions and average % error for 10% kaolin using the Hallbom modified Wilson & Thomas method – all rheologies

Hallbom: Partially rough wall turbulence (Pseudofluid) - Using Nikuradse

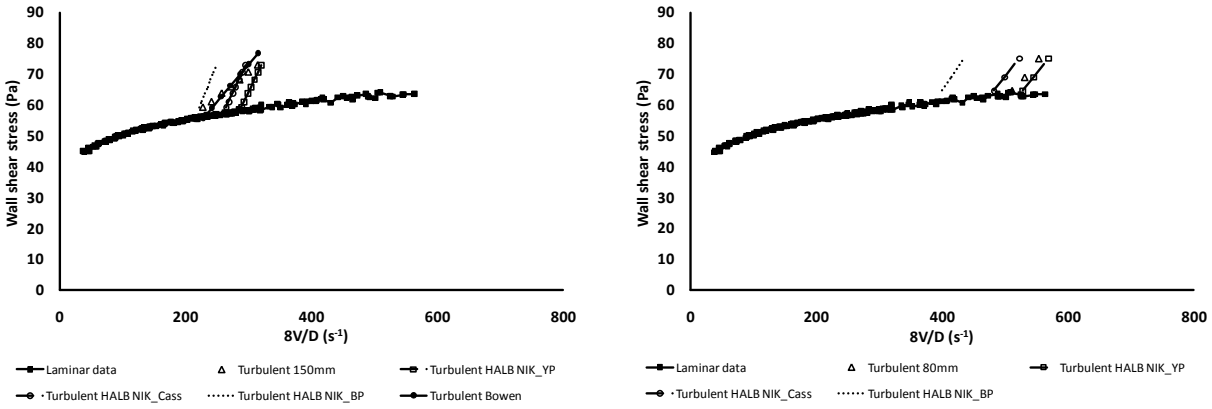

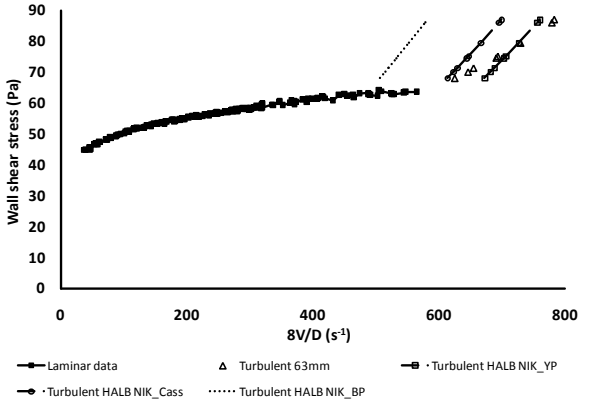

(8V/D) RMSE values - Hallbom Pseudo fluid NIK				
Pipe diameter	BP	CASS	YP	BOWEN (To)
100mm	12.7%	6.7%	12.9%	3.2%
80mm	21.7%	5.8%	2.9%	N/A
63mm	21.6%	5.3%	3.7%	N/A
Ave	18.7%	5.9%	6.5%	3.2%

Figure H.4 Turbulent flow predictions and average % error for 10% kaolin using the Hallbom Nikuradse pseudofluid method – all rheologies

Newtonian approximation

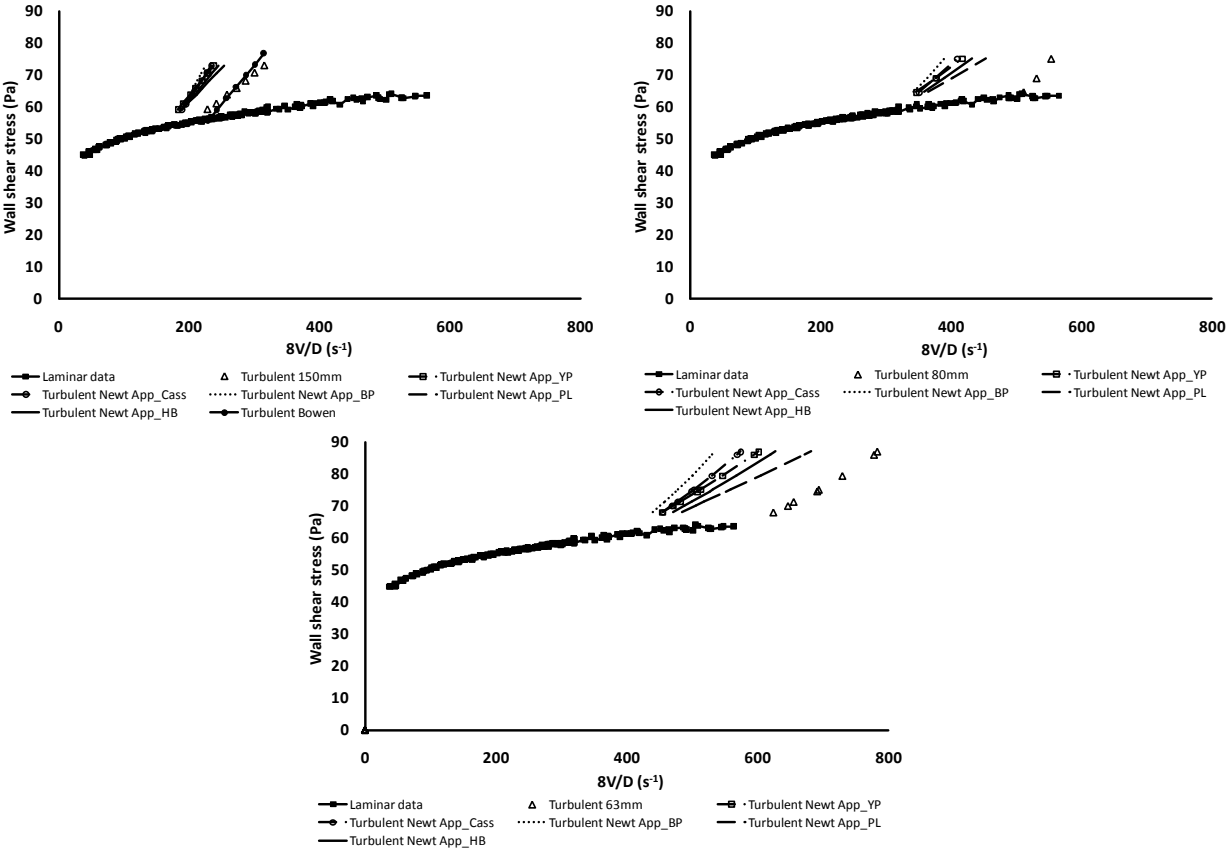

(8V/D) RMSE values - Newtonian Approximation method						
Pipe diameter	HB	BP	PL	CASS	HALL_YP	BOWEN (To)
100mm	20.2%	23.7%	18.7%	22.0%	22.7%	3.2%
80mm	26.1%	31.3%	23.7%	28.8%	28.6%	N/A
63mm	23.7%	30.6%	20.3%	27.4%	26.4%	N/A
Ave	23.3%	28.5%	20.9%	26.1%	25.9%	3.2%

Figure H.5 Turbulent flow predictions and average % error for 10% kaolin using the Newtonian approximation method – all rheologies

Torrance

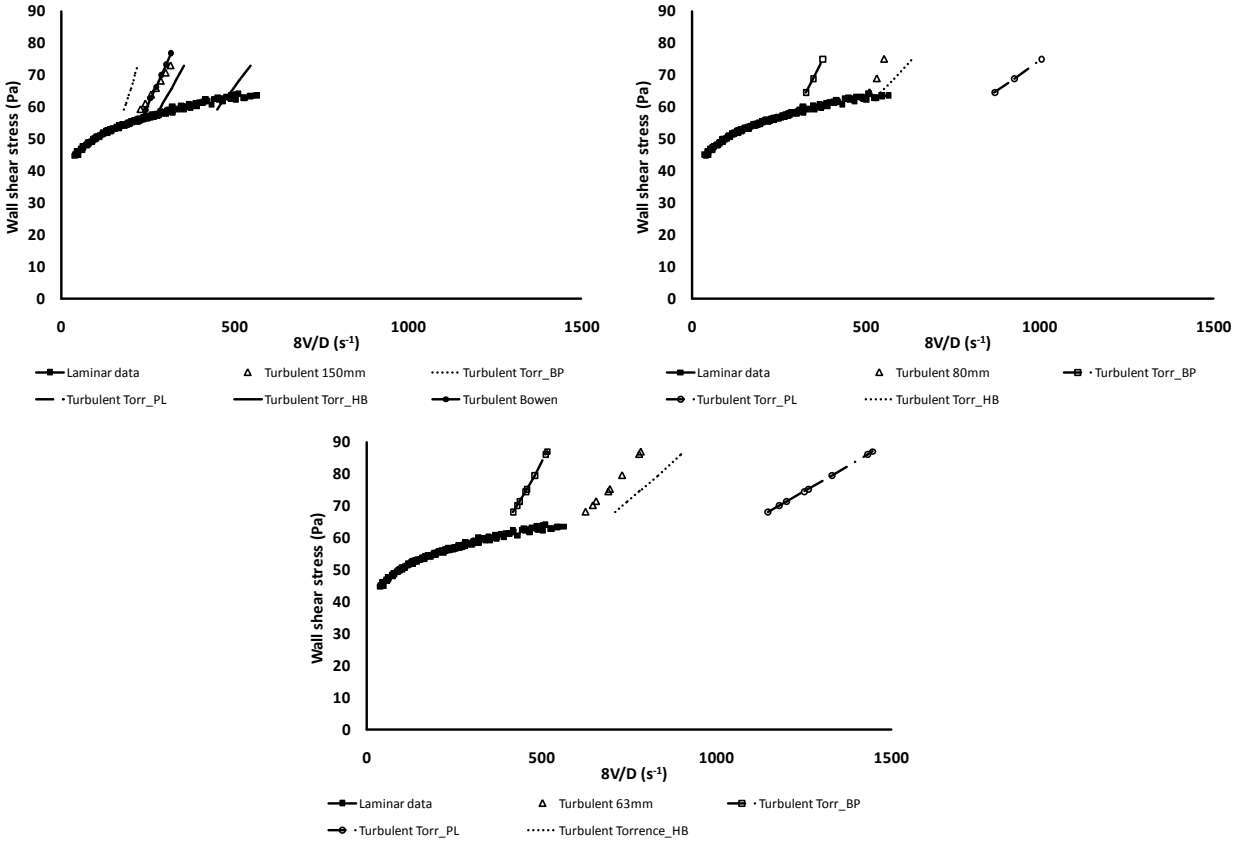

(8V/D) RMSE values - Torrance method				
Pipe diameter	HB	BP	PL	BOWEN (To)
100mm	17.2%	26.1%	83.4%	3.2%
80mm	9.9%	34.2%	75.4%	N/A
63mm	13.5%	33.8%	82.3%	N/A
Ave	13.5%	31.4%	80.4%	3.2%

Figure H.6 Turbulent flow predictions and average % error for 10% kaolin using the Torrance method – all rheologies

One rheology plotted for all techniques

Bingham plastic

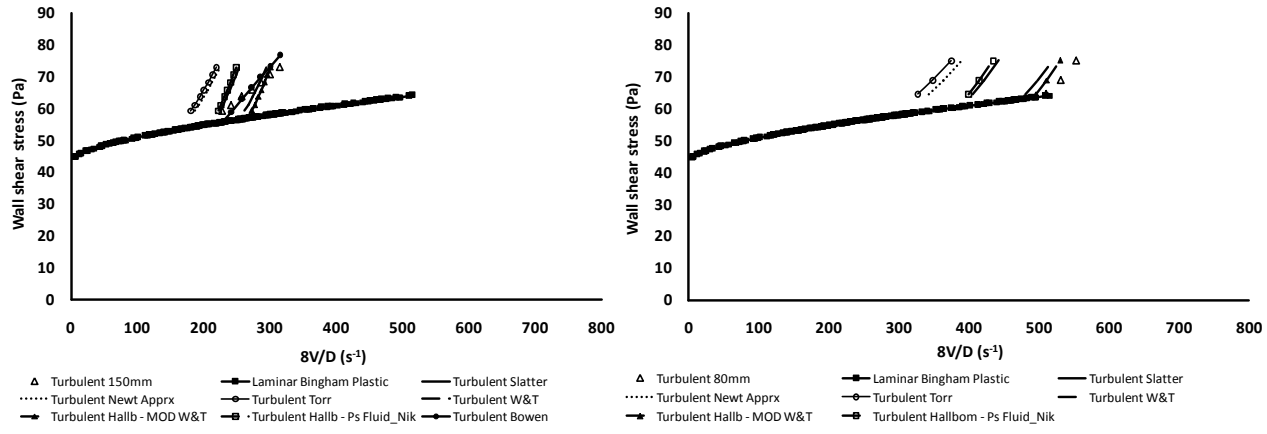

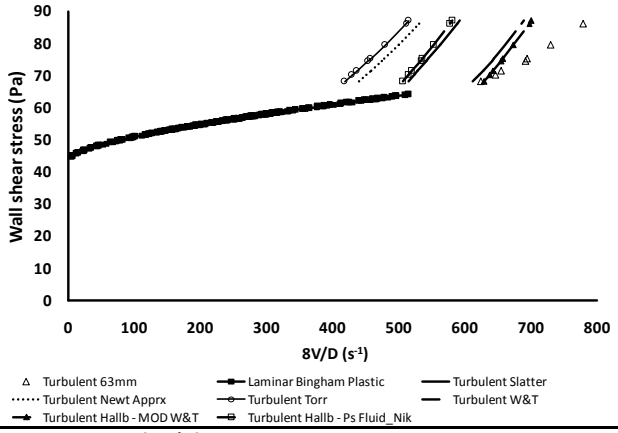

(8V/D) RMSE values - Bingham Plastic								
Pipe diameter	W&T	NEWT	TORR	D&M	SLATT	BOWEN (To)	MOD_W&T	Ps Fld_Nik
150mm	6.4%	23.7%	26.1%	N/A	11.3%	3.2%	8.1%	12.7%
80mm	5.9%	31.3%	34.2%	N/A	20.4%	N/A	3.6%	21.7%
63mm	5.6%	30.6%	33.8%	N/A	20.3%	N/A	3.7%	21.6%
Ave	6.0%	28.5%	31.4%	N/A	17.4%	3.2%	5.1%	18.7%

Figure H.7 10% kaolin turbulent flow predictions and average % error using the Bingham plastic rheology – all techniques

Power law

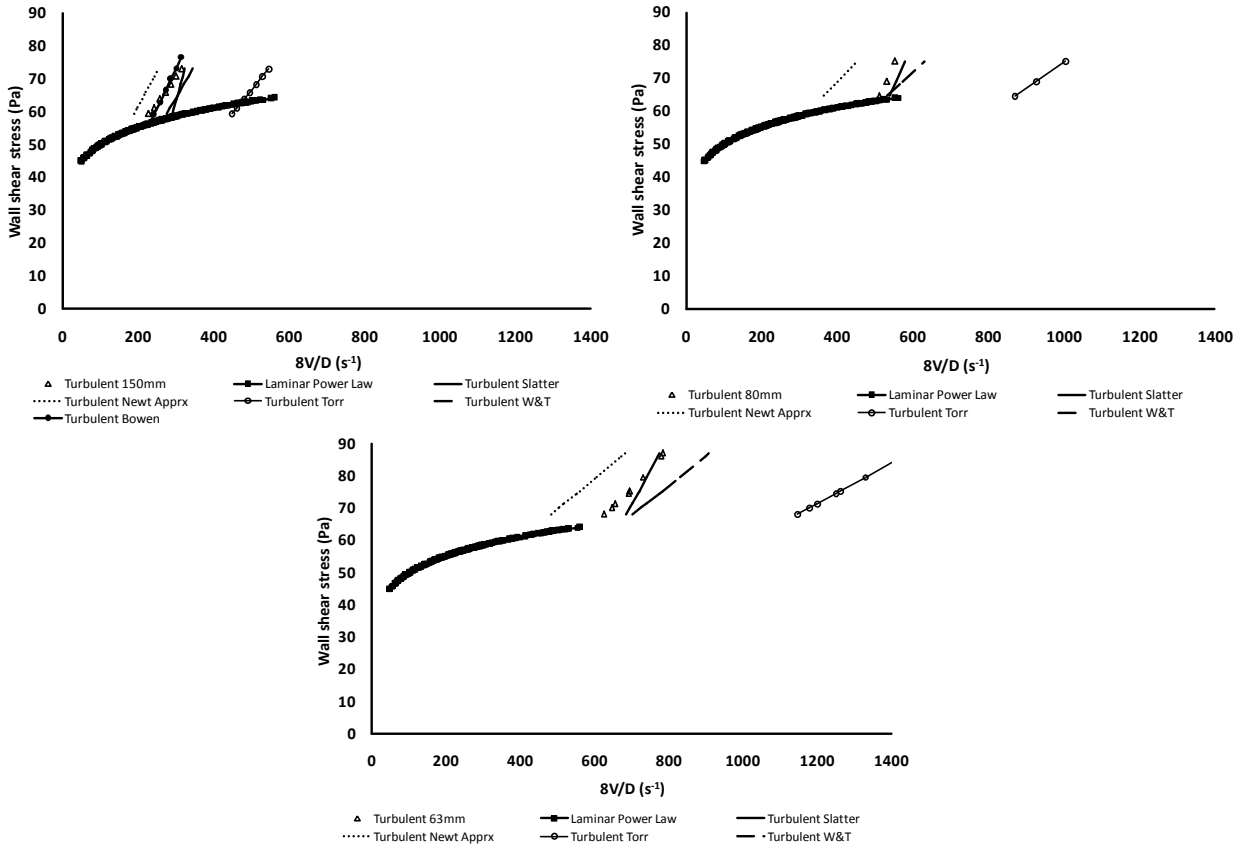

(8V/D) RMSE values - Power Law						
Pipe diameter	W&T	NEWT	TORR	D&M	SLATT	BOWEN (To)
150mm	14.4%	18.7%	83.4%	N/A	14.0%	3.2%
80mm	8.7%	23.7%	75.4%	N/A	4.9%	N/A
60mm	12.7%	20.3%	82.3%	N/A	5.5%	N/A
Ave	11.9%	20.9%	80.4%	N/A	8.1%	3.2%

Figure H.8 10% kaolin turbulent flow predictions and average % error using the power law rheology – all techniques

Herschel-Bulkley

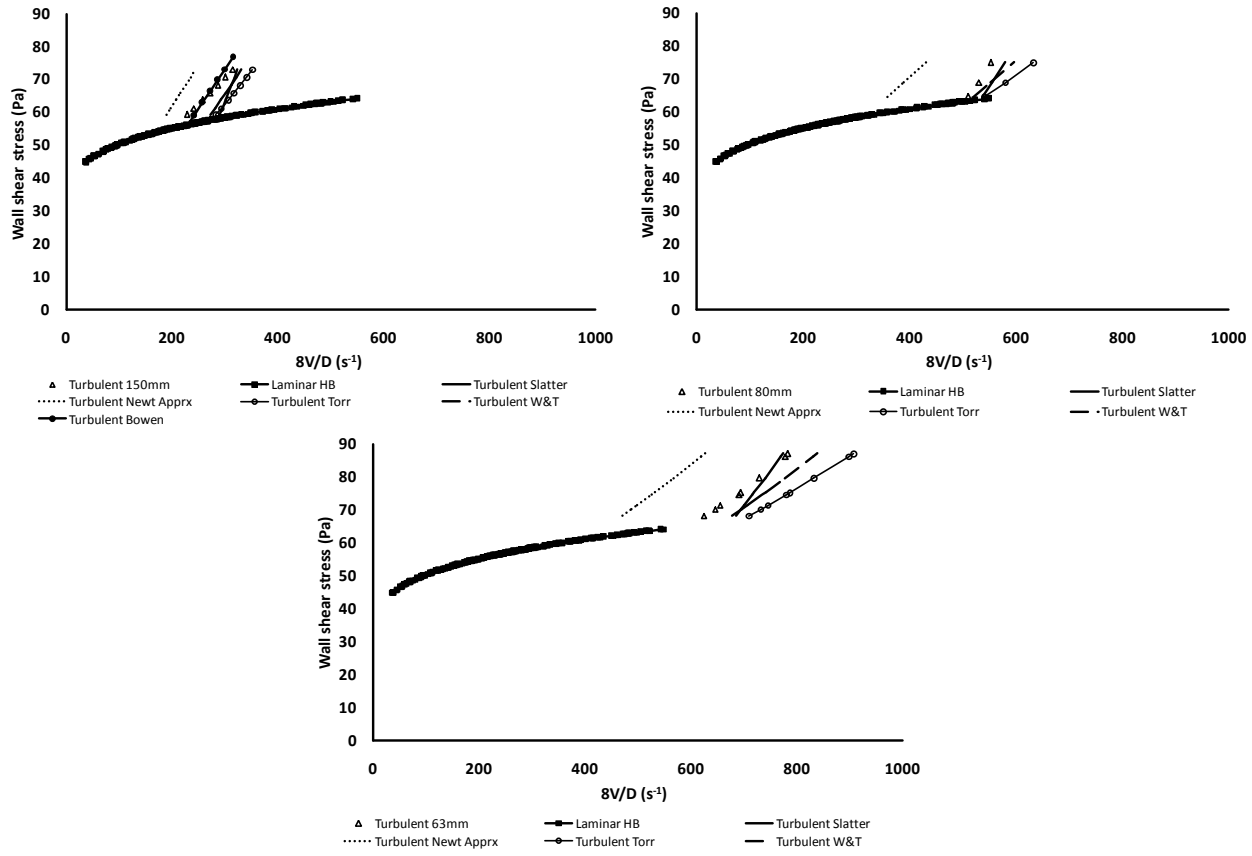

(8V/D) RMSE values - Herschelle-Bulkley						
Pipe diameter	W&T	NEWT	TORR	D&M	SLATT	BOWEN (To)
150mm	11.6%	20.2%	17.2%	N/A	13.9%	3.2%
80mm	4.6%	26.1%	9.9%	N/A	4.9%	N/A
63mm	7.4%	23.7%	13.5%	N/A	5.5%	N/A
Ave	7.9%	23.3%	13.5%	N/A	8.1%	3.2%

Figure H.9 10% kaolin turbulent flow predictions and average % error using the Herschel-Bulkley rheology – all techniques

Casson

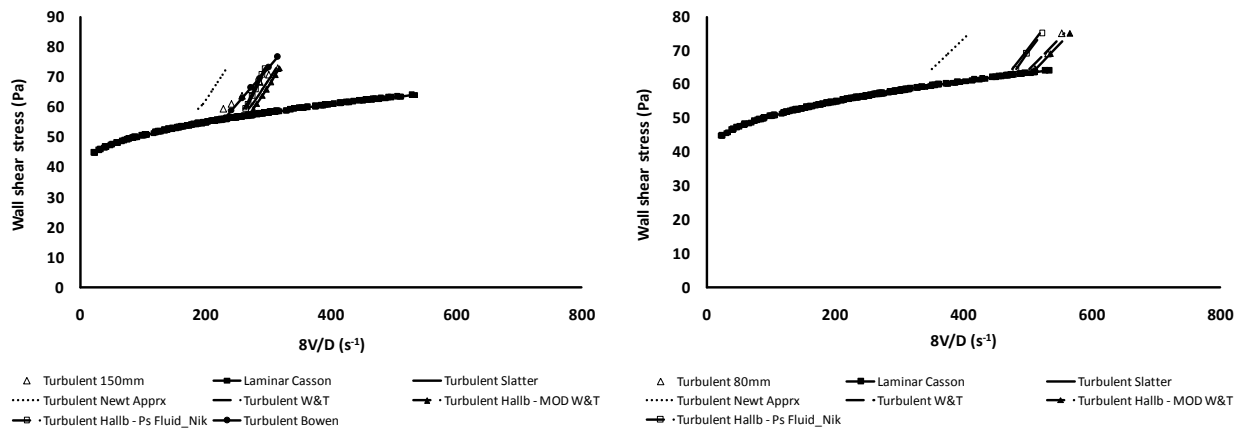

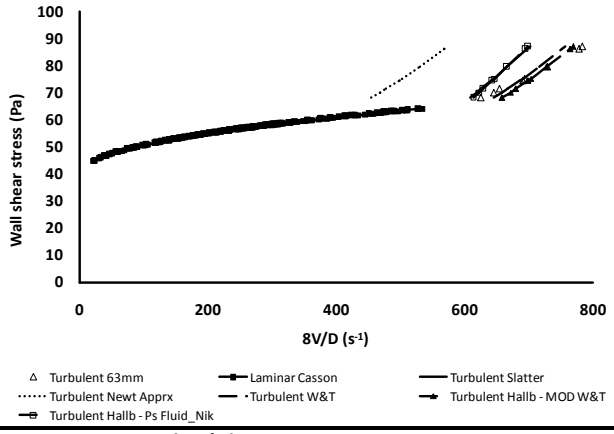

(8V/D) RMSE values - Casson								
Pipe diameter	W&T	NEWT	TORR	D&M	SLATT	BOWEN (To)	MOD_W&T	Ps Fld_Nik
150mm	7.9%	22.0%	N/A	N/A	6.2%	3.2%	9.9%	6.7%
80mm	1.2%	28.8%	N/A	N/A	6.6%	N/A	1.2%	5.8%
63mm	1.7%	27.4%	N/A	N/A	5.7%	N/A	2.6%	5.3%
Ave	3.6%	26.1%	N/A	N/A	6.2%	3.2%	4.6%	5.9%

Figure H.10 10% kaolin turbulent flow predictions and average % error using the Casson rheology – all techniques

Hallbom yield plastic

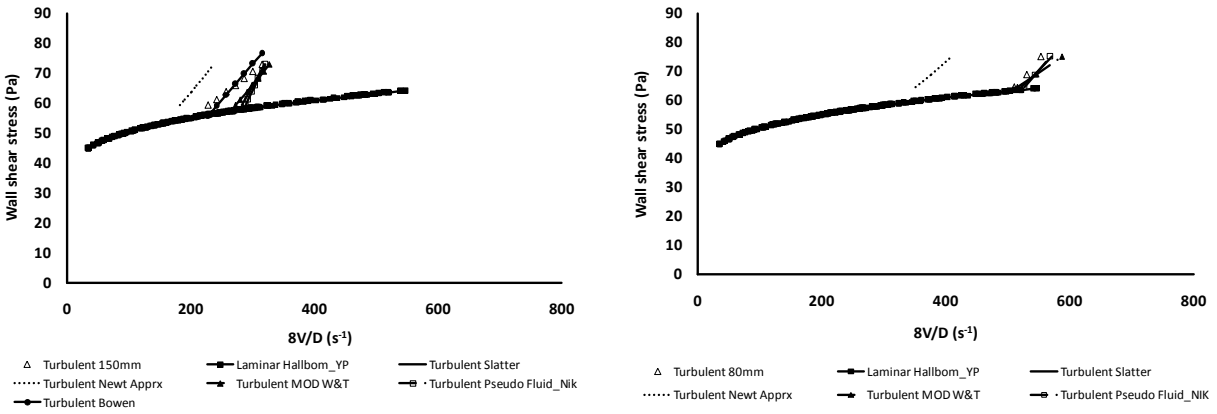

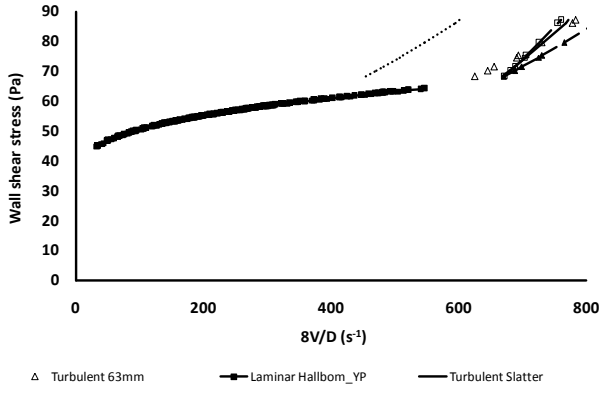

(8V/D) RMSE values - Hallbom_Yield plastic					
Pipe diameter	MOD_W&T	NEWT	Ps Fld_Nik	SLATT	BOWEN (To)
150mm	10.8%	22.7%	12.9%	11.4%	3.2%
80mm	3.3%	28.6%	2.9%	2.6%	N/A
63mm	5.9%	26.4%	3.7%	3.6%	N/A
Ave	6.7%	25.9%	6.5%	5.9%	3.2%

Figure H.11 10% kaolin turbulent flow predictions and average % error using the Hallbom yield plastic rheology – all techniques

15% kaolin

One technique plotted for all rheologies

Wilson & Thomas

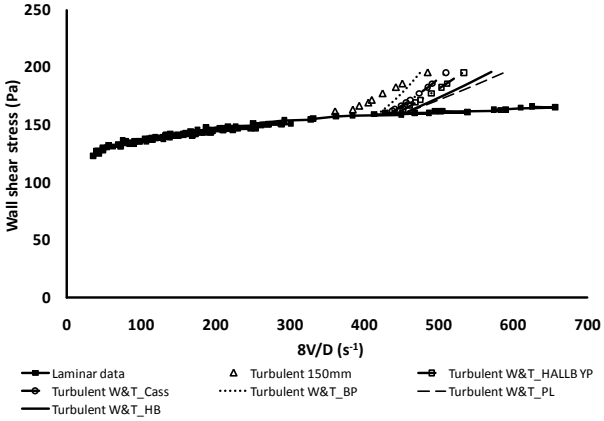

(8V/D) RMSE values - W&T(PRW) method					
Pipe diameter	HB	BP	PL	CASS	HALL_YP(SW)
100mm	20.7%	7.5%	22.8%	12.4%	15.9%
Ave	20.7%	7.5%	22.8%	12.4%	15.9%

Figure H.12 Turbulent flow predictions and average % error for 15% kaolin using the Wilson & Thomas method – all rheologies

Slatter

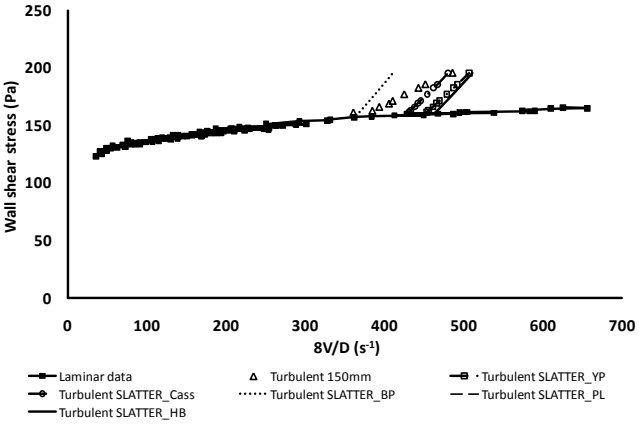

(8V/D) RMSE values - Slatter method					
Pipe diameter	HB	BP	PL	CASS	HALL_YP
150mm	16.1%	7.9%	16.1%	8.5%	14.2%
Ave	16.1%	7.9%	16.1%	8.5%	14.2%

Figure H.13 Turbulent flow predictions and average % error for 15% kaolin using the Slatter method – all rheologies

Hallbom: Smooth wall turbulence – Modified Wilson & Thomas

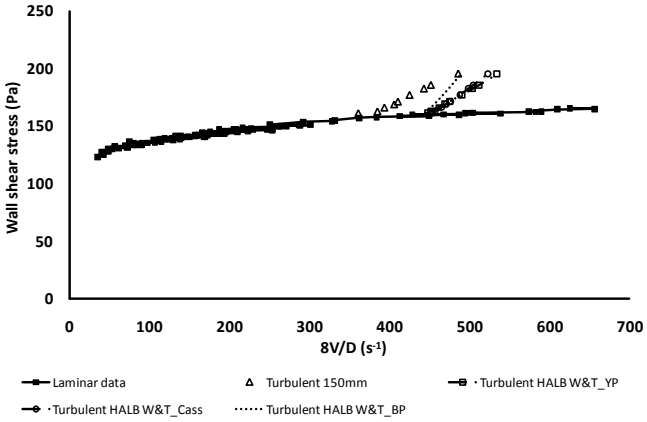

(8V/D) RMSE values - Hallb Mod W&T (SW)			
Pipe diameter	BP	CASS	YP
100mm	11.5%	15.7%	15.9%
Ave	11.5%	15.7%	15.9%

Figure H.14 Turbulent flow predictions and average % error for 15% kaolin using the Hallbom modified Wilson & Thomas – all rheologies

Hallbom: Partially rough wall turbulence (Pseudofluid) - Using Nikuradse

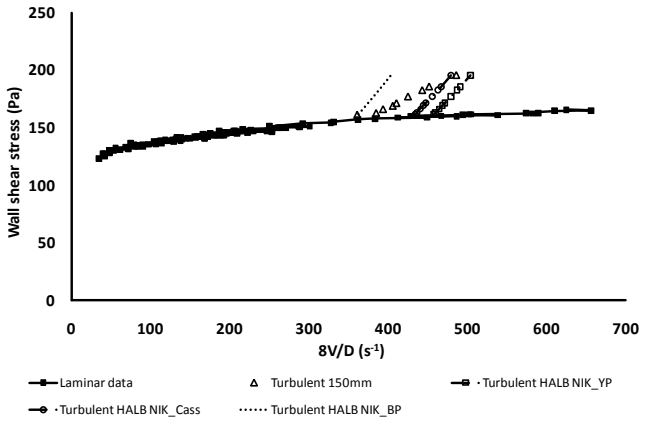

(8V/D) RMSE - Hallbom Pseudo fluid NIK			
Pipe diameter	BP	CASS	YP
100mm	9.0%	9.0%	14.5%
Ave	9.0%	9.0%	14.5%

Figure H.15 Turbulent flow predictions and average % error for 15% kaolin using the Hallbom Nikuradse pseudofluid method – all rheologies

Newtonian approximation

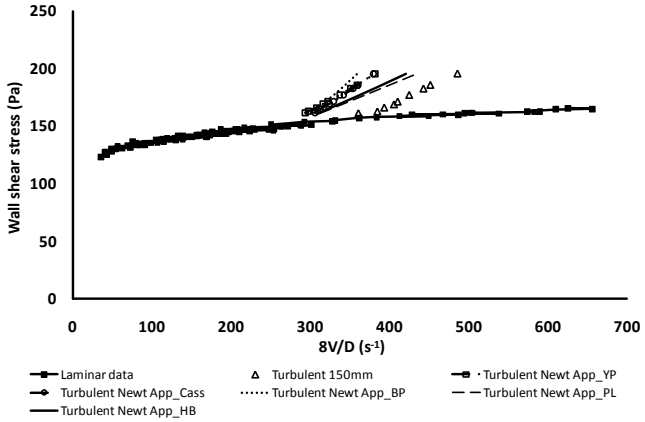

(8V/D) RMSE values - Newtonian Approximation method					
Pipe diameter	HB	BP	PL	CASS	HALL_YP
100mm	15.2%	22.1%	13.9%	19.5%	21.0%
Ave	15.2%	22.1%	13.9%	19.5%	21.0%

Figure H.16 Turbulent flow predictions and average % error for 15% kaolin using the Newtonian approximation method – all rheologies

Torrance

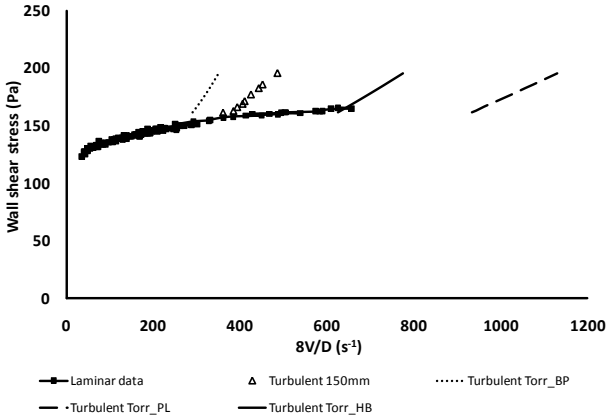

(8V/D) RMSE values - Torrance method			
Pipe diameter	HB	BP	PL
100mm	64.0%	24.4%	142.5%
Ave	64.0%	24.4%	142.5%

Figure H.17 Turbulent flow predictions and average % error for 15% kaolin using the Torrance method – all rheologies

One technique plotted for all rheologies

Bingham plastic

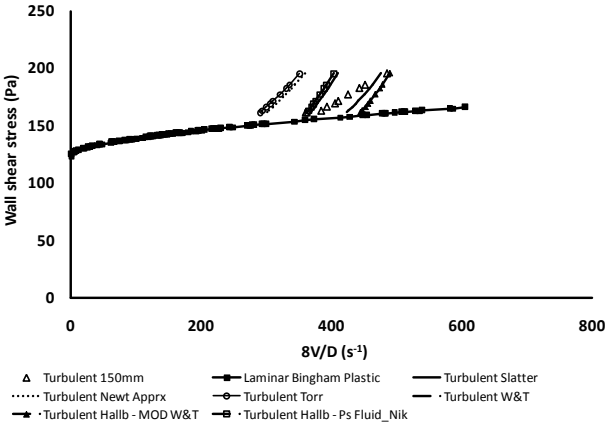

(8V/D) RMSE values - Bingham Plastic								
Pipe diameter	W&T	NEWT	TORR	D&M	SLATT	BOWEN (To)	MOD_W&T	Ps Fld_Nik
150mm	7.5%	22.1%	24.4%	N/A	7.9%	N/A	11.5%	9.0%
Ave	7.5%	22.1%	24.4%	N/A	7.9%	N/A	11.5%	9.0%

Figure H.18 15% kaolin turbulent flow predictions and average % error using the Bingham plastic rheology – all techniques

Power law

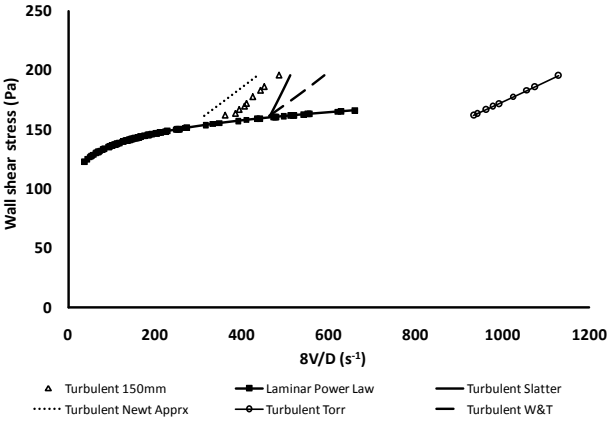

(8V/D) RMSE values - Power Law						
Pipe diameter	W&T	NEWT	TORR	D&M	SLATT	BOWEN (To)
150mm	22.8%	13.9%	142.5%	N/A	16.1%	N/A
Ave	22.8%	13.9%	142.5%	N/A	16.1%	N/A

Figure H.19 15% kaolin turbulent flow predictions and average % error using the power law rheology – all techniques

Herschel-Bulkley

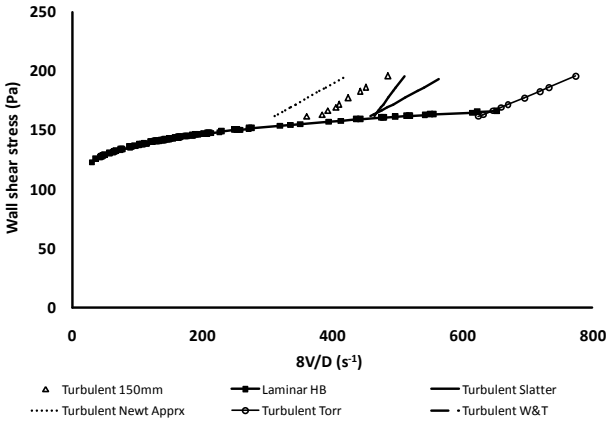

(8V/D) RMSE values - Herschelle-Bulkley						
Pipe diameter	W&T	NEWT	TORR	D&M	SLATT	BOWEN (To)
150mm	20.7%	15.2%	64.0%	N/A	16.1%	N/A
Ave	20.7%	15.2%	64.0%	N/A	16.1%	N/A

Figure H.20 15% kaolin turbulent flow predictions and average % error using the Herschel-Bulkley rheology – all techniques

Casson

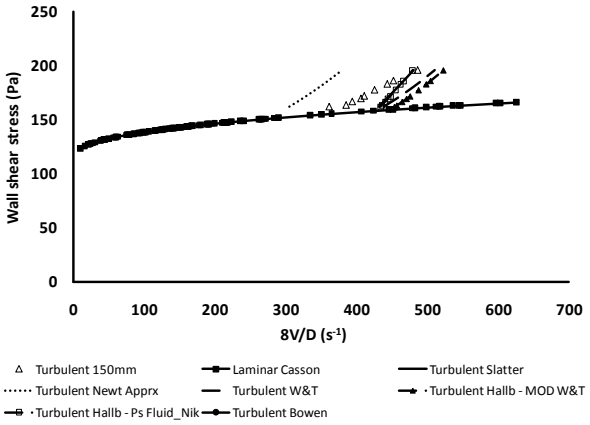

(8V/D) RMSE values - Casson								
Pipe diameter	W&T	NEWT	TORR	D&M	SLATT	BOWEN (To)	MOD_W&T	Ps Fld_Nik
150mm	12.4%	19.5%	N/A	N/A	8.5%	N/A	15.7%	9.0%
Ave	12.4%	19.5%	N/A	N/A	8.5%	N/A	15.7%	9.0%

Figure H.21 15% kaolin turbulent flow predictions and average % error using the Casson rheology – all techniques

Hallbom yield plastic

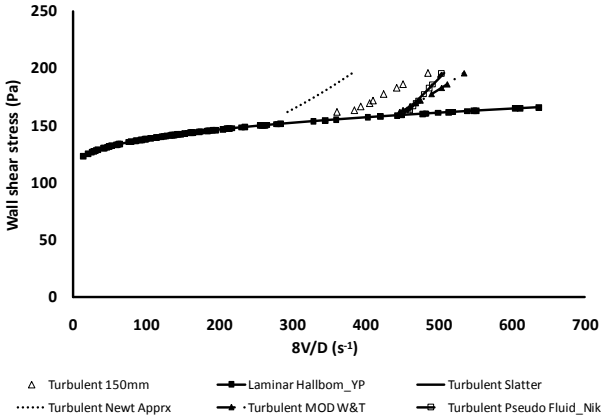

(8V/D) RMSE values - Hallbom_Yield plastic					
Pipe diameter	MOD_W&T	NEWT	Ps Fld_Nik	SLATT	BOWEN (To)
150mm	15.9%	21.0%	14.5%	14.2%	N/A
Ave	15.9%	21.0%	14.5%	14.2%	N/A

Figure H.22 15% kaolin turbulent flow predictions and average % error using the Hallbom yield plastic rheology – all techniques

Appendix I. Turbulent flow analysis and results: bentonite

The results for the 6% and 9% bentonite turbulent flow predictions are presented here.

6% bentonite

One technique plotted for all rheologies

Wilson & Thomas

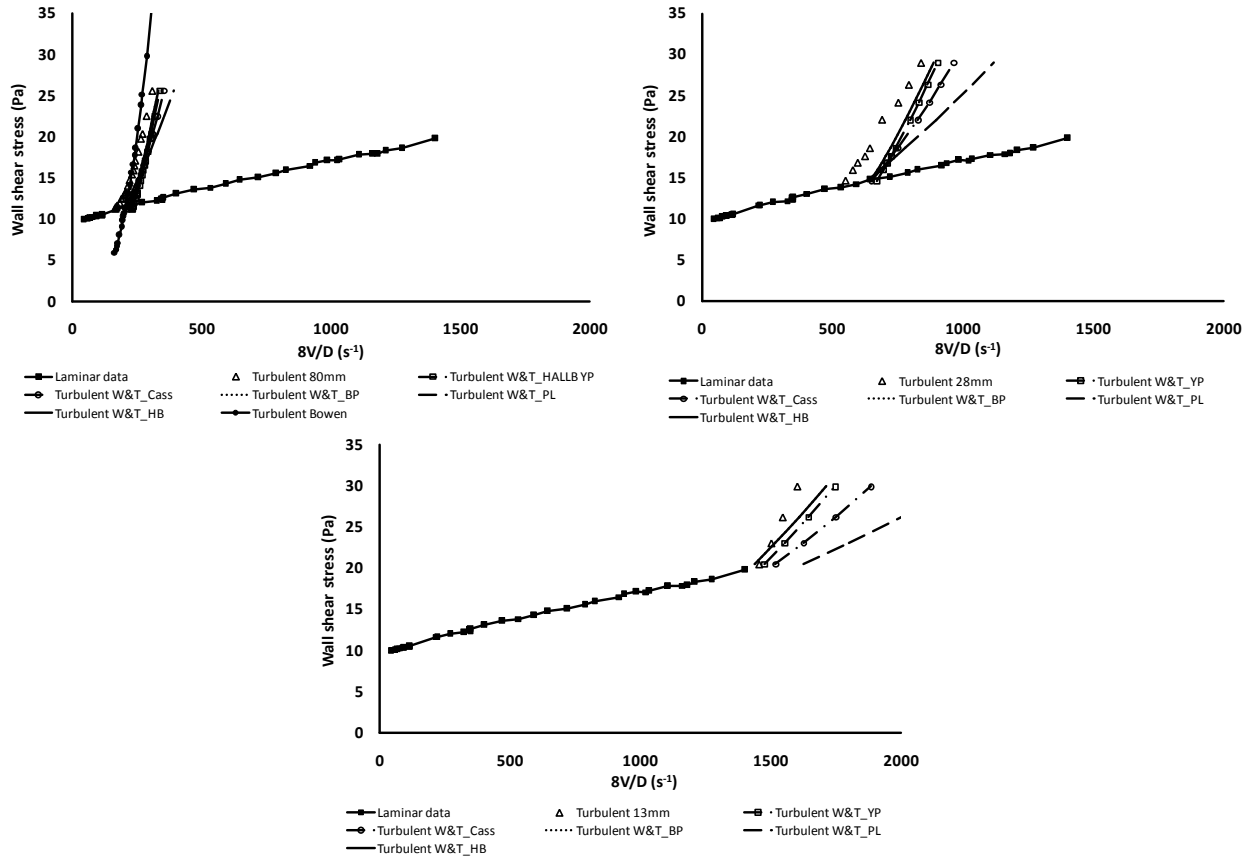

(8V/D) RMSE values - W&T(PRW) method						
Pipe diameter	HB	BP	PL	CASS	HALL_YP(SW)	BOWEN (To)
80mm	19.0%	19.0%	16.8%	19.3%	23.5%	22.7%
28mm	13.6%	13.6%	21.6%	17.5%	16.8%	N/A
13mm	2.1%	2.1%	20.4%	8.5%	7.1%	N/A
Ave	11.6%	11.6%	19.6%	15.1%	15.8%	22.7%

Figure I.1 6% bentonite turbulent flow predictions and average % error using the Wilson & Thomas method – all rheologies

Slatter

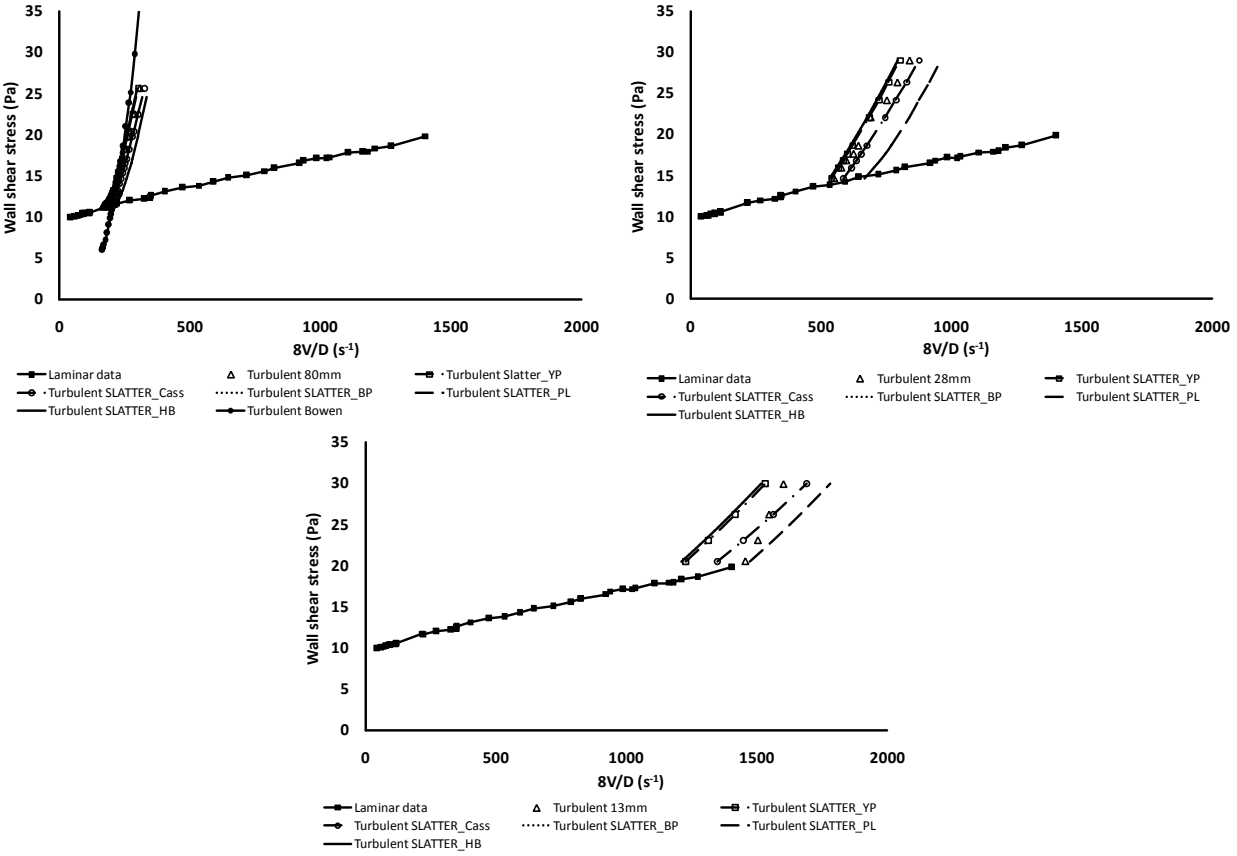

(8V/D) RMSE values - Slatter method						
Pipe diameter	HB	BP	PL	CASS	HALL_YP	BOWEN (To)
80mm	4.8%	4.8%	19.8%	10.2%	4.8%	22.7%
28mm	3.6%	3.7%	20.8%	5.9%	2.6%	N/A
13mm	13.2%	13.2%	4.4%	4.0%	12.2%	N/A
Ave	7.2%	7.2%	15.0%	6.7%	6.5%	22.7%

Figure I.2 6% bentonite turbulent flow predictions and average % error using the Slatter method – all rheologies

Hallbom: Smooth wall turbulence – Modified Wilson & Thomas

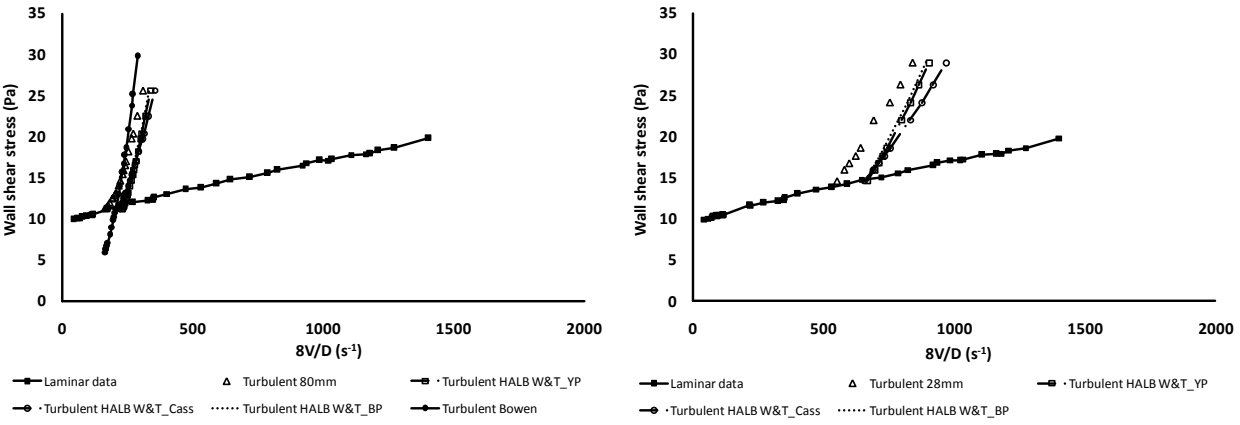

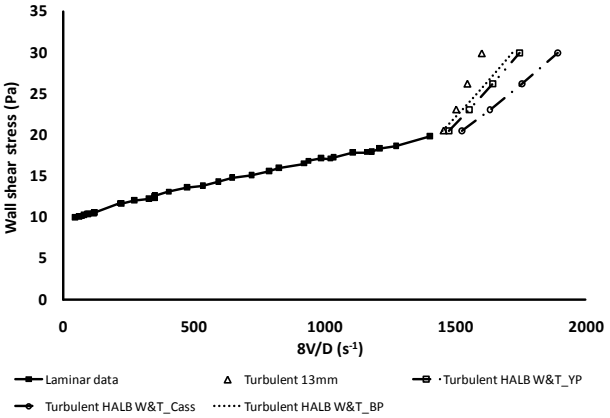

(8V/D) RMSE values - Hallb Mod W&T (SW)				
Pipe diameter	BP	CASS	YP	BOWEN (To)
80mm	22.1%	20.6%	23.5%	22.7%
28mm	15.0%	18.3%	16.8%	N/A
13mm	5.3%	12.7%	7.1%	N/A
Ave	14.1%	17.2%	15.8%	22.7%

Figure I.3 6% bentonite turbulent flow predictions and average % error using the Hallbom modified Wilson & Thomas method – all rheologies

Hallbom: Partially rough wall turbulence (pseudofluid) - Using Nikuradse

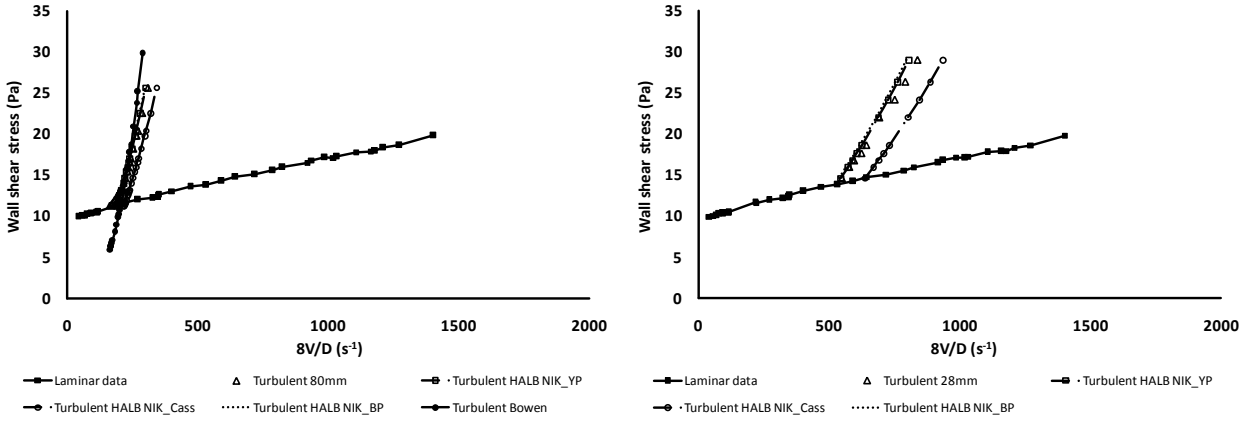

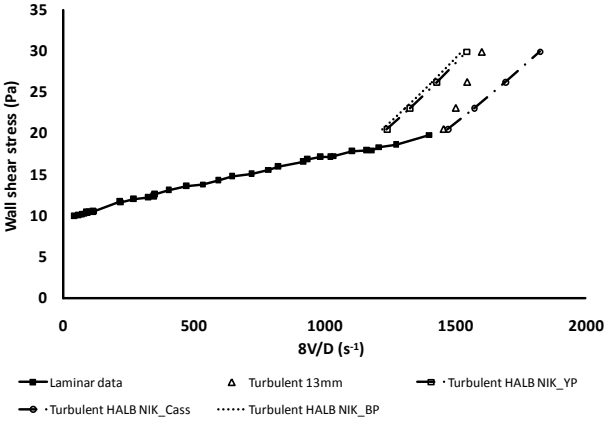

(8V/D) RMSE values - Hallbom_Nikuradse				
Pipe diameter	BP	CASS	YP	BOWEN (To)
80mm	4.9%	18.1%	5.0%	22.7%
28mm	3.0%	14.7%	1.9%	N/A
13mm	12.5%	5.1%	11.4%	N/A
Ave	6.8%	12.6%	6.1%	22.7%

Figure I.4 6% bentonite turbulent flow predictions and average % error using the Hallbom Nikuradse pseudo fluid method – all rheologies

Dodge & Metzner

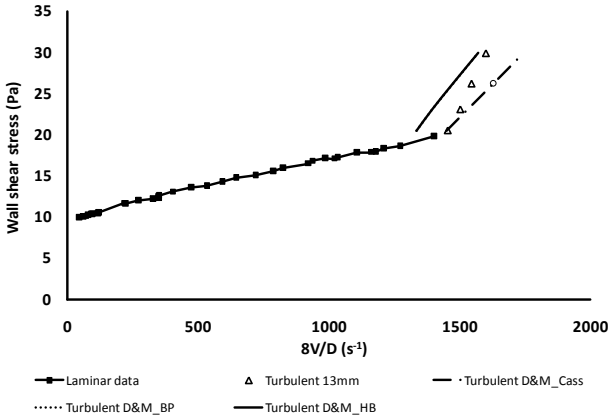

(8V/D) RMSE values - D&M method					
Pipe diameter	HB	BP	PL	CASS	BOWEN (To)
80mm	N/A	N/A	N/A	N/A	22.7%
28mm	N/A	N/A	N/A	N/A	N/A
13mm	6.6%	6.6%	N/A	2.6%	N/A
Ave	6.6%	6.6%	N/A	2.6%	22.7%

Figure I.5 6% bentonite turbulent flow predictions and average % error using the Dodge & Metzner method – all rheologies

Newtonian approximation

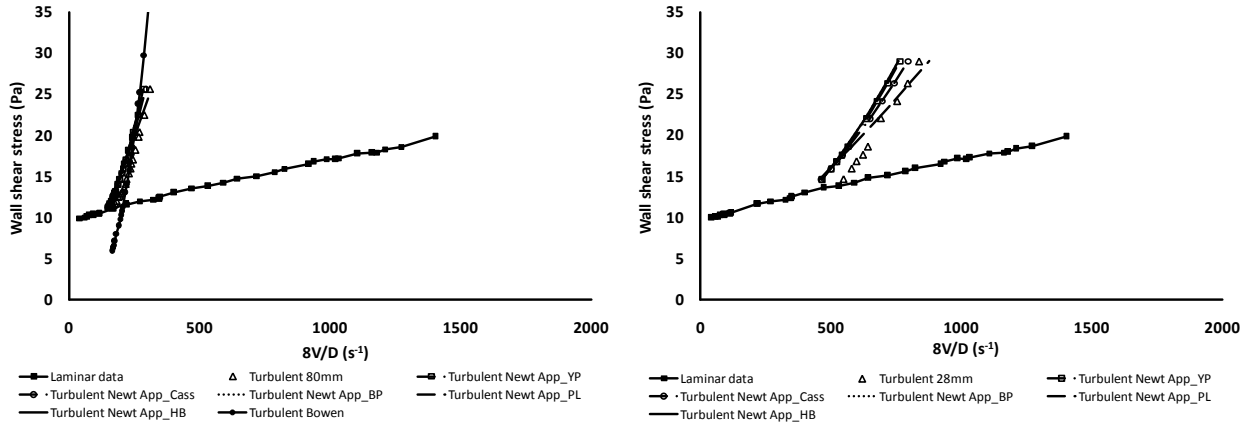

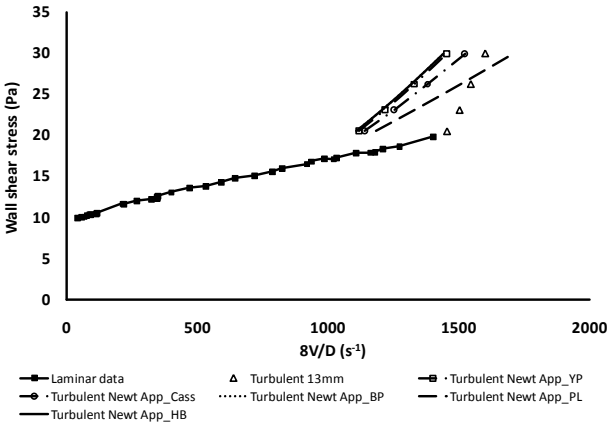

(8V/D) RMSE values - Newtonian Approximation						
Pipe diameter	HB	BP	PL	CASS	HALL_YP	BOWEN (To)
80mm	11.2%	11.2%	12.0%	11.6%	11.4%	22.7%
28mm	12.6%	12.6%	9.6%	11.3%	12.1%	N/A
13mm	19.4%	19.4%	10.8%	16.3%	18.7%	N/A
Ave	14.4%	14.4%	10.8%	13.1%	14.1%	22.7%

Figure I.6 6% bentonite turbulent flow predictions and average % error using the Newtonian approximation method – all rheologies

Torrance

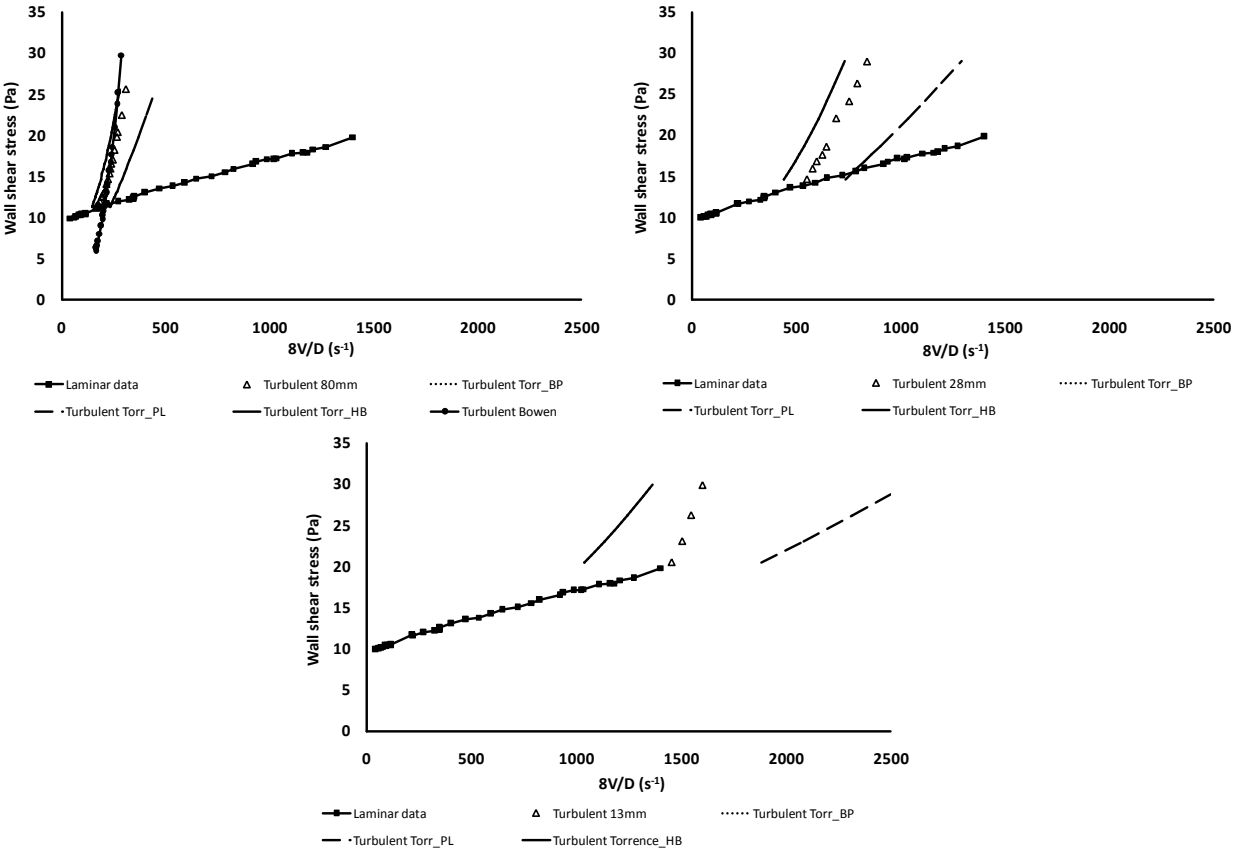

(8V/D) RMSE values - Torrance method				
Pipe diameter	HB	BP	PL	BOWEN (To)
80mm	14.1%	14.1%	35.0%	22.7%
28mm	16.7%	16.7%	40.7%	N/A
13mm	24.3%	24.3%	39.3%	N/A
Ave	18.3%	18.3%	38.3%	22.7%

Figure I.7 6% bentonite turbulent flow predictions and average % error using the Torrance method – all rheologies

One rheology plotted for all techniques

Bingham plastic

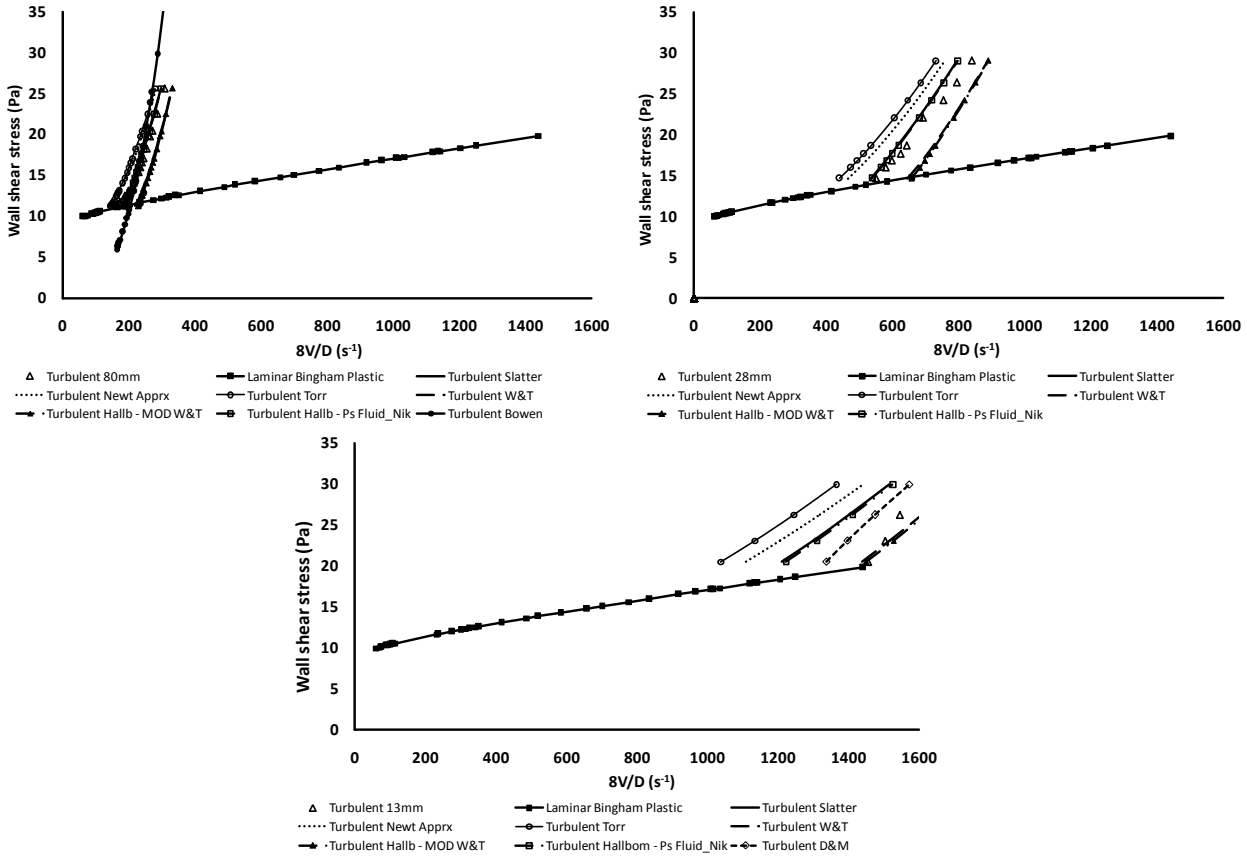

(8V/D) RMSE values - Bingham Plastic]								
Pipe diameter	W&T	NEWT	TORR	D&M	SLATT	BOWEN (To)	MOD_W&T	Ps Fld_Nik
80mm	19.0%	11.2%	14.1%	N/A	4.8%	22.7%	22.1%	4.9%
28mm	13.6%	12.6%	16.7%	N/A	3.7%	N/A	15.0%	3.0%
13mm	2.1%	19.4%	24.3%	6.6%	13.2%	N/A	5.3%	12.5%
Ave	11.6%	14.4%	18.3%	6.6%	7.2%	22.7%	14.1%	6.8%

Figure I.8 6% bentonite turbulent flow predictions and average % error using the Bingham plastic rheology – all techniques

Casson

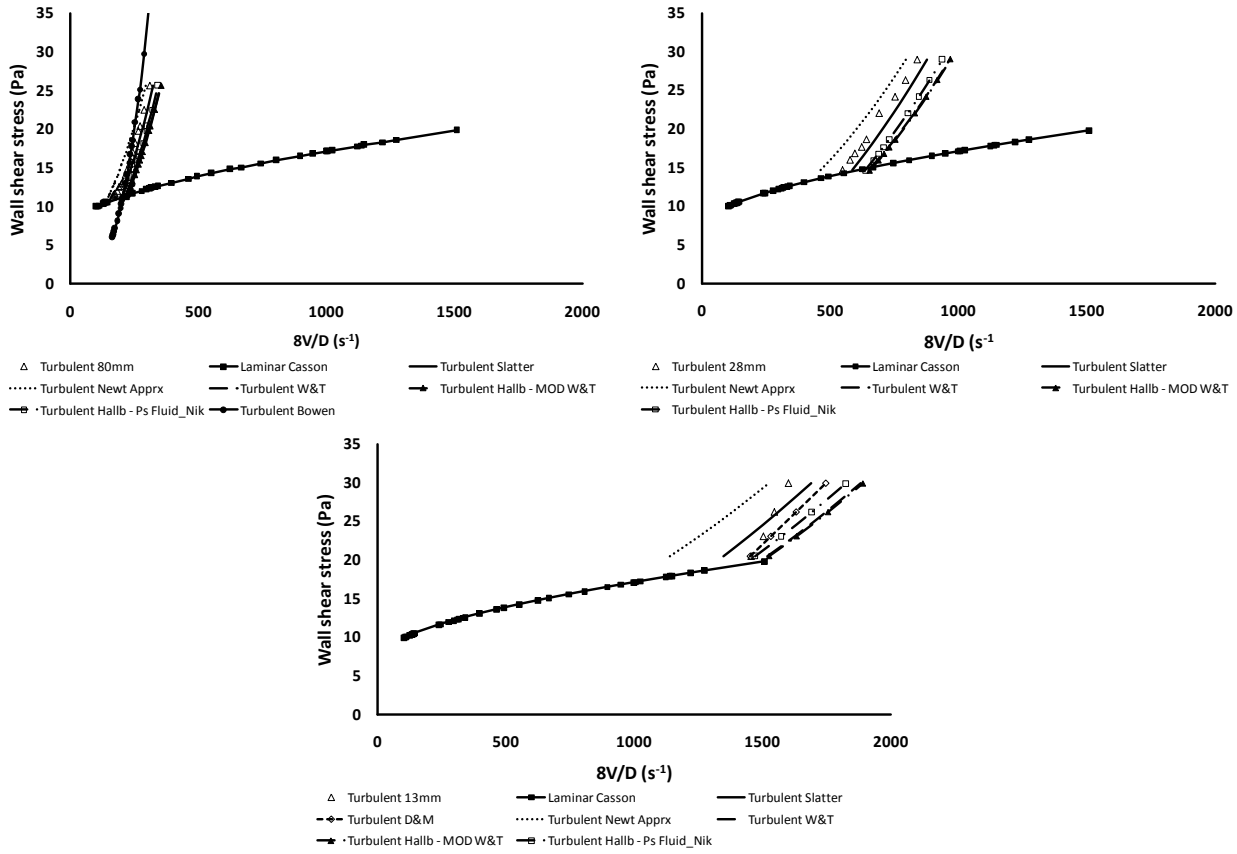

(8V/D) RMSE values - Casson								
Pipe diameter	W&T	NEWT	TORR	D&M	SLATT	BOWEN (To)	MOD_W&T	Ps Fld_Nik
80mm	19.3%	11.6%	N/A	N/A	10.2%	22.7%	20.6%	18.1%
28mm	17.5%	11.3%	N/A	N/A	5.9%	N/A	18.3%	14.7%
13mm	8.5%	16.3%	N/A	2.6%	4.0%	N/A	12.7%	5.1%
Ave	15.1%	13.1%	N/A	2.6%	6.7%	22.7%	17.2%	12.6%

Figure I.9 6% bentonite turbulent flow predictions and average % error using the Casson rheology – all techniques

9% bentonite

One technique plotted for all rheologies

Wilson & Thomas

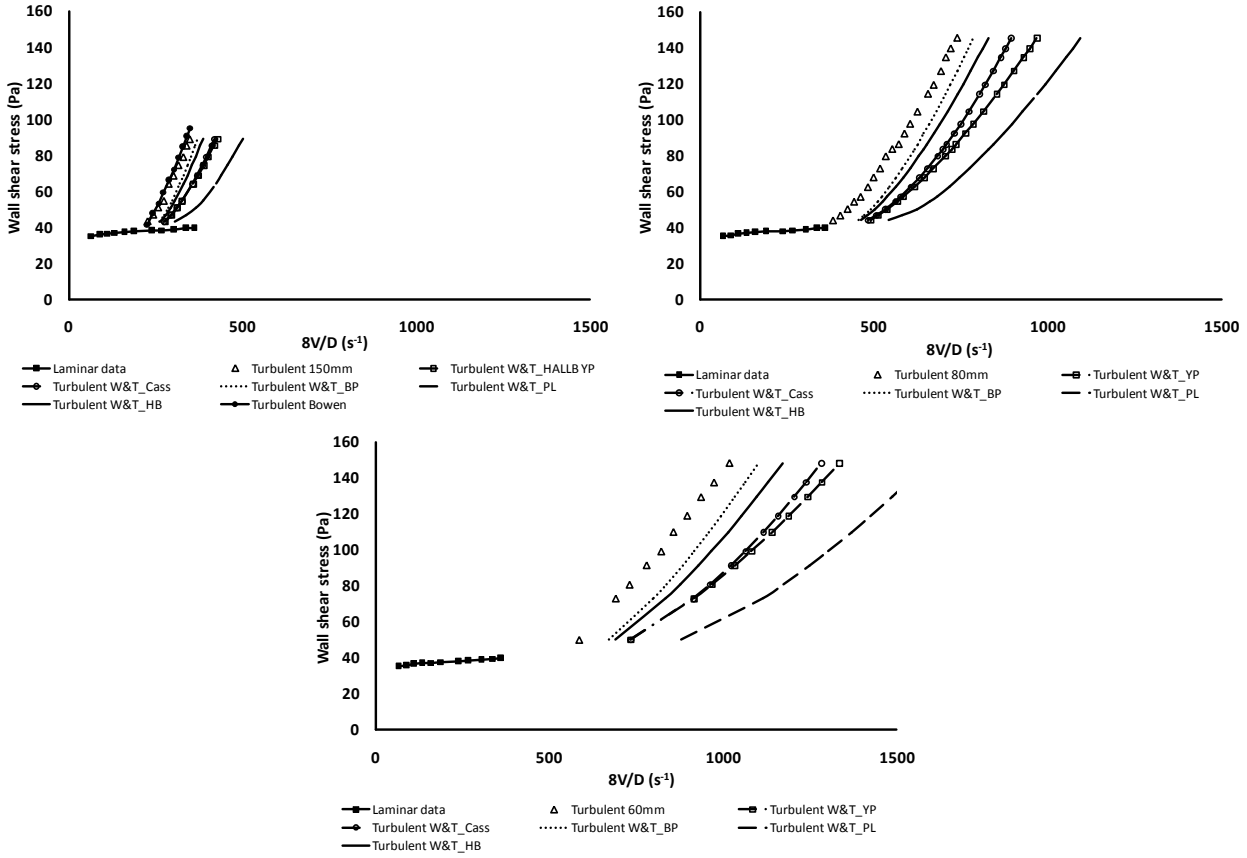

(8V/D) RMSE values - W&T(PRW) method						
Pipe diameter	HB	BP	PL	CASS	HALL_YP(SW)	BOWEN (To)
150mm	15.5%	13.4%	38.9%	21.2%	21.9%	3.1%
80mm	19.8%	17.5%	44.5%	25.8%	27.5%	N/A
60mm	19.5%	15.1%	57.5%	29.8%	30.1%	N/A
Ave	18.3%	15.3%	47.0%	25.6%	26.5%	3.1%

Figure I.10 9% bentonite turbulent flow predictions and average % error using the Wilson & Thomas method – all rheologies

Slatter

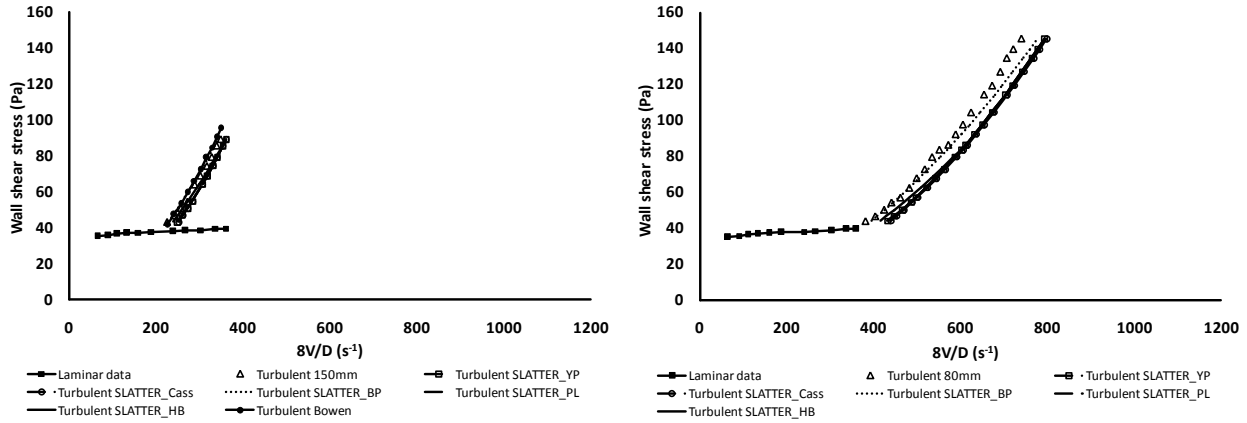

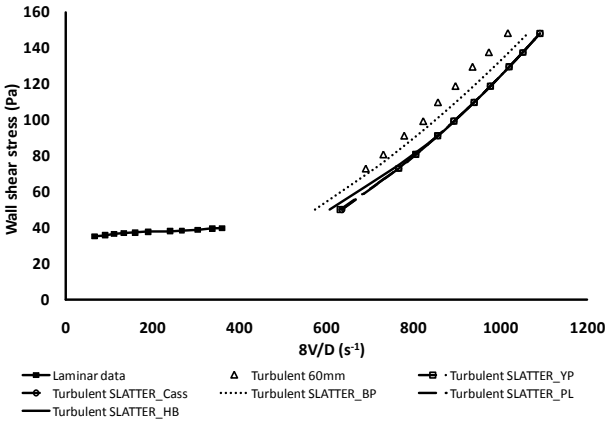

(8V/D) RMSE values - Slatter method						
Pipe diameter	HB	BP	PL	CASS	HALL_YP	BOWEN (To)
150mm	3.9%	1.7%	8.8%	8.8%	7.7%	3.1%
80mm	7.0%	1.7%	12.0%	12.7%	11.1%	N/A
60mm	7.3%	2.7%	9.8%	9.8%	9.6%	N/A
Ave	6.0%	2.1%	10.2%	10.4%	9.5%	3.1%

Figure I.11 9% bentonite turbulent flow predictions and average % error using the Slatter method – all rheologies

Hallbom: Smooth wall turbulence – Modified Wilson & Thomas

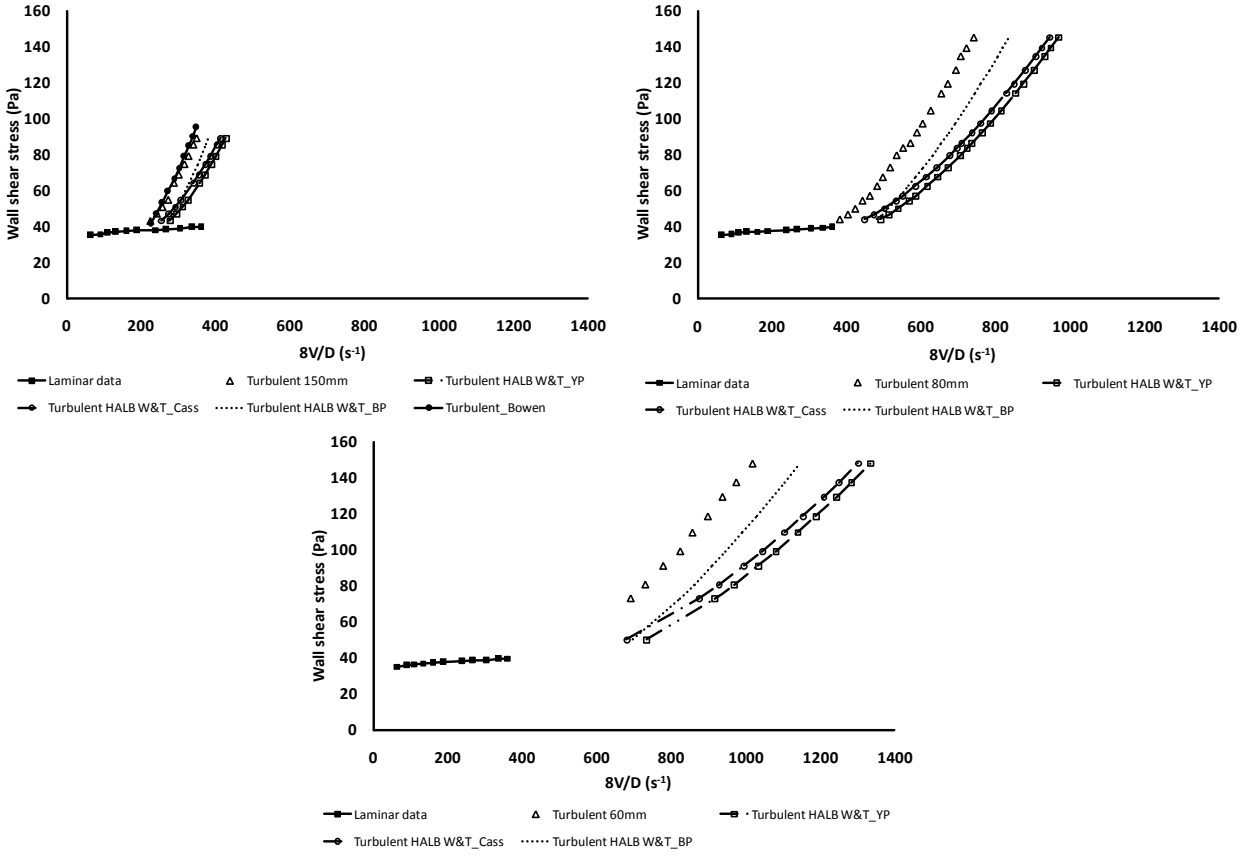

(8V/D) RMSE values - Hallb Mod W&T (SW)				
Pipe diameter	BP	CASS	YP	BOWEN (To)
150mm	18.1%	12.9%	21.9%	3.1%
80mm	23.2%	17.5%	27.5%	N/A
60mm	18.6%	23.2%	30.1%	N/A
Ave	20.0%	17.9%	26.5%	3.1%

Figure I.12 9% bentonite turbulent flow predictions and average % error using the Hallbom modified Wilson & Thomas method – all rheologies

Hallbom: Partially rough wall turbulence (Pseudofluid) - Using Nikuradse

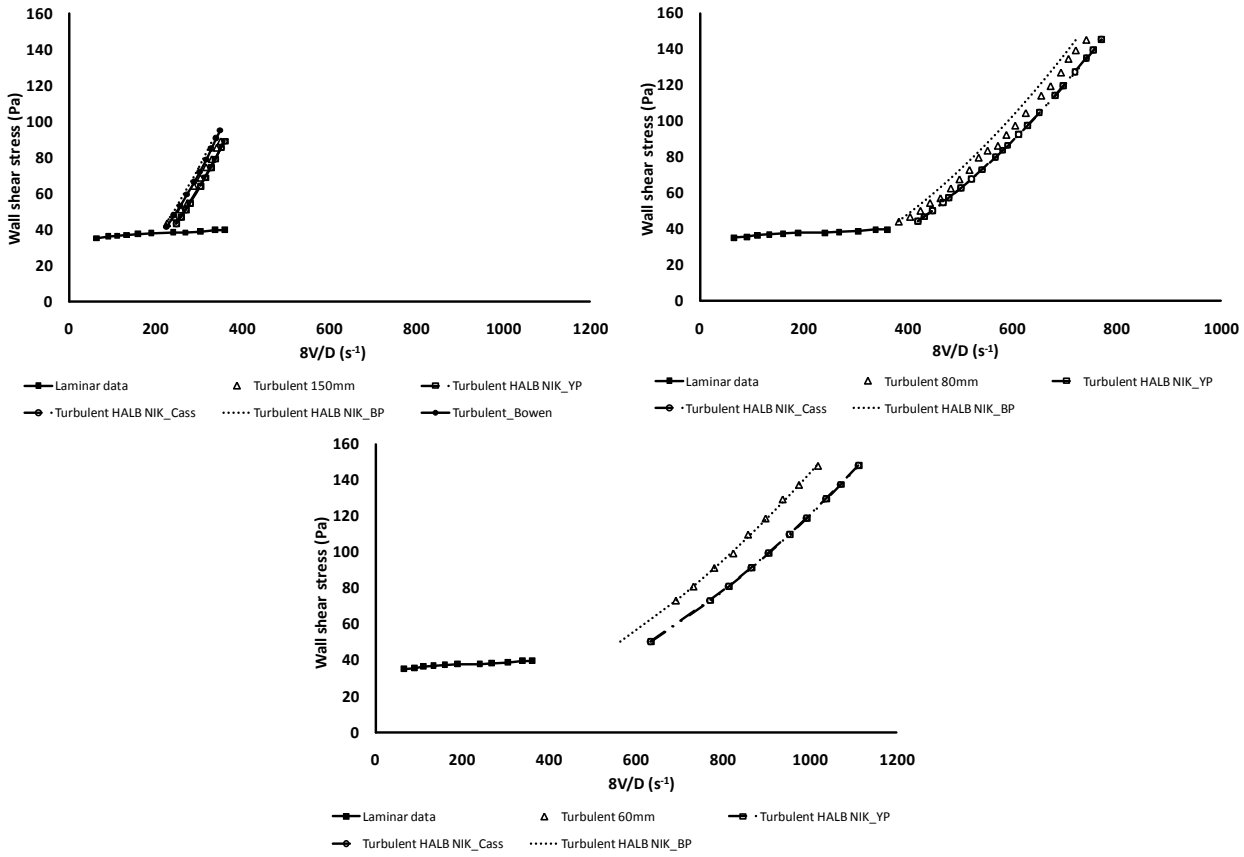

(8V/D) RMSE values - Hallbom_Nikuradse				
Pipe diameter	BP	CASS	YP	BOWEN (To)
150mm	3.5%	6.6%	6.8%	3.1%
80mm	2.2%	7.2%	7.3%	N/A
60mm	1.4%	10.2%	10.4%	N/A
Ave	2.3%	8.0%	8.2%	3.1%

Figure I.13 9% bentonite turbulent flow predictions and average % error using the Hallbom Nikuradse pseudo fluid method – all rheologies

Newtonian Approximation

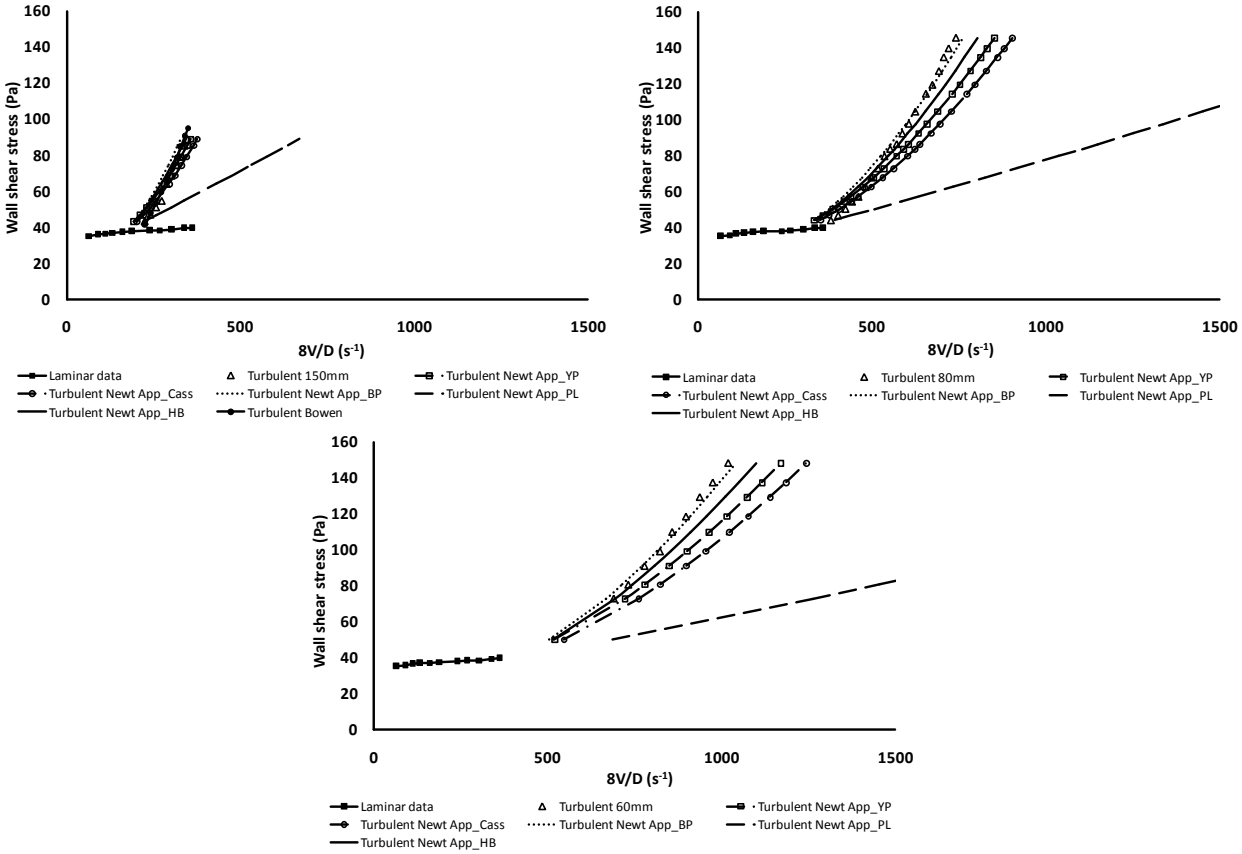

(8V/D) RMSE values - Newtonian Approximation						
Pipe diameter	HB	BP	PL	CASS	HALL_YP	BOWEN (To)
150mm	12.2%	13.6%	8.5%	8.5%	12.6%	3.1%
80mm	10.6%	12.1%	10.5%	6.4%	11.0%	N/A
60mm	4.7%	6.6%	66.4%	9.9%	7.5%	N/A
Ave	9.2%	10.7%	28.5%	8.2%	10.3%	3.1%

Figure I.14 9% bentonite turbulent flow predictions and average % error using the Newtonian Approximation method – all rheologies

Torrance

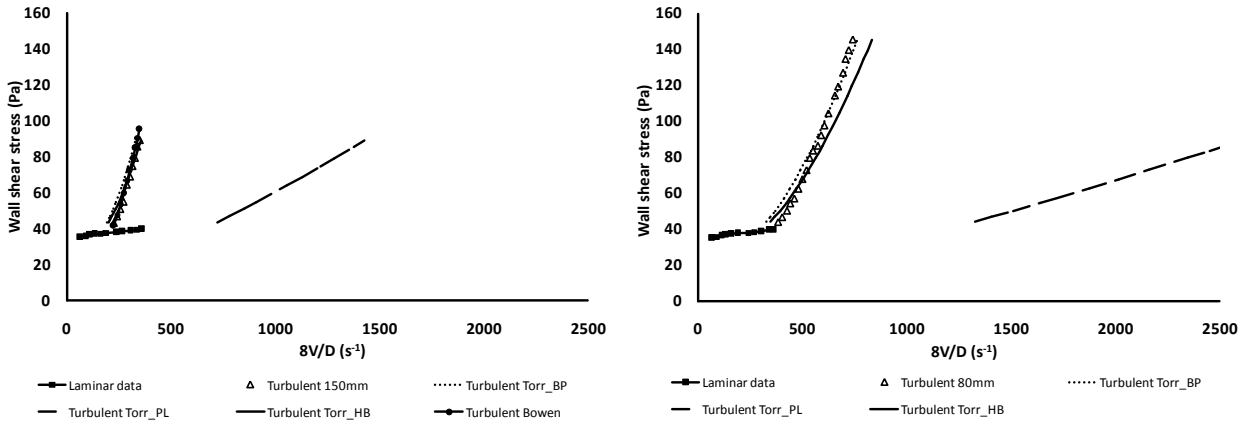

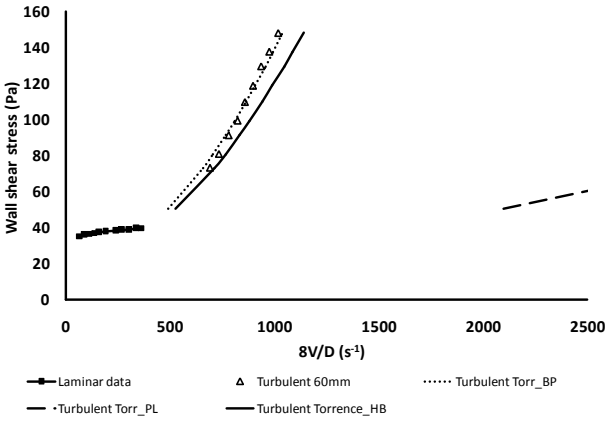

(8V/D) RMSE values - Torrance method				
Pipe diameter	HB	BP	PL	BOWEN (To)
150mm	10.0%	14.6%	224.5%	3.1%
80mm	9.0%	14.1%	250.7%	N/A
60mm	6.0%	8.2%	316.1%	N/A
Ave	8.3%	12.3%	263.8%	3.1%

Figure I.15 9% bentonite turbulent flow predictions and average % error using the Torrance method – all rheologies

One rheology plotted for all techniques

Bingham plastic

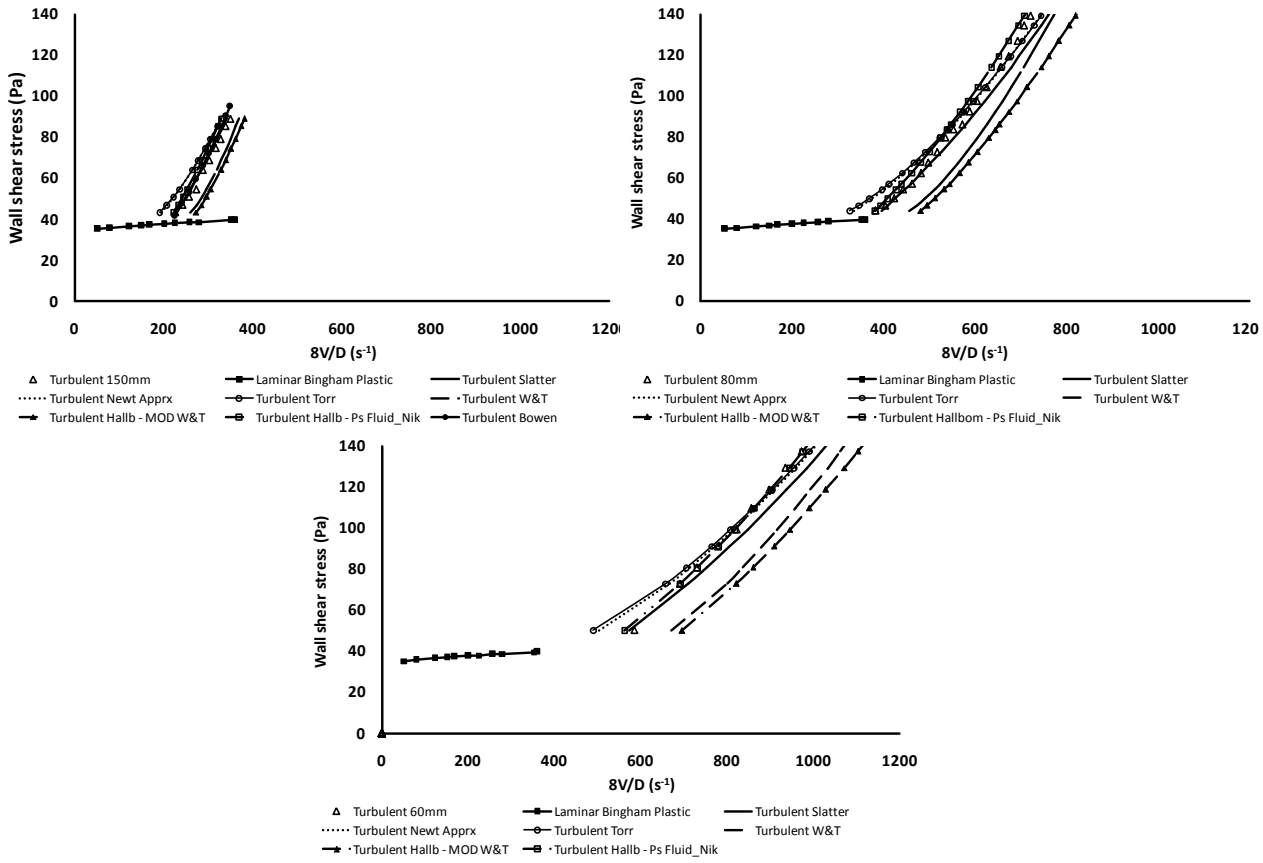

(8V/D) RMSE values - Bingham Plastic								
Pipe diameter	W&T	NEWT	TORR	D&M	SLATT	BOWEN (To)	MOD_W&T	Ps Fld_Nik
150mm	13.4%	13.6%	14.6%	N/A	1.7%	3.1%	18.1%	3.5%
80mm	17.5%	12.1%	14.1%	N/A	1.7%	N/A	23.2%	2.2%
60mm	15.1%	6.6%	8.2%	N/A	2.7%	N/A	18.6%	1.4%
Ave	15.3%	10.7%	12.3%	N/A	2.1%	3.1%	20.0%	2.3%

Figure I.16 9% bentonite turbulent flow predictions and average % error using the Bingham plastic rheology – all techniques

Casson

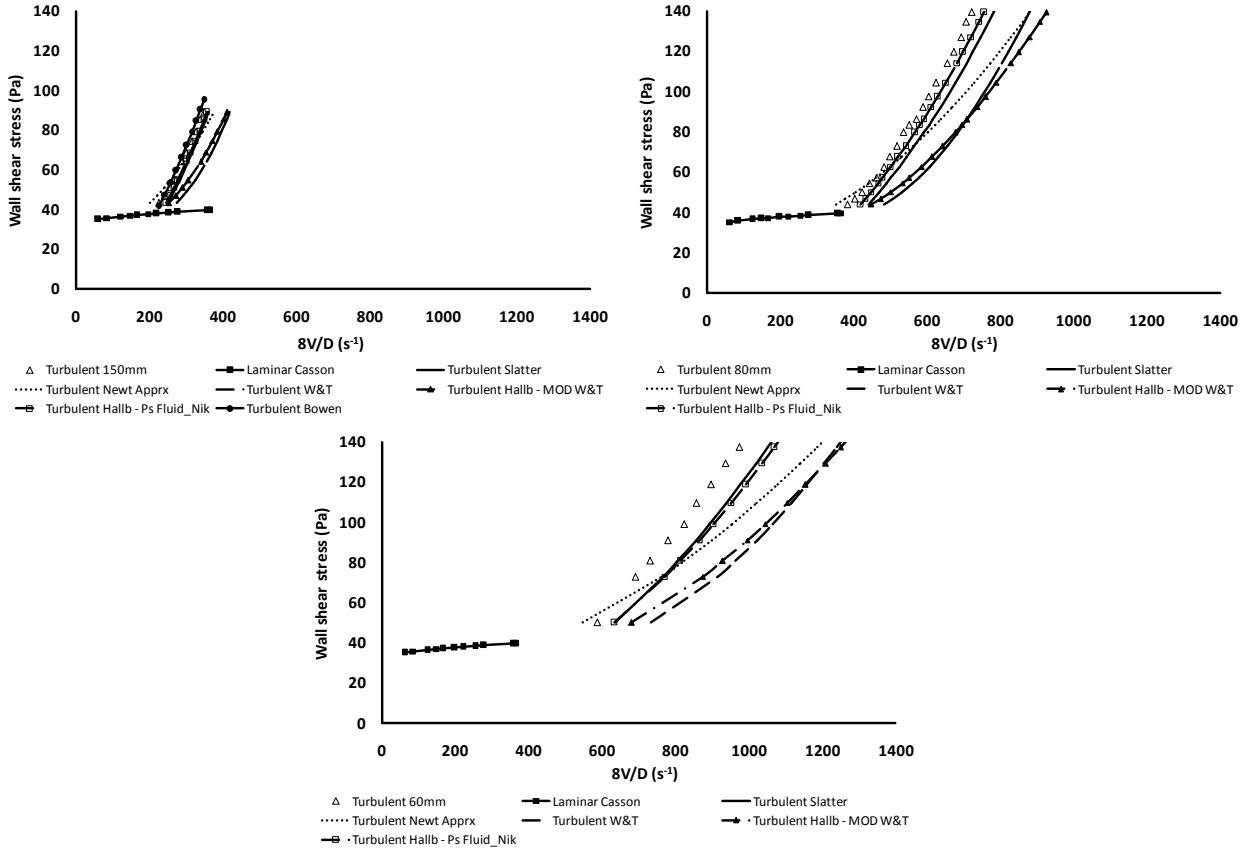

(8V/D) RMSE values - Casson								
Pipe diameter	W&T	NEWT	TORR	D&M	SLATT	BOWEN (To)	MOD_W&T	Ps Fld_Nik
150mm	21.2%	8.5%	N/A	N/A	8.8%	3.1%	12.9%	6.6%
80mm	25.8%	6.4%	N/A	N/A	12.7%	N/A	17.5%	7.2%
60mm	29.8%	9.9%	N/A	N/A	9.8%	N/A	23.2%	10.2%
Ave	25.6%	8.2%	N/A	N/A	10.4%	3.1%	17.9%	8.0%

Figure I.17 9% bentonite turbulent flow predictions and average % error using the Casson rheology – all techniques

Appendix J. Turbulent flow analysis and results: CMC

The results for the 3% and 8% CMC turbulent flow predictions are presented here.

3% CMC

One technique plotted for all rheologies

Wilson & Thomas

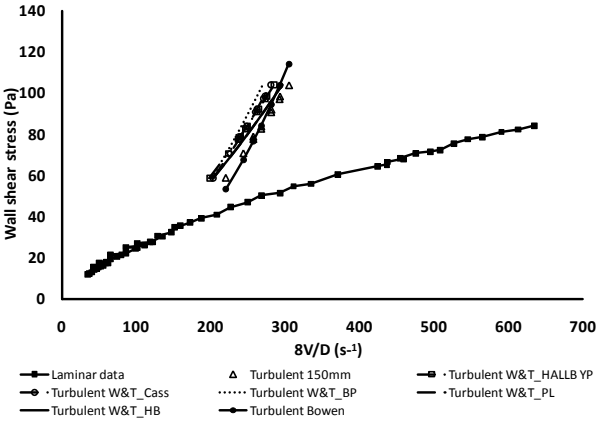

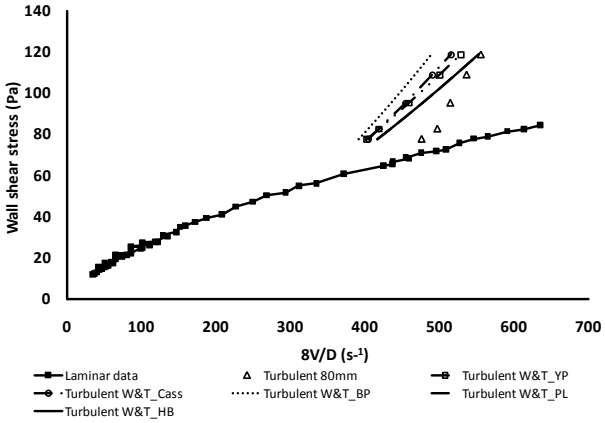

(8V/D) RMSE values - W&T(PRW) method						
Pipe diameter	HB	BP	PL	CASS	HALL_YP(SW)	BOWEN (To)
150mm	4.2%	10.2%	4.2%	7.3%	7.2%	4.3%
80mm	8.9%	16.1%	8.9%	12.8%	12.2%	N/A
Ave	6.5%	13.2%	6.5%	10.0%	9.7%	4.3%

Figure J.1 3% CMC turbulent flow predictions and average % error using the Wilson & Thomas method – all rheologies

Slatter

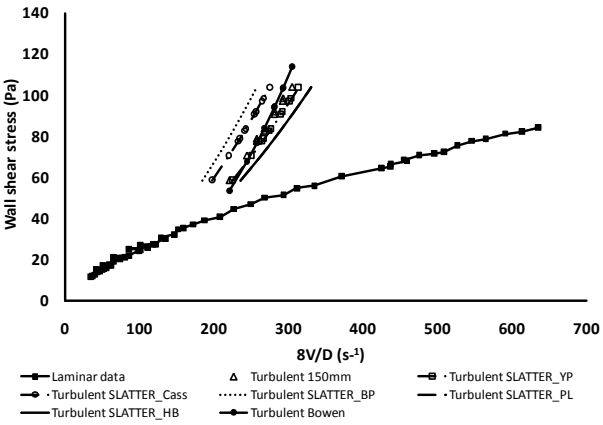

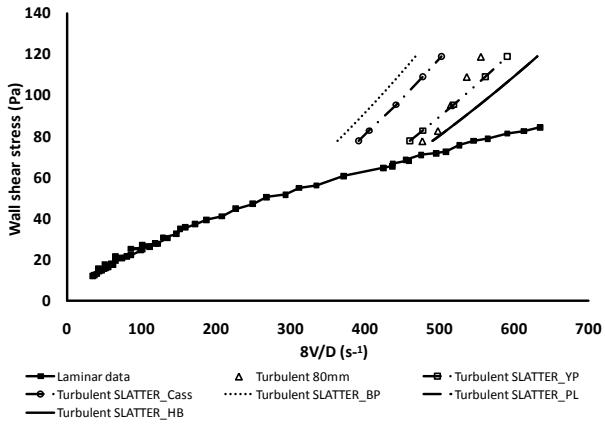

(8V/D) RMSE values - Slatter method						
Pipe diameter	HB	BP	PL	CASS	HALL_YP	BOWEN (To)
150mm	8.3%	15.5%	8.3%	9.7%	2.9%	4.3%
80mm	6.2%	21.4%	6.2%	15.3%	3.3%	N/A
Ave	7.3%	18.4%	7.3%	12.5%	3.1%	4.3%

Figure J.2 3% CMC turbulent flow predictions and average % error using the Slatter method – all rheologies

Hallbom: Smooth wall turbulence – Modified Wilson & Thomas

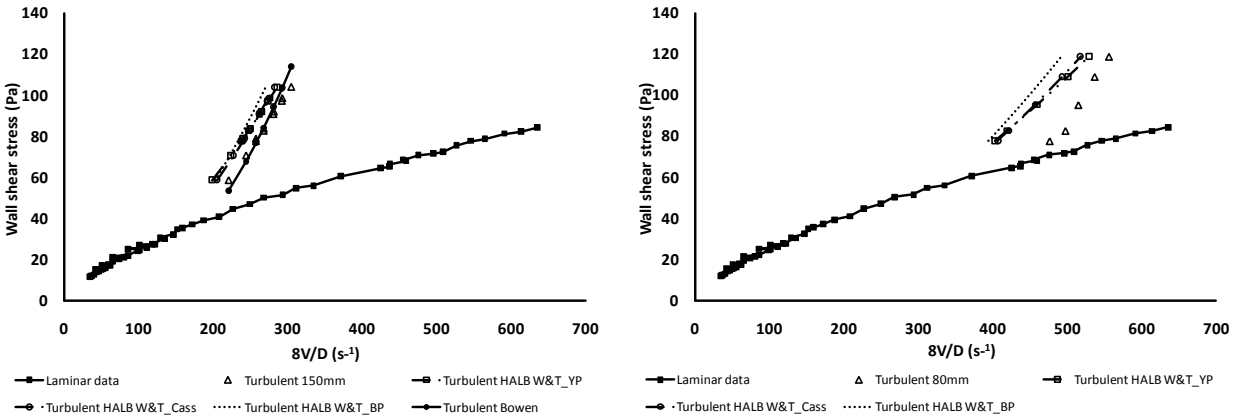

(8V/D) RMSE values - Hallb Mod W&T (SW)				
Pipe diameter	BP	CASS	YP	BOWEN (To)
150mm	9.4%	6.9%	7.2%	4.3%
80mm	15.8%	12.4%	12.2%	N/A
Ave	12.6%	9.6%	9.7%	4.3%

Figure J.3 3% CMC turbulent flow predictions and average % error using the Modified Wilson & Thomas method – all rheologies

Hallbom: Partially rough wall turbulence (Pseudofluid) - Using Nikuradse

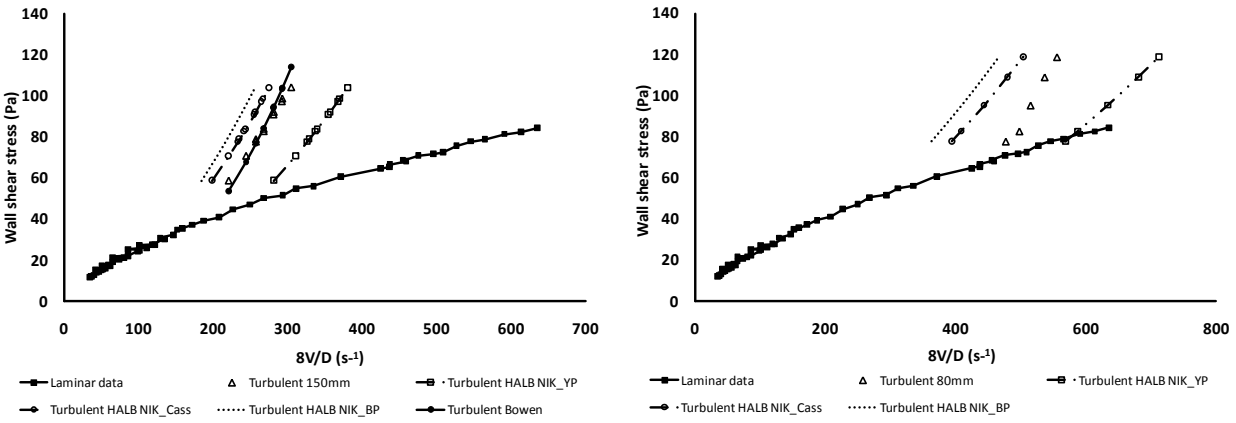

(8V/D) RMSE values - Hallbom_Nikuradse				
Pipe diameter	BP	CASS	YP	BOWEN (To)
150mm	15.8%	9.4%	26.4%	4.3%
80mm	21.5%	15.0%	21.7%	N/A
Ave	18.7%	12.2%	24.1%	4.3%

Figure J.4 3% CMC turbulent flow predictions and average % error using the Hallbom Nikuradse pseudo fluid method – all rheologies

Dodge & Metzner

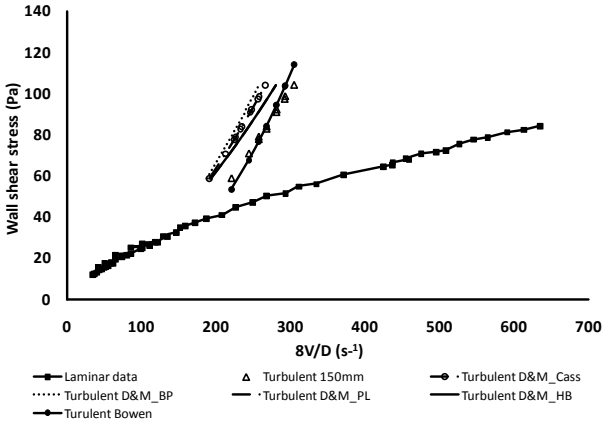

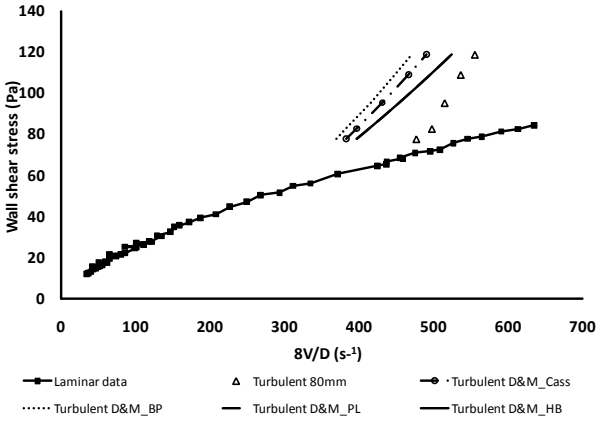

(8V/D) RMSE values - Dodge & Metzner					
Pipe diameter	HB	BP	PL	CASS	BOWEN (To)
150mm	9.3%	15.0%	9.3%	12.5%	4.3%
80mm	13.4%	20.4%	13.4%	17.4%	N/A
Ave	11.3%	17.7%	11.3%	14.9%	4.3%

Figure J.5 3% CMC turbulent flow predictions and average % error using the Dodge & Metzner method – all rheologies

Newtonian approximation

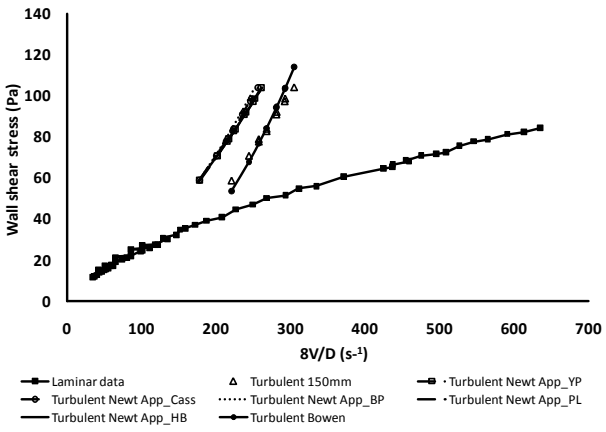

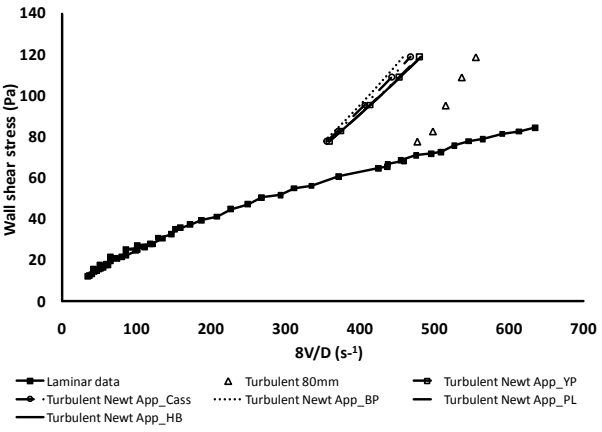

(8V/D) RMSE - Newtonian Approximation						
Pipe diameter	HB	BP	PL	CASS	HALL_YP	BOWEN (To)
150mm	15.9%	17.8%	15.9%	16.9%	15.9%	4.3%
80mm	21.2%	23.5%	21.2%	22.5%	21.2%	N/A
Ave	18.5%	20.6%	18.5%	19.7%	18.5%	4.3%

Figure J.6 3% CMC turbulent flow predictions and average % error using the Newtonian approximation method – all rheologies

Torrance

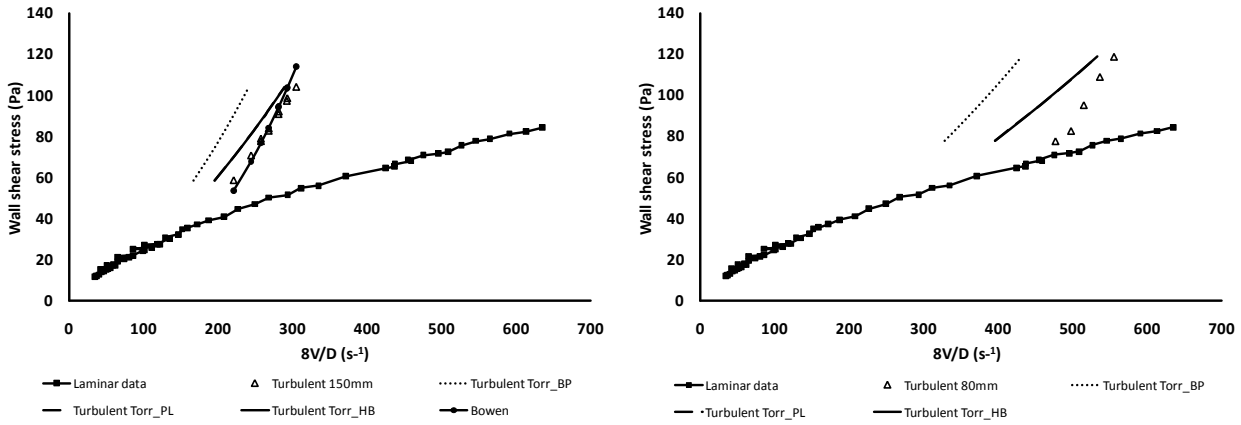

(8V/D) RMSE values - Torrance method				
Pipe diameter	HB	BP	PL	BOWEN (To)
150mm	7.0%	21.7%	7.0%	4.3%
80mm	12.9%	28.5%	12.9%	N/A
Ave	10.0%	25.1%	10.0%	4.3%

Figure J.7 3% CMC turbulent flow predictions and average % error using the Torrance method – all rheologies

One rheology plotted for all techniques

Power law

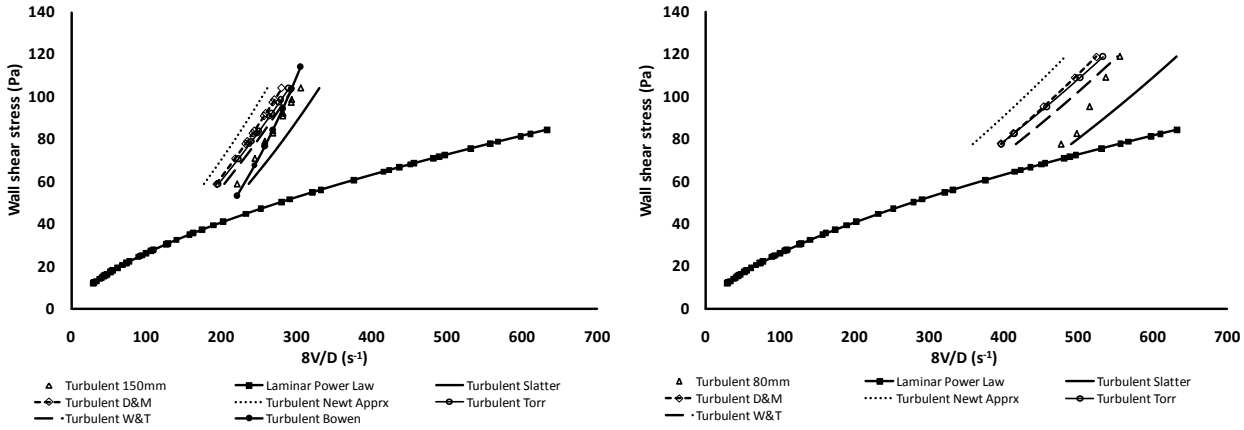

(8V/D) RMSE values - Power Law						
Pipe diameter	W&T	NEWT	TORR	D&M	SLATT	BOWEN (To)
150mm	4.2%	15.9%	7.0%	9.3%	8.3%	4.3%
80mm	8.8%	21.2%	12.9%	13.4%	6.2%	N/A
Ave	6.5%	18.5%	10.0%	11.3%	7.3%	4.3%

Figure J.8 3% CMC turbulent flow predictions and average % error using the power law rheology – all techniques

8% CMC

One technique plotted for all rheologies

Wilson & Thomas

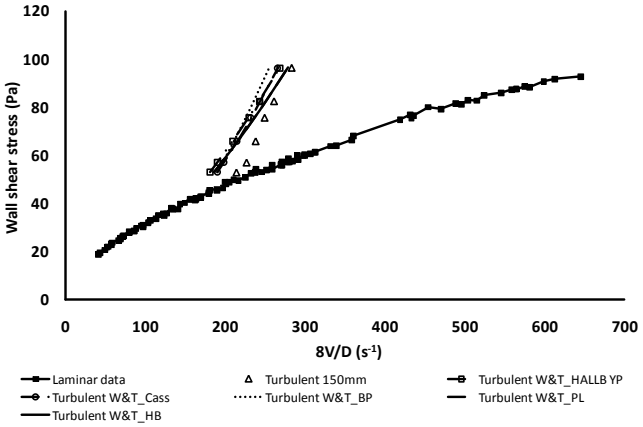

(8V/D) RMSE values - W&T(PRW) method					
Pipe diameter	HB	BP	PL	CASS	HALL_YP(SW)
150mm	7.8%	10.5%	7.8%	8.7%	10.5%
Ave	7.8%	10.5%	7.8%	8.7%	10.5%

Figure J.9 8% CMC turbulent flow predictions and average % error using the Wilson & Thomas method – all rheologies

Slatter

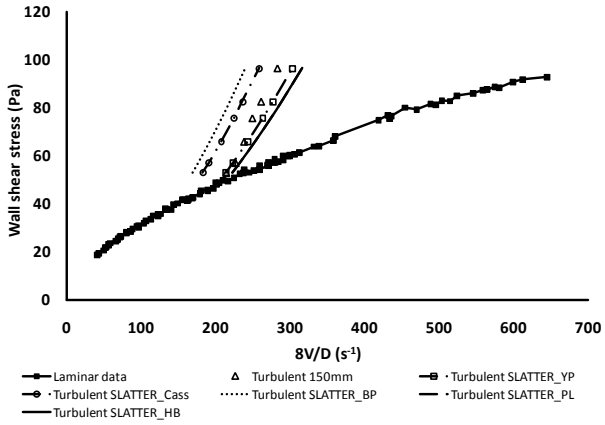

(8V/D) RMSE values - Slatter method					
Pipe diameter	HB	BP	PL	CASS	HALL_YP
150mm	7.6%	18.4%	7.6%	11.8%	3.8%
Ave	7.6%	18.4%	7.6%	11.8%	3.8%

Figure J.10 8% CMC turbulent flow predictions and average % error using the Slatter method – all rheologies

Hallbom: Smooth wall turbulence – Modified Wilson & Thomas

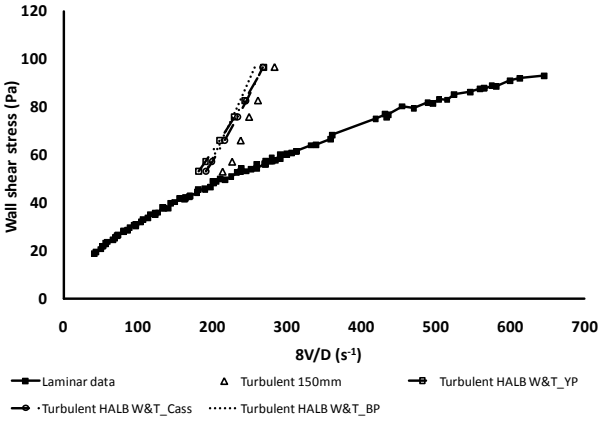

(8V/D) RMSE values - Hallb Mod W&T (SW)			
Pipe diameter	BP	CASS	YP
150mm	10.0%	8.3%	10.5%
Ave	10.0%	8.3%	10.5%

Figure J.11 8% CMC turbulent flow predictions and average % error using the Modified Wilson & Thomas method – all rheologies

Hallbom: Partially rough wall turbulence (pseudofluid) - Using Nikuradse

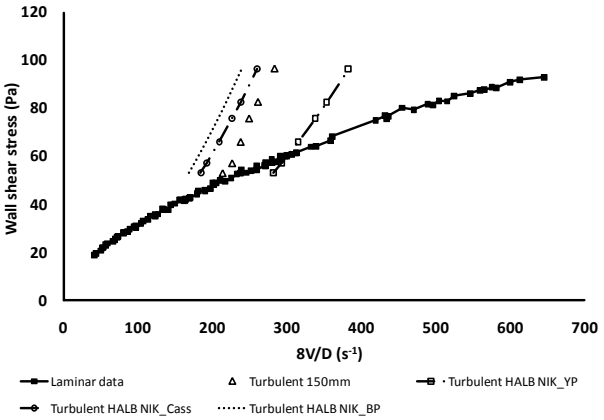

(8V/D) RMSE values - Hallbom_Nik method			
Pipe diameter	BP	CASS	YP
150mm	18.6%	11.3%	33.4%
Ave	18.6%	11.3%	33.4%

Figure J.12 8% CMC turbulent flow predictions and average % error using the Hallbom Nikuradse pseudo fluid method – all rheologies

Dodge & Metzner

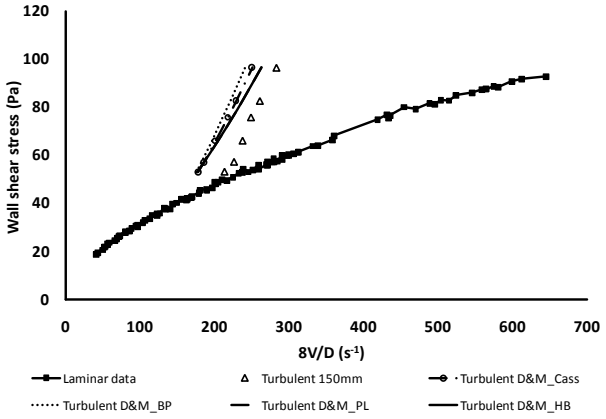

(8V/D) RMSE values - Dodge & Metzner method				
Pipe diameter	HB	BP	PL	CASS
150mm	12.6%	16.5%	11.7%	14.1%
Ave	12.6%	16.5%	11.7%	14.1%

Figure J.13 8% CMC turbulent flow predictions and average % error using the Dodge & Metzner method – all rheologies

Newtonian approximation

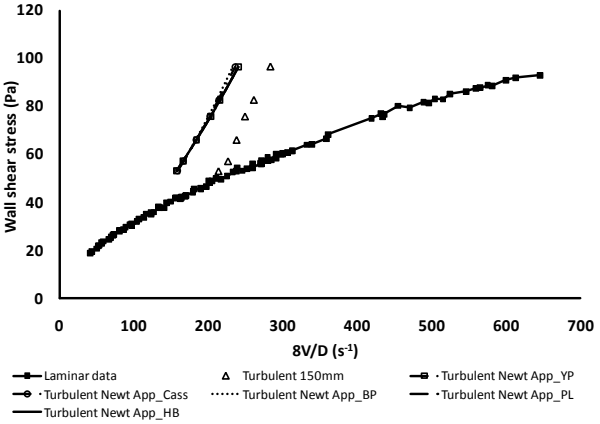

(8V/D) RMSE values - Newtonian Approximation method					
Pipe diameter	HB	BP	PL	CASS	HALL_YP
150mm	21.2%	21.9%	21.2%	21.5%	21.0%
Ave	21.2%	21.9%	21.2%	21.5%	21.0%

Figure J.14 8% CMC turbulent flow predictions and average % error using the Newtonian approximation method – all rheologies

Torrance

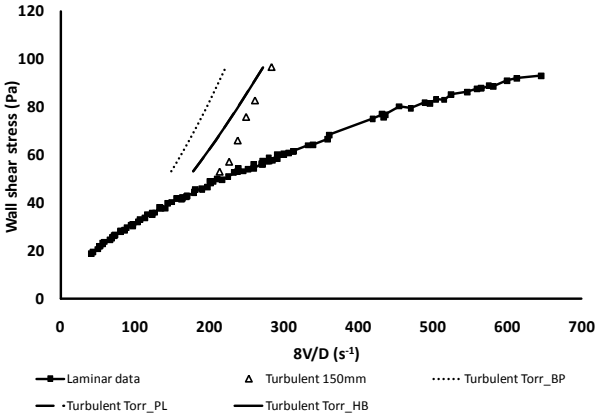

(8V/D) RMSE values - Torrance method			
Pipe diameter	HB	BP	PL
150mm	10.7%	26.3%	10.7%
Ave	10.7%	26.3%	10.7%

Figure J.15 8% CMC turbulent flow predictions and average % error using the Torrance method – all rheologies

One rheology plotted for all techniques

Power law

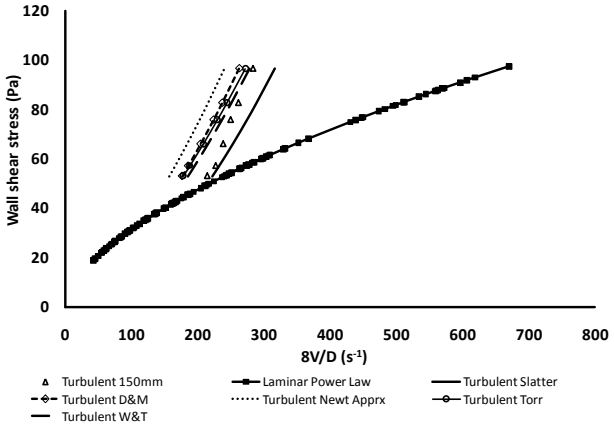

(8V/D) RMSE values - Power Law					
Pipe diameter	W&T	NEWT	TORR	D&M	SLATT
150mm	7.8%	21.2%	10.7%	11.7%	7.6%
Ave	7.8%	21.2%	10.7%	11.7%	7.6%

Figure J.16 6% bentonite turbulent flow predictions and average % error using the power law rheology – all techniques